Evolution of the Indo-Asian Orogen:

Insights from the Deformation of the Northern Tibetan Plateau,

Mass Balance Calculations, and Volcanic Geochemistry

by

Petr V. Yakovlev

A dissertation submitted in partial fulfillment
of the requirements for the degree of
Doctor of Philosophy
(Geology)
in the University of Michigan
2015

Doctoral Committee:

      Associate Professor Marin Kristen Clark, Chair
      Associate Professor Catherine E. Badgley
      Assistant Professor Eric A. Hetland
      Professor Rebecca Ann Lange
      Associate Professor Nathan A. Niemi

ACKNOWLEDGEMENTS

I would first like to thank my advisor, Marin Clark, for her continued support, and encouragement over the last five years, which helped me become more confident in my abilities as a scientist. I would also like to thank Nathan Niemi for his openness, and willingness to discuss a myriad of topics in tectonics, and the broader earth sciences. Our discussions helped me develop a broad awareness of new techniques, approaches, and ideas for the investigation of orogenic development, as well as a more in depth understanding of structural geology, and crustal deformation. My committee members, Rebecca Lange, Eric Hetland, and Catherine Badgley helped to broaden my understanding of geological processes, and aided me in incorporating ideas external to my specialty in developing interpretations. Faculty for whom I was a graduate instructor, Nathan Niemi, John Geissman, Marin Clark, Jeroen Ritsema, Rob van der Voo, and Nathan Sheldon helped develop my understanding of pedagogical methods, and gain confidence in my teaching abilities.

This thesis would have been impossible if not for the continued collaboration, and support of our colleagues at the Institute of Earth Environment, Chinese Academy of Sciences, Xi'An. Funding from the National Science Foundation of China under grant number 40921120406, and a commitment to the success of this project from institute director An Zhisheng were critical in accomplishing field work. Prof. Chang Hong was instrumental in managing the logistics of field excursions, navigating permitting issues, and was critical in developing our understanding of the Hoh Xil and Kumkuli Basins through his extensive knowledge of the regional scientific literature, and magnetostratigraphy. Jiang Yi was an impeccable field assistant, translator, and most of all, friend. I wish him, and his partner the best of luck in Beijing. Numerous others helped me in my travels in China, and Tibet, and I am incredibly thankful to them all for their kindness, and hard work.

My friends in grad school have been instrumental in shaping my understanding of the broader earth sciences, and in my ability to get through the highs and lows of grad school. Lydia Staisch was great to have in both the field, and in the lab. Grad school would have been significantly more challenging without her. Discussions with Tom Hudgins regarding melt generation, magmatic processes, and the mantle were vital to my ability to write my fourth chapter, and intelligently discuss geochemistry. Clay Tabor, Rich Fiorella, Ethan Hyland, and Tim Gallagher helped answer my

TABLE OF CONTENTS

LIST OF FIGURES

LIST OF TABLES

LIST OF APPENDICES

ABSTRACT

The Indo-Asian orogen is the world's largest region of high topography, which affects both regional climate and mammalian speciation. How and when it achieved modern elevations and crustal thicknesses remains controversial, though there is agreement that ~40-50 Ma collision between India and Asia led to widespread crustal thickening and some amount of elevation gain since that time. Development of pre-collisional topography, the structural mechanisms of crustal thickening since collision, and the role of mantle lithosphere removal in producing elevation gain are common processes by which we interpret the topographic history of the orogen. In chapter 2, I address pre-collisional topography by reconstructing crustal volume before collision using total plate convergence estimates since 40 Ma. Results show that modern crustal volumes are 30% less than those estimated for 40 Ma using a pre-collisional crustal thickness of ~40 km (global average). I argue that this imbalance can be eliminated if the majority of Asian and Indian crust now found within the boundaries of the orogen was 23-32 km thick and consequentially at low elevations prior to collision. Chapter 3 focuses on mechanisms of recent faulting from a rare occurrence of thrusting at high elevation in the Guaizi Liang of northern Tibet. (~5000 m asl). We document 9 km (20%) shortening since Pliocene time and Quaternary shortening rates of 1.7 mm/yr based on balanced cross-sections and ^{36}Cl cosmogenic radionuclide dating of a folded alluvial surface. Observed structural trends suggest that thrust faulting is related to simple shear between the Altyn Tagh and Kunlun/Manyi strike-slip faults, which need not produce crustal thickening. In chapter 4, I investigate the modification of the mantle lithosphere through a compilation of new and published geochemistry data from volcanic rocks across the plateau. I interpret slab flattening to have occurred at 40-30 Ma to drive widespread metasomatism of the Asian lithospheric mantle by melts from subducted Indian sediments. Removal of the slab at 30 Ma generated widespread volcanism across the plateau and likely thinned or removed them mantle lithosphere. Termination of volcanism in the southern Tibetan Plateau suggests renewed Indian underthrusting since 15 Ma.

Chapter 1: Introduction

1.1 Motivation

The Indo-Asian orogen is the largest contiguous region of high topography in the world, and includes the Himalaya and the Tibetan Plateau. It thus provides the strongest signal of mountain building in modern time, and is thus a key site for the investigation of the geodynamic and topographic development of mountain belts. The topographic evolution of the plateau reflects the geodynamic processes that accommodate continental convergence, as well as having a pronounced effect on modern and paleo-climate and the evolution and diversification of mammalian species (

We provide an additional constraint on the generation of metasomatism beneath the Tibetan Plateau using Pb isotopes. In the northern hemisphere, mid-ocean ridge basalts (MORBs) show a distinct linear relationship in $^{206}Pb/^{204}Pb$ vs $^{207}Pb/^{204}Pb$ space and $^{206}Pb/^{204}Pb$ vs $^{208}Pb/^{204}Pb$ space, which is termed the northern hemisphere reference line (NHRL) (Hart, 1984). Continental crust and sediments generally lie above this line. We investigate Pb isotopes by first calculating the Δ7/4 and Δ8/4 values of samples which have been analyzed for $^{207}Pb/^{204}Pb$, $^{206}Pb/^{204}Pb$, and $^{208}Pb/^{204}Pb$ ratios. The Δ7/4 value represents the difference between the observed $^{207}Pb/^{204}Pb$ ratio of a sample, and the $^{207}Pb/^{204}Pb$ of the NHRL at a $^{206}Pb/^{204}Pb$ ratio identical to that measured in the sample (Hart, 1984; Figure 7). Similarly, the Δ8/4 value is the difference between the $^{208}Pb/^{204}Pb$ ratio of a sample, and the $^{208}Pb/^{204}Pb$ of the NHRL at the sample's $^{206}Pb/^{204}Pb$ ratio (Hart, 1984). Group B lavas have generally high Δ7/4 and Δ8/4 values (above 15 and 100, respectively). These require input of old highly radiogenic continental crust and/or sediments, such as those from the passive margin of the northern Indian subcontinent, into the mantle source region of the lavas. However, the Δ7/4 and Δ8/4 values of group B lavas are higher than those of Himalayan sediments, suggesting an additional highly radiogenic and therefore older source. Δ7/4 and Δ8/4 values of lavas in the central, and northern Tibetan Plateau are lower than that of those in the southern Tibetan Plateau, indicating a lower contribution of continental sediments into their mantle source regions.

1.1.1 Summary of Interpretations

Major, trace and isotopic compositions of lavas in the Tibetan plateau constrain melt source compositions, and the geodynamic drivers of magmatism. Prior to 40 Ma lavas were produced during

subduction and arc volcanism, while lavas erupted since 30 Ma were generated by low-degree melting of a metasomatized mantle lithosphere. Metasomatism of the mantle lithosphere or thin mantle wedge beneath the Tibetan Plateau likely occurred between 30 and 40 Ma, as a consequence of the incorporation of sediments from the northern margin of India into the mantle, and migration of partial melts and/or fluids through the mantle lithosphere.

1.2 Discussion and Geodynamic Interpretation

We interpret the geodynamic evolution of the Indo-Asian orogen based on the timing and compositions of lavas from the Tibetan Plateau, and the distribution of faulting. We discuss specific ~10-15 Ma time windows in which we describe active patterns of deformation, as well as sources and drivers of magmatism. Volcanism prior to the ~50 Ma Indian collision was driven by northward subduction of Tethyian oceanic crust, resulting in pervasive plutonism and group A volcanism in the Gangdese arc of the southern Tibetan Plateau. Concurrent plutonism and group A volcanism in the Tanggula Shan of the central Tibetan Plateau are likely the result of the reactivation of a south-directed fossilized Mesozoic subduction zone (Roger et al., 2000). Magmatism in both regions was most likely driven by subduction and dehydration of oceanic crust, and mantle lithosphere. In the Tangula Shan subduction of Mesozoic marine sediments of the Songpan-Ganzi terrane may have also contributed to melt generation (Wang et al., 2010). Subduction of Songpan-Ganzi crust is broadly compatible with evidence for Eocene to Oligocene deformation of Cenozoic terrestrial sediments which had been deposited near the suture between the Songpan-Ganzi and Qiangtang terranes (Li et al., 2012; Staisch et al., 2014).

The arrival of continental crust of the Indian passive margin at the trench between 56 and 40 Ma (e.g. Bouilhol et al., 2013; Sciunnach and Garzanti, 2012), potentially resulted in flattening of the Tethyian slab and metasomatism of a frozen mantle wedge or lithospheric mantle beneath much of the Tibetan Plateau by 30 Ma. A modern analog may be the Trans-Mexican Volcanic Belt, where a flat Cocos slab drives dehydration melting, and resulting volcanism > 200 km into the continental interior (Jödicke et al., 2006; Pérez-Campos et al., 2008). In Mexico, slab flattening is hypothesized to have been caused by hydration of the mantle wedge, which generated a low viscosity channel that now prevents coupling between the Cocos sab and overriding North American crust (Manea and Gurnis, 2007; Pérez-Campos et al., 2008). Influx of Indian sediment into the mantle during subduction would have provided a mechanism to rapidly hydrate and metasomatize the mantle wedge, drive slab flattening, and prevent coupling with overriding Asian crust, which did not undergo significant crustal shortening between 40 and 30 Ma (Figure 4.1, Figure 4.2, Figure 4.11). A general northerly decrease

in $\Delta 7/4$, $\Delta 8/4$, $^{87}Sr/^{86}Sr$ and an increase in $^{144}Nd/^{143}Nd$ in high MgO (>6 wt%) group B magmas is then indicative of a lower magnitude of metasomatism further away from the southern plate margin, likely due to the incorporation of fewer sedimentary rocks subducted at the plate margin into the mantle beneath those regions.

Flattening of the Tehyian slab may have also resulted in a northward migration of volcanism between to the central Tibetan Plateau between 40 and 30 Ma (Figure 4.1, Figure 4.11). The location of volcanism in this time interval suggests that the Tethyian slab reached past the BNS, and up to ~300 km away from the Asian plate boundary. An absence of volcanism in the Tanggula Shan during this time period indicates that southward directed subduction of Songpan-Ganzi crust must have stopped, with convergence instead accommodated by continued crustal shortening and deformation of basin sediments (Li et al., 2012; Staisch et al., 2014).

A large-scale transition in the composition and extent of volcanism occurred at ~30 Ma, as group B volcanism initiated across the entirety of the Tibetan Plateau. This shift in the spatial distribution of magmatism is roughly concurrent with the termination of upper crustal shortening in the northern Tibetan Plateau and is 10-15 Myr earlier than the development of extensional faulting (Blisniuk et al., 2001; Li et al., 2012; Ratschbacher et al., 2011; Staisch et al., 2014; Sun et al., 2005; Wu et al., 2008; Yuan et al., 2013). Previous authors have hypothesized a coeval initiation of volcanism and normal faulting linked to the removal of a dense lithospheric root and the attainment of elevations of ~5000 m at 10-15 Ma (e.g. Molnar et al., 1993). Our results show that normal faulting and volcanism did not initiate coevally and thus argue strongly against a middle-Miocene timing of lithospheric removal.

Potentially, the initiation of volcanism at ~30 Ma was driven by the rollback and/or breakoff of the Tethyian slab, rather than convective removal of the mantle lithosphere. Removal of the Tethyian slab likely precipitated an influx of hot asthenosphere to regions beneath the Tibetan Plateau, resulting in widespread alkali magmatism and thermal erosion of the mantle lithosphere. Upwelling of hot asthenosphere into regions previously insulated by the Tethyian slab is compatible with petrological data showing a rapid pulse of advective heating of the crust in Oligocene time and a hydrated mantle at temperatures in excess of 1000°C in middle Miocene time beneath the southern Tibetan Plateau (Liu et al., 2011; Mahéo et al., 2002). Furthermore, this time period marks the termination of prograde metamorphism of sediments now exhumed in Himalayan gneiss domes, and the initiation of a period of rapid near isothermal exhumation, providing evidence for heightened geotherms, and the reorganization of deformation styles at the northern margin on the Indian plate

(e.g. Langille et al., 2012; Zhang et al., 2015). In the northern Tibetan Plateau, the correspondence of lavas in our compilation with melts derived from the spinel stability field suggests that melting depths were above ~80 km (Green and Ringwood, 1967; Holbig and Grove, 2008). Given the 60-70 km thick crust in the region today (Zhang et al., 2011), an ~80 km depth of melting would imply that the mantle lithosphere was highly thinned by ~24 Ma.

A final transition took place at 10-15 Ma, with the termination of volcanism in the southern and central Tibetan Plateau. We interpret this shift as being the consequence of Indian underthrusting, which drove the hydrated mantle wedge to the north, and thickened the mantle lithosphere in the southern to south-central Tibetan Plateau to a point where dehydration reactions were no longer favored, thereby removing previous drivers of melt generation. In this interpretation, strain in lithospheric mantle necessarily localizes south of the Tanggula Shan, creating a significant contrast in lithospheric thicknesses between the central and northern Tibetan Plateau. This contrast may help increase rates of volcanism in the northern Tibetan Plateau through shear driven upwelling as has been suggested for the Colorado Plateau of western North America (Ballmer et al., 2015), with a metasomatized mantle wedge acting as a low viscosity pocket and source for melting.

Indian underthrusting may have also precipitated the development of normal faulting by bringing the Tibetan Plateau to gravitationally unstable elevations of over ~4000 m, and contributing to the flow of lower crustal material to the periphery of the orogen (e.g. Styron et al., 2015). Continued crustal shortening then focused north of the Tibetan Plateau, as material in the plateau interior was moved laterally on newly initiated or reactivated strike-slip faults (Duvall et al., 2013; Liu et al., 2007; Lu et al., 2014; Murphy et al., 2000; Sun et al., 2005; Yuan et al., 2013; Zhang et al., 2012; Zheng et al., 2006). This then resulted in the distribution of faulting and volcanism observed in modern time, with volcanism limited to the northern Tibetan Plateau, dominance of normal faulting above elevations of 5000 m, and strike slip and thrust faulting elsewhere.

60 Ma

India Lhasa Q-T S-G

50 Ma

India Lhasa Q-T S-G

40 Ma

India Lhasa Q-T S-G

30 Ma

India Lhasa Q-T S-G

20 Ma

India Lhasa Q-T S-G

10 Ma

India Lhasa Q-T S-G

0 Ma

India Lhasa Q-T S-G

Legend

- Indian Crust
- Oceanic Crust
- Asian Crust
- Basin Sediments
- Mantle Wedge
- Mantle Lithosphere
- ▲ Volcanism
- Faulting
- → Mantle Flow

). However, the timing, and mechanisms by which the Indo-Asian orogen achieved modern elevations remain controversial, and are areas of active research by the tectonics community. In this thesis, I address three aspects of the tectonic evolution of the Tibetan Plateau that bear on the elevation of this region: the reconstruction of the mass balance of the orogen (Chapter 2), the gravitational stability of the crust and the interaction of major strike-slip faults in the northern Tibetan Plateau (Chapter 3), and the age and geochemistry of volcanic rocks with respect to modification of the mantle lithosphere beneath the Tibetan Plateau (Chapter 4).

The Indo-Asian orogen has been an area of geologic research for nearly a century (Argand, 1924), and in the last four decades has been a source for numerous hypotheses on the development of major mountain belts (e.g. Powell and Conaghan, 1975; Tapponnier et al., 1982; England and Houseman, 1988; Molnar et al., 1993; Clark and Royden, 2000; Tapponnier et al., 2001). These proposals have been applied to other orogens across the world, and in geologic time (e.g. Nironen,

1997; Chalot-Prat and Girbacea, 2000; Wells and Hoisch, 2008; Ducea and Saleeby, 2010), highlighting the importance of the region in improving our understanding of orogenic processes. An interpretation common to all studies of the Tibetan plateau is that some, if not all, of the modern topography and crustal thicknesses are the consequence of collision between Asia, and the Indian subcontinent. Evidence from Tethyian sedimentary sequences (Rowley, 1998; Sciunnach and Garzanti, 2012), pressure-temperature-time (P-T-t) paths of Himalayan metamorphic rocks (Guillot et al., 2008; Smit et al., 2014), paleomagnetic studies (Dupont-Nivet et al., 2010), and changes in volcanic geochemistry at the south Asian margin (Bouilhol et al., 2013) have recently converged on a collision age of 40-55 Ma between Indian and Asian crust.
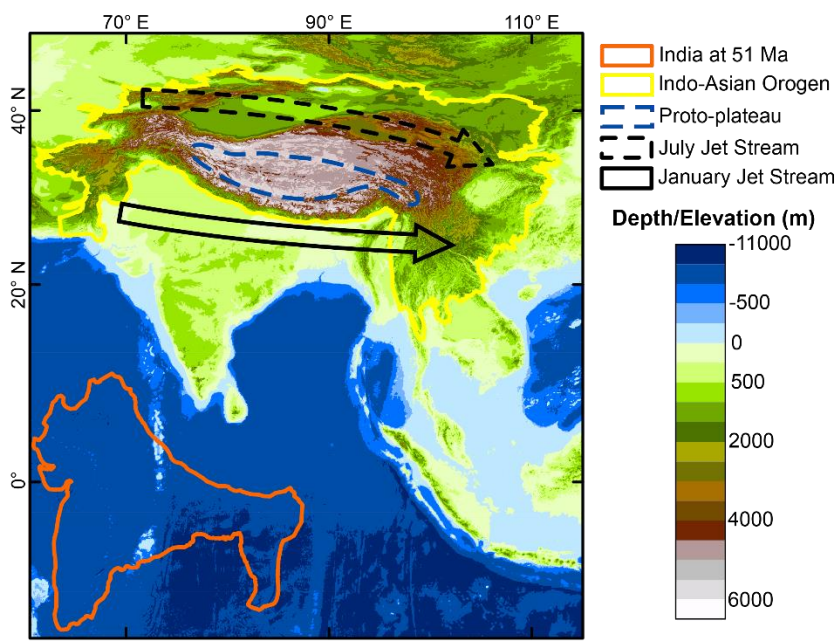
Figure 1.1 – Topographic map of east Asia, with July and January jet streams (Molnar et al., 2010), position of India at 51 Ma (van Hinsbergen, Steinberger, et al., 2011), and regions of pre-existing high crustal thicknesses ("Proto-plateau").

It is generally accepted that deformation of the southern margin of Asia during accretion of continental blocks and island arcs in Mesozoic time likely resulted in some high topography prior to continental collision (Dewey et al., 1988; Murphy et al., 1997; Yin and Harrison, 2000; Hoke et al., 2014). Evidence for a high "proto-plateau" comes from two areas of inquiry: balanced cross sections of deformed strata in the southern Tibetan Plateau show minimal post-Eocene shortening indicating that the crust was already thick prior to collision (e.g. Murphy et al., 1997; Kapp, DeCelles, Gehrels, et al., 2007; Kapp, DeCelles, Leier, et al., 2007), and stable isotope estimates of paleoelevation, which suggest that the Tibetan plateau was at elevations of over 3000 m in Paleogene to Eocene time (Quade et al., 2011; Bershaw et al., 2012; Hoke et al., 2014). Deformation and crustal thickening accompanied arc magmatism due to subduction of Tethyan oceanic crust in Jurassic though Paleocene time (Dewey et al., 1988), which resulted in extensive magmatism in the Lhasa terrane of the southern Tibetan Plateau (e.g. Wen et al., 2008; Ji et al., 2009),

and likely resulted in a tectonic setting analogous to the ~4000 m tall Andes Mountains today (e.g. Murphy et al., 1997; Figure 1-1).
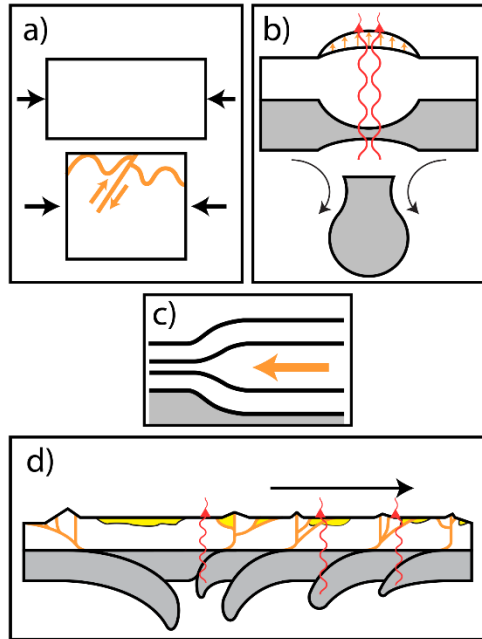
Figure 1.2 – Mechanisms for crustal thickening and plateau formation. a) Crustal shortening b) Removal of mantle lithosphere, resulting in topographic gain, and volcanism with lithospheric mantle shown in grey (Molnar et al., 1993) c) Flow of a ductile lower crustal channel (Clark and Royden, 2000) d) Subduction of continental lithosphere, resulting in progressive crustal thickening, and volcanic eruption (Tapponnier et al., 2001)

Once continental collision commenced, shortening of the northern Tibetan Plateau occurred over a broad region that roughly encompasses the area of modern deformation today(Clark, 2012). Crustal shortening occurred in the Hoh Xil basin of the northern Tibetan Plateau in Eocene to Oligocene time (Li et al., 2011; Staisch et al., 2014) with concurrent deformation in the Qilian Shan (Yin et al., 2008; Zheng et al., 2010; Zhuang et al., 2011) and the Kunlun and West Qilian Shan regions (Clark et al., 2010; Duvall et al., 2011). At the same time, crustal shortening was absent in the southern and central Tibetan Plateau (e.g. Murphy et al., 1997; Kapp, DeCelles, Gehrels, et al., 2007; Kapp, DeCelles, Leier, et al., 2007), which suggests that stresses were largely transmitted through regions of pre-existing thick crust near the Indus-Tsangpo suture to thinner foreland basins to the north. A relatively stationary boundary to the distal margin of the plateau challenges classical interpretations of collisional orogens as being generally time-transgressive, with high topography built progressively away from a plate margin (Clark, 2012). Many existing ideas for plateau development are based on this basic notion that deformation and topography propagate in space and time away from the plate boundary (i.e. England and Houseman, 1988; Tapponnier et al., 2001; Figure 1-2).

A large-scale transition from north-south shortening and thrust faulting to east-west extension in the Tibetan Plateau occurred by middle to late Miocene time, as evidenced by the initiation of major normal and strike-slip faults (Armijo et al., 1986; Mercier et al., 1987; Harrison et al., 1995; Murphy et al., 2000; Blisniuk et al., 2001; Phillips et al., 2004; Sun et al., 2005; Liu et al., 2007; Duvall et al., 2013). This shift in deformation mechanisms has typically been linked to the attainment gravitationally unstable crustal thicknesses in the Tibetan Plateau (e.g. Kapp and Guynn, 2004). Modern fault mechanisms show that normal faults are generally localized at elevations above 4000 m, providing a

possible threshold beyond which the crust may be considered unstable. Thrust faults typically lie below this elevation (e.g. Molnar and Tapponnier, 1978; Taylor and Yin, 2009), suggesting that crustal shortening alone can not bring the crust to elevations seen in modern time. However, how and when the plateau reached elevations of over 5000 m is a matter of debate, with current proposals leveraging lithospheric removal (Molnar et al., 1993) and lower crustal flow (Clark and Royden, 2000) to bring the crust to thicknesses unattainable by older episodes of crustal shortening (**Error! Reference source ot found.**).

Prominent descriptions of plateau development incorporate both fault styles, and the timing and compositions of volcanism observed at the earth's surface to support mechanisms such as the removal or subduction of Asian lithosphere (Molnar et al., 1993; Tapponnier et al., 2001; Figure 1-2). Geochemical studies often cite detached or subducted lithosphere, or a molten lower crust as possible sources of lavas erupted across the Tibetan Plateau (Roger et al., 2000; Holbig and Grove, 2008; Wang et al., 2012; Xia et al., 2011; Chen et al., 2012; Chung et al., 2005). Proposed drivers for volcanism include continental subduction (e.g. Arnaud et al., 1992; Yang and Ding, 2013), removal of lithospheric mantle (e.g. Turner et al., 1996; Chen et al., 2013), and upwelling of the asthenosphere beneath the Tibetan Plateau (e.g. Guo et al., 2006; Wang et al., 2010). A critical component of these interpretations is the thickness of the lithospheric mantle, and its evolution in Cenozoic time. Asthenospheric upwelling should result in thermal erosion of overlying lithosphere leading to decreased lithospheric thickness (e.g. Molnar, 1988). Recent removal of the lithospheric mantle would be also be expected to leave a region of thinned mantle lithosphere and but additionally result in an area of high seismic wave velocities where mantle lithosphere is now entrained in the mantle (e.g. Turner et al., 1993a; Hatzfeld and Molnar, 2010). Lastly, subduction of continental lithosphere would produce "slabs" of subducted or underthrust material, which may be recognized as topography on the lithosphere-asthenospheric boundary (Tapponnier et al., 2001). However, geophysical studies diverge widely in their interpretations of Asian lithospheric thickness, and have been used to support each of these mechanisms (e.g. Kind et al., 2002; Haines et al., 2003; Shi et al., 2004; Nábelek et al., 2009). Mineralogies of xenoliths sourced from the lithospheric mantle during Miocene volcanic eruptions in the southern and central Tibetan Plateau provide evidence for a hot and possibly thinned mantle but are limited in their spatial and temporal extent (Ding et al., 2007; Liu et al., 2011).

1.3 Role of topographic development on regional climate and speciation

The extent of high topography in the Indo-Asian orogen has strong implications on the climate of the region in Cenozoic time, and had a significant impact on mammalian speciation and the

origin of cold-adapted species. The Himalaya isolate warm moist tropical air from the cold dry air of the subtropics acting to strengthen the south Asian monsoon (e.g. Boos and Kuang, 2010), which provides nearly 80% of annual precipitation in the Indian subcontinent (Mooley and Parthasarathy, 1984). The Tibetan Plateau controls the position of the jet stream, which rapidly shifts from its southern margin in January, to its northern limit in July, thereby strongly affecting patterns of precipitation in eastern Asia (e.g. Molnar et al., 2010). The north-south extent of this region of high topography therefore likely had a strong impact on regional precipitation in Cenozoic time. The extreme elevations and high aridity of the Tibetan Plateau also provided physical forcing to promote speciation and diversification of mammals since Miocene time. The plateau then acted as a source for cold-adapted species during Holocene time, with primitive lineages found in the Tibetan Plateau identified as progenitors of both extinct Ice Age megafauna such as the wooly rhinoceros and extant species such as the arctic fox (Wang et al., 2015).

1.4 Thesis Outline

Subsequent chapters address three outstanding areas of inquiry regarding the development of the Indo-Asian orogen and the respective consequences on the development of high topography in southern Asia. Chapter 2 investigates the mass balance of the Indo-Asian orogen, which discusses proposed convergence estimates between India and Asia since the time of collision, evaluates possible crustal thicknesses of input material required to achieve mass balance, and highlights the importance of mass redistribution within the orogen. Chapter 3 focuses on the Guaizi Liang of the northern Tibetan Plateau, where field investigations reveal a unique example of active contractional shortening at elevations of ~5000 m. Interpretation of the magnitude and orientation of contractional structures in the Guaizi Liang suggests that deformation is likely driven by simple shear between the Altyn Tagh, and Kunlun/Manyi faults of the northern Tibetan Plateau. As simple shear would not produce crustal thickening, gravitational potential energy of the region would not increase, providing a viable mechanism of generating thrust faulting at high elevation. Furthermore, this interpretation suggests that slip on the Manyi Fault began at ~5 Ma, synchronous with the initiation of shortening in the Guaizi Liang. Chapter 4 investigates the evolution of the Tibetan Plateau through the spatial and temporal evolution of the compositions of volcanic rocks. New geochemical, and geochronological data from are synthesized with ~800 published samples from across the Tibetan Plateau. End-member lava compositions are then characterized using major- and trace- element abundances and isotopic ratios, which are used to infer melt source mineralogies, and possible drivers of melt generation. These interpretations are combined with observed changes in the spatial distribution of lavas, and integrated

with orogen-scale shifts in the timing and style of upper crustal deformation in order to provide a comprehensive geodynamic interpretation of the evolution of the Indo-Asian orogen. Chapter V summarizes the findings of Chapters 2 through 4, and integrates the implications of preceding chapters for the evolution of the Indo-Asian orogen. Outstanding issues, and possible avenues for future work are discussed. Appendices for chapter 4 are located at the end of the document.

1.5 References

Argand, E., 1924, La tectonique de l'Asie, in Proceedings of the 13th International Geological Congress, p. 170–372.

Armijo, R., Tapponnier, P., Mercier, J.-L.L., Han, T.-L., and Tong-Lin, H., 1986, Quaternary extension in southern Tibet: Field observations and tectonic implications: Journal of Geophysical Research, v. 91, p. 13803, doi: 10.1029/JB091iB14p13803.

Arnaud, N.O., Vidal, P., Tapponnier, P., Matte, P., and Deng, W.M., 1992, The high K2O volcanism of northwestern Tibet: Geochemistry and tectonic implications: Earth and Planetary Science Letters, v. 111, p. 351–367, doi: 10.1016/0012-821X(92)90189-3.

Bershaw, J., Penny, S.M., and Garzione, C.N., 2012, Stable isotopes of modern water across the Himalaya and eastern Tibetan Plateau: Implications for estimates of paleoelevation and paleoclimate: Journal of Geophysical Research, v. 117, p. 1–18, doi: 10.1029/2011JD016132.

Blisniuk, P.M., Hacker, B.R., Glodny, J., Ratschbacher, L., Bi, S., Wu, Z., McWilliams, M.O., and Calvert, A., 2001, Normal faulting in central Tibet since at least 13.5 Myr ago.: Nature, v. 412, p. 628–32, doi: 10.1038/35088045.

Boos, W.R., and Kuang, Z., 2010, Dominant control of the South Asian monsoon by orographic insulation versus plateau heating.: Nature, v. 463, p. 218–22, doi: 10.1038/nature08707.

Bouilhol, P., Jagoutz, O.E., Hanchar, J.M., and Dudas, F.O., 2013, Dating the India–Eurasia collision through arc magmatic records: Earth and Planetary Science Letters, v. 366, p. 163–175, doi: 10.1016/j.epsl.2013.01.023.

Chalot-Prat, F., and Girbacea, R., 2000, Partial delamination of continental mantle lithosphere, uplift-related crust–mantle decoupling, volcanism and basin formation: a new model for the Pliocene–Quaternary evolution of the southern East-Carpathians, Romania: Tectonophysics, v. 327, p. 83–107, doi: 10.1016/S0040-1951(00)00155-4.

Chen, J., Wu, J., Xu, J., Dong, Y., Wang, B., and Kang, Z., 2013, Geochemistry of Eocene high-Mg# adakitic rocks in the northern Qiangtang terrane, central Tibet: Implications for early uplift of the plateau: Geological Society of America Bulletin, v. 125, p. 1800–1819, doi: 10.1130/B30755.1.

Chen, J.-L., Xu, J.-F., Wang, B.-D., and Kang, Z.-Q., 2012, Cenozoic Mg-rich potassic rocks in the Tibetan Plateau: Geochemical variations, heterogeneity of subcontinental lithospheric mantle and tectonic implications: Journal of Asian Earth Sciences, v. 53, p. 115–130, doi: 10.1016/j.jseaes.2012.03.003.

Chung, S.-L., Chu, M.-F., Zhang, Y., Xie, Y., Lo, C.-H., Lee, T.-Y., Lan, C.-Y., Li, X., Zhang, Q., and Wang, Y., 2005, Tibetan tectonic evolution inferred from spatial and temporal variations in post-collisional magmatism: Earth-Science Reviews, v. 68, p. 173–196, doi: 10.1016/j.earscirev.2004.05.001.

Clark, M.K., 2012, Continental collision slowing due to viscous mantle lithosphere rather than topography: Nature, v. 483, p. 74–77, doi: 10.1038/nature10848.

Clark, M.K., Farley, K.A., Zheng, D., Wang, Z., and Duvall, A.R., 2010, Early Cenozoic faulting of the northern Tibetan Plateau margin from apatite (U–Th)/He ages: Earth and Planetary Science Letters, v. 296, p. 78–88, doi: 10.1016/j.epsl.2010.04.051.

Clark, M.K., and Royden, L.H., 2000, Topographic ooze: Building the eastern margin of Tibet by lower crustal flow: Geology, v. 28, p. 703, doi: 10.1130/0091-7613(2000)28<703:TOBTEM>2.0.CO;2.

Dewey, J.F., Shackleton, R.M., Chengfa, C., and Yiyin, S., 1988, The Tectonic Evolution of the Tibetan Plateau: Philosophical Transactions of the Royal Society A: Mathematical, Physical and Engineering Sciences, v. 327, p. 379–413, doi: 10.1098/rsta.1988.0135.

Ding, L., Kapp, P.A., Yue, Y., and Lai, Q., 2007, Postcollisional calc-alkaline lavas and xenoliths from the southern Qiangtang terrane, central Tibet: Earth and Planetary Science Letters, v. 254, p. 28–38, doi: 10.1016/j.epsl.2006.11.019.

Ducea, M., and Saleeby, J., 2010, A Case for Delamination of the Deep Batholithic Crust beneath the Sierra Nevada , California A Case for Delamination of the Deep Batholithic Crust beneath the Sierra Nevada , California: International Geology Review, v. 40, p. 37–41.

Dupont-Nivet, G., Lippert, P.C., Van Hinsbergen, D.J.J., Meijers, M.J.M., and Kapp, P.A., 2010, Palaeolatitude and age of the Indo-Asia collision: palaeomagnetic constraints: Geophysical Journal International, v. 182, p. 1189–1198, doi: 10.1111/j.1365-246X.2010.04697.x.

Duvall, A.R., Clark, M.K., Kirby, E., Farley, K. a., Craddock, W.H., Li, C., and Yuan, D.-Y., 2013, Low-temperature thermochronometry along the Kunlun and Haiyuan Faults, NE Tibetan Plateau: Evidence for kinematic change during late-stage orogenesis: Tectonics, v. 32, p. 1190–1211, doi: 10.1002/tect.20072.

Duvall, A.R., Clark, M.K., van der Pluijm, B. a., and Li, C., 2011, Direct dating of Eocene reverse faulting in northeastern Tibet using Ar-dating of fault clays and low-temperature thermochronometry: Earth and Planetary Science Letters, v. 304, p. 520–526, doi: 10.1016/j.epsl.2011.02.028.

England, P., and Houseman, G.A., 1988, The Mechanics of the Tibetan Plateau [and Discussion]: Philosophical Transactions of the Royal Society A: Mathematical, Physical and Engineering Sciences, v. 326, p. 301–320, doi: 10.1098/rsta.1988.0089.

Guillot, S., Mahéo, G., de Sigoyer, J., Hattori, K.H., and Pêcher, A., 2008, Tethyan and Indian subduction viewed from the Himalayan high- to ultrahigh-pressure metamorphic rocks: Tectonophysics, v. 451, p. 225–241, doi: 10.1016/j.tecto.2007.11.059.

Guo, Z., Wilson, M., Liu, J., and Mao, Q., 2006, Post-collisional, Potassic and Ultrapotassic Magmatism of the Northern Tibetan Plateau: Constraints on Characteristics of the Mantle Source, Geodynamic Setting and Uplift Mechanisms: Journal of Petrology, v. 47, p. 1177–1220, doi: 10.1093/petrology/egl007.

Haines, S.S., Klemperer, S.L., Brown, L.D., Guo, J., Mechie, J., Meissner, R., Ross, A., and Zhao, W., 2003, INDEPTH III seismic data: From surface observations to deep crustal processes in Tibet: Tectonics, v. 22, p. 1–18, doi: 10.1029/2001TC001305.

Harrison, T.M., Copeland, P., Kidd, W.S.F., and Lovera, O.M., 1995, Activation of the Nyainqentanghla Shear Zone: Implications for uplift of the southern Tibetan Plateau: Tectonics, v. 14, p. 658–676, doi: 10.1029/95TC00608.

Hatzfeld, D., and Molnar, P., 2010, Comparisons of the kinematics and deep structures of the Zagros and Himalaya and of the Iranian and Tibetan plateaus and geodynamic implications: Reviews of Geophysics, v. 48, doi: 10.1029/2009RG000304.

van Hinsbergen, D.J.J., Steinberger, B., Doubrovine, P. V., and Gassmöller, R., 2011, Acceleration and deceleration of India-Asia convergence since the Cretaceous: Roles of mantle plumes and

continental collision: Journal of Geophysical Research, v. 116, p. 1–20, doi: 10.1029/2010JB008051.

Hoke, G.D., Liu-Zeng, J., Hren, M.T., Wissink, G.K., and Garzione, C.N., 2014, Stable isotopes reveal high southeast Tibetan Plateau margin since the Paleogene: Earth and Planetary Science Letters, v. 394, p. 270–278, doi: 10.1016/j.epsl.2014.03.007.

Holbig, E.S., and Grove, T.L., 2008, Mantle melting beneath the Tibetan Plateau: Experimental constraints on ultrapotassic magmatism: Journal of Geophysical Research, v. 113, p. B04210, doi: 10.1029/2007JB005149.

Ji, W., Wu, F., Liu, C., and Chung, S., 2009, Geochronology and petrogenesis of granitic rocks in Gangdese batholith, southern Tibet: Science in China Series D: Earth Sciences, v. 52, p. 1240–1261, doi: 10.1007/s11430-009-0131-y.

Kapp, P.A., DeCelles, P.G., Gehrels, G.E., Heizler, M., and Ding, L., 2007, Geological records of the Lhasa-Qiangtang and Indo-Asian collisions in the Nima area of central Tibet: Geological Society of America Bulletin, v. 119, p. 917, doi: 10.1130/B26033.1.

Kapp, P.A., DeCelles, P.G., Leier, A.L., Fabijanic, J.M., He, S., Pullen, A., Gehrels, G.E., and Ding, L., 2007, The Gangdese retroarc thrust belt revealed: GSA Today, v. 17, p. 4–9, doi: 10.1130/GSAT01707A.1.

Kapp, P.A., and Guynn, J.H., 2004, Indian punch rifts Tibet: Geology, v. 32, p. 993, doi: 10.1130/G20689.1.

Kind, R., Yuan, X., Saul, J., Nelson, D., Sobolev, S. V, Mechie, J., Zhao, W., Kosarev, G., Ni, J., Achauer, U., and Jiang, M., 2002, Seismic images of crust and upper mantle beneath Tibet: evidence for Eurasian plate subduction.: Science, v. 298, p. 1219–1221.

Li, Y., Wang, C., Ma, C., Xu, G., and Zhao, X., 2011, Balanced cross-section and crustal shortening analysis in the Tanggula-Tuotuohe Area, Northern Tibet: Journal of Earth Science, v. 22, p. 1–10, doi: 10.1007/s12583-011-0152-2.

Liu, Y., Neubauer, F., Genser, J., Ge, X., Takasu, A., Yuan, S., Chang, L., and Li, W., 2007, Geochronology of the initiation and displacement of the Altyn Strike-Slip Fault, western China: Journal of Asian Earth Sciences, v. 29, p. 243–252, doi: 10.1016/j.jseaes.2006.03.002.

Liu, C.-Z., Wu, F.-Y., Chung, S.-L., and Zhao, Z.-D., 2011, Fragments of hot and metasomatized mantle lithosphere in Middle Miocene ultrapotassic lavas, southern Tibet: Geology, v. 39, p. 923–926, doi: 10.1130/G32172.1.

Mercier, J.-L., Armijo, R., Tapponnier, P., Carey-Gailhardis, E., and Lin, H.T., 1987, Change from Late Tertiary compression to Quaternary extension in southern Tibet during the India-Asia Collision: Tectonics, v. 6, p. 275, doi: 10.1029/TC006i003p00275.

Molnar, P., 1988, A Review of Geophysical Constraints on the Deep Structure of the Tibetan Plateau, the Himalaya and the Karakoram, and their Tectonic Implications: Philosophical Transactions of the Royal Society A: Mathematical, Physical and Engineering Sciences, v. 326, p. 33–88, doi: 10.1098/rsta.1988.0080.

Molnar, P., Boos, W.R., and Battisti, D.S., 2010, Orographic Controls on Climate and Paleoclimate of Asia: Thermal and Mechanical Roles for the Tibetan Plateau: Annual Review of Earth and Planetary Sciences, v. 38, p. 77–102, doi: 10.1146/annurev-earth-040809-152456.

Molnar, P., England, P., and Martinod, J., 1993, Mantle dynamics, uplift of the Tibetan Plateau, and the Indian Monsoon: Reviews of Geophysics, v. 31, p. 357–396, doi: 10.1029/93RG02030.

Molnar, P., and Tapponnier, P., 1978, Active tectonics of Tibet: Journal of Geophysical Research, v. 83, p. 5361, doi: 10.1029/JB083iB11p05361.

Mooley, D. a., and Parthasarathy, B., 1984, Fluctuations in All-India summer monsoon rainfall during 1871-1978: Climatic Change, v. 6, p. 287–301, doi: 10.1007/BF00142477.

Murphy, M.A., Yin, A., Harrison, T.M., Durr, S.B., Chen, Z., Ryerson, F.J., Kidd, W.S.F., Wang, X., and Zhou, X., 1997, Did the Indo-Asian collision alone create the Tibetan plateau? Geology, v. 25, p. 719–722, doi: 10.1130/0091-7613(1997)025<0719:DTIACA>2.3.CO;2.

Murphy, M.A., Yin, A., Kapp, P.A., Harrison, T.M., Lin, D., and Jinghui, G., 2000, Southward propagation of the Karakoram fault system, southwest Tibet: Timing and magnitude of slip: Geology, v. 28, p. 451, doi: 10.1130/0091-7613(2000)28<451:SPOTKF>2.0.CO;2.

Nábelek, J., Hetényi, G., Vergne, J., Sapkota, S., Kafle, B., Jiang, M., Su, H., Chen, J., and Huang, B.-S., 2009, Underplating in the Himalaya-Tibet collision zone revealed by the Hi-CLIMB experiment.: Science (New York, N.Y.), v. 325, p. 1371–4, doi: 10.1126/science.1167719.

Nironen, M., 1997, The Svecofennian Orogen: a tectonic model: Precambrian Research, v. 86, p. 21–44, doi: 10.1016/S0301-9268(97)00039-9.

Phillips, R.J., Parrish, R.R., and Searle, M.P., 2004, Age constraints on ductile deformation and long-term slip rates along the Karakoram fault zone, Ladakh: Earth and Planetary Science Letters, v. 226, p. 305–319, doi: 10.1016/j.epsl.2004.07.037.

Powell, C.M., and Conaghan, P.J., 1975, Tectonic models of the Tibetan plateau: Geology, v. 3, p. 727, doi: 10.1130/0091-7613(1975)3<727:TMOTTP>2.0.CO;2.

Quade, J., Breecker, D.O., Daeron, M., and Eiler, J.M., 2011, The paleoaltimetry of Tibet: An isotopic perspective: American Journal of Science, v. 311, p. 77–115, doi: 10.2475/02.2011.01.

Roger, F., Tapponnier, P., Arnaud, N., Schärer, U., Brunel, M., Zhiqin, X., and Jingsui, Y., 2000, An Eocene magmatic belt across central Tibet: mantle subduction triggered by the Indian collision? Terra Nova, v. 12, p. 102–108, doi: 10.1046/j.1365-3121.2000.123282.x.

Rowley, D.B., 1998, Minimum Age of Initiation of Collision Between India and Asia North of Everest Based on the Subsidence History of the Zhepure Mountain Section: The Journal of Geology, v. 106, p. 220–235, doi: 10.1086/516018.

Sciunnach, D., and Garzanti, E., 2012, Subsidence history of the Tethys Himalaya: Earth-Science Reviews, v. 111, p. 179–198, doi: 10.1016/j.earscirev.2011.11.007.

Shi, D., Zhao, W., Brown, L.D., Nelson, D., Zhao, X., Kind, R., Ni, J., Xiong, J., Mechie, J., Guo, J., Klemperer, S., and Hearn, T., 2004, Detection of southward intracontinental subduction of Tibetan lithosphere along the Bangong-Nujiang suture by P-to-S converted waves: Geology, v. 32, p. 209, doi: 10.1130/G19814.1.

Smit, M. a., Hacker, B.R., and Lee, J., 2014, Tibetan garnet records early Eocene initiation of thickening in the Himalaya: Geology, v. 42, p. 591–594, doi: 10.1130/G35524.1.

Staisch, L.M., Niemi, N.A., Hong, C., Clark, M.K., Rowley, D.B., and Currie, B., 2014, A Cretaceous-Eocene depositional age for the Fenghuoshan Group, Hoh Xil Basin: Implications for the tectonic evolution of the northern Tibet Plateau: Tectonics, v. 33, p. 281–301, doi: 10.1002/2013TC003367.

Sun, J., Zhu, R., and An, Z., 2005, Tectonic uplift in the northern Tibetan Plateau since 13.7 Ma ago inferred from molasse deposits along the Altyn Tagh Fault: Earth and Planetary Science Letters, v. 235, p. 641–653, doi: 10.1016/j.epsl.2005.04.034.

Tapponnier, P., Peltzer, G., Le Dain, A.Y., Armijo, R., and Cobbold, P.R., 1982, Propagating extrusion tectonics in Asia: New insights from simple experiments with plasticine: Geology, v. 10, p. 611, doi: 10.1130/0091-7613(1982)10<611:PETIAN>2.0.CO;2.

Tapponnier, P., Zhiqin, X., Roger, F., Meyer, B., Arnaud, N.O., Wittlinger, G., and Jingsui, Y., 2001, Oblique stepwise rise and growth of the Tibet plateau.: Science (New York, N.Y.), v. 294, p. 1671–7, doi: 10.1126/science.105978.

Taylor, M.H., and Yin, A., 2009, Active structures of the Himalayan-Tibetan orogen and their relationships to earthquake distribution, contemporary strain field, and Cenozoic volcanism: Geosphere, v. 5, p. 199–214, doi: 10.1130/GES00217.1.

Turner, S., Arnaud, N., Liu, J., Rogers, N., Hawkesworth, C., Harris, N., Kelley, S.P., van Calsteren, P., and Deng, W., 1996, Post-collision, Shoshonitic Volcanism on the Tibetan Plateau: Implications for Convective Thinning of the Lithosphere and the Source of Ocean Island Basalts: Journal of Petrology, v. 37, p. 45–71, doi: 10.1093/petrology/37.1.45.

Turner, S., Hawkesworth, C., Liu, J., Rogers, N., Kelley, S.P., and van Calsteren, P., 1993, Timing of Tibetan uplift constrained by analysis of volcanic rocks: Nature, v. 364, p. 50–54, doi: 10.1038/364050a0.

Wang, Q., Chung, S.-L., Li, X., Wyman, D.A., Li, Z.-X., Sun, W., Qiu, H.-N., Liu, Y.-S., and Zhu, Y., 2012, Crustal Melting and Flow beneath Northern Tibet: Evidence from Mid-Miocene to Quaternary Strongly Peraluminous Rhyolites in the Southern Kunlun Range: Journal of Petrology, v. 53, p. 2523–2566, doi: 10.1093/petrology/egs058.

Wang, X., Wang, Y., Li, Q., Tseng, Z.J., Takeuchi, G.T., Deng, T., Xie, G., Chang, M., and Wang, N., 2015, Cenozoic vertebrate evolution and paleoenvironment in Tibetan Plateau: Progress and prospects: Gondwana Research, v. 27, p. 1335–1354, doi: 10.1016/j.gr.2014.10.014.

Wang, Q., Wyman, D. a., Li, Z.-X., Sun, W., Chung, S.-L., Vasconcelos, P.M., Zhang, Q., Dong, H., Yu, Y., and Pearson, N., 2010, Eocene north–south trending dikes in central Tibet: New constraints on the timing of east–west extension with implications for early plateau uplift? Earth and Planetary Science Letters, v. 298, p. 205–216, doi: 10.1016/j.epsl.2010.07.046.

Wells, M.L., and Hoisch, T.D., 2008, The role of mantle delamination in widespread Late Cretaceous extension and magmatism in the Cordilleran orogen, western United States: Geological Society of America Bulletin, v. 120, p. 515–530, doi: 10.1130/B26006.1.

Wen, D.-R., Chung, S.-L., Song, B., Iizuka, Y., Yang, H.-J., Ji, J., Liu, D., and Gallet, S., 2008, Late Cretaceous Gangdese intrusions of adakitic geochemical characteristics, SE Tibet: Petrogenesis and tectonic implications: Lithos, v. 105, p. 1–11, doi: 10.1016/j.lithos.2008.02.005.

Xia, L., Li, X., Ma, Z., Xu, X., and Xia, Z., 2011, Cenozoic volcanism and tectonic evolution of the Tibetan plateau: Gondwana Research, v. 19, p. 850–866, doi: 10.1016/j.gr.2010.09.005.

Yang, D., and Ding, L., 2013, Geochronology and geochemistry of the high magnesium and high potassium ultrabasic leucite basanite in northern Tibetan Plateau: Chinese Journal of Geology, v. 48, p. 449–467.

Yin, A., Dang, Y.-Q., Wang, L.-C., Jiang, W.-M., Zhou, S.-P., Chen, X.-H., Gehrels, G.E., and McRivette, M.W., 2008, Cenozoic tectonic evolution of Qaidam basin and its surrounding regions (Part 1): The southern Qilian Shan-Nan Shan thrust belt and northern Qaidam basin: Geological Society of America Bulletin, v. 120, p. 813, doi: 10.1130/B26180.1.

Yin, A., and Harrison, T.M., 2000, Geologic Evolution of the Himalayan-Tibetan Orogen: Annual Review of Earth and Planetary Sciences, v. 28, p. 211–280, doi: 10.1146/annurev.earth.28.1.211.

Zheng, D., Clark, M.K., Zhang, P., Zheng, W., and Farley, K.A., 2010, Erosion, fault initiation and topographic growth of the North Qilian Shan (northern Tibetan Plateau): Geosphere, v. 6, p. 937–941, doi: 10.1130/GES00523.1.

Zhuang, G., Hourigan, J.K., Ritts, B.D., and Kent-Corson, M.L., 2011, Cenozoic multiple-phase tectonic evolution of the northern Tibetan Plateau: Constraints from sedimentary records from Qaidam basin, Hexi Corridor, and Subei basin, northwest China: American Journal of Science, v. 311, p. 116–152, doi: 10.2475/02.2011.02.

Chapter 2: Conservation and redistribution of crust during the Indo-Asian collision[1]

2.1 Abstract

We evaluate the mass balance of the Indo-Asian orogen by reconstructing the Indian and Asian margins prior to collision using recently published paleomagnetic and surface shortening constraints, and subtracting modern crustal volumes derived from gravity inversions and deep seismic soundings. Results show a 27-30% deficit between original and modern orogen volumes if the average global crustal thickness of 41 km is assumed prior to collision, even once eastward extrusion and crustal flow are considered. Such a large discrepancy requires crustal recycling of a magnitude that is approximately equal to one half of the modern orogenic mass, as others have previously suggested. Proposals for extensive high elevations prior to or soon after the collision further exacerbate this mismatch and dramatically increase the volume of material necessary to be placed into the mantle. However, we show that this discrepancy can be eliminated with a 23-32 km thick crust within the orogen prior to collision along with a thick southern Tibet margin (the Lhasa and Qiangtang terranes). Because of the relatively low magnitude of surface shortening in Asia, an initially thin crust would require underplating of Indian crust in southern Tibet and displacement of a highly mobile lower crust to the north and east in order to explain modern crustal thicknesses. The contrast between a proposed thinner Asian interior and older and thicker lithosphere of the North China block may have defined the distal extent of deformation at the time of collision and since.

2.2 Introduction

Collisional plate margins induce deformation for hundreds to over a thousand kilometers inboard of the plate boundary as a consequence of plate convergence. During the past three decades, study of the Tibetan Plateau has served as a natural laboratory for numerous descriptions of post-collisional topographic growth and their relation to geodynamic processes (Tapponnier et al., 1982; England and Houseman, 1988; Molnar et al., 1993; Clark and Royden, 2000; Tapponnier et al., 2001; DeCelles et al., 2002). Fundamentally, these studies attempt to provide a mechanism by which ~ 2500

---

km of India's northward motion has been accommodated by continental deformation since the ~50 Ma collision with Asia (e.g. Garzanti and Van Haver, 1988; Liebke et al., 2013). While these studies vary in terms of rheology and degree of coupling between the crust and mantle lithosphere, it is generally thought that India acts as a rigid indenter moving northward into the weaker southern margin of Asia, which accommodates the bulk of convergence. Deformation within the Indian plate is limited to its pre-collisional thinned northern margin now represented by the Himalaya, while crust in the southern margin of Asia has thickened to ~ 2x normal thicknesses within the Tibetan Plateau.

Recently, paleomagnetic studies from terrestrial sedimentary and volcanic rocks have confirmed that less than half of the overall Indo-Asian convergence since collision is accommodated by shortening within Asia (e.g. Dupont-Nivet et al., 2010; Cogne et al., 2013; van Hinsbergen, Kapp, et al., 2011), which is consistent with structural reconstructions of the upper crust that observe low magnitude strain or crustal shortening that is limited in geographical extent(e.g. Yin et al., 2008; Li et al., 2011 Figure 2.1; Table 2.4). These findings present a paradox: the southern Asian continental margin had to be relatively thick prior to collision if low amounts of shortening within Asia led to modern crustal thicknesses (e.g. Lease et al., 2012), but thick pre-collisional crust would require the removal of crustal mass in excess of its modern volume in order to accommodate ~2500 km of continental convergence since collision (Molnar and Stock, 2009; Dupont-Nivet et al., 2010; Cogne et al., 2013). The missing crustal mass, or "mass deficit" is made larger if regions of high crustal thickness in Asia existed prior to or soon after collision, as suggested by estimates of pre-collisional crustal shortening (e.g. Murphy et al., 1997; Kapp, DeCelles, Leier, et al., 2007) and high-standing early Cenozoic paleoelevation estimates for the northern and eastern Tibetan Plateau (Rowley and Currie, 2006; Quade et al., 2011; Bershaw et al., 2012; Hoke et al., 2014).

Calculations of mass deficit are sensitive to the approximation of collision age because of the rapid northward velocity of India near ~ 50 Ma (90-150 mm/yr) (e.g Molnar and Stock, 2009; van Hinsbergen, Steinberger, et al., 2011). Previously published mass balance calculations (Le Pichon et al., 1992; Replumaz et al., 2010) are based on a 45 Ma collision age, which is younger than the canonical age of 55-50 Ma supported by sedimentary evidence (e.g. Garzanti and Van Haver, 1988; Sciunnach and Garzanti, 2012). More recently published, albeit controversial, studies suggest a much younger age for collision at 34 Ma (Aitchison et al., 2007) or even 25-20 Ma. These collision ages would strongly influence the assumed mass input, with the total net convergence for a younger (or older) collision decreasing (or increasing) the total volume of mass added to the orogen.

In an attempt to resolve the mass balance problem, several earlier studies appeal to methods by which mass was removed from the orogen since ~50 Ma. Proposed solutions include the eastward extrusion of Asian affinity crustal blocks (Tapponnier et al., 1982; Le Pichon et al., 1992; Replumaz and Tapponnier, 2003) and recycling of Indian (Le Pichon et al., 1992; van Hinsbergen et al., 2012) or Asian (Tapponnier et al., 2001) crust into the mantle. In this study, we evaluate these and other processes affecting calculations of crustal volumes, which have not been previously quantitatively considered, including that an Andean-style, thick crust existed beneath the southern Tibet prior to collision (Murphy et al., 1997; Kapp, DeCelles, Leier, et al., 2007). We incorporate published extrusion values based on tomography and plate reconstructions (Leloup et al., 1995; Replumaz and Tapponnier, 2003), lower crustal flow into eastern Tibet (Clark and Royden, 2000), and new estimates of modern crustal thicknesses (Zhang, Yang, et al., 2011; e.g Steffen et al., 2011) (Figure 2.1). In order to avoid uncertainties associated with a precise collision age, we use independent estimates of Asian shortening (Dupont-Nivet et al., 2010) and the size of the pre-collisional Indian subcontinent (Gibbons et al., 2012) to constrain the crustal volume input (Figure 2.2). However, these are generally compatible with the 2000-2500 km of Indo-Asian convergence observed since 40 Ma (van Hinsbergen, Steinberger, et al., 2011), a collision age suggested by Bouilhol et al., (2013). We also calculate pre-collisional crustal thicknesses for Asia and India assuming that crustal volume is conserved in order to test the viability of a thin pre-collisional crust as an alternative to crustal recycling.

2.3 Methods

We investigate the mass balance of the Indo-Asian orogen by first defining the extent of the orogen and calculating its volume based on a compilation of published geophysical estimates of crustal thicknesses. We then calculate the Indian and Asian components of areal input during collsion from published paleomagnetic datasets (Gibbons et al., 2012; Dupont-Nivet et al., 2010). Next, we subtract the input crustal volume by multiplying the areal input by a global average for crustal thickness (~41 km) with or without a thicker, Andean-style margin for southern Eurasia. Finally, we use the modern orogenic volume to estimate the pre-collisional crustal thicknesses in India and Asia that would be compatible with orogen-scale mass conservation.

2.3.1 Calculating modern volumes

In order to investigate the balance between input and modern volumes, we first define the extent of the Indo-Asian orogen in the modern. This allows us to clearly delineate regions that were thickened during collision, and must have increased in mass due to input from Indian or Asian shortening. We define the areal limits of the modern orogen using the extent of high modern strain

rates and/or post-collisional crustal thickening (Figure 2.2) and use crustal thicknesses determined from geophysical data for this region to estimate the modern crustal volume (Figure 2.1). We estimate the northeastern extent of the Indo-Eurasian orogen at approximately ~ 40°N and the northwestern boundary north of the Tien Shan, which define the position of a relatively stationary northern boundary since the time of collision (Clark, 2012) and the modern limit of concentrated strain, respectively. Following the region of high GPS velocities in the Asian interior that correlate with regions of high topography (Gan et al., 2007) and crustal thickening, we use the 1000 m contour in the western half of the orogen. This relationship is more ambiguous in eastern Tibet, where we follow the 500 m contour due to the more diffuse nature of topography in that region and ambiguity between small amounts of post and pre collisional thickening. The southern and southeastern boundaries are in turn defined by the Main Frontal Thrust in India and the Saigaing Fault in Burma, respectively.

Our definition differs from previous studies (Le Pichon et al., 1992; Replumaz et al., 2010), which include the Altai in the definition of the Indo-Asian orogen. We recognize that large historic earthquakes and Quaternary fault slip occur farther north within the Gobi corridor (Mongolia) (Baljinnyam et al., 1993; Cunningham, 2013). However, Cenozoic shortening in the Altai did not begin until Pliocene time (e.g. Tapponnier and Molnar, 1979; e.g. De Grave and Van den haute, 2002; Glorie et al., 2012) and must account for a negligible amount of the overall convergence between India and Eurasia, and consequentially, the modern crustal thickness of up to 50 km in this area (Zorin et al., 1990) is difficult to wholly attribute to India-Asia collision and may in part be attributed to Mesozoic mountain building events. Further, our chosen extent omits large regions of Indonesia incorporated by Replumaz et al., (2010), as the inclusion of significant regions of oceanic crust will skew input estimates based on continental crustal volumes.
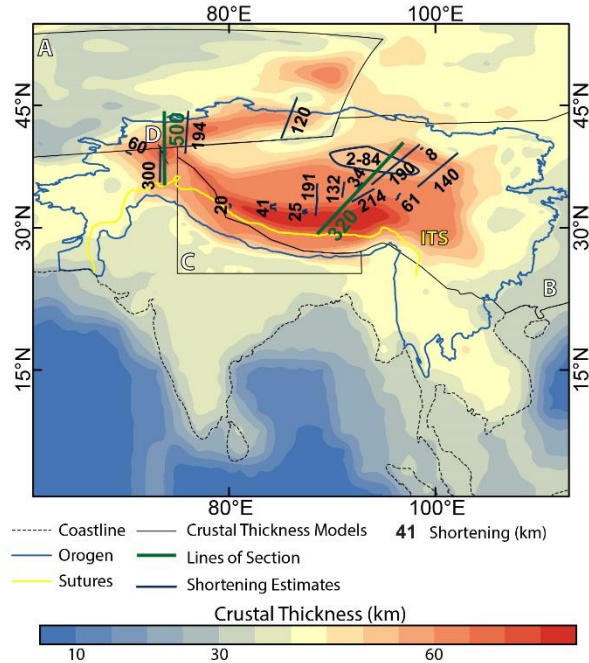
Figure 2.1 – Crustal thickness model and outline of the Indo-Asian orogen. Regional crustal thickness reconstructions used in our interpolation: Steffen et al., (2011)(A), Zhang, Yang, et al., (2011)(B), Zhang, Deng, et al., (2011)(C) and Mechie et al., (2011)(D). Crustal thicknesses in all other areas estimated from interpolation of the Crust 2.0 model (Bassin et al., 2000). Currently available upper crustal shortening estimates for Tibet totaling ~320 km of north-south shortening in eastern Tibet and ~500 km in the Pamir and Tien Shan along the lines of section shown. A summary of values and sources can be found in Table 2-4. ITS – Indus-Tsangpo Suture.

We use two compilations to derive crustal thicknesses from seismic soundings, gravity inversion and surface wave tomography, one extending over Tibet and the Himalayan front (Zhang, Deng, et al., 2011) and another covering China (Zhang, Yang, et al., 2011). We further incorporate a published gravity inversion model of the Tien Shan (Steffen et al., 2011), seismic refraction data from the Pamir (Mechie et al., 2012) and use the CRUST 2.0 global model (Bassin et al., 2000) where higher resolution data are not available. Due to significant discrepancies between the individual datasets they are clipped to their primary areas of focus, with individual extents shown in Figure 2.1. We approximate an average error in Moho depths for our model as ± 5 km, based on uncertainties reported in the data sources. Finally, we add the volume of material eroded from the orogen since collision, by combining the solid phase volume held in the Indus, Ganges, Pakistan, Bengal, and Andaman basins, as well as the Gulf of Thailand (Métivier et al., 2002).

In lieu of making blanket assumptions of crustal density profiles for the orogen in order to evaluate crustal mass, we note that typical density contrasts are sufficiently small to be neglected. The ~7% density difference between upper crustal rocks (e.g. granite) and the granodiorite or granulite

19

compositions typically inferred for the lower crust (e.g. Jackson, 2002; Burov and Watts, 2006) would only change resulting estimates of the modern orogenic mass by ~5% if localized to depths beneath 35 km. As such, we use the terms "mass" and "volume" interchangeably, with all input and modern volumes assumed to have homogenous densities at the orogen scale.

Table 2-1 – Mass balance calculations for alternative reconstructions of Asia based on paleomagnetic data and our compiled upper crustal shortening estimates.

Author	Asian Shortening	Areal Input (x 10^6 km^2)	Crustal Thickness[a]	Mass deficit (x 10^6 km^3)[a]
Dupont-Nivet et al. (2010)	1100 km	3.6	23-27 km	190-260
Tan et al. (2010)	810 km	2.8	24-29 km	160-230
van Hinsbergen et al. (2011b)	600 km/1050 km[c]	2.9	26-31 km	120-190
Sun et al. (2012)	1700 km	5.9	20-23 km	290-360
Cogne et al. (2013)	1450 km	4.4	22-26 km	220-290
van Hinsbergen et al. (2012)	600 km/1050 km[c]	2.9	30-36 km[b]	50-120[b]
This paper	320km/500 km[c]	2.3	27-33 km	100-170

a – Crustal thickness of Asia and greater India prior to collision required if mass is conserved. Range stated is for cases with 60 km thick Lhasa and 60 km Lhasa and Qiangtang, as in columns 2 and 3 of Table 3. Errors on crustal thickness are typically 5-6 km with 2σ uncertainty.
b – Calculated using input of India (2.5 x 10^6 km^2) from van Hinsbergen et al. (2012).
c – Calculated for two cross-sections in the west and east of the orogen, respectively.

2.3.2 Estimating crustal volume prior to collision

We derive the input volume to the orogen from the extent and thickness of pre-collisional India and Asia separately minus geological constraints on eastward extrusion. Material that is extruded eastward absorbs net convergence but does not contribute to the modern orogen volume so it is subtracted from the areal input (Table 2-3). Input volumes are based on the areal extent of India determined from marine magnetic anomalies (Gibbons et al., 2012) (Table 2-3) and the areal extent of Asia determined both from paleo-latitude estimates from paleomagnetism of continental volcanic and sedimentary rocks (Dupont-Nivet et al., 2010; Tan et al., 2010; Sun et al., 2010; Cogne et al., 2013) and palinspastic reconstructions of upper crustal shortening (Table 2-4). By using geologic constraints for the original continental geometry of India and Asia, we avoid reliance on determining a precise collision age in order to determine the total net convergence.

In estimating mass balance, and pre-collisional crustal thicknesses, we assume that a 60 km thick crust existed beneath southern Tibet (Lhasa and Qiangtang terranes) as has been suggested by >40-60% of Cretaceous shortening in the two terranes (Murphy et al., 1997; Kapp, DeCelles, Leier, et al., 2007). For other regions within the orogen, we use a pre-collisional thickness equal to the global average 41 km thick crust (Christensen and Mooney, 1995) as a reference value. However, we note

that some authors have proposed that northern Tibet may have been ≥ 4 km high (e.g. Rowley and Currie, 2006) or that eastern Tibet may have been 45 ± 5 km thick (Lease et al., 2012), suggesting that using crustal thickness values from the global average may underestimate crustal input.
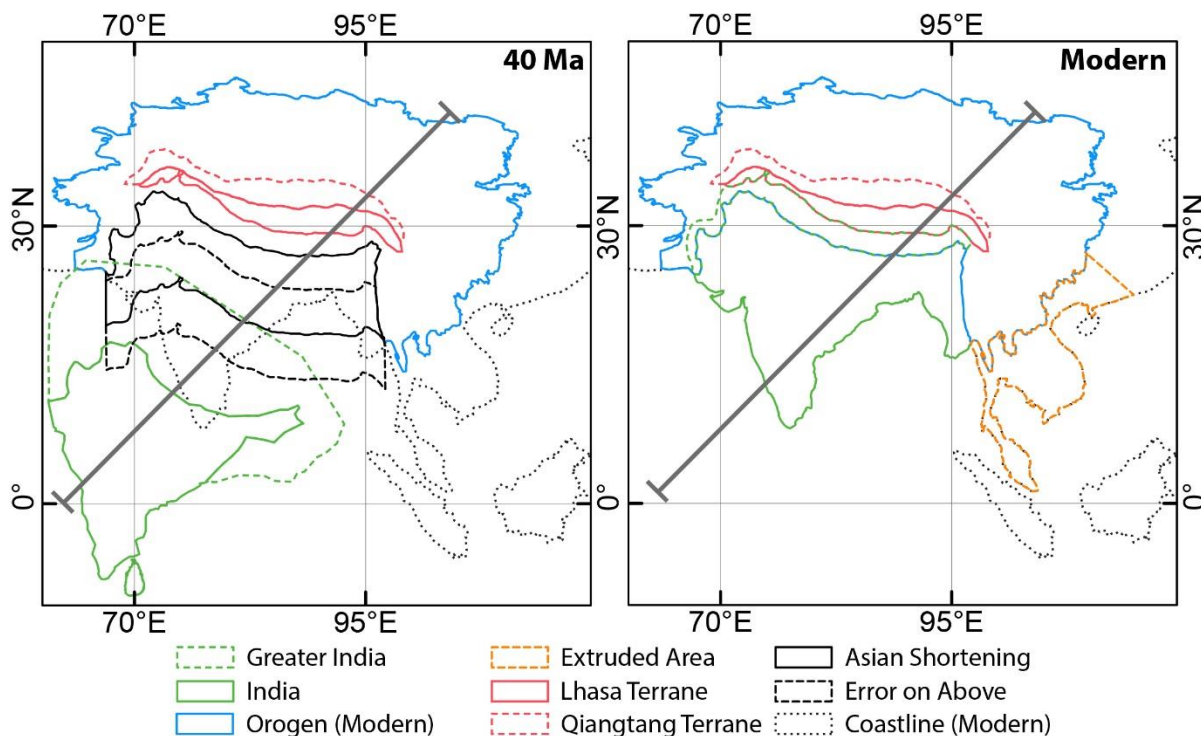
Figure 2.2 – Input areas for our calculations. Greater India is derived from Gibbons et al., (2012) with position at 40 Ma using their paleomagnetic reconstruction and a stable Eurasia in gPlates (Williams et al., 2012). Asian shortening estimates are from Dupont-Nivet et al., (2010), with the ITS moved directly south to define an area. Areas of possible pre-collisional crustal thickening are outlined in red. A schematic estimate of extruded material is in dashed orange. Note that this is not meant to show specific areas that were extruded from the collision with India, but rather to illustrate the relative importance of this process. Gray lines indicate sections used in Figure 2.4.

2.3.2.1 Input volume from India

To determine the areal input of India, we use the greater India of Gibbons et al., (2012) who follow previous authors (e.g Ali and Aitchison, 2005) in defining the northern extent of India by the Zenith and Wallaby plateaus, and incorporate a newly discovered Jurassic sliver of oceanic crust now isolated in the Indian ocean. The resulting geometry extends greater India ~1100 km past the modern extent of the subcontinent, yielding an area of ~4.2 x 10^6 km^2. We add a 10% error to this estimate in order to account for proposals of a late Cretaceous island arc collision with northern India (e.g. Reuber, 1986; Jagoutz et al., 2009), and any magmatic addition to continental crust added during extension, typically thought to be < 4 km in width (Buck, 2006).

2.3.2.2 Input volume from Asia

Reconstructing the areal extent of Asia is accomplished from changes in paleo-latitude or undoing shortening values associated with upper crustal deformation. We use the paleomagnetic estimate of post-Cretaceous convergence within Asia of 1100 ± 500 km from the Linzizong volcanic sequence in the Lhasa Terrane (Dupont-Nivet et al., 2010) as a median point of reference. While this estimate is one of many published over the last several years, it accounts for known problems with inclination shallowing and averaging of secular variation found in many previously published datasets that may overestimate convergence values. However, we also tested several convergence estimates from other recent publications (Table 2-2).

We further consider published palinpastic reconstructions of the Tibetan interior from structural geology studies, which reflect the portion of convergence recorded by upper crustal shortening in Asia (Figure 2.1). We assume a 50% uncertainty in stratigraphic thicknesses, which is likely given the typically low number of stratigraphic measurements in a given map area and heterogeneities in crustal thickness within intermontaine basins. Under area-balancing considerations, such uncertainties directly translate to a ~50% shortening error, which we apply to all palinspastic reconstructions of deformed sedimentary strata in Tibet (Table 2-4). We compile these data along two lines of section: through the Pamir and Tien Shan in the west, and from Indus-Yarlung Suture (TYS) to the Qilian Shan in the east (Figure 2.1).

Using the Indus-Tsangpo suture as the surface boundary between Asian and Indian affinity crust (e.g. Gansser, 1964) and a comparable suture zone in Pakistan as defined by Ahmed and Ernst (1999), we translate Asian shortening estimates into those of areal input by a generally southward migration of the suture. Our compilation of Asian upper crustal shortening estimates yields ~500 ± 250 km and ~320 ± 160 km of north-south upper crustal shortening at the west, and east ends of the orogen, respectively (Figure 2.1). These lie at or below the lower limit of convergence determined from paleomagnetism (Table 2-1). Uncertainties in shortening budgets are likely owed to a lack of subsurface and stratigraphic control across extensive regions and understudied regions potentially account for the lower total shortening value from cross-sections compared to the paleomagnetic data.

Another contribution in estimating the areal input into the orogen is the possibility of extrusion of large crustal blocks (Tapponnier et al., 1982; Leloup et al., 1995; Replumaz and Tapponnier, 2003) from the interior of the orogen to areas outside its margins. We obtain an upper bound of net extrusion area since collision from estimates by Replumaz and Tapponnier [2003]under the assumption that rates have remained constant between 40 and 50 Ma to. However, the large

displacements on strike-slip faults used in this work have been challenged by other authors (e.g. Cowgill, 2007; Leloup et al., 2011; van Hinsbergen, Kapp, et al., 2011). As such, we average this value with the smaller one proposed by Leloup et al., (1995) to obtain the 2.4×10^6 km^2 used in our calculations. As this is still an order of magnitude greater than that suggested by van Hinsbergen et al., (2011b) (which amounts to $\sim.1 \times 10^6$ km^2, using our definition of the boundaries of the orogen), we also include cases with no extrusion in our estimates of pre-collisional crustal thicknesses (Table 2-2). Using the larger estimate of Replumaz and Tapponnier (2003) alone would decrease the mass input slightly, leading to only a 7% increase in estimated crustal areal input because more crust is extruded eastward.

2.4 Results

Given the above constraints, our volume balance calculation is simply the volume input, defined by the net area prior to collision times the global average crustal thickness (41 km), minus the modern orogen volume. Under this assumption of average crustal thickness, the input volume due to the convergence between Asia and India is greater than the volume of crust presently within the orogen, yielding an overall mass deficit in the modern (Table 2-1). For example, using the median paleomagetism estimate (1100 ± 500 km, Dupont-Nivet et al., 2010) and assuming a 60 km thick Qiangtang and Lhasa terranes, with 41 km thick crust in the remainder of the orogen yields a deficit of 200×10^6 km^3 or $\sim$30% less crust in the modern than expected to have been present prior to collision. This value over half of the modern orogenic volume which we estimate as $390 \pm 40 \times 10^6$ km^3 based on our compilation of regional crustal thickness models (Figure 2.1). By comparison, using the lower Asia shortening estimates determined from upper crustal shortening (320 – 500 km) would produce smaller values of crustal input and correspondingly lower estimates of volume deficit (75– 150×10^6 km^3), or equivalent to about one third of the modern orogen volume. Although these lower values likely reflect an underestimate of crustal input due to unstudied regions of crustal shortening compared to the estimates of Asian shortening from paleomagnetism.

We also test the case by which mass is conserved. Instead of assuming a crustal thickness prior to collision equal to the global average, we calculate what the pre-collisional thickness of India and Asia must be in order to conserve crustal volume based on modern volumes divided by the pre-collisional area of India and Asia (Table 2-1). We calculate values based on a uniform thickness, as well as the case where the southern Asian margin is thickened prior to collision (Qiangtang and/or Lhasa block) and additionally consider cases with both our mean extrusion value, and where extrusion was negligible ("No Extrusion"). In order to conserve crustal volumes, the Indian and Asian crust

would have needed to be ~23-32 km thick prior to collision (Table 2-2). Cases with no extrusion yield smaller values of 23-26 km, than those including it (26 – 32 km). Similarly, cases which include a larger area of thick crust prior to collision require thinner crust (23 – 27 km) elsewhere in the orogen.

Table 2-2 – Average crustal thicknesses necessary to balance modern volume using Asian convergence estimates of Dupont-Nivet et al., (2010) and greater India of Gibbons et al (2012).

	No Lhasaplano	60 km Lhasa	60 km Lhasa & Qiangtang
No Extrusion	26 ± 5 km	25 ± 5 km	23 ± 6 km
Extrusion	29 ± 6 km	27 ± 6 km	26 ± 6 km
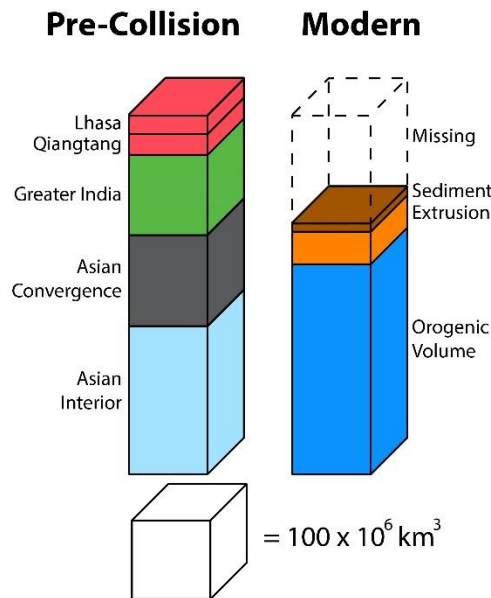
Figure 2.3 – Diagram of mass balance results, assuming 60 km thick Lhasa and Qiangtang terranes, and 41 km thick crust elsewhere prior to collision. We use Asian shortening values of Dupont-Nivet et al., (2010), and size of India from Gibbons et al., (2012). The volume of each rectangular prism is scaled to accurately represent the volume of each component.

Furthermore, due to significant differences in methods and terminology between this study and previous work, we attempt to put our calculations into a common framework (Table 2-3). LePichon et al., (1992) use topography as an analog for crustal thickness and necessary crustal shortening, under the assumption that $T = (h \times 7) + 35$. Where T is crustal thickness and h is topographic elevation. We combine his estimates of the mean elevation and surface area of Tibet to yield an equivalent crustal volume. Replumaz et al., (2010) perform density corrections on volumes used in their calculations, with a 17% decrease in volume for sediments and a 7% increase for crust below 35 km. We found a < 1% increase in volume for our dataset making similar corrections, and so state their estimates without such correction.

24

Table 2-3 – Comparison of our study with previous work (in units of 10^6 km^2).

Variable	This Study	Le Pichon, 1992	Replumaz et al., 2010
Area of Asia (collision)	12.5 ± 2.8	14.6	15[a]
Area of Asia (modern)	7.9	10.7	10.3[a]
Change in Asian Area[b]	3.6 ± 2.8	3.9[a]	4.7
Area of Greater India (collision)	4.2 ± 0.4	2.6-2.5[a]	3.1
Area of Greater India (modern)	-	-	0.8
Extrusion	0.8 – 2.1	-	-
Net Area Prior to Collision	15.7 ± 2.8	16.2-17.1	18.1
Modern Volume	390 ± 80[c]	530[a,c]	480[b,c]
Sediment Volume	17[c]	-	22[c]
Area of Lhasa Terrane	0.58	-	-
Area of Qiangtang Terrane	0.64	-	-

a – Values not explicitly stated, and derived via methods described in text.
b – Excludes volume of sediment moved out of the orogen.
c – Units are of 10^6 km^3

There are key differences in methodologies between our approach and previous studies and we compile these a comparable framework in Table 3. Le Pichon et al., (1992) argues for 2.8-3.0 x 10^6 km^2 of missing area, which would equate to 74-123 x 10^6 km^3 if the crust was 41 km thick) and Replumaz et al.,(2010) suggesting a mismatch of 11-14 x 10^6 km^3 of Asian and ~119-149 x 10^6 km^3 of Indian crust. Le Pichon et al., (1992) overestimate the modern orogenic volume by ~37% and use a Greater India that is only 38-67% of the area proposed by Gibbons et al., (2012). Consequently, their proportion of mass deficit is lower and the crustal thickness estimates needed for volume conservation are 5-7 km higher than in our study. Replumaz et al., (2010) suggest that the majority of mass imbalance in the orogen is due to Indian-derived crust, and argue against a mass transfer beneath Tibet and in favor of recycling. However, their work implicitly transfers mass from the Indo-Asian orogen to the Altai, amounting to 8% of the overall orogenic volume, without providing a mechanism by which such a transfer could have occurred. Furthermore, our estimates incorporate published estimates of crustal extrusion away from the orogen. This is implicated as a possible solution to mass imbalance by Le Pichon et al., (1992), and implicitly incorporated by Replumaz et al., (2010). However in the latter work, the area of the "Indochina Block" located east of the path of the eastern Himalayan syntaxis does not increase between 45 Ma and modern, indicating that overall area loss is accommodated by crustal shortening rather than extrusion.

Table 2-4 – Crustal shortening estimates used in this study.

Location	Source	Shortening (km)[a]	Azimuth
Pamir	Burtman and Molnar, (1993)	300	-
Tien Shan	Avouac et al., (1993)	194	16
Tien Shan	Avouac et al., (1993)	120	3
Peter the First Range	Hamburger et al., (1992)	60	40
Lhasa Block	Kapp et al., (2003)	20	5
Qiangtang	Kapp et al., (2005)	41	2
Qiangtang	Kapp et al., (2005)	16	0
Qiangtang	Kapp et al., (2007a)	25	0
Lhasa and Qiangtang	Wu et al., (2012)	191	-
Songpan-Ganzi	Li et al., (2011)	132	6
Songpan-Ganzi	Li et al., (2011)	214	50
Hoh Xil Basin	Wang et al., (2002)	34	30
Yushu-Nangqian	Spurlin et al., (2005)	61	45
Northeast Tibet	Meyer et al., (1998)	140	42
Northeast Tibet	Meyer et al., (1998)	190	44
Qilian Shan	Zheng et al., (2010)	8	38
Qaidam Basin	Yin et al., (2008)	2.6-50	-
Qaidam Basin	Liu et al., (2009)	19-60	-
Qaidam Basin	Zhou et al., (2006)	1-18	-

a – In cases where a cross section is comprised of multiple segments, the longer section is used.

2.5 Discussion

Our results show that a mass balance between modern, and pre-collisional volumes is impossible to achieve given a global average to thick crust prior to collision (≥41 km). Such a discrepancy can be accounted for in two primary ways: (1) Recycling of crustal material into the mantle or (2) A thin Indo-Asian crust prior to collision averaging ~23-32 km. Deep seismicity in the Pamir is often cited as evidence of crustal subduction (Burtman and Molnar, 1993), and to a limited extent, this mechanism has been proposed for Tibet based on geologic constraints (e.g. Tapponnier et al., 2001). However, we stress that the subducted volume necessary to balance an initial average thickness crust is equal to more than half the volume of crust currently within the orogen today and more than an order of magnitude greater than the $\sim$11-14 x 10^6 km^3 proposed for Asian continental subduction (Tapponnier et al., 2001; Replumaz et al., 2010) or the $\sim$15 x 10^6 km^3 estimated for Indian underplating and eclogitization (Hetényi et al., 2007; Replumaz et al., 2010; e.g. DeCelles et al., 2002). Furthermore, proposals of an extensive high plateau prior to or soon after collision (Rowley and Currie, 2006; Quade et al., 2011; Bershaw et al., 2012; Hoke et al., 2014) exacerbate the imbalance. If the majority of the high topography, and therefore modern crustal volume, was already in place by Eocene to Oliogocene time then all or most of the input volume (amounting to $\sim$ 3 x 10^8 km^3) would need to be recycled

26

into the mantle. Thus in our opinion, consideration of plate motions and crustal volume balance seriously challenge the interpretation from recent isotopic proxies for high paleoelevations in northern and eastern Tibet during Eocene and Oligocene time because these would require the recycling of an untenable amount of crustal material to the mantle.

As an alternative to crustal subduction, we hypothesize that a thin crust existed across much of the orogen prior to collision, which was likely near sea level. A thin pre-collisional crust is consistent with sedimentalogical, geomorphic and paleoclimatic constraints: Greater Indian sediments were deposited below sea level during the Jurassic and remained so during its drift from Gondwana (Sciunnach and Garzanti, 2012). Similarly, extensive regions in the northwest part of the orogen, encompassing the modern Tajik, Tarim and eastern Qaidam basins, were part of an inland sea that did not reach modern elevations until Eocene or Miocene time. (Ritts et al., 2008; Bosboom et al., 2011) Other areas such as the modern Xining-Minhe-Lingzhong basin complex located at the northeast end of the orogen, were unlikely to be at high elevations during Eocene time as evidenced by sedimentary sequences indicative of externally drained distal fluvial to lacustrine depositional environments (e.g. Ren et al., 2002; Horton et al., 2004). Lastly, relict erosional surfaces at the extreme southeast end of the orogen provide evidence for generally low relief and subdued topography connected to sea level (Clark et al., 2006). A thin crust with reasonable, albeit relatively low density, and a thin mantle lithosphere could reasonably support above sea level elevations (Clark et al., 2012), which would be consistent with the lack of Cretaceous age and younger marine strata within the interior of Tibet. Today, similarly thin crust can be observed in northern Ireland (24-30 km) (Davis et al., 2012), and Indonesia (16-44 km) (Macpherson et al., 2012). If the regions of Asia north of Qiangtang terrane were thin prior to Indian collision, a stationary northern boundary to the plateau (Clark et al., 2010; Clark, 2012) may be explained in part by this inherited rheologic contrast.

Our solution to the mass balance paradox is in contrast to one proposed by Van Hinsbergen et al., (2012) who use paleolatitudes of Indian terranes and mantle tomography to propose a microcontinent collision at ~50 Ma and subduction of oceanic crust over the next ~25 myr, eliminating ~2300 km of continental crust from total convergence budgets. Using the methods outlined in this paper, and Asian and Indian shortening constraints from their work, we estimate that a 30-36 km crust prior to collision in areas of the orogen outside of southern Tibet would conserve crustal volume, as compared to 23-32 km using our chosen estimates from Gibbons et al., (2012) and Dupont-Nivet et al., (2010) (Table 2-1). However, this value will still not provide a volume balance if extensive regions of high topography existed in northern and eastern Tibet (e.g. Rowley and Currie,

2006; Quade et al., 2011; Bershaw et al., 2012; Lease et al., 2012; Hoke et al., 2014) despite the resulting mass imbalance being obviously smaller due to the reduction of Indian mass input (Table 2-1).

Thin crust in India and the Asian interior prior to collision requires a consideration of crustal shortening estimates in order to discern between viable models (Tapponnier et al., 1982; England and Houseman, 1988; Molnar et al., 1993; Clark and Royden, 2000; Tapponnier et al., 2001; DeCelles et al., 2002) for plateau development. Our compilation of Asian upper crustal shortening estimates yields a smaller value for Asian crustal input (300-500 km) than the total convergence within Asia by paleomagnetic studies (~1000 km, e.g. Dupont-Nivet et al., 2010; Cogne et al., 2013), which suggest that Asia absorbed about half (or less) of the total convergence of India with Eurasia since ~ 50 Ma. In addition, our values are smaller than those suggested by van Hinsbergen et al., (2011b) (600-1000 km) due to our reliance solely on estimates of upper crustal shortening (as opposed to incorporation of paleomagnetic estimates), lack of interpolation of shortening values across unquantified regions, and use of recently published palinspastic reconstructions in the plateau interior (e.g. Li et al., 2011; Wu et al., 2012). The discrepancy between paleomagnetic estimates and those solely from upper crustal shortening values may be due to two primary factors: (1) systematic overestimates of Asian convergence from paleomagnetic data, and (2) the paucity of data from the Tibetan interior, which may underestimate total crustal shortening. Recent paleomagnetic studies have begun accounting for known problems that contributed to older values of upwards of ~2000 km of inter-Asian convergence (e.g. Dupont-Nivet et al., 2010; Sun et al., 2012) and generally agree on estimates of over 600 km (see Cogne et al., 2013).

Our upper crustal shortening compilation contains data along nearly the complete line of section, suggesting that there are no significant data gaps. As such, additional studies are unlikely to double the current net shortening value to bring it in line with paleomagnetic estimates. In order to conserve crustal volume, low amounts of upper crustal shortening imply that more than half of the net Asian convergence had to be accommodated without being recorded in the upper crust. This is supported by evidence of a viscous lower crust, which moves material from areas of high crustal thickness near the collision boundary to thinner areas at the margins that have experienced insufficient post-Eocene shortening to bring them to modern elevations (e.g. Clark and Royden, 2000; Wang et al., 2005; Le Pape et al., 2012). Similarly, the ~1100 km width of Greater India prior to rifting from Gondwana is greater than the 600-900 km of shortening seen in the Himalaya (DeCelles et al., 2002; Robinson et al., 2006; Yin et al., 2009; Long et al., 2011), and supports the underthrusting of Indian

28

crust north of the ITS (Nábelek et al., 2009; Ceylan et al., 2012; Agius and Lebedev, 2013) and mass redistribution at depth (Zhao and Morgan, 1987; DeCelles et al., 2002) (Figure 2.4).
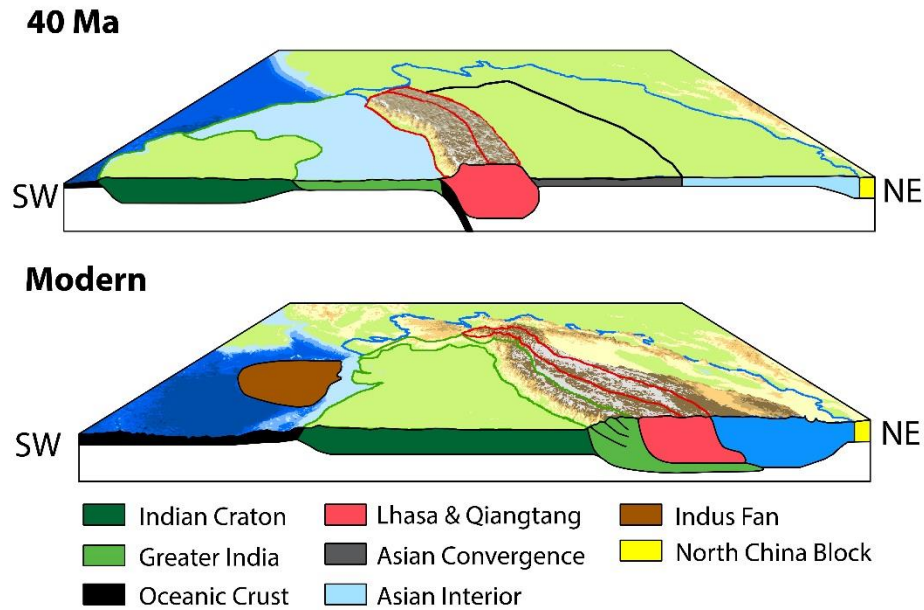
Figure 2.4 – Geodynamic cartoon of processes and distances mentioned in text. Top shows the scenario near the time of collision, with thinned greater India and Asian interior. The Lhasa and Qiang-Tang terranes are thickened prior to collision. Lower portion shows the modern state of the orogen, with convergence accommodated by Indian underthrusting, and Asian shortening and lower crustal flow. Colors used are same as in Figure 2.3, and lines of section are shown in Figure 2.2.

2.6 Conclusions

Current estimates from geologic and paleomagnetic records suggest that half or less of the overall Indo-Asian convergence since collision has been absorbed by Asian shortening. If average crustal thicknesses are assumed, this can directly account for doubling of Asian crust to modern values of 60-80 km, leaving nearly half of India's convergence unaccounted for in the modern mass of the orogen. Mass balance calculations with a 41 km crust and a high "Lhasaplano" at the Asian margin prior to collision yield a 27-30% or ~200 x 10^6 km^3 mismatch between modern and input volumes for the Indo-Asian orogen. These are an order of magnitude larger than proposed estimates of Asian continental subduction and eclogitization of underthrust Indian crust (Replumaz et al., 2010), and incorporate a range of extrusion values. Proposals for thick crust in northern and eastern Tibet prior to or soon after collision (Rowley and Currie, 2006; Quade et al., 2011; Bershaw et al., 2012; Hoke et al., 2014) further increase the mismatch, and require an untenable amount of material to be placed into the mantle. We propose that crustal conservation can be achieved with a ~23-32 km crust across the pre-collisional Asian interior and greater India, with the notable exceptions of the Lhasa and

Qiangtang terranes. As a direct consequence, the ~1100 km of Asian convergence suggested by paleomagnetic studies would be insufficient to build modern crustal volumes, and would require addition of Indian material and mass redistribution at depth. The long-lived northern boundary of the plateau, located at ~ 40°N, is then the result of a rheologic contrast with older, thicker, lithosphere of the North China block.

2.7 References

Agius, M.R., and Lebedev, S., 2013, Tibetan and Indian lithospheres in the upper mantle beneath Tibet: Evidence from broadband surface-wave dispersion: Geochemistry, Geophysics, Geosystems, v. 14, p. 4260–4281, doi: 10.1002/ggge.20274.

Ahmed, Z., and Ernst, W.G., 1999, Island Arc–Related, Back-Arc Basinal, and Oceanic-Island Components of the Bela Ophiolite-Mélange Complex, Pakistan: International Geology Review, v. 41, p. 739–763, doi: 10.1080/00206819909465167.

Ali, J.R., and Aitchison, J.C., 2005, Greater India: Earth-Science Reviews, v. 72, p. 169–188, doi: 10.1016/j.earscirev.2005.07.005.

Avouac, J.-P., Tapponnier, P., Bai, M., You, H., and Wang, G., 1993, Active Thrusting and Folding Along the Northern Tien Shan and Late Cenozoic Rotation of the Tarim Relative to Dzungaria and Kazakhstan: Journal of Geophysical Research, v. 98, p. 6755–6804, doi: 10.1029/92JB01963.

Baljinnyam, I., Bayasgalan, A., Borisov, B.A., Cisternas, A., Dem'yanovich, M.G., Ganbaatar, L., Kochetkov, V.M., Kurushin, R.A., Molnar, P., Philip, H., and Vashchilov, Y.Y., 1993, Ruptures of Major Earthquakes and Active Deformation in Mongolia and Its Surroundings: Geological Society of America.

Bassin, C., Laske, G., and Masters, G., 2000, The Current Limits of resolution for surface wave tomography in North America: EOS Trans AGU, v. 82.

Bershaw, J., Penny, S.M., and Garzione, C.N., 2012, Stable isotopes of modern water across the Himalaya and eastern Tibetan Plateau: Implications for estimates of paleoelevation and paleoclimate: Journal of Geophysical Research, v. 117, p. 1–18, doi: 10.1029/2011JD016132.

Bosboom, R.E., Dupont-Nivet, G., Houben, A.J.P., Brinkhuis, H., Villa, G., Mandic, O., Stoica, M., Zachariasse, W.J., Guo, Z., and Li, C., 2011, Late Eocene sea retreat from the Tarim Basin (west China) and concomitant Asian paleoenvironmental change: Palaeogeography, Palaeoclimatology, Palaeoecology, v. 299, p. 385–398, doi: 10.1016/j.palaeo.2010.12.019.

Bouilhol, P., Jagoutz, O.E., Hanchar, J.M., and Dudas, F.O., 2013, Dating the India–Eurasia collision through arc magmatic records: Earth and Planetary Science Letters, v. 366, p. 163–175, doi: 10.1016/j.epsl.2013.02.023.

Buck, W.R., 2006, The role of magma in the development of the Afro-Arabian Rift System: Geological Society, London, Special Publications, v. 259, p. 43–54, doi: 10.1144/GSL.SP.2006.259.02.05.

Burov, E.B., and Watts, A.., 2006, The long-term strength of continental lithosphere: "jelly sandwich" or "crème brûlée"? GSA Today, v. 16, p. 4, doi: 10.1130/1052-5173(2006)016<4:TLTSOC>2.0.CO;2.

Burtman, V.S., and Molnar, P., 1993, Geological and geophysical evidence for deep subduction of continental crust beneath the Pamir: Geological Society of America Special Papers, v. 287.

Ceylan, S., Ni, J., Chen, J.Y., Zhang, Q., Tilmann, F., and Sandvol, E., 2012, Fragmented Indian plate and vertically coherent deformation beneath eastern Tibet: Journal of Geophysical Research, v. 117, p. 1–11, doi: 10.1029/2012JB009210.

Christensen, N.I., and Mooney, W.D., 1995, Seismic velocity structure and composition of the continental crust: A global view: Journal of Geophysical Research, v. 100, p. 9761, doi: 10.1029/95JB00259.

Clark, M.K., 2012, Continental collision slowing due to viscous mantle lithosphere rather than topography: Nature, v. 483, p. 74–77, doi: 10.1038/nature10848.

Clark, M.K., and Royden, L.H., 2000, Topographic ooze: Building the eastern margin of Tibet by lower crustal flow: Geology, v. 28, p. 703, doi: 10.1130/0091-7613(2000)28<703:TOBTEM>2.0.CO;2.

Clark, M.K., Royden, L.H., Whipple, K.X., Burchfiel, B.C., Zhang, X., and Tang, W., 2006, Use of a regional, relict landscape to measure vertical deformation of the eastern Tibetan Plateau: Journal of Geophysical Research, v. 111, p. F03002, doi: 10.1029/2005JF000294.

Cogne, J.-P., Besse, J., Chen, Y., and Hankard, F., 2013, A new Late Cretaceous to Present APWP for Asia and its implications for paleomagnetic shallow inclinations in Central Asia and Cenozoic Eurasian plate deformation: Geophysical Journal International, v. 192, p. 1000–1024, doi: 10.1093/gji/ggs104.

Cowgill, E., 2007, Impact of riser reconstructions on estimation of secular variation in rates of strike–slip faulting: Revisiting the Cherchen River site along the Altyn Tagh Fault, NW China: Earth and Planetary Science Letters, v. 254, p. 239–255, doi: 10.1016/j.epsl.2006.09.015.

Cunningham, D., 2013, Mountain building processes in intracontinental oblique deformation belts: Lessons from the Gobi Corridor, Central Asia: Journal of Structural Geology, v. 46, p. 255–282, doi: 10.1016/j.jsg.2012.08.010.

Davis, M.W., White, N.J., Priestley, K.F., Baptie, B.J., and Tilmann, F.J., 2012, Crustal structure of the British Isles and its epeirogenic consequences: Geophysical Journal International, v. 190, p. 705–725, doi: 10.1111/j.1365-246X.2012.05485.x.

DeCelles, P.G., Robinson, D.M., and Zandt, G., 2002, Implications of shortening in the Himalayan fold-thrust belt for uplift of the Tibetan Plateau: Tectonics, v. 21, p. 12–1–12–25, doi: 10.1029/2001TC001322.

Dupont-Nivet, G., Lippert, P.C., Van Hinsbergen, D.J.J., Meijers, M.J.M., and Kapp, P.A., 2010, Palaeolatitude and age of the Indo-Asia collision: palaeomagnetic constraints: Geophysical Journal International, v. 182, p. 1189–1198, doi: 10.1111/j.1365-246X.2010.04697.x.

England, P., and Houseman, G.A., 1988, The Mechanics of the Tibetan Plateau [and Discussion]: Philosophical Transactions of the Royal Society A: Mathematical, Physical and Engineering Sciences, v. 326, p. 301–320, doi: 10.1098/rsta.1988.0089.

Gan, W., Zhang, P., Shen, Z.-K., Niu, Z., Wang, M., Wan, Y., Zhou, D., and Cheng, J., 2007, Present-day crustal motion within the Tibetan Plateau inferred from GPS measurements: Journal of Geophysical Research, v. 112, p. 1–14, doi: 10.1029/2005JB004120.

Gansser, A., 1964, Geology of the Himalayas: New York, John Wiley & Sons.

Garzanti, E., and Van Haver, T., 1988, The indus clastics: forearc basin sedimentation in the Ladakh Himalaya (India): Sedimentary Geology, v. 59, p. 237–249, doi: 10.1016/0037-0738(88)90078-4.

Gibbons, A.D., Barckhausen, U., van den Bogaard, P., Hoernle, K., Werner, R., Whittaker, J.M., and Müller, R.D., 2012, Constraining the Jurassic extent of Greater India: Tectonic evolution of the West Australian margin: Geochemistry Geophysics Geosystems, v. 13, p. 1–25, doi: 10.1029/2011GC003919.

Glorie, S., De Grave, J., Buslov, M.M., Zhimulev, F.I., Elburg, M. a., and Van den haute, P., 2012, Structural control on Meso-Cenozoic tectonic reactivation and denudation in the Siberian Altai: Insights from multi-method thermochronometry: Tectonophysics, v. 544-545, p. 75–92, doi: 10.1016/j.tecto.2012.03.035.

De Grave, J., and Van den haute, P., 2002, Denudation and cooling of the Lake Teletskoye Region in the Altai Mountains (South Siberia) as revealed by apatite fission-track thermochronology: Tectonophysics, v. 349, p. 145–159, doi: 10.1016/S0040-1951(02)00051-3.

Hamburger, M.W., Sarewitz, D.R., Pavlis, T.L., Popandopulo, G.A., and Sciences, G., 1992, Structural and seismic evidence for intracontinental subduction in the Peter the First Range, Central Asia: Geological Society of America Bulletin, v. 104, p. 397–408, doi: 10.1130/0016-7606(1992)104<0397:SASEFI>2.3.CO;2.

Hetényi, G., Cattin, R., Brunet, F., Bollinger, L., Vergne, J., Nábělek, J.L., and Diament, M., 2007, Density distribution of the India plate beneath the Tibetan plateau: Geophysical and petrological constraints on the kinetics of lower-crustal eclogitization: Earth and Planetary Science Letters, v. 264, p. 226–244, doi: 10.1016/j.epsl.2007.09.036.

Van Hinsbergen, D.J.J., Kapp, P.A., Dupont-Nivet, G., Lippert, P.C., DeCelles, P.G., and Torsvik, T.H., 2011, Restoration of Cenozoic deformation in Asia and the size of Greater India: Tectonics, v. 30, p. 1–31, doi: 10.1029/2011TC002908.

Van Hinsbergen, D.J.J., Lippert, P.C., Dupont-Nivet, G., McQuarrie, N., Doubrovine, P. V., Spakman, W., and Torsvik, T.H., 2012, Greater India Basin hypothesis and a two-stage Cenozoic collision between India and Asia: Proceedings of the National Academy of Sciences, v. 109, doi: 10.1073/pnas.1117262109.

Van Hinsbergen, D.J.J., Steinberger, B., Doubrovine, P. V., and Gassmöller, R., 2011, Acceleration and deceleration of India-Asia convergence since the Cretaceous: Roles of mantle plumes and continental collision: Journal of Geophysical Research, v. 116, p. 1–20, doi: 10.1029/2010JB008052.

Hoke, G.D., Liu-Zeng, J., Hren, M.T., Wissink, G.K., and Garzione, C.N., 2014, Stable isotopes reveal high southeast Tibetan Plateau margin since the Paleogene: Earth and Planetary Science Letters, v. 394, p. 270–278, doi: 10.1016/j.epsl.2014.03.007.

Horton, B.K., Dupont-Nivet, G., Zhou, J., Waanders, G.L., Butler, R.F., and Wang, J., 2004, Mesozoic-Cenozoic evolution of the Xining-Minhe and Dangchang basins, northeastern Tibetan Plateau: Magnetostratigraphic and biostratigraphic results: Journal of Geophysical Research, v. 109, p. 1–15, doi: 10.1029/2003JB002913.

Jackson, J., 2002, Strength of the continental lithosphere: Time to abandon the jelly sandwich? GSA Today, v. 12, p. 4, doi: 10.1130/1052-5173(2002)012<0004:SOTCLT>2.0.CO;2.

Jagoutz, O.E., Burg, J.-P., Hussain, S., Dawood, H., Pettke, T., Iizuka, T., and Maruyama, S., 2009, Construction of the granitoid crust of an island arc part I: geochronological and geochemical constraints from the plutonic Kohistan (NW Pakistan): Contributions to Mineralogy and Petrology, v. 158, p. 739–755, doi: 10.1007/s00410-009-0408-3.

Kapp, P.A., DeCelles, P.G., Gehrels, G.E., Heizler, M., and Ding, L., 2007, Geological records of the Lhasa-Qiangtang and Indo-Asian collisions in the Nima area of central Tibet: Geological Society of America Bulletin, v. 119, p. 917, doi: 10.1130/B26033.2.

Kapp, P.A., DeCelles, P.G., Leier, A.L., Fabijanic, J.M., He, S., Pullen, A., Gehrels, G.E., and Ding, L., 2007, The Gangdese retroarc thrust belt revealed: GSA Today, v. 17, p. 4–9, doi: 10.1130/GSAT01707A.2.

Kapp, P.A., Murphy, M.A., Yin, A., and Harrison, T.M., 2003, Mesozoic and Cenozoic tectonic evolution of the Shiquanhe area of western Tibet: Tectonics, v. 22, doi: 10.1029/2001TC001332.

Kapp, P.A., Yin, A., Harrison, T.M., and Ding, L., 2005, Cretaceous-Tertiary shortening, basin development, and volcanism in central Tibet: Geological Society of America Bulletin, v. 117, p. 865, doi: 10.1130/B25595.2.

Lease, R.O., Burbank, D.W., Zhang, H., Liu, J., and Yuan, D., 2012, Cenozoic shortening budget for the northeastern edge of the Tibetan Plateau: Is lower crustal flow necessary? Tectonics, v. 31, p. 1–16, doi: 10.1029/2011TC003066.

Leloup, P.H., Boutonnet, E., Davis, W.J., and Hattori, K.H., 2011, Long-lasting intracontinental strike-slip faulting: new evidence from the Karakorum shear zone in the Himalayas: Terra Nova, p. no–no, doi: 10.1111/j.1365-3122.2012.00988.x.

Leloup, P.H., Lacassin, R., Tapponnier, P., Schärer, U., Zhong, D., Liu, X., Zhang, L., Ji, S., and Trinh, P.T., 1995, The Ailao Shan-Red River shear zone (Yunnan, China), Tertiary transform boundary of Indochina: Tectonophysics, v. 251, p. 3–84, doi: 10.1016/0040-1951(95)00070-4.

Li, Y., Wang, C., Ma, C., Xu, G., and Zhao, X., 2011, Balanced cross-section and crustal shortening analysis in the Tanggula-Tuotuohe Area, Northern Tibet: Journal of Earth Science, v. 22, p. 1–10, doi: 10.1007/s12583-011-0152-2.

Liebke, U., Appel, E., Ding, L., and Zhang, Q., 2013, Age constraints on the India–Asia collision derived from secondary remanences of Tethyan Himalayan sediments from the Tingri area: Journal of Asian Earth Sciences, v. 62, p. 329–340, doi: 10.1016/j.jseaes.2012.10.012.

Liu, D., Fang, X., Gao, J., Wang, Y., Zhang, W., Miao, Y., Liu, Y., and Zhang, Y., 2009, Cenozoic Stratigraphy Deformation History in the Central and Eastern of Qaidam Basin by the Balance Section Restoration and its Implication: Acta Geologica Sinica, v. 83, p. 359–371, doi: 10.1111/j.1755-6724.2009.00024.x.

Long, S., McQuarrie, N., Tobgay, T., and Grujic, D., 2011, Geometry and crustal shortening of the Himalayan fold-thrust belt, eastern and central Bhutan: Geological Society of America Bulletin, v. 123, p. 1427–1447, doi: 10.1130/B30203.2.

Macpherson, K. a., Hidayat, D., and Goh, S.H., 2012, Receiver function structure beneath four seismic stations in the Sumatra region: Journal of Asian Earth Sciences, v. 46, p. 161–176, doi: 10.1016/j.jseaes.2012.12.005.

Mechie, J., Yuan, X., Schurr, B., Schneider, F., Sippl, C., Ratschbacher, L., Minaev, V., Gadoev, M., Oimahmadov, I., Abdybachaev, U., Moldobekov, B., Orunbaev, S., and Negmatullaev, S., 2012, Crustal and uppermost mantle velocity structure along a profile across the Pamir and southern Tien Shan as derived from project TIPAGE wide-angle seismic data: Geophysical Journal International, v. 188, p. 385–407, doi: 10.1111/j.1365-246X.2012.05278.x.

Métivier, F., Gaudemer, Y., Tapponnier, P., and Klein, M., 2002, Mass accumulation rates in Asia during the Cenozoic: Geophysical Journal International, v. 137, p. 280–318, doi: 10.1046/j.1365-246X.1999.00802.x.

Meyer, B., Tapponnier, P., Bourjot, L., Métivier, F., Gaudemer, Y., Peltzer, G., Shunmin, G., and Zhitai, C., 1998, Crustal thickening in Gansu-Qinghai, lithospheric mantle subduction, and oblique, strike-slip controlled growth of the Tibet plateau: Geophysical Journal International, v. 135, p. 1–47, doi: 10.1046/j.1365-246X.1998.00567.x.

Molnar, P., England, P., and Martinod, J., 1993, Mantle dynamics, uplift of the Tibetan Plateau, and the Indian Monsoon: Reviews of Geophysics, v. 31, p. 357–396, doi: 10.1029/93RG02030.

Molnar, P., and Stock, J.M., 2009, Slowing of India's convergence with Eurasia since 20 Ma and its implications for Tibetan mantle dynamics: Tectonics, v. 28, p. 1–11, doi: 10.1029/2008TC002272.

Murphy, M.A., Yin, A., Harrison, T.M., Durr, S.B., Chen, Z., Ryerson, F.J., Kidd, W.S.F., Wang, X., and Zhou, X., 1997, Did the Indo-Asian collision alone create the Tibetan plateau? Geology, v. 25, p. 719–722, doi: 10.1130/0091-7613(1997)025<0719:DTIACA>2.3.CO;2.

Nábelek, J., Hetényi, G., Vergne, J., Sapkota, S., Kafle, B., Jiang, M., Su, H., Chen, J., and Huang, B.-S., 2009, Underplating in the Himalaya-Tibet collision zone revealed by the Hi-CLIMB experiment.: Science (New York, N.Y.), v. 325, p. 1371–4, doi: 10.1126/science.1167719.

Le Pape, F., Jones, A.G., Vozar, J., and Wenbo, W., 2012, Penetration of crustal melt beyond the Kunlun Fault into northern Tibet: Nature Geoscience, v. 5, p. 330–335, doi: 10.1038/ngeo1449.

Le Pichon, X., Fournier, M., and Jolivet, L., 1992, Kinematics, Topography, Shortening, and Extrusion in the India-Eurasia Collision: Tectonics, v. 11, p. 1085–1098.

Quade, J., Breecker, D.O., Daeron, M., and Eiler, J.M., 2011, The paleoaltimetry of Tibet: An isotopic perspective: American Journal of Science, v. 311, p. 77–115, doi: 10.2475/02.2012.02.

Ren, J., Tamaki, K., Li, S., and Junxia, Z., 2002, Late Mesozoic and Cenozoic rifting and its dynamic setting in Eastern China and adjacent areas: Tectonophysics, v. 344, p. 175–205, doi: 10.1016/S0040-1951(01)00271-2.

Replumaz, A., Negredo, A.M., Guillot, S., der Beek, P. Van, Villaseñor, A., and van Der Beek, P., 2010, Crustal mass budget and recycling during the India/Asia collision: Tectonophysics, v. 492, p. 99–107, doi: 10.1016/j.tecto.2010.05.023.

Replumaz, A., and Tapponnier, P., 2003, Reconstruction of the deformed collision zone Between India and Asia by backward motion of lithospheric blocks: Journal of Geophysical Research, v. 108, doi: 10.1029/2001JB000662.

Reuber, I., 1986, Geometry of accretion and oceanic thrusting of the Spongtang Ophiolite, Ladakh-Himalaya: Nature, v. 321, p. 592–596, doi: 10.1038/321592a0.

Ritts, B.D., Yue, Y., Graham, S. a., Sobel, E.R., Abbink, A.O., and Stockli, D.F., 2008, From sea level to high elevation in 15 million years: Uplift history of the northern Tibetan Plateau margin in the Altun Shan: American Journal of Science, v. 308, p. 657–678, doi: 10.2475/05.2008.02.

Robinson, D.M., DeCelles, P.G., and Copeland, P., 2006, Tectonic evolution of the Himalayan thrust belt in western Nepal: Implications for channel flow models: Geological Society of America Bulletin, v. 118, p. 865–885, doi: 10.1130/B25912.2.

Rowley, D.B., and Currie, B.S., 2006, Palaeo-altimetry of the late Eocene to Miocene Lunpola basin, central Tibet.: Nature, v. 439, p. 677–81, doi: 10.1038/nature04506.

Sciunnach, D., and Garzanti, E., 2012, Subsidence history of the Tethys Himalaya: Earth-Science Reviews, v. 111, p. 179–198, doi: 10.1016/j.earscirev.2012.12.007.

Spurlin, M.S., Yin, A., Horton, B.K., Zhou, J., and Wang, J., 2005, Structural evolution of the Yushu-Nangqian region and its relationship to syncollisional igneous activity, east-central Tibet: Geological Society of America Bulletin, v. 117, p. 1293, doi: 10.1130/B25572.2.

Steffen, R., Steffen, H., and Jentzsch, G., 2011, A three-dimensional Moho depth model for the Tien Shan from EGM2008 gravity data: Tectonics, v. 30, doi: 10.1029/2011TC002886.

Sun, Z., Jiang, W., Li, H., Pei, J., and Zhu, Z., 2010, New paleomagnetic results of Paleocene volcanic rocks from the Lhasa block: Tectonic implications for the collision of India and Asia: Tectonophysics, v. 490, p. 257–266, doi: 10.1016/j.tecto.2010.05.012.

Sun, Z., Pei, J., Li, H., Xu, W., Jiang, W., Zhu, Z., Wang, X., and Yang, Z., 2012, Palaeomagnetism of late Cretaceous sediments from southern Tibet: Evidence for the consistent palaeolatitudes of the southern margin of Eurasia prior to the collision with India: Gondwana Research, v. 21, p. 53–63, doi: 10.1016/j.gr.2012.08.003.

Tan, X., Gilder, S., Kodama, K.P., Jiang, W., Han, Y., Zhang, H., Xu, H., and Zhou, D., 2010, New paleomagnetic results from the Lhasa block: Revised estimation of latitudinal shortening across Tibet and implications for dating the India–Asia collision: Earth and Planetary Science Letters, v. 293, p. 396–404, doi: 10.1016/j.epsl.2010.03.013.

Tapponnier, P., and Molnar, P., 1979, Active faulting and cenozoic tectonics of the Tien Shan, Mongolia, and Baykal Regions: Journal of Geophysical Research, v. 84, p. 3425, doi: 10.1029/JB084iB07p03425.

Tapponnier, P., Peltzer, G., Le Dain, A.Y., Armijo, R., and Cobbold, P.R., 1982, Propagating extrusion tectonics in Asia: New insights from simple experiments with plasticine: Geology, v. 10, p. 611, doi: 10.1130/0091-7613(1982)10<611:PETIAN>2.0.CO;2.

Tapponnier, P., Zhiqin, X., Roger, F., Meyer, B., Arnaud, N.O., Wittlinger, G., and Jingsui, Y., 2001, Oblique stepwise rise and growth of the Tibet plateau.: Science (New York, N.Y.), v. 294, p. 1671–7, doi: 10.1126/science.105978.

Wang, C., Liu, Z., Yi, H., Liu, S., and Zhao, X., 2002, Tertiary crustal shortening and peneplanation in the Hoh Xil region: implications for the tectonic history of the northern Tibetan Plateau: Journal of Asian Earth Sciences, v. 20, p. 211–223, doi: 10.1016/S1367-9120(01)00051-7.

Wang, Q., McDermott, F., Xu, J., Bellon, H., and Zhu, Y., 2005, Cenozoic K-rich adakitic volcanic rocks in the Hohxil area, northern Tibet: Lower-crustal melting in an intracontinental setting: Geology, v. 33, p. 465, doi: 10.1130/G21522.2.

Williams, S.E., Müller, R.D., Landgrebe, T.C.W., and Whittaker, J.M., 2012, An open-source software environment for visualizing and refining plate tectonic reconstructions using high-resolution geological and geophysical data sets: GSA Today, v. 22, p. 4–9, doi: 10.1130/GSATG139A.2.

Wu, Z., Ye, P., Barosh, P.J., Hu, D., Lu, L., and Zhang, Y., 2012, Early Cenozoic Mega Thrusting in the Qiangtang Block of the Northern Tibetan Plateau: Acta Geologica Sinica - English Edition, v. 86, p. 799–809, doi: 10.1111/j.1755-6724.2012.00707.x.

Yin, A., Dang, Y.-Q., Wang, L.-C., Jiang, W.-M., Zhou, S.-P., Chen, X.-H., Gehrels, G.E., and McRivette, M.W., 2008, Cenozoic tectonic evolution of Qaidam basin and its surrounding regions (Part 1): The southern Qilian Shan-Nan Shan thrust belt and northern Qaidam basin: Geological Society of America Bulletin, v. 120, p. 813, doi: 10.1130/B26180.2.

Yin, A., Dubey, C.S., Webb, A.A.G., Kelty, T.K., Grove, M., Gehrels, G.E., and Burgess, W.P., 2009, Geologic correlation of the Himalayan orogen and Indian craton: Part 2. Structural geology, U-Pb zircon geochronology, and tectonic evolution of the Shillong Plateau and its neighboring regions in NE India: Geological Society of America Bulletin, v. 122, p. 336–359, doi: 10.1130/B26460.2.

Zhang, Z., Deng, Y., Teng, J., Wang, C., Gao, R., Chen, Y., and Fan, W., 2011, An overview of the crustal structure of the Tibetan plateau after 35 years of deep seismic soundings: Journal of Asian Earth Sciences, v. 40, p. 977–989, doi: 10.1016/j.jseaes.2010.03.010.

Zhang, Z., Yang, L., Teng, J., and Badal, J., 2011, An overview of the earth crust under China: Earth-Science Reviews, v. 104, p. 143–166, doi: 10.1016/j.earscirev.2010.10.003.

Zhao, W.-L., and Morgan, W.J., 1987, Injection of Indian crust into Tibetan lower crust: A two-dimensional finite element model study: Tectonics, v. 6, p. 489–504, doi: 10.1029/TC006i004p00489.

Zheng, D., Clark, M.K., Zhang, P., Zheng, W., and Farley, K.A., 2010, Erosion, fault initiation and topographic growth of the North Qilian Shan (northern Tibetan Plateau): Geosphere, v. 6, p. 937–941, doi: 10.1130/GES00523.2.

Zhou, J., Xu, F., Wang, T., Cao, A., and Yin, C., 2006, Cenozoic deformation history of the Qaidam Basin, NW China: Results from cross-section restoration and implications for Qinghai–Tibet Plateau tectonics: Earth and Planetary Science Letters, v. 243, p. 195–210, doi: 10.1016/j.epsl.2005.12.033.

Zorin, Y.A., Novoselova, M.R., Turutanov, E.K., and Kozhevnikov, V.M., 1990, Structure of the lithosphere of the Mongolian-Siberian mountainous province: Journal of Geodynamics, v. 11, p. 327–342, doi: 10.1016/0264-3707(90)90015-M.

Chapter 3: Pliocene to Recent Shortening at the Northern Margin of the Tibetan Plateau: Generating High Elevation Compressional Faulting though Simple Shear[2]

3.1 Abstract

Post-Miocene deformation in the high (>4000 m) Tibetan plateau is dominated by normal and strike-slip faulting. The cessation of thrust faulting and the initiation of normal and strike-slip faulting within the Tibetan interior is thought to result from the crust having reached elevations at which contractional faulting is inhibited by gravity and no longer continues to thicken despite ongoing continental convergence. We present evidence of active thrust faulting in the northern margin of the Tibetan Plateau at elevations of ~5000 m underlain by 60 km thick crust. We present new geologic mapping and a balanced cross section of the Guaizi Liang, a range formed through the deformation of the Oligo-Pliocene Kumkuli Basin, to the southwest of the Qaidam Basin. Results reveal ~20 %, or ~9 km, of post-Pliocene north-south shortening on active east-west and northwest-southeast striking thrust faults. Observed structural trends are used to infer a compressive stress orientation of ~020°. A ^{36}Cl cosmogenic radionuclide depth profile from a folded Quaternary fan surface yields a vertical uplift rate of ~3.4 mm/yr. When this rate is integrated with our palinspastically-restored cross-section, a horizontal shortening rate of ~1.7 mm/yr is inferred. These rates are among the fastest dip-slip fault rates documented in the northern Tibetan Plateau.

The mechanisms driving contraction in this region can be elucidated from the structural trends of active faults, which are broadly compatible with slip transfer and shear between the Altyn Tagh and Kunlun/Manyi left-lateral strike slip faults. We conclude that the Guaizi Liang accommodates a relatively low amount of crustal shortening and may likely be related to the simple shear, where localized crustal thickening is balanced by distributed extension elsewhere such that no changes in crustal thickness occur. This interpretation provides a viable explanation for observed thrust faulting at ~5 km elevation because simple shear does not lead to increasing gravitational potential energy by

---

crustal thickening. This implies that the modern thick crust and resultant high elevations were likely present in the northern Tibetan Plateau prior to the onset of regional shear and active thrust faulting in the Guaizi Liang and that the modern strain field is not analogous to earlier tectonic phases that thickened the plateau crust. The ~5 Ma initiation age may also provide an upper bound on the initiation of the Manyi segment of the Kunlun fault system.

3.2 Introduction

Modes of active deformation in the Tibetan Plateau, the world's largest region of high topography, are partitioned by elevation (Molnar and Tapponnier, 1978; Figure 1). Both earthquake focal mechanisms and geologic observations indicate a prevalence of normal and strike-slip faults at elevations of > 4000 m in the plateau interior, while thrust faults are prevalent below this elevation and are generally located near the margins of the orogen (Molnar and Tapponnier, 1978; Taylor and Yin, 2009). This relationship between fault mechanisms and topography has led to the interpretation that the crust is gravitationally unstable above 4000 m, and that cessation of thrust faulting in the plateau interior and initiation of normal or strike-slip faulting is mechanistically related to the attainment of high elevations (Harrison et al., 1992; Molnar et al., 1993; Kapp and Guynn, 2004). A prediction of this hypothesis is that the initiation ages of normal and strike-slip faults can be used to constrain the timing of topographic growth across the Tibetan Plateau. Such constraints are relevant to both the geodynamics of plateau formation, as well as the perturbation of climate due to the presence of high terrain (Harrison et al., 1992; Molnar et al., 1993; Clark and Royden, 2000; Zhisheng et al., 2001; Yin, 2010; Molnar et al., 2010) .

The initiation or re-initiation of major strike slip and normal faults in late Miocene time has been argued to indicate the time period during which the crust may have attained modern elevations and crustal thicknesses (Armijo et al., 1986; Mercier et al., 1987; Harrison et al., 1992, 1995; Murphy et al., 2000; Blisniuk et al., 2001; Phillips et al., 2004; Sun et al., 2005; Liu et al., 2007; Duvall et al., 2013; Styron et al., 2013; Lu et al., 2014). As such, the temporal progression of faulting styles within the Tibetan Plateau records the evolution of the strength of the lithosphere and should reflect the geodynamic mechanisms required to attain thick crust and high elevations. These mechanisms remain a matter of debate and include processes such as distributed compressional faulting in the upper and lower crust (e.g. Yin and Taylor, 2011), transpression between major strike-slip faults (Tapponnier et al., 2001), lithospheric removal (Molnar et al., 1993), or lower crustal flow (Clark and Royden, 2000) to bring the crustal column to modern thicknesses of 60-70 km and an elevation of 5000 m.
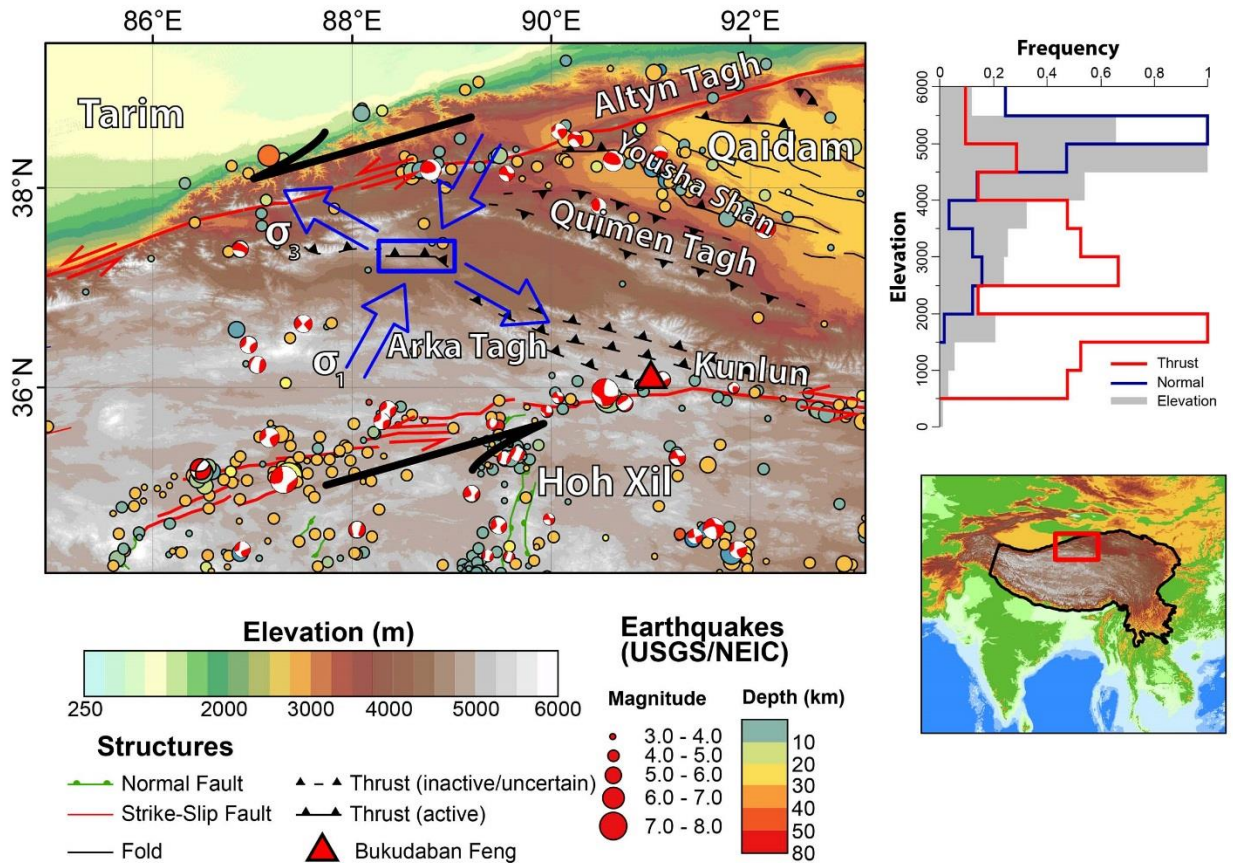
Figure 3.1 – Left: interpretation of regional tectonics in the vicinity of the Kumuli Basin. Map area (**Figure 3.4**) located in blue box. Blue arrows show inferred maximum compressive (σ_1) and least compressive (σ_3) stress directions inferred in the map area. Earthquake locations and depths for the Hoh Xil Basin sourced from the USGS NEIC database, and moment tensors from the global CMT database (Dziewonski et al., 1981; Ekström et al., 2012). The western most tensor on the Manyi Fault is reproduced from Molnar and Tapponnier, (1978). Faults are generalized from Taylor and Yin, (2009), with the exception of links between the Manyi and Kunlun Faults, which are based on our interpretations. Right: Frequency of earthquakes with $M_w > 5.5$ in Tibet, limited to region outlined in black in the index map below. Note that thrust faults above 4000 m are generally related to transpressional stepovers in major strike-slip faults, such as the Karakorum and Altyn Tagh. Focal mechanisms obtained from Global CMT catalog (Ekström et al., 2012).

While crustal thickening and presumably active plateau growth is currently focused on the plateau margins, thrust faulting in the northern Tibetan Plateau near the Qaidam Basin suggests that additional thickening may be ongoing in regions of already thick crust (Molnar and Tapponnier, 1978; Taylor and Yin, 2009). The ~5000 m high Guaizi Liang is a unique example of a high-elevation, post-Pliocene thrust belt (Figure 1). As such, it provides a venue to evaluate the relationship between elevation, crustal thickness, faulting style and the gravitational stability of a thickened lithosphere. Two

major strike-slip fault systems, the Altyn Tagh and Kunlun/Manyi, bound the Guaizi Liang to the north and south respectively (Figure 1). We investigate this unusual example of thrust faulting occurring in a region of thick crust and at high elevation by evaluating the role of the Altyn Tagh and Kunlun/Manyi faults in accommodating Indo-Asian convergence southwest of the Qaidam Basin, and their kinematic relationship with deformation in the Guaizi Liang. This kinematic description is compared to geologic observations, which include geologic mapping, balanced cross sections, and Quaternary shortening rates obtained on an actively growing fold in order to assess the potential contribution of thrust faulting to crustal thickening.

3.3 Tectonic Setting of the Kukuli Basin and Guaizi Liang

The high terrain southwest of the Qaidam Basin, including the regions surrounding Aqqikkol and Ayakkum lakes and Ulugh Muztagh, is composed of a series of west-northwest trending mountain ranges and intermontane basins. This region lies at altitudes of 4000-5000 m and merges with the high topography of the Tibetan Plateau interior. The region as a whole is bounded to the south by the Kunlun/Manyi fault system, and separated from the low elevation Tarim Basin to the north by the Altyn Tagh strike-slip fault. Prior to Oligocene time, a single unified basin extended ~500 km to the southwest of the Qaidam Basin and encompassed the present-day extents of both the Kumkuli Basin and the Hoh Xil Basin, a Cretaceous-Oligocene basin which is presently located within the interior of the Tibetan Plateau (Yin et al., 2007; Meng and Fang, 2008; Figure 1). Emergence of the earliest generation of thrust-related mountain ranges within and to the southwest of the Qaidam Basin occurred in Oligocene-early Miocene time. These ranges created isolated individual sub-basins, which continued to accumulate sediment through the late Miocene, when a Plio-Quaternary tectonic event generated the active thrust belt observed today, and deformed Oligo-Pliocene basin deposits.

The first phase of Cenozoic thrust faulting in our study area is associated with prominent high relief ranges, such as the Qimen Tagh and Arka Tagh. These basement-cored ranges are thought to have been active from Oligocene to early Miocene time (Yin et al., 2007). Development of the Qimen Tagh and Arka Tagh has been kinematically linked to left-lateral strike-slip faulting along the Altyn Tagh fault, similar to the proposed evolution of the Qilian Shan to the northeast of our study area (Yin et al., 2002; Cowgill et al., 2003). The onset of deformation associated with these ranges is coeval with the cessation of shortening across much of the northern Tibetan Plateau to the south, based on the presence of undeformed Miocene sediments and Oligocene lava flows that cap deformed strata of the Cretaceous-Eocene Hoh Xil Basin (Wu et al., 2008; Li et al., 2013; Staisch et al., 2014). This deformation also led to isolation of the paleo-Qaidam Basin from the Hoh Xil Basin in Oligocene

time, and led to the creation of the Kumkuli Basin from late Oligocene to Pliocene time (Yin et al., 2007).

Intermontane basins associated with the basement–cored Oligo-Miocene ranges continued to accumulate sediment through late Miocene to early Pliocene time, at which point they become deformed to form a younger set of ranges comprised solely of Cenozoic sedimentary strata. Such ranges include the Yousha Shan, and the Guaizi Liang. Emergence of these ranges likely initiated in Miocene or Pliocene time, and deformation continues to the present (Xiao et al., 2005; Yin et al., 2007; Meng and Fang, 2008). The Guaizi Liang is a particularly well-exposed example of such a range, and lies to the north of Aqqikkol Lake at a modern elevation of 5000 m. This range is comprised of deformed Oligo-Pliocene basin sediments that are a part of the Kumkuli Basin, and lies between the Qimen Tagh and Arka Tagh ranges to the north and south, respectively. The Guaizi Liang has 500-700 m of relief and is underlain by a series of broad east-west to northwest-southeast trending folds.

Deformation of ranges surrounding the northwestern Qaidam Basin has been linked solely to motion on the Altyn Tagh strike-slip fault. However, the Guaizi Liang is in equal proximity to the Kunlun fault system, which suggests that the Kunlun fault may also play a role in driving deformation of the Kumkuli Basin. Our present understanding of the Altyn Tagh and Kunlun fault systems would support simultaneous activity since at least 20 Ma with approximately ~10 mm/yr of left-lateral slip concentrated on each fault system (Van der Woerd et al., 1998; Cowgill, 2007; Ritts et al., 2008; Duvall et al., 2013). Because the Guaizi Liang lies between the Kunlun and Altyn Tagh faults, we hypothesize that deformation is related to westward propagation of the Kunlun fault since 20 Ma, which initiated a step-over or transfer of strain from the Kunlun to the Altyn Tagh fault. This behavior is similar to that observed in the northeastern Tibetan Plateau between the Kunlun and Haiyuan fault systems, and deformation within the Qaidam basin in modern time (Duvall and Clark, 2010).

3.4 Stratigraphy of the Guaizi Liang

The Guaizi Liang contains deformed Oligocene through Quaternary sedimentary rocks, which document basin isolation, infilling, and subsequent crustal shortening. Deposition of sedimentary strata in our study region, which is a part of the Kumkuli Basin, likely began with the Oligocene to early Miocene emergence of the Qimen Tagh range to the north and the Arka Tagh range to the south (Yin et al., 2007; Cheng et al., 2014). These topographic barriers isolated the paleo-Qaidam Basin from the Hoh Xil Basin, thus forming a new intermontane basin (i.e. the Kumkuli Basin) (Meng and Fang, 2008). Northerly paleocurrent directions in Oligo-Miocene strata suggest that sediment sources for the Kumkuli Basin lay to the south, in the present-day plateau interior (Xiao et al., 2005). Below we

describe the principal stratigraphic units in the Kumkuli Basin, as described by Xiao et al. (2005), supplemented with our own field observations.

Figure 3.2 – Artiodactyl track from the Shibiliang Formation. The track can be no older than Early Miocene, based on the oldest large Artiodactyls found in the region, located within the Tiejianggou Formation of the Qilian Shan (Wang et al., 2003). Protractor is 18 cm long.

Strata within the Kumkuli Basin are composed of the Oligo-Miocene sedimentary sequences, which are unconformably overlain by Quaternary strata. Xiao et al. (2005) classify these units as the Oligocene Shimagou Formation, Miocene Shibiliang Formation, and Pliocene Hongliang Formation. We depart from this stratigraphic classification by subsuming the Shimagou Formation into the Shibiliang Formation, based on the observation of along-strike grain size changes from conglomerates previously identified as the Shimagou Formation to fine grained sandstones and mudstones mapped by Li et al., (2002) as the Shibiliang Formation. This proposed along-strike facies transition suggests that strata identified as the Shimagou Formation by Xiao et al. (2005) are lateral equivalents of the lower portion of the Shibiliang Formation, and extends the temporal range of the Shibiliang Formation to include the Oligocene Epoch.

Age assignments for stratigraphic units in the Guaizi Liang were determined on the basis of pollen, ostracode, and gastropod assemblages found within each unit (Xiao et al., 2005; Zhang et al., 1996, 2001). However, in some cases, ages of key index fossils are determined from other sedimentary basins in the Tibetan Plateau with no clear isotopic or magnetostratigraphic age determination. As such, we first broadly corroborate the age range of sedimentary units in the Kumkuili Basin with artiodactyl footprints (Figure 3.2) located in an area mapped as Shibiliang Fm. (Li et al., 2002). The track must be no older than the early Miocene, based on the earliest medium-sized artiodactyl fossils

found in Qilian Shan to the north (Wang et al., 2003). However, modern tracks left by the Tibetan antelope (*Pantholops hodgsonii*) are identical to our trace fossil, preventing us from ruling out the possibility that strata are younger than suggested by previous authors.

Strata in the lower portion of the Shibiliang Formation in the western half of the map area are predominantly composed of a clast-supported pebble conglomerate with a coarse to medium sandstone matrix. Clasts are well-rounded, moderately well sorted, and composed predominantly of limestone; sandstone clasts are common, while clasts of chert, and granite are present, but subordinate. Greenstone and mudstone clasts are rare. The conglomerates are occasionally interbedded with coarse-grained, poorly sorted litharenites, of no more than 1 m thickness.

Conglomerates in the lower portion of the Shibiliang Formation grade to finer grained strata over 20-30 m of section, and over ~5 km along strike. Overlying and laterally equivalent strata make up the majority of the Shibiliang Formation and are constituted of red, fine to medium grained, well-sorted lith- to quartzarenites and siltstones, with subordinate interbedded gray siltstones, laminated limestones and thin (0.5-2.0 cm) gypsum layers. The presence of symmetric ripples, mud cracks, and channel scour indicates a fluvial to lacustrine depositional setting (Figure 3.3). A 12-km-long lenticular evaporite member in the eastern half of the map area marks a significant deviation from the typical sedimentology of the Shibiliang Formation. This unit is composed of 1-20 cm thick gypsum and halite layers, interbedded with gray siltstones and limestones. Due to the strong deformation within this unit, and in most overlying strata, the sedimentary thickness was not measured, but is estimated to be at least 200 m based on mapped outcrop patterns. Shortening estimates in later sections of this paper are therefore limited to the western half of the map area, where no thick evaporite sequences are observed.

The Pliocene Hongliang Formation conformably overlies the Shibiliang Formation and is composed of silty and/or carbonaceous red fine-grained sandstones to mudstones, with interbedded siltstones. We observed a rapid increase in grain size towards the top of the Hongliang Formation, which Xiao et al. (2005) document as culminating in a > 100 m thick conglomerate which caps the stratigraphic section below the Quaternary unconformity. Quaternary strata unconformably overlie the Hongliang Formation, and are composed of fluvial and colluvial deposits containing clasts eroded from the Oligo-Miocene formations, as well as basalt and granitoid clasts that are derived from the Kumbuyan Shan range to the northwest.

42
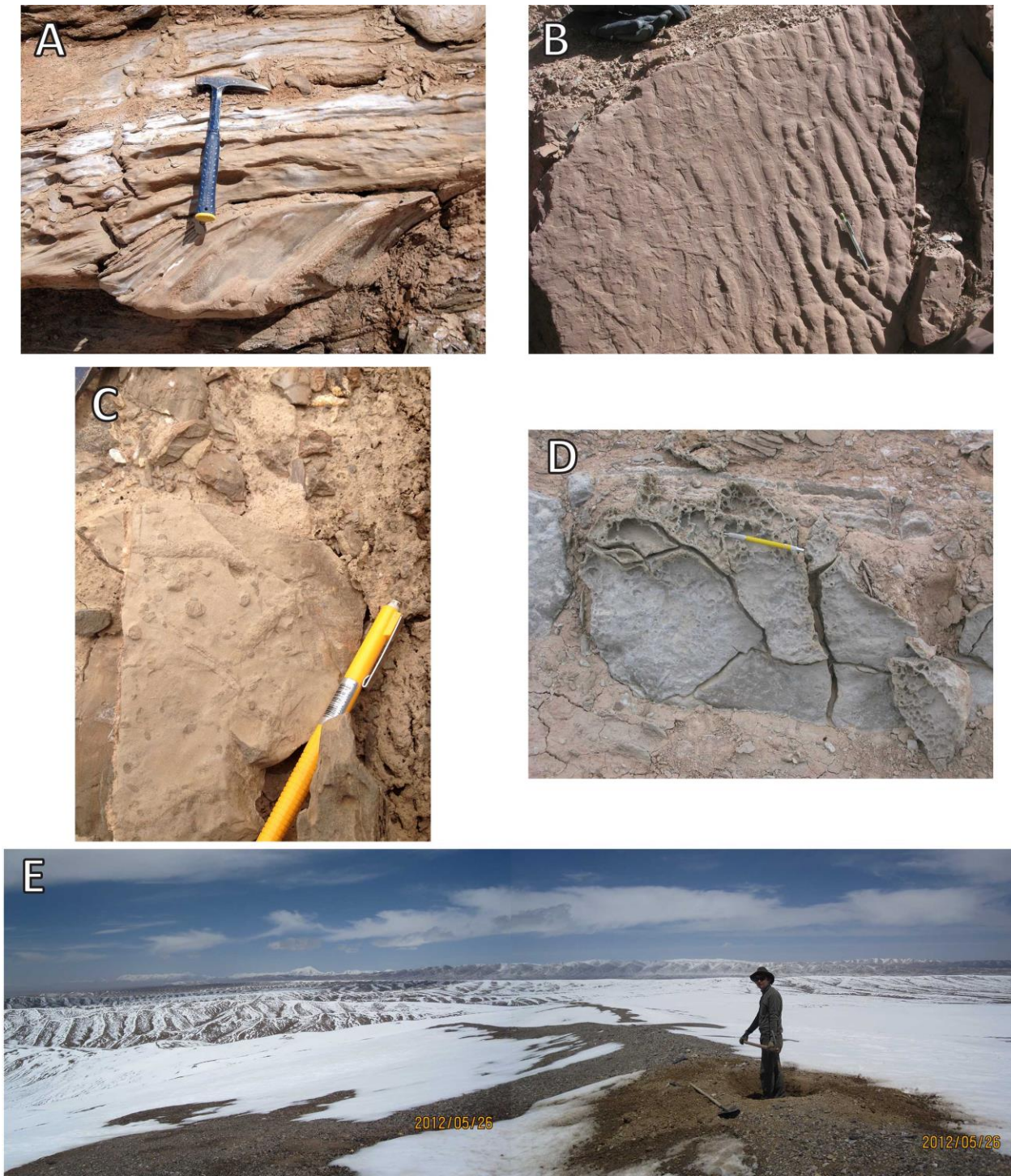
Figure 3.3 – (A-D) Sedimentary features of the Shibiliang Formation: (A) Trough crossbeds in sandstone. (B) Symmetric ripples and horizontal burrows in fine-grained sandstone. (C) Horizontal and vertical worm burrows in mudstone, filled with medium sand. (D) Gray carbonaceous siltstone with mudcracks. (E) Panoramic view from fault-bend fold, showing site of [36]Cl depth profile, and morphology of deformed alluvial surface.

Strata within the Kumkuli Basin document Oligo-Pliocene basin quiescence and infilling, which was terminated by the cessation of deposition and initiation of deformation of basin strata in Pliocene through Quaternary time. Chert and limestone clasts found in the lower portion of the Shibiliang Formation were likely sourced from Triassic marine sediments in the Hoh Xil Basin. This interpretation is consistent with generally northerly paleocurrent directions, and suggests that the Hoh Xil Basin was at higher elevations than the Kumkuli Basin in Oligo-Miocene time. The initiation of basin infilling during Oligocene time may also mark the isolation of the Kumkuli Basin from the Qiadam Basin to the northwest, concurrent with the emergence of the Qilian Shan, as suggested by previous authors (Yin et al., 2007; Meng and Fang, 2008). The fine grained sandstones, evaporites and lacustrine carbonates of the Shibiliang Formation and the lower portion of the Hongliang Formation suggest a period of tectonic quiescence within the Kumkuli Basin, with low stream gradients incapable of transporting coarse-grained strata, and continued basin infilling during Miocene through Pliocene time. A rapid transition to conglomeratic strata before an unconformity with Quaternary alluvium at the top of the Hongliang Formation suggests that deformation in the region began in Pliocene time, leading to increased stream power and transport of coarser grained sediments from more proximal sources.

3.5 Structural Intepretation of the Guaizi Liang

Since Pliocene time, deformation in the western Kumkuli Basin has formed the Guaizi Liang range. In order to quantify the amount of shortening and the geologic average shortening rate in the Guaizi Liang, we mapped an area of approximately 1800 km^2 and constructed a balanced cross-section through the range. We derive the total amount and rate of shortening from our cross-section, which can be compared to the Quaternary deformation documented from a folded fan surface presented in the next section. Our field work was focused was on the western two thirds of the map area (**Figure 3.4**), which includes a detailed structural transect along which we constructed a cross section. Due to the remote nature of this site and difficulty in traversing the region, we obtained supplementary structural data through remote sensing approaches. We used RIMS (Bernardin et al., 2006), a 3D visualization tool, in conjunction with ASTER multispectral satellite imagery and the SRTM digital elevation dataset to create "virtual strike dips" to supplement our understanding of deformation in the region. In areas with both field and remote measurements of bedding inclinations, we found that virtual strikes were within 10° and dips were within 15° of nearby field measurements, as compatible with previously published work (Bernardin et al., 2006). ASTER VNIR and SWIR band ratios (e.g. Yamaguchi and Naito, 2003) were used to distinguish between map units and individual alluvial fan

surfaces in order to delineate geologic contacts. Previous mapping in the region, overlapping with the eastern half of our map area, was completed at a scale of 1:250,000 and does not include a balanced and restored cross-section (Li et al., 2002).

3.5.1 Deformation Styles

Deformation in the western half of our map area is dominated by large, kilometer-scale east-west trending folds (Figure 3.5A). A lower hemisphere stereographic projection of poles to bedding measurements collected throughout the field area shows that folds are upright, with populations of both north and south steeply dipping axial planes (**Figure 3.4**, inset). The region contains two major surface-breaking faults with remaining deformation accommodated by blind thrusts. In the southern half of the map area, a north-dipping surface-breaking fault accommodates ~4.5 km of shortening, and contains an overturned drag fold in the hanging wall. The other major surface-breaking fault is located in the northern portion of the map area, accommodates ~2.5 km of shortening and dips to the south. In order to palinspastically balance our cross-section, we require 2 km of additional north-south shortening to be accommodated by blind thrusts along the line of section, which result in major east-west trending folds at the surface. Additional deformation occurs in small, meter-scale open north-south trending folds (Figure 3.5C), which are oblique to the main east-west trending faults and folds in the western half of the map area. This suggests that deformation is not due to, or caused solely by, north-south compression but rather by northeast-southwest directed compression.

The eastern portion of the Guaizi Liang shows a distinct change in structural trend from the western portion of the range, and contains off-fault deformation, as evidenced by at least one isoclinal fold (**Figure 3.5**B). Off-fault folding may be related to the presence of evaporites in this part of the map area. However, the poor quality of outcrop, and fine grain size of the strata typically lead to an absence of sedimentary structures that may be used to infer stratigraphic up, precluding us from eliminating the presence of additional isoclinal folds. Observed folds along a structural transect in this area, which we term the Salt River Transect, have fold axes which trend ~towards ~115° and bedding orientations in the limbs which strike 110° ± 5°. The smaller scale north-south trending folds that we observe in the western portion of the map area are not present along this transect. Remote sensing analysis indicates that beds further to the east of the Salt River transect dip towards ~50°, suggesting a progressive turn in the structural grain of the belt.
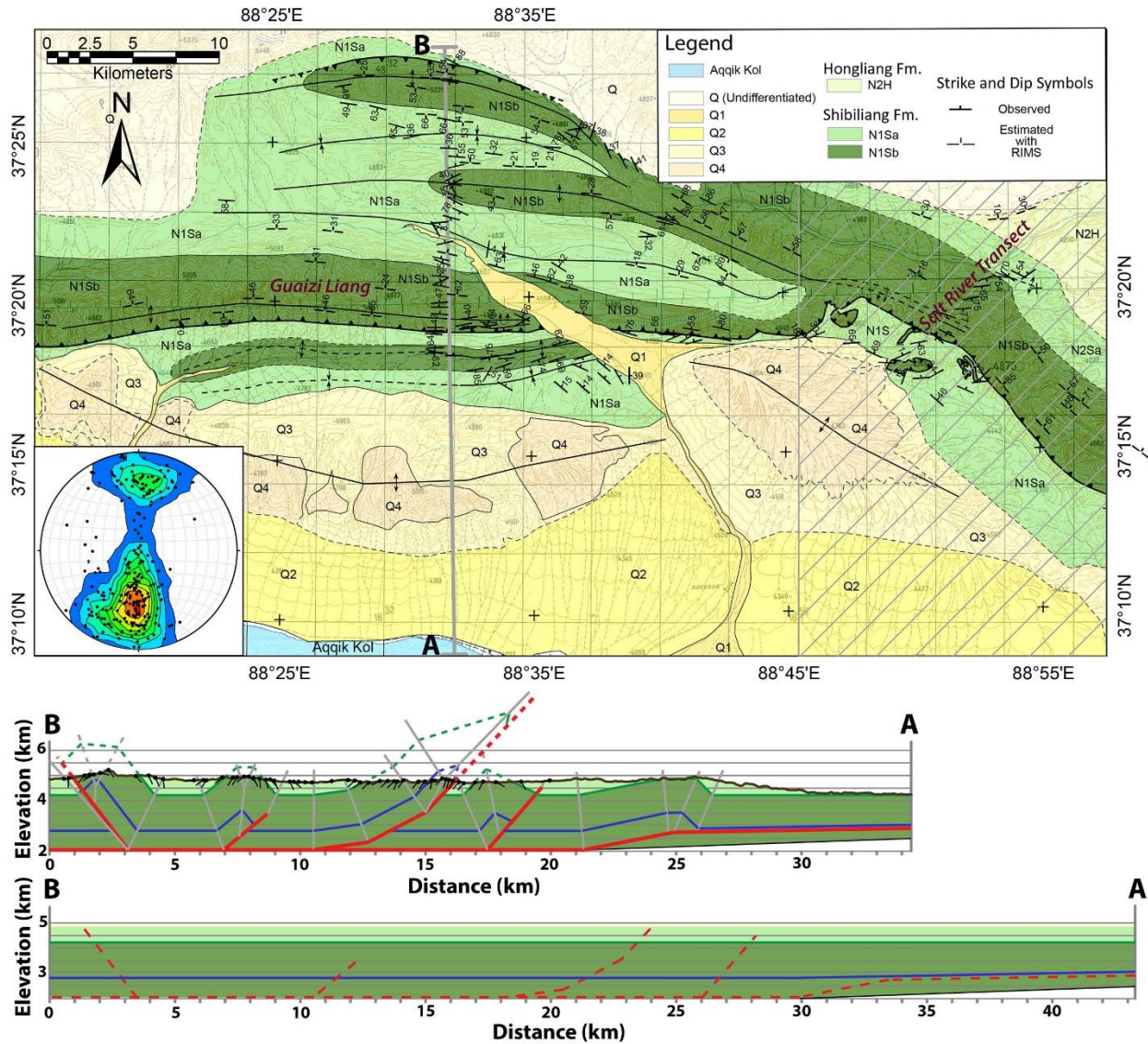
Figure 3.4 – Geologic map and cross section of the Guaizi Liang. Geology in the striped region is largely based on remote sensing in RIMS (Bernardin et al., 2006) and previous mapping in the region (Li et al., 2002). Blue horizon on cross section has no stratigraphic significance, and is plotted solely for clarification of structural features. Green line denotes contact between upper and lower units of the Shibiliang Formation. Note that Quaternary sediments are inferred to be <100 m thick, and are thus not plotted on the cross section. A lower hemisphere projection of poles to bedding collected in the western two thirds of the map area, and 2σ Kamb contours presented in bottom left corner of map. Stereonet plot constructed using Stereonet 9 software (Cardozo and Allmendinger, 2013).

Figure 3.5 – Dominant deformation styles in the Guaizi Liang: (A) Broad east-west running folds. (B) Tight to isoclinal folding with fold axis trending towards ~115°. (C) Meter-scale folding with north-south trending fold axes. Photo is taken looking east near the top of a anticline, which has an east-west trending fold axis. (D) Small magnitude (<10 m) faulting, estimated to be no more than 2 m in this outcrop based on marker bed outlined in white.

3.5.2 Shortening Estimates and Stratigraphic Thicknesses

The Kumkuli Basin has undergone 9 ± 2 km (20 ± 5 %) of north-south shortening, based on our balanced cross section for the western half of the region (**Figure 3.4**). Error on the above shortening estimates is based on uncertainties in stratigraphic thicknesses applied to our cross section using AreaErrorProp (Judge and Allmendinger, 2011). We estimate that the lower member of the Shibiliang Formation is 2.1 ± 0.5 km thick, based on bedding dip orientations, and outcrop patterns in the central portion of the map area, which is within error of published estimates by Xiao et al., (2005). As this unit makes up the bulk of deformed strata in our map area, we use the ~24 %

uncertainty for the stratigraphic thickness of the lower Shibiliang Formation as an estimate of the overall error in our cross section. Our estimated depth to décollement of ~3 km is significantly less than published stratigraphic thicknesses of ~7 km, but is consistent with the depth to basement estimated in a magnetotelluric transect of the Kumkuli Basin (Xiao et al., 2005; He et al., 2009; Figure 4). This is likely due to three major factors: First, the stratigraphic section measured by Xiao et al. (2005) in the eastern part of the range includes ~2 km of Pliocene Hongliang Formation. This unit is absent in the western portion of the map area, either due to erosion, or nondeposition. Second, we estimate the Shibiliang Formation as ~0.8-1.2 km thick, or ~1 km thinner than published values of Xiao et al., (2005). Finally, a reclassification of the ~0.9 km thick Shimagou Formation as a coarser grained and more proximal portion of the Shibiliang Formation reduces the total stratigraphic thickness estimated by Xiao et al., (2005).

Conglomerates at the top of the Pliocene Hongliang Formation may indicate an increase in stream power related to the initiation of shortening. The presence of deformed, and uplifted Quaternary alluvial fan surfaces indicates that deformation is still active. Initiation of shortening in Pliocene time (5.3-2.6 Ma) implies an average shortening rate of 2.3 ± 0.9 mm/yr.

3.6 Quaternary Deformation of the Guaizi Liang

3.6.1 Quaternary Vertical Uplift

We identify three folded alluvial fan surfaces at the southern end of the map area (**Figure 3.4**), which we use to estimate the magnitude of Quaternary uplift. These surfaces have been deformed as part of an actively growing fault-bend fold that has its tip line to the south of the range front. In order to calculate vertical offset of the fold, we extract stream profiles for two streams that wrap around the western end of this fault bend fold using the ASTER GDEM2 elevation model (Tachikawa et al., 2011), and verify stream paths with available topographic maps (**Figure 3.6**). We infer that these modern stream profiles approximate the elevation of the original alluvial surface prior to deformation, as aggradation rates in hyperarid regions like the Kumkuli Basin should be minimal (e.g. Jungers et al., 2013 report 2m/Myr in the Atacama Desert). The difference between the elevation of the modern streams and a point on the fold at the same latitude then approximates the total vertical displacement of that point since deformation began, amounting to 720 m of uplift of the alluvial surface relative to stream B and 670 m relative to stream C, or an average value of 695 ± 25 m.
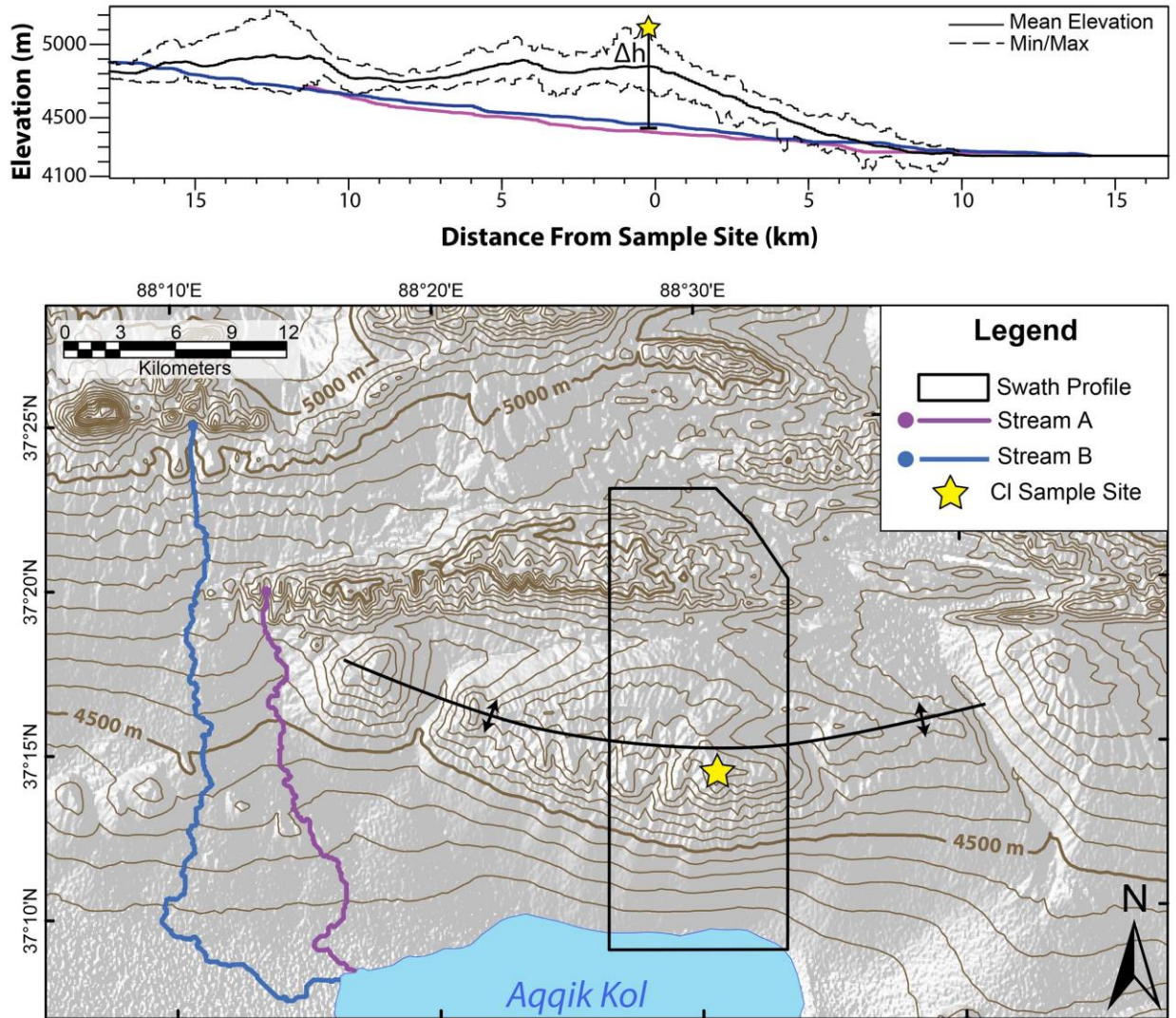
Figure 3.6 – Geomorphic estimate for total uplift of sampled alluvial surface, Δh. Topography of the Guaizi Liang is shown along with two streams (A) – Stream starting in older Plio-Quaternary range front to the north of Quaternary folding. (B) – undisturbed stream west of deformed Cenozoic strata. Both streams are intermittent and likely only active during storm events or during periods of snow melt. Note that stream profiles at top are smoothed with a 15 pixel running average (1 pix~28 m).

3.6.2 [36]Cl Cosmogenic Radionuclide Dating

In order to determine the age of the folded alluvial surface, we collected six samples for cosmogenic radionuclide dating from a soil pit on the fold crest. Samples were obtained from depths ranging from 10 to 150 cm (**Figure 3.3**E, **Figure 3.6**). Due to localized disturbances at the crest during construction of a nearby survey marker, no samples were collected at zero depth. Clasts within sampled material were predominantly limestone and mudstone, for which we used the [36]Cl chronometer. Bulk material at each sample level was collected in the field, and 2-5 mm carbonate

grains were subsequently separated for analysis. Grains were ground in a BICO disk mill, washed with 18 MΩ water and dried at 85ºC for 8-10 hours. Three gram aliquots were set aside for major and trace element analysis via XRF and LA-ICP-MS by ActLabs, Inc. (Table 3-1). The remaining material, and a sample blank, were digested overnight with trace metal grade HNO_3 after the addition of ~1 g of ^{35}Cl enriched carrier. The digested sample was then centrifuged for 10 minutes at 3600 rpm, and the supernatant decanted. $AgNO_3$ solution was added to the supernatant to produce an $AgCl_2$ precipitate after overnight refrigeration. Solids were separated from solution after an additional 10 minutes of centrifugation at 3600 rpm. Anion exchange chromatography was then performed on the samples to yield a pure $AgCl_2$ precipitate that was dried, weighed to ±0.0001 g and packed for AMS analysis at Purdue University's PRIME Lab (results in

Table **3-2**, methods described in detail by Desilets et al., 2006).

We derive diffusion lengths, in addition to attenuation and production rate coefficients, using the spreadsheet calculator of Schimmelpfennig et al. (2009). We then incorporate their formulas for total production of ^{36}Cl into a model that predicts ^{36}Cl concentration as a function of depth, surface age, rock density and ^{36}Cl inheritance. The most likely values for these parameters were then determined using a Bayesian approach by comparison of the predicted ^{36}Cl concentrations to observed concentrations across a wide range of potential parameter space. We assume that erosion at the top of the fold is negligible, based on the presence of a well-developed desert pavement. This assumption is generally compatible with low erosion rates of ≤ 12 mm/ka seen in other internally drained regions of the Tibetan plateau (Lal et al., 2004; Strobl et al., 2012). We further note that when erosion is included as parameter in a high-resolution (1000 models per parameter) grid search, the resulting best-fit model has a zero erosion rate. Reported sample densities were measured on disaggregated material in the laboratory, and may underestimate actual densities of the *in situ* closely-packed alluvium. As such, our model included a priori density values between that of disaggregated sediments (~1.6 g/cm^3) and the maximum expected value for the limestone that dominates the alluvial fan clasts (~2.8 g/cm^3). A priori ^{36}Cl inheritance values are between zero and the ^{36}Cl concentration measured for the deepest sample. A priori surface exposure ages were assumed to be between zero and 500 ka. In estimating misfit and calculating likelihoods, we use an L2 norm, and test 2×10^7 random models with uniformly distributed priors. We chose the number of tested models in order to consistently retain ~4000 likely models. In the absence of direct measurements, we assume that samples have a 10 weight percent water content, which represents an upper bound for barren Tibetan soils (Xie et al., 2012; Genxu et al., 2009).

To estimate ^{36}Cl production rates, we use the scaling relationships of Desilets and Zreda, (2003) and topographic shielding calculated from CosmoCalc (Vermeesch, 2007). However, estimates of snow shielding are problematic due to the lack of adequate information on the depth, density, and longevity of snow pack in Pleistocene time. Previous work has suggested that snow shielding may increase uncorrected ages by 6-14 % (Benson et al., 2004; Schildgen et al., 2005). We thus apply an approximate upper bound for average yearly snow cover in the Kumkuli Basin in order to account for uncertainties and variations in snow pack. NCEP reanalysis climate averages for 1980-2010 (Kalnay et al., 1996, http://www.esrl.noaa.gov/psd/; Schneider et al., 2011, GPCC v6 surface data) suggest that the Kumkuli Basin typically experiences ~1.2 cm/mo of precipitation during months where the region remains below freezing (Oct-April). However, high sublimation rates of 2-7 cm/mo in arid mountain ranges would ensure that average snow cover remained low (Hood et al., 1999; Schulz and de Jong, 2004). We do not expect drastic increases in snowpack during glacial intervals, as significant advances and growth of major glaciers have not been observed in the Tibetan Plateau during the last glacial maximum (Lehmkuhl et al., 1998), and there being no geomorphic evidence for significant ice cover in the Kumkuli Basin. We use 24 cm of average yearly snow cover, which represents two months of precipitation assuming a snow density of 0.1 g/cm^3. This density is typical for freshly fallen snow in comparably arid regions of the central Rockies (Judson and Doesken, 2000). This thickness and density of mean annual snow pack then yields a snow shielding factor 0.985 using CosmoCalc (Vermeesch, 2007).

Table 3-1 – Major and trace element data for cosmogenic calculations

Element	Units	12CC02	12CC03	12CC04	12CC05	12CC06	12CC07
SiO2	%	11.94	10.98	10.88	11.59	11.5	10.21
Al2O3	%	1.51	1.33	1.35	1.55	1.16	0.86
Fe2O3(t)	%	0.87	0.81	0.77	0.81	0.76	0.63
MnO	%	0.025	0.024	0.022	0.024	0.023	0.02
MgO	%	11.63	11.96	13.12	12.81	11.75	13.92
CaO	%	34.1	34.65	33.08	33.14	34.54	32.97
Na2O	%	0.11	0.13	0.13	0.18	0.12	0.08
K2O	%	0.22	0.21	0.22	0.25	0.16	0.14
TiO2	%	0.08	0.08	0.08	0.09	0.07	0.05
P2O5	%	0.02	0.02	0.03	0.03	0.03	0.02
Cr2O3	%	0.01	0.01	0.01	0.01	0.01	0.02
V2O5	%	0.004	0.004	0.006	< 0.003	0.004	0.003
LOI	%	39.45	39.99	40.17	39.72	39.75	40.91
Total	%	99.96	100.2	99.87	100.2	99.88	99.84
Li	ppm	3.8	3.6	3.8	4.2	4	3
B	ppm	4	5	6	5	5	4

Bi	ppm	0.04	0.04	0.03	0.03	0.03	0.02
Sc	ppm	1.1	1	0.9	1	0.9	0.7
V	ppm	10	9	9	11	11	9
Cr	ppm	6.6	6	5.2	6.1	5.4	5.4
Mn	ppm	200	186	159	175	186	143
Co	ppm	1.9	1.7	1.5	1.7	1.6	1.3
Ni	ppm	8.9	8.7	7.9	9.3	8.9	7.9
Cu	ppm	15.9	26.5	12.4	11.7	10.1	11.5
Zn	ppm	13.1	21.2	11.4	12.9	16.3	9.8
Ga	ppm	0.43	0.53	0.57	0.64	0.47	0.43
As	ppm	2.7	2.6	2.3	2.3	3	1.8
Rb	ppm	3.2	3.3	3.2	3.4	3.1	2.4
Sr	ppm	177	178	165	175	217	178
Y	ppm	3.81	3.26	3.14	3.3	3.6	2.77
Zr	ppm	1.3	1.4	1.2	1.8	1.4	1.1
Mo	ppm	0.77	0.74	0.61	0.64	0.64	0.56
Ag	ppm	0.059	0.058	0.049	0.041	0.057	0.039
Cd	ppm	0.13	0.09	0.08	0.08	0.09	0.09
Sn	ppm	0.17	0.23	0.14	0.2	0.19	0.13
Sb	ppm	0.2	0.16	0.16	0.16	0.16	0.14
Cs	ppm	0.53	0.54	0.56	0.61	0.39	0.3
Ba	ppm	106	62.5	54.8	60.3	70.3	47.4
La	ppm	3.7	3.2	3.1	3.1	2.9	2.4
Ce	ppm	6.37	5.66	5.63	5.77	5.26	4.27
Pr	ppm	0.9	0.8	0.7	0.8	0.8	0.6
Nd	ppm	3.48	3.09	3.03	3.15	3.14	2.4
Sm	ppm	0.8	0.7	0.7	0.8	0.7	0.6
Eu	ppm	0.2	0.2	0.2	0.2	0.2	0.1
Gd	ppm	0.8	0.7	0.7	0.7	0.8	0.6
Dy	ppm	0.7	0.6	0.6	0.6	0.7	0.5
Er	ppm	0.4	0.3	0.3	0.3	0.3	0.2
Yb	ppm	0.3	0.2	0.2	0.2	0.2	0.2
Pb	ppm	4.52	3.81	2.97	3.55	4.45	2.73
Th	ppm	1.2	0.9	0.9	0.9	0.7	0.6
U	ppm	0.8	0.8	0.8	0.8	0.8	0.8

Table 3-2 – ^{36}Cl Cosmogenic Radionuclide Data

Sample	Depth (cm)	Density (g/cm^3)	Sample Weight (g)	Added Carrier (mg)	^{36}Cl/Cl (x 10^{-15})	^{36}Cl/Cl 1σ uncertainty (x 10^{-15})	^{35}Cl/^{37}Cl	^{35}Cl/^{37}Cl 1σ uncertainty
12CC02	150		23.012	1.0125	2190	40	5.44	0.101
12CC03	120		25.8559	1.0328	2360	60	5.15	0.015
12CC04	90		31.6669	1.0207	2650	130	4.12	0.010
12CC05	60		27.4571	1.014	4160	70	4.33	0.008
12CC06	30	1.6	21.6889	1.015	4140	110	4.11	0.011
12CC07	10	1.6	24.9557	1.0252	8800	180	4.84	0.022
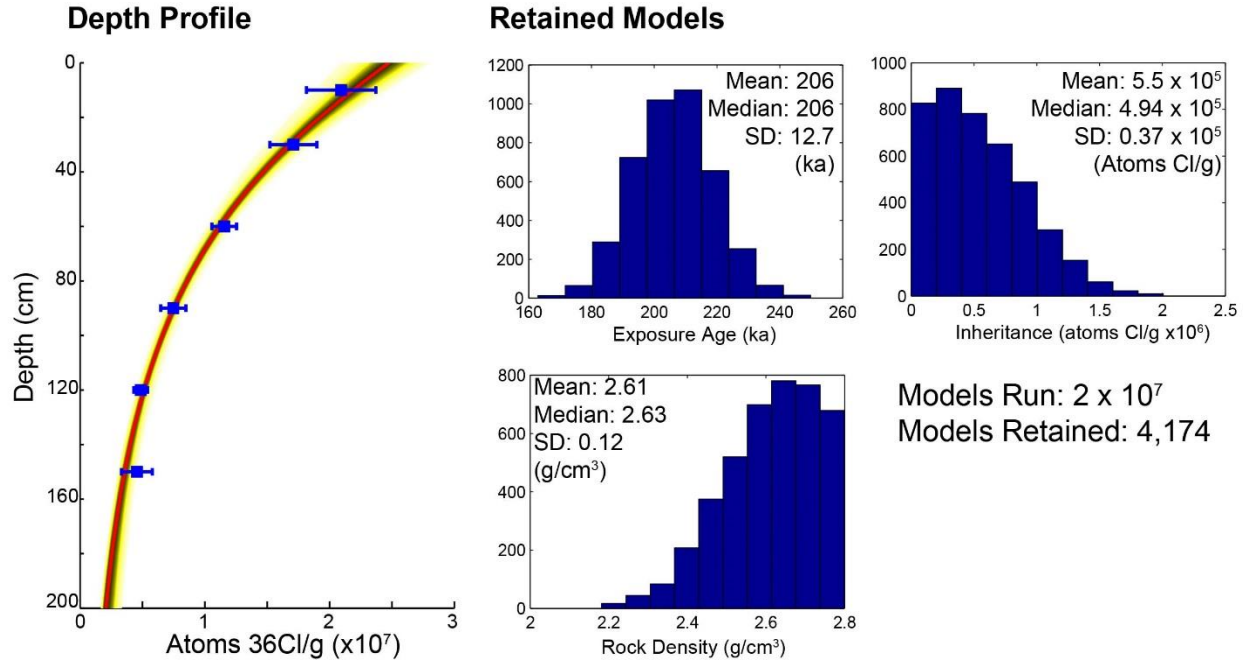
Figure 3.7 – [36]Cl cosmogenic radionuclide depth profile and retained models with individual statistics for each parameter. Red line in depth profile represents best fit model, yellow colors represent models with likelihoods between the lowest likelihood model and the highest likelihood model, and black colors show models between the midpoint and the highest likelihood model.

Modeling results yield a mean age of 206 ± 26 ka (2σ uncertainty) for the alluvial surface. The estimated density of sampled material is 2.61 ± 0.24 g/cm^{3} with an inherited [36]Cl concentration of 5.5 ± 0.7 x 10^{5} atoms [36]Cl/g (**Figure 3.7**). Model runs performed using a snow shielding factor of 1, representing negligible annual snow pack, produce a 10 ka or ~5 % decrease in the mean exposure age of the sampled surface. This decrease in mean exposure age is within the uncertainties of our model, suggesting that our estimated exposure age is robust under a variety of paleo-precipitation conditions.

3.6.3 Quaternary Uplift and Shortening Rates

Quaternary uplift and shortening rates can be estimated from the 206 ± 26 ka age of the fan surface, total uplift since its deposition, and our balanced cross section. As the surface has experienced 695 ± 25 m of uplift, this translates into a vertical uplift rate of 3.4 ± 0.4 mm/yr. We can combine this uplift rate with our structural cross section to estimate the amount of Quaternary shortening as 350 ± 84 m, subject to the limitations on our certainty on stratigraphic thicknesses, and yield a Quaternary north-south shortening rate of 1.7 ± 0.5 mm/yr. Given ~9 km of total north-south shortening, these rates yield an initiation age for deformation of ~5 Ma. These results are consistent with structural and stratigraphic constraints, which suggest an initiation age of 5.3-2.6 Ma and a

shortening rate of 2.3 ± 0.9 mm/yr. Overall shortening rates may be higher than our north-south estimate, as we do not consider out of plane shortening evidenced by small scale north-south trending folds in the western half of the map area.

3.7 Discussion

We explore possible causes of thrust faulting in the Guaizi Liang, and the consequences of deformation to the gravitational potential energy in the region. We first assess a Plio-Quaternary compressive stress direction for the study area by integrating observed orientations of folding and faulting in the Guaizi Liang. We then discuss possible geometries of the Kunlun fault, its relationship with the Manyi Fault, and how slip transfer between the Manyi/Kunlun fault system and the Altyn Tagh may relate to contraction in the Guaizi Liang. The resulting kinematic interpretation of deformation southwest of the Qaidam Basin has implications for local crustal thickening and changes in gravitational potential energy.

3.7.1 Stress orientation inferred from Plio-Quaternary Shortening in the Guaizi Liang

We use the structural styles and trends of the Guaizi Liang to estimate the principle strain axes by which we infer a maximum compressive stress direction for deformation within the map area. In the eastern portion of our map area, axes of isoclinal folds in the Salt River transect trend towards the ~115°, and beds have strikes of 110° ± 5°. We assume that the observed fold axis trends and limb bedding orientations represent a principle strain axis, which is perpendicular to the maximum compressive stress direction oriented at 020° ± 5°. Deformation in this part of the map area is likely localized above Miocene evaporite deposits of the Shibiliang Formation, which locally act as a décollement, and generate structures oriented perpendicular to the maximum compressive stress direction. These evaporite units are absent in the western portion of the map area, where deformation is accommodated by km-scale east-west trending folds, and m-scale north-south trending folds. An absence of both crosscutting relationships and major north-south trending structures suggests that these orthogonal structural trends formed coevally and represent a single principal strain axis orientation. From the relative scales of folding observed for both fold trends, we estimate a principal strain axis oriented west-northwest. We assume that this principal strain axis direction is perpendicular to a maximum compressive stress directed north-northeast, which is consistent with the 020° ± 5° orientation of the maximum compressive stress inferred in the Salt River transect.

We suggest that the major east-west trending faults in the western portion of the map area were inherited from an earlier phase of deformation observed immediately to the west of our study

area (Aylik Tagh) where fault trends are east-west. Thus we interpret that the subsurface structures beneath the Guaizi Liang were reactivated during Plio-Quaternary time, by a maximum compressive stress oriented $020° \pm 5°$ resulting in strain partitioning between fault slip on pre-existing faults and orthogonal m-scale folding. The presence of older, reactivated structures is supported by a magnetotelluric transect of the Kumkuli Basin, which shows basement faults offsetting Oligo-Pliocene strata (He et al., 2009).

The proximity of the Guaizi Liang to the Altyn Tagh, Kunlun and Manyi faults suggests that the north-northeast directed contraction observed in the Guaizi Liang may be related to these major structures. As such, we propose a geometric relationship between the Altyn Tagh, Kunlun and Manyi faults on which our interpretation of the Guaizi Liang rests. We follow Taylor and Yin (2009), who suggest that the Kunlun fault connects to the Manyi fault via a series of fault relays. This interpretation is supported by a southwesterly turn in the Kunlun fault south of Bukadaban Feng that ruptured during the 2001 M_w 7.8 Kokoxili earthquake (Lasserre et al., 2005; Klinger et al., 2005). Smaller magnitude earthquakes in the USGS and NEIC databases also outline a link with the Manyi Fault, which experienced two large (M_w >7) earthquakes in the last forty years (Molnar and Tapponnier, 1978; Peltzer, 1999; Figure 1). However, observation of a thoroughgoing historic rupture that directly links the Kunlun and Manyi fault systems is lacking. (**Figure 3.1**). Despite a lack of direct linkage, we propose that minor seismicity and fault trends between the Kunlun fault and the Manyi fault suggest that they act as a single, integrated system, which we refer to as the Kunlun/Manyi fault system. This fault system has been previously suggested as one of several western continuations or terminations of the Kunlun fault (Tapponnier et al., 1982; Jolivet et al., 2003; Lasserre et al., 2005; Taylor and Yin, 2009).

3.7.2 Comparison to regional fault slip rates and gravitational potential energy

Contraction in the Guaizi Liang has two possible origins. First, thrust faults could accommodate simple shear in the intervening region between the Altyn Tagh and Kunlun/Manyi fault. Alternatively, thrust faults could be related to compression and crustal thickening on structures oriented favorably with ~020° directed Indo-Asian convergence. The interpretation that contraction in the Guazi Liang is driven by slip transfer between the Altyn Tagh and Kunlun/Manyi faults predicts that deformation is dominated by simple shear, while crustal thickening would be supported by the dominance of pure shear. Only in the case of the latter would we expect gravitational potential energy to increase due to the observed thrust faulting.

The Guaizi Liang is located west of the southwesterly turn of the Kunlun fault at Bukadaban Feng, north of the Manyi Fault and south of the Altyn Tagh fault (**Figure 3.1**). If the Kunlun/Manyi fault system and the Altyn Tagh fault act to form a broad area of simple shear that encompasses the Kumkuli Basin and the Guaizi Liang, we would anticipate that the orientation of principal strain axes for the Guaizi Liang would lie at 45° to the strike of the Altyn Tagh and Kunlun/Manyi faults. Based on the ~066° strike of the Altyn Tagh and Manyi faults, we predict that the principal strain axes in the Guaizi Liang would be oriented towards ~110°, which is compatible with the estimated direction of the principal strain axis (110° ± 5°) calculated from the orientation of contractional structures in our map area (**Figure 3.4**, **Figure 3.8**). This interpretation would also require that simple shear is accommodated by extension. Extension must be distributed elsewhere in the region of shear, as no specific extensional structures have been identified in our study area. In addition, if the inference of regional simple shear related to simultaneous motion of the Altyn Tagh and Kunlun/Manyi faults is correct, then the initiation of contraction in the Kumkuli Basin during Pliocene time may provide a minimum age for the Manyi fault segment.

Orogen-scale strain rates and fault slip estimates of major structures can also be used to evaluate our hypothesis that contraction in the Guaizi Liang may be due primarily to simple shear between the Kunlun/Manyi and Altyn Tagh faults. We assess the amount of north-south shortening that can account for deformation seen in the Guaizi Liang by calculating the amount of north-south shortening that can be accommodated by slip on the Altyn Tagh, and Kunlun/Manyi faults, and comparing this value to the estimated bulk strain rates for the area (**Figure 3.8**). Slip rates on the Altyn Tagh at ~87°E, ~100 km northwest of the Guaizi Liang, are estimated as ~9.4 mm/yr (Cowgill, 2007), and can account for ~4 mm/yr of north-south shortening given the fault trend of ~66°. Slip along the Manyi fault is less well constrained, but is likely zero near its westerly termination at ~86°E longitude. Available slip rates for the Kunlun fault at ~94°E longitude are ~12 mm/yr (Van der Woerd et al., 2000; Duvall and Clark, 2010). We estimate slip rates along the Kunlun/Manyi fault system by assuming that slip linearly decreases along the ~650 km fault parallel distance between measured slip rates on the Kunlun fault and the termination of the Manyi fault. This yields a slip rate of ~4 mm/yr and ~2mm/yr of north-south shortening near the Kumkuli Basin, which is located ~200 km east along fault strike, and 200 km north of the termination of the Manyi Fault. We thus estimate that slip on the Kunlun/Manyi, and Altyn Tagh faults can jointly accommodate ~6 mm/yr of north-south shortening, or more, if our estimate for slip on the Manyi fault is too low. This shortening rate may be compared to the expected north-south shear strain due to Indo-Asian convergence. The long term

bulk strain rate across the Indo-Asian orogen has been determined to be 7 x 10^{-16} s^{-1} (Clark, 2012). When applied to the ~270 km north-south width of the region between the Altyn Tagh and Manyi faults, this strain rate results in a north – south shortening rate of ~6 mm/yr. This shortening rate is compatible with the north-south shortening strain accommodated by slip on the Kunlun/Manyi and Altyn Tagh faults. As such, minimum deformation between the Kunlun/Manyi and Altyn Tagh faults is permitted unless strain is more highly concentrated in our study region compared to average, or if the slip rates on the Altyn Tagh and Kunlun/Manyi faults are dramatically higher than reported here.

Alternatively, the inferred primary stress direction in the Guazi Liang, which is parallel to the ~20° orientation of Indo-Asian convergence, may be accommodating crustal thickening by pure shear. We observe 20 % local crustal shortening in the Guaizi Liang, but other zones of equally young deformation southwest of the Qaidam Basin are not recognized in neither Chinese geologic maps nor on satellite imagery. If the Guaizi Liang is the only region across the ~250 km north-south distance between the Altyn Tagh and Kunlun/Manyi faults that accommodates pure shear, then the bulk strain in the region may be as low as ~3 % (**Figure 3.8**). If pure shear dominates, then the low percent strain suggests that the contribution of surface faulting in the Guaizi Liang to crustal thickening between the Altyn Tagh and Kunlun/Manyi faults is low.

If contraction between the Altyn Tagh and Kunlun/Manyi faults occurs by simple shear, we do not expect changes in regional crustal thickening and topographic growth. Therefore, the observed thrust faulting in the Guaizi Liang is unlikely to have led to changes in the gravitational potential energy of the crust. The idea that thick crust and high elevation topography inhibits thrust faulting may not apply to the Guaizi Liang because simple shear can explain the unexpected observation of thrust faulting at 5000 m elevation. However, a lack of crustal thickening generated by post-Pliocene thrust faulting in the Guaizi Liang would suggest that modern elevations of ~5000 m were attained by mechanisms other than crustal shortening, and/or at an older period of geologic time. An Eocene to early Miocene phase of deformation and crustal shortening (Yin et al., 2007; Wu et al., 2008; Li et al., 2013; Staisch et al., 2014), may have been obscured by infilling of the Kumkuli Basin in Oligocene through Pliocene time. Topographic gain by injection of lower crustal material from the high plateau (Clark and Royden, 2000), or removal of a lithospheric root (Molnar et al., 1993) may have also contributed to crustal thickening and elevation gain.
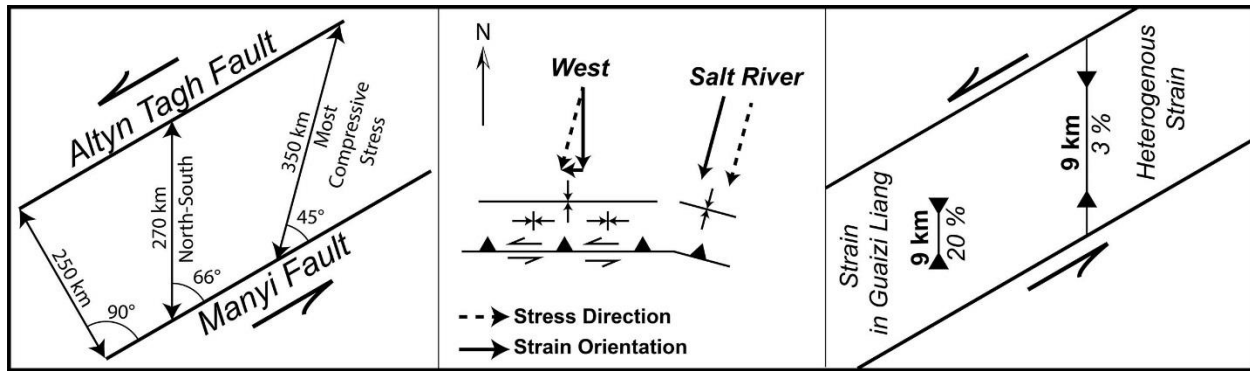
Figure 3.8 – Diagrams of interpreted regional deformation kinematics (Left) – Widths of shear zone discussed in text, and orientation of Indo-Asian convergence with respect to shear zone. (Center) Interpreted orientations of maximum compressive stress direction, and associated principal strain axes in the Guaizi Liang. (Right) Calculation of strain across the shear zone for a case of heterogeneous shear. Shorter line represents values assessed for the Guaizi Liang, longer line shows interpreted shortening across the entire width of the shear zone.

3.8 Conclusions

Geologic mapping, balanced cross-sections and geomorphic constraints on Quaternary folding allow us to constrain the deformation history of the Guaizi Liang since Pliocene time. The Guaizi Liang has experienced ~9 km or ~20 % shortening, with ~350 m of shortening accommodated on a Quaternary fault-bend fold. Alluvial surfaces at the peak of this fold were deposited at 206 ± 26 ka and have been uplifted by ~700 m, yielding a vertical surface uplift rate of ~3.4 mm/yr and a shortening rate of ~1.7 mm/yr. Combined with the total shortening estimate from our cross section, this shortening rate suggests that deformation likely initiated in Pliocene time, as supported by a transition from fluvial and lacustrine strata to conglomeratic strata at the top of the Pliocene Hongliang Formation (Xiao et al., 2005). Shortening in the Guaizi Liang is likely the result of the interaction of the Kunlun/Manyi (~200 km to the southeast) and Altyn Tagh (~80 km north) faults, which act as a broad regional of shear. Using bulk orogenic strain rates, slip rates on the Kunlun/Manyi and Altyn Tagh faults, observed fault orientations and the estimated magnitude of shortening, we posit that deformation in the Guaizi Liang occurs primarily by simple shear. Further, the initiation of shortening in the Kumkuli Basin and the formation of the Guaizi Liang at ~5 Ma may reflect the initiation of the Manyi Fault, and the formation of this region of shear in Pliocene time. We conclude that high-elevation thrust faulting is compatible with simple shear because it is not expected to cause crustal shortening or changes in gravitational potential energy. The exclusion of regional crustal thickening in the Guaizi Liang since Pliocene time suggests that the modern elevation of ~5000 m must be the consequence of deformation events that pre-date the deformed Oligo-Pliocene sequences,

or be the result of events that do not leave a record of upper crustal deformation, such as the removal of a dense lithospheric root (Molnar et al., 1993), and/or potentially crustal thickening due to influx of material into the lower crust (Clark and Royden, 2000).

3.9 References

Allmendinger, R.W., Cardozo, N., and Fisher, D.M., 2011, Structural Geology Algorithms: Vectors and Tensors: Cambridge University Press.

Armijo, R., Tapponnier, P., Mercier, J.-L.L., Han, T.-L., and Tong-Lin, H., 1986, Quaternary extension in southern Tibet: Field observations and tectonic implications: Journal of Geophysical Research, v. 91, p. 13803, doi: 10.1029/JB091iB14p13803.

Benson, L., Madole, R., Phillips, W., Landis, G., Thomas, T., and Kubik, P., 2004, The probable importance of snow and sediment shielding on cosmogenic ages of north-central Colorado Pinedale and pre-Pinedale moraines: Quaternary Science Reviews, v. 23, p. 193–206, doi: 10.1016/j.quascirev.2003.07.002.

Bernardin, T., Cowgill, E., Gold, R., Hamann, B., Kreylos, O., and Schmitt, A., 2006, Interactive mapping on 3-D terrain models: Geochemistry Geophysics Geosystems, v. 7, p. 1–12, doi: 10.1029/2006GC001335.

Blisniuk, P.M., Hacker, B.R., Glodny, J., Ratschbacher, L., Bi, S., Wu, Z., McWilliams, M.O., and Calvert, A., 2001, Normal faulting in central Tibet since at least 13.5 Myr ago.: Nature, v. 412, p. 628–32, doi: 10.1038/35088045.

Cheng, F., Jolivet, M., Fu, S., Zhang, Q., Guan, S., Yu, X., and Guo, Z., 2014, Northward growth of the Qimen Tagh Range: A new model accounting for the Late Neogene strike-slip deformation of the SW Qaidam Basin: Tectonophysics, v. 632, p. 32–47, doi: 10.1016/j.tecto.2014.05.034.

Clark, M.K., 2012, Continental collision slowing due to viscous mantle lithosphere rather than topography: Nature, v. 483, p. 74–77, doi: 10.1038/nature10848.

Clark, M.K., and Royden, L.H., 2000, Topographic ooze: Building the eastern margin of Tibet by lower crustal flow: Geology, v. 28, p. 703, doi: 10.1130/0091-7613(2000)28<703:TOBTEM>2.0.CO;2.

Cowgill, E., 2007, Impact of riser reconstructions on estimation of secular variation in rates of strike–slip faulting: Revisiting the Cherchen River site along the Altyn Tagh Fault, NW China: Earth and Planetary Science Letters, v. 254, p. 239–255, doi: 10.1016/j.epsl.2006.09.015.

Cowgill, E., Yin, A., Harrison, T.M., and Xiao-Feng, W., 2003, Reconstruction of the Altyn Tagh fault based on U-Pb geochronology: Role of back thrusts, mantle sutures, and heterogeneous crustal strength in forming the Tibetan Plateau: Journal of Geophysical Research, v. 108, doi: 10.1029/2002JB002080.

Desilets, D., and Zreda, M., 2003, Spatial and temporal distribution of secondary cosmic-ray nucleon intensities and applications to in situ cosmogenic dating: Earth and Planetary Science Letters, v. 206, p. 21–42, doi: 10.1016/S0012-821X(02)01088-9.

Desilets, D., Zreda, M., Almasi, P.F., and Elmore, D., 2006, Determination of cosmogenic 36Cl in rocks by isotope dilution: innovations, validation and error propagation: Chemical Geology, v. 233, p. 185–195, doi: 10.1016/j.chemgeo.2006.03.001.

Duvall, A.R., and Clark, M.K., 2010, Dissipation of fast strike-slip faulting within and beyond northeastern Tibet: Geology, v. 38, p. 223–226, doi: 10.1130/G30711.1.

Duvall, A.R., Clark, M.K., Kirby, E., Farley, K. a., Craddock, W.H., Li, C., and Yuan, D.-Y., 2013, Low-temperature thermochronometry along the Kunlun and Haiyuan Faults, NE Tibetan Plateau: Evidence for kinematic change during late-stage orogenesis: Tectonics, v. 32, p. 1190–1211, doi: 10.1002/tect.20072.

Genxu, W., Shengnan, L., Hongchang, H., and Yuanshou, L., 2009, Water regime shifts in the active soil layer of the Qinghai–Tibet Plateau permafrost region, under different levels of vegetation: Geoderma, v. 149, p. 280–289, doi: 10.1016/j.geoderma.2008.12.008.

Harrison, T.M., Copeland, P., Kidd, W.S.F., and Lovera, O.M., 1995, Activation of the Nyainqentanghla Shear Zone: Implications for uplift of the southern Tibetan Plateau: Tectonics, v. 14, p. 658–676, doi: 10.1029/95TC00608.

Harrison, T.M., Copeland, P., Kidd, W.S., and Yin, A., 1992, Raising tibet.: Science (New York, N.Y.), v. 255, p. 1663–70, doi: 10.1126/science.255.5052.1663.

He, B., Xu, Z., Jiao, C., Cui, J., Wang, S., Wang, G., Li, Z., and Qiu, Z., 2009, Structural architecture and evolution of Kumkuli basin, north Tibet: Journal of Earth Science, v. 20, p. 464–476, doi: 10.1007/s12583-009-0038-8.

Hood, E., Williams, M., and Cline, D., 1999, Sublimation from a seasonal snowpack at a continental, mid-latitude alpine site: Hydrological Processes, v. 13, p. 1781–1797, doi: 10.1002/(SICI)1099-1085(199909)13:12/13<1781::AID-HYP860>3.0.CO;2-C.

Jolivet, M., Brunel, M., Seward, D., Xu, Z., Yang, J., Malavieille, J., Roger, F., Leyreloup, A., Arnaud, N., and Wu, C., 2003, Neogene extension and volcanism in the Kunlun Fault Zone, northern Tibet: New constraints on the age of the Kunlun Fault: Tectonics, v. 22, doi: 10.1029/2002TC001428.

Judge, P.A., and Allmendinger, R.W., 2011, Assessing uncertainties in balanced cross sections: Journal of Structural Geology, v. 33, p. 458–467, doi: 10.1016/j.jsg.2011.01.006.

Judson, A., and Doesken, N., 2000, Density of Freshly Fallen Snow in the Central Rocky Mountains: Bulletin of the American Meteorological Society, v. 81, p. 1577–1587, doi: 10.1175/1520-0477(2000)081<1577:DOFFSI>2.3.CO;2.

Jungers, M.C., Heimsath, A.M., Amundson, R., Balco, G., Shuster, D., and Chong, G., 2013, Active erosion–deposition cycles in the hyperarid Atacama Desert of Northern Chile: Earth and Planetary Science Letters, v. 371-372, p. 125–133, doi: 10.1016/j.epsl.2013.04.005.

Kalnay, E., Kanamitsu, M., Kistler, R., Collins, W., Deaven, D., Gandin, L., Iredell, M., Saha, S., White, G., Woollen, J., Zhu, Y., Leetmaa, A., Reynolds, R., Chelliah, M., et al., 1996, The NCEP/NCAR 40-Year Reanalysis Project: Bulletin of the American Meteorological Society, v. 77, p. 437–471, doi: 10.1175/1520-0477(1996)077<0437:TNYRP>2.0.CO;2.

Kapp, P.A., and Guynn, J.H., 2004, Indian punch rifts Tibet: Geology, v. 32, p. 993, doi: 10.1130/G20689.1.

Klinger, Y., Xu, X., Tapponnier, P., van der Woerd, J., Lasserre, C., and King, G., 2005, High-Resolution Satellite Imagery Mapping of the Surface Rupture and Slip Distribution of the Mw 7.8, 14 November 2001 Kokoxili Earthquake, Kunlun Fault, Northern Tibet, China: Bulletin of the Seismological Society of America, v. 95, p. 1970–1987, doi: 10.1785/0120040233.

Lal, D., Harris, N.B.., Sharma, K.K., Gu, Z., Ding, L., Liu, T., Dong, W., Caffee, M.W., and Jull, A.J.., 2004, Erosion history of the Tibetan Plateau since the last interglacial: constraints from the first studies of cosmogenic 10Be from Tibetan bedrock: Earth and Planetary Science Letters, v. 217, p. 33–42, doi: 10.1016/S0012-821X(03)00600-9.

Lasserre, C., Peltzer, G., Crampé, F., Klinger, Y., van der Woerd, J., and Tapponnier, P., 2005, Coseismic deformation of the 2001 M w = 7.8 Kokoxili earthquake in Tibet, measured by synthetic aperture radar interferometry: Journal of Geophysical Research, v. 110, doi: 10.1029/2004JB003500.

Lehmkuhl, F., Owen, L.A., and Derbyshire, E., 1998, Late Quaternary Glacial History of Northeast Tibet: Quaternary Proceedings, v. 6, p. 121–142.

Li, D., Li, X., Wang, X., Zhou, X., Dai, X., Gao, X., Wang, Y., Wang, X., Du, S., Cui, J., Zhang, B., and Chang, H., 2002, Geologic map of the Ayakakum Kul Basin (at 1:250,000 scale):.

Li, Y.L., Zhu, L.D., Dai, J.G., Wang, L.C., Yang, W.G., and Wei, Y.S., 2013, Sedimentation and deformation of the Yanghu basin and its tectonic implications in the western Hoh Xil, Central Tibet: Acta Petrologica Sinica, v. 29, p. 1017–1026.

Liu, Y., Neubauer, F., Genser, J., Ge, X., Takasu, A., Yuan, S., Chang, L., and Li, W., 2007, Geochronology of the initiation and displacement of the Altyn Strike-Slip Fault, western China: Journal of Asian Earth Sciences, v. 29, p. 243–252, doi: 10.1016/j.jseaes.2006.03.002.

Lu, H., Wang, E., and Meng, K., 2014, Paleomagnetism and anisotropy of magnetic susceptibility of the Tertiary Janggalsay section (southeast Tarim basin): Implications for Miocene tectonic evolution of the Altyn Tagh Range: Tectonophysics, doi: 10.1016/j.tecto.2014.01.031.

Meng, Q., and Fang, X., 2008, Cenozoic tectonic development of the Qaidam Basin in the northeastern Tibetan Plateau: Geological Society of America Special Papers, v. 444, p. 1–24, doi: 10.1130/2008.2444(01).

Mercier, J.-L., Armijo, R., Tapponnier, P., Carey-Gailhardis, E., and Lin, H.T., 1987, Change from Late Tertiary compression to Quaternary extension in southern Tibet during the India-Asia Collision: Tectonics, v. 6, p. 275, doi: 10.1029/TC006i003p00275.

Molnar, P., Boos, W.R., and Battisti, D.S., 2010, Orographic Controls on Climate and Paleoclimate of Asia: Thermal and Mechanical Roles for the Tibetan Plateau: Annual Review of Earth and Planetary Sciences, v. 38, p. 77–102, doi: 10.1146/annurev-earth-040809-152456.

Molnar, P., England, P., and Martinod, J., 1993, Mantle dynamics, uplift of the Tibetan Plateau, and the Indian Monsoon: Reviews of Geophysics, v. 31, p. 357–396, doi: 10.1029/93RG02030.

Molnar, P., and Tapponnier, P., 1978, Active tectonics of Tibet: Journal of Geophysical Research, v. 83, p. 5361, doi: 10.1029/JB083iB11p05361.

Murphy, M.A., Yin, A., Kapp, P.A., Harrison, T.M., Lin, D., and Jinghui, G., 2000, Southward propagation of the Karakoram fault system, southwest Tibet: Timing and magnitude of slip: Geology, v. 28, p. 451, doi: 10.1130/0091-7613(2000)28<451:SPOTKF>2.0.CO;2.

Peltzer, G., 1999, Evidence of Nonlinear Elasticity of the Crust from the Mw7.6 Manyi (Tibet) Earthquake: Science, v. 286, p. 272–276, doi: 10.1126/science.286.5438.272.

Phillips, R.J., Parrish, R.R., and Searle, M.P., 2004, Age constraints on ductile deformation and long-term slip rates along the Karakoram fault zone, Ladakh: Earth and Planetary Science Letters, v. 226, p. 305–319, doi: 10.1016/j.epsl.2004.07.037.

Ritts, B.D., Yue, Y., Graham, S. a., Sobel, E.R., Abbink, A.O., and Stockli, D.F., 2008, From sea level to high elevation in 15 million years: Uplift history of the northern Tibetan Plateau margin in the Altun Shan: American Journal of Science, v. 308, p. 657–678, doi: 10.2475/05.2008.01.

Schildgen, T.F., Phillips, W.M., and Purves, R.S., 2005, Simulation of snow shielding corrections for cosmogenic nuclide surface exposure studies: Geomorphology, v. 64, p. 67–85, doi: 10.1016/j.geomorph.2004.05.003.

Schimmelpfennig, I., Benedetti, L., Finkel, R.C., Pik, R., Blard, P.-H., Bourlès, D., Burnard, P., and Williams, A., 2009, Sources of in-situ 36Cl in basaltic rocks. Implications for calibration of production rates: Quaternary Geochronology, v. 4, p. 441–461, doi: 10.1016/j.quageo.2009.06.003.

Schneider, U., Becker, A., Finger, P., Meyer-Christoffer, A., Rudolf, B., and Ziese, M., 2011, GPCC Full Data Reanalysis Version 6.0 at 0.5°: Monthly Land-Surface Precipitation from Rain-Gauges built on GTS-based and Historic Data: , doi: 10.5676/DWD_GPCC/FD_M_V6_050.

Schulz, O., and de Jong, C., 2004, Snowmelt and sublimation: field experiments and modelling in the High Atlas Mountains of Morocco: Hydrology and Earth System Sciences, v. 8, p. 1076–1089.

Staisch, L.M., Niemi, N.A., Hong, C., Clark, M.K., Rowley, D.B., and Currie, B., 2014, A Cretaceous-Eocene depositional age for the Fenghuoshan Group, Hoh Xil Basin: Implications for the

tectonic evolution of the northern Tibet Plateau: Tectonics, v. 33, p. 281–301, doi: 10.1002/2013TC003367.

Strobl, M., Hetzel, R., Niedermann, S., Ding, L., and Zhang, L., 2012, Landscape evolution of a bedrock peneplain on the southern Tibetan Plateau revealed by in situ-produced cosmogenic 10Be and 21Ne: Geomorphology, v. 153-154, p. 192–204, doi: 10.1016/j.geomorph.2012.02.024.

Styron, R.H., Taylor, M.H., Sundell, K.E., Stockli, D.F., Oalmann, J. a. G., Möller, A., McCallister, A.T., Liu, D., and Ding, L., 2013, Miocene initiation and acceleration of extension in the South Lunggar rift, western Tibet: Evolution of an active detachment system from structural mapping and (U-Th)/He thermochronology: Tectonics, v. 32, p. n/a–n/a, doi: 10.1002/tect.20053.

Sun, J., Zhu, R., and An, Z., 2005, Tectonic uplift in the northern Tibetan Plateau since 13.7 Ma ago inferred from molasse deposits along the Altyn Tagh Fault: Earth and Planetary Science Letters, v. 235, p. 641–653, doi: 10.1016/j.epsl.2005.04.034.

Tachikawa, T., Hato, M., Kaku, M., and Iwasaki, A., 2011, Characteristics of ASTER GDEM version 2, in 2011 IEEE International Geoscience and Remote Sensing Symposium, IEEE, p. 3657–3660.

Tapponnier, P., Peltzer, G., Le Dain, A.Y., Armijo, R., and Cobbold, P.R., 1982, Propagating extrusion tectonics in Asia: New insights from simple experiments with plasticine: Geology, v. 10, p. 611, doi: 10.1130/0091-7613(1982)10<611:PETIAN>2.0.CO;2.

Taylor, M.H., and Yin, A., 2009, Active structures of the Himalayan-Tibetan orogen and their relationships to earthquake distribution, contemporary strain field, and Cenozoic volcanism: Geosphere, v. 5, p. 199–214, doi: 10.1130/GES00217.1.

Vermeesch, P., 2007, CosmoCalc: An Excel add-in for cosmogenic nuclide calculations: Geochemistry Geophysics Geosystems, v. 8, p. Q08003, doi: 10.1029/2006GC001530.

Wang, X., Wang, B., Qiu, Z., Xie, G., Xie, J., Downs, W., Qiu, Z., and Deng, T., 2003, Danghe area (western Gansu, China) biostratigraphy and implications for depositional history and tectonics of northern Tibetan Plateau: Earth and Planetary Science Letters, v. 208, p. 253–269, doi: 10.1016/S0012-821X(03)00047-5.

Van der Woerd, J., Ryerson, F.J., Tapponnier, P., Gaudemer, Y., Finkel, R.C., Caffee, M., Guoguang, Z., and He, Q., 1998, Holocene left-slip rate determined by cosmogenic surface dating on the Xidatan segment of the Kunlun fault (Qinghai , China): Geology, v. 26, p. 695–698, doi: 10.1130/0091-7613(1998)026<0695:HLSRDB>2.3.CO;2.

Van der Woerd, J., Ryerson, F.J., Tapponnier, P., Meriaux, A., Gaudemer, Y., Meyer, B., Finkel, R.C., Caffee, M.W., Guoguang, Z., and Zhiqin, X., 2000, Uniform sliprate along the Kunlun Fault: Implications for seismic behaviour and large-scale tectonics: Geophysical Research Letters, v. 27, p. 2353, doi: 10.1029/1999GL011292.

Wu, Z., Barosh, P.J., Zhonghai, W., Hu, D., Xun, Z., and Peisheng, Y., 2008, Vast early Miocene lakes of the central Tibetan Plateau: Geological Society of America Bulletin, v. 120, p. 1326, doi: 10.1130/B26043.1.

Xiao, A., Li, D., Li, X., Zhou, X., and Di, S.-X., 2005, Evolution of the Kumkuli Basin in Xinjiang: Geology of Shaanxi, v. 23, p. 59–69.

Xie, C., Zhao, L., Wu, T., and Dong, X., 2012, Changes in the thermal and hydraulic regime within the active layer in the Qinghai-Tibet Plateau: Journal of Mountain Science, v. 9, p. 483–491, doi: 10.1007/s11629-012-2352-3.

Yamaguchi, Y., and Naito, C., 2003, Spectral indices for lithologic discrimination and mapping by using the ASTER SWIR bands: International Journal of Remote Sensing, v. 24, p. 4311–4323, doi: 10.1080/01431160110070320.

Yin, A., 2010, Cenozoic tectonic evolution of Asia: A preliminary synthesis: Tectonophysics, v. 488, p. 293–325, doi: 10.1016/j.tecto.2009.06.002.

Yin, A., Rumelhart, P.E., Butler, R.F., Cowgill, E., Harrison, T.M., Foster, D.A., Ingersoll, R.V., Qing, Z., Xian-Qiang, Z., Xiao-Feng, W., Hanson, A., and Raza, A., 2002, Tectonic history of the Altyn Tagh fault system in northern Tibet inferred from Cenozoic sedimentation: Geological Society of America Bulletin, v. 114, p. 1257–1295, doi: 10.1130/0016-7606(2002)114<1257:THOTAT>2.0.CO;2.

Yin, A., and Taylor, M.H., 2011, Mechanics of V-shaped conjugate strike-slip faults and the corresponding continuum mode of continental deformation: Geological Society of America Bulletin, v. 123, p. 1798–1821, doi: 10.1130/B30159.1.

Yin, A., Zhang, M., McRivette, M.W., and Burgess, W.P., 2007, Cenozoic tectonic evolution of Qaidam basin and its surrounding regions (Part 2): Wedge tectonics in southern Qaidam basin and the Eastern Kunlun Range: Geological Society of America Special Papers, v. 433, p. 369–390, doi: 10.1130/2007.2433(18).

Zhang, Y., Che, Z., and Liu, L., 2001, Cenozoic Sedimentary Sequence in the Kumkal Basin, Xinjiang and New Evidence for the Late Quaternary Uplift of the Qinghai-Tibetan Plateau: The Geological Review, v. 47, p. 218–222.

Zhang, Y., Che, Z., Liu, L., and Luo, J., 1996, Tertiary in the Kumkol Basin, Xinjiang: Regional geology of China, v. 4, p. 311–316.

Zhisheng, a, Kutzbach, J.E., Prell, W.L., and Porter, S.C., 2001, Evolution of Asian monsoons and phased uplift of the Himalaya-Tibetan plateau since Late Miocene times.: Nature, v. 411, p. 62–6, doi: 10.1038/35075035.

Chapter 4: The Geochemistry of Tibetan Lavas: Spatial and Temporal Relationships, Tectonic Links and Geodynamic Implications[3]

4.1 Abstract

The evolution of volcanism in the Tibetan Plateau since Eocene time has been a key component for interpretations of the development of the Indo-Eurasian orogen. Conversely, proposed geodynamic mechanisms of plateau development have been incorporated in interpretations of the geochemical compositions of lavas erupted in the region. We combine the temporal and spatial evolution of volcanic compositions with recorded shifts in fault styles and distributions to create a unified history of the lithospheric evolution of the Indo-Asian orogen, and to address proposals for a ~10-15 Ma episode of lithospheric removal. We present a compilation of published geochemical and geochronologic data for lavas from across the orogen, in addition to twenty-seven new analyses from the Hoh Xil Basin of the northern Tibetan Plateau. We characterize compiled data into two compositional end-members, interpret their source compositions, and discuss the tectonic implications of temporal shifts between identified end-members. Proposed sources of volcanic material in the Tibetan Plateau include the asthenosphere, the lower crust, and a metasomatized lithospheric mantle. We term one end-member group A, which has major- and trace- element compositions typical of arc volcanism, and isotopic compositions consistent with melting of the asthenospheric mantle. Group A lavas are dominant prior to 40 Ma in the southern and central Tibetan Plateau, with volcanism at the southern margin of the orogen driven by subduction of the Tethyian oceanic slab. The presence of group A volcanism and coeval plutonism in the central Tibetan Plateau suggests the presence of a second southerly directed slab between ~60 and 40 Ma, possibly as a consequence of the reactivation of a fossilized subduction zone. Volcanism between 40 and 30 Ma is limited to low volume eruptions in the central Tibetan Plateau, consistent with flattening of the Tethyian slab or thinning of the mantle wedge. A 30 Ma flare-up of volcanism across the entirety of the Tibetan Plateau is dominated by an alternative end-member, termed group B. These lavas have Cr

---

and Ni concentrations, as well as Th/La ratios incompatible with melting of the lower crust. Trace element compositions of Group B lavas are compatible with low-degree melting of a metasomatized mantle lithosphere. Sr and Nd isotopic compositions lie on a mixing line with Himalayan sediments, suggesting that metasomatism involved the fluxing of rmelts and/or fluids derived from the subduction of Indian sediments through the overlying mantle. The absence of group B lavas prior to 30 Ma, and the dominance of group A volcanism prior to 40 Ma suggest that metasomatism must have taken place during this 10 Myr window. The coeval initiation of group B volcanism across the plateau at ~30 Ma may have been driven by rollback or detachment of the Tethyian slab and an influx of hot asthenosphere. This long-lived volcanic flare-up is 20 Myr earlier than a lithospheric removal event suggested in earlier studies, and appears to be unrelated to the initiation of normal faulting. Shutoff of volcanism in the southern Tibetan Plateau at ~10 Ma may be attributed to Indian underthrusting, and/or strain localization in the lithospheric mantle beneath the southern and central Tibetan Plateau. Termination of volcanism is concurrent with or postdates the initiation of extensional faulting, suggesting that Indian underthrusting may be a key driver in the late Miocene evolution of the southern Indo-Eurasian orogen.

4.2 Introduction

The Tibetan Plateau is the largest region of high elevation, low relief topography in the world, and has been the subject of prominent mechanisms of orogenic development for nearly a century (see England and McKenzie, 1982; Powell and Conaghan, 1975; Tapponnier et al., 1982). More recent proposals link the evolution of faulting, elevation gain and/or volcanism in the geodynamic development of the plateau (Clark and Royden, 2000; Molnar et al., 1993; Tapponnier et al., 2001). Proposed geodynamic mechanisms have in turn, been cited to explain the geochemical compositions of Cenozoic volcanism across the orogen (Chen et al., 2012; Chung et al., 2005; Holbig and Grove, 2008; Roger et al., 2000; Wang et al., 2012; Xia et al., 2011). However, few studies have attempted to connect the large scale transitions in deformation styles since the ~50 Ma Indian collision, with the spatial, temporal and geochemical evolution of volcanism across the plateau. Moreover, the large number of geochemical datasets published over the last five years, and a new understanding of the tectonic development of the northern Tibetan Plateau prompt a re-evaluation of previous syntheses (Ding et al., 2003; Mo et al., 2006; Staisch et al., 2014; Yuan et al., 2013).

We first broadly describe the tectonic evolution of the Indo-Asian orogen in Cenozoic time, and then summarize proposed mechanisms of melt generation in the region. Prior to Indo-Asian collision, the southern Tibetan Plateau, encompassing the Lhasa and parts of the Qiangtang terranes,

was likely at high elevations and had a thick crust based on paleoaltimetry studies and estimates of Cretaceous to Eocene crustal shortening (DeCelles et al., 2007; Kapp et al., 2007, 2003; Murphy et al., 1997; Quade et al., 2011; Rowley and Currie, 2006). Continental collision of the Indian subcontinent at ~ 50 Ma resulted in the initiation of thrust faults over ~1000 km north of the Indo-Asian plate boundary, reaching as far as the Qilian Shan and the north Qilian Shan, which represent the modern northern boundary of the orogen (Duvall et al., 2011; Li et al., 2012; Staisch et al., 2014; Yin et al., 2008; Zhuang et al., 2011). Deformation in the intervening region occurred during Eocene to Oligocene time and was likely focused in the Hoh Xil Basin, where Cretaceous to Eocene strata experienced 40-60% shortening (Li et al., 2012, 2011; Wang et al., 2002). Flat lying basalts dated to ~27 Ma and undeformed Miocene lacustrine sequences suggest that crustal shortening terminated in the Hoh Xil Basin by Oligocene time, coincident with the initiation of shortening in the Qaidam Basin to the north along the Kunlun Shan (Clark et al., 2010; Y. L. Li et al., 2013; Staisch et al., 2014; Wu et al., 2008; Yin et al., 2007).

Normal faulting in the southern and central Tibetan Plateau began between 15 and 10 Ma and may have marked the cessation of a period of apparent tectonic quiescence or reduced fault activity as well as the beginning of large-scale structural reorganization of the orogen (e.g. Blisniuk et al., 2001; Harrison et al., 1995; Ratschbacher et al., 2011; Styron et al., 2013; Figure 1). North of the Kunlun Suture, this shift is recorded by the initiation of shortening in Cenozoic sedimentary basins (Craddock et al., 2011; W. Li et al., 2013; Zhang et al., 2012), increased exhumation rates (Zheng et al., 2006), and the regional development of strike-slip faulting (e.g. Duvall et al., 2013; Lu et al., 2014; Sun et al., 2005; Yuan et al., 2011). However, how this transition from tectonic quiescence to extension and the Oligocene termination of shortening are linked to the volcanic history of the orogen have not been previously evaluated.

Proposed mechanisms of melt generation in the Tibetan Plateau may be divided into three groups: continental subduction (Arnaud et al., 1992; Ding et al., 2007; Wang et al., 2010; Yang and Ding, 2013), lithospheric removal (Chen et al., 2013; Y. Li et al., 2013; Turner et al., 1996), and asthenospheric upwelling (Guo et al., 2006; Wang et al., 2010; L. Zhang et al., 2014). Mechanisms incorporating continental subduction generally drive melt generation through dehydration of subducting continental crust and/or lithosphere, with the later possibly incorporating hydrous mineral phases during the Mesozoic development of the south Asian margin (Arnaud et al., 1992; Ding et al., 2003). While some geophysical studies propose that continental subduction is active along major sutures within the orogen, others instead argue for discrete changes in lithospheric thickness or flow

of the lower crust and the absence of subduction in identical localities (Agius and Lebedev, 2013; Haines et al., 2003; Karplus et al., 2011; Kind et al., 2002; Le Pape et al., 2012; Nábelek et al., 2009; Shi et al., 2004; Z. Zhang et al., 2014; Zhao et al., 2011; Zhu and Helmberger, 1998).
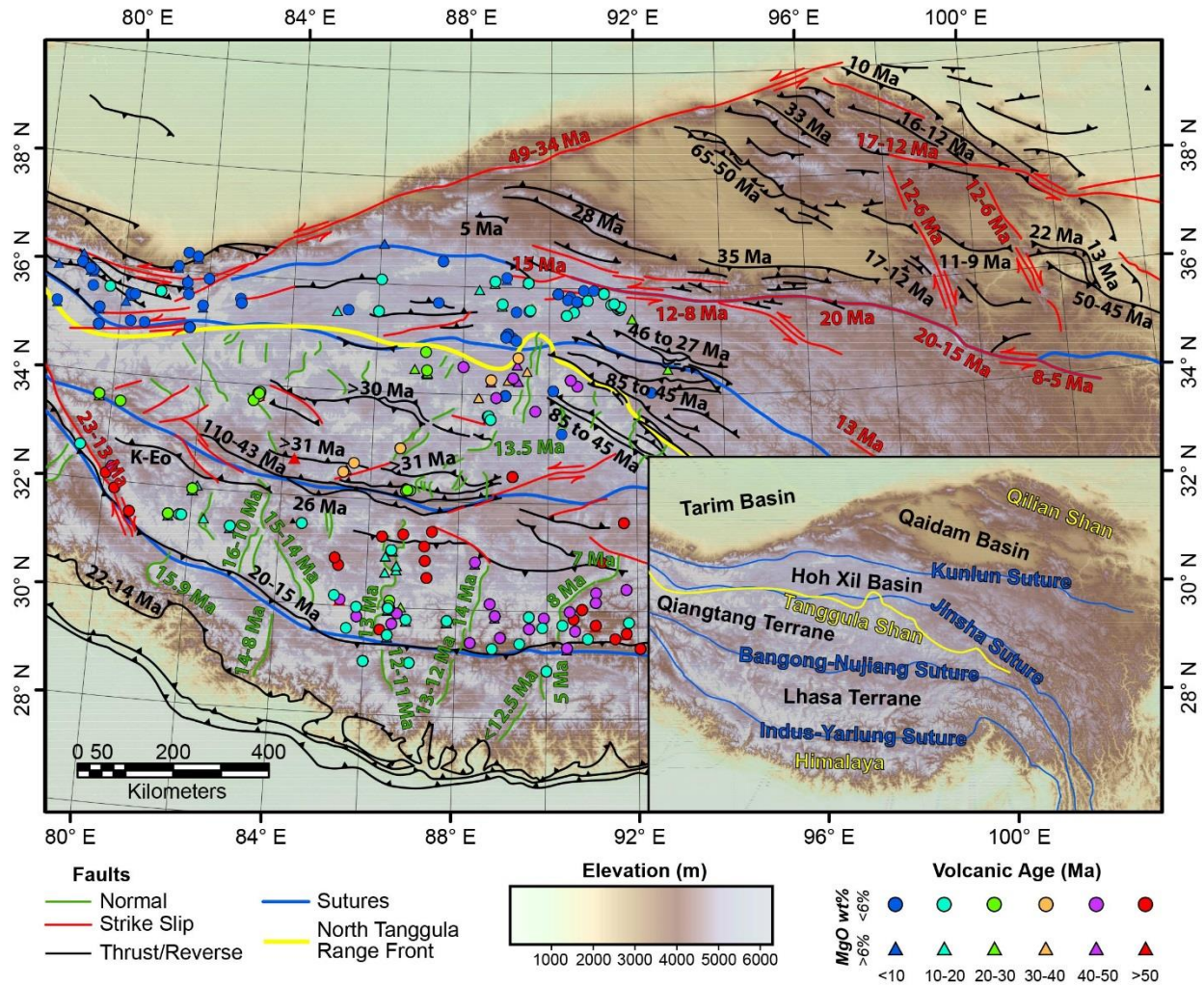
Figure 4.1 – Map of major faults in the Tibetan Plateau, and their periods of activity (e.g. 46 to 27 Ma), or initiation with uncertainty (e.g. 22-14 Ma) (Cowgill et al., 2003; Jolivet et al., 2003; Taylor and Yin, 2009; Wang et al., 2004; Yuan et al., 2013). Circles and triangles represent volcanic samples used in our compilation.

Thinning of the mantle lithosphere has been proposed as a driver of melt generation in both Cretaceous and Miocene time (Y. Li et al., 2013; Turner et al., 1996; Xia et al., 2011). Integrated geophysical and petrological modeling, as well as high surface heat flows suggest that the northern Tibetan Plateau may currently have a thin mantle lithosphere (Vozar et al., 2014; Yang, 2012). While high equilibration temperatures and an absence of hydrous minerals in crustal xenoliths have been used to argue against lithospheric removal in the central Tibetan Plateau (Hacker et al., 2000), hydrous

mantle xenoliths in the southern Tibetan Plateau have instead been used to support the presence of this process in Middle Miocene time (Liu et al., 2011).

Lastly, proposals for asthenospherically-driven volcanism generally incorporate the dynamics of the Indian or Asian mantle lithosphere to generate upwelling and resulting mantle melting (Guo et al., 2006; Mahéo et al., 2002; Wang et al., 2010; L. Zhang et al., 2014). The locations of Indian and Asian lithosphere in modern time have been interpreted from modeled seismic wave speeds beneath the Tibetan Plateau by seismic tomography studies. However, the low velocity contrast between the lithosphere and upper asthenospheric mantle, as well as a sparse seismic network in the region, have complicated ongoing efforts. Proposed hypotheses include the presence of hot asthenosphere beneath the majority of the Tibetan Plateau north of the Jinsha Suture, and its limitation solely to the northwestern quarter of the plateau (e.g. Agius and Lebedev, 2013; Liang et al., 2012; Nunn et al., 2013). A recent integrated geophysical-petrological study by Vozar et al., (2014) may provide an alternative in assessing the extent of thick mantle lithosphere and locations of asthenospheric upwelling by leveraging both seismic and magnetotulluric datasets, though it is limited to the vicinity of the Bangong-Nujiang Suture (BNS). As such, additional geophysical and petrological data would be necessary to resolve whether, and when, asthenospherically driven volcanism was present in the Tibetan Plateau.

Here, we present new major- and trace- element contents, Sr, Nd Pb, and Hf isotopic compositions, and age dates for twenty seven samples from four volcanic fields in the northern Tibetan Plateau together with a compilation of ~800 previously published geochemical data and respective eruption ages (see Appendices A and B). We first define end member lava compositions, and interpret possible melt source compositions. We then combine our interpretations of this geochemical dataset with the timing and styles of upper crustal deformation in order to propose a new, integrated geodynamic proposal for the evolution of the Tibetan Plateau.

4.3 Compilation Methodology

We use the following steps to ensure consistency between datasets in compiling our data with geochemical analyses from previous studies across the Tibetan Plateau. We re-calculate the Mg# and FeO(t) of every sample, assuming 85% ferric iron when total iron is reported. When the eruption or emplacement age of an individual sample is not available in a publication, we average the ages of dated samples stratigraphically above and below the given sample within the same volcanic sequence. When stratigraphic order is unclear, we follow source literature in inferring that geographically proximal samples in the same volcanic field have similar ages. The latitude and longitude of individual samples

are generally based on positions on geologic maps accompanying published sources. These frequently lack sufficient detail to provide highly accurate location coordinates, and thus may have an uncertainty of kilometers. Given the large number of samples and localities, we divide the Tibetan Plateau into three major regions: The southern Tibetan Plateau, limited to the Lhasa terrane between the Indus-Yarlung Suture (IYS) and the Bangong-Nujiang Suture (BNS). The central Tibetan Plateau, defined by the BNS in the south and the Tanggula Shan in the north, encompassing approximately two thirds of the Qiangtang terrane. The northern Tibetan Plateau is limited to the Qiangtang terrane north of the Tanggula Shan, the Songpan Ganzi terrane, and the West Kunlun Shan.

4.4 Synthesis of Tibetan Volcanic Geochemistry and Geochronology

We investigate the compiled geochemical and geochronologic data, interpret possible melt sources, and propose geodynamic mechanisms for melt generation and lithospheric development. We first broadly describe the timing and distribution of volcanism in the Tibetan Plateau. We then investigate major element compositions of two end-members, and compare them with petrological experiments in order to constrain source mineralogies and mechanisms of melt generation. Trace element contents of these end-members are utilized to support interpretations from major element compositions, and investigate possible processes that produced hypothesized melt source compositions. Additional constraints on melt generation and source alteration of the two end-members are then obtained from Sr, Nd Pb, and Hf isotopic compositions. We then summarize our interpretations of volcanism in the Tibetan Plateau, and implications for the geodynamic evolution of the Indo-Asian orogen.

4.4.1 Timing of Volcanism

Volcanism in the Tibetan Plateau underwent several major shifts since Indo-Asian collision, including periods of widespread volcanic activity, and quiescence. Prior to 40 Ma, Cenozoic volcanism was generally limited to the southern and central Tibetan Plateau (Figure 4.1, Figure 4.2). From 40 Ma to ~30 Ma volcanism was then limited to only to the south central Tibetan Plateau, roughly equidistant between previous centers of magmatism in the Lhasa terrane and the Tanggula Shan. This period of volcanic quiescence sharply terminated in a plateau-wide pulse of alkalic volcanism at ~30 Ma. In the Hoh Xil Basin, three of our samples represent some of the oldest evidence of volcanism in the region, having been dated between to ~24 Ma by whole rock $^{40}Ar/^{39}Ar$ (Appendix A). Volcanism in the southern Tibetan Plateau ended abruptly by ~10 Ma, while regions to the north have continued to be volcanically active through Pleistocene time.

69
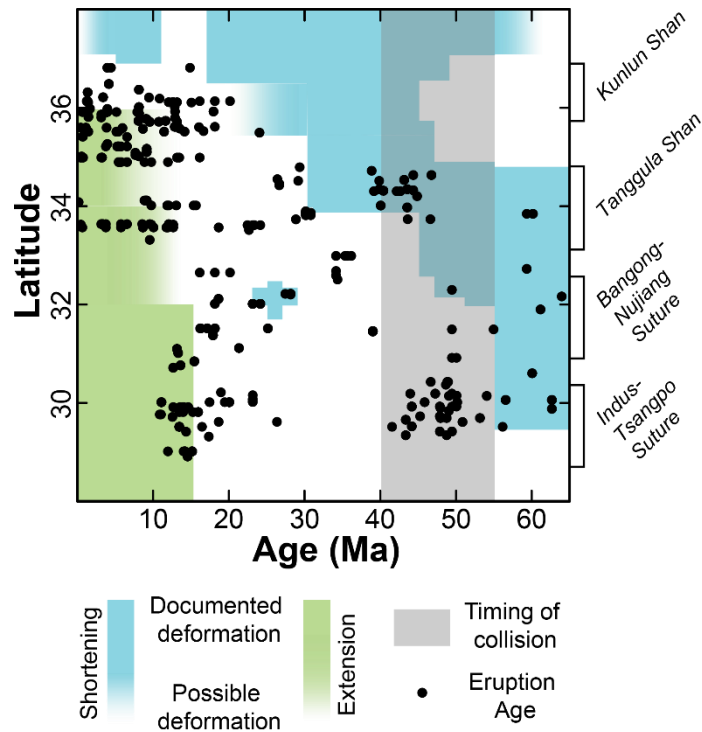
Figure 4.2 – Ages of erupted lavas in the Tibetan plateau. Each dot represents one dated sample of volcanic rock in our compilation. Note period of volcanic quiescence in the southern and northern Tibetan Plateau at approximately ~30-40 Ma, and the termination of volcanism in the region at ~10 Ma. Depiction of time progressive crustal shortening is modified from Staisch et al., (2015). Timing of extension based on oldest ages reported at a given latitude (e.g. Blisniuk et al., 2001; McCallister et al., 2014; Ratschbacher et al., 2011; Styron et al., 2013)

4.4.2 Major Element Compositions

Major element compositions of lavas in the Tibetan Plateau can be divided into two end-member compositions, termed groups A and B, which are then used to interpret possible melt sources. These groups are best represented by lavas erupted in the southern Tibetan Plateau (Figure 4.3, Figure 4.5, Figure 4.6). Group A is best described by lavas erupted prior to 40 Ma while group B is wholly limited to lavas erupted since 30 Ma. Group A lavas are generally sub-alkaline, have high Al_2O_3, CaO, FeO(t) and low SiO_2 at similar MgO contents relative to group B lavas. These trends remain consistent when considering solely samples with MgO wt% of 6 or greater, suggesting that differences between the two groups are not due to the effects of crustal contamination or fractional crystallization of mantle melts (Figure 4.4).

We compare the major element concentrations of group A and B end members and intermediate lavas with petrological experiments which may provide analogs for melt source compositions. Group A lavas have major element compositions consistent with melts generated from

70

a mantle wedge in an arc volcanic setting, and are in part analogous to melting experiments performed on naturally occurring lherzholites (Hirose and Kawamoto, 1995). Group B lava compositions are comparable to those determined by Wang and Gaetani (2008) for melts generated from eclogite partial melts hosted in an olivine crucible, as an analog for source materials in a metasomatized mantle. Lavas from the northern and central Tibetan Plateau have compositions that lie between group A and B endmembers. The compositions of lavas in the northern Tibetan Plateau are compatible with experiments performed on primitive leucitites from both the plateau and the Sierra Nevada (USA). These experiments suggest source compositions of Spinel + Garnet Pyroxenite and Phlogopite + Clinopyroxene Peridotite, respectively, likely hosted in a metasomatized mantle lithosphere (Elkins-Tanton and Grove, 2003; Holbig and Grove, 2008). Compositions of lavas in the central Tibetan Plateau may be due to a temporal transition between end-member compositions at 40-30 Ma, as we discuss in the next section.
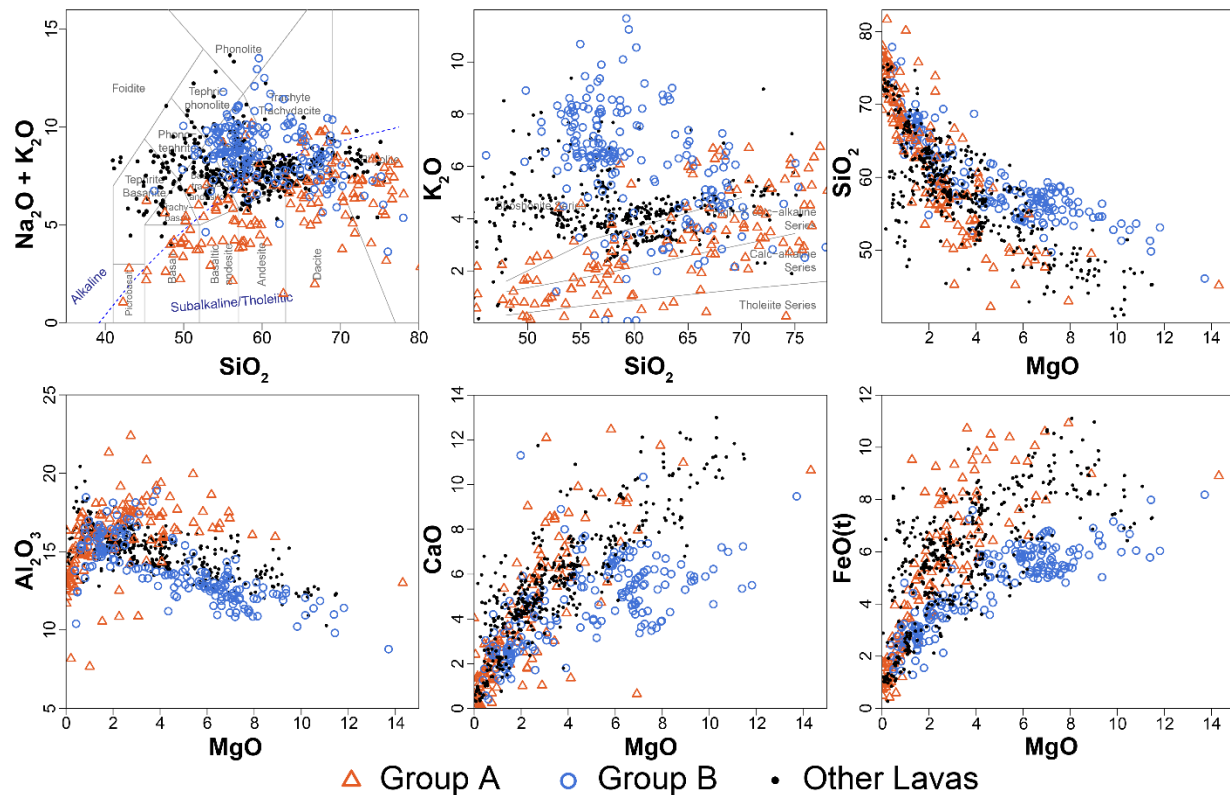
Figure 4.3 – End-member major element compositions of lavas from the Tibetan Plateau. Group A includes lavas from the southern Tibetan Plateau erupted prior to 40 Ma. Group B is limited to lavas from the southern Tibetan Plateau erupted since 30 Ma. See text for definitions of zone boundaries.
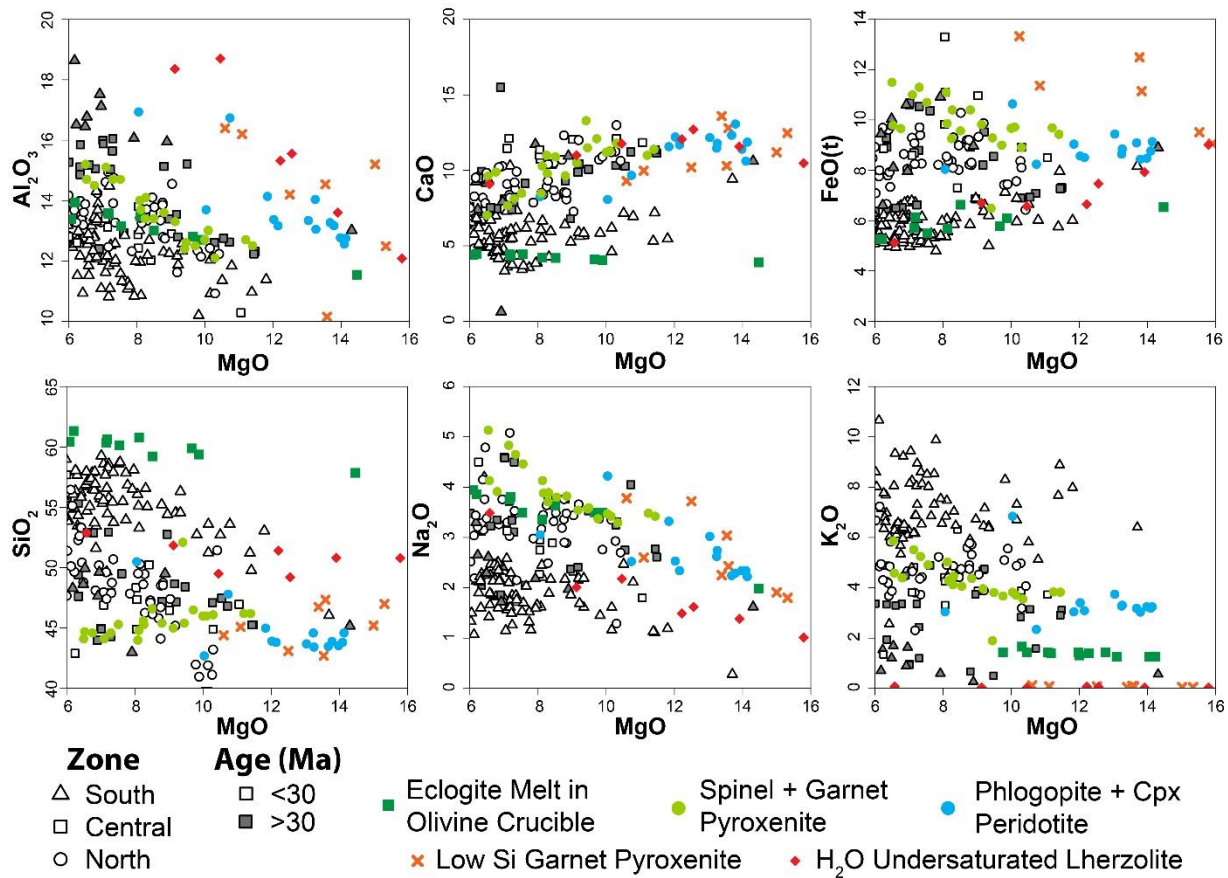
Figure 4.4 – Major element compositions for high MgO (>6 wt. %) lavas in the Tibetan Plateau. Black and white symbols denote geographic regions of the Tibetan Plateau, as delineated in text. Filled symbols show lavas erupted prior to 30 Ma, and open symbols denote lavas erupted since 30 Ma. Note that group A lavas are shown as filled triangles, and group B as open triangles. Colored symbols denote results of petrologic experiments analogous to source compositions of melts generated beneath the Tibetan Plateau. Green squares show compositions of melts generated by partial equilibration of silica-rich eclogite melts with an Olivine crucible, as a possible analog for subduction metasomatism (Wang and Gaetani, 2008). Light green circles denote compositions of partial melts from primitive olivine leucitite sampled in the northern Tibetan Plateau and likely sourced from a Spinel + Garnet Peridotite in a metasomatized mantle lithosphere (Holbig and Grove, 2008). Light blue circles show results of phase equilibrium experiments on a primitive olivine leucitite from the Sierra Nevada, USA, sourced from a metasomatized lithospheric mantle comprised of Phlogopite + Cpx Peridotite (Elkins-Tanton and Grove, 2003). Orange diagonal crosses denote silica-deficient garnet pyroxenite melts Pilet et al., (2008), compositions thought to be analogous for melting of recycled oceanic crust in the asthenosphere. Red diamonds are partial melts of a naturally occurring H_2O undersaturated lherzolite (Hirose and Kawamoto, 1995), an analog for asthenospheric melting.

0-30 Ma 30-40 Ma >40 Ma

Figure 4.5

73
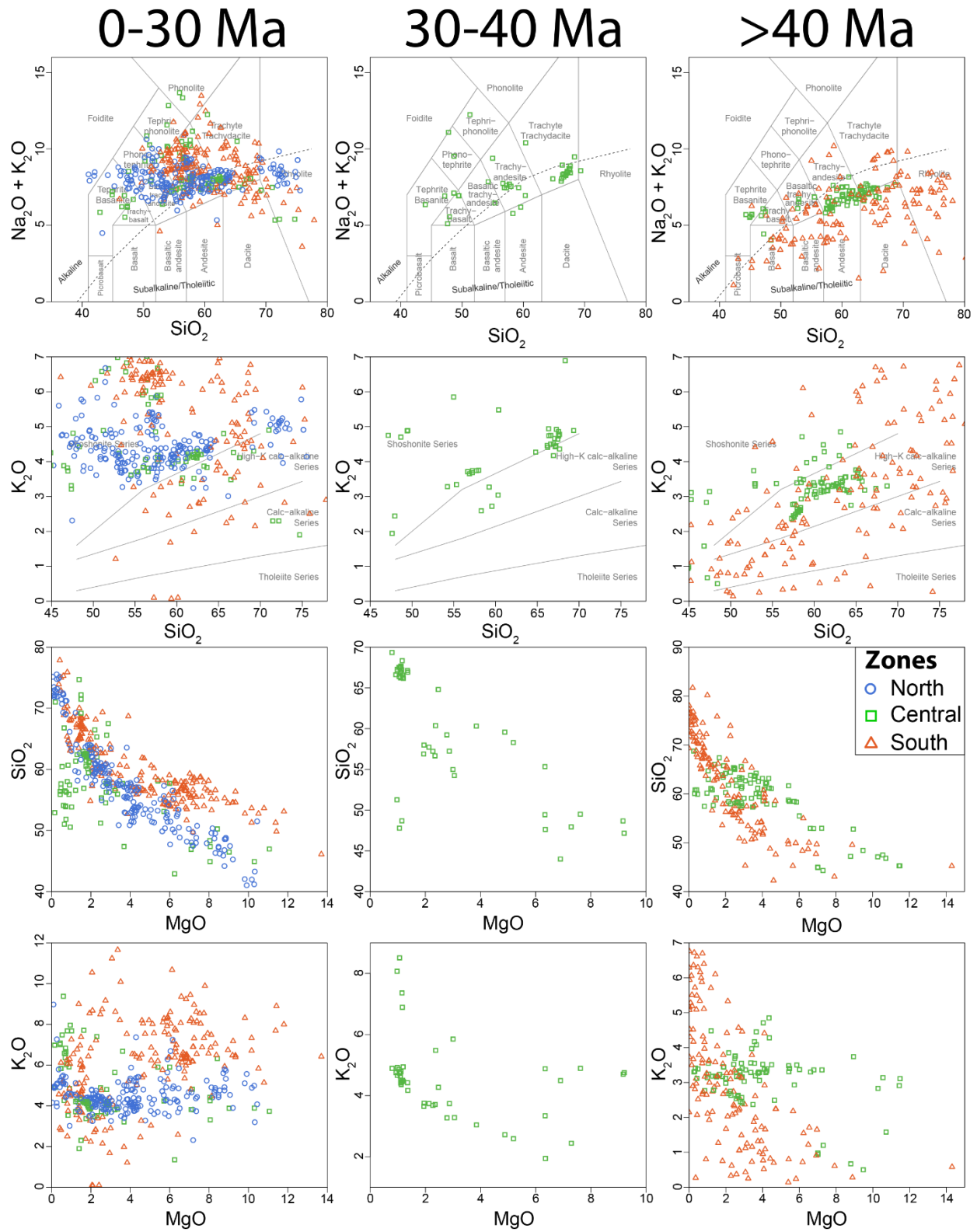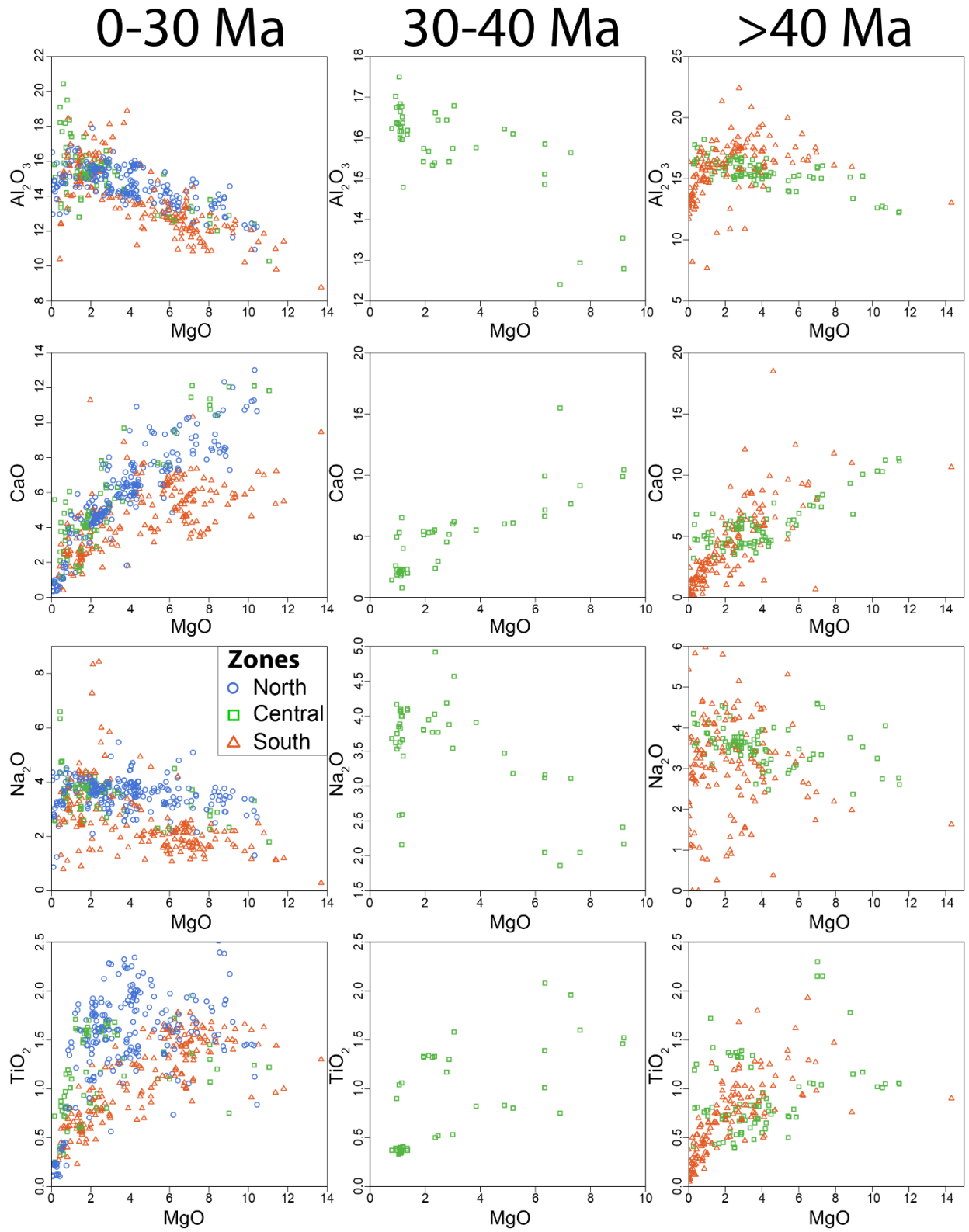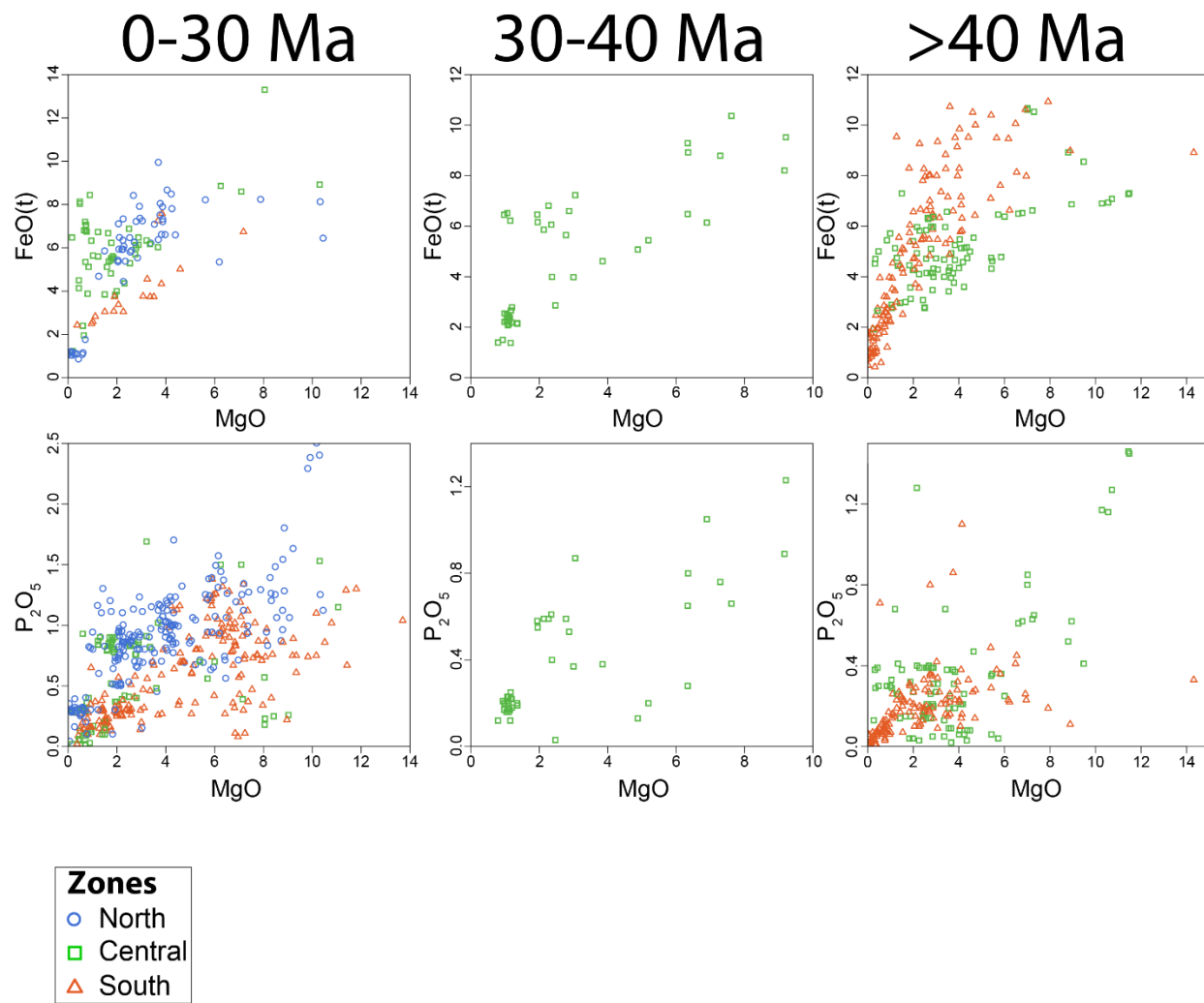
Figure 4.5

Figure 4.5 – Major element compositions of lavas in the Tibetan Plateau, sorted by eruption age.
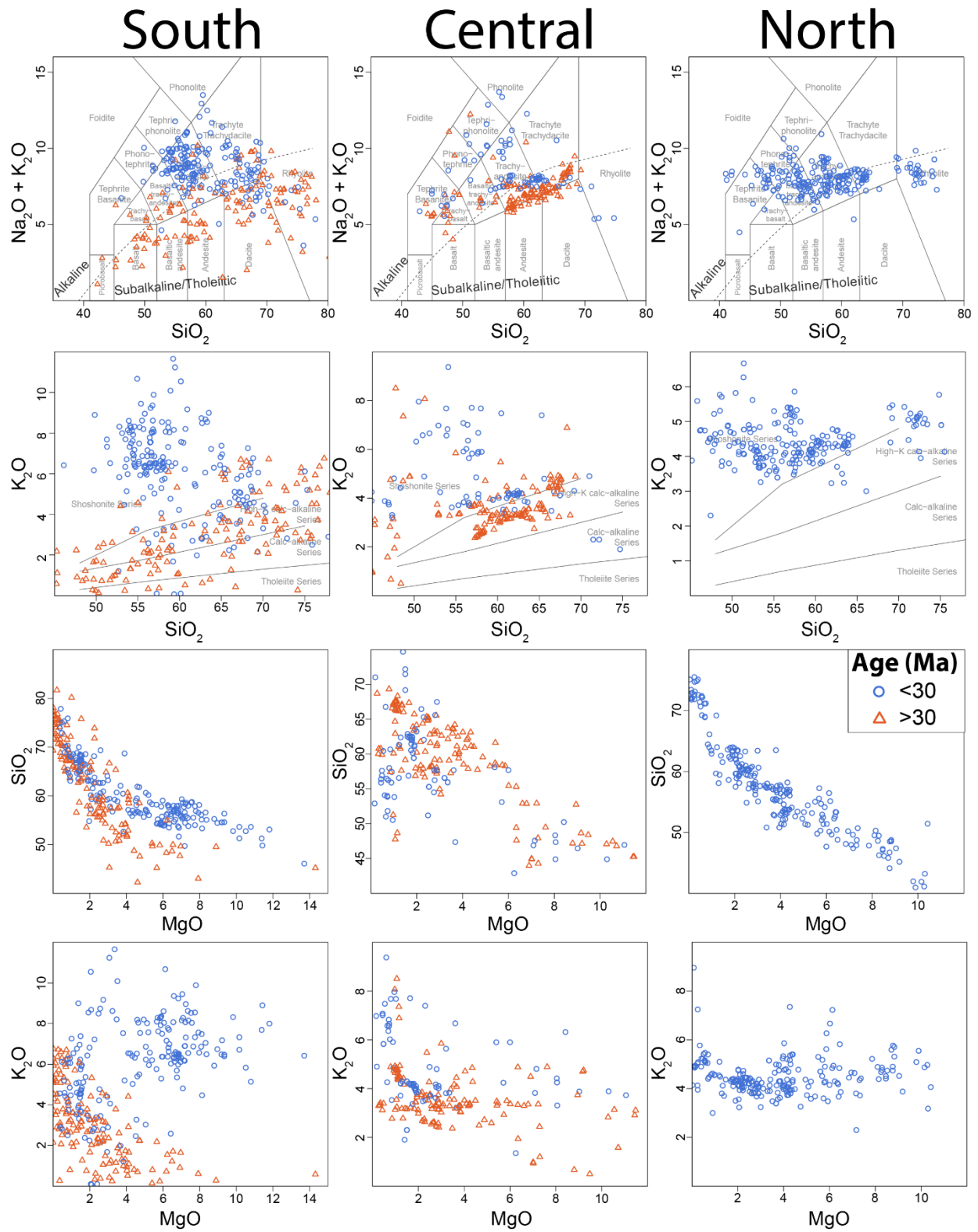
Figure 4.6
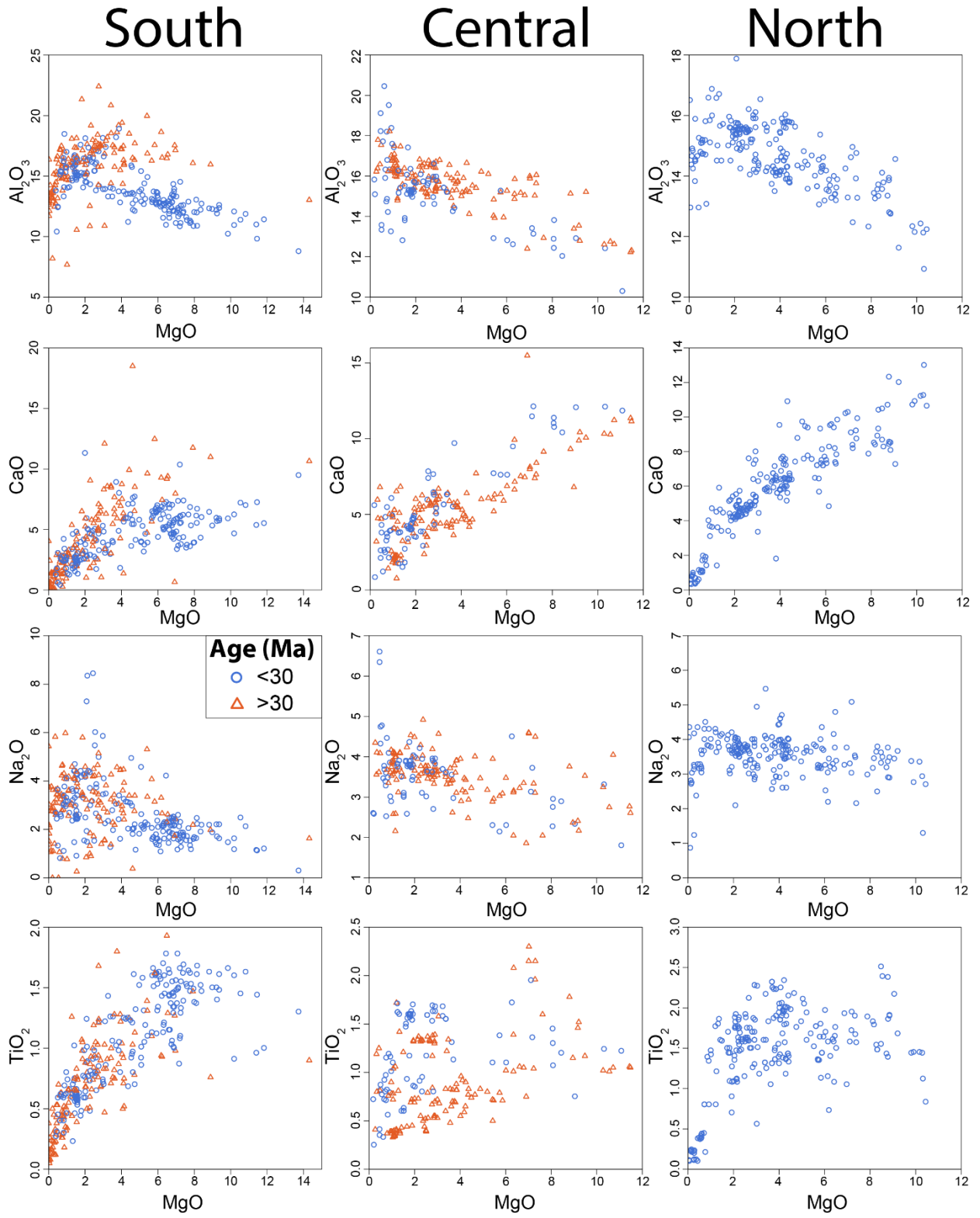
Figure 4.6
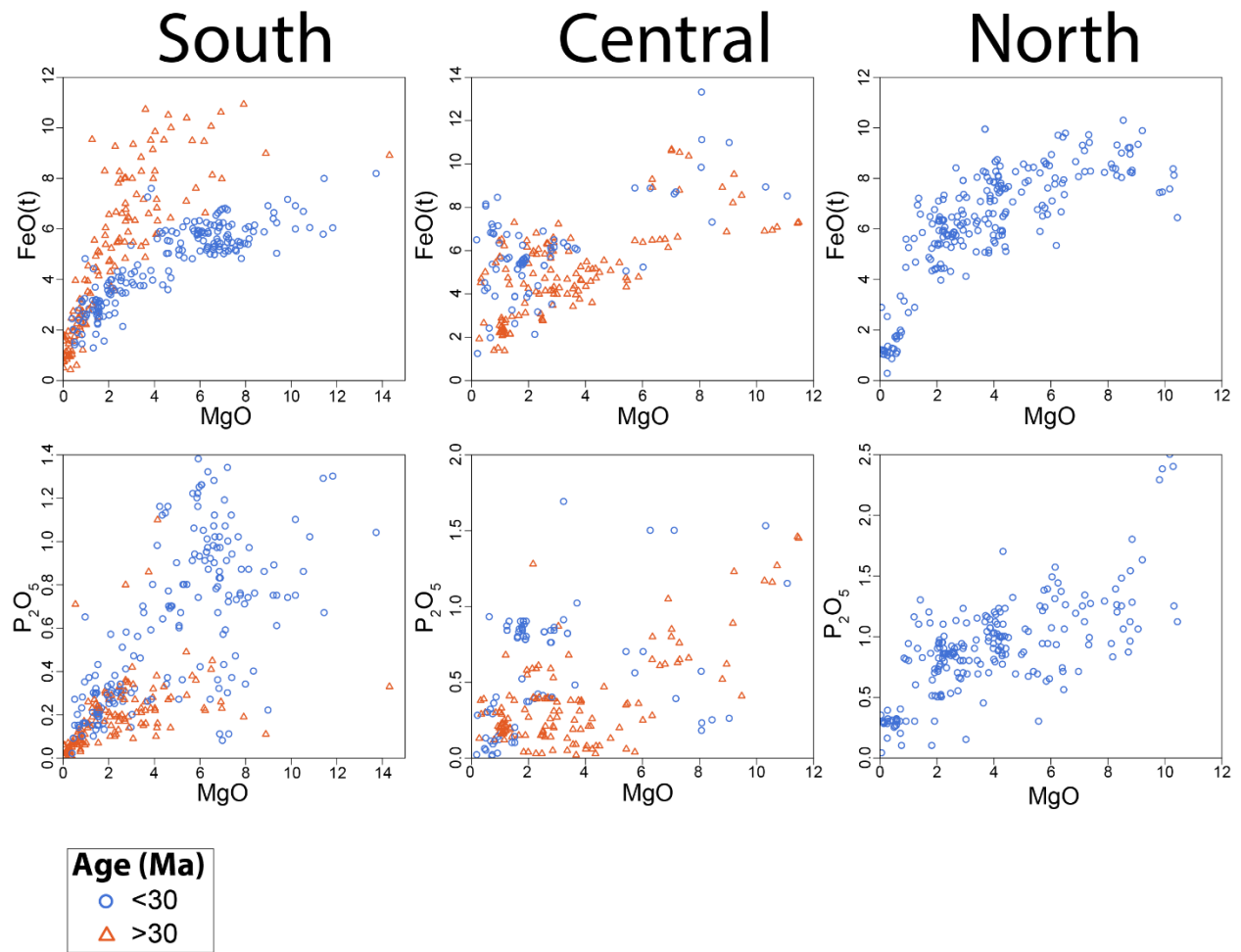
Figure 4.6 – Major element compositions of lavas in the Tibetan Plateau, sorted by zone.
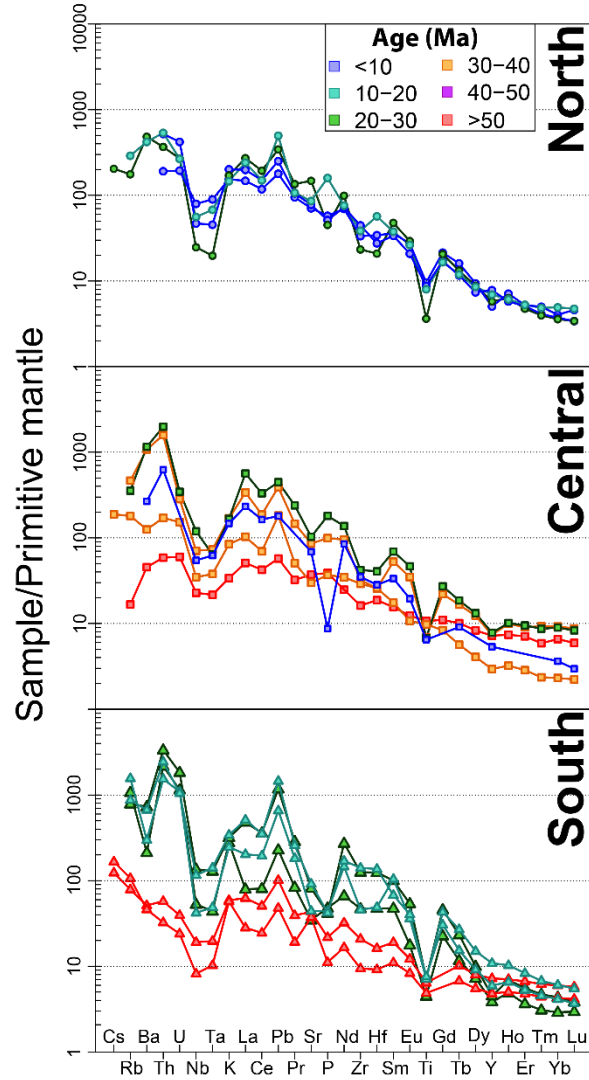
Figure 4.7 – Representative primitive mantle normalized (McDonough and Sun, 1995) trace element compositions of Tibetan lavas with MgO compositions of 7 ± 1 wt%. Lavas erupted in the southern Tibetan plateau prior to 40 Ma fall into group A, and are typical of arc volcanism. Lavas erupted since 30 Ma in the southern Tibetan Plateau are classified into group B, and suggest low-degree melting of a metasomatized mantle lithosphere. See Figure 4.1 and text for definitions of zones within the Tibetan Plateau.

4.4.3 Trace Element Compositions

We investigate the trace element compositions of lavas in our compilation in order to constrain the relative degree of melting for source material, and provide further support for source compositions interpreted from major element concentrations. We evaluate lavas with MgO 7 ± 1 wt% in primitive mantle normalized incompatible trace element (ITE) diagrams, as this compositional range has the largest amount of samples while maintaining similar MgO values (Figure 4.7). Group A lavas show patterns typical of arc volcanism: enrichment of ITEs and negative anomalies of high field strength

elements (HFSEs) such as Nb and Ta. Group B lavas have significantly higher enrichment of ITEs (up to 2000 times primitive mantle values), with extremely negative HFSE anomalies. The high ITE enrichment and highly negative HFSE anomalies of group B lavas are compatible with low-degree melting of a metasomatized mantle lithosphere or a cold mantle wedge.

In the central Tibetan Plateau, the transition between group A and group B end-members appears to take place between 40 and 30 Ma, with both end-member compositions observed in this time interval. Younger lavas in the central Tibetan Plateau show similar ITE patterns to group B lavas, but with slightly lower enrichment and less pronounced, though still prominent, HFSE anomalies. Lavas erupted in the northern Tibetan Plateau near 27 Ma are generally similar to group B lavas, but with younger lavas having progressively smaller negative HFSE element anomalies, possibly indicating a depletion of the metasomatized mantle lithospheric source.
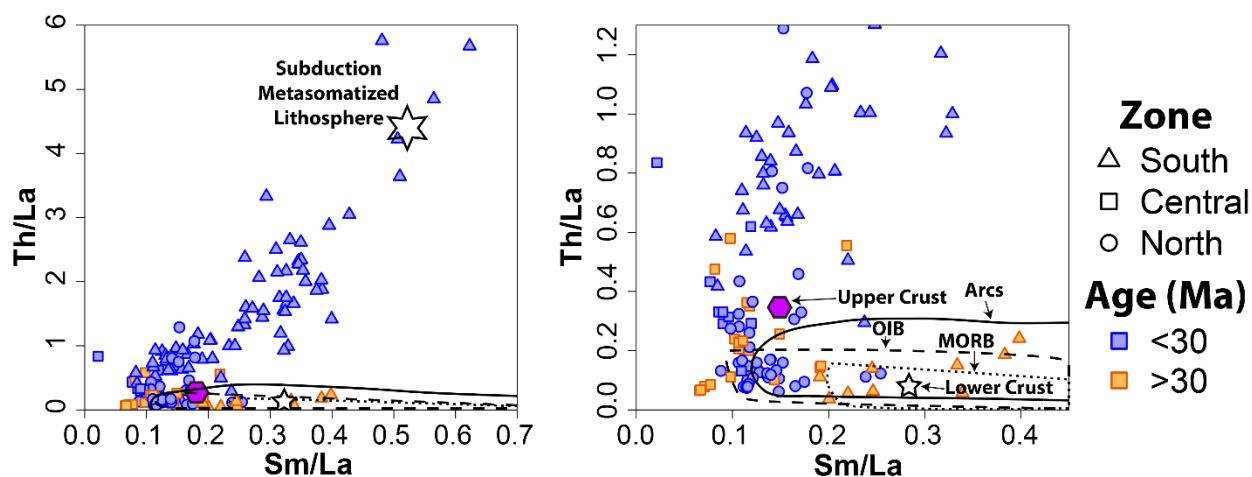
Figure 4.8 – Trace element compositions of lavas erupted in the Tibetan Plateau with MgO>6 wt%. Lavas erupted prior to 30 Ma generally fall in a range of compositions typical of arc volcanism, best shown by group A lavas (orange triangles). Note that lavas erupted since 30 Ma have a distinctly positive trend, with group B lavas (blue triangles) containing the highest Th/La ratios. Lines and symbols of figure on left are identical to those on right.

Trace element ratios are then used to constrain a processes which generated metasomatism of the group B source, and further support an absence of significant crustal contamination. The Sm/La and Th/La ratios of high MgO samples (>6 wt%) in group A lavas are compatible with mantle melting in any tectonic setting (MORB, OIB and Arc volcanism). Group B lavas, however, display a strong positive trend between Sm/La and Th/La ratios (Figure 4.8). This strongly positive trend is observed in a wide swath of primitive lavas in the Tethyan realm, and is interpreted to be the result of subduction of peri-Gondwanan sediments, metasomatism of overlying mantle lithosphere or a cold mantle wedge by melts sourced from these sedimentary units, and subsequent reheating of the subduction

metasomatized mantle to generate low-degree partial melting and volcanism (Tommasini et al., 2011). We suggest that an identical process, mantle metasomatism generated by the subduction of peri-Gondwanan sediments, is applicable to group B lavas. At MgO >6 wt%, group B lavas have Ni concentrations of 150-550 ppm and Cr concentrations of ~400-650 ppm (Figure 4.9). These concentrations are high compared to bulk crustal averages of 105 and 185 ppm, indicating that melts are not strongly contaminated by or sourced directly from crustal material (Taylor and McLennan, 1995).
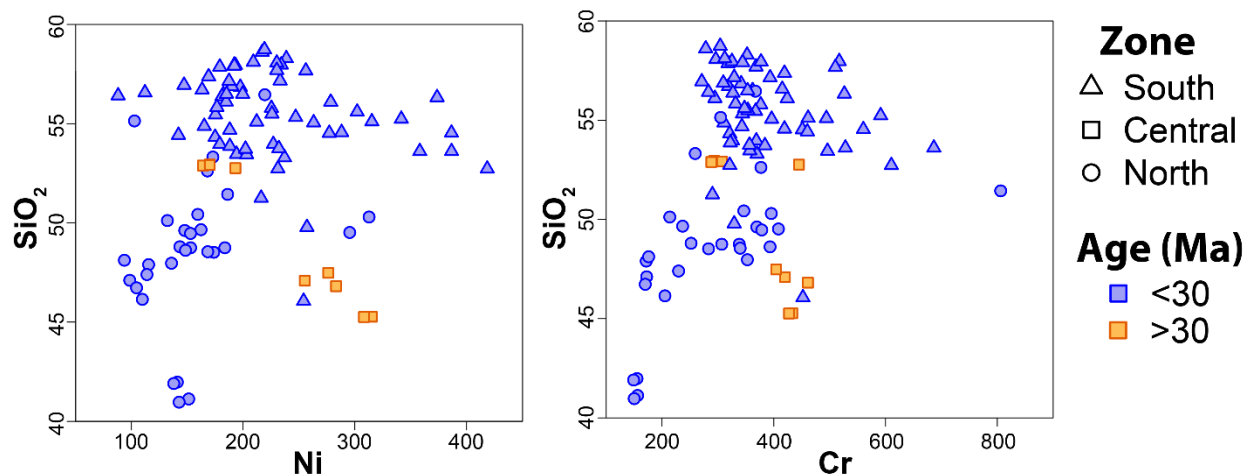
Figure 4.9 – Ni and Cr compositions of lavas erupted in the Tibetan Plateau. Note positive slopes in lavas younger than 30 Ma, and values greater than crustal averages of 105 and 185 ppm (Taylor and McLennan, 1995).

4.4.4 Isotopic Compositions

We use the Sr, Nd, and Pb isotopic compositions of end-member lavas to further support melt source compositions, and elaborate on mechanisms by which the mantle lithosphere beneath the Tibetan Plateau would become metasomatized. $^{87}Sr/^{86}Sr$ and $^{143}Nd/^{144}Nd$ isotopic compositions of group A lavas fall along typical arc volcanic trends and lie close to primitive mantle values when considering samples with high MgO (>6 wt%) compositions (Figure 4.10). Group B lavas however, generally have $^{87}Sr/^{86}Sr$ values above 0.71 and $^{143}Nd/^{144}Nd$ values below 0.5120, compatible with a crustal origin of the isotopic signature. These isotopic compositions fall on a mixing line between primitive mantle values, and averages for Himalayan sediments. As Himalayan sediments represent the northern margin of India prior to collision, which was formed at the northern margin of Gondwana in Mesozoic time, we infer that metasomatism of the mantle beneath the Tibetan Plateau was generated by the subduction of sedimentary rocks deposited on the passive margin of the Indian subcontinent.
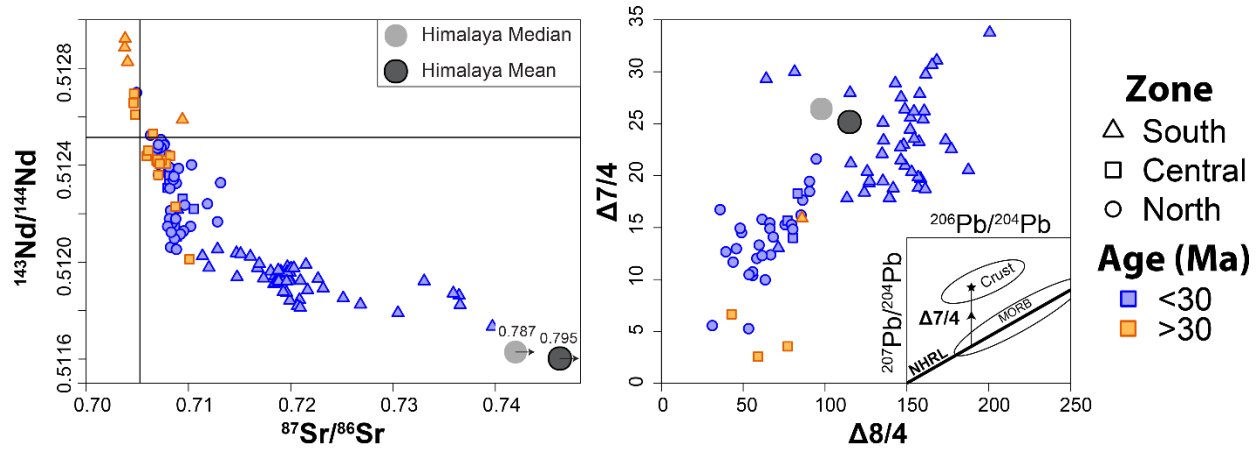
Figure 4.10 – Isotopic compositions for Tibetan lavas. Black lines on figure at left represent $^{87}Sr/^{86}Sr$ and $^{143}Nd/^{144}Nd$ of the primitive mantle. Light gray circles represent the median composition of Himalayan sediments, and dark grey circles the mean composition. Inset in right panel schematically depicts method of calculating delta values with respect to the Northern Hemisphere Reference Line (NHRL of Hart, 1984)

We provide an additional constraint on the generation of metasomatism beneath the Tibetan Plateau using Pb isotopes. In the northern hemisphere, mid-ocean ridge basalts (MORBs) show a distinct linear relationship in $^{206}Pb/^{204}Pb$ vs $^{207}Pb/^{204}Pb$ space and $^{206}Pb/^{204}Pb$ vs $^{208}Pb/^{204}Pb$ space, which is termed the northern hemisphere reference line (NHRL) (Hart, 1984). Continental crust and sediments generally lie above this line. We investigate Pb isotopes by first calculating the Δ7/4 and Δ8/4 values of samples which have been analyzed for $^{207}Pb/^{204}Pb,^{206}Pb/^{204}Pb$, and $^{208}Pb/^{204}Pb$ ratios. The Δ7/4 value represents the difference between the observed $^{207}Pb/^{204}Pb$ ratio of a sample, and the $^{207}Pb/^{204}Pb$ of the NHRL at a $^{206}Pb/^{204}Pb$ ratio identical to that measured in the sample (Hart, 1984; Figure 7). Similarly, the Δ8/4 value is the difference between the $^{208}Pb/^{204}Pb$ ratio of a sample, and the $^{208}Pb/^{204}Pb$ of the NHRL at the sample's $^{206}Pb/^{204}Pb$ ratio (Hart, 1984). Group B lavas have generally high Δ7/4 and Δ8/4 values (above 15 and 100, respectively). These require input of old highly radiogenic continental crust and/or sediments, such as those from the passive margin of the northern Indian subcontinent, into the mantle source region of the lavas. However, the Δ7/4 and Δ8/4 values of group B lavas are higher than those of Himalayan sediments, suggesting an additional highly radiogenic and therefore older source. Δ7/4 and Δ8/4 values of lavas in the central, and northern Tibetan Plateau are lower than that of those in the southern Tibetan Plateau, indicating a lower contribution of continental sediments into their mantle source regions.

4.4.5 Summary of Interpretations

Major, trace and isotopic compositions of lavas in the Tibetan plateau constrain melt source compositions, and the geodynamic drivers of magmatism. Prior to 40 Ma lavas were produced during subduction and arc volcanism, while lavas erupted since 30 Ma were generated by low-degree melting of a metasomatized mantle lithosphere. Metasomatism of the mantle lithosphere or thin mantle wedge beneath the Tibetan Plateau likely occurred between 30 and 40 Ma, as a consequence of the incorporation of sediments from the northern margin of India into the mantle, and migration of partial melts and/or fluids through the mantle lithosphere.

4.5 Discussion and Geodynamic Interpretation

We interpret the geodynamic evolution of the Indo-Asian orogen based on the timing and compositions of lavas from the Tibetan Plateau, and the distribution of faulting. We discuss specific ~10-15 Ma time windows in which we describe active patterns of deformation, as well as sources and drivers of magmatism. Volcanism prior to the ~50 Ma Indian collision was driven by northward subduction of Tethyian oceanic crust, resulting in pervasive plutonism and group A volcanism in the Gangdese arc of the southern Tibetan Plateau. Concurrent plutonism and group A volcanism in the Tanggula Shan of the central Tibetan Plateau are likely the result of the reactivation of a south-directed fossilized Mesozoic subduction zone (Roger et al., 2000). Magmatism in both regions was most likely driven by subduction and dehydration of oceanic crust, and mantle lithosphere. In the Tangula Shan subduction of Mesozoic marine sediments of the Songpan-Ganzi terrane may have also contributed to melt generation (Wang et al., 2010). Subduction of Songpan-Ganzi crust is broadly compatible with evidence for Eocene to Oligocene deformation of Cenozoic terrestrial sediments which had been deposited near the suture between the Songpan-Ganzi and Qiangtang terranes (Li et al., 2012; Staisch et al., 2014).

The arrival of continental crust of the Indian passive margin at the trench between 56 and 40 Ma (e.g. Bouilhol et al., 2013; Sciunnach and Garzanti, 2012), potentially resulted in flattening of the Tethyian slab and metasomatism of a frozen mantle wedge or lithospheric mantle beneath much of the Tibetan Plateau by 30 Ma. A modern analog may be the Trans-Mexican Volcanic Belt, where a flat Cocos slab drives dehydration melting, and resulting volcanism > 200 km into the continental interior (Jödicke et al., 2006; Pérez-Campos et al., 2008). In Mexico, slab flattening is hypothesized to have been caused by hydration of the mantle wedge, which generated a low viscosity channel that now prevents coupling between the Cocos sab and overriding North American crust (Manea and Gurnis, 2007; Pérez-Campos et al., 2008). Influx of Indian sediment into the mantle during subduction would

have provided a mechanism to rapidly hydrate and metasomatize the mantle wedge, drive slab flattening, and prevent coupling with overriding Asian crust, which did not undergo significant crustal shortening between 40 and 30 Ma (Figure 4.1, Figure 4.2, Figure 4.11). A general northerly decrease in $\Delta7/4$, $\Delta8/4$, $^{87}Sr/^{86}Sr$ and an increase in $^{144}Nd/^{143}Nd$ in high MgO (>6 wt%) group B magmas is then indicative of a lower magnitude of metasomatism further away from the southern plate margin, likely due to the incorporation of fewer sedimentary rocks subducted at the plate margin into the mantle beneath those regions.

Flattening of the Tehyian slab may have also resulted in a northward migration of volcanism between to the central Tibetan Plateau between 40 and 30 Ma (Figure 4.1, Figure 4.11). The location of volcanism in this time interval suggests that the Tethyian slab reached past the BNS, and up to ~300 km away from the Asian plate boundary. An absence of volcanism in the Tanggula Shan during this time period indicates that southward directed subduction of Songpan-Ganzi crust must have stopped, with convergence instead accommodated by continued crustal shortening and deformation of basin sediments (Li et al., 2012; Staisch et al., 2014).

A large-scale transition in the composition and extent of volcanism occurred at ~30 Ma, as group B volcanism initiated across the entirety of the Tibetan Plateau. This shift in the spatial distribution of magmatism is roughly concurrent with the termination of upper crustal shortening in the northern Tibetan Plateau and is 10-15 Myr earlier than the development of extensional faulting (Blisniuk et al., 2001; Li et al., 2012; Ratschbacher et al., 2011; Staisch et al., 2014; Sun et al., 2005; Wu et al., 2008; Yuan et al., 2013). Previous authors have hypothesized a coeval initiation of volcanism and normal faulting linked to the removal of a dense lithospheric root and the attainment of elevations of ~5000 m at 10-15 Ma (e.g. Molnar et al., 1993). Our results show that normal faulting and volcanism did not initiate coevally and thus argue strongly against a middle-Miocene timing of lithospheric removal.

Potentially, the initiation of volcanism at ~30 Ma was driven by the rollback and/or breakoff of the Tethyian slab, rather than convective removal of the mantle lithosphere. Removal of the Tethyian slab likely precipitated an influx of hot asthenosphere to regions beneath the Tibetan Plateau, resulting in widespread alkali magmatism and thermal erosion of the mantle lithosphere. Upwelling of hot asthenosphere into regions previously insulated by the Tethyian slab is compatible with petrological data showing a rapid pulse of advective heating of the crust in Oligocene time and a hydrated mantle at temperatures in excess of 1000°C in middle Miocene time beneath the southern Tibetan Plateau (Liu et al., 2011; Mahéo et al., 2002). Furthermore, this time period marks the

termination of prograde metamorphism of sediments now exhumed in Himalayan gneiss domes, and the initiation of a period of rapid near isothermal exhumation, providing evidence for heightened geotherms, and the reorganization of deformation styles at the northern margin on the Indian plate (e.g. Langille et al., 2012; Zhang et al., 2015). In the northern Tibetan Plateau, the correspondence of lavas in our compilation with melts derived from the spinel stability field suggests that melting depths were above ~80 km (Green and Ringwood, 1967; Holbig and Grove, 2008). Given the 60-70 km thick crust in the region today (Zhang et al., 2011), an ~80 km depth of melting would imply that the mantle lithosphere was highly thinned by ~24 Ma.

A final transition took place at 10-15 Ma, with the termination of volcanism in the southern and central Tibetan Plateau. We interpret this shift as being the consequence of Indian underthrusting, which drove the hydrated mantle wedge to the north, and thickened the mantle lithosphere in the southern to south-central Tibetan Plateau to a point where dehydration reactions were no longer favored, thereby removing previous drivers of melt generation. In this interpretation, strain in lithospheric mantle necessarily localizes south of the Tanggula Shan, creating a significant contrast in lithospheric thicknesses between the central and northern Tibetan Plateau. This contrast may help increase rates of volcanism in the northern Tibetan Plateau through shear driven upwelling as has been suggested for the Colorado Plateau of western North America (Ballmer et al., 2015), with a metasomatized mantle wedge acting as a low viscosity pocket and source for melting.

Indian underthrusting may have also precipitated the development of normal faulting by bringing the Tibetan Plateau to gravitationally unstable elevations of over ~4000 m, and contributing to the flow of lower crustal material to the periphery of the orogen (e.g. Styron et al., 2015). Continued crustal shortening then focused north of the Tibetan Plateau, as material in the plateau interior was moved laterally on newly initiated or reactivated strike-slip faults (Duvall et al., 2013; Liu et al., 2007; Lu et al., 2014; Murphy et al., 2000; Sun et al., 2005; Yuan et al., 2013; Zhang et al., 2012; Zheng et al., 2006). This then resulted in the distribution of faulting and volcanism observed in modern time, with volcanism limited to the northern Tibetan Plateau, dominance of normal faulting above elevations of 5000 m, and strike slip and thrust faulting elsewhere.

Figure 4.11 – Proposed geodynamic evolution of the Tibetan plateau over the last 60 Myr. See text for details.

4.6 Conclusions

We present a combined dataset of geochemical, and geochronologic studies from the Tibetan Plateau, and investigate the possible melt source compositions, and geodynamic drivers of volcanism, and mantle metasomatism. Major element, trace element, and isotopic compositions of lavas erupted prior to 40 Ma (group A) are compatible with melt generation in an arc volcanic setting due to northward subduction of Tethyian oceanic crust, and the 40-50 Ma reactivation of a fossilized south directed subduction zone in the central Tibetan Plateau. Lavas erupted since 30 Ma (group B) have compositions indicative of low-degree melting of a metasomatized mantle lithosphere, or cold mantle wedge, as suggested by previous authors (e.g. Mahéo et al., 2002; Turner et al., 1993). Based on Sm/La and Th/La trace element ratios, and Sr, Nd and Pb isotopes, we suggest that mantle metasomatism

was generated by subduction of Indian sediments and flattening of the Tethyian oceanic slab between 40 and 30 Ma. The initiation of widespread volcanism across the plateau at 30 Ma, and low-degree melting of subduction metasomatized mantle may have been the result of rollback and/or breakoff of the Tethyian slab. The initiation of volcanism is ~15-20 Myr earlier than a proposed middle Miocene lithospheric removal event suggesting that the initiation of normal faulting and volcanism may not be linked. We propose that the shutoff of volcanism in the southern, and central Tibetan Plateau and the initiation of extensional faulting at 10-15 Ma were likely related to Indian underthrusting and resulting lithospheric thickening.

4.7 References

Agius, M.R., Lebedev, S., 2013. Tibetan and Indian lithospheres in the upper mantle beneath Tibet: Evidence from broadband surface-wave dispersion. Geochemistry, Geophys. Geosystems 14, 4260–4281. doi:10.1002/ggge.20274

Arnaud, N.O., Vidal, P., Tapponnier, P., Matte, P., Deng, W.M., 1992. The high K2O volcanism of northwestern Tibet: Geochemistry and tectonic implications. Earth Planet. Sci. Lett. 111, 351–367. doi:10.1016/0012-821X(92)90189-3

Ballmer, M.D., Conrad, C.P., Smith, E.I., Johnsen, R., 2015. Intraplate volcanism at the edges of the Colorado Plateau sustained by shear-driven upwelling. Geochemistry, Geophys. Geosystems 15, 6744. doi:10.1002/2014GC005641

Blisniuk, P.M., Hacker, B.R., Glodny, J., Ratschbacher, L., Bi, S., Wu, Z., McWilliams, M.O., Calvert, A., 2001. Normal faulting in central Tibet since at least 13.5 Myr ago. Nature 412, 628–32. doi:10.1038/35088045

Bouilhol, P., Jagoutz, O.E., Hanchar, J.M., Dudas, F.O., 2013. Dating the India–Eurasia collision through arc magmatic records. Earth Planet. Sci. Lett. 366, 163–175. doi:10.1016/j.epsl.2013.01.023

Chen, J., Wu, J., Xu, J., Dong, Y., Wang, B., Kang, Z., 2013. Geochemistry of Eocene high-Mg# adakitic rocks in the northern Qiangtang terrane, central Tibet: Implications for early uplift of the plateau. Geol. Soc. Am. Bull. 125, 1800–1819. doi:10.1130/B30755.1

Chen, J.-L., Xu, J.-F., Wang, B.-D., Kang, Z.-Q., 2012. Cenozoic Mg-rich potassic rocks in the Tibetan Plateau: Geochemical variations, heterogeneity of subcontinental lithospheric mantle and tectonic implications. J. Asian Earth Sci. 53, 115–130. doi:10.1016/j.jseaes.2012.03.003

Chung, S.-L., Chu, M.-F., Zhang, Y., Xie, Y., Lo, C.-H., Lee, T.-Y., Lan, C.-Y., Li, X., Zhang, Q., Wang, Y., 2005. Tibetan tectonic evolution inferred from spatial and temporal variations in post-collisional magmatism. Earth-Science Rev. 68, 173–196. doi:10.1016/j.earscirev.2004.05.001

Clark, M.K., Farley, K.A., Zheng, D., Wang, Z., Duvall, A.R., 2010. Early Cenozoic faulting of the northern Tibetan Plateau margin from apatite (U–Th)/He ages. Earth Planet. Sci. Lett. 296, 78–88. doi:10.1016/j.epsl.2010.04.051

Clark, M.K., Royden, L.H., 2000. Topographic ooze: Building the eastern margin of Tibet by lower crustal flow. Geology 28, 703. doi:10.1130/0091-7613(2000)28<703:TOBTEM>2.0.CO;2

Cowgill, E., Yin, A., Harrison, T.M., Xiao-Feng, W., 2003. Reconstruction of the Altyn Tagh fault based on U-Pb geochronology: Role of back thrusts, mantle sutures, and heterogeneous crustal strength in forming the Tibetan Plateau. J. Geophys. Res. 108. doi:10.1029/2002JB002080

Craddock, W., Kirby, E., Zhang, H., 2011. Late Miocene-Pliocene range growth in the interior of the northeastern Tibetan Plateau. Lithosphere 3, 420–438. doi:10.1130/L159.1

DeCelles, P.G., Quade, J., Kapp, P.A., Fan, M., Dettman, D.L., Ding, L., 2007. High and dry in central Tibet during the Late Oligocene. Earth Planet. Sci. Lett. 253, 389–401. doi:10.1016/j.epsl.2006.11.001

Ding, L., Kapp, P.A., Yue, Y., Lai, Q., 2007. Postcollisional calc-alkaline lavas and xenoliths from the southern Qiangtang terrane, central Tibet. Earth Planet. Sci. Lett. 254, 28–38. doi:10.1016/j.epsl.2006.11.019

Ding, L., Kapp, P.A., Zhong, D., Deng, W., 2003. Cenozoic Volcanism in Tibet: Evidence for a Transition from Oceanic to Continental Subduction. J. Petrol. 44, 1833–1865. doi:10.1093/petrology/egg061

Duvall, A.R., Clark, M.K., Kirby, E., Farley, K. a., Craddock, W.H., Li, C., Yuan, D.-Y., 2013. Low-temperature thermochronometry along the Kunlun and Haiyuan Faults, NE Tibetan Plateau: Evidence for kinematic change during late-stage orogenesis. Tectonics 32, 1190–1211. doi:10.1002/tect.20072

Duvall, A.R., Clark, M.K., van der Pluijm, B. a., Li, C., 2011. Direct dating of Eocene reverse faulting in northeastern Tibet using Ar-dating of fault clays and low-temperature thermochronometry. Earth Planet. Sci. Lett. 304, 520–526. doi:10.1016/j.epsl.2011.02.028

Elkins-Tanton, L.T., Grove, T.L., 2003. Evidence for deep melting of hydrous metasomatized mantle: Pliocene high-potassium magmas from the Sierra Nevadas. J. Geophys. Res. 108. doi:10.1029/2002JB002168

England, P., McKenzie, D., 1982. A thin viscous sheet model for continental deformation. Geophys. J. Int. 70, 295–321. doi:10.1111/j.1365-246X.1982.tb04969.x

Green, D.H., Ringwood, A.E., 1967. The stability fields of aluminous pyroxene peridotite and garnet peridotite and their relevance in upper mantle structure. Earth Planet. Sci. Lett. 3, 151–160. doi:10.1016/0012-821X(67)90027-1

Guo, Z., Wilson, M., Liu, J., Mao, Q., 2006. Post-collisional, Potassic and Ultrapotassic Magmatism of the Northern Tibetan Plateau: Constraints on Characteristics of the Mantle Source, Geodynamic Setting and Uplift Mechanisms. J. Petrol. 47, 1177–1220. doi:10.1093/petrology/egl007

Hacker, B.R., Gnos, E., Ratschbacher, L., Grove, M., Mcwilliams, M., Sobolev, S. V, Wan, J., Zhenhan, W., 2000. Hot and Dry Deep Crustal Xenoliths from Tibet. Science (80-.). 287, 2463–2466. doi:10.1126/science.287.5462.2463

Haines, S.S., Klemperer, S.L., Brown, L.D., Guo, J., Mechie, J., Meissner, R., Ross, A., Zhao, W., 2003. INDEPTH III seismic data: From surface observations to deep crustal processes in Tibet. Tectonics 22, 1–18. doi:10.1029/2001TC001305

Harrison, T.M., Copeland, P., Kidd, W.S.F., Lovera, O.M., 1995. Activation of the Nyainqentanghla Shear Zone: Implications for uplift of the southern Tibetan Plateau. Tectonics 14, 658–676. doi:10.1029/95TC00608

Hart, S.R., 1984. A large-scale isotope anomaly in the Southern Hemisphere mantle. Nature 309, 753–757. doi:10.1038/309753a0

Hirose, K., Kawamoto, T., 1995. Hydrous partial melting of lherzolite at 1 GPa: The effect of H2O on the genesis of basaltic magmas. Earth Planet. Sci. Lett. 133, 463–473. doi:10.1016/0012-821X(95)00096-U

Holbig, E.S., Grove, T.L., 2008. Mantle melting beneath the Tibetan Plateau: Experimental constraints on ultrapotassic magmatism. J. Geophys. Res. 113, B04210. doi:10.1029/2007JB005149

Jödicke, H., Jording, A., Ferrari, L., Arzate, J., Mezger, K., Rüpke, L., 2006. Fluid release from the subducted Cocos plate and partial melting of the crust deduced from magnetotelluric studies

in southern Mexico: Implications for the generation of volcanism and subduction dynamics. J. Geophys. Res. Solid Earth 111, 1–22. doi:10.1029/2005JB003739

Jolivet, M., Brunel, M., Seward, D., Xu, Z., Yang, J., Malavieille, J., Roger, F., Leyreloup, A., Arnaud, N., Wu, C., 2003. Neogene extension and volcanism in the Kunlun Fault Zone, northern Tibet: New constraints on the age of the Kunlun Fault. Tectonics 22. doi:10.1029/2002TC001428

Kapp, P.A., DeCelles, P.G., Gehrels, G.E., Heizler, M., Ding, L., 2007. Geological records of the Lhasa-Qiangtang and Indo-Asian collisions in the Nima area of central Tibet. Geol. Soc. Am. Bull. 119, 917. doi:10.1130/B26033.1

Kapp, P.A., Murphy, M.A., Yin, A., Harrison, T.M., 2003. Mesozoic and Cenozoic tectonic evolution of the Shiquanhe area of western Tibet. Tectonics 22. doi:10.1029/2001TC001332

Karplus, M.S., Zhao, W., Klemperer, S.L., Wu, Z., Mechie, J., Shi, D., Brown, L.D., Chen, C., 2011. Injection of Tibetan crust beneath the south Qaidam Basin: Evidence from INDEPTH IV wide-angle seismic data. J. Geophys. Res. 116, 1–23. doi:10.1029/2010JB007911

Kind, R., Yuan, X., Saul, J., Nelson, D., Sobolev, S. V, Mechie, J., Zhao, W., Kosarev, G., Ni, J., Achauer, U., Jiang, M., 2002. Seismic images of crust and upper mantle beneath Tibet: evidence for Eurasian plate subduction. Science (80-.). 298, 1219–1221.

Langille, J.M., Jessup, M.J., Cottle, J.M., Lederer, G., Ahmad, T., 2012. Timing of metamorphism, melting and exhumation of the Leo Pargil dome, northwest India. J. Metamorph. Geol. 30, 769–791. doi:10.1111/j.1525-1314.2012.00998.x

Le Pape, F., Jones, A.G., Vozar, J., Wenbo, W., 2012. Penetration of crustal melt beyond the Kunlun Fault into northern Tibet. Nat. Geosci. 5, 330–335. doi:10.1038/ngeo1449

Li, W., Dong, Y., Guo, A., Liu, X., Zhou, D., 2013. Chronology and tectonic significance of Cenozoic faults in the Liupanshan Arcuate Tectonic Belt at the northeastern margin of the Qinghai–Tibet Plateau. J. Asian Earth Sci. 73, 103–113. doi:10.1016/j.jseaes.2013.04.026

Li, Y., He, J., Wang, C., Santosh, M., Dai, J., Zhang, Y., Wei, Y., Wang, J., 2013. Late Cretaceous K-rich magmatism in central Tibet: Evidence for early elevation of the Tibetan plateau? Lithos 160-161, 1–13. doi:10.1016/j.lithos.2012.11.019

Li, Y., Wang, C., Ma, C., Xu, G., Zhao, X., 2011. Balanced cross-section and crustal shortening analysis in the Tanggula-Tuotuohe Area, Northern Tibet. J. Earth Sci. 22, 1–10. doi:10.1007/s12583-011-0152-2

Li, Y., Wang, C., Zhao, X., Yin, A., Ma, C., 2012. Cenozoic thrust system, basin evolution, and uplift of the Tanggula Range in the Tuotuohe region, central Tibet. Gondwana Res. 22, 482–492. doi:10.1016/j.gr.2011.11.017

Li, Y.L., Zhu, L.D., Dai, J.G., Wang, L.C., Yang, W.G., Wei, Y.S., 2013. Sedimentation and deformation of the Yanghu basin and its tectonic implications in the western Hoh Xil, Central Tibet. Acta Petrol. Sin. 29, 1017–1026.

Liang, X., Sandvol, E., Chen, Y.J., Hearn, T., Ni, J., Klemperer, S., Shen, Y., Tilmann, F., 2012. A complex Tibetan upper mantle: A fragmented Indian slab and no south-verging subduction of Eurasian lithosphere. Earth Planet. Sci. Lett. 333-334, 101–111. doi:10.1016/j.epsl.2012.03.036

Liu, C.-Z., Wu, F.-Y., Chung, S.-L., Zhao, Z.-D., 2011. Fragments of hot and metasomatized mantle lithosphere in Middle Miocene ultrapotassic lavas, southern Tibet. Geology 39, 923–926. doi:10.1130/G32172.1

Liu, Y., Neubauer, F., Genser, J., Ge, X., Takasu, A., Yuan, S., Chang, L., Li, W., 2007. Geochronology of the initiation and displacement of the Altyn Strike-Slip Fault, western China. J. Asian Earth Sci. 29, 243–252. doi:10.1016/j.jseaes.2006.03.002

Lu, H., Wang, E., Meng, K., 2014. Paleomagnetism and anisotropy of magnetic susceptibility of the Tertiary Janggalsay section (southeast Tarim basin): Implications for Miocene tectonic evolution of the Altyn Tagh Range. Tectonophysics. doi:10.1016/j.tecto.2014.01.031

Mahéo, G., Guillot, S., Blichert-Toft, J., Rolland, Y., Pêcher, A., 2002. A slab breakoff model for the neogene thermal evolution of South Karakorum and South Tibet. Earth Planet. Sci. Lett. 195, 45–58. doi:10.1016/S0012-821X(01)00578-7

Manea, V., Gurnis, M., 2007. Subduction zone evolution and low viscosity wedges and channels. Earth Planet. Sci. Lett. 264, 22–45. doi:10.1016/j.epsl.2007.08.030

McCallister, A.T., Taylor, M.H., Murphy, M.A., Styron, R.H., Stockli, D.F., 2014. Thermochronologic constraints on the late Cenozoic exhumation history of the Gurla Mandhata metamorphic core complex, Southwestern Tibet. Tectonics 33, 27–52. doi:10.1002/2013TC003302

McDonough, W.F., Sun, S. -s., 1995. The composition of the Earth. Chem. Geol. 120, 223–253. doi:10.1016/0009-2541(94)00140-4

Mo, X., Zhao, Z., Deng, J., Flower, M.F.J., Yu, X., Luo, Z., Li, Y., Zhou, S., Dong, G., Zhu, D., Wang, L., 2006. Petrology and geochemistry of postcollisional volcanic rocks from the Tibetan plateau: Implications for lithosphere heterogeneity and collision-induced asthenospheric mantle flow. Geol. Soc. Am. Spec. Pap. 409. doi:10.1130/2006.2409(24)

Molnar, P., England, P., Martinod, J., 1993. Mantle dynamics, uplift of the Tibetan Plateau, and the Indian Monsoon. Rev. Geophys. 31, 357–396. doi:10.1029/93RG02030

Murphy, M.A., Yin, A., Harrison, T.M., Durr, S.B., Chen, Z., Ryerson, F.J., Kidd, W.S.F., Wang, X., Zhou, X., 1997. Did the Indo-Asian collision alone create the Tibetan plateau? Geology 25, 719–722. doi:10.1130/0091-7613(1997)025<0719:DTIACA>2.3.CO;2

Murphy, M.A., Yin, A., Kapp, P.A., Harrison, T.M., Lin, D., Jinghui, G., 2000. Southward propagation of the Karakoram fault system, southwest Tibet: Timing and magnitude of slip. Geology 28, 451. doi:10.1130/0091-7613(2000)28<451:SPOTKF>2.0.CO;2

Nábelek, J., Hetényi, G., Vergne, J., Sapkota, S., Kafle, B., Jiang, M., Su, H., Chen, J., Huang, B.-S., 2009. Underplating in the Himalaya-Tibet collision zone revealed by the Hi-CLIMB experiment. Science 325, 1371–4. doi:10.1126/science.1167719

Nunn, C., Roecker, S.W., Tilmann, F.J., Priestley, K.F., Heyburn, R., Sandvol, E. a., Ni, J.F., Chen, Y.J., Zhao, W., Team, T.I., 2013. Imaging the lithosphere beneath NE Tibet: teleseismic P and S body wave tomography incorporating surface wave starting models. Geophys. J. Int. 196, 1724–1741. doi:10.1093/gji/ggt476

Pérez-Campos, X., Kim, Y.H., Husker, A., Davis, P.M., Clayton, R.W., Iglesias, A., Pacheco, J.F., Singh, S.K., Manea, V.C., Gurnis, M., 2008. Horizontal subduction and truncation of the Cocos Plate beneath central Mexico. Geophys. Res. Lett. 35, 1–6. doi:10.1029/2008GL035127

Pilet, S., Baker, M.B., Stolper, E.M., 2008. Metasomatized lithosphere and the origin of alkaline lavas. Science 320, 916–9. doi:10.1126/science.1156563

Powell, C.M., Conaghan, P.J., 1975. Tectonic models of the Tibetan plateau. Geology 3, 727. doi:10.1130/0091-7613(1975)3<727:TMOTTP>2.0.CO;2

Quade, J., Breecker, D.O., Daeron, M., Eiler, J.M., 2011. The paleoaltimetry of Tibet: An isotopic perspective. Am. J. Sci. 311, 77–115. doi:10.2475/02.2011.01

Ratschbacher, L., Krumrei, I., Blumenwitz, M., Staiger, M., Gloaguen, R., Miller, B. V., Samson, S.D., Edwards, M. a., Appel, E., 2011. Rifting and strike-slip shear in central Tibet and the geometry, age and kinematics of upper crustal extension in Tibet. Geol. Soc. London, Spec. Publ. 353, 127–163. doi:10.1144/SP353.8

Roger, F., Tapponnier, P., Arnaud, N., Schärer, U., Brunel, M., Zhiqin, X., Jingsui, Y., 2000. An Eocene magmatic belt across central Tibet: mantle subduction triggered by the Indian collision? Terra Nov. 12, 102–108. doi:10.1046/j.1365-3121.2000.123282.x

Rowley, D.B., Currie, B.S., 2006. Palaeo-altimetry of the late Eocene to Miocene Lunpola basin, central Tibet. Nature 439, 677–81. doi:10.1038/nature04506

Sciunnach, D., Garzanti, E., 2012. Subsidence history of the Tethys Himalaya. Earth-Science Rev. 111, 179–198. doi:10.1016/j.earscirev.2011.11.007

Shi, D., Zhao, W., Brown, L.D., Nelson, D., Zhao, X., Kind, R., Ni, J., Xiong, J., Mechie, J., Guo, J., Klemperer, S., Hearn, T., 2004. Detection of southward intracontinental subduction of Tibetan lithosphere along the Bangong-Nujiang suture by P-to-S converted waves. Geology 32, 209. doi:10.1130/G19814.1

Staisch, L.M., Niemi, N.A., Hong, C., Clark, M.K., Rowley, D.B., Currie, B., 2014. A Cretaceous-Eocene depositional age for the Fenghuoshan Group, Hoh Xil Basin: Implications for the tectonic evolution of the northern Tibet Plateau. Tectonics 33, 281–301. doi:10.1002/2013TC003367

Styron, R.H., Taylor, M.H., Sundell, K., 2015. Accelerated extension of Tibet linked to the northward underthrusting of Indian crust. Nat. Geosci. 8, 131–134. doi:10.1038/ngeo2336

Styron, R.H., Taylor, M.H., Sundell, K.E., Stockli, D.F., Oalmann, J. a. G., Möller, A., McCallister, A.T., Liu, D., Ding, L., 2013. Miocene initiation and acceleration of extension in the South Lunggar rift, western Tibet: Evolution of an active detachment system from structural mapping and (U-Th)/He thermochronology. Tectonics 32, n/a–n/a. doi:10.1002/tect.20053

Sun, J., Zhu, R., An, Z., 2005. Tectonic uplift in the northern Tibetan Plateau since 13.7 Ma ago inferred from molasse deposits along the Altyn Tagh Fault. Earth Planet. Sci. Lett. 235, 641–653. doi:10.1016/j.epsl.2005.04.034

Tapponnier, P., Peltzer, G., Le Dain, A.Y., Armijo, R., Cobbold, P.R., 1982. Propagating extrusion tectonics in Asia: New insights from simple experiments with plasticine. Geology 10, 611. doi:10.1130/0091-7613(1982)10<611:PETIAN>2.0.CO;2

Tapponnier, P., Zhiqin, X., Roger, F., Meyer, B., Arnaud, N.O., Wittlinger, G., Jingsui, Y., 2001. Oblique stepwise rise and growth of the Tibet plateau. Science 294, 1671–7. doi:10.1126/science.105978

Taylor, M.H., Yin, A., 2009. Active structures of the Himalayan-Tibetan orogen and their relationships to earthquake distribution, contemporary strain field, and Cenozoic volcanism. Geosphere 5, 199–214. doi:10.1130/GES00217.1

Taylor, S.R., McLennan, S.M., 1995. The geochemical evolution of the continental crust. Rev. Geophys. 33, 241. doi:10.1029/95RG00262

Tommasini, S., Avanzinelli, R., Conticelli, S., 2011. The Th/La and Sm/La conundrum of the Tethyan realm lamproites. Earth Planet. Sci. Lett. 301, 469–478. doi:10.1016/j.epsl.2010.11.023

Turner, S., Arnaud, N., Liu, J., Rogers, N., Hawkesworth, C., Harris, N., Kelley, S.P., van Calsteren, P., Deng, W., 1996. Post-collision, Shoshonitic Volcanism on the Tibetan Plateau: Implications for Convective Thinning of the Lithosphere and the Source of Ocean Island Basalts. J. Petrol. 37, 45–71. doi:10.1093/petrology/37.1.45

Turner, S., Hawkesworth, C., Liu, J., Rogers, N., Kelley, S., van Calsteren, P., 1993. Timing of Tibetan uplift constrained by analysis of volcanic rocks. Nature 364, 50–54. doi:10.1038/364050a0

Vozar, J., Jones, A.G., Fullea, J., Agius, M.R., Lebedev, S., Le Pape, F., Wei, W., 2014. Integrated geophysical-petrological modeling of lithosphere-asthenosphere boundary in central Tibet using electromagnetic and seismic data. Geochemistry, Geophys. Geosystems 15, 3965–3988. doi:10.1002/2014GC005365

Wang, C., Liu, Z., Yi, H., Liu, S., Zhao, X., 2002. Tertiary crustal shortening and peneplanation in the Hoh Xil region: implications for the tectonic history of the northern Tibetan Plateau. J. Asian Earth Sci. 20, 211–223. doi:10.1016/S1367-9120(01)00051-7

Wang, F., Lo, C., Li, Q., Yeh, M., Wan, J., Zheng, D., Wang, E., 2004. Onset timing of significant unroofing around Qaidam basin, northern Tibet, China: constraints from 40Ar/39Ar and FT thermochronology on granitoids. J. Asian Earth Sci. 24, 59–69. doi:10.1016/j.jseaes.2003.07.004

Wang, Q., Chung, S.-L., Li, X., Wyman, D.A., Li, Z.-X., Sun, W., Qiu, H.-N., Liu, Y.-S., Zhu, Y., 2012. Crustal Melting and Flow beneath Northern Tibet: Evidence from Mid-Miocene to Quaternary Strongly Peraluminous Rhyolites in the Southern Kunlun Range. J. Petrol. 53, 2523–2566. doi:10.1093/petrology/egs058

Wang, Q., Wyman, D. a., Li, Z.-X., Sun, W., Chung, S.-L., Vasconcelos, P.M., Zhang, Q., Dong, H., Yu, Y., Pearson, N., 2010. Eocene north–south trending dikes in central Tibet: New constraints on the timing of east–west extension with implications for early plateau uplift? Earth Planet. Sci. Lett. 298, 205–216. doi:10.1016/j.epsl.2010.07.046

Wang, Z., Gaetani, G. a., 2008. Partitioning of Ni between olivine and siliceous eclogite partial melt: experimental constraints on the mantle source of Hawaiian basalts. Contrib. to Mineral. Petrol. 156, 661–678. doi:10.1007/s00410-008-0308-y

Wu, Z., Barosh, P.J., Zhonghai, W., Hu, D., Xun, Z., Peisheng, Y., 2008. Vast early Miocene lakes of the central Tibetan Plateau. Geol. Soc. Am. Bull. 120, 1326. doi:10.1130/B26043.1

Xia, L., Li, X., Ma, Z., Xu, X., Xia, Z., 2011. Cenozoic volcanism and tectonic evolution of the Tibetan plateau. Gondwana Res. 19, 850–866. doi:10.1016/j.gr.2010.09.005

Yang, D., Ding, L., 2013. Geochronology and geochemistry of the high magnesium and high potassium ultrabasic leucite basanite in northern Tibetan Plateau. Chinese J. Geol. 48, 449–467.

Yang, W., 2012. Thermal State and Strength of the Lithosphere Beneath the Chinese Mainland. Acta Geol. Sin. - English Ed. 86, 810–827. doi:10.1111/j.1755-6724.2012.00708.x

Yin, A., Dang, Y.-Q., Wang, L.-C., Jiang, W.-M., Zhou, S.-P., Chen, X.-H., Gehrels, G.E., McRivette, M.W., 2008. Cenozoic tectonic evolution of Qaidam basin and its surrounding regions (Part 1): The southern Qilian Shan-Nan Shan thrust belt and northern Qaidam basin. Geol. Soc. Am. Bull. 120, 813. doi:10.1130/B26180.1

Yin, A., Zhang, M., McRivette, M.W., Burgess, W.P., 2007. Cenozoic tectonic evolution of Qaidam basin and its surrounding regions (Part 2): Wedge tectonics in southern Qaidam basin and the Eastern Kunlun Range. Geol. Soc. Am. Spec. Pap. 433, 369–390. doi:10.1130/2007.2433(18)

Yuan, D.-Y., Champagnac, J.-D., Ge, W.-P., Molnar, P., Zhang, P.-Z., Zheng, W.-J., Zhang, H.-P., Liu, X.-W., 2011. Late Quaternary right-lateral slip rates of faults adjacent to the lake Qinghai, northeastern margin of the Tibetan Plateau. Geol. Soc. Am. Bull. 123, 2016–2030. doi:10.1130/B30315.1

Yuan, D.-Y., Ge, W.-P., Chen, Z.-W., Li, C.-Y., Wang, Z.-C., Zhang, H.-P., Zhang, P.-Z., Zheng, D.-W., Zheng, W.-J., Craddock, W.H., Dayem, K.E., Duvall, A.R., Hough, B.G., Lease, R.O., Champagnac, J.-D., Burbank, D.W., Clark, M.K., Farley, K. a., Garzione, C.N., Kirby, E., Molnar, P., Roe, G.H., 2013. The growth of northeastern Tibet and its relevance to large-scale continental geodynamics: A review of recent studies. Tectonics 32, 1358–1370. doi:10.1002/tect.20081

Zhang, H.-P., Craddock, W.H., Lease, R.O., Wang, W., Yuan, D.-Y., Zhang, P.-Z., Molnar, P., Zheng, D.-W., Zheng, W.-J., 2012. Magnetostratigraphy of the Neogene Chaka basin and its implications for mountain building processes in the north-eastern Tibetan Plateau. Basin Res. 24, 31–50. doi:10.1111/j.1365-2117.2011.00512.x

Zhang, L., Ducea, M.N., Ding, L., Pullen, A., Kapp, P.A., Hoffman, D., 2014. Southern Tibetan Oligocene–Miocene adakites: A record of Indian slab tearing. Lithos 210-211, 209–223. doi:10.1016/j.lithos.2014.09.029

Zhang, Z., Wang, Y., Houseman, G. a., Xu, T., Wu, Z., Yuan, X., Chen, Y., Tian, X., Bai, Z., Teng, J., 2014. The Moho beneath western Tibet: Shear zones and eclogitization in the lower crust. Earth Planet. Sci. Lett. 408, 370–377. doi:10.1016/j.epsl.2014.10.022

Zhang, Z., Xiang, H., Dong, X., Ding, H., He, Z., 2015. Long-lived high-temperature granulite-facies metamorphism in the Eastern Himalayan orogen, south Tibet. Lithos 212-215, 1–15. doi:10.1016/j.lithos.2014.10.009

Zhang, Z., Yang, L., Teng, J., Badal, J., 2011. An overview of the earth crust under China. Earth-Science Rev. 104, 143–166. doi:10.1016/j.earscirev.2010.10.003

Zhao, W., Kumar, P., Mechie, J., Kind, R., Meissner, R., Wu, Z., Shi, D., Su, H., Xue, G., Karplus, M., Tilmann, F., 2011. Tibetan plate overriding the Asian plate in central and northern Tibet. Nat. Geosci. 4, 870–873. doi:10.1038/ngeo1309

Zheng, D., Zhang, P.-Z., Wan, J., Yuan, D., Li, C., Yin, G., Zhang, G., Wang, Z., Min, W., Chen, J., 2006. Rapid exhumation at ~8 Ma on the Liupan Shan thrust fault from apatite fission-track thermochronology: Implications for growth of the northeastern Tibetan Plateau margin. Earth Planet. Sci. Lett. 248, 198–208. doi:10.1016/j.epsl.2006.05.023

Zhu, L., Helmberger, D. V., 1998. Moho Offset Across the Northern Margin of the Tibetan Plateau. Science (80-.). 281, 1170–1172. doi:10.1126/science.281.5380.1170

Zhuang, G., Hourigan, J.K., Ritts, B.D., Kent-Corson, M.L., 2011. Cenozoic multiple-phase tectonic evolution of the northern Tibetan Plateau: Constraints from sedimentary records from Qaidam basin, Hexi Corridor, and Subei basin, northwest China. Am. J. Sci. 311, 116–152. doi:10.2475/02.2011.02

.

Chapter 5: Summary and Conclusions

5.1 Summary of primary dissertation results

Results of this dissertation focus on resolving outstanding issues regarding the evolution of the Indo-Asian orogen over the last 50 Myr. Chapter 2 focuses on orogen-scale mass balance, shows that the northern Indian margin and the Asian interior must have been 23-29 km thick at the time of collision, and strongly supports the redistribution of Indian material beneath the Tibetan Plateau through underplating or lower crustal flow. Chapter investigates the Guaizi Liang of northern Tibet, which are a unique example of thrust faulting at ~5000 m elevation. Based on the orientation and magnitude of shortening in the area, we suggest that slip transfer between the nearby Altyn Tagh and Kunlun/Manyi faults generates a broad region of simple shear. As simple shear does not result in crustal thickening, it does not result in changes in gravitational potential energy, and provides a mechanism for thrust faulting to occur at high elevations. Chapter 4 includes new geochemical and geochronologic data, which is synthesized with previous studies to investigate the evolution of the lithosphere in the Tibetan Plateau. Results show that volcanism was likely generated by oceanic subduction prior to collision. After a ~10 Ma period of quiescence, removal of a flat Tethyian slab likely resulted in an influx of hot asthenosphere and melting of subduction metasomatized lithosphere. Subsequent Indian underthrusting led to the termination of volcanism in the southern Tibetan Plateau by thickening the lithosphere and insulating Asian crust. Overall, results of this thesis support the redistribution of Indian crust beneath the Tibetan Plateau, and flow of lower crustal material to the margins of the orogen.

5.1.1 Chapter 2 summary

This chapter investigates the mass balance of the Indo-Eurasian orogen and pre-existing regions of high topography prior to the time of collision. The modern volume of the Indo-Asian orogen is estimated at ~390 x 10^6 km^3 using a compilation of regional geophysical studies which constrain the crustal thickness of specific portions of the orogen. The area of the orogen at the time of collision is constrained using a range of published estimates for Indo-Asian convergence. A synthesis of published cross sections and shortening values shows that only 320-500 km of the ~2500 km total convergence between India and Asia was accommodated in Asian crust. If input areas

had a crustal thickness equal to the modern global average of ~41 km, then the inferred volume of the orogen prior to collision is ~200 x 10^6 km^3 greater than that estimated for the modern, requiring recycling of a volume equal to half of the modern orogen into the mantle. However, if input areas were 23-32 km thick, as is compatible with sedimentologic, geomorphic, and paloclimatic records, this imbalance is eliminated. This result argues strongly against studies which suggest that large swaths of the eastern and northern Tibetan Plateau had thick crust and were at high elevations prior to the time of collision. A thin crust in the northern Tibetan Plateau and India, a thick crust in the southern Tibetan Plateau prior to collision, and limited Asian shortening since the time of collision, require underplating of India beneath the Tibetan Plateau and transfer of material beneath the plateau through the flow of a ductile lower crustal channel.

5.1.2 Chapter 3 summary

Chapter 3 focuses on the Guaizi Liang of the northern Tibetan Plateau, a young, active thrust belt located at elevations of ~5000 m. I assess 9 km or 20% shortening in the Guaizi Liang using a balanced cross section, and note that deformation must have begun in Pliocene time based on a transition from fine-grained basin sediments to conglomerates at the top of the deformed Pliocene Hongliang Formation. The age of a folded alluvial surface, and its total surface uplift are derived using a ^{36}Cl cosmogenic radionuclide depth profile, and a geomorphic reconstruction of its elevation at the time of deposition, respectively. These suggest that surface uplift rates over the last 206 ka average ~3.4 mm/yr, and shortening rates are ~1.7 mm/yr. Using the estimated ~9 km of total shortening in the region, shortening rates confirm a Pliocene initiation age for deformation. Compressional shortening is likely generated by slip transfer between the Altyn Tagh and Kunlun/Manyi faults, which I suggest form a broad region of simple shear. Simple shear provides a mechanism for generating thrust faulting without necessarily thickening the crust, and increasing its gravitational potential energy. Pure shear and crustal thickening southwest of the Qaidam Basin should be minimal, as we estimate that slip on the Altyn Tagh and Kunlun/Manyi faults can accommodate the entirety of north-south strain due to Indo-Asian convergence. Similarly, an absence of other young contractional mountain belts on Chinese geologic maps of the region suggests that overall pure shear, and crustal thickening is minimal in the recent geological record. Observations in the Guaizi Liang therefore do not contradict those made in the remainder of the orogen, where crustal shortening is limited to elevations below 4000 m. Deformation in the Guaizi Liang as then also provides the first published age constraint on the Manyi fault, which I suggest initiated at ~5 Ma.

5.1.3 Chapter 4 summary

Chapter 4 investigates the temporal and spatial changes in the geochemistry of lavas in the Tibetan Plateau, and their geodynamic implications. I compile 27 new samples from the northern Tibetan Plateau with over 800 previously published data to define end-member compositions of volcanism in the region. Results show that lavas can generally be categorized in two groups. Group A lavas are widespread prior to 40 Ma, and show geochemical signatures typical of subduction and arc volcanism. These are present in both the northern and central portions of the Tibetan Plateau. Arc volcanism at the southern end of the orogen is likely due to subduction of the Tethyian oceanic slab prior to collision. In the central Tibetan Plateau arc volcanism and coeval plutonism may have been driven by the reactivation of a fossilized subduction zone between ~60 and 40 Ma. Group B lavas generally erupted after 30 Ma and have compositions indicative of low-degree melting of a subduction metasomatized mantle lithosphere. Sr, Nd, and Pb isotopic ratios suggest that metasomatism likely involved partial melting of sediments from the northern Indian margin which were subducted beneath the Tibetan Plateau. As evidence of metasomatism is wholly absent in group A lavas, metasomatism must have taken place between 30 and 40 Ma, which we link to the flattening of the Tethyian slab or thinning of the mantle wedge during the initial stages of Indian collision. Subsequent removal or rollback of the Tethyain slab at 30 Ma then resulted in asthenospheric upwelling and widespread volcanism across the plateau sourced from subduction metasomatized mantle lithosphere. New data from the northern Tibetan Plateau provides evidence for volcanism at ~28 Ma. This is 8-13 Myr older than prosed a proposed 10-15 Ma episodes of lithospheric removal which has been linked to the initiation of volcanism and normal faulting in the region. I instead suggest that the initiation of normal faulting, and coeval termination of volcanism in the southern and south central Tibetan Plateau are due to Indian underthrusting, and thickening of the lithosphere.

5.2 Implications for the Indo-Asian orogen and directions for future work

Results from this thesis strongly support proposals for the redistribution of lower crust across the Indo-Eurasian orogen (e.g. Clark and Royden, 2000), likely occurring near 10 Ma in northern, and the eastern Tibetan Plateau (Duvall et al., 2012). Chapter 2 shows that the Indian contribution to orogenic volumes must be transferred beneath Asian crust, likely via underplating and the development of a lower crustal channel. Results in chapter 4 argue strongly against a coeval episode of lithospheric removal and extensional faulting by pushing back the onset of volcanism across the plateau to 30 Ma, 10-20 Myr prior to the initiation of extension across the orogen. This contrasts with earlier work which suggested that an episode of lithospheric removal and an influx of hot

asthenosphere resulted in topographic gain, crustal extension, and widespread volcanism at ~10 Ma (e.g. Molnar et al., 1993; Turner et al., 1993). Chapter 3 points to the necessity of mechanisms other than crustal shortening to bring portions of the Tibetan Plateau to modern elevations of over 5000 m, by proposing that compression in the ~5000 m high Guaizi Liang is driven by simple shear, and that crustal thickening must have either occurred earlier or by a mechanism that did not involve shortening the upper crust.

In chapter 4, I propose that Indian underthrusting may be the cause of flow of lower crustal material beneath the northern, and eastern portions of the Tibetan Plateau. The emplacement of Indian crust beneath the southern Tibetan Plateau would thicken the crustal column, increase its gravitational potential energy, and result in extension. A ~70-80 km thick crust may also result in low-degree melting of the lower crust, decreasing its strength, and thereby lowering its viscosity sufficiently to allow it to flow to the margins of the orogen. Future work should seek to assess this hypothesis by using geophysical studies to investigate the state of the lithosphere beneath Tibet, geochemically fingerprint Indian vs Asian crustal compositions, and link them to observed chemistries of lower-crust derived melts. The results of this thesis argue against a Miocene episode of lithospheric removal, and suggest that this process occurred earlier in the orogen's history. High surface heat flows, pervasive volcanism, and geophysical data, suggest that the lithosphere is thin beneath the northern Tibetan Plateau today (Yang, 2012; Vozar et al., 2014). New data from chapter 4 suggest that this process may have occurred near 27 Ma, and additional data from further sites in the region would strengthen this conclusion. Overall, how, and when the lithosphere beneath the northern Tibetan Plateau became thinned should be a focus of additional research.

Gaps in datasets which were presented and compiled in this thesis highlight the need for continuing work in remote regions of the Tibetan Plateau. Further work should focus on western regions of the central and northern Tibetan Plateau where previous studies suggest that the region contains nearly continuous records of sedimentation, paleoenvironmental conditions, deformation and volcanism going back as far as Cretaceous time (Kapp et al., 2005; Chung et al., 2005; Zhang et al., 2008; Ratschbacher et al., 2011). This may provide an abundance and length of potential datasets which are unequaled in other parts of the orogen, and may aid in combining disparate hypotheses developed at the margins of the Tibetan Plateau. However, studies investigating these regions are sparse, with only a few data points in a region the size of the US state of Texas. As such, there is ample potential for further work which would investigate and integrate these records to elucidate the tectonic and topographic evolution of the Indo-Asian orogen. As an example, the western Tibetan Plateau

should contain the along-strike equivalent of the syncollisional plutonism observed in the Tanggula Shan (Roger et al., 2000) and related volcanism, deformation, and sedimentation. Additional investigations would test the proposed subduction of Songpan-Ganzi oceanic crust proposed in Chapter 4, and aid in evaluating whether the shutoff of volcanism in the southern Tibetan Plateau at 10 Ma was related to Indian underthrusting. Geophysical studies seeking to estimate the depth of the lithosphere-asthenosphere boundary in the region would be critical in making these assessments. This thesis provides a strong contribution to our understanding of the evolution of the Indo-Asian orogen, but also highlights the abundance of opportunities for further investigation.

5.3 References

Chung, S.-L., Chu, M.-F., Zhang, Y., Xie, Y., Lo, C.-H., Lee, T.-Y., Lan, C.-Y., Li, X., Zhang, Q., and Wang, Y., 2005, Tibetan tectonic evolution inferred from spatial and temporal variations in post-collisional magmatism: Earth-Science Reviews, v. 68, p. 173–196, doi: 10.1016/j.earscirev.2004.05.001.

Clark, M.K., and Royden, L.H., 2000, Topographic ooze: Building the eastern margin of Tibet by lower crustal flow: Geology, v. 28, p. 703, doi: 10.1130/0091-7613(2000)28<703:TOBTEM>2.0.CO;2.

Duvall, A.R., Clark, M.K., Avdeev, B., Farley, K. a., and Chen, Z., 2012, Widespread late Cenozoic increase in erosion rates across the interior of eastern Tibet constrained by detrital low-temperature thermochronometry: Tectonics, v. 31, doi: 10.1029/2011TC002969.

Kapp, P.A., Yin, A., Harrison, T.M., and Ding, L., 2005, Cretaceous-Tertiary shortening, basin development, and volcanism in central Tibet: Geological Society of America Bulletin, v. 117, p. 865, doi: 10.1130/B25595.1.

Molnar, P., England, P., and Martinod, J., 1993, Mantle dynamics, uplift of the Tibetan Plateau, and the Indian Monsoon: Reviews of Geophysics, v. 31, p. 357–396, doi: 10.1029/93RG02030.

Ratschbacher, L., Krumrei, I., Blumenwitz, M., Staiger, M., Gloaguen, R., Miller, B. V., Samson, S.D., Edwards, M. a., and Appel, E., 2011, Rifting and strike-slip shear in central Tibet and the geometry, age and kinematics of upper crustal extension in Tibet: Geological Society, London, Special Publications, v. 353, p. 127–163, doi: 10.1144/SP353.8.

Roger, F., Tapponnier, P., Arnaud, N., Schärer, U., Brunel, M., Zhiqin, X., and Jingsui, Y., 2000, An Eocene magmatic belt across central Tibet: mantle subduction triggered by the Indian collision? Terra Nova, v. 12, p. 102–108, doi: 10.1046/j.1365-3121.2000.123282.x.

Turner, S., Hawkesworth, C., Liu, J., Rogers, N., Kelley, S.P., and van Calsteren, P., 1993, Timing of Tibetan uplift constrained by analysis of volcanic rocks: Nature, v. 364, p. 50–54, doi: 10.1038/364050a0.

Vozar, J., Jones, A.G., Fullea, J., Agius, M.R., Lebedev, S., Le Pape, F., and Wei, W., 2014, Integrated geophysical-petrological modeling of lithosphere-asthenosphere boundary in central Tibet using electromagnetic and seismic data: Geochemistry, Geophysics, Geosystems, v. 15, p. 3965–3988, doi: 10.1002/2014GC005365.

Yang, W., 2012, Thermal State and Strength of the Lithosphere Beneath the Chinese Mainland: Acta Geologica Sinica - English Edition, v. 86, p. 810–827, doi: 10.1111/j.1755-6724.2012.00708.x.

Zhang, K.X., Wang, G.C., Cao, K., Liu, C., Xiang, S.Y., Hong, H.L., Kou, X.H., Xu, Y.D., Chen, F.N., Meng, Y.N., and Chen, R.M., 2008, Cenozoic sedimentary records and geochronological constraints of differential uplift of the Qinghai-Tibet Plateau: Science in China, Series D: Earth Sciences, v. 51, p. 1658–1672, doi: 10.1007/s11430-008-0132-2.

.

Appendix A: New Data from the Hoh Xil Basin

We collected twenty seven samples from the Hoh Xil Basin of the northern Tibetan Plateau from four eruptive centers (Figure A.1). Samples were analyzed for their major and trace element compositions, with a subset analyzed for their Pb, Nd, Sr, and Hf isotopic compositions. Age constraints on individual volcanic fields was obtained through $^{40}Ar/^{39}Ar$, zircon U-Pb, and apatite (U-Th)/He dating. Two samples (12HXV01 and 12HXV33) were collected at a single cinder cone, measuring ~150 m in diameter. Remaining samples are from larger volcanic fields ranging in size from 12-1200 km^2 which record multiple eruption cycles. Each field contained a suite of volcanic compositions, ranging from trachyandesites to rhyolites. Sampling and geochemical analysis focused on more mafic end-members in order to obtain the most primitive compositions, and reduce crustal contamination.
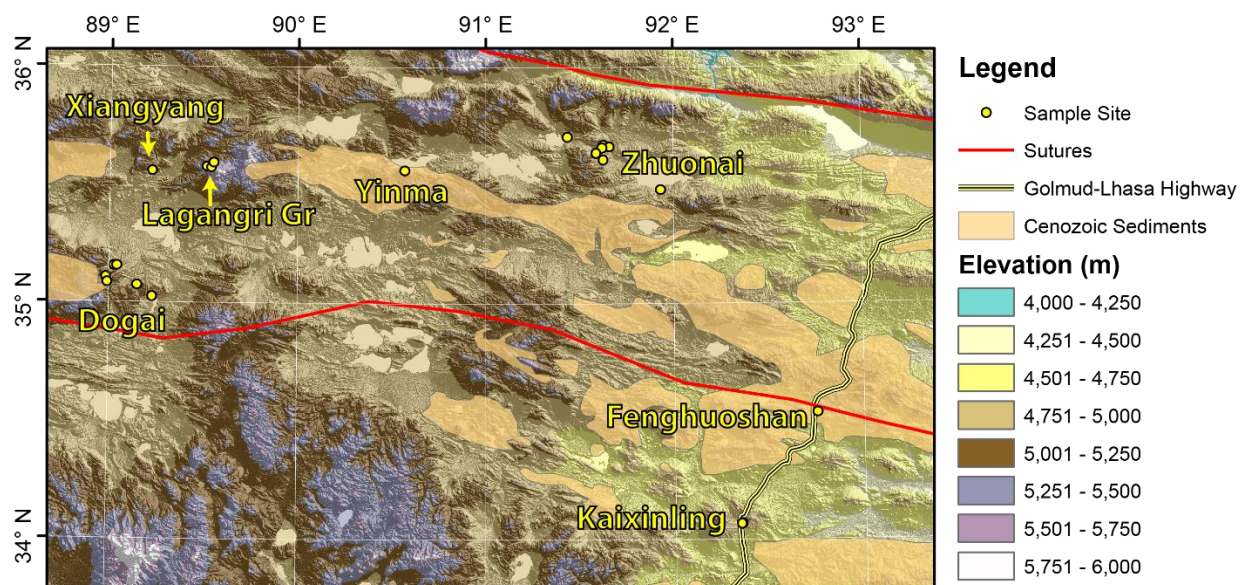
Figure A.1 – Sample sites in the Hoh Xil Basin. Mapped sutures are the Kunlun (north) and Jinsha (south). Yellow text denotes locality names. Map uses an Albers equal area conic projection with a central meridian at 91°E and standard parallels of 22°N and 42°N. Elevation from the SRTM Dataset.

A.1 Analytical Methods

We analyzed the major and trace element compositions of all collected samples showing minimal alteration and weathering. A subset of these samples, focusing on more mafic compostions, was chosen for detailed Hf, Sr, Nd, and Pb isotope analysis. Major and trace element analyses were performed by ALS Labs, Inc. for samples beginning with 13DV, 13LG and 13XV. Oxides were measured using lithium-borate fusion XRF, and trace element compositions were analyzed using LA-ICPMS[4]. Sample names starting with 12H were analyzed at the Washington State GeoAnalytical lab, with major elements determined using XRF (see Johnson et al., 1999 for detailed methodology), and trace element using an Agilent 7700 LA-ICPMS[5]. Precision for trace element analysis is 10% for rare earth elements, and 5% for other trace elements. Major element compositions of samples in the 11UMT series we analyzed by tetraborate fusion XRF at Act Labs, Inc. using methods and standards of Norrish and Hutton, (1969). Trace element compostions of samples in the 11UMT series were analyzed at the Washington State GeoAnalytical lab by LA-ICPMS. One sample, 12HXV33 was analyzed at both Washington State and ALS Labs to ensure inter-lab consistency.

Pb, Sr, Nd and Hf isotopic measurements were performed at the Mass Spectrometer Analytical Facility, Brown University. About 1 gm of sample powders were leached with 6N double distilled HCl for about 1 hour at 100° C and triple rinsed with 18 MΩ H_2O. Samples were centrifuged between each rinsing step to ensure removal of acid. Samples were then dried, and ~100 mg of powder was dissolved in a double distilled 3:1 $HF:HNO_3$ mixture. Pb was separated from the matrix using AG1-X8 (100-200 mesh, BIO-RAD) resin. Hf was separated using using Ln resin (Eichrom). The remaining matrix was passed through TRU-spec resin (Eichrom) to separate Rb-Sr from REE. The Rb-Sr fraction was then passed through Sr-spec resin (Eichrom) to get a clean Sr fraction. The remaining REE fraction was then passed through Ln resin (Eichrom) to get a clean Nd fraction.

Isotopic compositions were measured on a Thermo Scientific Neputne Plus MC-ICP-MS. Sr, Nd and Hf were introduced into the plasma using a PFA nebulizer with a flow rate of ~70 μl/min coupled with a glass spray chamber, while Pb was introduced with an APEX-IR introduction system to enhance the sensitivity. The mass spectrometer was equipped with an H-skimmer cone and H-sampler cone. The baseline measurement was taken at -0.5 amu. $^{87}Sr/^{86}Sr$, $^{143}Nd/^{144}Nd$, and $^{176}Hf/^{177}Hf$

---

[4] Detailed methods, and analytical precision for individual analyses may be found at http://www.alsglobal.com/en/Our-Services/Minerals/Geochemistry/Downloads. Samples were submitted for the "Complete Characterization" package.
[5] See http://environment.wsu.edu/facilities/geolab/technotes/icp-ms_method.html for detailed methods.

were corrected for instrumental mass fractionation using values of $^{88}Sr/^{86}Sr = 0.1194$, $^{146}Nd/^{144}Nd = 0.7219$ and $^{176}Hf/^{177}Hf = 0.7325$ with an exponential law. Pb solution was spiked with NBS SRM-997 Tl standard prior to analysis with a $Pb/Tl = 4$ to correct for the mass fractionation using an exponential law with a $^{203}Tl/^{205}Tl = 0.418922$. Sr, Nd and Hf were measured at 200 ppb concentration whereas Pb was measured at 75 ppb concentration level. $^{87}Sr/^{86}Sr$, $^{143}Nd/^{144}Nd$ and $^{176}Hf/^{177}Hf$ of samples are reported relative to NBS SRM 987 $^{87}Sr/^{86}Sr = 0.71024$, JNd-i Nd standard $^{143}Nd/^{144}Nd = 0.512115$ and JMC-475 Hf standard $^{176}Hf/^{177}Hf = 0.282160$ respectively. $^{206}Pb/^{204}Pb$, $^{207}Pb/^{204}Pb$, $^{208}Pb/^{204}Pb$ are reported relative to the NBS 981 standard $^{206}Pb/^{204}Pb = 16.9356$, $^{207}Pb/^{204}Pb = 15.4891$, and $^{208}Pb/^{204}Pb = 36.7006$ (Todt et al., 1996). The external precision on the ratios over the course of two years is 30 ppm for Sr (2σ, n = 75) and Nd (2σ, n = 104), 40 ppm for Hf (2σ, n = 89) and 45-80 ppm (2σ, n = 75) Pb. The Sr and Pb blanks were < 50 pg, and Nd and Hf blanks were < 30 pg. The USGS reference material BIR-1 was processed during sample preparation and measured with the same instrument set up. Measured Sr, Nd, Hf and Pb isotope ratios for BIR-1 are in agreement with those reported in the GeoRem database.

We performed $^{40}Ar/^{39}Ar$, zircon U-Pb and apatite (U-Th)/He dating on a subset of samples from each volcanic field in order to constrain sample eruption ages. U-Pb dating was performed at the University of Arizona LaserChron Center using a Nu Instrument MC-ICPMS with a 30 micron spot size and 15 micron pit depth (see Gehrels et al., 2008 for detailed methods). Prior to analysis, mineral separates and standards were placed in 1" epoxy mounts, sanded to a depth of 20 microns, polished, imaged using cathode-luminescence, and cleaned.

Whole rock $^{40}Ar/^{39}Ar$ dating for samples 12HXV01, 12HXV03, 12HXV11, 12HXV17, and 13XV05 was performed at the USGS $^{40}Ar/^{39}Ar$ Laboratory in Denver, Co. using a Thermo Scientific ARGUSVI mass spectrometer. All data were corrected for blanks, radioactive decay, nucleogenic interferences, mass discrimination, and detector intercalibration. Ages were calculated using most recent constraints on decay constants, atmospheric $^{40}Ar/^{36}Ar$, and the age of the Fish Canyon sanidine standard (Min et al., 2000; Lee et al., 2006; Kuiper et al., 2008). Argon isotope data for masses 40-37 were collected simultaneously on a faraday collector, with mass 36 collected on an ion counter.

Samples 13DV22 and 13DV13 were analyzed at the University of Michigan Argon Geochronology Laboratory. ~2 mm chips of clean, unaltered rock were packed in pure Al foil irradiated at location 8C of the McMaster Nuclear Reactor for 90 MWhr in package mc46. Hornblende MMhb-1 was used as a neutron fluence monitor with an assumed age of 520.4 Ma (Samson and Alexander, 1987). Samples were heated for 30 second increments with a Coherent Innova 70 5W

continuous argon-ion laser until complete fusion was achieved. Ar isotopic measurements were performed using a VG1200S noble gas mass spectrometer operating at 150 μA total emission and equipped with a Daly detector. Fusion blanks were run every five fusion steps and blank levels from argon masses 36 through 40 were subtracted from sample gas fractions. Corrections were made for the decay of ^{37}Ar and ^{39}Ar, interfering nucleogenic reactions from K, Ca and Cl, as well as the production of ^{36}Ar from the decay of ^{36}Cl.

Apatite (U-Th)/He dating was performed at the University of Michigan on an ASI Alphachron quadruple mass spectrometer via ^{3}H isotope dilution mass spectrometry. Single grain inclusion-free aliquots were handpicked from mineral separates, and placed in individual pre-cleaned platinum tubes. Tubes were heated to 900°C with a 980 nm diode laser for five minutes in vacuum to release contained helium. Temperature was verified with a built-in Impac pyrometer. Gas was then extracted to the mass spectrometer and the chamber cleared. A second heating step was then performed to test for the presence of hereto unrecognized radiogenic inclusions, with grains showing helium content above baseline rejected from further analysis Parent isotope (U, Th, Sm) measurement was performed on an Element2 single-collector high-resolution ICP-MS at the University of Arizona following methodology of Reiners and Nicolescu, (2006). Measured lengths, and widths of each individual grain were then used to obtain an Ft correction (Farley et al., 1996), and calculate individual grain ages.

A.2 Geochronology Results

Results of geochemical analyses may be found in Appendix B. Geochronological results are summarized below (**Error! Reference source not found.**), with additional data tables (Table A.2, Table A.3) and figures (Figure A.2, Figure A.3, Figure A.4) for individual techniques. Results show that samples collected in the Dogai Volcanic field erupted between 7.53 and ~9.0 Ma based on the range of plateau ages from whole rock ^{40}Ar/^{39}Ar analyses for two samples, and their replicates. Two tuffs collected in the Lagangri Graben are estimated as having erupted at 1.96 Ma based on Apatite (U-Th)/He analyses. This low temperature thermochronometer should be sensitive to the rapid cooling of an air fall tuff. As sampled units were unburied, ages should be representative of the time of eruption. Eruption ages in the Xiangyang Hu Volcanic Filed are estimated at ~8.5 Ma using both whole rock ^{40}Ar/^{39}Ar, and zircon (U-Pb) ages (**Error! Reference source not found.**). A single whole rock ^{40}Ar/^{39}Ar age constrains the eruption age of lavas in a prominent mesa near Yinma Hu to 13.36 Ma. A small cinder cone found near Zhuonai Hu erupted at ~23.89 Ma based on a single biotite ^{40}Ar/^{39}Ar age. This predates the eruption of a large volcanic field to the northwest by ~10 My, where

volcanism occurred at ~13 Ma based on both whole rock ^{40}Ar/^{39}Ar and zircon U-Pb age dates (**Error! Reference source not found.**).

Table A.1 – Summary of age data, and associated uncertainties.

Sample	Locality	Age (Ma)	Uncertainty (Ma)	Method
13DV13	Dogai Volcanics	9.004	±0.069	WR Ar/Ar Pl
13DV13	Dogai Volcanics	8.93	±0.06	WR Ar/Ar Pl
13DV22	Dogai Volcanics	7.53	±0.086	WR Ar/Ar Pl
13DV22	Dogai Volcanics	7.943	±0.073	WR Ar/Ar Pl
12HG06	Lagangri Graben	1.96	±0.05	Ap He
13XV05	Xiangyang Hu Volcanics	8.46	±0.03	WR Ar/Ar Pl
13XV06	Xiangyang Hu Volcanics	8.5	+0.21/-0.14	Zr U-Pb
12HXV11	Yinma Volcanics	13.36	±0.011	WR Ar/Ar Int
12HXV01	Zhuonai Cinder Cone	23.89	±0.04	Bio Ar/Ar
12HXV03	Zhuonai Volcanic Field	12.97	±0.009	WR Ar/Ar Int
12HXV17	Zhuonai Volcanic Field	13	±0.007	WR Ar/Ar Int
12HXV24	Zhuonai Volcanic Field	13.69	+0.21/-0.28	Zr U-Pb
12HXV32	Zhuonai Volcanic Field	13	+0.31/-0.23	Zr U-Pb

Abbreviations for methods are as follows: Ap He – Apatite (U-Th)/He, Zr U-Pb – Zircon U-Pb via LA-ICPMS, Bio Ar/Ar – Biotite ^{40}Ar/^{39}Ar plateau age, WR Ar/Ar Pl – Whole rock ^{40}Ar/^{39}Ar plateau age, WR Ar/Ar Int – Whole rock ^{40}Ar/^{39}Ar integrated age. Uncertainties for ^{40}Ar/^{39}Ar results are at the 2-σ level, for U-Pb analysis at confidence level shown in individual plots in Figure A.2 as determined by the TuffZirc algorithm of Ludwig, (2008), and for (U-Th)/He data represented by standard error of analyzed grains.
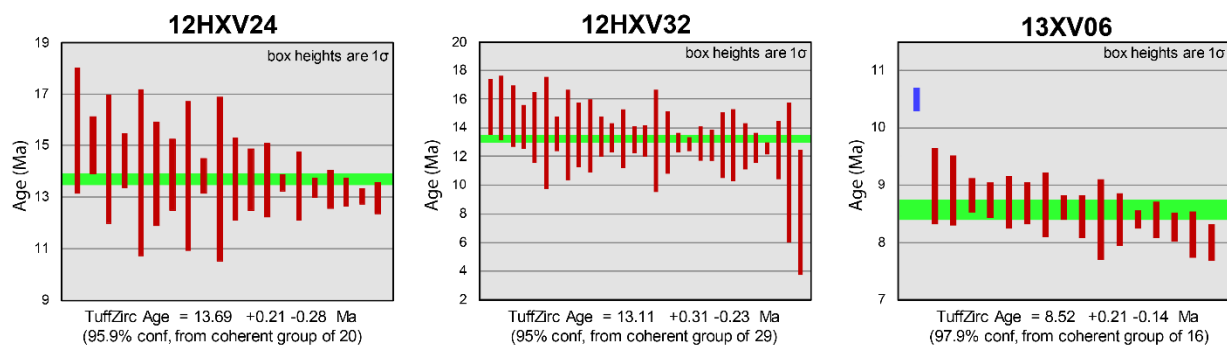
Figure A.2– Zircon U-Pb age distributions, and eruption ages calculated with TuffZirc (Ludwig, 2008). See **Table A.2** – Zircon U-Pb analyses.Table A.2 for individual grain ages.
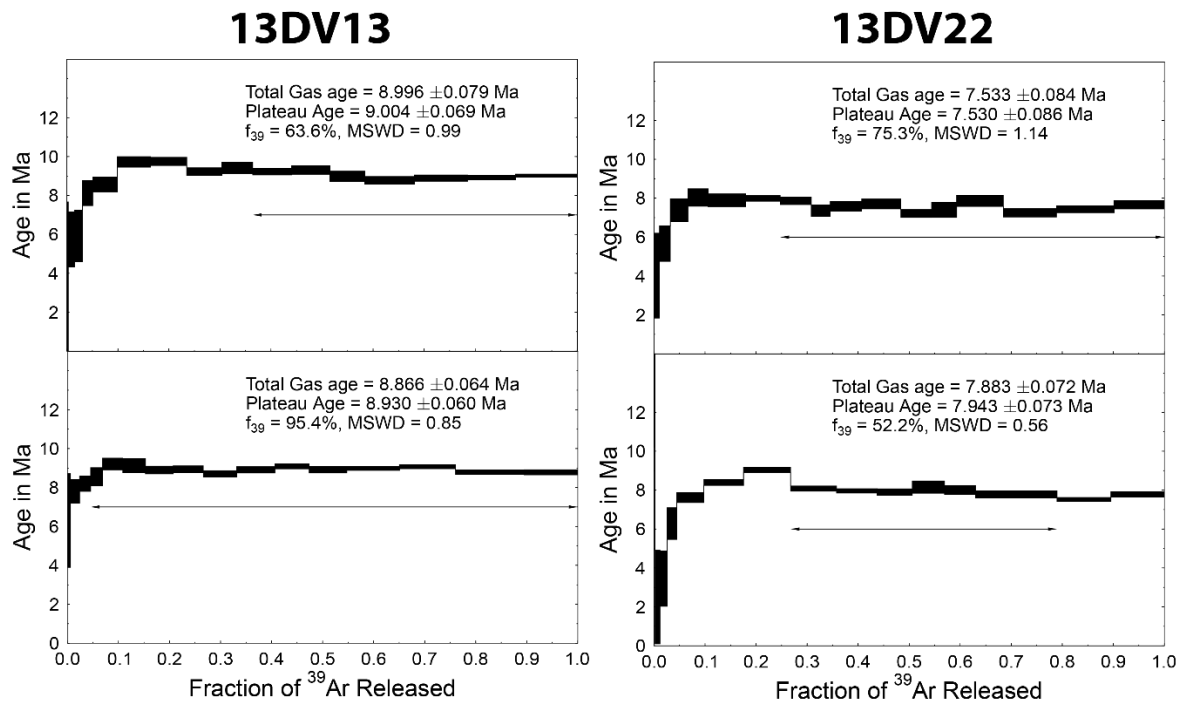
Figure A.3 – $^{40}Ar/^{39}Ar$ age spectra for samples analyzed at the University of Michigan. Note that each sample has two replicates.
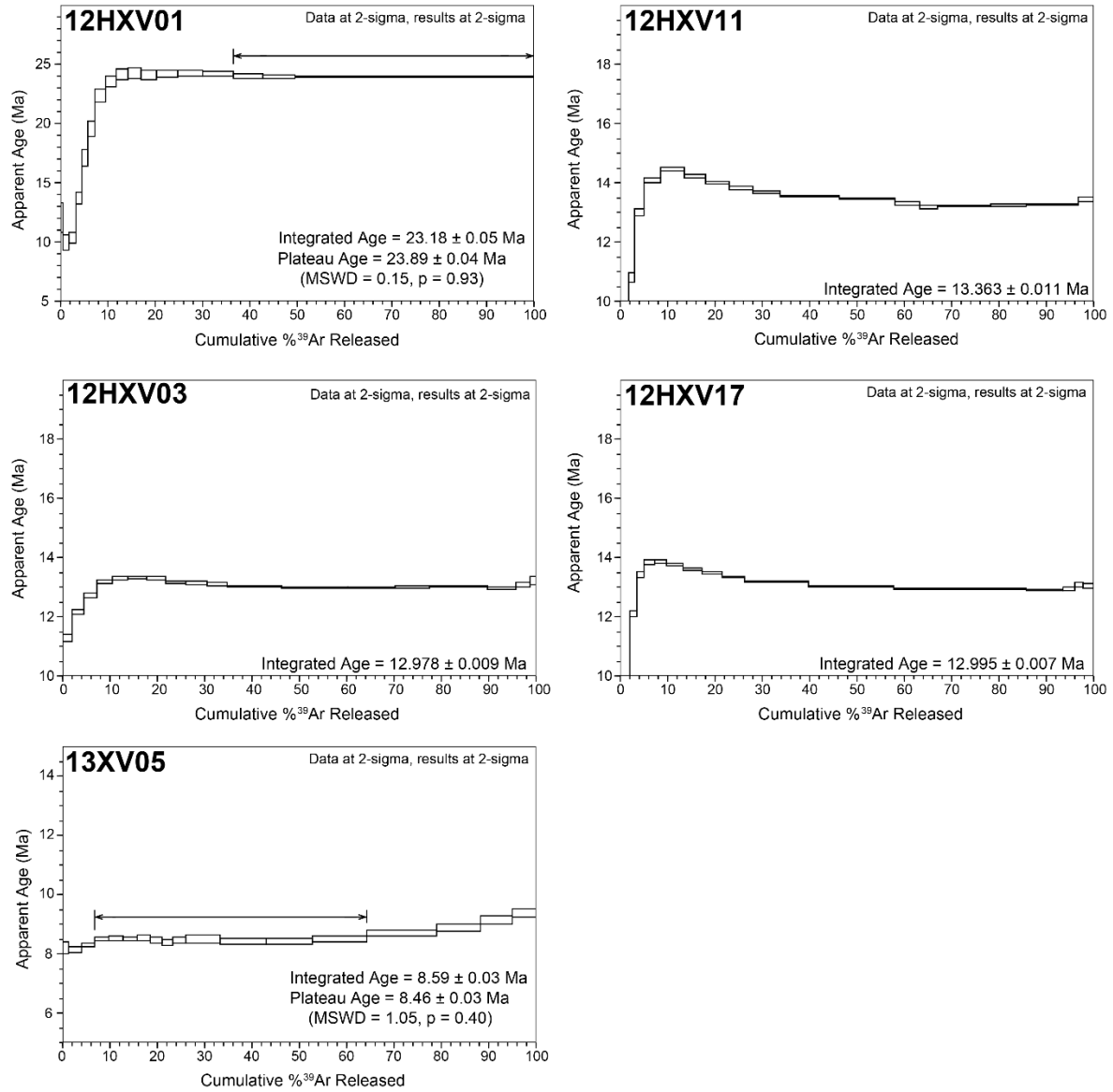
Figure A.4 – $^{40}Ar/^{39}Ar$ age spectra for samples analyzed at the USGS.

.

Table A.2 – Zircon U-Pb analyses.

Analysis	U (ppm)	206Pb 204Pb	U/Th	Isotope ratios							Apparent ages (Ma)							
				206Pb* 207Pb*	± (%)	207Pb* 235U*	± (%)	206Pb* 238U	± (%)	error corr.	206Pb* 238U*	± (Ma)	207Pb* 235U	± (Ma)	206Pb* 207Pb*	± (Ma)	Best age (Ma)	± (Ma)
12HXV24																		
12HXV24-01	474	3926	1.8	28.4976	23.0	0.0104	27.2	0.0022	14.5	0.53	13.9	2.0	10.5	2.8	-701.4	644.8	13.9	2.0
12HXV24-01	406	5742	1.8	24.7068	65.4	0.0125	65.8	0.0022	7.3	0.11	14.4	1.1	12.6	8.2	-320.6	1873.0	14.4	1.1
12HXV24-01	1641	19016	3.4	23.1769	12.7	0.0120	12.9	0.0020	2.2	0.17	13.0	0.3	12.1	1.6	-159.1	317.4	13.0	0.3
12HXV24-01	352	2720	1.1	9.7112	111.6	0.0302	113.9	0.0021	23.2	0.20	13.7	3.2	30.2	33.9	1678.4	66.1	13.7	3.2
12HXV24-05	369	3122	1.2	15.2172	32.0	0.0193	34.0	0.0021	11.6	0.34	13.7	1.6	19.4	6.5	797.3	687.3	13.7	1.6
12HXV24-06	550	6413	1.5	32.5712	49.3	0.0088	50.3	0.0021	9.8	0.20	13.4	1.3	8.9	4.5	NA	NA	13.4	1.3
12HXV24-07	1410	13002	3.5	22.6154	14.8	0.0127	15.1	0.0021	2.8	0.19	13.4	0.4	12.8	1.9	-98.5	365.5	13.4	0.4
12HXV24-09	1085	13940	1.7	25.6832	51.3	0.0113	51.3	0.0021	2.3	0.04	13.5	0.3	11.4	5.8	-421.0	1426.4	13.5	0.3
12HXV24-10	632	4657	1.1	23.8875	29.6	0.0135	30.5	0.0023	7.4	0.24	15.0	1.1	13.6	4.1	-234.8	759.7	15.0	1.1
12HXV24-11	1936	20925	2.7	22.3673	17.8	0.0126	18.3	0.0020	4.2	0.23	13.2	0.5	12.7	2.3	-71.5	437.6	13.2	0.5
12HXV24-12	1049	8175	4.7	26.2525	22.7	0.0108	23.4	0.0021	5.6	0.24	13.3	0.8	11.0	2.6	-478.8	609.2	13.3	0.8
12HXV24-13	680	5216	1.5	19.9812	18.1	0.0139	18.7	0.0020	4.8	0.26	13.0	0.6	14.0	2.6	197.2	423.5	13.0	0.6
12HXV24-14	852	7425	1.8	24.1519	37.0	0.0121	38.0	0.0021	8.6	0.23	13.7	1.2	12.2	4.6	-262.6	966.0	13.7	1.2
12HXV24-15	264	2149	0.8	12.3417	39.2	0.0251	42.9	0.0022	17.2	0.40	14.5	2.5	25.2	10.7	1222.1	803.0	14.5	2.5
12HXV24-16	231	1491	0.7	7.8156	116.0	0.0381	118.3	0.0022	23.2	0.20	13.9	3.2	38.0	44.1	2070.0	288.1	13.9	3.2
12HXV24-17	468	3320	0.6	21.5173	35.1	0.0138	36.5	0.0022	10.0	0.27	13.9	1.4	13.9	5.0	22.3	866.0	13.9	1.4
12HXV24-18	235	5104	0.7	8.5056	97.7	0.0392	99.0	0.0024	15.5	0.16	15.6	2.4	39.1	37.9	1919.6	NA	15.6	2.4
12HXV24-19	224	3632	0.5	13.0328	45.8	0.0227	50.3	0.0021	20.9	0.42	13.8	2.9	22.8	11.4	1114.1	966.5	13.8	2.9
12HXV24-21	500	6531	1.2	17.1760	38.8	0.0170	40.2	0.0021	10.4	0.26	13.7	1.4	17.1	6.8	538.1	881.4	13.7	1.4
12HXV24-22	1012	5289	1.7	21.9360	26.7	0.0135	27.1	0.0021	4.8	0.18	13.8	0.7	13.6	3.7	-24.1	655.7	13.8	0.7
~~12HXV24-08~~	~~573~~	~~9047~~	~~1.3~~	~~20.2224~~	~~15.2~~	~~0.0433~~	~~20.9~~	~~0.0063~~	~~14.2~~	~~0.68~~	~~40.8~~	~~5.8~~	~~43.0~~	~~8.8~~	~~169.2~~	~~357.7~~	~~40.8~~	~~5.8~~
12HXV32																		
12HXV32-21	525	506	1.2	10.8363	80.7	0.0160	96.7	0.0013	53.4	0.55	8.1	4.3	16.1	15.4	1473.2	1964.0	8.1	4.3
12HXV32-18	956	3182	1.5	17.0892	47.1	0.0136	65.1	0.0017	44.9	0.69	10.9	4.9	13.7	8.9	549.2	1087.8	10.9	4.9
12HXV32-04	209	742	1.6	11.0317	88.4	0.0242	89.8	0.0019	15.9	0.18	12.4	2.0	24.2	21.5	1439.2	52.6	12.4	2.0
12HXV32-26	1320	2785	1.0	22.2287	19.2	0.0121	19.4	0.0019	2.9	0.15	12.6	0.4	12.2	2.4	-56.3	472.4	12.6	0.4
12HXV32-32	274	2812	1.5	21.0417	71.1	0.0128	71.6	0.0020	8.0	0.11	12.6	1.0	13.0	9.2	75.7	1952.4	12.6	1.0
12HXV32-06	300	3886	1.3	13.9694	158.8	0.0195	159.3	0.0020	12.5	0.08	12.7	1.6	19.6	30.9	974.1	707.9	12.7	1.6

Analysis	U (ppm)	206Pb 204Pb	U/Th	Isotope ratios 206Pb* 207Pb*	± (%)	207Pb* 235U*	± (%)	206Pb* 238U	± (%)	error corr.	Apparent ages (Ma) 206Pb* 238U*	± (Ma)	207Pb* 235U	± (Ma)	206Pb* 207Pb*	± (Ma)	Best age (Ma)	± (Ma)
12HXV32 (cont'd)																		
12HXV32-20	195	1025	0.4	-1.8458	648.4	-0.1481	648.7	0.0020	19.5	0.03	12.8	2.5	-162.8	NA	NA	NA	12.8	2.5
12HXV32-02	346	1862	1.5	25.0584	49.3	0.0109	52.4	0.0020	17.6	0.34	12.8	2.2	11.0	5.7	-357.0	1347.7	12.8	2.2
12HXV32-22	261	6542	1.0	14.8506	95.7	0.0185	96.0	0.0020	8.4	0.09	12.8	1.1	18.6	17.7	848.2	377.9	12.8	1.1
12HXV32-11	354	2778	1.6	17.4073	68.8	0.0158	69.4	0.0020	9.2	0.13	12.9	1.2	16.0	11.0	508.7	1737.7	12.9	1.2
12HXV32-05	1693	8782	4.6	21.8406	8.1	0.0126	8.7	0.0020	3.3	0.38	12.9	0.4	12.7	1.1	-13.6	195.4	12.9	0.4
12HXV32-30	1772	23698	5.1	20.7378	8.7	0.0134	10.0	0.0020	4.8	0.48	13.0	0.6	13.5	1.3	110.1	206.6	13.0	0.6
12HXV32-03	183	1256	1.0	13.2675	110.7	0.0209	111.9	0.0020	16.6	0.15	13.0	2.2	21.0	23.3	1078.4	323.8	13.0	2.2
12HXV32-27	96	431	0.5	5.3032	267.3	0.0528	268.7	0.0020	27.3	0.10	13.1	3.6	52.3	137.8	2729.7	127.9	13.1	3.6
12HXV32-15	1331	15327	2.2	23.5384	15.2	0.0119	17.2	0.0020	8.0	0.47	13.1	1.1	12.0	2.1	-197.8	381.8	13.1	1.1
12HXV32-14	401	3010	0.7	29.4942	74.4	0.0096	74.7	0.0020	7.0	0.09	13.2	0.9	9.7	7.2	-797.9	2444.6	13.2	0.9
12HXV32-07	304	2028	1.0	26.8234	58.5	0.0106	60.5	0.0021	15.4	0.25	13.2	2.0	10.7	6.4	-536.2	1700.5	13.2	2.0
12HXV32-08	755	6361	2.6	28.3995	38.4	0.0100	39.1	0.0021	7.5	0.19	13.3	1.0	10.1	3.9	-691.9	1096.7	13.3	1.0
12HXV32-19	315	3435	1.2	21.5031	62.1	0.0133	63.0	0.0021	10.2	0.16	13.4	1.4	13.5	8.4	23.9	1647.9	13.4	1.4
12HXV32-31	161	2211	2.1	7.5908	180.5	0.0379	181.5	0.0021	18.9	0.10	13.4	2.5	37.7	67.3	2121.2	23.6	13.4	2.5
12HXV32-12	150	790	0.8	7.7564	138.3	0.0373	139.3	0.0021	16.6	0.12	13.5	2.2	37.2	50.9	2083.4	187.7	13.5	2.2
12HXV32-25	95	755	0.5	3.8479	145.9	0.0752	147.7	0.0021	23.0	0.16	13.5	3.1	73.6	105.3	3246.0	863.2	13.5	3.1
12HXV32-17	771	10840	2.8	20.4284	13.1	0.0142	15.8	0.0021	8.9	0.56	13.6	1.2	14.4	2.3	145.5	308.8	13.6	1.2
12HXV32-29	99	1020	0.5	6.9377	80.9	0.0422	85.8	0.0021	28.5	0.33	13.7	3.9	41.9	35.3	2277.5	594.4	13.7	3.9
12HXV32-10	291	1921	1.4	17.8790	118.2	0.0168	119.4	0.0022	17.3	0.14	14.0	2.4	16.9	20.0	449.6	835.5	14.0	2.4
12HXV32-16	450	3609	3.1	21.5816	46.8	0.0140	48.0	0.0022	10.9	0.23	14.1	1.5	14.1	6.7	15.1	1183.8	14.1	1.5
12HXV32-09	378	996	2.6	21.5743	39.8	0.0147	42.3	0.0023	14.3	0.34	14.8	2.1	14.8	6.2	15.9	990.6	14.8	2.1
12HXV32-13	520	2752	2.0	17.5716	79.6	0.0188	80.9	0.0024	14.5	0.18	15.4	2.2	18.9	15.1	488.0	2176.7	15.4	2.2
12HXV32-28	274	3306	1.9	24.1425	63.8	0.0137	65.0	0.0024	12.4	0.19	15.5	1.9	13.8	8.9	-261.6	1795.3	15.5	1.9
~~12HXV32-23~~	~~102~~	~~20431~~	~~0.9~~	~~19.9503~~	~~8.9~~	~~0.2766~~	~~11.0~~	~~0.0400~~	~~6.4~~	~~0.58~~	~~252.9~~	~~15.9~~	~~247.9~~	~~24.1~~	~~200.8~~	~~206.6~~	~~252.9~~	~~15.9~~

Analysis	U (ppm)	206Pb/204Pb	U/Th	Isotope ratios							Apparent ages (Ma)							
				206Pb*/207Pb*	± (%)	207Pb*/235U*	± (%)	206Pb*/238U	± (%)	error corr.	206Pb*/238U*	± (Ma)	207Pb*/235U	± (Ma)	206Pb*/207Pb*	± (Ma)	Best age (Ma)	± (Ma)
13XV06																		
13XV06-02	472	3127	7.9	23.7587	62.8	0.0076	63.4	0.0013	8.3	0.13	8.4	0.7	7.7	4.8	-221.1	1747.4	8.4	0.7
13XV06-109	480	675	0.7	31.5180	11.2	0.0054	11.9	0.0012	3.9	0.33	8.0	0.3	5.5	0.7	990.1	332.5	8.0	0.3
13XV06-105	146	383	2.4	118.1367	53.4	0.0015	53.6	0.0013	4.9	0.09	8.1	0.4	1.5	0.8	0.0	1541.2	8.1	0.4
13XV06-91	1558	2116	4.9	25.1180	9.8	0.0070	10.2	0.0013	3.0	0.30	8.3	0.3	7.1	0.7	363.1	253.0	8.3	0.3
13XV06-106	844	35939	0.6	22.7817	8.2	0.0079	9.0	0.0013	3.8	0.42	8.4	0.3	8.0	0.7	116.6	202.3	8.4	0.3
13XV06-104	1247	3550	2.3	21.4587	8.4	0.0084	8.6	0.0013	1.9	0.22	8.4	0.2	8.5	0.7	28.8	201.0	8.4	0.2
13XV06-98	1437	1594	1.8	25.8252	6.9	0.0070	8.8	0.0013	5.3	0.61	8.4	0.4	7.0	0.6	435.5	182.7	8.4	0.4
13XV06-101	457	1163	1.6	32.7813	9.7	0.0055	10.7	0.0013	4.4	0.42	8.4	0.4	5.6	0.6	1107.9	295.9	8.4	0.4
13XV06-93	826	1845	1.5	6.9513	31.0	0.0265	31.1	0.0013	2.4	0.08	8.6	0.2	26.5	8.1	2274.2	548.1	8.6	0.2
13XV06-90	315	1872	0.9	25.5450	12.7	0.0073	14.2	0.0013	6.4	0.45	8.7	0.5	7.3	1.0	406.9	334.0	8.7	0.5
13XV06-102	293	1285	1.3	18.4140	11.9	0.0101	12.6	0.0013	4.1	0.33	8.7	0.4	10.2	1.3	383.8	267.6	8.7	0.4
13XV06-103	896	3811	2.0	15.4681	13.2	0.0120	14.2	0.0014	5.2	0.37	8.7	0.5	12.2	1.7	762.9	279.3	8.7	0.5
13XV06-107	386	416	0.6	75.6940	10.0	0.0025	10.6	0.0014	3.5	0.33	8.7	0.3	2.5	0.3	0.0	0.0	8.7	0.3
13XV06-108	1032	12437	3.6	20.0540	7.1	0.0094	7.9	0.0014	3.4	0.43	8.8	0.3	9.5	0.7	188.7	165.2	8.8	0.3
13XV06-82	104	2246	3.5	23.8422	15.9	0.0080	17.3	0.0014	6.8	0.39	8.9	0.6	8.1	1.4	230.0	402.3	8.9	0.6
13XV06-95	256	979	1.0	29.7795	11.6	0.0065	13.7	0.0014	7.3	0.53	9.0	0.7	6.5	0.9	825.3	331.8	9.0	0.7
13XV06-99	5014	9691	123.6	18.0197	8.2	0.0125	8.4	0.0016	1.9	0.23	10.5	0.2	12.6	1.1	432.2	182.5	10.5	0.2
~~13XV06-100~~	~~26864~~	~~39966~~	~~67.9~~	~~18.2235~~	~~13.9~~	~~-0.0027~~	~~304.6~~	~~-0.0004~~	~~304.2~~	~~1.00~~	~~2.3~~	~~7.0~~	~~2.7~~	~~8.3~~	~~407.1~~	~~313.5~~	~~2.3~~	~~7.0~~
~~13XV06-05~~	~~91~~	~~596~~	~~0.4~~	~~4.0655~~	~~236.7~~	~~0.0441~~	~~240.9~~	~~0.0013~~	~~44.7~~	~~0.19~~	~~8.4~~	~~3.7~~	~~43.8~~	~~103.7~~	~~3159.0~~	~~507.7~~	~~8.4~~	~~3.7~~
~~13XV06-01~~	~~186~~	~~1140~~	~~0.4~~	~~2.3874~~	~~612.9~~	~~0.0845~~	~~613.3~~	~~0.0015~~	~~23.6~~	~~0.04~~	~~9.4~~	~~2.2~~	~~82.4~~	~~528.3~~	~~3978.3~~	~~279.1~~	~~9.4~~	~~2.2~~

Analyses with strike through are excluded from the mean age calculation of a specific sample due to high analytical uncertainties.

Table A.3 – Apatite (U-Th)/He results for sample 12HG06.

Analysis	He (ncc)	U (ppm)	Th (ppm)	Sm (ppm)	He (ppm)	Mass (µg)	Width (µm)	Length (µm)	Ft corr.	Uncorr. Age	**Corrected Age**
12HG06a	0.1289	235.59	737.21	122.33	3.38	1.70	86.58	112.672	0.7210	1.53	**2.12**
12HG06b	0.1917	152.96	1150.87	157.58	3.00	2.85	80.406	219.097	0.7219	1.31	**1.81**
12HG06c	0.0954	212.94	1053.42	146.33	3.21	1.33	77.736	109.096	0.6939	1.28	**1.85**
12HG06d	0.1231	232.40	580.05	142.38	2.90	1.90	89.715	117.046	0.7304	1.45	**1.99**
12HG06e	0.5638	214.24	1324.64	154.04	4.40	5.72	97.621	298.242	0.7708	1.54	**2.00**
12HG06f	0.2170	182.82	1275.73	162.17	3.49	2.78	66.694	310.062	0.6775	1.33	**1.97**

A.3 References

Farley, K.A., Wolf, R.A., and Silver, L.T., 1996, The effects of long alpha-stopping distances on (U-Th)/He ages: Geochimica et Cosmochimica Acta, v. 60, p. 4223–4229, doi: 10.1016/S0016-7037(96)00193-7.

Gehrels, G.E., Valencia, V. a., and Ruiz, J., 2008, Enhanced precision, accuracy, efficiency, and spatial resolution of U-Pb ages by laser ablation-multicollector-inductively coupled plasma-mass spectrometry: Geochemistry, Geophysics, Geosystems, v. 9, doi: 10.1029/2007GC001805.

Johnson, D.M., Hooper, P.R., and Conrey, R.M., 1999, XRF analysis of rocks and minerals for major and trace elements on a single low dilution Li-tetraborate fused bead: Advances in X-ray Analysis, v. 41, p. 843–867.

Kuiper, K.F., Deino, A., Hilgen, F.J., Krijgsman, W., Renne, P.R., and Wijbrans, J.R., 2008, Synchronizing Rock Clocks of Earth History: Science, v. 320, p. 500–504, doi: 10.1126/science.1154339.

Lee, J.Y., Marti, K., Severinghaus, J.P., Kawamura, K., Yoo, H.S., Lee, J.B., and Kim, J.S., 2006, A redetermination of the isotopic abundances of atmospheric Ar: Geochimica et Cosmochimica Acta, v. 70, p. 4507–4512, doi: 10.1016/j.gca.2006.06.1563.

Ludwig, K.R., 2008, User's Manual for Isoplot 3.70: A Geochronological Toolkit for Microsoft Excel: Berkeley Geochronology Center Special Publication No. 4,.

Min, K., Mundil, R., Renne, P.R., and Ludwig, K.R., 2000, A test for systematic errors in 40Ar/39Ar geochronology through comparison with U/Pb analysis of a 1.1-Ga rhyolite: Geochimica et Cosmochimica Acta, v. 64, p. 73–98, doi: 10.1016/S0016-7037(99)00204-5.

Norrish, K., and Hutton, J.., 1969, An accurate X-ray spectrographic method for the analysis of a wide range of geological samples: Geochimica et Cosmochimica Acta, v. 33, p. 431–453, doi: 10.1016/0016-7037(69)90126-4.

Reiners, P.W., and Nicolescu, S., 2006, Measurement of parent nuclides for (U-Th)/He chronometry by solution sector ICP-MS: ARHDL Report 1,.

Samson, S.D., and Alexander, E.C., 1987, Calibration of the interlaboratory 40Ar-39Ar dating standard, MMhb-1: Chemical Geology: Isotope Geoscience section, v. 66, p. 27–34, doi: 10.1016/0168-9622(87)90025-X.

Todt, W., Cliff, R., Hanser, A., and Hofmann, A., 1996, Evaluation of a 202Pb–205Pb double spike for high - precision lead isotope analysis, in Geophysical Monograph Series, p. 429–437.

Appendix B:Compiled Geochemistry Data for the Tibetan Plateau

B.1 Tables of Compiled Geochemistry Data

Tables below contain the compiled geochemical database of lavas in the Tibetan Plateau described in chapter 4, including new geochemical data from the Hoh Xil basin. Analytical methods may be found in Appendix A, and cited references. The compiled dataset is split into seven tables, containing the locations of samples, major and trace element compositions, isotopic values, and calculated parameters from published datasets. Subsequent to Table B.1, all tables contain columns with reference, and sample numbers for indexing purposes.

Table B.1 – Location and age information for compiled lavas from the Tibetan Plateau.

Reference	Ref. #	Sample	Lat	Long	Locality	Terrane	Zone	Age (Ma)
Arnaud et al 1992	1	K89G185	35.20	79.50		Songpan-Ganzi	North	5.6
Arnaud et al 1992	1	K89G186	35.20	79.50		Songpan-Ganzi	North	5.6
Arnaud et al 1992	1	K89G189	35.20	79.50		Songpan-Ganzi	North	5.1
Arnaud et al 1992	1	K89G190	35.20	79.50		Songpan-Ganzi	North	5.3
Arnaud et al 1992	1	KB9G191	35.20	79.50		Songpan-Ganzi	North	5.3
Arnaud et al 1992	1	K89G192	35.20	79.50		Songpan-Ganzi	North	5.3
Arnaud et al 1992	1	K189G193	35.20	79.50		Songpan-Ganzi	North	5.3
Arnaud et al 1992	1	K89G197	35.20	79.50		Songpan-Ganzi	North	6.4
Arnaud et al 1992	1	K89G200	35.20	79.50		Songpan-Ganzi	North	3.6
Chen et al 2012	2	05S2-4	32.10	82.10	Sailipu	Lhasa	South	18.48
Chen et al 2012	2	05S2-6	32.10	82.10	Sailipu	Lhasa	South	18.48
Chen et al 2012	2	05S2-9	32.10	82.10	Sailipu	Lhasa	South	18.48
Chen et al 2012	2	05SLP5-1	32.10	82.10	Sailipu	Lhasa	South	18.48
Chen et al 2012	2	05SLP5-2	32.10	82.10	Sailipu	Lhasa	South	18.48
Chen et al 2012	2	05SLP5-4	32.10	82.10	Sailipu	Lhasa	South	18.48
Chen et al 2012	2	CM10-04-04	30.70	86.40	Mibale	Lhasa	South	12.5
Chen et al 2012	2	CM10-04-09	30.70	86.40	Mibale	Lhasa	South	12.5
Chen et al 2012	2	CM10-04-12	30.70	86.40	Mibale	Lhasa	South	12.5
Chen et al 2012	2	04DYH-01	34.50	89.50	Dongyuehu	Qiangtang	Central	39.7
Chen et al 2012	2	D3141	34.50	86.90	Bamaoqunzong	Qiangtang	Central	29
Chen et al 2013	3	04LQS-2	34.52	88.02	Luangingshan	Qiangtang	Central	43
Chen et al 2013	3	04LQS-3	34.52	88.02	Luangingshan	Qiangtang	Central	43
Chen et al 2013	3	04LQS-6	34.52	88.02	Luangingshan	Qiangtang	Central	43
Chen et al 2013	3	04LQS-14	34.52	88.02	Luangingshan	Qiangtang	Central	43
Chen et al 2013	3	04LQS-16	34.52	88.02	Luangingshan	Qiangtang	Central	43
Chen et al 2013	3	04YJL-05	33.96	88.79	Yuenjinla	Qiangtang	Central	43.4
Chen et al 2013	3	04YJL-07	33.96	88.79	Yuenjinla	Qiangtang	Central	43.4
Chen et al 2013	3	04YJL-06	33.96	88.79	Yuenjinla	Qiangtang	Central	43.4

Reference	Ref. #	Sample	Lat	Long	Locality	Terrane	Zone	Age (Ma)
Chen et al 2013	3	04YJL-09	33.96	88.79	Yuenjinla	Qiangtang	Central	43.4
Chen et al 2013	3	04DN30-2	34.33	89.17	Dongyuehu	Qiangtang	Central	43.4
Chen et al 2013	3	04DN30-3	34.33	89.17	Dongyuehu	Qiangtang	Central	43.4
Chen et al 2013	3	04DN31-1	34.33	89.17	Dongyuehu	Qiangtang	Central	43.4
Chen et al 2013	3	04DN32-1	34.33	89.17	Dongyuehu	Qiangtang	Central	43.4
Chen et al 2013	3	04DN32-2	34.33	89.17	Dongyuehu	Qiangtang	Central	43.4
Chen et al 2013	3	04DN35-2	34.33	89.17	Dongyuehu	Qiangtang	Central	43.4
Chen et al 2013	3	04DN36-3	34.33	89.17	Dongyuehu	Qiangtang	Central	43.4
Chen et al 2013	3	04DN37-2	34.33	89.17	Dongyuehu	Qiangtang	Central	43.4
Chen et al 2013	3	04DN39	34.33	89.17	Dongyuehu	Qiangtang	Central	43.4
Chen et al 2013	3	04DN40	34.33	89.17	Dongyuehu	Qiangtang	Central	43.4
Chen et al 2013	3	04DY44-2	34.33	89.17	Dongyuehu	Qiangtang	Central	43.4
Chen et al 2013	3	04DY44-4	34.33	89.17	Dongyuehu	Qiangtang	Central	43.4
Chen et al 2013	3	04DY44-7	34.33	89.17	Dongyuehu	Qiangtang	Central	43.4
Chen et al 2013	3	04D6441	33.72	89.69	Meiriqiecuo	Qiangtang	Central	43.46
Chen et al 2013	3	04D6437	33.72	89.69	Meiriqiecuo	Qiangtang	Central	46.46
Ding 2003	4	2T394	33.83	83.35	Bangdaco	Qiangtang	Central	59.18
Ding 2003	4	2T395	33.83	83.35	Bangdaco	Qiangtang	Central	60
Ding 2003	4	2T396	33.83	83.35	Bangdaco	Qiangtang	Central	60
Ding 2003	4	98T03	32.71	84.25	Lagala	Qiangtang	Central	59.18
Ding 2003	4	98T04	32.71	84.25	Lagala	Qiangtang	Central	59.18
Ding 2003	4	98T07	33.88	83.37	Bangdaco	Qiangtang	Central	30
Ding 2003	4	98T15	33.88	83.37	Bangdaco	Qiangtang	Central	30
Ding 2003	4	98T16	33.87	83.35	Bangdaco	Qiangtang	Central	30
Ding 2003	4	98T33	33.80	83.35	Bangdaco	Qiangtang	Central	30
Ding 2003	4	98T38	33.80	83.35	Bangdaco	Qiangtang	Central	30
Ding 2003	4	98T43	33.81	83.32	Bangdaco	Qiangtang	Central	30
Ding 2003	4	98T44	33.80	83.35	Bangdaco	Qiangtang	Central	30.66
Ding 2003	4	98T46	33.87	83.34	Bangdaco	Qiangtang	Central	30
Ding 2003	4	98T49	33.85	83.35	Yulinshan	Qiangtang	Central	30

Reference	Ref. #	Sample	Lat	Long	Locality	Terrane	Zone	Age (Ma)
Ding 2003	4	98T51	33.85	83.35	Yulinshan	Qiangtang	Central	30
Ding 2003	4	98T52	33.85	83.35	Yulinshan	Qiangtang	Central	30
Ding 2003	4	98T53	33.85	83.35	Yulinshan	Qiangtang	Central	30.67
Ding 2003	4	98T54	33.85	83.35	Yulinshan	Qiangtang	Central	30
Ding 2003	4	98T57	33.85	83.35	Yulinshan	Qiangtang	Central	30
Ding 2003	4	98T69	33.86	83.37	Yulinshan	Qiangtang	Central	30
Ding 2003	4	98T70	33.85	83.34	Yulinshan	Qiangtang	Central	30.33
Ding 2003	4	98T71	33.86	83.33	Yulinshan	Qiangtang	Central	30
Ding 2003	4	98T73	33.85	83.32	Yulinshan	Qiangtang	Central	30
Ding 2003	4	99T132	30.06	86.78	Chazi	Lhasa	South	23
Ding 2003	4	99T134	30.14	86.53	Chazi	Lhasa	South	23
Ding 2003	4	99T145	30.00	86.49	Chazi	Lhasa	South	23
Ding 2003	4	99T152	30.01	86.53	Chazi	Lhasa	South	23
Ding 2003	4	99T154	30.05	86.52	Chazi	Lhasa	South	23
Ding 2003	4	99T53	31.08	86.52	Wenbu	Lhasa	South	13
Ding 2003	4	99T56	31.08	86.52	Wenbu	Lhasa	South	13
Ding 2003	4	99T57	31.08	86.52	Wenbu	Lhasa	South	13
Ding 2003	4	99T60	31.08	86.52	Wenbu	Lhasa	South	13
Ding 2003	4	99T62	31.08	86.52	Wenbu	Lhasa	South	13
Ding 2007	5	2002T1021	32.97	86.64	Yibuchaka	Qiangtang	Central	35.5
Ding 2007	5	2002T1022	32.97	86.64	Yibuchaka	Qiangtang	Central	35.2
Ding 2007	5	2002T1023	32.97	86.64	Yibuchaka	Qiangtang	Central	36
Ding 2007	5	2002T1024	32.97	86.64	Yibuchaka	Qiangtang	Central	36
Ding 2007	5	2002T1025	32.97	86.64	Yibuchaka	Qiangtang	Central	34
Ding 2007	5	2002T1026	32.97	86.64	Yibuchaka	Qiangtang	Central	34
Ding 2007	5	2003T373	32.57	85.44	Nading Co	Qiangtang	Central	34
Ding 2007	5	2003T374	32.58	85.44	Nading Co	Qiangtang	Central	34
Ding 2007	5	2003T375	32.67	85.60	Nading Co	Qiangtang	Central	34
Ding 2007	5	2003T380	32.49	85.37	Nading Co	Qiangtang	Central	34.2
Ding 2007	5	2003T483	32.20	86.89	Ejumaima	Qiangtang	Central	28

Reference	Ref. #	Sample	Lat	Long	Locality	Terrane	Zone	Age (Ma)
Ding 2007	5	2003T485	32.20	86.83	Ejumaima	Qiangtang	Central	28
Ding 2007	5	2003T486	32.20	86.83	Ejumaima	Qiangtang	Central	27.3
Ding 2007	5	2003T487	32.21	86.83	Ejumaima	Qiangtang	Central	28
Ding 2007	5	2003T488	32.21	86.83	Ejumaima	Qiangtang	Central	28
Ding 2007	5	2003T492	32.19	86.80	Ejumaima	Qiangtang	Central	28
Gao et al 2007	6	Tl/10	30.00	86.50	Mibale	Lhasa	South	19.9
Gao et al 2007	6	Tl/11	30.00	86.50	Mibale	Lhasa	South	19.9
Gao et al 2007	6	Tl/18	30.00	86.50	Mibale	Lhasa	South	19.9
Gao et al 2007	6	Tl/13	30.00	86.50	Mibale	Lhasa	South	19.9
Gao et al 2007	6	Tl/03	30.00	86.50	Mibale	Lhasa	South	19.9
Gao et al 2007	6	Tl/08	30.00	86.50	Mibale	Lhasa	South	19.9
Gao et al 2007	6	Tl/17	30.00	86.50	Mibale	Lhasa	South	19.9
Gao et al 2007	6	Tl/06	30.00	86.50	Mibale	Lhasa	South	19.9
Gao et al 2007	6	Tl/59	30.00	86.50	Mibale	Lhasa	South	19.9
Gao et al 2007	6	CHZ-1	29.50	86.50	Chazi	Lhasa	South	13.3
Gao et al 2007	6	CHZ-2	29.50	86.50	Chazi	Lhasa	South	13.3
Gao et al 2007	6	CHZ-3	29.50	86.50	Chazi	Lhasa	South	13.3
Gao et al 2007	6	CHZ-4	29.50	86.50	Chazi	Lhasa	South	13.3
Gao et al 2007	6	CHZ-5	29.50	86.50	Chazi	Lhasa	South	13.3
Gao et al 2007	6	CHZ-6	29.50	86.50	Chazi	Lhasa	South	13.3
Gao et al 2007	6	CHZ-7	29.50	86.50	Chazi	Lhasa	South	13.3
Gao et al 2007	6	CHZ-8	29.50	86.50	Chazi	Lhasa	South	13.3
Gao et al 2007	6	CHZ-9	29.50	86.50	Chazi	Lhasa	South	13.3
Gao et al 2007	6	CHZ-10	29.50	86.50	Chazi	Lhasa	South	13.3
Gao et al 2007	6	CHZ-11	29.50	86.50	Chazi	Lhasa	South	13.3
Gao et al 2007	6	CHZ-12	29.50	86.50	Chazi	Lhasa	South	13.3
Guo 2006	7	AH-7	35.58	81.55	Songpan-Ganzi	Songpan-Ganzi	North	0.96
Guo 2006	7	G26	33.72	83.23	North Qiangtang	Qiangtang	Central	28.7
Guo 2006	7	G68	33.72	83.23	North Qiangtang	Qiangtang	Central	28.7
Guo 2006	7	G98-0	34.44	87.18	North Qiangtang	Qiangtang	Central	26.5

Reference	Ref. #	Sample	Lat	Long	Locality	Terrane	Zone	Age (Ma)
Guo 2006	7	G98-1	34.44	87.18	North Qiangtang	Qiangtang	Central	26.5
Guo 2006	7	G98-14	34.44	87.18	North Qiangtang	Qiangtang	Central	26.5
Guo 2006	7	G98-3	34.44	87.18	North Qiangtang	Qiangtang	Central	26.5
Guo 2006	7	G98-6	34.43	87.20	North Qiangtang	Qiangtang	Central	26.5
Guo 2006	7	G98-9	34.41	87.19	North Qiangtang	Qiangtang	Central	26.5
Guo 2006	7	HH72	36.00	88.36	Songpan-Ganzi	Songpan-Ganzi	North	12.7
Guo 2006	7	HS07	35.58	82.77	Songpan-Ganzi	Songpan-Ganzi	North	3.7
Guo 2006	7	HS-69	35.58	82.77	Songpan-Ganzi	Songpan-Ganzi	North	3.7
Guo 2006	7	JC9719	34.00	88.39	North Qiangtang	Qiangtang	Central	39.9
Guo 2006	7	JC973	34.00	88.39	North Qiangtang	Qiangtang	Central	39.9
Guo 2006	7	JC975	34.00	88.39	North Qiangtang	Qiangtang	Central	39.9
Guo 2006	7	JC978	34.33	89.06	North Qiangtang	Qiangtang	Central	39.7
Guo 2006	7	JH6	36.17	89.49	Songpan-Ganzi	Songpan-Ganzi	North	10.7
Guo 2006	7	KX84	35.96	78.44	Songpan-Ganzi	Songpan-Ganzi	North	3.8
Guo 2006	7	PL-58	36.09	81.26	North Kunlun	Kunlun	North	1.27
Guo 2006	7	PL-7	36.09	81.26	North Kunlun	Kunlun	North	1.27
Guo 2006	7	QQ08	36.09	86.05	Songpan-Ganzi	Songpan-Ganzi	North	14.9
Guo 2006	7	QS22	35.39	80.10	Songpan-Ganzi	Songpan-Ganzi	North	6.4
Guo 2006	7	XT16	36.19	88.99	Songpan-Ganzi	Songpan-Ganzi	North	9.3
Guo 2006	7	XT8	36.19	88.99	Songpan-Ganzi	Songpan-Ganzi	North	9.3
Guo 2006	7	XY03	35.70	88.90	Songpan-Ganzi	Songpan-Ganzi	North	10.6
Guo 2006	7	XY05	35.70	88.90	Songpan-Ganzi	Songpan-Ganzi	North	10.6
Guo 2006	7	YS02	35.51	85.04	Songpan-Ganzi	Songpan-Ganzi	North	16.5
Guo 2006	7	YS72	35.58	79.30	Songpan-Ganzi	Songpan-Ganzi	North	0.28
Guo 2006	7	ZF91	34.19	90.65	North Qiangtang	Qiangtang	Central	44.7
Guo 2006	7	ZF96	34.19	90.65	North Qiangtang	Qiangtang	Central	44.7
Guo et al 2007	8	ZF09	33.50	80.20	Shiquanhe	Qiangtang	Central	22.5
Guo et al 2007	8	GUO62	31.50	81.80	Gegar	Lhasa	South	17
Guo et al 2007	8	GUO51	31.50	81.80	Gegar	Lhasa	South	17
Guo et al 2007	8	GUO48	29.60	85.60	Daggyai	Lhasa	South	18.5

Reference	Ref. #	Sample	Lat	Long	Locality	Terrane	Zone	Age (Ma)
Guo et al 2007	8	GUO37	29.30	88.80	Xigaze	Lhasa	South	17.2
Guo et al 2007	8	G09	29.40	89.40	Wuyu	Lhasa	South	14.2
Guo et al 2007	8	ZFG17	29.70	89.90	Majiang	Lhasa	South	12.4
Guo et al 2007	8	G006	29.50	90.90	Nanmu	Lhasa	South	16.3
Guo et al 2007	8	G019	29.80	91.80	Jiama	Lhasa	South	15.1
Guo et al 2007	8	G016	29.80	91.80	Jiama	Lhasa	South	15.1
Guo et al 2007	8	G025	29.60	94.60	Linzhi	Lhasa	South	26.2
Guo et al 2013	9	DY-7	31.10	86.55	Garwa	Lhasa	South	21.18
Guo et al 2013	9	DC2	31.10	86.55	Garwa	Lhasa	South	21.18
Guo et al 2013	9	D509	31.10	86.55	Garwa	Lhasa	South	21.18
Guo et al 2013	9	DG43	31.10	86.55	Garwa	Lhasa	South	21.18
Guo et al 2013	9	YE51	30.75	86.65	Yaqian	Lhasa	South	13.46
Guo et al 2013	9	YC08	30.75	86.65	Yaqian	Lhasa	South	13.46
Guo et al 2013	9	YG13	30.75	86.65	Yaqian	Lhasa	South	13.46
Guo et al 2013	9	YF12	30.75	86.65	Yaqian	Lhasa	South	13.46
Guo et al 2013	9	YA32	30.75	86.65	Yaqian	Lhasa	South	13.46
Guo et al 2013	9	MH78	30.83	86.65	Mibale	Lhasa	South	15.29
Guo et al 2013	9	MH69	30.83	86.65	Mibale	Lhasa	South	15.29
Guo et al 2013	9	MG-3	30.83	86.65	Mibale	Lhasa	South	15.29
Guo et al 2013	9	MY1	30.83	86.65	Mibale	Lhasa	South	15.29
Guo et al 2013	9	MK09	30.83	86.65	Mibale	Lhasa	South	15.29
Guo et al 2013	9	MR21	30.83	86.65	Mibale	Lhasa	South	15.29
Guo et al 2013	9	MA75	30.83	86.65	Mibale	Lhasa	South	15.29
Guo et al 2013	9	MX5	30.83	86.65	Mibale	Lhasa	South	15.29
Guo et al 2013	9	2003T534	31.00	86.40	Yiqian	Lhasa	South	13.15
Guo et al 2013	9	2003T536	31.00	86.40	Yiqian	Lhasa	South	13.15
Guo et al 2013	9	2003T539	31.00	86.40	Yiqian	Lhasa	South	13.15
Guo et al 2013	9	G8	30.00	86.50	Chazi	Lhasa	South	10.94
Guo et al 2013	9	C10	30.00	86.50	Chazi	Lhasa	South	10.94
Guo et al 2013	9	CV5	30.00	86.50	Chazi	Lhasa	South	10.94

Reference	Ref. #	Sample	Lat	Long	Locality	Terrane	Zone	Age (Ma)
Guo et al 2013	9	C76	30.00	86.50	Chazi	Lhasa	South	10.94
Guo et al 2013	9	CH4	30.00	86.50	Chazi	Lhasa	South	10.94
Guo et al 2013	9	CH7	30.00	86.50	Chazi	Lhasa	South	10.94
Guo et al 2013	9	C03	30.00	86.50	Chazi	Lhasa	South	10.94
Guo et al 2013	9	CX38	30.00	86.50	Chazi	Lhasa	South	10.94
Guo et al 2013	9	C25	30.00	86.50	Chazi	Lhasa	South	10.94
Guo et al 2014	10	CT09	35.20	79.50	Tianshuihai	Songpan-Ganzi	North	5.2
Guo et al 2014	10	CT12	35.20	79.50	Tianshuihai	Songpan-Ganzi	North	5.2
Guo et al 2014	10	CT17	35.20	79.50	Tianshuihai	Songpan-Ganzi	North	5.2
Guo et al 2014	10	CT05	35.20	79.50	Tianshuihai	Songpan-Ganzi	North	5.2
Guo et al 2014	10	CT23	35.20	79.50	Tianshuihai	Songpan-Ganzi	North	5.2
Guo et al 2014	10	QS12	35.50	80.20	Quanshuigou	Songpan-Ganzi	North	5.23
Guo et al 2014	10	QS27	35.50	80.20	Quanshuigou	Songpan-Ganzi	North	5.23
Guo et al 2014	10	QS19	35.50	80.20	Quanshuigou	Songpan-Ganzi	North	5.23
Guo et al 2014	10	QS23	35.50	80.20	Quanshuigou	Songpan-Ganzi	North	5.23
Guo et al 2014	10	QS18	35.50	80.20	Quanshuigou	Songpan-Ganzi	North	5.23
Guo et al 2014	10	QS24	35.50	80.20	Quanshuigou	Songpan-Ganzi	North	5.23
Guo et al 2014	10	KY03	35.40	81.90	Keliya	Songpan-Ganzi	North	0.56
Guo et al 2014	10	KY02	35.40	81.90	Keliya	Songpan-Ganzi	North	0.56
Guo et al 2014	10	KY06	35.40	81.90	Keliya	Songpan-Ganzi	North	0.56
Guo et al 2014	10	KY01	35.40	81.90	Keliya	Songpan-Ganzi	North	0.56
Guo et al 2014	10	HS041	35.50	82.80	Heishibei	Songpan-Ganzi	North	1.28
Guo et al 2014	10	HS046	35.50	82.80	Heishibei	Songpan-Ganzi	North	1.28
Guo et al 2014	10	HS047	35.50	82.80	Heishibei	Songpan-Ganzi	North	1.28
Guo et al 2014	10	HS028	35.50	82.80	Heishibei	Songpan-Ganzi	North	1.28
Guo et al 2014	10	AH607	35.90	81.50	Ashikule	Songpan-Ganzi	North	1.07
Guo et al 2014	10	AH605	35.90	81.50	Ashikule	Songpan-Ganzi	North	1.07
Guo et al 2014	10	AH609	35.90	81.50	Ashikule	Songpan-Ganzi	North	1.07
Guo et al 2014	10	AH602	35.90	81.50	Ashikule	Songpan-Ganzi	North	1.07
Guo et al 2014	10	AH618	35.90	81.50	Ashikule	Songpan-Ganzi	North	1.07

Reference	Ref. #	Sample	Lat	Long	Locality	Terrane	Zone	Age (Ma)
Guo et al 2014	10	AH615	35.90	81.50	Ashikule	Songpan-Ganzi	North	1.07
Guo et al 2014	10	YS74	35.90	79.20	Dahongliutan	Songpan-Ganzi	North	3.78
Guo et al 2014	10	YS78	35.90	79.20	Dahongliutan	Songpan-Ganzi	North	3.78
Guo et al 2014	10	YS05	35.90	79.20	Dahongliutan	Songpan-Ganzi	North	3.78
Guo et al 2014	10	YS79	35.90	79.20	Dahongliutan	Songpan-Ganzi	North	3.78
Guo et al 2014	10	YS07	35.90	79.20	Dahongliutan	Songpan-Ganzi	North	3.78
Guo et al 2014	10	KX44	36.20	79.00	Kangxiwa	Songpan-Ganzi	North	3.24
Guo et al 2014	10	KX51	36.20	79.00	Kangxiwa	Songpan-Ganzi	North	3.24
Guo et al 2014	10	KX80	36.20	79.00	Kangxiwa	Songpan-Ganzi	North	3.24
Guo et al 2014	10	KX49	36.20	79.00	Kangxiwa	Songpan-Ganzi	North	3.24
Guo et al 2014	10	KX62	36.20	79.00	Kangxiwa	Songpan-Ganzi	North	3.24
Guo et al 2014	10	PL53	36.30	81.70	Pulu	Songpan-Ganzi	North	1.2
Guo et al 2014	10	PL61	36.30	81.70	Pulu	Songpan-Ganzi	North	1.2
Guo et al 2014	10	PL3	36.30	81.70	Pulu	Songpan-Ganzi	North	1.2
Guo et al 2014	10	PL18	36.30	81.70	Pulu	Songpan-Ganzi	North	1.2
Guo et al 2014	10	PL92	36.30	81.70	Pulu	Songpan-Ganzi	North	1.2
Guo et al 2014	10	PL43	36.30	81.70	Pulu	Songpan-Ganzi	North	1.2
Harris et al 1988	11	G10	29.50	91.50	Gangdese Granite (Quxu)	Lhasa	South	41.4
Harris et al 1988	11	G15A	29.50	91.50	Gangdese Tonalite (Dagze)	Lhasa	South	56
Harris et al 1988	11	S70C	30.00	90.50	Nyainqentanglha Granite gneiss	Lhasa	South	50
Harris et al 1988	11	S70D	30.00	90.50	Nyainqentanglha Fol. granite	Lhasa	South	50
Hébert et al 2014	12	07-SA-21	29.00	87.00		Lhasa	South	15
Hébert et al 2014	12	07-SA-26A	29.00	87.00		Lhasa	South	15
Hébert et al 2014	12	07-SA-26B	29.00	87.00		Lhasa	South	15
Hébert et al 2014	12	07-SG-03	29.00	86.00		Lhasa	South	14.03
Hébert et al 2014	12	07-SG-04A	29.00	86.00		Lhasa	South	14.03
Hébert et al 2014	12	07-SG-05	29.00	86.00		Lhasa	South	14.03
Hébert et al 2014	12	07-SG-06	29.00	86.00		Lhasa	South	14.03
Hébert et al 2014	12	07-SG-29	29.00	86.00		Lhasa	South	14.03

Reference	Ref. #	Sample	Lat	Long	Locality	Terrane	Zone	Age (Ma)
Hébert et al 2014	12	07-SG-30	29.00	86.00		Lhasa	South	14.03
Hébert et al 2014	12	07-SG-31A	29.00	86.00		Lhasa	South	15
Hébert et al 2014	12	07-SG-31B	29.00	86.00		Lhasa	South	15
Hébert et al 2014	12	07-SG-48A	29.00	86.00		Lhasa	South	15
Hébert et al 2014	12	07-SG-48B	29.00	86.00		Lhasa	South	15
Hébert et al 2014	12	07-SG-52A	29.00	86.00		Lhasa	South	15
Hébert et al 2014	12	07-SG-66	29.00	86.00		Lhasa	South	11.8
Hébert et al 2014	12	06-SA-28C	29.00	87.00		Lhasa	South	15
Hébert et al 2014	12	06-SA-48A	29.00	87.00		Lhasa	South	15
Hébert et al 2014	12	06-SG-200	29.00	86.00		Lhasa	South	15
Hébert et al 2014	12	06-SG-201	29.00	86.00		Lhasa	South	13.87
Hébert et al 2014	12	07-SA-25	29.00	87.00		Lhasa	South	15
Jiang et al 2006	13	NQ2-1*	31.44	97.46	East Qiangtang	Qiangtang	Central	38.86
Jiang et al 2006	13	NQ21-4*	31.44	97.46	East Qiangtang	Qiangtang	Central	38.86
Jiang et al 2006	13	NQ7-1*	31.44	97.46	East Qiangtang	Qiangtang	Central	38.86
Jiang et al 2006	13	Y1-11	31.45	97.46	East Qiangtang	Qiangtang	Central	38.86
Jiang et al 2006	13	Y1-12	31.44	97.46	East Qiangtang	Qiangtang	Central	38.86
Jiang et al 2006	13	Y1-13	31.45	97.46	East Qiangtang	Qiangtang	Central	38.86
Jiang et al 2006	13	Y1-14	31.45	97.46	East Qiangtang	Qiangtang	Central	38.86
Jiang et al 2006	13	Y1-15	31.45	97.46	East Qiangtang	Qiangtang	Central	38.86
Jiang et al 2006	13	Y115-90	31.44	97.46	East Qiangtang	Qiangtang	Central	38.86
Jiang et al 2006	13	Y1-16	31.45	97.46	East Qiangtang	Qiangtang	Central	38.86
Jiang et al 2006	13	Y1-18	31.44	97.46	East Qiangtang	Qiangtang	Central	38.86
Jiang et al 2006	13	Y1-8	31.45	97.46	East Qiangtang	Qiangtang	Central	38.86
Jiang et al 2006	13	Y1-9	31.45	97.46	East Qiangtang	Qiangtang	Central	38.86
Jiang et al 2006	13	Y2-1	31.44	97.46	East Qiangtang	Qiangtang	Central	38.86
Jiang et al 2006	13	Y2-2	31.44	97.46	East Qiangtang	Qiangtang	Central	38.86
Jiang et al 2006	13	Y2-3	31.45	97.46	East Qiangtang	Qiangtang	Central	38.86
Jiang et al 2006	13	Y2-4	31.45	97.46	East Qiangtang	Qiangtang	Central	38.86
Jiang et al 2006	13	Y2-5	31.45	97.46	East Qiangtang	Qiangtang	Central	38.86

Reference	Ref. #	Sample	Lat	Long	Locality	Terrane	Zone	Age (Ma)
Jiang et al 2006	13	Y2-6	31.44	97.46	East Qiangtang	Qiangtang	Central	38.86
Jiang et al 2006	13	Y2-7	31.45	97.46	East Qiangtang	Qiangtang	Central	38.86
Jiang et al 2006	13	Y2-8	31.45	97.46	East Qiangtang	Qiangtang	Central	38.86
Jiang et al 2006	13	Y2-9	31.45	97.46	East Qiangtang	Qiangtang	Central	38.86
Jiang et al 2006	13	Z96-2*	31.44	97.46	East Qiangtang	Qiangtang	Central	38.86
Jiang et al 2008	14	KK06003	35.72	91.51	1	Songpan-Ganzi	North	11.49
Jiang et al 2008	14	KK06004	35.72	91.51	1	Songpan-Ganzi	North	11.49
Jiang et al 2008	14	KK06005	35.72	91.51	1	Songpan-Ganzi	North	11.49
Jiang et al 2008	14	KK06006	35.72	91.51	1	Songpan-Ganzi	North	11.49
Jiang et al 2008	14	KK06007	35.72	91.51	1	Songpan-Ganzi	North	11.49
Jiang et al 2008	14	KK06008	35.72	91.51	1	Songpan-Ganzi	North	11.49
Jiang et al 2008	14	KK06009	35.72	91.51	1	Songpan-Ganzi	North	11.49
Jiang et al 2008	14	KK06010	35.72	91.51	1	Songpan-Ganzi	North	11.49
Jiang et al 2008	14	KK06011	35.72	91.51	1	Songpan-Ganzi	North	7.89
Jiang et al 2008	14	KK06012	35.72	91.51	1	Songpan-Ganzi	North	7.89
Jiang et al 2008	14	KK06013	35.91	91.27	2	Songpan-Ganzi	North	17.82
Jiang et al 2008	14	KK06014	35.91	91.27	2	Songpan-Ganzi	North	17.82
Jiang et al 2008	14	KK06016	35.91	91.27	2	Songpan-Ganzi	North	17.82
Jiang et al 2008	14	KK06018	35.91	91.27	2	Songpan-Ganzi	North	17.82
Jiang et al 2008	14	KK06019	35.91	91.27	2	Songpan-Ganzi	North	17.82
Jiang et al 2008	14	KK06022	35.91	91.27	2	Songpan-Ganzi	North	17.82
Jiang et al 2008	14	KK06024	35.91	91.27	2	Songpan-Ganzi	North	12.74
Jiang et al 2008	14	KK06025	35.78	90.89	3	Songpan-Ganzi	North	12.74
Jiang et al 2008	14	KK06026	35.78	90.89	3	Songpan-Ganzi	North	12.74
Jiang et al 2008	14	KK06027	35.50	90.40	4	Songpan-Ganzi	North	11.3
Jiang et al 2008	14	KK06028	35.50	90.40	4	Songpan-Ganzi	North	11.3
Jiang et al 2008	14	KK06029	35.50	90.40	4	Songpan-Ganzi	North	11.3
Jiang et al 2008	14	KK06030	35.50	90.40	4	Songpan-Ganzi	North	11.3
Jiang et al 2008	14	KK06031	35.50	90.40	4	Songpan-Ganzi	North	11.3
Jiang et al 2008	14	KK06032	35.76	90.64	5	Songpan-Ganzi	North	8.91

Reference	Ref. #	Sample	Lat	Long	Locality	Terrane	Zone	Age (Ma)
Jiang et al 2008	14	KK06033	35.76	90.64	5	Songpan-Ganzi	North	8.91
Jiang et al 2008	14	KK06034	35.76	90.64	5	Songpan-Ganzi	North	8.91
Jiang et al 2008	14	KK06038	35.90	90.20	6	Songpan-Ganzi	North	7.77
Jiang et al 2008	14	KK06039	35.90	90.20	6	Songpan-Ganzi	North	7.77
Jiang et al 2008	14	KK06040	35.90	90.20	6	Songpan-Ganzi	North	7.77
Jiang et al 2008	14	KK06041	35.90	90.20	6	Songpan-Ganzi	North	7.77
Jiang et al 2008	14	KK06042	35.90	90.20	6	Songpan-Ganzi	North	7.77
Jiang et al 2008	14	KK06043	35.90	90.20	6	Songpan-Ganzi	North	7.77
Jiang et al 2008	14	KK06046	35.90	90.20	6	Songpan-Ganzi	North	7.77
Jiang et al 2008	14	KK06047	35.90	90.20	6	Songpan-Ganzi	North	7.77
Lai and Qin 2013	15	Z02H1	34.30	90.50	Wulanwula	Qiangtang	Central	40.25
Lai and Qin 2013	15	Z07H	34.30	90.50	Wulanwula	Qiangtang	Central	40.25
Lai and Qin 2013	15	Z07H1	34.30	90.50	Wulanwula	Qiangtang	Central	40.25
Lai and Qin 2013	15	Z07H2	34.30	90.50	Wulanwula	Qiangtang	Central	40.25
Lai and Qin 2013	15	Z07H3	34.30	90.50	Wulanwula	Qiangtang	Central	40.25
Lai and Qin 2013	15	Z07H4	34.30	90.50	Wulanwula	Qiangtang	Central	40.25
Lai and Qin 2013	15	Z07H5	34.30	90.50	Wulanwula	Qiangtang	Central	40.25
Lai and Qin 2013	15	Z07H6	34.30	90.50	Wulanwula	Qiangtang	Central	40.25
Lai and Qin 2013	15	Z08H1	34.30	90.50	Wulanwula	Qiangtang	Central	40.25
Lai and Qin 2013	15	Z08H2	34.30	90.50	Wulanwula	Qiangtang	Central	40.25
Lai and Qin 2013	15	Z08H3	34.30	90.50	Wulanwula	Qiangtang	Central	40.25
Lai and Qin 2013	15	Z08H4	34.30	90.50	Wulanwula	Qiangtang	Central	40.25
Lai and Qin 2013	15	Z08H6	34.30	90.50	Wulanwula	Qiangtang	Central	40.25
Lai and Qin 2013	15	Z12H3	34.30	90.50	Wulanwula	Qiangtang	Central	40.25
Lai and Qin 2013	15	Z15H1	34.30	90.50	Wulanwula	Qiangtang	Central	40.25
Lai and Qin 2013	15	Z15H2	34.30	90.50	Wulanwula	Qiangtang	Central	40.25
Lai and Qin 2013	15	Z15H3	34.30	90.50	Wulanwula	Qiangtang	Central	40.25
Lai and Qin 2013	15	Z15H5	34.30	90.50	Wulanwula	Qiangtang	Central	40.25
Lai and Qin 2013	15	Z15H6	34.30	90.50	Wulanwula	Qiangtang	Central	40.25
Lai and Qin 2013	15	Z19H1	34.30	90.50	Wulanwula	Qiangtang	Central	40.25

Reference	Ref. #	Sample	Lat	Long	Locality	Terrane	Zone	Age (Ma)
Lai and Qin 2013	15	Z19H4	34.30	90.50	Wulanwula	Qiangtang	Central	40.25
Lai and Qin 2013	15	Z19H5	34.30	90.50	Wulanwula	Qiangtang	Central	40.25
Lai and Qin 2013	15	Z19H6	34.30	90.50	Wulanwula	Qiangtang	Central	40.25
Lai and Qin 2013	15	Z06H	34.30	90.50	Wulanwula	Qiangtang	Central	40.25
Lai and Qin 2013	15	Z08H5	34.30	90.50	Wulanwula	Qiangtang	Central	40.25
Lai and Qin 2013	15	Z10H	34.30	90.50	Wulanwula	Qiangtang	Central	40.25
Lai and Qin 2013	15	Z11H1	34.30	90.50	Wulanwula	Qiangtang	Central	40.25
Lai and Qin 2013	15	Z11H2	34.30	90.50	Wulanwula	Qiangtang	Central	40.25
Lai and Qin 2013	15	Z12H1	34.30	90.50	Wulanwula	Qiangtang	Central	40.25
Lai and Qin 2013	15	Z12H2	34.30	90.50	Wulanwula	Qiangtang	Central	40.25
Lai and Qin 2013	15	Z15H7	34.30	90.50	Wulanwula	Qiangtang	Central	40.25
Lai and Qin 2013	15	Z15H11	34.30	90.50	Wulanwula	Qiangtang	Central	40.25
Lee et al 2012	16	ET021B	29.60	91.75	Lhasa	Lhasa	South	87
Lee et al 2012	16	ET021C	29.60	91.75	Lhasa	Lhasa	South	105.5
Lee et al 2012	16	ET022A	29.60	91.75	Lhasa	Lhasa	South	105.5
Lee et al 2012	16	ET024	29.60	91.75	Lhasa	Lhasa	South	105.5
Lee et al 2012	16	ST052B	30.17	91.07	Lhasa	Lhasa	South	47.1
Lee et al 2012	16	ST053	30.17	91.07	Lhasa	Lhasa	South	47.1
Lee et al 2012	16	ST054	30.17	91.07	Lhasa	Lhasa	South	47.1
Lee et al 2012	16	ST055A	30.17	91.07	Lhasa	Lhasa	South	49.3
Lee et al 2012	16	ST055B	30.17	91.07	Lhasa	Lhasa	South	49.3
Lee et al 2012	16	ST055C	30.17	91.07	Lhasa	Lhasa	South	43.8
Lee et al 2012	16	ST057A	30.41	91.75	Lhasa	Lhasa	South	46.5
Lee et al 2012	16	ST058	30.41	91.75	Lhasa	Lhasa	South	46.5
Lee et al 2012	16	ST059A	30.41	91.75	Lhasa	Lhasa	South	48.8
Lee et al 2012	16	ST060A	30.41	91.75	Lhasa	Lhasa	South	48.7
Lee et al 2012	16	ST060C	30.41	91.75	Lhasa	Lhasa	South	48.7
Lee et al 2012	16	ST061A	30.41	91.75	Lhasa	Lhasa	South	48.7
Lee et al 2012	16	ST062	30.35	91.08	Lhasa	Lhasa	South	48.5
Lee et al 2012	16	ST101B	29.32	92.05	Lhasa	Lhasa	South	105.5

Reference	Ref. #	Sample	Lat	Long	Locality	Terrane	Zone	Age (Ma)
Lee et al 2012	16	ST102B	29.32	92.05	Lhasa	Lhasa	South	105.5
Lee et al 2012	16	ST109	29.32	92.05	Lhasa	Lhasa	South	105.5
Lee et al 2012	16	ST119A	29.32	92.05	Lhasa	Lhasa	South	105.5
Lee et al 2012	16	ST119B	29.32	92.05	Lhasa	Lhasa	South	105.5
Lee et al 2012	16	ST121	29.32	92.05	Lhasa	Lhasa	South	105.5
Lee et al 2012	16	ST122	29.32	92.05	Lhasa	Lhasa	South	105.5
Lee et al 2012	16	T006B1	30.00	92.40	Lhasa	Lhasa	South	45.7
Lee et al 2012	16	T006B2	30.00	92.40	Lhasa	Lhasa	South	45.7
Lee et al 2012	16	T034A	29.33	90.44	Lhasa	Lhasa	South	43.2
Lee et al 2012	16	T034B	29.33	90.44	Lhasa	Lhasa	South	43.2
Lee et al 2012	16	T036D	29.33	90.44	Lhasa	Lhasa	South	48.6
Lee et al 2012	16	T038F	29.71	86.59	Lhasa	Lhasa	South	47.7
Lee et al 2012	16	T038G	29.71	86.59	Lhasa	Lhasa	South	45.1
Lee et al 2012	16	T038M	29.71	86.59	Lhasa	Lhasa	South	47.7
Lee et al 2012	16	T039	29.71	86.59	Lhasa	Lhasa	South	47.7
Lee et al 2012	16	T040A	29.40	88.32	Lhasa	Lhasa	South	47.7
Lee et al 2012	16	T040B	29.40	88.32	Lhasa	Lhasa	South	47.7
Lee et al 2012	16	T041 J	29.40	88.32	Lhasa	Lhasa	South	49.3
Lee et al 2012	16	T041F	29.40	88.32	Lhasa	Lhasa	South	49.3
Lee et al 2012	16	T041H	29.40	88.32	Lhasa	Lhasa	South	49.3
Lee et al 2012	16	T042C	29.91	88.85	Lhasa	Lhasa	South	49.9
Lee et al 2012	16	T042D	29.91	88.85	Lhasa	Lhasa	South	49.3
Lee et al 2012	16	T046A	29.91	88.85	Lhasa	Lhasa	South	44
Lee et al 2012	16	T047	29.91	88.85	Lhasa	Lhasa	South	44
Lee et al 2012	16	T048B	29.91	88.85	Lhasa	Lhasa	South	44
Lee et al 2012	16	T049A	29.91	88.85	Lhasa	Lhasa	South	44
Lee et al 2012	16	T049B	29.91	88.85	Lhasa	Lhasa	South	44
Lee et al 2012	16	T049C	29.91	88.85	Lhasa	Lhasa	South	44
Lee et al 2012	16	T051B	29.91	88.85	Lhasa	Lhasa	South	44
Lee et al 2012	16	T051C	29.91	88.85	Lhasa	Lhasa	South	44

Reference	Ref. #	Sample	Lat	Long	Locality	Terrane	Zone	Age (Ma)
Lee et al 2012	16	T052	29.91	88.85	Lhasa	Lhasa	South	44
Lee et al 2012	16	T054A	29.91	88.85	Lhasa	Lhasa	South	44
Lee et al 2012	16	T055A	29.51	88.98	Lhasa	Lhasa	South	44
Lee et al 2012	16	T055B	29.51	88.98	Lhasa	Lhasa	South	44
Lee et al 2012	16	T056A	29.51	88.98	Lhasa	Lhasa	South	44
Lee et al 2012	16	T056B	29.51	88.98	Lhasa	Lhasa	South	44
Lee et al 2012	16	T062B	29.68	89.61	Lhasa	Lhasa	South	47.8
Lee et al 2012	16	T062C	29.68	89.61	Lhasa	Lhasa	South	47.8
Lee et al 2012	16	T063	29.68	89.61	Lhasa	Lhasa	South	47.8
Lee et al 2012	16	T064A	29.68	89.61	Lhasa	Lhasa	South	47.8
Lee et al 2012	16	T065A	29.68	89.61	Lhasa	Lhasa	South	48.6
Lee et al 2012	16	T065B	29.68	89.61	Lhasa	Lhasa	South	48.6
Lee et al 2012	16	T066	29.68	89.61	Lhasa	Lhasa	South	48.6
Lee et al 2012	16	T068	29.88	89.93	Lhasa	Lhasa	South	47.8
Lee et al 2012	16	T070A	29.88	89.93	Lhasa	Lhasa	South	47.8
Lee et al 2012	16	T072A	31.65	91.70	Lhasa	Lhasa	South	105.5
Lee et al 2012	16	T072D	31.65	91.70	Lhasa	Lhasa	South	105.5
Lee et al 2012	16	T072E	31.65	91.70	Lhasa	Lhasa	South	105.5
Lee et al 2012	16	T073	31.65	91.70	Lhasa	Lhasa	South	105.5
Lee et al 2012	16	T078B	29.75	91.07	Lhasa	Lhasa	South	97.3
Lee et al 2012	16	T079A	29.75	91.07	Lhasa	Lhasa	South	105.5
Lee et al 2012	16	T079B	29.75	91.07	Lhasa	Lhasa	South	105.5
Lee et al 2012	16	T079C	29.75	91.07	Lhasa	Lhasa	South	105.5
Lee et al 2012	16	T080	29.60	91.75	Lhasa	Lhasa	South	105.5
Lee et al 2012	16	T082A	29.64	90.62	Lhasa	Lhasa	South	43.2
Lee et al 2012	16	T082B	29.64	90.62	Lhasa	Lhasa	South	43.2
Lee et al 2012	16	T083B	29.64	90.62	Lhasa	Lhasa	South	43.2
Lee et al 2012	16	T083C	29.64	90.62	Lhasa	Lhasa	South	43.2
Lee et al 2012	16	T084C	29.64	90.62	Lhasa	Lhasa	South	43.2
Lee et al 2012	16	T102A	29.68	89.61	Lhasa	Lhasa	South	53

Reference	Ref. #	Sample	Lat	Long	Locality	Terrane	Zone	Age (Ma)
Lee et al 2012	16	T103	29.68	89.61	Lhasa	Lhasa	South	47.8
Lee et al 2012	16	T104	29.68	89.61	Lhasa	Lhasa	South	53
Lee et al 2012	16	T105A	29.68	89.61	Lhasa	Lhasa	South	53
Lee et al 2012	16	T110A	30.13	88.74	Lhasa	Lhasa	South	49.9
Lee et al 2012	16	T110B	30.13	88.74	Lhasa	Lhasa	South	49.9
Lee et al 2012	16	T111	30.13	88.74	Lhasa	Lhasa	South	49.9
Lee et al 2012	16	T112	30.13	88.74	Lhasa	Lhasa	South	49.9
Lee et al 2012	16	T113	30.13	88.74	Lhasa	Lhasa	South	49.9
Lee et al 2012	16	T116A	30.90	88.39	Lhasa	Lhasa	South	49.3
Lee et al 2012	16	T117	30.90	88.39	Lhasa	Lhasa	South	49.9
Lee et al 2012	16	T127B	31.44	87.41	Lhasa	Lhasa	South	105.5
Lee et al 2012	16	T129A	31.17	87.25	Lhasa	Lhasa	South	105.5
Lee et al 2012	16	T130	30.90	87.28	Lhasa	Lhasa	South	105.5
Lee et al 2012	16	T131A	30.90	87.28	Lhasa	Lhasa	South	112.3
Lee et al 2012	16	T134	30.59	87.32	Lhasa	Lhasa	South	59.9
Lee et al 2012	16	T136A	30.59	87.32	Lhasa	Lhasa	South	59.9
Lee et al 2012	16	T136B	30.59	87.32	Lhasa	Lhasa	South	59.9
Lee et al 2012	16	T138D	31.38	86.78	Lhasa	Lhasa	South	105.5
Lee et al 2012	16	T139	31.33	86.30	Lhasa	Lhasa	South	85.8
Lee et al 2012	16	T140A	31.33	86.30	Lhasa	Lhasa	South	105.5
Lee et al 2012	16	T140B	31.33	86.30	Lhasa	Lhasa	South	105.6
Lee et al 2012	16	T140D	31.33	86.30	Lhasa	Lhasa	South	105.5
Lee et al 2012	16	T140E	31.33	86.30	Lhasa	Lhasa	South	105.5
Lee et al 2012	16	T142	30.90	85.27	Lhasa	Lhasa	South	71.1
Lee et al 2012	16	T143	30.90	85.27	Lhasa	Lhasa	South	105.5
Lee et al 2012	16	T144A	30.90	85.27	Lhasa	Lhasa	South	105.5
Lee et al 2012	16	T144B	30.90	85.27	Lhasa	Lhasa	South	105.5
Lee et al 2012	16	T144C	30.90	85.27	Lhasa	Lhasa	South	105.5
Lee et al 2012	16	T144D	30.90	85.27	Lhasa	Lhasa	South	105.5
Lee et al 2012	16	T146	30.76	85.36	Lhasa	Lhasa	South	105.5

Reference	Ref. #	Sample	Lat	Long	Locality	Terrane	Zone	Age (Ma)
Lee et al 2012	16	T147	30.76	85.36	Lhasa	Lhasa	South	105.5
Lee et al 2012	16	T151	30.13	85.43	Lhasa	Lhasa	South	53.9
Lee et al 2012	16	T152A	30.13	85.43	Lhasa	Lhasa	South	48.9
Lee et al 2012	16	T152B	30.13	85.43	Lhasa	Lhasa	South	53.9
Lee et al 2012	16	T155	29.82	85.81	Lhasa	Lhasa	South	48.9
Lee et al 2012	16	T160A	29.91	86.70	Lhasa	Lhasa	South	47.7
Lee et al 2012	16	T160B	29.91	86.70	Lhasa	Lhasa	South	47.7
Lee et al 2012	16	T169A	29.82	85.81	Lhasa	Lhasa	South	110.4
Lee et al 2012	16	T169B	29.82	85.81	Lhasa	Lhasa	South	105.5
Lee et al 2012	16	T169C	30.92	91.21	Lhasa	Lhasa	South	105.5
Lee et al 2012	16	T233A	30.05	90.77	Lhasa	Lhasa	South	62.5
Lee et al 2012	16	T233B	30.05	90.77	Lhasa	Lhasa	South	62.5
Lee et al 2012	16	T233C	30.05	90.77	Lhasa	Lhasa	South	62.5
Lee et al 2012	16	T234A	30.05	90.77	Lhasa	Lhasa	South	56.4
Lee et al 2012	16	T234B	30.05	90.77	Lhasa	Lhasa	South	56.4
Lee et al 2012	16	T234C	30.05	90.77	Lhasa	Lhasa	South	56.4
Lee et al 2012	16	T235A	30.05	90.77	Lhasa	Lhasa	South	56.4
Lee et al 2012	16	T235B	30.05	90.77	Lhasa	Lhasa	South	56.4
Lee et al 2012	16	T238B	30.05	90.77	Lhasa	Lhasa	South	62.5
Lee et al 2012	16	T239	29.86	90.58	Lhasa	Lhasa	South	62.5
Lee et al 2012	16	T240B	29.86	90.58	Lhasa	Lhasa	South	62.5
Li 2013	17	GGL01	32.50	89.19	Qiangtang	Qiangtang	Central	79.9
Li 2013	17	GGL02	32.50	89.19	Qiangtang	Qiangtang	Central	79.9
Li 2013	17	GGL03	32.50	89.19	Qiangtang	Qiangtang	Central	79.9
Li 2013	17	GGL04	32.50	89.19	Qiangtang	Qiangtang	Central	79.9
Li 2013	17	GGL05	32.50	89.19	Qiangtang	Qiangtang	Central	79.9
Li 2013	17	GGL06	32.50	89.19	Qiangtang	Qiangtang	Central	79.9
Li 2013	17	GGL07	32.50	89.19	Qiangtang	Qiangtang	Central	79.9
Li 2013	17	GGL08	32.50	89.19	Qiangtang	Qiangtang	Central	79.9
Li 2013	17	GGL09	32.50	89.19	Qiangtang	Qiangtang	Central	79.9

Reference	Ref. #	Sample	Lat	Long	Locality	Terrane	Zone	Age (Ma)
Li 2013	17	GGL10	32.50	89.19	Qiangtang	Qiangtang	Central	79.9
Li 2013	17	GGL11	32.50	89.19	Qiangtang	Qiangtang	Central	79.9
Li 2013	17	GGL12	32.50	89.19	Qiangtang	Qiangtang	Central	79.9
Li 2013	17	GGL13	32.50	89.19	Qiangtang	Qiangtang	Central	79.9
Li 2013	17	GGL14	32.50	89.19	Qiangtang	Qiangtang	Central	79.9
Li 2013	17	GGL15	32.50	89.19	Qiangtang	Qiangtang	Central	75.9
Liu et al 2014	18	GJ0601	32.00	82.00	Xungba	Lhasa	South	23
Liu et al 2014	18	GJ0602	32.00	82.00	Xungba	Lhasa	South	23
Liu et al 2014	18	GJ0605	32.00	82.00	Xungba	Lhasa	South	23
Liu et al 2014	18	GJ0606	32.00	82.00	Xungba	Lhasa	South	23
Liu et al 2014	18	08YR04	32.00	82.00	Xungba	Lhasa	South	23
Liu et al 2014	18	GJ0614	32.00	82.00	Xungba	Lhasa	South	23
Liu et al 2014	18	GJ0617	32.00	82.00	Xungba	Lhasa	South	23
Liu et al 2014	18	GJ0619	32.00	82.00	Xungba	Lhasa	South	23
Liu et al 2014	18	GJ0620	32.00	82.00	Xungba	Lhasa	South	23
Liu et al 2014	18	GJ0624	32.00	82.00	Xungba	Lhasa	South	23
Liu et al 2014	18	GJ0627	32.00	82.00	Xungba	Lhasa	South	23
Liu et al 2014	18	GJ0628	32.00	82.00	Xungba	Lhasa	South	23
Liu et al 2014	18	GJ0629	32.00	82.00	Xungba	Lhasa	South	23
Liu et al 2014	18	10XB03	32.00	82.00	Xungba	Lhasa	South	24
Liu et al 2014	18	10XB04	32.00	82.00	Xungba	Lhasa	South	24
Liu et al 2014	18	10XB07	32.00	82.00	Xungba	Lhasa	South	24
Liu et al 2014	18	08YR05	32.00	82.00	Xungba	Lhasa	South	23
Liu et al 2014	18	10XB10	32.00	82.00	Xungba	Lhasa	South	23
Liu et al 2014	18	10XB12	32.00	82.00	Xungba	Lhasa	South	23
Liu et al 2014	18	10XB13	32.00	82.00	Xungba	Lhasa	South	23
Liu et al 2014	18	10YR01	32.00	82.00	Xungba	Lhasa	South	24
Liu et al 2014	18	10YR02	32.00	82.00	Xungba	Lhasa	South	24
Liu et al 2014	18	10YR04	32.00	82.00	Xungba	Lhasa	South	24
Liu et al 2014	18	10YR04a	32.00	82.00	Xungba	Lhasa	South	24

Reference	Ref. #	Sample	Lat	Long	Locality	Terrane	Zone	Age (Ma)
Liu et al 2014	18	10YR07	32.00	82.00	Xungba	Lhasa	South	24
McKenna & Walker 1990	19	MV1B			Ulugh Mutztagh	Songpan-Ganzi	Central	4
McKenna & Walker 1990	19	MV2	36.47	87.48	Ulugh Mutztagh	Songpan-Ganzi	North	4
McKenna & Walker 1990	19	UM1B	36.47	87.4797	Ulugh Mutztagh	Songpan-Ganzi	North	4
McKenna & Walker 1990	19	UM3V	36.47	87.4797	Ulugh Mutztagh	Songpan-Ganzi	North	4
McKenna & Walker 1990	19	UMQP	36.47	87.48	Ulugh Mutztagh	Songpan-Ganzi	North	4
McKenna & Walker 1990	19	UMVU	36.47	87.4797	Ulugh Mutztagh	Songpan-Ganzi	North	4
Miller et al 1999	20	TE008/93	32.00	82	Xungba	Lhasa	South	23
Miller et al 1999	20	TE011/93	32.00	82	Xungba	Lhasa	South	23
Miller et al 1999	20	TE125/93	32.00	82	Xungba	Lhasa	South	23
Miller et al 1999	20	TE126/93	32.00	82	Xungba	Lhasa	South	23
Miller et al 1999	20	TE127/93	32.00	82	Xungba	Lhasa	South	23
Miller et al 1999	20	TE131/93	32.00	82	Xungba	Lhasa	South	23
Miller et al 1999	20	TE137/93	32.00	82	Xungba	Lhasa	South	18
Miller et al 1999	20	TE138/93	31.50	81.5	Xungba	Lhasa	South	18
Miller et al 1999	20	TE117/93	31.50	82.3	E Jarga	Lhasa	South	18
Miller et al 1999	20	TE118/93	31.50	82.3	E Jarga	Lhasa	South	18
Miller et al 1999	20	TE007/93	32.00	82	Xungba	Lhasa	South	23
Miller et al 1999	20	TE025/93	32.00	82	Xungba	Lhasa	South	23
Miller et al 1999	20	TE136/93	32.00	82	Xungba	Lhasa	South	18
Miller et al 1999	20	TE148/93	31.50	81.5	Bongba	Lhasa	South	25
Miller et al 1999	20	TE150/93	31.50	81.5	Bongba	Lhasa	South	25
Miller et al 1999	20	TE153/93	31.50	81.5	Bongba	Lhasa	South	25
Miller et al 1999	20	TE154/93	31.50	81.5	Bongba	Lhasa	South	25
Miller et al 1999	20	TE047/93	31.50	81.75	Gegar	Lhasa	South	17
Miller et al 1999	20	TE189/93	31.50	81.5	Mana-sarowar	Lhasa	South	17

Reference	Ref. #	Sample	Lat	Long	Locality	Terrane	Zone	Age (Ma)
Miller et al 1999	20	TE192/93	31.50	81.5	Mana-sarowar	Lhasa	South	17
Miller et al 1999	20	TE194/94	31.50	81.5	Mana-sarowar	Lhasa	South	17
Nomade et al 2004	21	Y-2	29.75	90.34	Yangying	Lhasa	South	10.72
Nomade et al 2004	21	Y-4	29.75	90.34	Yangying	Lhasa	South	10.88
Nomade et al 2004	21	ZB1	31.50	84.5	Zabuye	Lhasa	South	16.16
Nomade et al 2004	21	ZB4	31.50	84.5	Zabuye	Lhasa	South	16.12
Nomade et al 2004	21	ZB10	31.50	84.5	Zabuye	Lhasa	South	16.06
Nomade et al 2004	21	ZB12	31.50	84.5	Zabuye	Lhasa	South	16.06
Turner 1993	22	K732	34.97	81.6316		Songpan-Ganzi	North	13.3
Turner 1993	22	K738	34.97	81.6316		Songpan-Ganzi	North	13
Turner 1993	22	K89G185	34.88	79.5223		Songpan-Ganzi	North	11.8
Turner 1993	22	K89G200	34.88	79.5223		Songpan-Ganzi	North	9.6
Turner 1993	22	K9007	33.62	88.6244		Songpan-Ganzi	Central	9.4
Turner 1993	22	K9008	33.55	88.6702		Songpan-Ganzi	Central	8.5
Turner 1993	22	K9021	33.55	88.6702		Songpan-Ganzi	Central	5.6
Turner 1993	22	K9024	33.55	88.6702		Songpan-Ganzi	Central	3.6
Turner 1993	22	K9031	33.55	88.6702		Songpan-Ganzi	Central	0.5
Turner 1993	22	K9038	33.61	88.5997		Songpan-Ganzi	Central	0.3
Turner 1996	23	Bb-105	33.62	88.6244	VIII	Qiangtang	Central	5.6
Turner 1996	23	Bb-107	33.62	88.6244	VIII	Qiangtang	Central	3
Turner 1996	23	Bb-109	33.62	88.6244	VIII	Qiangtang	Central	3.1
Turner 1996	23	Bb-114	33.62	88.6244	VIII	Qiangtang	Central	3.2
Turner 1996	23	Bb-88	33.62	88.6244	VIII	Qiangtang	Central	3.2
Turner 1996	23	Bb-89	33.62	88.6244	VIII	Qiangtang	Central	6.4
Turner 1996	23	Bb94-2	33.62	88.6244	VIII	Qiangtang	Central	3.6
Turner 1996	23	Bb-95	33.62	88.6244	VIII	Qiangtang	Central	3
Turner 1996	23	Bg 121	35.50	86.0107	VI	Songpan-Ganzi	North	14
Turner 1996	23	Bg 124	35.50	86.0107	VI	Songpan-Ganzi	North	14
Turner 1996	23	COUL311	28.90	90	XI	Lhasa	South	14.4
Turner 1996	23	COUL326	28.90	90	XI	Lhasa	South	14.4

Reference	Ref. #	Sample	Lat	Long	Locality	Terrane	Zone	Age (Ma)
Turner 1996	23	COUL328	28.90	90	XI	Lhasa	South	14.4
Turner 1996	23	COUL338	28.90	90	XI	Lhasa	South	14.4
Turner 1996	23	COUL339	28.90	90	XI	Lhasa	South	14.4
Turner 1996	23	k705	34.97	81.6316	IV	Kunlun	North	0.3
Turner 1996	23	k708	34.97	81.6316	IV	Kunlun	North	0.5
Turner 1996	23	K713	34.97	81.6316	IV	Kunlun	North	0.4
Turner 1996	23	K716	34.97	81.6316	IV	Kunlun	North	3.1
Turner 1996	23	K718	34.97	81.6316	IV	Kunlun	North	3
Turner 1996	23	K720	34.97	81.6316	IV	Kunlun	North	3.1
Turner 1996	23	K723	34.97	81.6316	IV	Kunlun	North	0.6
Turner 1996	23	K732	34.97	81.6316	IV	Kunlun	North	0.3
Turner 1996	23	K738	34.97	81.6316	IV	Kunlun	North	0.5
Turner 1996	23	K89G159	32.64	79.3847	X	Lhasa	South	16
Turner 1996	23	K89G162	32.64	79.3847	X	Lhasa	South	18
Turner 1996	23	K89G163	32.64	79.3847	X	Lhasa	South	20
Turner 1996	23	K89G185	34.88	79.5223	I	Kunlun	North	5.6
Turner 1996	23	K89G186	34.88	79.5223	I	Kunlun	North	5.6
Turner 1996	23	K89G191	34.88	79.5223	I	Kunlun	North	5.3
Turner 1996	23	K89G192	34.88	79.5223	I	Kunlun	North	5.3
Turner 1996	23	K89G193	34.88	79.5223	I	Kunlun	North	5.3
Turner 1996	23	K89G197	34.88	79.5223	I	Kunlun	North	6.4
Turner 1996	23	K89G200	34.88	79.5223	I	Kunlun	North	8.7
Turner 1996	23	K9002	34.00	89	V-IX	Qiangtang	Central	11.7
Turner 1996	23	K9006	33.30	90.2981	VIII	Qiangtang	Central	9.4
Turner 1996	23	K9007	33.62	88.6244	VIII	Qiangtang	Central	8.4
Turner 1996	23	K9008	33.55	88.6702	VIII	Qiangtang	Central	9.9
Turner 1996	23	K9016	33.55	88.6702	VIII	Qiangtang	Central	8.5
Turner 1996	23	K9017	34.00	89	V-IX	Qiangtang	Central	12.9
Turner 1996	23	K9018	33.55	88.6702	VIII	Qiangtang	Central	18.5
Turner 1996	23	K9019	34.00	89	V-IX	Qiangtang	Central	11.9

Reference	Ref. #	Sample	Lat	Long	Locality	Terrane	Zone	Age (Ma)
Turner 1996	23	K9021	33.55	88.6702	VIII	Qiangtang	Central	11.8
Turner 1996	23	K9024	34.00	89	IX	Qiangtang	Central	9.6
Turner 1996	23	K9026	33.55	88.6702	VIII	Qiangtang	Central	12.5
Turner 1996	23	K9027	34.00	89	V-IX	Qiangtang	Central	15.5
Turner 1996	23	K9028	33.55	88.6702	VIII	Qiangtang	Central	18.5
Turner 1996	23	K9029	34.00	89	V-IX	Qiangtang	Central	15.2
Turner 1996	23	K9031	33.55	88.6702	VIII	Qiangtang	Central	11.6
Turner 1996	23	K9032	33.62	88.6244	VIII	Qiangtang	Central	11.9
Turner 1996	23	K9038	33.61	88.5997	VIII	Qiangtang	Central	9.6
Turner 1996	23	K9039	33.61	88.5997	VIII	Qiangtang	Central	12.5
Turner 1996	23	Kp 35-10	36.12	88.7161	VII	Kunlun	North	1.07
Turner 1996	23	Kp12-58	34.97	81.6316	IV	Kunlun	North	16
Turner 1996	23	Kp23-2	36.12	88.7161	VII	Kunlun	North	1.2
Turner 1996	23	Kp24-1	35.00	80.577	III	Kunlun	North	0.4
Turner 1996	23	Kp39-3	36.12	88.7161	VII	Kunlun	North	16
Turner 1996	23	Kp47-2	36.12	88.7161	VII	Kunlun	North	18
Turner 1996	23	Kp47-5	36.12	88.7161	VII	Kunlun	North	20
Wang 2012	24	2303	35.75	90.6631	Southern Malanshan	Songpan-Ganzi	North	9
Wang 2012	24	2509	35.97	90.8017	Bukadaban	Songpan-Ganzi	North	1.5
Wang 2012	24	1P2JD7-1	35.79	90.4275	Hudongliang	Songpan-Ganzi	North	3
Wang 2012	24	1P2JD7-1a	35.85	90.4844	Hudongliang	Songpan-Ganzi	North	3
Wang 2012	24	2011a	35.79	90.4275	Hudongliang	Songpan-Ganzi	North	3
Wang 2012	24	2059a	35.97	90.8017	Bukadaban	Songpan-Ganzi	North	1.5
Wang 2012	24	2303a	35.75	90.6564	Southern Malanshan	Songpan-Ganzi	North	9
Wang 2012	24	2511-1	35.97	91.0333	Bukadaban	Songpan-Ganzi	North	1.5
Wang et al 2010	25	04wq-1	34.62	89.2686	Duogecuoren	Qiangtang	Central	46.6
Wang et al 2010	25	04wq-2	34.62	89.2686	Duogecuoren	Qiangtang	Central	46.6
Wang et al 2010	25	04wq-3	34.62	89.2686	Duogecuoren	Qiangtang	Central	46.6
Wang et al 2010	25	04wq-4	34.62	89.2686	Duogecuoren	Qiangtang	Central	44.2
Wang et al 2010	25	04wq-5	34.62	89.2686	Duogecuoren	Qiangtang	Central	44.2

Reference	Ref. #	Sample	Lat	Long	Locality	Terrane	Zone	Age (Ma)
Wang et al 2010	25	04wq-6	34.31	89.3	Duogecuoren	Qiangtang	Central	44.2
Wang et al 2010	25	04wq-7	34.31	89.3	Duogecuoren	Qiangtang	Central	44.2
Wang et al 2010	25	4086-1	34.31	89.3	Duogecuoren	Qiangtang	Central	44.2
Wang et al 2010	25	8528	34.29	88.6653	Duogecuoren	Qiangtang	Central	42.5
Wang et al 2010	25	8518-1	34.29	88.6653	Duogecuoren	Qiangtang	Central	39
Wang et al 2010	25	8518-2	34.29	88.6653	Narigongma	Qiangtang	Central	42
Wang et al 2010	25	9063-GS2	34.71	89.2833	Lianghe	Qiangtang	Central	38.7
Wang et al 2010	25	9063-GS3	34.71	89.2833	Lushui	Qiangtang	Central	38.7
Wang et al 2010	25	D3145	34.78	87.1431	Bamaoquongzhong	Qiangtang	Central	29.2
Wang et al 2014	26	05S2-7	31.36	82.9	Sailipu	Lhasa	South	17.75
Wang et al 2014	26	05S2-8-1	31.36	82.9	Sailipu	Lhasa	South	17.75
Wang et al 2014	26	05SLP5-3	31.36	82.9	Sailipu	Lhasa	South	17.75
Wang et al 2014	26	05SLP5-05	31.36	82.9	Sailipu	Lhasa	South	17.75
Wang et al 2014	26	05SLP5-06	31.36	82.9	Sailipu	Lhasa	South	17.75
Wang et al 2014	26	05SLP5-7	31.36	82.9	Sailipu	Lhasa	South	17.75
Wang et al 2014	26	05SLP5-8	31.36	82.9	Sailipu	Lhasa	South	17.75
Wang et al 2014	26	05SLP5-09	31.36	82.9	Sailipu	Lhasa	South	17.75
Wang et al 2014	26	S05SLP5-10	31.36	82.9	Sailipu	Lhasa	South	17.75
Wang et al 2014	26	05SLP5-11	31.36	82.9	Sailipu	Lhasa	South	17.75
Wang et al 2014	26	05SLP5-16	31.36	82.9	Sailipu	Lhasa	South	17.75
Wang et al 2014	26	05SLP4-01	31.36	82.9	Sailipu	Lhasa	South	17.75
Wang et al 2014	26	05SLP4-02	31.36	82.9	Sailipu	Lhasa	South	17.75
Wang et al 2014	26	05SLP4-03	31.36	82.9	Sailipu	Lhasa	South	17.75
Wang et al 2014	26	05SLP4-04	31.36	82.9	Sailipu	Lhasa	South	17.75
Wang et al 2014	26	05S2-7	31.36	82.9	Sailipu	Lhasa	South	17.75
Wang et al 2014	26	05S2-8-1	31.36	82.9	Sailipu	Lhasa	South	17.75
Wang et al 2015	27	WR-12-48	32.28	80.1472	Gaer	Lhasa	South	49.3
Wang et al 2015	27	WR-12-47	32.15	80.025	Zhada	Lhasa	South	63.8
Wang et al 2015	27	WR-12-44	31.89	80.25	Yajie	Lhasa	South	61
Wang et al 2015	27	WR-12-45	31.89	80.25	Yajie	Lhasa	South	61

Reference	Ref. #	Sample	Lat	Long	Locality	Terrane	Zone	Age (Ma)
Wang et al 2015	27	WR-12-40	31.48	80.6278	Ganre	Lhasa	South	49.3
Wang et al 2015	27	WR-12-42	31.48	80.6278	Ganre	Lhasa	South	54.8
Wang et al 2015	27	WR-12-33	29.60	86.3333	Sangsang-Saga	Lhasa	South	50.7
Wang et al 2015	27	WR-12-35	29.60	86.3333	Sangsang-Saga	Lhasa	South	50.7
Williams et al 2001	28	T2A/98	29.80	86.9	Pabbai Z.	Lhasa	South	13.8
Williams et al 2001	28	T3b/98	29.80	86.9	Pabbai Z.	Lhasa	South	13.8
Williams et al 2001	28	T4A/98	29.80	86.9	Pabbai Z.	Lhasa	South	13.3
Williams et al 2001	28	T5A/98	29.80	86.9	Pabbai Z.	Lhasa	South	13.3
Williams et al 2001	28	T11B/98	30.00	85.8	Daggya Tso	Lhasa	South	17.3
Williams et al 2001	28	JPT 14.2	30.00	85.8	Daggya Tso	Lhasa	South	19.3
Williams et al 2004	29	JPT24A	33.60	79.7	Shiquanhe	Lhasa	Central	23.2
Williams et al 2004	29	JPT24B	33.60	79.7	Shiquanhe	Lhasa	Central	22.3
Williams et al 2004	29	JPT24C	33.60	79.7	Shiquanhe	Lhasa	Central	24
Williams et al 2004	29	JPT22	33.60	79.7	Shiquanhe	Lhasa	Central	23
Williams et al 2004	29	K89G162	33.60	79.7	Shiquanhe	Lhasa	Central	23.13
Williams et al 2004	29	20E39A	35.60	79.7	Shiquanhe	Lhasa	North	18
Williams et al 2004	29	JPT7	29.80	87.8	P.Z.	Lhasa	South	15.8
Williams et al 2004	29	T5B/98	29.80	87.8	P.Z.	Lhasa	South	15.8
Williams et al 2004	29	JPT14.1	30.20	85.3	Daggyai Tso	Lhasa	South	18.8
Williams et al 2004	29	JPT3	29.90	89.6	Namling	Lhasa	South	13.9
Williams et al 2004	29	JPT4	29.90	89.6	Namling	Lhasa	South	13.4
Williams et al 2004	29	JPT5.2	29.90	89.6	Namling	Lhasa	South	12.5
Williams et al 2004	29	JPT8	29.90	89.6	Namling	Lhasa	South	13.8
Williams et al 2004	29	95RAS11.3	29.90	89.6	Namling	Lhasa	South	14.48
Williams et al 2004	29	T2A	29.80	87.8	P.Z.	Lhasa	South	15.8
Williams et al 2004	29	T3B	29.80	87.8	P.Z.	Lhasa	South	15.8
Williams et al 2004	29	T4A	29.80	87.8	P.Z.	Lhasa	South	15.8
Williams et al 2004	29	T5A	29.80	87.8	P.Z.	Lhasa	South	15.8
Williams et al 2004	29	912	35.90	82	Ash	Kunlun	North	1.2
Williams et al 2004	29	1105	35.90	82	Ash	Kunlun	North	5

Reference	Ref. #	Sample	Lat	Long	Locality	Terrane	Zone	Age (Ma)
Williams et al 2004	29	K702	35.90	82	Ash	Kunlun	North	0.5
Williams et al 2004	29	K703	35.90	82	Ash	Kunlun	North	0.5
Williams et al 2004	29	K89G185	35.50	80.3	Tien	Songpan-Ganzi	North	5
Williams et al 2004	29	K89G186	35.50	80.3	Tien	Songpan-Ganzi	North	5
Williams et al 2004	29	K89G200	35.50	80.3	Tien	Songpan-Ganzi	North	5
Williams et al 2004	29	KP 12.6	35.50	85.3	Hei	Songpan-Ganzi	North	
Williams et al 2004	29	KP47-2	35.50	85.3	Hei	Songpan-Ganzi	North	
Williams et al 2004	29	KP47-5	35.50	85.3	Hei	Songpan-Ganzi	North	
Williams et al 2004	29	Bb 124	35.60	80.9	Qiang	Kunlun	North	12.7
Williams et al 2004	29	Bb121	35.60	80.9	Qiang	Kunlun	North	12.7
Williams et al 2004	29	Bq137	35.60	80.9	Qiang	Kunlun	North	12.7
Williams et al 2004	29	Bb119	35.60	80.9	Qiang	Kunlun	North	12.7
Williams et al 2004	29	Bb122	35.60	80.9	Qiang	Kunlun	North	12.7
Williams et al 2004	29	Bb135	35.60	80.9	Qiang	Kunlun	North	12.7
Williams et al 2004	29	Bg142	35.70	87.4	Yong	Songpan-Ganzi	North	9.4
Williams et al 2004	29	Bq140	35.70	87.4	Yong	Songpan-Ganzi	North	9.4
Williams et al 2004	29	Bq141	35.70	87.4	Yong	Songpan-Ganzi	North	9.4
Williams et al 2004	29	K9024	36.10	89.5	Kunlun	Kunlun	North	12.47
Williams et al 2004	29	K9026	36.10	89.5	Kunlun	Kunlun	North	12.4
Williams et al 2004	29	K9027	36.10	89.5	Kunlun	Kunlun	North	12.47
Williams et al 2004	29	K9028	36.10	89.5	Kunlun	Kunlun	North	12.47
Williams et al 2004	29	K9029	36.10	89.5	Kunlun	Kunlun	North	13
Williams et al 2004	29	K9031	36.10	89.5	Kunlun	Kunlun	North	12.47
Williams et al 2004	29	K9032	36.10	89.5	Kunlun	Kunlun	North	11.9
Williams et al 2004	29	K9038	36.10	89.5	Kunlun	Kunlun	North	12.47
Williams et al 2004	29	K9039	36.10	89.5	Kunlun	Kunlun	North	12.5
Williams et al 2004	29	K9041	36.10	89.5	Kunlun	Kunlun	North	12.47
Williams et al 2004	29	K9001	34.10	90.1	Dogai C.	Qiangtang	Central	8.9
Williams et al 2004	29	K9002	34.10	90.1	Dogai C.	Qiangtang	Central	8.7
Williams et al 2004	29	K9006	34.10	90.1	Dogai C.	Qiangtang	Central	8.9

Reference	Ref. #	Sample	Lat	Long	Locality	Terrane	Zone	Age (Ma)
Williams et al 2004	29	K9007	34.10	90.1	Dogai C.	Qiangtang	Central	8.9
Williams et al 2004	29	K9008	34.10	90.1	Dogai C.	Qiangtang	Central	8.9
Williams et al 2004	29	K9016	34.10	90.1	Dogai C.	Qiangtang	Central	8.9
Williams et al 2004	29	K9017	34.10	90.1	Dogai C.	Qiangtang	Central	9
Williams et al 2004	29	K9018	34.10	90.1	Dogai C.	Qiangtang	Central	8.9
Williams et al 2004	29	K9019	34.10	90.1	Dogai C.	Qiangtang	Central	9
Williams et al 2004	29	K9021	34.10	90.1	Dogai C.	Qiangtang	Central	8.9
Yang and Ding 2013	30	2007k251	36.80	86.07	Silver Mountain	Songpan-Ganzi	North	3.799
Yang and Ding 2013	30	2007k252	36.80	86.07	Silver Mountain	Songpan-Ganzi	North	3.799
Yang and Ding 2013	30	2007k253	36.80	86.07	Silver Mountain	Songpan-Ganzi	North	4.28
Yang and Ding 2013	30	2007k254	36.80	86.07	Silver Mountain	Songpan-Ganzi	North	14.71
Zhang et al 2008	31	DHLT-10	35.87	79.2834	West Kunlun	Kunlun	North	7.97
Zhang et al 2008	31	DHLT-2	35.87	79.2834	West Kunlun	Kunlun	North	7.97
Zhang et al 2008	31	DHLT-4	35.87	79.2834	West Kunlun	Kunlun	North	7.97
Zhang et al 2008	31	DHLT-5	35.87	79.2834	West Kunlun	Kunlun	North	7.97
Zhang et al 2008	31	DHLT-7	35.87	79.2834	West Kunlun	Kunlun	North	7.97
Zhang et al 2008	31	DHLT-9	35.87	79.2834	West Kunlun	Kunlun	North	7.97
Zhang et al 2008	31	PL-12	36.35	81.475	West Kunlun	Kunlun	North	7.97
Zhang et al 2008	31	PL-2	36.35	81.475	West Kunlun	Kunlun	North	7.97
Zhang et al 2008	31	PL-3	36.35	81.475	West Kunlun	Kunlun	North	7.97
Zhang et al 2008	31	PL-5	36.35	81.475	West Kunlun	Kunlun	North	7.97
Zhang et al 2008	31	PL-7	36.35	81.475	West Kunlun	Kunlun	North	7.97
Zhang et al 2008	31	PL-9	36.35	81.475	West Kunlun	Kunlun	North	7.97
Zhang et al 2008	31	YCN-1	36.00	79	West Kunlun	Kunlun	North	7.97
Zhang et al 2008	31	YCN-2	36.00	79	West Kunlun	Kunlun	North	7.97
Zhang et al 2008	31	YCN-3	36.00	79	West Kunlun	Kunlun	North	7.97
Zhang et al 2008	31	YCN-4	36.00	79	West Kunlun	Kunlun	North	7.97
Zhang et al 2008	31	YCN-6	36.00	79	West Kunlun	Kunlun	North	7.97
Zhang et al 2008	31	YCN-7	36.00	79	West Kunlun	Kunlun	North	7.97
Zhang et al 2008	31	YCN-8	36.00	79	West Kunlun	Kunlun	North	7.97

Reference	Ref. #	Sample	Lat	Long	Locality	Terrane	Zone	Age (Ma)
Zhang et al 2008	31	KP24-1	35.80	81.5	Ashikule	Kunlun	North	1.3
Zhang et al 2008	31	KP25-3	35.80	81.5	Ashikule	Kunlun	North	1.3
Zhang et al 2008	31	KP28-1	35.80	81.5	Ashikule	Kunlun	North	1.3
Zhang et al 2008	31	KP33-3	35.80	81.5	Ashikule	Kunlun	North	1.3
Zhang et al 2008	31	KP39-1	35.25	78.5	Kangxiwa	Kunlun	North	3.8
Zhang et al 2008	31	KP39-4	35.25	78.5	Kangxiwa	Kunlun	North	3.8
Zhang et al 2008	31	KP47-1	35.00	80.25	Quanshiguo	Kunlun	North	7.97
Zhang et al 2008	31	KP47-4	35.00	80.25	Quanshiguo	Kunlun	North	7.97
Zhang et al 2008	31	KP47-7	35.00	80.25	Quanshiguo	Kunlun	North	7.97
This Study	32	11UMT14	34.07	92.3515	Kaixinling	Songpan-Ganzi	North	0
This Study	32	11UMT15	34.07	92.35	Kaixinling	Songpan-Ganzi	North	0
This Study	32	11UMT17-a	34.54	92.7533	Fenghuoshan	Songpan-Ganzi	North	26.25
This Study	32	12HG04	35.57	89.5165	LagangriGr	Songpan-Ganzi	North	5.8
This Study	32	12HG06	35.57	89.5398	LagangriGr	Songpan-Ganzi	North	5.8
This Study	32	12HXV01	35.48	91.9333	ZhuonaiCC	Songpan-Ganzi	North	23.89
This Study	32	12HXV08	35.64	91.5913	ZhuonaiVF	Songpan-Ganzi	North	13
This Study	32	12HXV09	35.56	90.5711	Yinma	Songpan-Ganzi	North	13.36
This Study	32	12HXV12	35.70	91.4392	ZhuonaiVF	Songpan-Ganzi	North	13
This Study	32	12HXV15	35.67	91.6366	ZhuonaiVF	Songpan-Ganzi	North	13
This Study	32	12HXV19	35.67	91.6292	ZhuonaiVF	Songpan-Ganzi	North	13
This Study	32	12HXV21A	35.66	91.6629	ZhuonaiVF	Songpan-Ganzi	North	13
This Study	32	12HXV23	35.66	91.622	ZhuonaiVF	Songpan-Ganzi	North	13
This Study	32	12HXV24	35.61	91.6291	ZhuonaiVF	Songpan-Ganzi	North	13
This Study	32	12HXV32	35.64	91.5928	ZhuonaiVF	Songpan-Ganzi	North	13
This Study	32	12HXV33	35.48	91.9331	ZhuonaiCC	Songpan-Ganzi	North	23.89
This Study	32	13DV05	35.15	89.0299	DogaiVF	Songpan-Ganzi	North	9
This Study	32	13DV04	35.15	89.0438	DogaiVF	Songpan-Ganzi	North	9
This Study	32	13DV11	35.11	88.9855	DogaiVF	Songpan-Ganzi	North	9
This Study	32	13DV13	35.08	88.9927	DogaiVF	Songpan-Ganzi	North	9
This Study	32	13DV14	35.08	88.9926	DogaiVF	Songpan-Ganzi	North	9

Reference	Ref. #	Sample	Lat	Long	Locality	Terrane	Zone	Age (Ma)
This Study	32	13DV15	35.08	88.9927	DogaiVF	Songpan-Ganzi	North	9
This Study	32	13DV23	35.07	89.1521	DogaiVF	Songpan-Ganzi	North	7.5
This Study	32	13DV29	35.02	89.2317	DogaiVF	Songpan-Ganzi	North	7.5
This Study	32	13LG07	35.59	89.552	LagangriGr	Songpan-Ganzi	North	15.9
This Study	32	13XV01	35.56	89.226	XiangyangVF	Songpan-Ganzi	North	8.5
This Study	32	13XV02	35.56	89.226	XiangyangVF	Songpan-Ganzi	North	8.5

Table B.2 – Major element compositions of compiled geochemical data for the Tibetan Plateau. See sources for methods.

Ref. #	Sample	SiO2	Al2O3	TiO2	Fe2O3	Fe2O3(t)	FeO	FeO(t)	MnO	CaO	MgO	K2O	Na2O	P2O5	LOI	Total
1	K89G185	51.42	14.62	1.85	3.35		3.02		0.14	7.59	4.03	4.77	4.6			99.76
1	K89G186	49.8	13.65	1.77	3.27		2.94		0.12	7.2	5.6	4.7	3.8	1.25		100.24
1	K89G189	52.2	14.6	1.79	3.29		2.96		0.12	7.56	4.21	4.69	3.79			99.01
1	K89G190	56.05	13.77	1.33	2.83		2.55		0.11	6.59	4.4	4.35	3.69			99.02
1	KB9G191	56.95	14.1	1.36	2.86		2.57		0.1	6.45	3.8	4.75	3.89	0.99		100.01
1	K89G192	57.5	14.15	1.32	2.82		2.54		0.09	5.85	3.36	5.15	4.1	0.97		99.84
1	K189G193	57.09	14.31	1.31	2.81		2.53		0.09	6.74	3.67	4.99	4.06			99.66
1	K89G197	75.1	12.95	0.1	1.6		1.44		0.01	0.6	0.04	4.9	4.35	0.04		99.44
1	K89G200	56.67	13.8	1.43	2.93		2.64		0.1	6.35	4.37	5.4	4.02			99.04
2	05S2-4	58.63	11.64	1.5		5.68			0.06	3.64	7.09	8.28	1.57	0.59		100.09
2	05S2-6	57.89	11.3	1.47		5.93			0.08	3.59	7.74	8.55	1.53	0.75		99.55
2	05S2-9	58.62	12.54	1.33		6.75			0.08	3.77	7.24	7.32	1.86	0.11		100.14
2	05SLP5-1	55.77	13.29	1.48		6.92			0.09	4.81	6.99	6.31	2.34	0.57		99.75
2	05SLP5-2	59.31	12	1.37		5.56			0.07	3.36	7.02	8.16	1.79	0.43		100.07
2	05SLP5-4	56.97	13.45	1.45		6.54			0.08	4.35	6.75	6.52	2.37	0.36		99.55
2	CM10-04-04	56.63	10.83	1.66		6.07			0.08	5.49	7.18	6.89	1.75	0.3		99.96
2	CM10-04-09	56.25	10.95	1.78		5.55			0.08	5.2	6.42	2.58	4.21	0.27		99.39
2	CM10-04-12	55.99	11.1	1.56		7.53			0.08	5.84	6.96	6.11	1.77	0.08		99.49
2	04DYH-01	55.33	15.11	1.01		7.2			0.17	6.64	6.34	3.34	3.12	0.28		100.05
2	D3141	46.96	10.28	1.22		9.45			0.16	11.84	11.06	3.73	1.8	1.15		99.58
3	04LQS-2	61.64	14.84	0.5		4.8			0.07	5.2	5.43	3.31	3.95	0.06	0.86	100.67
3	04LQS-3	63.15	15	0.55		4.83			0.04	4.68	4.01	3.52	3.95	0.06	1.73	101.5
3	04LQS-6	57.77	15.41	0.77		6.16			0.09	7.71	4.65	2.49	4.01	0.47	2.28	101.81
3	04LQS-14	67.38	15.88	0.44		3.33			0.05	3.17	1.66	3.23	4.24	0.15	0.25	99.79
3	04LQS-16	64.4	16.26	0.55		4.56			0.05	4.56	2.26	2.75	4.29	0.03	1.05	100.74
3	04YJL-05	58.44	15.19	0.79		7.18			0.09	6.34	5.73	2.93	3.03	0.04	0.63	100.39
3	04YJL-07	61.2	15.2	0.83		5.26			0.07	4.48	4.37	4.28	2.94	0.08	0.67	99.36
3	04YJL-06	62.99	15.89	0.83		4.71			0.06	4.31	3.56	4.17	3.34	0.09	0.55	100.49

Ref. #	Sample	SiO2	Al2O3	TiO2	Fe2O3	Fe2O3(t)	FeO	FeO(t)	MnO	CaO	MgO	K2O	Na2O	P2O5	LOI	Total
3	04YJL-09	64.22	14.51	0.7		4.4			0.06	3.63	3.66	4.45	2.62	0.09	1.72	100.04
3	04DN30-2	55.47	15.27	1.02		7.09			0.1	6.87	6.01	3.37	3.48	0.25	1.2	100.13
3	04DN30-3	61.07	15.53	0.74		5.55			0.08	4.66	4.49	3.51	3.23	0.08	1	99.94
3	04DN31-1	62.17	16.06	0.83		5.2			0.08	4.43	3.36	3.29	3.5	0.05	0.62	99.61
3	04DN32-1	64.17	16.03	0.69		4.73			0.03	4.36	1.99	3.12	4.49	0.04	0.85	100.48
3	04DN32-2	63.91	16.15	0.69		4.95			0.03	4.13	1.83	3.17	4.54	0.04	0.93	100.37
3	04DN35-2	62.83	15.96	0.79		5.24			0.05	4.11	2.57	3.3	3.46	0.14	1.64	100.1
3	04DN36-3	60.93	15.9	0.92		5.7			0.09	5	4.1	3.38	3.17	0.21	1.19	100.57
3	04DN37-2	57.91	16.65	0.9		5.72			0.12	6.4	4.24	3.39	3.43	0.06	1.21	100.03
3	04DN39	62.9	15.89	0.84		5.67			0.09	4.51	2.78	3.29	3.44	0.14	0.84	100.41
3	04DN40	65.55	15.27	0.55		3.86			0.04	4.04	2.85	3.55	3.33	0.05	1.34	100.41
3	04DY44-2	59.41	16.11	0.88		5.84			0.07	5.81	3.83	3.29	3.11	0.19	1.57	100.1
3	04DY44-4	63.77	15.32	0.6		4.44			0.17	4.21	3.36	3.56	3.58	0.13	0.82	99.97
3	04DY44-7	60.04	15.79	0.82		5.48			0.05	5.74	3.67	4.08	3.43	0.02	0.76	99.88
3	04D6441	63.15	14.12	0.77		5.74			0.09	4.17	4.35	4.85	2.48	0.03	0.12	99.86
3	04D6437	58.53	15.19	0.96		6.09			0.06	5.3	4.04	4.71	2.9	0.08	1.51	99.37
4	2T394	44.98	15.99	2.15	11.79			10.61	0.18	7.99	7.01	0.98	4.6	0.8	2.97	99.44
4	2T395	44.3	16.05	2.15	11.7			10.53	0.19	8.4	7.3	1.2	4.5	0.65	3.2	99.6
4	2T396	44.91	15.88	2.3	11.86			10.67	0.16	8.13	7.02	0.94	4.58	0.85	2.91	99.54
4	98T03	48.41	15.21	1.17	9.5			8.55	0.17	10.07	9.48	0.5	3.53	0.41	1.76	100.21
4	98T04	47.2	15.13	1.78	9.91			8.92	0.15	9.32	8.8	0.67	3.76	0.52	2.46	99.7
4	98T07	53.84	17.41	1.1	6.27			5.64	0.17	4.04	1.02	7.68	3.89	0.17	3.84	99.43
4	98T15	51.2	15.53	1.17	7.65			6.88	0.2	5.95	2.49	4.89	3.01	0.41	5.61	98.11
4	98T16	55.91	13.24	0.79	9.38			8.44	0.25	3.93	0.89	5.91	3.85	0.03	4.8	98.98
4	98T33	51.83	16.78	1.15	7.85			7.06	0.21	3.5	0.73	6.66	2.52	0.09	7.09	98.41
4	98T38	57.62	13.56	0.82	9.04			8.13	0.27	3.78	0.48	5.83	4.74	0.05	3.4	99.59
4	98T43	56.94	13.32	0.87	8.93			8.04	0.25	4.28	0.48	5.83	4.32	0.13	3.74	99.09
4	98T44	47.78	17.5	1.04	7.25			6.52	0.19	5.29	1.06	8.51	2.58	0.23	5.74	97.17
4	98T46	56.46	14.72	0.8	8			7.2	0.32	3.25	0.69	6.36	3.39	0.01	4.35	98.35

Ref. #	Sample	SiO2	Al2O3	TiO2	Fe2O3	Fe2O3(t)	FeO	FeO(t)	MnO	CaO	MgO	K2O	Na2O	P2O5	LOI	Total
4	98T49	54	18.18	0.97	5.95			5.35	0.17	3.71	0.71	6.83	3.28	0.02	5.68	99.5
4	98T51	53.87	14.85	0.71	7.55			6.79	0.26	5.46	0.72	6.57	3.6	0.29	5.93	99.81
4	98T52	47.37	14.4	1.13	6.7			6.03	0.12	9.69	3.68	3.21	2.97	1.02	6.49	96.97
4	98T53	51.27	16.75	0.9	7.17			6.45	0.21	4.94	0.97	8.07	4.17	0.17	4.17	98.79
4	98T54	54.09	20.44	0.33	2.67			2.4	0.34	2.63	0.6	9.38	3.46	0.93	4.31	99.18
4	98T57	51.02	16.31	0.92	7.57			6.81	0.22	4.81	0.65	6.58	3.68	0.11	6.04	97.91
4	98T69	50.54	17.58	1.01	7.04			6.33	0.19	4.92	0.95	7.96	2.89	0.12	5.25	98.45
4	98T70	48.68	16.77	1.06	6.91			6.22	0.17	6.52	1.15	7.36	2.16	0.12	7.06	97.96
4	98T71	56.26	14.2	0.82	7.5			6.75	0.25	2.65	0.76	6.02	4.46	0.36	4.55	97.83
4	98T73	52.91	15.81	0.72	7.2			6.48	0.21	5.59	0.16	6.98	2.6	0.02	6.4	98.6
4	99T132	49.71	11.85	1.08	7.49			6.74	0.24	10.34	7.18	6.17	1.62	1.34	1.78	99.41
4	99T134	68.54	14.07	0.66	3.15			2.83	0.14	1.24	1.11	6.54	2.68	0.37	1.06	100
4	99T145	65.02	14.67	0.66	3.39			3.05	0.16	2.26	1.5	7.38	2.57	0.43	4.18	99.38
4	99T152	60.45	13.71	0.98	4.82			4.34	0.17	4.86	3.82	7.53	2.41	0.59	1.18	99.66
4	99T154	56.81	12.71	0.97	5.58			5.02	0.19	7.12	4.59	8.19	1.8	0.77	1.01	99.57
4	99T53	60.15	14.47	1.24	3.76			3.38	0.12	2.79	2.06	10.55	1.92	0.57	2.63	99.65
4	99T56	59.45	13.91	1.22	4.19			3.77	0.13	3.04	3.07	11.24	2.24	0.47	1.21	99.71
4	99T57	56.79	13.29	1.43	5.07			4.56	0.16	3.7	3.24	8.62	2.34	0.56	1.76	99.8
4	99T60	59.22	14.02	1.26	4.16			3.74	0.13	2.95	3.36	11.66	1.26	0.46	0.67	100
4	99T62	58.9	13.93	1.26	4.16			3.74	0.16	3.92	3.51	10.09	1.96	0.67	1.16	99.89
5	2002T1021	57.72	15.67	1.34	6.51			5.86	0.12	5.29	2.13	3.74	3.95	0.59	2.93	99.56
5	2002T1022	56.66	15.39	1.33	6.73			6.06	0.14	5.51	2.35	3.71	4.03	0.61	3.35	99.39
5	2002T1023	57.23	15.42	1.3	7.33			6.6	0.1	5.15	2.87	3.74	3.88	0.53	2.33	99.34
5	2002T1024	57.22	15.33	1.32	7.57			6.81	0.13	5.33	2.27	3.68	3.77	0.59	2.88	99.53
5	2002T1025	57.98	15.74	1.32	6.85			6.16	0.11	5.12	1.95	3.75	3.8	0.55	2.65	99.36
5	2002T1026	56.89	15.42	1.33	7.18			6.46	0.15	5.4	1.94	3.65	3.81	0.58	3.51	99.39
5	2003T373	47.62	15.85	2.08	9.91			8.92	0.12	7.15	6.35	1.94	3.16	0.8	4.67	99.65
5	2003T374	47.94	15.64	1.96	9.77			8.79	0.14	7.64	7.29	2.44	3.11	0.76	2.87	99.55
5	2003T375	54.24	16.79	1.58	8.04			7.23	0.08	6.18	3.05	3.28	4.57	0.87	1.12	99.8

Ref. #	Sample	SiO2	Al2O3	TiO2	Fe2O3	Fe2O3(t)	FeO	FeO(t)	MnO	CaO	MgO	K2O	Na2O	P2O5	LOI	Total
5	2003T380	59.23	16.44	1.17	6.28			5.65	0.09	4.53	2.78	3.27	4.19	0.59	0.99	99.55
5	2003T483	60.54	16.34	1.17	5.36			4.82	0.08	4.04	1.75	3.37	4.36	0.52	2.13	99.66
5	2003T485	63.61	15.67	0.86	4.26			3.83	0.05	3.52	1.92	3.83	4.03	0.37	1.47	99.59
5	2003T486	63.25	15.64	0.85	4.45			4	0.05	3.49	1.99	3.87	3.99	0.37	1.45	99.39
5	2003T487	62.05	15.72	0.95	4.85			4.36	0.05	3.84	2.31	3.52	3.94	0.42	1.85	99.5
5	2003T488	66.78	15.89	0.72	2.18			1.96	0.01	2.47	0.64	4.26	3.77	0.32	2.32	99.36
5	2003T492	60.68	16.31	1.19	5.69			5.12	0.03	3.89	0.84	3.53	4.09	0.4	2.97	99.61
6	Tl/10	53.33	10.87	1.68	2.64		3.22		0.1	6.69	8.13	4.47	2.22	0.97	4.57	
6	Tl/11	54	11.09	1.62	3.59		2.22		0.09	6.83	7.74	7.33	1.33	0.76	2.37	
6	Tl/18	56.72	13.4	1.58	3.34		2.42		0.07	5.27	5.13	8.02	2.08	0.67	0.61	
6	Tl/13	54.36	12.18	1.45	4.59		1.68		0.1	6.74	6.34	6.99	2.29	0.87	1.37	
6	Tl/03	54.72	11.53	1.43	5.05		1.58		0.08	7.06	6.6	6.34	2.26	0.9	1.66	
6	Tl/08	56.64	13.49	1.61	4.56		1.4		0.07	5.42	4.65	8.05	2.04	0.69	0.56	
6	Tl/17	60.7	13.29	1.06	2.37		1.98		0.07	4.04	3.47	8.21	2.78	0.7	0.46	
6	Tl/06	60.92	14.16	1.22	3.11		1.05		0.06	3.26	2.74	9.17	2.49	0.58	0.49	
6	Tl/59	62.62	13.79	0.92	2.25		1.42		0.07	2.58	2.57	8.74	2.65	0.51	0.63	
6	CHZ-1	54.28	12.82	1.6	3.39		2.95		0.11	6.48	5.66	8.1	1.59	1.22	0.84	
6	CHZ-2	54.42	12.75	1.62	3.29		2.85		0.11	6.48	5.87	7.92	1.79	1.22	0.8	
6	CHZ-3	55.2	12.98	1.66	2.69		3.48		0.1	6.1	5.71	8.29	1.66	1.06	0.28	
6	CHZ-4	54.18	13.59	1.53	2.7		3.88		0.12	6.54	5.95	7.5	1.61	0.93	0.66	
6	CHZ-5	54.37	13.7	1.51	2.89		3.67		0.11	6.36	5.74	7.62	1.67	0.94	0.61	
6	CHZ-6	55.66	13.71	1.52	3.11		3.02		0.09	5.78	4.95	8.2	1.81	0.9	0.43	
6	CHZ-7	54	12.79	1.59	3.3		2.93		0.12	6.64	6.05	8.04	1.51	1.26	0.73	
6	CHZ-8	54.15	12.76	1.6	3.25		2.82		0.12	6.67	5.84	8.27	1.46	1.2	0.84	
6	CHZ-9	54.07	12.64	1.62	3.43		2.68		0.12	6.79	5.9	8.36	1.37	1.38	0.78	
6	CHZ-10	53.9	12.73	1.63	3.51		2.68		0.11	6.59	6.03	8.61	1.34	1.26	0.73	
6	CHZ-11	53.5	12.57	1.6	3.28		2.92		0.1	7.12	6.32	7.7	1.61	1.32	0.91	
6	CHZ-12	54.58	12.78	1.61	3.31		2.95		0.11	6.37	5.88	8.32	1.61	1.16	0.51	
7	AH-7	57.52	13.73	1.05		9.19			0.08	6.24	3.61	4.65	3.48	0.45	0.7	

Ref. #	Sample	SiO2	Al2O3	TiO2	Fe2O3	Fe2O3(t)	FeO	FeO(t)	MnO	CaO	MgO	K2O	Na2O	P2O5	LOI	Total
7	G26	57.69	14.24	1.31		6.77			0.15	5.5	3.61	6.68	3.55	0.48	2.55	
7	G68	57.44	18.37	1.16		7.92			0.13	6.06	0.91	4.85	3.01	0.14	2.33	
7	G98-0	53.11	15.26	1.38		9.86			0.14	7.6	5.71	4.24	2.14	0.56	1.33	
7	G98-1	50.24	12.02	1.2		8.11			0.14	10.4	8.42	6.32	2.89	0.25	1.24	
7	G98-14	47.58	13.12	1.36		9.66			0.09	12.12	7.15	4.81	3.72	0.39	2.41	
7	G98-3	47.36	13.8	1.07		12.34			0.11	10.76	8.06	3.31	2.95	0.23	0.62	
7	G98-6	46.47	12.9	0.75		12.19			0.12	12.06	9.02	3.88	2.33	0.26	1.48	
7	G98-9	48.34	12.87	1.45		10.92			0.11	11.01	8.04	4.42	2.27	0.57	2.11	
7	HH72	47.29	13.56	1.55		8.91			0.14	10.48	8.46	4.51	3.62	1.48	1.91	
7	HS07	54.46	13.57	1.6		9.33			0.07	7.76	5.19	3.58	3.77	0.67	2.46	
7	HS-69	45.82	13.34	1.43		10.22			0.14	10.7	8.7	5.59	3.19	0.87	1.19	
7	JC9719	48.66	13.54	1.46		9.12			0.17	9.88	9.17	4.7	2.41	0.89	2.87	
7	JC973	49.43	14.86	1.39		10.32			0.14	9.93	6.34	4.88	2.05	0.65	1.83	
7	JC975	47.16	12.79	1.52		10.58			0.15	10.43	9.21	4.75	2.17	1.23	2.03	
7	JC978	49.49	12.93	1.6		11.52			0.09	9.14	7.62	4.89	2.05	0.66	0.46	
7	JH6	46.26	13.33	1.48		10.34			0.12	10.41	8.3	4.76	3.79	1.2	1.15	
7	KX84	44.12	13.93	1.39		9.94			0.15	12.32	8.76	4.9	3.36	1.12	2.34	
7	PL-58	55.97	14.51	1.68		9			0.11	7.26	4.13	3.86	2.6	0.88	0.68	
7	PL-7	45.19	11.62	1.68		10.97			0.16	12.01	9.19	3.88	3.66	1.63	0.79	
7	QQ08	57.62	16.53	1.18		6.43			0.13	6.68	3.11	4	3.53	0.8	1.82	
7	QS22	50.7	13.27	1.57		9.19			0.14	9.92	7.37	4.42	2.15	1.27	1.14	
7	XT16	52.92	14.23	1.13		9.53			0.15	8.13	5.82	4.29	3.16	0.63	1.21	
7	XT8	53.35	13.4	1.08		10.69			0.16	7.38	6.4	3.67	3.15	0.71	0.34	
7	XY03	52.28	13.99	1.61		7.4			0.11	9.39	6.34	4.23	3.29	1.37	2.57	
7	XY05	62.08	15.82	1.44		6.87			0.06	4	1.82	4.26	3.01	0.64	0.16	
7	YS02	50.2	13.28	1.05		8.95			0.14	10.28	6.95	4.66	3.76	0.71	2.75	
7	YS72	56.64	14.29	1.18		6.58			0.12	5.15	4.27	7.35	3.56	0.84	0.59	
7	ZF91	61.77	16.46	0.73		5.48			0.13	4.75	2.16	3.85	3.4	1.28	1.39	
7	ZF96	59.1	15.19	1.22		6.63			0.09	6.41	3.41	3.97	3.32	0.68	0.54	

Ref. #	Sample	SiO2	Al2O3	TiO2	Fe2O3	Fe2O3(t)	FeO	FeO(t)	MnO	CaO	MgO	K2O	Na2O	P2O5	LOI	Total
8	ZF09	66.47	16.07	0.91		2.35			0.07	3.85	2.2	3.48	4.21	0.39	1.53	99.78
8	GUO62	65.93	18.11	0.64		2.86			0.05	3.74	1.99	2.24	4.16	0.27	0.36	99.52
8	GUO51	68.15	16.31	0.48		2.95			0.07	2.88	2.24	2.83	3.7	0.38	0.27	100.47
8	GUO48	62.68	17.02	0.85		3.84			0.07	4.63	2.72	2.79	4.98	0.41	0.66	99.54
8	GUO37	59.22	18.13	0.74		5.93			0.07	5.28	2.95	1.68	5.85	0.14	1.29	99.91
8	G09	67.29	16.18	0.63		2.46			0.06	3.69	1.49	3.7	4.28	0.22	0.47	99.76
8	ZFG17	69.36	17.08	0.65		2.36			0.1	1.71	2.59	2.15	3.72	0.26	1.06	99.63
8	G006	70.02	16.07	0.46		2.02			0.02	1.86	1.41	3.31	4.69	0.13	0.52	99.89
8	G019	68.56	15.25	0.48		1.72			0.06	2.49	1.77	5.37	4.16	0.13	1.82	100.04
8	G016	68.82	16.01	0.23		1.42			0.03	1.74	1.3	6.77	3.57	0.1	0.87	99.93
8	G025	66.52	17.57	0.44		2.8			0.05	3.95	1.73	2.38	4.41	0.16	1.68	99.64
9	DY-7	56.52	12.08	1.46		5.72			0.12	5.56	6.83	9.24	1.61	0.86	1.05	
9	DC2	54.91	12.46	1.57		6.13			0.17	5.83	6.12	10.68	1.08	1.05	0.79	
9	D509	55.36	12.17	1.78		5.84			0.09	5.91	7.05	9.45	1.16	1.19	0.84	
9	DG43	55.82	12.53	1.55		6.22			0.11	5.55	7.24	8.96	1.27	0.75	1.34	
9	YE51	58.32	11.1	1.29		5.68			0.04	6.06	7.22	8.07	1.5	0.72	1.67	
9	YC08	56.74	11.86	1.44		6.01			0.09	4.96	6.59	9.36	1.67	1.28	0.98	
9	YG13	56.88	11.18	1.53		5.35			0.03	5.31	7.79	9.89	1.17	0.87	1.07	
9	YF12	55.49	11.94	1.62		5.78			0.03	6.19	7.35	8.62	1.86	1.12	1.29	
9	YA32	56.41	11.53	1.7		6.93			0.07	6.24	6.26	7.78	2.13	0.95	0.83	
9	MH78	55.27	12.31	1.63		6.52			0.08	6.43	8.79	5.93	2.18	0.86	1.17	
9	MH69	56.36	12.59	1.61		5.58			0.1	5.72	9.34	6.47	1.62	0.61	1.46	
9	MG-3	56.91	12.57	1.65		5.74			0.06	6.03	6.56	8.07	1.43	0.98	1.2	
9	MY1	53.79	12.04	1.69		6.85			0.07	7.37	7.38	8.15	1.72	0.94	0.46	
9	MK09	55.14	11.97	1.61		6.75			0.08	5.52	8.11	7.49	2.46	0.87	0.62	
9	MR21	55.53	12.86	1.64		6.1			0.08	6.21	7.65	6.87	2.04	1.02	0.73	
9	MA75	54.57	11.89	1.4		7.37			0.11	5.67	9.22	7.18	1.7	0.89	0.65	
9	MX5	56.13	13.03	1.37		5.98			0.06	6.12	8.08	6.86	1.63	0.74	1.02	
9	2003T534	55.09	12.7	1.47		6.82			0.1	6	8.37	6.49	2.18	0.76	0.87	

Ref. #	Sample	SiO2	Al2O3	TiO2	Fe2O3	Fe2O3(t)	FeO	FeO(t)	MnO	CaO	MgO	K2O	Na2O	P2O5	LOI	Total
9	2003T536	54.56	12.18	1.5		7.1			0.11	5.94	9.19	6.48	2.2	0.75	1.15	
9	2003T539	54.6	12.34	1.48		6.92			0.11	5.88	9.34	6.39	2.2	0.75	1.05	
9	G8	57.81	13.67	1.12		6.24			0.11	6.44	5.9	5.29	2.68	0.74	1.28	
9	C10	56.14	12.57	1.43		6.47			0.14	6.85	6.19	7.16	2.14	0.91	0.79	
9	CV5	55.76	13.35	1.31		6.56			0.13	6.98	5.94	6.37	2.35	1.25	0.92	
9	C76	55.87	12.77	1.52		6.83			0.12	7.25	6.43	6.03	2.26	0.92	1.16	
9	CH4	56.53	12.84	1.55		7.35			0.11	7.01	6.76	5.35	1.83	0.67	1.04	
9	CH7	52.76	11.37	1.45		7.42			0.13	7.19	10.51	5.83	2.48	0.86	0.58	
9	C03	53.64	11.85	1.63		6.71			0.11	6.99	10.79	5.14	2.12	1.02	0.49	
9	CX38	55.63	12.34	1.49		7.56			0.09	7.34	7.08	4.81	2.59	1.07	0.72	
9	C25	57.18	12.09	1.62		5.52			0.14	6.75	6.61	6.49	2.48	1.12	0.93	
10	CT09	55.04	14	1.52		7.5			0.13	6.47	5.51	5.3	3.85	0.69	1.12	
10	CT12	52.62	13.38	1.58		8.66			0.12	8.19	6.38	4.18	4.15	0.74	0.79	
10	CT17	53.32	13.19	1.65		8.81			0.14	7.29	6.43	4.84	3.76	0.56	0.68	
10	CT05	52.45	14.33	1.44		7.29			0.08	7.19	5.86	5.62	4.35	1.39	1.21	
10	CT23	50.43	13.61	1.76		8.16			0.11	7.83	6.45	5.82	4.79	1.06	0.94	
10	QS12	50.3	15.36	1.35		9.63			0.14	9.32	5.74	3.6	3.18	1.38	0.82	
10	QS27	48.8	13.88	1.5		10.86			0.12	9.84	6.49	3.86	3.38	1.26	1.01	
10	QS19	49.66	13.27	1.4		10.77			0.13	9.58	6.23	4.3	3.21	1.44	1.34	
10	QS23	47.97	14.61	1.58		10.33			0.13	9.1	7.09	4.64	3.3	1.25	0.76	
10	QS18	48.75	14.75	1.67		10.45			0.11	8.75	7.33	3.72	3.48	0.99	0.59	
10	QS24	49.62	14.95	1.72		10.09			0.12	8.38	7.16	3.8	3.03	1.12	1.32	
10	KY03	54.71	14.13	1.64		7.58			0.13	7.32	5.77	4.25	3.23	1.24	1.18	
10	KY02	52.26	14.26	1.83		8.27			0.12	9.73	4.95	4.37	3.36	0.85	0.46	
10	KY06	56.46	13.49	1.15		8.62			0.14	4.83	6.12	4.84	3.04	1.31	0.75	
10	KY01	55.58	14.53	1.36		7.69			0.11	6.43	5.68	4.51	3.17	0.94	0.98	
10	HS041	53.18	14.67	1.68		9.36			0.15	7.56	5.37	3.68	3.64	0.71	1.14	
10	HS046	53.43	14.34	1.76		9.17			0.12	8.78	4.74	3.26	3.71	0.69	1.02	
10	HS047	53.33	14.81	2.11		9.5			0.16	7.58	5.02	3.73	2.89	0.87	0.51	

146

Ref.#	Sample	SiO2	Al2O3	TiO2	Fe2O3	Fe2O3(t)	FeO	FeO(t)	MnO	CaO	MgO	K2O	Na2O	P2O5	LOI	Total
10	HS028	54.16	13.18	1.64		9.43			0.14	7.7	5.93	3.48	3.69	0.65	0.77	
10	AH607	47.9	13.91	1.9		10.79			0.18	9.21	7.31	4.35	3.53	0.93	0.82	
10	AH605	46.15	13.78	2.39		11.43			0.16	8.28	8.52	4.74	3.49	1.06	1.57	
10	AH609	48.12	14.24	1.93		9.61			0.14	10.21	6.85	4.45	3.26	1.19	0.68	
10	AH602	47.11	14.1	2.51		9.99			0.15	8.68	8.46	4.41	3.32	1.25	0.66	
10	AH618	46.73	13.85	2.38		10.23			0.16	8.43	8.76	4.74	3.76	0.96	1.79	
10	AH615	47.4	14.55	2.17		10.37			0.17	7.27	9.04	4.52	3.44	1.06	2.05	
10	YS74	51.37	14.61	1.44		8.45			0.13	7.19	5.87	6.27	3.73	0.94	1.37	
10	YS78	57.26	13.05	1.35		7.22			0.11	5.67	5.69	5.18	3.26	1.21	1.78	
10	YS05	50.12	13.87	1.58		8.89			0.14	8.28	6.13	7.23	2.19	1.57	0.84	
10	YS79	57.03	14.72	1.36		6.54			0.11	6.38	4.28	5.36	3.45	0.77	0.8	
10	YS07	57.49	14.18	1.42		6.04			0.12	6.87	4.02	5.86	3.21	0.79	1.43	
10	KX44	48.75	12.76	1.9		9.12			0.15	8.08	8.83	5.71	2.89	1.8	0.74	
10	KX51	48.62	13.55	1.54		9.3			0.12	8.91	8.25	4.68	3.64	1.39	1.46	
10	KX80	49.47	13.71	1.48		9			0.13	9.32	8.29	4.86	2.49	1.26	1.13	
10	KX49	48.52	12.79	1.86		9.15			0.14	8.56	8.77	5.77	2.9	1.54	0.71	
10	KX62	48.55	12.74	1.91		9.23			0.15	8.52	8.83	5.31	3.48	1.28	0.86	
10	PL53	50.3	13.25	1.79		9.33			0.12	8.4	8.15	4.39	3.45	0.83	0.75	
10	PL61	49.52	13.43	1.83		9.5			0.11	8.51	8.1	4.89	3.17	0.94	1.08	
10	PL3	53.79	15.78	2.15		8.43			0.12	6.73	4.39	4.27	3.49	0.85	1.17	
10	PL18	51.37	14.47	2.05		8.69			0.13	9.46	5.08	4.08	3.61	1.06	1.35	
10	PL92	51.25	14.36	1.94		8.77			0.11	9.38	5.19	4.29	3.67	1.04	1.22	
10	PL43	52.63	15.62	2.18		7.84			0.12	7.41	4.64	4.78	3.46	1.32	0.77	
11	G10															
11	G15A															
11	S70C															
11	S70D															
12	07-SA-21	59.03	15.86	0.92		5.57			0.08	3.61	4.51	2.46	4.94	0.34	2.3	
12	07-SA-26A	60.13	16.48	0.91		4.53			0.05	4.86	2.41	0.1	8.44	0.31	2.7	

147

Ref. #	Sample	SiO2	Al2O3	TiO2	Fe2O3	Fe2O3(t)	FeO	FeO(t)	MnO	CaO	MgO	K2O	Na2O	P2O5	LOI	Total
12	07-SA-26B	59.34	16.34	0.89		4.42			0.05	5.04	2.1	0.07	8.34	0.31	3.6	
12	07-SG-03	54.82	14.93	0.76		4.29			0.06	11.3	1.97	3.27	4.28	0.28	3.8	
12	07-SG-04A	59.92	15.42	0.77		4.37			0.06	5.02	2.51	4.22	5.46	0.29	2.1	
12	07-SG-05	60.57	16.09	0.79		4.83			0.07	4.08	2.59	3.45	3.86	0.31	3.3	
12	07-SG-06	58.9	15.98	0.8		4.51			0.07	4.17	2.53	4.77	6.01	0.3	1.6	
12	07-SG-29	66.66	15.07	0.59		3.49			0.04	1.32	1.57	4.84	4.05	0.22	2.1	
12	07-SG-30	67.06	15.12	0.58		3.42			0.04	2.12	1.54	4.73	3.4	0.24	1.3	
12	07-SG-31A	67.28	14.86	0.56		3.06			0.04	1.51	1.42	4.52	4.04	0.2	2.6	
12	07-SG-31B	65.98	14.82	0.58		3.17			0.04	1.97	1.49	4.57	3.61	0.22	3.5	
12	07-SG-48A	65.13	16.57	0.73		3.43			0.04	2.63	1.37	3.86	4.4	0.29	0.9	
12	07-SG-48B	64.88	16.7	0.75		3.53			0.05	2.45	1.4	3.97	4.43	0.3	1	
12	07-SG-52A	58.09	15.72	0.95		6.14			0.09	5.42	4.55	3.27	2.97	0.37	2.8	
12	07-SG-66	65.81	16.25	0.53		3.17			0.04	3.03	1.55	3.66	4.28	0.21	0.9	
12	06-SA-28C	57.2	15.39	0.92		5.73			0.08	3.93	5.05	3.03	4.57	0.27	3.2	
12	06-SA-48A	57.25	15.94	0.88		4.41			0.05	5.91	2.06	0.1	7.28	0.3	4.9	
12	06-SG-200	57.8	17.38	0.86		4.77			0.06	3.28	3.11	4.06	3.47	0.32	3.8	
12	06-SG-201	59.2	16.15	0.78		4.78			0.07	4.57	2.35	3.39	3.16	0.3	4.1	
12	07-SA-25															
13	NQ2-1*	43.99	12.4	0.75	3.59		2.91		0.13	15.5	6.9	4.49	1.86	1.05	5.51	99.08
13	NQ21-4*	54.98	15.74	0.53	3.16		1.14		0.09	6	3	5.85	3.54	0.37	4.85	99.25
13	NQ7-1*	66.17	14.79	0.41	2.1		0.9		0.03	4	1.2	4.46	3.43	0.18	1.48	99.15
13	Y1-11	66.61	17.02	0.39	0.88		0.71		0.03	2.57	0.93	4.75	3.62	0.21	1.83	99.54
13	Y1-12	66.58	16.52	0.4	1.64		1.19		0.03	2.27	1.17	4.5	3.66	0.22	1.38	99.57
13	Y1-13	67.28	16.36	0.37	1.42		0.93		0.02	1.84	0.98	4.92	3.53	0.2	1.68	99.52
13	Y1-14	66.92	16.65	0.37	1.59		0.94		0.04	2.29	1.1	4.5	3.82	0.2	1.24	99.66
13	Y1-15	67.07	16.38	0.39	1.74		0.98		0.03	2.3	0.98	4.66	3.75	0.2	1.21	99.7
13	Y115-90	64.8	16.44	0.52	1.23		1.76		0.06	2.94	2.47	4.27	3.77	0.03	1.47	99.76
13	Y1-16	69.35	16.23	0.37	1.07		0.43		0.01	1.42	0.79	4.89	3.68	0.12	1.62	99.98
13	Y1-18	68.34	15.96	0.37	0.81		0.65		0.01	0.77	1.16	6.89	2.59	0.25	1.78	99.57

Ref. #	Sample	SiO2	Al2O3	TiO2	Fe2O3	Fe2O3(t)	FeO	FeO(t)	MnO	CaO	MgO	K2O	Na2O	P2O5	LOI	Total
13	Y1-8	66.24	16.84	0.4	1.73		0.88		0.02	2.19	1.1	4.41	3.63	0.23	2.04	99.73
13	Y1-9	66.39	16.77	0.39	1.71		0.96		0.02	2.08	1.05	4.74	3.57	0.21	1.64	99.53
13	Y2-1	66.93	16.19	0.37	1.5		0.79		0.04	1.97	1.36	4.17	4.09	0.19	1.92	99.5
13	Y2-2	66.35	16.37	0.41	1.56		0.78		0.02	2.25	1.19	4.94	4	0.22	1.98	100.06
13	Y2-3	67.65	16.26	0.34	1.18		1.06		0.03	1.76	1.11	4.78	4.1	0.16	1.02	99.43
13	Y2-4	67.22	16.15	0.35	1.52		1.01		0.03	1.92	1.14	4.45	4	0.17	1.25	99.22
13	Y2-5	67.66	16.28	0.34	1.46		0.96		0.03	2.25	1.12	4.36	4.07	0.17	1.22	99.93
13	Y2-6	67.14	16.08	0.39	1.29		1		0.04	2.29	1.35	4.42	4.11	0.2	1.26	99.57
13	Y2-7	67.55	16.16	0.34	1.05		1.13		0.03	2.21	1.08	4.73	3.89	0.17	1.11	99.45
13	Y2-8	67.53	16.34	0.33	1.62		0.79		0.04	1.98	1.04	4.86	3.85	0.16	1.36	99.91
13	Y2-9	67.45	16	0.34	1.34		1.02		0.03	2.15	1.09	4.64	4.08	0.17	1.31	99.62
13	Z96-2*	60.37	16.62	0.5	2.68		1.58		0.07	2.37	2.37	5.48	4.92	0.4	1.4	98.76
14	KK06003	60.29	15.51	1.59		6.38			0.08	4.69	2.65	4.31	3.66	0.83	0.9	
14	KK06004	60.42	15.57	1.58		6.34			0.07	4.63	2.35	4.43	3.76	0.85	0.4	
14	KK06005	60.71	15.55	1.58		6.29			0.07	4.51	2.2	4.41	3.8	0.86	0.18	
14	KK06006	60.97	15.6	1.58		5.84			0.08	4.39	2.48	4.36	3.85	0.84	1.17	
14	KK06007	61.43	15.5	1.47		5.99			0.04	4.34	2.1	4.57	3.79	0.77	0.38	
14	KK06008	60.13	15.54	1.61		6.4			0.09	4.68	2.55	4.4	3.76	0.85	0.33	
14	KK06009	60.15	15.47	1.63		6.51			0.08	4.74	2.59	4.28	3.7	0.86	2.08	
14	KK06010	60.29	15.54	1.61		6.43			0.07	4.69	2.3	4.46	3.74	0.86	0.6	
14	KK06011	60.42	15.43	1.63		6.29			0.09	4.56	2.52	4.43	3.76	0.87	0.95	
14	KK06012	60.3	15.52	1.61		6.38			0.07	4.72	2.39	4.45	3.69	0.86	0.65	
14	KK06013	63.85	15.58	1.09		4.81			0.04	4.23	1.81	4.4	3.69	0.51	0.68	
14	KK06014	63.98	15.51	1.08		4.86			0.05	4.17	1.92	4.32	3.6	0.51	0.47	
14	KK06016	63.8	15.37	1.09		4.93			0.06	4.36	2	4.39	3.63	0.5	0.73	
14	KK06018	63.5	15.74	1.12		4.4			0.04	4.32	2.12	4.38	3.71	0.52	0.55	
14	KK06019	63.46	15.7	1.08		4.91			0.05	4.22	2.14	4.31	3.64	0.5	0.45	
14	KK06022	63.39	15.54	1.11		5.1			0.04	4.23	2.11	4.31	3.65	0.51	0.6	
14	KK06024	63.3	15.44	1.15		4.78			0.08	4.37	2.46	4.22	3.67	0.53	1.5	

Ref. #	Sample	SiO2	Al2O3	TiO2	Fe2O3	Fe2O3(t)	FeO	FeO(t)	MnO	CaO	MgO	K2O	Na2O	P2O5	LOI	Total
14	KK06025	58.12	15.37	1.85		7.95			0.1	5.72	2.2	4.02	3.57	1.1	2.15	
14	KK06026	59.46	15.65	1.86		8			0.07	4.64	1.34	4.12	3.77	1.1	0.93	
14	KK06027	59.64	15.61	1.75		7			0.08	4.85	2.04	4.1	3.99	0.94	0.18	
14	KK06028	59.36	15.42	1.74		7.02			0.09	5.11	2.18	4.18	3.94	0.95	1.4	
14	KK06029	59.19	15.51	1.77		7.06			0.08	5.17	2.17	4.08	4.02	0.95	1	
14	KK06030	59.7	15.35	1.75		6.99			0.08	4.91	2.07	4.13	4.03	0.97	0.22	
14	KK06031	59.63	15.41	1.77		7.07			0.07	4.87	2.06	4.11	4.06	0.95	0.22	
14	KK06032	72.18	15.17	0.39		1.96			0.03	1.1	0.57	5.14	3.15	0.31	2.68	
14	KK06033	72.58	15.25	0.38		1.41			0.01	1.14	0.41	5.23	3.28	0.31	1.05	
14	KK06034	72.19	15.19	0.38		1.92			0.03	1.09	0.56	5.11	3.21	0.32	2.2	
14	KK06038	63.44	15.45	1.27		4.89			0.07	4.2	1.91	4.36	3.67	0.73	1.53	
14	KK06039	64.46	16.58	1.39		3.48			0.03	4.01	0.83	4.57	3.83	0.82	1.35	
14	KK06040	63.45	16.87	1.47		2.97			0.04	4.71	0.98	4.55	4.01	0.94	2.93	
14	KK06041	58.63	15.95	1.7		7.19			0.05	5.13	1.74	4.38	4.12	1.11	0.85	
14	KK06042	62.4	15.6	1.44		5.31			0.07	4.41	1.76	4.36	3.8	0.86	1.67	
14	KK06043	59.68	16.57	1.77		6.23			0.04	4.51	1.18	4.54	4.3	1.16	0.92	
14	KK06046	62.93	15.99	1.42		5.83			0.05	3.63	0.99	4.57	3.78	0.8	0.72	
14	KK06047	63.99	15.83	1.34		4.96			0.07	3.68	0.89	4.62	3.81	0.81	0.75	
15	Z02H1	61.13	15.62	0.7		4.6			0.06	5.6	3.75	3.27	3.79	0.38	1.28	100.18
15	Z07H	66.04	15.58	0.43		3.29			0.08	3.24	1.42	3.18	3.62	0.14	2.65	99.67
15	Z07H1	58.71	14.03	0.72		5.28			0.08	5.99	5.42	3.48	2.89	0.35	2.89	99.84
15	Z07H2	58.3	13.95	0.71		5.31			0.08	5.9	5.86	3.5	3.09	0.36	3.03	100.09
15	Z07H3	62.09	15.24	0.59		5.09			0.08	4.89	4.18	3.29	3.47	0.21	1.14	100.27
15	Z07H4	58.44	13.92	0.71		5.14			0.08	6.31	5.47	3.4	2.96	0.36	2.78	99.57
15	Z07H5	62.31	15.3	0.65		4			0.06	4.62	4.23	3.33	3.12	0.26	1.94	99.82
15	Z07H6	63.58	15.28	0.65		4.85			0.05	4.58	3.61	3.19	3.41	0.25	0.83	100.28
15	Z08H1	62.54	15.3	0.69		4.18			0.06	4.52	3.79	3.3	3.61	0.31	1.22	99.52
15	Z08H2	63.33	15.78	0.67		4.61			0.03	4.04	2.76	3.33	3.55	0.26	1.36	99.72
15	Z08H3	63.22	15.49	0.7		4.44			0.05	4.42	2.89	3.4	3.67	0.31	1.31	99.72

Ref. #	Sample	SiO2	Al2O3	TiO2	Fe2O3	Fe2O3(t)	FeO	FeO(t)	MnO	CaO	MgO	K2O	Na2O	P2O5	LOI	Total
15	Z08H4	63.39	15.96	0.72		3.97			0.04	4.42	1.87	3.45	3.74	0.32	1.82	99.7
15	Z08H6	62.66	15.38	0.68		4.76			0.07	4.39	3.08	3.36	3.65	0.31	1.36	99.7
15	Z12H3	59.1	15.71	0.72		5.25			0.09	6.69	3	3.03	3.63	0.27	2.28	99.77
15	Z15H1	61.15	15.22	0.53		4.61			0.14	5.76	2.86	3.14	3.88	0.21	2.01	99.51
15	Z15H2	61.63	15.27	0.53		4.61			0.08	5.57	2.59	3.17	3.77	0.21	2.1	99.53
15	Z15H3	61.46	15.36	0.55		4.8			0.18	5.62	2.89	3.16	3.76	0.2	1.85	99.83
15	Z15H5	65.74	15.34	0.45		3.47			0.03	3.75	1.89	3.44	3.99	0.15	1.34	99.59
15	Z15H6	65.36	15.18	0.44		3.42			0.05	3.68	2.43	3.52	3.65	0.15	1.62	99.5
15	Z19H1	63.7	14.91	0.48		3.8			0.06	4.12	3.56	3.55	3.72	0.19	1.59	99.68
15	Z19H4	65.18	15.1	0.4		3.1			0.05	3.51	2.49	3.69	3.77	0.15	2.32	99.76
15	Z19H5	65.27	15.13	0.4		3.07			0.05	3.51	2.5	3.75	3.68	0.17	2.45	99.98
15	Z19H6	64.99	14.95	0.39		3.07			0.05	3.51	2.51	3.76	3.59	0.18	2.54	99.54
15	Z06H	57.44	18.22	0.76		6.05			0.04	5.02	0.85	2.77	3.35	0.3	4.72	99.52
15	Z08H5	64.69	16.23	0.72		3.21			0.02	4.09	1.05	3.55	3.86	0.33	1.79	99.54
15	Z10H	60.78	17.79	0.8		5.23			0.01	4.74	0.34	3.41	4.11	0.29	2.16	99.66
15	Z11H1	59.92	17.54	0.81		5.56			0.01	4.7	0.48	3.39	4.09	0.3	2.76	99.56
15	Z11H2	60.12	16.88	0.78		6.35			0.01	4.8	0.99	3.14	3.88	0.3	2.29	99.54
15	Z12H1	60.24	15.82	0.73		6.01			0.06	6.02	2	2.98	3.66	0.27	2.08	99.87
15	Z12H2	62.94	17.09	0.78		3.07			0.06	5.28	1.06	3.24	4.12	0.29	1.62	99.55
15	Z15H7	68.72	16.22	0.41		2.14			0.01	3.2	0.27	3.3	4.35	0.13	1.06	99.81
15	Z15H11	61.09	14.89	1.72		5.7			0.05	4.51	1.2	4.48	3.68	0.68	1.51	99.51
16	ET021B	49.55	15.96	0.76		9.99			0.18	10.99	8.89	0.28	1.98	0.11	1.3	99.99
16	ET021C	58.53	16.34	0.78		7.15			0.11	6.53	4.71	2.24	2.76	0.14	0.93	100.22
16	ET022A	70.36	13.17	0.31		1.93			0.07	1.41	0.49	2.52	3.68	0.06	2.29	96.28
16	ET024	71.64	12.71	0.23		1.142			0.07	1.54	0.39	2.97	3.64	0.05	1.68	96.06
16	ST052B	67.51	16.62	0.53		2.18			0.06	1.85	0.48	6.3	3.46	0.09	0.63	99.71
16	ST053	65.26	17.49	0.63		2.75			0.06	2.53	0.7	5.88	3.45	0.13	0.59	99.46
16	ST054	65.78	17.19	0.61		2.5			0.06	2.33	0.61	6.16	3.38	0.11	0.7	99.42
16	ST055A	70.69	15.18	0.45		1.77			0.05	1.09	0.28	6.72	3.1	0.05	0.99	100.37

Ref. #	Sample	SiO2	Al2O3	TiO2	Fe2O3	Fe2O3(t)	FeO	FeO(t)	MnO	CaO	MgO	K2O	Na2O	P2O5	LOI	Total
16	ST055B	68.02	16.38	0.53		2.18			0.06	1.73	0.43	6.61	3.25	0.08	0.33	99.6
16	ST055C	52.92	17.49	0.92		7.96			0.17	6.34	4.1	4.41	2.66	0.38	2.97	100.3
16	ST057A	59.69	17.64	0.8		5.82			0.07	4.21	2.11	5.33	2.83	0.29	0.87	99.66
16	ST058	65.37	14.41	0.71		5.9			0.04	3.03	3.42	3.79	1.37	0.16	1.32	99.52
16	ST059A	65.02	17.17	0.63		2.76			0.07	2.53	0.66	6	3.25	0.12	0.98	99.21
16	ST060A	67.34	15.84	0.48		2.35			0.09	1.59	0.73	6.7	3.07	0.07	1.32	99.59
16	ST060C	68.39	15.16	0.47		2.51			0.08	1.35	0.81	6.4	2.82	0.07	0.84	98.89
16	ST061A	55	18.42	1.03		8.9			0.1	2.53	2.69	4.57	4.66	0.27	0.57	98.74
16	ST062	65.45	15.89	0.6		3.83			0.07	2.72	1.19	5.71	3.01	0.15	0.6	99.22
16	ST101B	57.43	17.92	0.83		7.04			0.05	6.3	3.15	1.25	3.82	0.27	2.5	100.55
16	ST102B	57.44	17.54	0.76		7.96			0.16	5.46	3.52	1.87	2.29	0.15	3.43	100.57
16	ST109	67.18	15.92	0.46		3.09			0.07	3.31	1.11	3	3.63	0.16	2.51	100.44
16	ST119A	49.92	17.57	1.62		8.46			0.15	12.48	5.82	0.24	3.15	0.36	1.79	101.55
16	ST119B	54.07	18.63	1.8		7.34			0.28	5.92	3.75	1.32	4.57	0.86	1.7	100.23
16	ST121	56.19	17.4	1.68		7.01			0.17	4.87	2.74	2.25	5.15	0.8	2.33	100.58
16	ST122	50.28	19.97	1.39		7.89			0.25	4.74	5.4	0.14	5.31	0.49	4.72	100.57
16	T006B1	54.98	16.53	0.93		7.37			0.11	7.44	6.23	1.55	2.66	0.22	2.7	100.71
16	T006B2	47.69	17.54	1.27		11.8			0.2	0.66	6.92	0.91	1.73	0.26	1.3	100.27
16	T034A	59.87	15.92	0.52		7.02			0.12	5.86	4.14	1.09	3.93	1.1	1.02	99.58
16	T034B	60.65	14.36	0.5		6.42			0.12	5.84	4.07	0.52	3.61	0.1	1.7	97.89
16	T036D	48.34	18.65	0.94		10.52			0.16	9.28	6.18	0.72	3.31	0.23	0.51	98.83
16	T038F	66.98	16.26	0.73		4.78			0.11	1.02	2.06	4.42	0.85	0.1	2.01	99.31
16	T038G	63.62	16.17	1.05		5.98			0.29	3.25	1.86	2.67	3.42	0.22	0.95	99.49
16	T038M	75.59	13.17	0.24		1.03			0.04	0.79	0.17	5.19	2.75	0.03	0.31	99.31
16	T039	68.84	14.49	0.29		1.72			0.1	1.57	0.4	5.09	3.09	0.06	5.63	101.26
16	T040A	64.39	16.6	0.76		4.6			0.1	3.45	1.56	3.18	3.91	0.22	1.31	100.08
16	T040B	65.98	16.41	0.66		3.91			0.27	3.02	1.08	3.63	3.59	0.16	0.98	99.69
16	T041 J	51.65	19.41	0.95		10.95			0.15	7.52	4.03	0.77	2.97	0.22	1.53	100.15
16	T041F	52.25	19.2	0.87		10.57			0.14	7.23	3.84	1	3.06	0.23	1.63	100.03

Ref. #	Sample	SiO2	Al2O3	TiO2	Fe2O3	Fe2O3(t)	FeO	FeO(t)	MnO	CaO	MgO	K2O	Na2O	P2O5	LOI	Total
16	T041H	50.66	20.85	0.92		9.82			0.13	8.6	3.42	0.73	3.24	0.23	1.37	99.96
16	T042C	48.76	18.51	1.25		10.58			0.2	9.92	4.42	0.82	3.4	0.33	0.97	99.15
16	T042D	45.22	13.03	0.9		9.91			0.18	10.65	14.31	0.58	1.63	0.33	3.63	100.37
16	T046A	59.73	14.27	0.94		7.79			0.13	5.78	2.73	1.05	3.45	0.31	1.12	97.3
16	T047	50.87	22.41	1.24		7.53			0.11	6.33	2.75	2.55	4.25	0.35	0.96	99.35
16	T048B	59.1	17.25	0.81		6.09			0.09	4.99	2.7	2.2	3	0.18	3.85	100.25
16	T049A	75.82	10.56	0.39		2.79			0.09	1.97	1.54	2.94	0.26	0.07	3.42	99.86
16	T049B	56.29	16.54	0.88		7.3			0.17	5.91	2.01	1.67	4.19	0.27	5.64	100.86
16	T049C	55.71	17.49	0.94		8.85			0.14	4.19	2.52	2.12	4.22	0.28	4.3	100.76
16	T051B	69.33	13.62	0.38		1.9			0.07	4.05	0	2.15	5.44	0.06	3.67	100.67
16	T051C	74.06	13.28	0.16		0.93			0.08	1.35	0.16	5.51	2.87	0.02	1.72	100.13
16	T052	68.19	15.17	0.43		3.06			0.08	2.37	0.84	4.16	3.35	0.11	2.28	100.03
16	T054A	56.49	17.64	1.21		8.92			0.19	7.09	2.74	1.06	3.19	0.36	0.71	99.59
16	T055A	62.71	19.18	0.93		7.41			0.07	4.62	2.32	0.62	0.9	0.11	0.98	99.86
16	T055B	56.6	18.09	1.26		10.6			0.25	5.37	1.27	2.16	3.07	0.23	1.18	100.27
16	T056A	53.56	21.35	1.07		9.22			0.14	6.5	1.82	0.75	3.38	0.17	2.05	99.99
16	T056B	56.23	16.91	0.87		10.3			0.22	9.05	2.28	0.33	1.84	0.2	1.76	100
16	T062B	57.87	17.13	0.91		6.72			0.15	3.21	1.86	3.79	5.8	0.3	2.5	100.25
16	T062C	51.96	17.23	1.04		9.21			0.16	8.75	4.02	0.95	2.8	0.23	2.2	98.54
16	T063	57.88	15.91	0.68		5.23			0.1	5.25	2.01	2.75	4.59	0.21	3.32	97.91
16	T064A	56.35	17.08	0.66		6.07			0.08	5.8	2.36	2.08	3.17	0.19	4.38	98.22
16	T065A	73.9	10.87	0.51		3.95			0.07	1.8	2.26	3.09	1	0.1	1.91	99.45
16	T065B	75.87	13.82	0.29		2.16			0.03	1.15	0.22	4.52	2.77	0.07	0.94	101.84
16	T066	54.13	15.5	1.28		10.16			0.29	4.27	3.93	1.32	4.45	0.28	3.94	99.54
16	T068	71.79	13.43	0.26		1.9			0.07	2.42	0.06	4.3	2.08	0.06	0.06	99.63
16	T070A	65.76	16.14	0.44		3.33			0.17	2.18	1.28	2.74	4.59	0.19	1.41	98.23
16	T072A	51.91	16.91	0.82		5.42			0.06	6.7	3.6	2.61	3.43	0.22	6.38	98.05
16	T072D	57.68	15.76	0.75		6.07			0.09	6.26	3.62	1.99	2.19	0.16	2.02	96.6
16	T072E	58.49	16.04	0.75		6.47			0.1	5.89	4.14	1.66	2.41	0.16	3.26	99.36

153

Ref. #	Sample	SiO2	Al2O3	TiO2	Fe2O3	Fe2O3(t)	FeO	FeO(t)	MnO	CaO	MgO	K2O	Na2O	P2O5	LOI	Total
16	T073	58.1	15.76	0.76		5.37			0.09	5.12	2.72	3.18	2.54	0.17	3.86	97.66
16	T078B	63.65	15.7	0.35		2.74			0.05	3.04	0.92	0.8	5.98	0.17	5.29	98.67
16	T079A	43.04	16.08	1.47		12.15			0.19	11.76	7.92	0.61	2.19	0.19	3.11	98.71
16	T079B	47.6	17.71	1.13		11.12			0.1	8.52	4.73	2.24	3.4	0.28	1.3	98.14
16	T079C	42.27	16.5	1.03		11.68			0.25	18.5	4.61	0.7	0.38	0.27	0.95	97.15
16	T080	45.25	16.27	1.1		10.55			0.24	5.66	5.66	2.18	4.08	0.38	6.84	98.22
16	T082A	71.48	12.91	0.18		1.33			0.06	1.4	0.23	3.67	3.63	0.05	1.5	96.44
16	T082B	72.27	13.6	0.23		1.62			0.04	1.36	0.24	4.17	2.9	0.05	1.26	97.73
16	T083B	74.57	13.54	0.13		1.28			0.06	0.56	0.13	6.06	1.13	0.03	0.67	98.15
16	T083C	50.85	17.39	1.28		11.93			0.29	7.67	3.61	1.63	3.15	0.26	0.83	98.88
16	T084C	70.72	15.35	0.43		2.18			0.03	1.67	0.42	5.49	2.69	0.06	0.4	99.45
16	T102A	62.72	16.49	0.65		6.17			0.08	3.47	1.37	2.87	4.11	0.27	0.13	98.33
16	T103	75.02	13.99	0.22		0.48			0.02	0.12	0.32	5.72	1.41	0.03	1.84	99.15
16	T104	71.54	14.81	0.29		2.89			0.02	0.69	0.76	4.32	0.79	0.03	2.1	98.24
16	T105A	57.47	17.15	1.19		9.19			0.1	2.23	2.47	2.32	4.5	0.33	4.08	101.03
16	T110A	64.88	15.8	0.69		7.14			0.08	1.05	2.89	4.46	1.4	0.14	2.04	100.58
16	T110B	71.82	12.53	0.6		5.02			0.08	1.84	2.26	3.28	1.32	0.12	1.31	100.17
16	T111	70.24	14.87	0.26		1.99			0.07	2.81	0.73	3.65	2.79	0.08	3.95	101.43
16	T112	65.03	15.53	0.75		5.47			0.07	2.76	1.43	3.58	2.96	0.17	2.09	99.84
16	T113	67.16	14.9	0.65		4.38			0.07	3.04	1.08	3.61	2.56	0.14	2.93	100.53
16	T116A	48.68	16.47	1.93		11.18			0.2	9.19	6.49	1.22	2.3	0.41	2.4	100.47
16	T117	80.18	7.68	0.34		2.46			0.03	2.17	1.01	2.11	0.77	0.07	3.63	100.43
16	T127B	65.32	15.33	0.5		4.12			0.06	2.53	2.1	2.03	4.37	0.15	2.73	99.23
16	T129A	55.62	17.98	1		8.68			0.12	3.62	2.42	2.74	3.57	0.13	3.34	99.21
16	T130	77.35	13.01	0.1		0.55			0	0.13	0.02	6.76	1.37	0.01	0.98	100.28
16	T131A	74.17	14.25	0.33		2.75			0.1	0.69	0.36	0.27	5.83	0.07	1.6	100.42
16	T134	72.57	14.79	0.28		0.67			0.02	2.94	0.59	5.34	1.06	0.06	0.98	99.29
16	T136A	72.8	16.37	0.13		1.99			0.05	0.42	0.02	5.16	2.18	0.01	1.69	100.82
16	T136B	70.21	16.02	0.7		4.4			0.05	1.03	0.54	3.79	0	0.71	3.77	101.22

Ref. #	Sample	SiO2	Al2O3	TiO2	Fe2O3	Fe2O3(t)	FeO	FeO(t)	MnO	CaO	MgO	K2O	Na2O	P2O5	LOI	Total
16	T138D	67.45	17.05	0.18		1.35			0.03	1.8	0.86	3.17	4.11	0.07	2.9	98.96
16	T139	78.04	11.71	0.08		0.82			0.01	0.32	0.02	5.08	1.51	0.01	1.05	98.64
16	T140A	70.63	15.1	0.38		3.05			0.06	2.89	0.44	2.07	3.44	0.07	1.48	99.61
16	T140B	57.53	17.86	1.05		7.35			0.15	5.94	2.58	0.37	3.52	0.2	3.51	100.07
16	T140D	67.52	15.64	0.51		4.42			0.1	2.79	0.95	2.65	3.02	0.11	2.03	99.72
16	T140E	76.59	12.77	0.07		0.84			0.02	0.68	0.02	3.73	3.03	0.01	1.57	99.33
16	T142	67.14	15.7	0.44		3.58			0.1	2.22	0.73	2.66	4.63	0.1	1.52	98.82
16	T143	68.56	16.61	0.41		3.17			0.13	1.29	0.72	3.55	4.23	0.09	1.58	100.32
16	T144A	74.52	13.81	0.26		2.25			0.06	0.27	0.76	2.73	4.67	0.04	1.08	100.45
16	T144B	59.22	16.32	0.71		7.6			0.32	1.37	4.11	2.92	4.48	0.14	3.07	100.25
16	T144C	76.78	13.16	0.12		1.08			0.04	0.15	0.24	6.36	1.1	0.03	1.21	100.26
16	T144D	72.19	14.72	0.32		2.52			0.07	0.95	0.96	3.26	4.08	0.06	1.36	100.47
16	T146	69.36	14.96	0.52		3.55			0.09	1.41	0.84	3.97	4.31	0.1	1.87	100.97
16	T147	72.71	13.69	0.17		1.95			0.05	1.45	0.15	3.5	3.77	0.03	0.57	98.04
16	T151	49.99	16.79	1.29		9.04			0.14	9.39	6.54	1.71	2.62	0.45	2.87	100.84
16	T152A	61.47	16.19	0.98		6.38			0.1	2.97	1.84	3.53	3.51	0.31	3.53	100.81
16	T152B	49.66	17.14	0.98		8.87			0.14	7.97	6.96	1.65	2.42	0.23	3.31	99.32
16	T155	69.57	16.17	0.44		2.87			0.08	2.26	0.81	5.11	3.39	0.13	0.57	101.39
16	T160A	63.41	18.14	0.83		5.69			0.1	2.97	1.53	4.04	2.6	0.2	1.26	100.76
16	T160B	76.57	14.24	0.08		1.06			0.01	0.23	0.09	5.28	1.06	0.02	1.65	100.27
16	T169A	74.6	12.63	0.16		1.74			0.02	0.53	0.01	6.29	2.17	0.02	0.9	99.06
16	T169B	76.27	12.97	0.16		1.14			0.04	0.26	0.03	5.94	1.83	0.02	1.1	99.74
16	T169C	81.7	8.19	0.5		1.04			0	0.1	0.21	2.9	0	0.03	4.49	99.16
16	T233A	66.71	10.89	0.47		6.08			0.13	3.4	3.07	0.43	1.57	0.09	6.17	99
16	T233B	58.73	16.78	0.74		6.11			0.13	3.99	2.43	2.36	4.19	0.17	2.5	98.12
16	T233C	45.31	16.84	1.03		10.39			0.17	12.1	3.07	1.12	1.54	0.34	9.48	101.38
16	T234A	54.33	17.49	0.68		7.21			0.14	6.49	2.85	3.14	3.11	0.35	2.89	98.67
16	T234B	50.23	17.55	0.83		8.89			0.15	8.31	3.03	2.37	2.86	0.42	3.91	98.54
16	T234C	66.26	14.66	0.55		5.04			0.07	2.88	1.1	1.93	4.18	0.26	2.35	99.3

Ref. #	Sample	SiO2	Al2O3	TiO2	Fe2O3	Fe2O3(t)	FeO	FeO(t)	MnO	CaO	MgO	K2O	Na2O	P2O5	LOI	Total
16	T235A	75.39	12.76	0.12		1.29			0.02	0.67	0.38	3.11	2.61	0.01	2.23	98.58
16	T235B	75.68	12.47	0.12		1.06			0.04	1.53	0.32	2.81	2.73	0.01	2.67	99.44
16	T238B	53.42	18.22	0.91		8.18			0.11	8.57	3.22	0.25	2.7	0.21	5.07	100.86
16	T239	57.06	17.6	0.9		6.53			0.1	6.86	2.85	1.49	2.34	0.19	3.16	99.07
16	T240B	59.37	17.39	0.84		6.25			0.11	5.53	2.47	3.35	1.72	0.19	1.93	99.15
17	GGL01	60.81	15.39	0.81		5.27			0.05	5.09	1.28	3.18	3.12	0.26	4.34	99.59
17	GGL02	60.04	16.38	1.19		5.02			0.1	5.97	0.32	3.32	3.56	0.38	3.01	99.29
17	GGL03	59.16	16.38	1.21		8.11			0.04	4.26	1.5	3.16	3.51	0.38	1.72	99.43
17	GGL04	60.8	16.58	1.25		2.95			0.09	6.8	0.43	3.12	3.62	0.39	3.1	99.13
17	GGL05	57.51	16.63	1.38		6.65			0.1	6.41	2.79	2.45	3.65	0.39	1.12	99.08
17	GGL06	57.61	16.71	1.39		7.08			0.1	5.94	2.89	2.41	3.64	0.39	1.08	99.25
17	GGL07	58.11	16.76	1.37		6.49			0.09	5.93	2.57	2.54	3.65	0.39	1.39	99.31
17	GGL08	57.29	16.55	1.34		7.3			0.1	5.88	3.48	2.37	3.44	0.38	0.95	99.08
17	GGL09	58.23	16.53	1.32		7.03			0.1	5.58	2.68	2.63	3.56	0.4	1.07	99.13
17	GGL10	58.29	16.53	1.34		6.99			0.1	5.76	2.66	2.61	3.58	0.39	1.1	99.35
17	GGL11	58.38	16.82	1.37		6.63			0.07	5.66	2.17	2.68	3.53	0.4	1.67	99.37
17	GGL12	58.34	16.57	1.33		7.03			0.08	5.67	2.64	2.6	3.55	0.39	1.13	99.34
17	GGL13	58.04	16.4	1.32		6.64			0.08	6.38	2.87	2.57	3.5	0.39	1.14	99.33
17	GGL14	57.95	16.53	1.34		6.47			0.09	6.26	2.28	2.63	3.58	0.39	1.39	98.9
17	GGL15	57.64	17.47	1.42		4.92			0.05	6.83	1.33	2.78	3.74	0.41	2.92	99.51
18	GJ0601	63.1	15.2	1.01		3.9			0.03	2.76	2.08	8.68	1.48	0.34	1.16	99.8
18	GJ0602	63.3	15.2	0.98		3.96			0.03	2.54	1.93	8.55	1.53	0.33	1.19	99.6
18	GJ0605	62.7	15.4	0.98		3.93			0.05	2.74	2.48	8.49	1.52	0.34	0.96	99.6
18	GJ0606	63.5	15.8	1.02		4.09			0.02	1.9	1.38	9	1.46	0.38	1.09	99.6
18	08YR04	65.1	15.9	0.61		2.87			0.03	2.55	1.45	6.96	2.58	0.3	1.3	99.6
18	GJ0614	68.9	15.4	0.62		3.07			0.01	2.63	0.63	4.59	2.61	0.15	1.75	100.3
18	GJ0617	68.1	15.2	0.62		2.96			0.05	2.41	1.47	4.36	2.42	0.15	2.64	100.4
18	GJ0619	68.4	15.3	0.62		3.01			0.05	2.42	1.52	4.54	2.48	0.15	1.75	100.2
18	GJ0620	70.1	15.3	0.6		2.63			0.02	2.49	0.66	4.43	2.53	0.14	1.45	100.4

Ref. #	Sample	SiO2	Al2O3	TiO2	Fe2O3	Fe2O3(t)	FeO	FeO(t)	MnO	CaO	MgO	K2O	Na2O	P2O5	LOI	Total
18	GJ0624	68.5	15.2	0.58		2.52			0.03	2.31	1.48	6.23	2.52	0.21	0.61	100.2
18	GJ0627	68.3	15	0.57		2.77			0.04	2.21	1.57	5.96	2.45	0.21	1.12	100.2
18	GJ0628	66.9	15	0.57		2.72			0.05	2.83	1.5	5.75	2.76	0.19	1.61	99.8
18	GJ0629	67.4	15	0.55		3.02			0.04	2.43	1.55	5.9	2.42	0.19	1.47	100.1
18	10XB03	67.3	14.8	0.62		3.08			0.05	2.01	1.27	5.06	2.35	0.21	2.56	99.3
18	10XB04	68.1	15.3	0.62		2.91			0.02	2.5	0.91	4.85	2.95	0.16	1.02	99.4
18	10XB07	66.6	15	0.63		3.25			0.05	2.42	1.65	5.11	2.6	0.23	1.89	99.4
18	08YR05	57.9	12.8	1.06		6.09			0.09	5.32	6.75	5.69	2.17	0.79	1.06	99.7
18	10XB10	58.7	13.1	1.19		5.38			0.08	4.62	5.28	6.57	2.28	0.8	1.35	99.3
18	10XB12	58	13	1.19		5.8			0.09	4.96	6.29	6.82	2.23	1.01	1.02	100.4
18	10XB13	57.7	12.7	1.21		5.87			0.09	5.06	6.31	6.63	2.15	0.97	1.07	99.8
18	10YR01	59.5	13.6	1.21		3.98			0.07	5.77	4.57	6.52	2.01	1.16	1.14	99.6
18	10YR02	58.2	13.1	1.13		5.34			0.08	5.9	5.64	5.76	2.05	0.91	1.52	99.6
18	10YR04	57.2	12.7	1.15		5.9			0.09	5.51	6.63	6.13	1.87	1.02	1.58	99.8
18	10YR04a	58.1	12.7	1.13		5.72			0.09	5.15	6.26	6.37	1.91	0.95	1.31	100.2
18	10YR07	58	12.9	1.15		5.85			0.1	5.34	6.58	6.3	1.9	1.07	1.02	100.2
19	MV1B	71.02	15.08	0.25	1.37			1.23		0.83	0.19	4.9	2.58	0.28	2.07	98.58
19	MV2	73.42	14.65	0.22	1.32			1.19		0.76	0.1	4.92	2.81	0.29	1.14	99.63
19	UM1B	72.08	14.24	0.21	1.3			1.17		0.98	0.15	4.9	3.03		1.63	98.52
19	UM3V	71.82	14.9	0.24	1.26			1.13		0.8	0.12	4.86	2.71	0.28	1.78	98.77
19	UMQP	72.05	14.37	0.23	1.15			1.03		0.32	0.08	8.96	0.86	0.3	0.54	98.86
19	UMVU	72.92	14.83	0.24	1.13			1.02		0.88	0.14	4.95	2.75	0.29	1.28	99.41
20	TE008/93	60.62	12.88	0.86		5.51			0.1	3.93	5.06	6.23	2.62	0.6	1.37	99.78
20	TE011/93	56.96	13.87	1.01		5.73			0.1	3.99	5.06	6.86	2.17	0.61	2.77	99.13
20	TE125/93	56.45	12.99	1.32		6.55			0.13	4.12	4.75	7.54	1.15	0.7	3.67	99.37
20	TE126/93	53.48	13.91	1.34		7.47			0.11	4.65	6.87	6.34	2.17	0.83	1.84	99.01
20	TE127/93	55.13	13.18	1.37		7.25			0.11	4.6	6.68	6.6	2.14	0.78	2.27	100.11
20	TE131/93	53.76	14.32	1.29		6.7			0.1	5.53	6.82	5.98	2.52	0.83	1.13	98.98
20	TE137/93	53.64	12.05	0.91		6.65			0.12	4.65	10.16	6.71	1.62	1.1	0.86	98.47

Ref. #	Sample	SiO2	Al2O3	TiO2	Fe2O3	Fe2O3(t)	FeO	FeO(t)	MnO	CaO	MgO	K2O	Na2O	P2O5	LOI	Total
20	TE138/93	57.73	12.18	0.87		6.31			0.12	4.27	7.14	6.19	2.11	0.91	1.08	98.91
20	TE117/93	57.98	12.14	1.01		5.87			0.12	4.64	6.83	6.48	2.51	1.02	0.64	99.24
20	TE118/93	57.41	12.35	1.03		6.21			0.15	4.62	6.72	6.29	2.47	0.97	0.72	98.94
20	TE007/93	64.07	13.9	0.72		4.67			0.09	3.91	2.96	4.4	3.44	0.3	0.11	98.57
20	TE025/93	64.91	14.51	0.59		3.81			0.1	3.18	1.99	6.82	2.48	0.25	0.59	99.23
20	TE136/93	67.16	15.26	0.63		3.54			0.02	2.72	1.41	5.1	3.3	0.32	1.4	100.86
20	TE148/93	64.11	15.75	0.62		3.59			0.03	2.4	0.92	6.3	3.15	0.35	1.3	98.52
20	TE150/93	65.38	16.47	0.59		3.49			0.03	2.36	0.79	6.26	2.99	0.23	0.97	99.56
20	TE153/93	69.42	14.06	0.61		3.44			0.06	2.4	0.82	6.06	3.04	0.28	0.36	100.55
20	TE154/93	65.48	15.95	0.59		3.52			0.08	2.71	1.45	6.01	2.98	0.21	0.39	99.37
20	TE047/93	77.86	10.39	0.31		2.23			0.05	1.76	0.42	2.9	2.43	0.09	1.1	99.54
20	TE189/93	64.75	18.46	0.69		2.55			0.02	3.39	0.84	3.75	3.76	0.16	0.77	99.14
20	TE192/93	72.89	12.45	0.59		1.67			0.03	3.04	0.48	2.82	3.63	0.15	1.15	98.9
20	TE194/94	66.85	14.6	0.59		3.51			0.07	3.37	1.27	3.54	3.66	0.15	2.82	100.43
21	Y-2	63.07	15.7	0.8		5.34			0.02	1.75	0.94	6.06	3.3	0.65	2.23	99.86
21	Y-4	75.03	12.4	0.45		1.56			0.01	0.57	0.48	6.12	1.32	0.27	2.41	100.62
21	ZB1	56.44	13.48	1.24		6.53			0.09	5.93	4.21	6.53	3.14	1.16	0.76	99.51
21	ZB4	55.9	13.52	1.25		6.46			0.09	5.92	4.32	6.41	3.12	1.12	0.73	98.84
21	ZB10	56.48	13.51	1.23		6.58			0.1	6.22	4.46	6.32	3.08	1.13	0.64	99.75
21	ZB12	57.13	13.71	1.25		6.22			0.09	5.62	4.1	6.54	3.25	0.98	0.77	99.66
22	K732	56.22	14.54	2.28		8.78			0.11	5.14	2.9	4.04	2.84		1.46	99.54
22	K738	55.44	14.12	2.32		11.04			0.14	6.33	3.67	3.39	2.56		1.1	101.23
22	K89G185	51.42	14.62	1.85		9.61			0.14	7.59	4.03	4.77	4.6	1.12	2.09	100.72
22	K89G200	56.67	13.8	1.43		7.31			0.1	6.35	4.37	5.4	4.02	1.23	0.32	99.77
22	K9007	59.44	15.3	1.54		6.13			0.09	4.75	1.87	3.93	3.42	0.78	2.97	100.22
22	K9008	61.34	15.15	1.62		6.22			0.09	3.77	1.23	4.21	3.82	0.84	0.94	99.23
22	K9021	62.02	15.14	1.57		5.92			0.08	3.99	1.77	4.12	3.77	0.84	0.81	100.03
22	K9024	56.57	15.41	1.58		7.05			0.1	5.64	3.21	3.81	3.69	0.91	1.82	99.79
22	K9031	55.95	15.19	1.55		6.86			0.1	6.3	3.35	3.83	3.61	0.82	1.99	99.55

158

Ref. #	Sample	SiO2	Al2O3	TiO2	Fe2O3	Fe2O3(t)	FeO	FeO(t)	MnO	CaO	MgO	K2O	Na2O	P2O5	LOI	Total
22	K9038	55.31	15.63	1.59		5.88			0.15	7.38	2.53	3.71	3.63	0.83	3.26	99.9
23	Bb-105	55.9	19.1	0.41				4.5	0.16	2.6	0.44	7.08	6.6	0.06	2.34	99.69
23	Bb-107	44.9	12.4	1.24				8.92	0.16	12.1	10.3	3.89	3.31	1.53	1.91	100.65
23	Bb-109	56.4	18.21	0.35				4.14	15	2.1	0.44	7.01	6.34	0.06	3.36	113.87
23	Bb-114	42.9	12.6	1.72				8.86	0.7	9.47	6.25	1.35	4.5	1.5	9.55	99.86
23	Bb-88	44.9	12.42	1.3				13.3	0.16	11.37	8.05	4.25	2.75	0.18	1.06	101.22
23	Bb-89	46.9	13.4	1.95				8.6	0.16	11.46	7.09	3.82	3.13	1.5	2.48	101.45
23	Bb94-2	58	19.5	0.56				3.88	0.07	2.12	0.8	7.68	3.48	0.11	1.98	98.61
23	Bb-95	56.9	17.4	0.93				6.68	0.09	3.38	1.64	7.71	2.58	0.83	1.98	100.86
23	Bg 121	60.8	15.2	1.5				7.2	0.08	4.94	2.76	3.85	3.41	0.66	0.97	102.17
23	Bg 124	57.6	14.2	1.26				5.52	0.09	7.28	2.82	3.68	3.18	0.65	1.89	98.96
23	COUL311	73.93	13.78	0.27				2.43	0.05	1.26	0.37	4.56	2.67	0.02	1.41	100.39
23	COUL326	67.96	16.97	0.46				2.5	0.03	2.66	0.96	4.47	4.1	0.16	0.62	100.17
23	COUL328	63.03	16.44	0.59				3.74	0.06	4.16	1.9	3.47	4.26	0.29	1.05	99.39
23	COUL338	62.07	18.19	1.02				7.25	0.16	8.9	3.68	1.98	3.04	0.26	1.33	98.59
23	COUL339	52.67	18.89	1.05				7.59	0.17	8	3.84	1.21	3.39	0.27	1.41	99.34
23	k705	52.79	13.49	1.87				7.5	0.1	7.15	3.74	3.83	2.76	1.04	5.11	100.2
23	k708	57.28	14.12	1.85				7.35	0.1	5.36	2.92	4.37	2.91	0.92	2.06	100.06
23	K713	55.09	14.42	2.27				7.23	0.11	6.28	3.02	3.69	3.24	1.11	2.62	99.88
23	K716	57.62	14.11	2.23				7.31	0.12	5.6	3.85	4.31	2.92	1.07	1.56	100.14
23	K718	57.98	14.04	2.12				8.4	0.11	5.07	2.65	4.12	3.01	1.13	0.91	100.47
23	K720	55.34	14.1	2.23				7.88	0.13	6.32	3.84	3.62	2.93	1.14	1.77	100.18
23	K723	55.25	14.21	2.23				8.03	0.15	6.35	3.75	3.57	3.11	1.16	1.78	100.48
23	K732	56.22	14.54	2.28				7.9	0.11	5.14	2.9	4.04	2.84	1.23	1.46	99.54
23	K738	55.44	14.12	2.32				9.93	0.14	6.33	3.67	3.39	2.56	1.12	1.1	101.23
23	K89G159	68.19	14.01	0.74				2.59	0.02	1.33	1.01	7.26	3.16		0.53	99.11
23	K89G162	63.78	14.3	0.81				3.05	0.05	2.88	2.26	7.22	2.99		2.1	99.78
23	K89G163	64.85	14.04	0.77				3.07	0.06	2.93	1.87	6.43	3.3		1.75	99.41
23	K89G185	51.42	14.62	1.85				8.65	0.14	7.59	4.03	4.77	4.6		2.09	100.72

Ref. #	Sample	SiO2	Al2O3	TiO2	Fe2O3	Fe2O3(t)	FeO	FeO(t)	MnO	CaO	MgO	K2O	Na2O	P2O5	LOI	Total
23	K89G186	49.8	13.65	1.77				8.2	0.12	7.2	5.6	4.7	3.8		4.15	99.9
23	K89G191	56.95	14.1	1.36				6.6	0.1	6.45	3.8	4.75	3.89		1.01	99.75
23	K89G192	57.5	14.15	1.32				6.2	0.09	5.85	3.36	5.15	4.1		1.15	99.56
23	K89G193	57.09	14.31	1.31				6.36	0.09	6.74	3.67	4.99	4.06		1.04	100
23	K89G197	75.1	12.95	0.1				0.85	0.01	0.6	0.4	4.9	4.35		0.5	99.5
23	K89G200	56.67	13.8	1.43				6.58	0.01	6.35	4.37	5.4	4.02		0.32	99.77
23	K9002	71.48	13.79	0.63				3.85	0.07	1.8	1.5	2.3	3.04	0.14	1.81	100.84
23	K9006	62.23	15.24	1.6				5.43	0.08	3.97	1.75	4.14	3.88	0.86	1.08	100.86
23	K9007	59.44	15.3	1.54				5.52	0.09	4.76	1.87	3.93	3.42	0.78	2.97	100.22
23	K9008	61.34	15.15	1.62				5.6	0.09	3.77	1.23	4.21	3.82	0.84	0.94	99.23
23	K9016	62.53	16.05	1.47				5.12	0.08	4.2	1.59	4.21	3.87	0.79	0.78	100.26
23	K9017	62.36	15.26	1.56				5.37	0.07	4.04	1.66	4.15	3.76	0.85	0.85	100.53
23	K9018	61.47	15.06	1.59				5.52	0.08	4.32	1.76	4.16	3.77	0.85	0.99	100.2
23	K9019	60.16	14.95	1.63				5.61	0.09	4.65	1.83	4.01	3.73	0.88	1.9	100.06
23	K9021	62.02	15.14	1.57				6.23	0.08	3.99	1.77	4.12	3.77	0.84	0.81	100.03
23	K9024	56.57	15.41	1.68				6.34	0.1	5.64	3.21	5.64	3.69	1.69	1.82	99.79
23	K9026	57.71	15.95	1.69				6.12	0.09	6.45	2.76	4.17	3.95	0.84	0.89	100.33
23	K9027	67.49	15.96	1.68				6.14	0.09	5.39	2.88	4.11	3.95	0.86	0.79	100.01
23	K9028	54.51	14.94	1.53				5.7	0.09	7.64	2.75	3.62	3.62	0.76	3.8	99.69
23	K9029	56.26	16.6	1.63				6.01	0.09	6.28	2.78	4.06	3.9	0.76	1.87	99.91
23	K9031	55.95	15.19	1.55				6.17	0.1	6.3	3.35	3.83	3.61	0.82	1.99	99.66
23	K9032	57.69	15.76	1.63				6.48	0.1	5.04	2.88	4.01	3.82	0.84	0.9	99.87
23	K9038	55.31	15.83	1.59				5.29	0.15	7.83	2.53	3.71	3.63	0.83	3.26	99.9
23	K9039	56.57	16.25	1.71				6.73	0.04	1.74	1.22	3.71	3.75	0.87	2.27	99.61
23	Kp 35-10	54.88	15.55	1.88				5.79	0.13	4.9	2.52	3.88	3.23	0.86	2.65	96.92
23	Kp12-58	59.56	14.24	1.75				7.32	0.1	4.43	2.23	4.33	3.49	1	1.05	101.32
23	Kp23-2	53.27	15.77	2.34				8.47	0.13	6	4.2	4.06	3.44	1.2	1	100.82
23	Kp24-1	56.56	14.49	1.9				7.19	0.11	5.6	3.85	4.31	2.92	1.07	0.93	99.19
23	Kp39-3	47.85	12.32	1.89				8.22	0.13	7.87	7.86	5.22	2.98	1.29	3.16	99.71

Ref. #	Sample	SiO2	Al2O3	TiO2	Fe2O3	Fe2O3(t)	FeO	FeO(t)	MnO	CaO	MgO	K2O	Na2O	P2O5	LOI	Total
23	Kp47-2	50.81	14.03	1.55				6.59	0.9	9.53	3.95	4.06	4.42	1.02	2.21	99
23	Kp47-5	52.97	13.89	1.57				7.79	0.12	7.21	4.23	4.18	3.43	0.91	2.58	99.75
24	2303	71.4	14.79	0.39		1.37			0.02	1.01	0.48	5.23	3.15	0.25	1.06	99.9
24	2509	73.13	14.49	0.23		1.49			0.02	0.67	0.26	5.08	3.21	0.32	0.84	100.04
24	1P2JD7-1	72.64	15.88	0.12		1.09			0.09	0.36	0.25	3.95	4.17	0.39	0.46	99.8
24	1P2JD7-1a	72.43	16.5	0.11		1.34			0.08	0.36	0.02	4.14	4.06	0.35	0.62	100
24	2011a	75.5	13.82	0.11		0.3			0.03	0.42	0.24	4.13	3.13	0.16	0.76	99.8
24	2059a	71.86	14.48	0.22		2.8			0.03	0.68	0.24	5.03	3.26	0.28	1.02	99.88
24	2303a	70.67	15.08	0.37		1.9			0.03	1.12	0.51	5.42	3.28	0.26	1.54	100.18
24	2511-1	69.24	15.1	0.43		1.82			0.04	1.02	0.57	5.47	3.04	0.32	1.5	99.8
25	04wq-1	46.81	12.62	1.05		7.87			0.13	11.23	10.72	1.58	4.05	1.27	2.1	99.44
25	04wq-2	47.09	12.61	1.02		7.67			0.12	10.33	10.28	2.83	3.25	1.17	2.15	98.51
25	04wq-3	45.27	12.31	1.05		8.12			0.13	11.15	11.48	3.11	2.61	1.45	2.69	99.38
25	04wq-4	47.48	12.75	1.01		7.71			0.12	10.28	10.55	3.14	2.75	1.16	2.43	99.39
25	04wq-5	45.26	12.23	1.06		8.08			0.13	11.36	11.44	2.91	2.77	1.46	2.34	99.03
25	04wq-6	52.94	15.03	1.04		7.36			0.1	7.39	7.23	3.36	3.34	0.63	0.94	99.36
25	04wq-7	52.89	15.05	1.05		7.25			0.09	7.46	6.79	3.36	3.35	0.62	0.91	98.82
25	4086-1	52.92	15.17	1.06		7.22			0.09	7.53	6.61	3.3	3.23	0.61	1.42	99.16
25	8528	52.76	13.39	1.15		7.63			0.08	6.8	8.95	3.74	2.37	0.62	2.17	99.67
25	8518-1	60.31	15.76	0.82		5.13			0.07	5.51	3.85	3.04	3.91	0.38	0.8	99.58
25	8518-2	60.02	15.7	0.82		5.18			0.07	5.46	3.83	3.06	3.91	0.37	0.67	99.08
25	9063-GS2	58.29	16.1	0.8		6.05			0.08	6.08	5.19	2.59	3.18	0.2	1.2	99.75
25	9063-GS3	59.57	16.22	0.83		5.64			0.08	6	4.88	2.72	3.47	0.13	0.74	100.26
25	D3145	60.45	17.7	0.77		4.73			0.14	1.2	0.54	7.48	4.77	0.3	1.41	99.48
26	05S2-7	58.64	11.59	1.53		5.74			0.07	3.47	7.53	8.53	1.54	0.47	0.89	100
26	05S2-8-1	58.77	11.34	1.51		5.68			0.07	3.71	7.57	8.04	1.71	0.73	1.1	100.24
26	05SLP5-3	60.19	12.66	1.31		5.71			0.06	3.15	5.2	7.57	2.01	0.36	1.26	99.47
26	05SLP5-05	58.14	12	1.38		6.66			0.09	3.91	7.97	6.57	1.67	0.34	0.58	99.3
26	05SLP5-06	57.95	12.58	1.39		6.06			0.08	4.35	7.37	6.55	1.77	0.37	0.62	99.1

Ref. #	Sample	SiO2	Al2O3	TiO2	Fe2O3	Fe2O3(t)	FeO	FeO(t)	MnO	CaO	MgO	K2O	Na2O	P2O5	LOI	Total
26	05SLP5-7	56.6	12.2	1.52		6.53			0.09	4.3	8.32	7.05	1.9	0.4	0.55	99.45
26	05SLP5-8	59.04	13.2	1.34		5.68			0.08	4.36	5.98	6.37	2.09	0.42	0.81	99.38
26	05SLP5-09	56.53	10.85	1.49		6.01			0.08	3.88	7.93	7.56	1.6	0.71	2.61	99.25
26	S05SLP5-10	56.45	13.32	1.34		6.93			0.09	4.73	6.81	6.37	2.43	0.32	0.78	99.58
26	05SLP5-11	56.98	13.39	1.43		6.78			0.09	4.2	6.84	6.41	2.35	0.11	0.48	99.06
26	05SLP5-16	54.46	12.26	1.5		7.67			0.1	5.3	8.96	6.74	1.87	0.22	0.37	99.45
26	05SLP4-01	46.1	8.77	1.3		9.09			0.13	9.47	13.7	6.42	0.29	1.04	3.05	99.36
26	05SLP4-02	51.29	10.93	1.6		7.67			0.11	6.22	10.16	7.33	1.17	0.75	2.66	99.89
26	05SLP4-03	49.82	9.8	1.44		8.87			0.12	7.23	11.42	8.9	1.12	0.67	0.9	100.29
26	05SLP4-04	52.77	10.21	1.66		7.95			0.1	5.89	9.82	8.32	1.46	0.74	1.15	100.08
26	05S2-7																
26	05S2-8-1																
27	WR-12-48	58.65	17.37	0.66		4.96			0.13	3.71	1.43	6.1	4.09	0.25	0.46	97.8
27	WR-12-47	76.43	12.12	0.05		0.86			0.02	0.45	0.04	4.52	3.73	0	0.42	98.64
27	WR-12-44	66.17	16.11	0.74		5.63			0.09	4.66	1.59	1.27	3.74	0.23	0.65	100.9
27	WR-12-45	49.68	16.87	1.31		11.55			0.19	9.63	5.42	0.8	3.35	0.29	1.01	100.10
27	WR-12-40	63.03	17.33	0.65		4.8			0.1	4.19	1.52	3.18	4.38	0.24	0.58	99.99
27	WR-12-42	52.54	18.54	1		9.2			0.24	8.47	3.43	1.16	4.27	0.21	1.22	100.30
27	WR-12-33	65.59	15.12	0.68		5.29			0.1	4.38	2.05	3.27	3.23	0.19	0.57	100.50
27	WR-12-35	54.3	17.24	1.22		8.88			0.17	6.94	3.95	1.73	4.47	0.32	0.96	100.20
28	T2A/98	51.27	10.98	0.96		6.42			0.11	5.35	11.38	7.69	1.14	1.29	2.50	99.09
28	T3b/98	56.05	14.37	1.05		6.74			0.10	3.73	5.23	5.96	2.14	0.80	3.25	99.41
28	T4A/98	51.66	13.70	1.00		6.03			0.08	5.75	6.86	6.52	2.14	0.97	4.10	98.97
28	T5A/98	56.97	11.19	0.683		4.19			0.09	7.08	4.34	5.03	2.02	0.641	7.380	99.61
28	T11B/98	62.60	16.50	0.73		3.96			0.06	4.65	2.23	2.82	4.35	0.25	2.27	100.41
28	JPT 14.2	61.54	17.33	0.77		4.05			0.06	4.96	2.16	2.70	4.41	0.26	0.99	99.23
29	JPT24A	65.6	14.6	0.8		3.9			0.1	4.3	2.8	4.8	2.7	0.4	2.5	
29	JPT24B	58.1	12.9	1.1		5.6			0.1	7.7	5.4	5.9	2.3	0.7	3.1	
29	JPT24C	57.7	12.8	1.1		5.8			0.1	7.6	6	5.9	2.3	0.7	2.8	

Ref. #	Sample	SiO2	Al2O3	TiO2	Fe2O3	Fe2O3(t)	FeO	FeO(t)	MnO	CaO	MgO	K2O	Na2O	P2O5	LOI	Total
29	JPT22	69.2	15.5	0.6		2.9			0.1	2.7	1.5	4.3	3	0.2	2.3	
29	K89G162	65.3	14.6	0.8		3.5			0.1	2.9	2.3	7.4	3.1		2.1	
29	20E39A	63.2	15.3	0.9		7.5			0.1	3.1	1.9	3.5	4.2	0.3	2.4	
29	JPT7	61.9	12.2	0.8		4.8			0.1	7.6	4.6	5.4	2	0.7	6.6	
29	T5B/98	68.7	12.8	0.8		4.4			0.1	1.8	3.9	5.2	1.6	0.8	3.6	
29	JPT14.1	63.2	16.6	0.7		4.3			0.1	4.8	3	2.9	4.1	0.2	0.6	
29	JPT3	64.7	15.7	0.7		4.9			0.2	4.6	1.3	4.6	3.2	0.3	3.2	
29	JPT4	70.3	16.2	0.4		2			0	2.8	0.8	4.1	3.4	0.1	2.5	
29	JPT5.2	67.6	16.4	0.6		3.2			0	4.8	1.5	4.7	0.9	0.2	8.1	
29	JPT8	75.3	15.1	0.4		2.1			0	0.4	0.6	5.2	0.8	0.2	3.1	
29	95RAS11.3	75.9	13.3	0.3		1.6			0	4.2	0.8	2.5	1.1	0.1	5	
29	T2A	53.1	11.4	1		6.7			0.1	5.5	11.8	8	1.2	1.3	2.5	
29	T3B	58.3	14.9	1.1		7			0.1	3.9	5.4	6.2	2.2	0.8	3.3	
29	T4A	54.5	14.5	1.1		6.4			0.1	6.1	7.2	6.9	2.3	1	4.1	
29	T5A	61.8	12.1	0.7		4.5			0.1	7.7	4.7	5.5	2.2	0.7	7.4	
29	912	58.2	14.3	1.8		7.2			0.1	5.6	4.3	5	2.6	1.1	0	
29	1105	62.7	15.1	0.7		6			0.1	5.4	1.9	4.3	3.2	0.7		
29	K702	53.2	13.9	1.9		7.2			0.2	10.9	4.3	3.8	3	1.7	2.4	
29	K703	56.4	14.9	2		7.9			0.1	6.4	4	4.1	2.9	1.2	1.1	
29	K89G185	52	14.3	1.8		9.5			0.1	7.5	5.8	4.9	4		4.2	
29	K89G186	52.1	14.8	1.9		9.7			0.1	7.7	4.1	4.8	4.7		2.1	
29	K89G200	57	13.9	1.4		7.4			0.1	6.4	4.4	5.4	4		0.32	
29	KP 12.6	61.4	13.8	2		7.2			0.1	5.7	2	4	3	0.9	0.8	
29	KP47-2	52.5	14.5	1.6		7.6			0.1	9.8	4.1	4.2	4.6	1.1	2.2	
29	KP47-5	54.5	14.3	1.6		8.9			0.1	7.4	4.4	4.3	3.5	0.9	2.6	
29	Bb 124	59.7	14.7	1.3		5.9			0.1	7.5	2.9	3.8	3.3	0.7	1.9	
29	Bb121	60.6	15.1	1.5		7.2			0.1	4.9	2.7	3.8	3.4	0.7	1	
29	Bq137	63.5	15.2	1.5		5.6			0.1	1.8	3.8	4.3	3.6	0.7	0.3	
29	Bb119	62.6	14.5	1.6		7.3			0.1	3.4	1.4	3.7	4.1	1.3	0.5	

Ref. #	Sample	SiO2	Al2O3	TiO2	Fe2O3	Fe2O3(t)	FeO	FeO(t)	MnO	CaO	MgO	K2O	Na2O	P2O5	LOI	Total
29	Bb122	63.9	14.5	1.5		5.8			0.1	5.2	1.8	4.1	3.1	0.1		
29	Bb135	63.6	15	1.5		5.4			0	3.4	1.7	4.3	4	1.2	1.1	
29	Bg142	68.9	15.8	0.8		2.2			0	1.9	0.7	5.4	4	0.2	1.4	
29	Bq140	69.2	14.5	0.8		3.2			0	1.4	1.2	5.1	4.2	0.3	1.2	
29	Bq141	69	14.7	0.8		3.7			0	1.9	0.7	4.4	4.3	0.4	1.1	
29	K9024	57.7	15.7	1.6		7.2			0.1	5.8	3.3	3.9	3.8	0.9	1.8	
29	K9026	58	16	1.7		6.8			0.1	5.5	2.8	4.2	4	0.8	0.9	
29	K9027	57.9	16.1	1.7		6.9			0.1	5.4	2.9	4.1	4	0.9	0.8	
29	K9028	56.9	15.6	1.6		6.6			0.1	8	2.9	3.8	3.8	0.8	3.8	
29	K9029	57.4	15.9	1.7		6.8			0.1	6.4	2.8	4.1	4	0.8	1.9	
29	K9031	57.3	15.6	1.6		7			0.1	6.5	3.4	3.9	3.7	0.8	2	
29	K9032	58.3	15.9	1.6		7.3			0.1	5.1	2.9	4.1	3.9	0.8	0.9	
29	K9038	57.2	16.2	1.6		6.1			0.2	7.6	2.6	3.8	3.8	0.9	3.3	
29	K9039	58.1	16.7	1.8		7.7			0	5.9	1.3	3.8	3.9	0.9	2.3	
29	K9041	66.1	15.1	0.8		6.2			0.1	3.1	0.9	3	4.3	0.3	0.4	
29	K9001	74.7	12.8	0.6		3.6			0.1	1.5	1.4	1.9	3.5	0.1	1.4	
29	K9002	72.2	13.9	0.6		4.3			0.1	1.8	1.5	2.3	3.1	0.1	1.8	
29	K9006	62.4	15.3	1.6		6			0.1	4	1.8	4.1	3.9	0.9	1.1	
29	K9007	61.1	15.7	1.6		6.3			0.1	4.9	1.9	4	3.5	0.8	3	
29	K9008	62.4	15.4	1.6		6.3			0.1	3.8	1.3	4.3	3.9	0.9	0.9	
29	K9016	62.9	15.1	1.5		5.7			0.1	4.2	1.6	4.2	3.9	0.8	0.8	
29	K9017	62.6	15.3	1.6		6			0.1	4.1	1.7	4.2	3.8	0.9	0.9	
29	K9018	62	15.2	1.6		6.2			0.1	4.4	1.8	4.2	3.8	0.9	1	
29	K9019	61.3	15.2	1.7		6.3			0.1	4.7	1.9	4.1	3.8	0.9	1.9	
29	K9021	62.5	15.3	1.6		6			0.1	4	1.8	4.2	3.8	0.8	0.8	
30	2007k251	41.13	12.12	1.44	5.55		3.37		0.15	11.26	10.27	4.97	2.93	2.40	3.46	99.05
30	2007k252	41.98	12.33	1.44	3.56		4.22		0.14	10.71	9.79	5.09	3.37	2.29	2.00	96.92
30	2007k253	41.91	12.42	1.45	4.03		3.94		0.14	11.21	10.15	4.87	3.35	2.5	2.08	98.06
30	2007k254	40.97	12.14	1.45	3.52		4.28		0.14	10.91	9.89	5.55	2.76	2.38	2.9	96.89

Ref. #	Sample	SiO2	Al2O3	TiO2	Fe2O3	Fe2O3(t)	FeO	FeO(t)	MnO	CaO	MgO	K2O	Na2O	P2O5	LOI	Total
31	DHLT-10	56.93	14.15	1.38	4.85		1.35		0.1	5.84	4.15	5.21	3.9	0.89		99.48
31	DHLT-2	57.76	14.12	1.31	3.14		2.69		0.09	5.34	3.98	5.33	3.98	0.81		99.18
31	DHLT-4	51.4	13.54	1.7	4.47		3.07		0.13	7.32	6.02	6.67	2.52	1.49		99.03
31	DHLT-5	57.11	14.15	1.39	3		3.04		0.1	5.8	3.96	5.24	3.96	0.9		99.16
31	DHLT-7	55.52	14	1.47	4.02		2.57		0.1	6.57	3.79	4.97	3.79	0.96		98.42
31	DHLT-9	56.39	14.04	1.37	4.75		1.47		0.1	5.99	4.27	5.17	3.83	0.86		98.95
31	PL-12	54.61	15.61	1.97	3.69		4.72		0.12	5.92	4.14	4.06	3.52	0.96		100.08
31	PL-2	50.81	15.48	2.17	6.71		1.99		0.1	5.71	3.39	4.13	5.46	1.15		98.07
31	PL-3	52.91	15.78	2.25	6.38		2.48		0.13	5.92	3.69	4.13	3.83	1.17		99.36
31	PL-5	53.11	15.89	2.25	4.39		4.31		0.13	5.99	4.05	4.14	3.99	1.18		99.92
31	PL-7	52.87	15.41	2.05	5.31		3.04		0.11	5.76	3.99	3.98	4.44	1.03		98.9
31	PL-9	55.18	15.45	1.94	2.74		5.38		0.12	5.82	3.97	4.14	3.64	0.94		99.68
31	YCN-1	53.7	15.77	1.95	4.47		3.39		0.11	6.47	4.16	3.73	3.7	1		99.34
31	YCN-2	53.8	16.02	1.96	4.22		3.68		0.12	6.44	4.21	3.74	3.5	1		99.38
31	YCN-3	53.71	15.79	2	3.58		4.36		0.12	6.41	4.36	3.94	3.8	1		99.49
31	YCN-4	53.75	15.8	2.01	3.42		4.51		0.12	6.42	4.28	3.94	3.7	1		99.56
31	YCN-6	54.08	15.76	1.98	2.47		5.44		0.12	6.38	4.49	3.98	3.62	0.99		100.08
31	YCN-7	53.44	15.75	2.06	5.44		2.66		0.12	6.36	4.1	3.96	3.81	1.02		99.21
31	YCN-8	52.96	15.58	2	7.9		0.59		0.12	6.24	4.23	3.94	3.93	0.99		99.06
31	KP24-1	56.56	14.49	1.9	1.21		5.98		0.12	5.6	3.85	4.31	2.92	1.07		98.9
31	KP25-3	59.28	14.49	1.87	1.18		5.66		0.1	4.87	2.85	4.19	2.99	0.94		98.93
31	KP28-1	60.63	14.34	1.51	1.11		5.26		0.1	4.44	3.04	4.24	3.17	0.69		98.76
31	KP33-3	47.67	14.17	1.97	1.72		7.38		0.14	7.51	6	4.15	3.26	1.07		98.27
31	KP39-1	47.42	12.46	1.95	5.28		3.5		0.14	8.19	7.17	2.3	5.08	1.34		97.29
31	KP39-4	63.42	14.21	0.56	0.21		3.92		0.06	3.35	3	3.24	4.94	0.15		99.95
31	KP47-1	71.17	13.07	0.21	0.72		1.25		0.02	1.41	0.74	4.47	4.5	0.1		99.22
31	KP47-4	58.04	14.27	1.25	0.92		5.09		0.1	5.91	3.42	4.37	4.02	0.69		99.73
31	KP47-7	51.33	14.5	1.93	3.94		4.12		0.11	7.44	4.15	4.37	3.84	1.23		99.18
32	11UMT14	45.43	14.31	1.04	9.13			8.22	0.11	11.74	2.72	0.17	6.17	0.55	8.19	99.62

Ref. #	Sample	SiO2	Al2O3	TiO2	Fe2O3	Fe2O3(t)	FeO	FeO(t)	MnO	CaO	MgO	K2O	Na2O	P2O5	LOI	Total
32	11UMT15	47.27	16.13	1.24	9.8			8.82	0.13	6.92	5.55	0.73	5.24	0.3	6.17	99.54
32	11UMT17-a	43.22	10.92	1.12	9.01			8.11	0.16	13	10.3	3.18	1.29	1.25	5	98.63
32	12HG04	74.84	14.65	0.119				1.08	0.04	0.49	0.34	5.77	2.37	0.302		95.427
32	12HG06	74.72	14.54	0.197				1.12	0.06	0.35	0.25	7.25	1.23	0.299		96.593
32	12HXV01	55.14	13.68	0.73				5.33	0.11	9.52	6.17	4.94	3.44	0.931		94.504
32	12HXV08	71.15	15.18	0.445				1.75	0.04	1.73	0.68	5.05	3.67	0.3		95.86
32	12HXV09	61.55	15.71	1.589				5.84	0.04	4.46	1.47	4.37	4.15	0.824		98.543
32	12HXV12	60.85	15.54	1.541				5.92	0.07	4.56	2.23	4.6	3.84	0.854		99.388
32	12HXV15	62.06	15.52	1.403				5.41	0.07	4.18	2.02	4.78	3.83	0.73		99.234
32	12HXV19	61.92	17.87	1.825				5.92	0.08	4.26	2.06	3.23	2.09	0.75		87.222
32	12HXV21A	62.53	15.63	1.465				4.43	0.08	4.24	2.24	4.73	3.87	0.793		98.04
32	12HXV23	62.67	15.23	1.351				5.34	0.07	4.08	2.02	4.75	3.77	0.711		98.679
32	12HXV24	72.41	14.72	0.409				1.06	0.03	1.7	0.56	5.16	3.68	0.267		98.852
32	12HXV32	72.18	14.73	0.439				1.14	0.02	1.97	0.59	5.07	3.57	0.3		97.139
32	12HXV33	51.44	12.23	0.833				6.43	0.13	10.64	10.42	4.06	2.7	1.12		96.34
32	13DV05	59.6	14.85	1.88	7.04			6.335	0.08	4.71	2.22	3.93	3.5	0.9	0.12	99.23
32	13DV04	58.9	14.9	1.92	7.18			6.461	0.08	4.76	2.08	3.94	3.52	0.91	0.61	99.46
32	13DV11	59.5	14.95	1.92	7.17			6.452	0.09	4.93	2.5	4.2	3.33	0.92	0.06	100
32	13DV13	59.3	15.2	1.75	6.93			6.236	0.09	4.85	2.69	3.84	3.59	0.91	0.3	99.91
32	13DV14	61	15.05	1.63	6.56			5.903	0.08	4.56	2.18	4.08	3.57	0.82	0.38	100.3
32	13DV15	60.1	14.9	1.69	6.73			6.056	0.08	4.64	2.26	4.06	3.6	0.86	0.23	99.57
32	13DV23	57.5	15.75	1.88	7.88			7.09	0.08	5.52	2.04	3.56	3.6	0.82	0.96	99.97
32	13DV29	57.4	15.05	1.83	7.86			7.072	0.11	5.69	3.51	3.48	3.43	0.77	0.66	100.2
32	13LG07	64	15	1.21	5.19			4.67	0.04	3.61	1.23	4.49	3.63	0.6	0.57	100
32	13XV01	61.2	15.1	1.48	5.96			5.363	0.07	4.31	2.32	4.24	3.62	0.74	0.18	99.65
32	13XV02	59.4	15.5	1.75	6.51			5.858	0.08	4.83	2.57	4.03	3.81	0.87	0.02	99.82

Table B.3 – Trace element compositions of compiled lavas in the Tibetan Plateau, part 1. Data typically obtained via ICPMS.

Ref.#	Sample	Ba	Be	Ce	Cl	Co	Cr	Cs	Cu	Dy	Er	Eu	Ga	Gd	Ge	Hf	Ho
1	K89G185	2563		333		24	88.0	2.00				4.30	21.6			8.0	
1	K89G186	2564		358		31	122.0	0.00		6.3	2.71	4.72	17.4	12.0		8.7	
1	K89G189	2350				13											
1	K89G190	1765				23											
1	KB9G191	2080		263		30	137.0	0.00		4.5	2.10	2.99	20.3	8.3		7.3	
1	K89G192	2091		290		35	109.0	14.40		4.9	2.35	3.24	20.9	9.2		10.0	
1	K189G193	1760		274		18	81.0	3.70				3.00	21.6			8.2	
1	K89G197	86		103		22	9.0	128.90		1.0	1.00	0.21	29.4	1.0		8.2	
1	K89G200	2076		287		20	83.0	6.00				3.60				9.8	
2	05S2-4	2914		190		19.5				5.3	2.03	4.73	20.7	13.8		17.7	0.81
2	05S2-6	2993		149		21.5				5.0	1.91	4.26	22.3	12.5		18.5	0.75
2	05S2-9	3284		76		23.5				3.9	1.57	4.40	19.4	8.1		14.4	0.63
2	05SLP5-1	2503		180		25.3				4.8	1.98	4.61	21.7	11.9		13.2	0.77
2	05SLP5-2	2797		169		18.8				4.0	1.56	4.52	21.0	11.0		17.2	0.60
2	05SLP5-4	2297		142		23.7				3.5	1.44	3.46	21.8	7.9		14.2	0.57
2	CM10-04-04	4465		260		24				4.5	1.81	3.16	22.4	9.9		26.9	0.65
2	CM10-04-09	4347		295		20.8				5.1	2.11	3.30	22.8	9.5		26.9	0.78
2	CM10-04-12	3626		153		30.4				3.7	1.62	2.37	18.8	7.7		20.5	0.57
2	04DYH-01	1845		119		42.1				3.2	1.48	2.11	17.6	4.4		7.0	0.58
2	D3141	4161		547		39				9.9	3.87	7.73	16.7	20.4		10.8	1.55
3	04LQS-2	1741		92						1.8	0.84	1.45		2.8		4.5	0.32
3	04LQS-3	1880		70						1.7	0.75	1.70		2.1		4.8	0.29
3	04LQS-6	1520		128						3.3	1.45	1.79		4.3		4.7	0.59
3	04LQS-14	1296		90						1.8	0.81	1.08		2.9		5.8	0.33
3	04LQS-16	1456		30						1.6	0.84	0.88		1.8		4.2	0.31
3	04YJL-05	1957		93						2.5	1.24	1.21		3.1		5.1	0.49
3	04YJL-07	1923		118						2.4	1.14	1.60		3.4		6.7	0.43
3	04YJL-06	2255		103						2.0	0.93	1.66		2.8		7.1	0.35

Ref.#	Sample	Ba	Be	Ce	Cl	Co	Cr	Cs	Cu	Dy	Er	Eu	Ga	Gd	Ge	Hf	Ho
3	04YJL-09	1844		110						2.7	1.32	1.43		3.4		6.5	0.50
3	04DN30-2	1786		112						3.2	1.51	2.16		4.2		6.9	0.60
3	04DN30-3	1838		89						2.0	0.99	1.38		2.5		5.9	0.37
3	04DN31-1	1757		70						1.7	0.80	1.38		2.1		5.9	0.31
3	04DN32-1	1968		46						1.7	0.88	1.02		2.0		5.1	0.34
3	04DN32-2	2064		44						1.7	0.87	1.15		2.2		4.9	0.34
3	04DN35-2	1356		47						1.5	0.70	1.16		1.8		5.4	0.28
3	04DN36-3	1290		74						2.4	1.13	1.41		3.2		5.4	0.44
3	04DN37-2	1447		33						1.7	0.84	1.39		2.2		5.5	0.32
3	04DN39	1300		58						1.7	0.93	1.00		2.0		4.5	0.33
3	04DN40	1483		93						2.1	1.01	1.23		2.9		5.3	0.38
3	04DY44-2	1358		76						2.4	1.22	1.44		3.0		5.1	0.45
3	04DY44-4	1952		91						2.0	0.97	1.27		2.7		5.1	0.37
3	04DY44-7	2120		82						1.7	0.86	1.44		2.5		4.9	0.33
3	04D6441	2757		86						2.0	0.95	0.97		2.5		4.5	0.36
3	04D6437	3648		106						2.4	1.00	1.85		3.3		6.3	0.40
4	2T394	911		120				1.70		5.0	2.50	2.80		7.0		5.5	1.00
4	2T395	894		118				1.60		5.4	2.70	2.80		7.2		5.6	1.00
4	2T396	300		71				39.00		5.6	3.10	1.90		6.1		5.3	1.10
4	98T03	391		80				46.00		5.9	3.30	2.10		6.5		6.4	1.20
4	98T04	929		121				1.70		5.6	2.80	3.00		7.3		5.9	1.10
4	98T07	3579		927				3.40		15.5	7.40	9.00		25.8		30.0	2.70
4	98T15	6903		672				1.60		12.1	5.20	7.30		20.4		18.0	2.10
4	98T16	1651		####				2.00		16.0	7.30	9.40		26.0		27.0	2.80
4	98T33	4553		852				1.60		12.3	5.00	8.30		19.4		16.0	1.90
4	98T38	1573		####				4.00		17.7	8.30	10.40		28.1		30.0	3.20
4	98T43	2102		####				1.60		16.1	7.30	9.50		26.0		26.0	2.90
4	98T44	15973		####				3.30		18.9	7.70	12.40		33.0		25.0	2.70
4	98T46	3354		####				2.60		13.9	6.40	7.80		20.0		27.0	2.30
4	98T49	6267		697				3.00		8.9	3.90	5.40		15.9		15.0	1.40

Ref.#	Sample	Ba	Be	Ce	Cl	Co	Cr	Cs	Cu	Dy	Er	Eu	Ga	Gd	Ge	Hf	Ho
4	98T51	2448		934				8.90		11.9	5.70	6.90		21.5		22.0	2.10
4	98T52	7609		707				3.70		10.4	4.20	6.80		20.4		12.0	1.60
4	98T53	3914		578				2.20		8.3	3.50	5.30		14.6		11.0	1.30
4	98T54	4264		474				11.00		5.8	2.30	4.40		12.0		2.4	0.80
4	98T57	3421		955				1.90		13.0	5.60	7.70		19.0		19.0	2.00
4	98T69	8175		725				2.10		10.0	4.30	6.20		19.0		13.0	1.60
4	98T70	7934		622				3.40		8.6	3.60	5.20		17.0		12.0	1.30
4	98T71	3466		967				2.10		12.0	5.70	7.50		22.0		25.0	2.20
4	98T73	2070		996				3.60		13.0	6.00	7.70		22.0		22.0	2.30
4	99T132	3648		486				14.00		5.5	2.70	5.80		17.0		30.0	0.80
4	99T134	3574		560				6.80		5.3	2.80	6.70		21.0		26.0	0.80
4	99T145	5160		591				26.00		6.9	3.50	7.90		24.0		40.0	1.20
4	99T152	3167		514				14.00		4.9	2.00	5.00		17.0		24.0	0.70
4	99T154	3035		507				6.20		5.2	2.40	5.60		19.0		19.0	0.80
4	99T53	3209		314				33.00		9.8	3.80	7.10		22.0		13.0	1.50
4	99T56	1256		198				17.00		3.5	1.40	2.70		5.6		6.3	0.50
4	99T57	1594		229				21.00		5.0	2.00	3.50		9.8		8.5	0.80
4	99T60	1757		250				33.00		5.9	2.30	4.20		11.0		9.7	0.90
4	99T62	2108		252				30.00		6.4	2.80	4.90		14.0		11.4	1.00
5	2002T1021	522		107				0.91		4.4	2.11	2.68		6.7		6.3	0.89
5	2002T1022	515		96				0.47		4.2	2.04	2.20		6.1		5.5	0.77
5	2002T1023	1150		167				0.57		3.7	1.67	2.83		7.1		6.2	0.68
5	2002T1024	701		113				5.38		3.4	1.65	1.86		5.3		5.6	0.64
5	2002T1025	798		124				6.99		2.9	1.28	1.90		5.2		7.2	0.50
5	2002T1026	715		108				7.10		2.6	1.20	1.54		4.4		6.6	0.45
5	2003T373	695		107				7.08		2.4	1.06	1.55		4.3		6.7	0.42
5	2003T374	827		117				3.95		2.7	1.25	1.65		4.6		7.3	0.48
5	2003T375	666		106				10.91		2.2	0.96	1.45		4.0		5.1	0.39
5	2003T380	585		104				4.50		3.0	1.46	1.78		4.6		6.0	0.55
5	2003T483	1100		152				114.30		4.0	2.00	2.27		6.6		8.3	0.74

Ref.#	Sample	Ba	Be	Ce	Cl	Co	Cr	Cs	Cu	Dy	Er	Eu	Ga	Gd	Ge	Hf	Ho
5	2003T485	969		164				129.68		3.9	1.83	2.06		6.4		8.9	0.69
5	2003T486	1017		163				106.45		4.0	1.89	2.09		6.7		9.4	0.71
5	2003T487	1010		162				139.46		4.1	1.91	2.09		6.8		8.8	0.71
5	2003T488	944		162				125.33		4.0	1.84	2.10		6.6		9.0	0.68
5	2003T492	997		164				130.60		4.3	2.07	2.10		7.0		8.8	0.74
6	Tl/10	3340		16		27.6	370.0	27.00		6.3		5.47	22.1	15.5		26.3	0.98
6	Tl/11	3931		15		26.6	368.6	4.30		6.3		5.47	22.3	15.2		26.5	0.97
6	Tl/18	2531		14		19.3	239.1	7.30		6.1		4.93	23.8	15.3		21.7	0.96
6	Tl/13	3452		11		24.5	320.9	17.10		6.0		4.73	20.6	13.0		23.3	0.98
6	Tl/03	3051		14		32.7	342.8	52.70		5.8		4.60	20.2	13.7		21.0	0.91
6	Tl/08	2537		14		22.1	239.2	6.60		5.9		4.80	23.8	14.7		21.6	0.92
6	Tl/17	2835		11		36.2	564.6	36.70		7.3		5.93	20.5	20.0		27.0	1.09
6	Tl/06	2369		13		11.6	89.4	13.10		4.7		3.90	27.1	11.0		25.8	0.73
6	Tl/59	2869		15		10.7	75.9	10.50		4.3		3.91	24.1	10.5		12.3	0.64
6	CHZ-1	2989		27		25.9	313.0	22.30		9.6		6.83	27.9	26.2		30.1	1.44
6	CHZ-2	2939		28		24.1	299.0	25.90		9.5		6.72	27.2	26.0		25.0	1.42
6	CHZ-3	2498		27		23.8	286.0	15.00		8.7		6.20	27.4	24.6		23.3	1.34
6	CHZ-4	2134		24		24.8	297.0	24.20		7.8		5.36	24.9	21.1		22.8	1.23
6	CHZ-5	2346		25		27	329.0	32.30		8.6		5.91	27.0	22.9		24.2	1.36
6	CHZ-6	2151		28		21.7	269.0	26.60		8.7		5.80	27.4	23.2		25.8	1.37
6	CHZ-7	3167		26		25	326.0	22.20		9.5		6.73	27.0	25.8		26.6	1.45
6	CHZ-8	3819		30		23.6	316.0	13.70		9.1		6.68	27.1	24.9		27.2	1.39
6	CHZ-9	3336		30		25.3	324.0	15.10		9.7		7.06	28.0	26.9		26.2	1.49
6	CHZ-10	3263		29		25.7	322.0	17.20		9.6		6.86	28.1	26.6		26.5	1.43
6	CHZ-11	3287		25		25.8	357.0	20.40		9.1		6.75	26.6	25.9		20.6	1.38
6	CHZ-12	2968		36		25.7	351.0	16.30		9.8		6.90	29.4	27.7		24.4	1.51
7	AH-7	1755		376						8.0	2.93	3.73		12.9		13.5	1.33
7	G26	6062		685						11.5	4.69	6.74		18.0		15.8	1.97
7	G68	6929		589						9.6	4.37	5.38		15.7		14.0	1.65
7	G98-0	4011		368						7.2	2.97	5.05		12.3		11.8	1.23

Ref.#	Sample	Ba	Be	Ce	Cl	Co	Cr	Cs	Cu	Dy	Er	Eu	Ga	Gd	Ge	Hf	Ho
7	G98-1	7504		658						9.7	4.02	8.61		18.5		10.6	1.56
7	G98-14	7627		554						8.9	4.16	7.17		15.1		11.5	1.51
7	G98-3	7434		715						10.3	4.27	9.31		19.3		8.2	1.64
7	G98-6	7544		625						9.3	3.97	8.46		17.2		12.9	1.35
7	G98-9	7569		462						7.1	4.11	6.49		12.9		12.8	1.48
7	HH72	1888		217						5.2	2.38	3.84		8.5		18.9	0.97
7	HS07	1188		217						4.3	2.03	2.14		6.0		13.5	0.81
7	HS-69	988		75						3.3	1.73	1.54		4.0		7.4	0.66
7	JC9719	6869		308						6.1	3.61	4.42		7.4		9.4	1.37
7	JC973	7108		314						8.3	3.96	5.36		12.2		7.3	1.48
7	JC975	6428		202						5.8	3.44	3.84		8.1		11.3	1.24
7	JC978	4985		77						4.3	2.51	2.28		4.7		9.2	0.86
7	JH6	2426		261						4.8	1.96	4.11		8.6		12.5	0.77
7	KX84	2003		238						4.2	1.87	4.47		6.9		10.1	0.75
7	PL-58	1673		369						8.8	2.87	4.28		15.7		11.0	1.27
7	PL-7	1372		235						7.9	3.03	4.27		10.9		15.7	1.31
7	QQ08	1695		286						5.7	2.09	2.67		9.5		14.3	0.96
7	QS22	2008		269						4.2	1.99	4.84		9.3		10.4	0.76
7	XT16	1246		216						5.8	2.72	2.64		9.2		10.1	1.07
7	XT8	1978		351						5.3	1.74	5.12		9.4		16.5	0.77
7	XY03	2777		251						5.8	2.31	4.06		9.2		16.1	0.91
7	XY05	1684		266						5.6	2.12	2.75		9.4		13.4	0.88
7	YS02	1846		342						5.0	1.97	4.64		8.7		8.9	0.86
7	YS72	2004		297						6.5	2.21	3.31		10.1		12.1	1.08
7	ZF91	1565		116						3.5	1.75	1.54		4.1		12.6	0.64
7	ZF96	1342		319						6.1	2.91	3.48		8.0		8.5	1.15
8	ZF09	840		55		5.77	59.0		10.3	2.3	0.91	1.89	18.6	3.1		6.7	0.39
8	GUO62	660		48		6.22	78.7		10.1	2.0	0.76	1.51	14.9	2.6		3.9	0.33
8	GUO51	762		46		6.03	52.2		10.3	1.5	0.70	1.68	16.7	2.3		4.8	0.28
8	GUO48	766		54		8.34	81.9		14.4	1.9	0.80	1.48	14.9	3.1		3.6	0.31

Ref.#	Sample	Ba	Be	Ce	Cl	Co	Cr	Cs	Cu	Dy	Er	Eu	Ga	Gd	Ge	Hf	Ho
8	GUO37	478		37		18.3	89.0		21.4	1.8	0.82	1.23	17.2	2.9		3.1	0.32
8	G09	819		41		11.5	46.9		12.6	1.6	0.72	1.24	16.0	2.9		4.5	0.28
8	ZFG17	845		36		8.66	57.9		13.9	1.7	0.78	1.38	16.8	3.9		4.2	0.31
8	G006	729		15		9.12	46.8		19.0	0.6	0.33	0.45	18.2	0.8		3.7	0.12
8	G019	783		50		28.3	42.7		124.0	1.1	0.49	0.79	15.2	1.6		3.5	0.20
8	G016	981		57		14.9	55.0		88.6	1.1	0.56	0.81	17.1	1.9		3.4	0.21
8	G025	461		69		18.9	56.8		53.5	1.3	0.59	1.19	16.1	2.7		6.4	0.22
9	DY-7	4829		601		26.09	361.4		56.0	6.7	2.44	8.30	25.4	25.4		35.2	1.03
9	DC2	3247		659		23.12	310.8		78.4	5.8	1.86	8.17	22.7	23.9		24.2	0.87
9	D509	3691		478		29.64	343.9		50.3	4.6	1.52	4.28	27.0	13.6		35.6	0.67
9	DG43	5618		894		27.83	376.5		63.1	5.7	1.83	6.32	24.6	17.5		48.3	0.74
9	YE51	4110		483		33.68	352.1		69.0	6.1	1.85	4.68	23.3	18.2		32.8	0.76
9	YC08	3581		398		27.51	318.9		58.5	6.0	1.61	4.89	25.9	17.5		22.5	0.70
9	YG13	4418		591		41.9	341.5		62.1	6.2	2.32	6.21	22.7	16.9		38.7	0.98
9	YF12	4283		535		52.18	367.3		67.3	6.0	1.95	5.97	24.6	16.2		25.6	0.88
9	YA32	2616		375		25.62	326.7		56.7	4.8	1.54	3.80	25.4	13.3		16.2	0.67
9	MH78	3212		408		29.43	591.2		67.2	6.1	2.18	4.71	24.7	17.2		25.8	0.94
9	MH69	3740		459		31.52	526.2		76.4	4.2	1.53	3.65	35.6	13.6		30.4	0.62
9	MG-3	2437		341		22.96	309.5		46.3	6.0	2.23	4.51	22.2	12.7		16.5	0.94
9	MY1	2702		442		24.17	356.4		63.9	6.2	2.24	4.27	20.6	13.6		20.4	0.98
9	MK09	1810		317		25.46	461.3		69.4	5.0	1.97	4.24	23.8	14.3		13.4	0.80
9	MR21	2237		226		28.19	353.6		60.5	3.5	1.24	2.15	25.1	7.7		15.1	0.56
9	MA75	3891		437		28.03	560.2		71.4	5.2	1.88	3.32	27.9	10.3		24.5	0.83
9	MX5	2689		271		28.54	423.9		64.7	5.4	2.37	2.55	26.5	8.4		18.4	0.93
9	2003T534	2455		315		33	396.0			5.6	2.35	4.70		15.0		21.0	0.93
9	2003T536	2548		307		33	451.0			5.4	2.24	4.80		15.0		24.0	0.85
9	2003T539	2495		303		33	419.0			5.3	1.98	4.80		15.0		24.0	0.80
9	G8	2620		365		31.38	278.5		61.8	8.9	2.94	6.11	27.2	25.8		21.6	1.39
9	C10	1973		328		26.84	294.4		58.3	10.1	3.64	5.55	26.5	23.9		13.9	1.53
9	CV5	1783		286		25.26	282.8		67.4	9.5	3.31	5.24	26.3	21.8		17.8	1.45

Ref.#	Sample	Ba	Be	Ce	Cl	Co	Cr	Cs	Cu	Dy	Er	Eu	Ga	Gd	Ge	Hf	Ho
9	C76	2376		342		25.63	331.5		34.3	7.6	3.01	6.87	28.4	22.6		24.7	1.17
9	CH4	3371		394		26.1	362.1		41.5	9.8	2.71	7.13	25.3	28.5		30.3	1.38
9	CH7	2433		410		61.95	610.3		39.6	9.6	2.76	8.18	18.7	34.7		22.4	1.34
9	C03	3516		388		53.81	686.4		41.2	9.6	2.98	6.80	21.4	26.4		16.9	1.32
9	CX38	2002		291		24.32	347.5		28.5	6.6	2.40	5.11	22.7	18.7		14.5	1.04
9	C25	1785		242		27.04	393.3		35.9	6.3	2.14	3.39	25.4	14.8		12.9	0.95
10	CT09			263		29.6	202.3		28.4	5.8	2.31	3.54	18.2	11.3		9.6	0.92
10	CT12			265		39.4	376.9		28.5	5.1	2.34	3.45	23.5	12.3		10.5	0.94
10	CT17			153		34.8	259.2		41.2	5.2	2.29	2.51	23.3	8.1		8.9	0.92
10	CT05			212		31.7	263.6		36.3	5.6	2.36	2.77	21.7	8.7		11.4	1.02
10	CT23			251		44.6	346.3		27.9	5.0	2.23	3.21	22.4	9.5		7.8	0.86
10	QS12			277		26.2	117.3		31.7	6.1	2.68	3.86	22.1	15.3		8.1	1.21
10	QS27			248		37.3	251.8		26.8	5.8	2.43	4.14	20.5	15.4		10.9	0.96
10	QS19			203		33.9	236.7		32.3	6.1	2.62	3.31	19.3	14.2		13.2	1.14
10	QS23			222		36.2	352.6		32.6	8.1	2.85	3.74	18.6	15.3		11.7	1.27
10	QS18			192		29.7	338.1		28.3	7.1	2.73	3.31	23.7	13.7		9.6	1.15
10	QS24			152		34.1	369.5		25.4	6.2	2.52	2.71	21.9	11.7		8.3	1.02
10	KY03			236		22.8	182.5		23.9	8.5	2.82	3.46	21.3	13.8		14.2	1.33
10	KY02			187		31.3	343.8		34.8	7.3	2.79	3.16	23.5	13.1		7.4	1.28
10	KY06			136		39.4	367.1		51.3	6.6	2.66	2.27	24.7	10.5		11.6	1.05
10	KY01			264		25.6	253.0		27.7	7.3	2.35	4.48	18.9	14.2		13.8	1.16
10	HS041			189		33.4	138.2		41.8	4.8	2.23	2.24	21.4	8.2		11.8	0.91
10	HS046			183		32.5	237.1		29.8	4.7	2.14	2.18	18.5	7.4		10.5	0.85
10	HS047			239		30.8	210.6		27.5	4.9	2.21	2.66	19.6	8.2		12.7	0.92
10	HS028			126		39.1	395.4		36.3	4.7	1.96	2.04	20.3	6.7		8.4	0.86
10	AH607			313		39.4	171.6		35.8	5.8	2.38	4.73	23.7	13.6		10.6	0.95
10	AH605			174		32.8	205.1		37.6	4.8	2.95	3.37	21.6	7.9		8.5	0.99
10	AH609			197		27.5	175.9		33.1	6.3	2.29	4.22	18.5	11.9		9.7	1.06
10	AH602			218		31.7	172.3		42.5	5.6	2.48	4.13	20.4	11.3		11.5	0.97
10	AH618			193		41.3	169.8		39.7	4.8	2.45	2.94	21.9	9.0		10.2	0.94

Ref.#	Sample	Ba	Be	Ce	Cl	Co	Cr	Cs	Cu	Dy	Er	Eu	Ga	Gd	Ge	Hf	Ho
10	AH615			204		35.2	229.5		38.3	6.4	2.56	4.09	21.3	12.7		8.9	1.01
10	YS74			409		28.4	172.9		28.6	8.2	2.72	6.48	24.1	14.3		14.9	1.32
10	YS78			383		31.9	185.0		25.3	7.3	2.46	5.32	20.5	13.2		15.8	1.13
10	YS05			315		36.5	213.7		34.9	7.8	2.53	5.94	19.4	12.2		17.3	1.26
10	YS79			426		24.1	138.6		22.7	8.1	2.43	6.82	18.9	15.3		28.6	1.27
10	YS07			278		22.6	163.4		20.3	5.2	1.68	3.43	22.6	9.1		16.7	0.74
10	KX44			251		32.9	306.7		39.6	8.2	3.17	6.53	18.3	17.2		13.2	1.34
10	KX51			242		40.5	393.2		36.8	4.8	1.96	4.02	21.1	7.3		12.6	0.88
10	KX80			247		38.9	378.4		35.1	7.3	2.38	5.81	21.6	15.3		11.8	1.10
10	KX49			249		31.3	283.1		40.8	8.8	3.25	6.46	19.0	17.1		14.1	1.51
10	KX62			282		36.5	339.7		36.4	6.6	2.69	4.83	22.3	12.3		12.8	1.28
10	PL53			318		53.5	395.4		36.1	7.4	2.63	4.97	21.3	14.2		16.2	1.15
10	PL61			343		51.8	408.2		34.8	7.1	2.45	5.13	18.6	14.7		17.9	1.02
10	PL3			251		28.4	91.6		25.3	5.5	2.18	3.89	25.7	8.8		10.4	0.82
10	PL18			313		41.7	251.3		26.8	6.4	2.31	4.25	23.5	13.3		13.8	1.03
10	PL92			345		38.6	263.8		31.7	5.5	2.36	4.94	20.4	13.3		11.6	0.96
10	PL43			231		31.5	167.2		28.9	5.0	2.13	3.46	24.8	9.5		12.1	0.78
12	07-SA-21	854		82		22	178.0			2.6	1.06	1.48	20.0	4.4		4.9	0.41
12	07-SA-26A	147		56		11	16.0			1.6	0.48	1.15	17.0	2.9		4.5	0.22
12	07-SA-26B	244		54		15	27.0			1.7	0.59	1.12	17.0	3.0		4.5	0.24
12	07-SG-03	860		114		10	25.0			2.6	0.94	1.36	19.0	4.6		5.1	0.39
12	07-SG-04A	803		120		15	29.0			2.9	1.10	1.56	21.0	5.1		6.1	0.46
12	07-SG-05	880		131		16	33.0			3.0	1.34	1.77	22.0	5.3		4.5	0.49
12	07-SG-06	948		120		10	25.0			2.8	1.05	1.65	19.0	5.1		5.0	0.43
12	07-SG-29	1288		114		14	54.0			2.8	1.14	1.51	18.0	4.6		5.1	0.45
12	07-SG-30	1229		120		8	61.0			2.7	1.10	1.56	20.0	4.8		5.3	0.43
12	07-SG-31A	1131		109		6	38.0			2.9	1.28	1.47	20.0	4.8		5.0	0.47
12	07-SG-31B	1162		115		11	37.0			2.9	1.26	1.57	21.0	4.9		5.5	0.48
12	07-SG-48A	1112		103		9	20.0			2.0	0.72	1.28	22.0	3.7		4.1	0.30
12	07-SG-48B	1152		104		6	24.0			2.0	0.79	1.30	22.0	3.8		4.6	0.33

Ref.#	Sample	Ba	Be	Ce	Cl	Co	Cr	Cs	Cu	Dy	Er	Eu	Ga	Gd	Ge	Hf	Ho
12	07-SG-52A	925		117		24	163.0			3.4	1.55	1.85	18.0	5.6		6.0	0.59
12	07-SG-66	977		50		10	24.0			1.5	0.60	0.92	22.0	2.6		3.9	0.23
12	06-SA-28C	703		49		22	167.0			2.4	1.09	1.19	15.0	3.4		3.7	0.40
12	06-SA-48A	243		44		11	24.0			1.5	0.55	0.95	14.0	2.7		3.7	0.23
12	06-SG-200	934		137		12	22.0			2.9	1.15	1.76	22.0	5.2		5.6	0.46
12	06-SG-201	866		129		14	25.0			3.1	1.30	1.76	21.0	5.2		5.0	0.50
13	NQ2-1*	3324		385						7.6	2.70	7.10		17.0		7.6	1.10
13	NQ21-4*	1960		269						4.8	2.30	3.30		8.9		9.0	0.75
13	NQ7-1*	1024		109						3.1	1.40	1.80		5.0		4.2	0.50
13	Y1-11	1038		142						2.8	1.30	1.70		5.3		5.6	0.49
13	Y1-12	966		139						2.8	1.40	1.80		5.6		6.1	0.50
13	Y1-13	1241		133						2.6	1.30	1.70		5.0		5.5	0.45
13	Y1-14	963		121						2.7	1.30	1.70		5.1		6.5	0.47
13	Y1-15	1057		129						2.9	1.40	1.90		5.4		5.9	0.52
13	Y1-16	865		59						1.1	0.58	0.91		2.2		6.2	0.20
13	Y1-18	871		96						2.0	0.93	1.30		3.8		6.0	0.34
13	Y1-8	977		139						3.4	1.60	2.00		6.2		6.7	0.60
13	Y1-9	1046		141						2.9	1.40	1.80		5.6		8.4	0.52
13	Y2-1	831		106						2.4	1.20	1.50		4.4		6.1	0.46
13	Y2-2	1120		104						2.6	1.30	1.50		4.5		6.5	0.46
13	Y2-3	1046		81						2.2	1.10	1.30		3.0		7.7	0.40
13	Y2-4	941		85						2.2	1.10	1.40		4.0		7.1	0.41
13	Y2-5	780		94						2.3	1.10	1.50		4.0		7.2	0.42
13	Y2-6	1182		111						2.5	1.20	1.50		4.6		7.6	0.44
13	Y2-7	1083		88						2.2	1.10	1.30		3.9		6.7	0.39
13	Y2-8	1091		101						2.3	1.10	1.40		4.1		5.8	0.40
13	Y2-9	974		87						2.1	1.10	1.20		3.7		6.4	0.39
13	Z96-2*	1507		195						4.4	2.30	3.40		8.1		4.4	0.77
14	KK06003	2051		284		12.9		4.72		5.0	2.10	2.86	23.6	10.3		11.8	
14	KK06004	1761		268		12.5		3.36		4.7	1.89	2.82	24.2	10.0		11.7	

175

Ref.#	Sample	Ba	Be	Ce	Cl	Co	Cr	Cs	Cu	Dy	Er	Eu	Ga	Gd	Ge	Hf	Ho
14	KK06005	1739		268		12.1		3.65		4.7	1.92	2.70	23.7	10.0		10.8	
14	KK06006	1811		279		13.3		4.37		4.9	1.99	2.75	24.3	10.3		11.3	
14	KK06007	1888		271		9.7		4.38		4.8	2.00	2.69	23.6	9.7		11.7	
14	KK06008	1888		296		16.2		3.20		5.2	2.10	2.90	24.4	10.6		11.5	
14	KK06009	1881		297		14.5		5.10		5.2	2.19	2.94	24.3	10.9		11.7	
14	KK06010	1919		280		14.4		3.34		5.2	2.12	2.91	24.5	10.4		11.8	
14	KK06011	1926		301		15.2		9.24		5.2	2.16	2.86	24.4	10.8		11.7	
14	KK06012	2018		285		13.6		2.42		5.0	1.99	2.95	24.9	10.5		12.0	
14	KK06013	1515		243		10.4		3.01		3.7	1.62	2.13	24.9	7.9		9.8	
14	KK06014	1489		254		11.5		2.89		3.8	1.64	2.21	25.1	8.1		9.8	
14	KK06016	1487		233		13.1		3.97		3.6	1.59	2.12	23.9	7.4		9.9	
14	KK06018	1528		241		11		3.60		3.6	1.48	2.17	24.7	7.7		9.7	
14	KK06019	1494		249		13.4		3.18		3.9	1.68	2.13	24.8	7.8		9.9	
14	KK06022	1422		245		14.9		3.55		3.9	1.74	2.14	24.4	7.8		9.8	
14	KK06024	1494		253		20.5		5.09		3.8	1.71	2.17	24.6	8.0		10.0	
14	KK06025	2262		318		14.3		5.08		6.1	2.53	3.60	25.2	12.5		11.5	
14	KK06026	2220		302		13.2		5.31		6.0	2.50	3.60	25.4	12.2		11.7	
14	KK06027	2050		288		11.6		2.23		5.4	2.23	3.22	25.6	10.8		12.6	
14	KK06028	2070		310		13.3		3.92		5.8	2.40	3.21	25.2	11.5		12.7	
14	KK06029	2021		286		12.7		3.02		5.6	2.34	3.09	24.1	10.8		12.9	
14	KK06030	2041		265		11.8		1.50		5.5	2.34	3.18	24.2	10.2		12.8	
14	KK06031	1968		298		10.7		1.54		5.4	2.29	3.14	24.0	11.1		12.4	
14	KK06032	274		98		3.57		41.50		2.1	0.82	0.58	25.6	4.5		6.1	
14	KK06033	306		102		3.52		13.60		1.9	0.75	0.58	25.4	4.5		5.8	
14	KK06034	270		101		3.42		42.70		2.1	0.85	0.61	25.9	4.9		5.8	
14	KK06038	2239		276		9.45		85.70		5.1	2.17	2.63	24.5	10.0		10.6	
14	KK06039	1945		299		8.32		106.00		5.6	2.35	3.02	26.4	11.0		11.2	
14	KK06040	2374		364		5.43		20.40		6.1	2.47	3.46	26.9	12.8		11.9	
14	KK06041	2237		325		12.1		4.41		5.9	2.48	3.44	25.1	11.8		11.9	
14	KK06042	2237		325		9.87		18.80		5.2	2.22	2.95	25.2	11.1		11.7	

Ref.#	Sample	Ba	Be	Ce	Cl	Co	Cr	Cs	Cu	Dy	Er	Eu	Ga	Gd	Ge	Hf	Ho
14	KK06043	2326		359		14.3		8.29		6.2	2.58	3.77	27.3	13.4		12.3	
14	KK06046	1894		309		14.7		5.34		5.1	2.10	3.03	25.9	10.4		11.7	
14	KK06047	1790		275		9.28		32.60		4.9	1.93	2.85	25.9	10.2		11.1	
15	Z02H1	1531		137		76.9		3.23		3.0	1.39	1.84		5.8		5.7	0.53
15	Z07H	1027		46		74.5		9.89		2.3	1.47	0.89		2.8		3.6	0.50
15	Z07H1	1690		127		69.8		9.41		3.4	1.63	1.92		6.2		5.1	0.62
15	Z07H2	1629		127		66.2		7.86		3.4	1.57	1.90		6.1		5.1	0.61
15	Z07H3	1877		91		69.7		11.50		2.8	1.51	1.42		4.5		4.7	0.56
15	Z07H4	1757		128		66.7		10.30		3.4	1.62	1.90		6.2		5.1	0.61
15	Z07H5	1589		107		57.8		15.50		3.0	1.53	1.55		4.9		4.9	0.56
15	Z07H6	1505		104		75.9		10.60		3.0	1.47	1.54		5.0		4.8	0.55
15	Z08H1	1732		123		58.7		3.98		3.4	1.62	1.82		5.8		5.1	0.60
15	Z08H2	1680		103		48.2		12.90		2.7	1.25	1.56		4.6		5.0	0.48
15	Z08H3	1736		124		47.8		4.43		3.4	1.54	1.88		5.8		5.3	0.58
15	Z08H4	1748		128		50.9		4.61		3.4	1.51	1.94		6.0		5.5	0.58
15	Z08H6	1695		123		53.4		4.10		3.3	1.54	1.80		5.7		5.3	0.58
15	Z12H3	1249		84		42.2		4.82		3.1	1.52	1.51		4.6		4.5	0.56
15	Z15H1	1755		106		42.5		4.60		3.2	1.65	1.71		5.2		4.0	0.60
15	Z15H2	1640		101		38.1		4.25		3.0	1.53	1.64		5.0		4.1	0.56
15	Z15H3	1815		104		43.9		4.57		3.1	1.60	1.68		5.2		4.2	0.58
15	Z15H5	1247		61		45.7		5.32		1.8	0.94	1.03		2.9		3.9	0.35
15	Z15H6	1158		58		60.5		8.07		2.1	1.08	0.98		3.1		4.0	0.41
15	Z19H1	1303		76		56.4		7.42		2.5	1.22	1.30		3.9		4.2	0.46
15	Z19H4	1160		54		63.6		8.42		1.9	0.98	0.97		2.9		3.7	0.37
15	Z19H5	1161		54		45.7		8.58		1.8	0.94	0.94		2.8		3.7	0.37
15	Z19H6	1172		54		46.5		8.55		1.9	0.95	0.96		2.9		3.8	0.37
15	Z06H	1623		118		23.1		17.40		3.2	1.64	1.59		5.5		5.5	0.60
15	Z08H5	1665		132		42.4		3.99		3.5	1.54	1.97		6.3		5.5	0.61
15	Z10H	1418		90		32.8		8.60		2.8	1.28	1.57		4.6		4.9	0.50
15	Z11H1	1455		88		29		5.09		2.8	1.32	1.57		4.5		4.9	0.50

Ref.#	Sample	Ba	Be	Ce	Cl	Co	Cr	Cs	Cu	Dy	Er	Eu	Ga	Gd	Ge	Hf	Ho
15	Z11H2	1533		90		37.2		4.85		3.2	1.52	1.66		4.9		4.9	0.57
15	Z12H1	1280		85		38.8		4.71		3.3	1.67	1.55		4.8		4.5	0.61
15	Z12H2	1358		88		44		9.09		2.8	1.32	1.62		4.6		4.7	0.52
15	Z15H7	1083		43		43.3		6.90		1.8	0.91	0.89		2.5		3.4	0.35
15	Z15H11	1784		264		30.6		3.19		5.4	2.04	2.96		11.1		13.6	0.85
16	ET021B	63		16				1.20		2.7	1.60	0.73				1.1	0.57
16	ET021C	314		35				2.90		3.5	2.10	0.96				0.7	0.74
16	ET022A	874		35				3.00		1.9	1.29	0.69				1.8	0.42
16	ET024	1212		39				2.00		1.9	1.28	0.72				1.7	0.42
16	ST052B	622		155				5.20		5.3	2.92	1.56				7.5	1.02
16	ST053	905		162				5.40		5.3	2.86	2.02				6.3	1.03
16	ST054	722		169				5.90		5.5	2.90	1.84				3.8	1.05
16	ST055A	213		186				7.60		6.1	3.37	1.03				7.8	1.18
16	ST055B	504		172				6.50		5.6	3.10	1.53				7.1	1.09
16	ST055C	657		94				5.70		5.4	2.72	2.19				3.8	1.01
16	ST057A	849		117				9.40		5.1	2.68	2.23				6.1	0.96
16	ST058	837		158				5.40		5.0	2.72	1.90				4.3	0.97
16	ST059A	420		116				14.30		5.6	3.07	1.38				4.3	1.10
16	ST060A	283		185				9.00		5.8	3.21	1.42				5.9	1.12
16	ST060C	219		198				12.00		6.5	3.61	1.15				7.1	1.26
16	ST061A	307		98				19.80		7.8	4.16	2.24				4.5	1.52
16	ST062	338		234				20.50		6.8	3.72	1.24				1.6	1.32
16	ST101B	144		48				1.20		2.6	1.46	1.08				2.9	0.52
16	ST102B	247		29				3.20		3.2	1.86	0.91				2.4	0.65
16	ST109	430		59				8.60		2.0	1.15	0.91				2.0	0.39
16	ST119A	82		37				0.40		4.7	2.72	1.46				3.4	0.96
16	ST119B	137		90				1.80		8.1	4.58	2.32				7.0	1.62
16	ST121	260		82				0.62		7.2	4.00	2.39				6.0	1.44
16	ST122	88		54				1.00		4.4	2.52	1.50				4.1	0.89
16	T006B1	263		42				5.10		3.3	1.87	1.15				3.5	0.67

Ref.#	Sample	Ba	Be	Ce	Cl	Co	Cr	Cs	Cu	Dy	Er	Eu	Ga	Gd	Ge	Hf	Ho
16	T006B2	128		44				6.40		4.3	2.51	1.41				1.7	0.90
16	T034A	171		18				0.19		2.7	1.66	0.76				2.1	0.57
16	T034B	107		18				0.14		2.6	1.61	0.72				1.7	0.56
16	T036D	229		19				1.10		2.7	1.54	1.01				0.6	0.56
16	T038F	248		83				22.80		4.8	2.81	1.23				3.9	0.98
16	T038G	410		65				13.30		5.1	3.05	1.42				4.5	1.06
16	T038M	285		68				7.90		2.8	1.99	0.33				1.0	0.63
16	T039	816		51				6.80		3.9	2.44	0.95				2.6	0.83
16	T040A	545		62				5.30		4.0	2.30	1.31				3.4	0.82
16	T040B	680		71				5.00		4.5	2.58	1.44				2.0	0.92
16	T041J	240		19				1.00		2.6	1.53	1.12				0.9	0.55
16	T041F	275		19				1.10		2.6	1.50	1.13				1.0	0.54
16	T041H	227		20				0.59		2.8	1.56	1.14				0.5	0.57
16	T042C	152		62				8.00		7.1	4.10	1.94				4.8	1.47
16	T042D	125		35				1.50		3.3	1.77	1.25				1.5	0.65
16	T046A	353		39				2.50		3.8	2.23	1.14				2.7	0.79
16	T047	459		55				18.30		4.7	2.61	1.54				1.9	0.96
16	T048B	471		61				13.00		3.7	2.17	1.22				4.6	0.77
16	T049A	504		68				7.40		3.6	2.21	0.88				2.9	0.76
16	T049B	354		59				5.10		2.9	1.62	1.23				3.7	0.58
16	T049C	478		64				6.50		3.2	1.82	1.41				4.0	0.65
16	T051B	479		62				1.30		3.2	1.79	1.21				1.5	0.63
16	T051C	296		73				2.10		2.7	1.82	0.57				3.4	0.58
16	T052	577		77				9.90		3.9	2.34	1.09				1.8	0.80
16	T054A	290		41				4.80		5.0	2.85	1.66				2.9	1.03
16	T055A	269		42				1.60		4.1	2.37	1.09				3.5	0.85
16	T055B	279		38				3.20		5.1	3.04	1.52				3.0	1.07
16	T056A	290		22				4.90		3.1	1.88	1.05				2.8	0.67
16	T056B	126		28				13.40		3.7	2.33	1.00				2.7	0.80
16	T062B	906		63				5.00		5.1	3.00	1.86				5.0	1.06

Ref.#	Sample	Ba	Be	Ce	Cl	Co	Cr	Cs	Cu	Dy	Er	Eu	Ga	Gd	Ge	Hf	Ho
16	T062C	358		38				3.10		3.5	1.97	1.24				2.9	0.72
16	T063	676		47				4.50		3.5	1.94	1.39				2.6	0.70
16	T064A	481		45				10.30		2.9	1.67	1.15				2.4	0.59
16	T065A	483		71				7.90		4.2	2.48	1.06				1.9	0.87
16	T065B	470		65				7.00		4.4	2.82	0.81				2.4	0.95
16	T066	449		64				1.50		5.0	2.92	1.50				4.2	1.04
16	T068	490		63				7.00		4.1	2.64	0.81				2.3	0.89
16	T070A	643		71				3.10		4.0	2.47	1.46				4.1	0.85
16	T072A	410		99				4.10		4.9	2.92	1.46				5.5	1.02
16	T072D	473		74				1.20		4.3	2.54	1.18				4.2	0.89
16	T072E	465		76				3.50		4.2	2.46	1.16				4.2	0.86
16	T073	459		72				5.90		4.1	2.41	1.13				4.3	0.86
16	T078B	164		62				5.00		1.4	0.79	0.85				3.4	0.27
16	T079A	233		28				9.20		3.9	2.06	1.38				1.8	0.78
16	T079B	239		41				23.90		4.3	2.46	1.64				2.6	0.89
16	T079C	260		36				1.30		4.4	2.63	1.30				2.8	0.93
16	T080	745		36				1.90		3.9	2.18	1.55				1.5	0.80
16	T082A	888		65				3.10		2.1	1.37	0.77				1.6	0.45
16	T082B	833		66				7.50		2.2	1.44	0.87				1.7	0.48
16	T083B	906		80				12.40		3.9	2.49	0.83				2.7	0.84
16	T083C	269		47				7.00		5.2	2.92	1.45				1.3	1.06
16	T084C	948		58				4.70		5.1	3.06	1.18				3.6	1.05
16	T102A	307		85				95.40		5.3	3.05	1.24				0.9	1.07
16	T103	779		281				10.20		7.2	3.74	2.26				3.4	1.38
16	T104	333		85				44.10		5.1	2.98	0.98				3.8	1.04
16	T105A	293		85				7.50		7.1	4.14	1.62				7.4	1.46
16	T110A	565		116				18.60		5.4	2.91	1.45				3.4	1.05
16	T110B	447		89				9.20		5.1	2.84	1.27				3.6	1.01
16	T111	384		54				14.40		2.5	1.42	0.79				1.7	0.49
16	T112	677		131				2.60		6.9	3.80	1.96				4.3	1.37

Ref.#	Sample	Ba	Be	Ce	Cl	Co	Cr	Cs	Cu	Dy	Er	Eu	Ga	Gd	Ge	Hf	Ho
16	T113	635		130				4.10		7.2	4.04	1.71				4.3	1.44
16	T116A	192		36				1.20		5.3	3.15	1.56				1.8	1.13
16	T117	497		61				4.50		3.6	2.06	0.95				3.9	0.73
16	T127B	279		54				1.40		2.6	1.45	0.88				3.5	0.52
16	T129A	298		39				2.10		4.3	2.63	1.01				3.1	0.91
16	T130	1137		53				3.10		5.3	3.84	0.97				5.3	1.21
16	T131A	102		79				0.31		5.7	3.30	1.36				3.2	1.19
16	T134	1186		187				2.90		9.6	5.56	2.03				5.0	1.95
16	T136A	1113		245				9.40		10.5	5.76	3.03				6.1	2.04
16	T136B	573		284				10.80		77.1	23.00	10.00				5.6	11.60
16	T138D	1144		14				6.90		0.8	0.33	0.59				1.1	0.13
16	T139	1158		55				4.00		3.3	1.94	1.02				3.7	0.65
16	T140A	373		70				3.70		4.7	2.91	1.18				4.9	0.99
16	T140B	182		83				4.30		4.7	2.60	1.57				5.1	0.94
16	T140D	394		65				5.70		4.4	2.68	1.19				4.3	0.92
16	T140E	293		47				3.00		7.1	4.30	0.57				3.5	1.48
16	T142	895		69				2.50		5.0	3.10	1.22				2.9	1.06
16	T143	689		80				1.80		5.4	3.36	1.36				3.0	1.13
16	T144A	543		78				0.88		11.6	6.38	2.00				4.9	2.35
16	T144B	717		54				1.90		5.6	3.35	1.46				4.2	1.17
16	T144C	551		62				3.90		3.6	2.64	0.52				3.2	0.81
16	T144D	755		102				2.30		3.8	2.37	1.26				2.7	0.80
16	T146	469		65				2.20		5.5	3.49	1.04				5.9	1.18
16	T147	436		83				1.30		7.1	4.38	1.24				4.1	1.49
16	T151	340		85				2.60		5.4	2.93	1.88				4.6	1.05
16	T152A	1006		106				11.30		5.8	3.26	2.37				7.4	1.17
16	T152B	304		41				3.50		3.7	2.09	1.28				2.6	0.75
16	T155	447		124				3.10		5.1	2.83	1.41				2.8	0.99
16	T160A	628		80				12.00		5.5	3.12	1.66				5.0	1.11
16	T160B	406		72				12.80		8.5	5.24	1.04				4.0	1.74

Ref.#	Sample	Ba	Be	Ce	Cl	Co	Cr	Cs	Cu	Dy	Er	Eu	Ga	Gd	Ge	Hf	Ho
16	T169A	217		112				14.80		7.1	4.26	0.78				5.2	1.45
16	T169B	199		494				13.70		16.0	6.64	2.47				5.2	2.78
16	T169C	911		66				2.80		4.0	2.24	0.96				3.2	0.80
16	T233A	121		42				0.83		2.3	1.29	0.86				2.2	0.46
16	T233B	458		47				2.70		3.9	2.23	1.17				3.5	0.81
16	T233C	624		87				3.20		6.0	2.79	2.17				2.9	1.08
16	T234A	943		85				0.37		4.4	2.23	2.12				4.0	0.83
16	T234B	735		88				1.40		4.7	2.35	2.25				3.7	0.87
16	T234C	124		82				2.10		3.5	1.67	1.51				4.0	0.63
16	T235A	440		88				3.20		5.8	3.08	1.13				4.2	1.14
16	T235B	330		96				3.30		5.0	2.86	0.95				3.4	0.99
16	T238B	217		38				9.50		4.2	2.39	1.22				3.9	0.86
16	T239	318		39				12.20		3.8	2.14	1.14				4.4	0.77
16	T240B	387		41				3.50		4.3	2.45	1.20				4.6	0.86
17	GGL01	565		89						4.7	2.47	1.45		5.5		5.9	0.90
17	GGL02	680		105						6.1	3.42	1.76		7.2		7.1	1.24
17	GGL03	574		98						5.5	2.98	1.58		6.8		6.6	1.05
17	GGL04	663		103						6.7	3.81	1.87		7.4		7.7	1.39
17	GGL05	501		84						5.9	3.18	1.86		6.4		6.6	1.18
17	GGL06	507		81						5.6	3.20	1.79		6.3		6.0	1.16
17	GGL07	495		83						5.8	3.19	1.74		6.3		6.3	1.19
17	GGL08	463		77						5.4	2.94	1.70		5.9		5.9	1.09
17	GGL09	567		89						5.9	3.20	1.82		6.6		6.6	1.18
17	GGL10	595		89						6.1	3.44	1.89		6.8		7.0	1.26
17	GGL11	519		86						5.7	3.11	1.79		6.4		6.5	1.14
17	GGL12	522		85						5.9	3.22	1.78		6.6		6.5	1.18
17	GGL13	547		90						6.0	3.31	1.88		6.8		7.1	1.23
17	GGL14	594		91						6.1	3.36	1.90		6.8		6.9	1.22
17	GGL15	533		89						5.4	2.80	1.82		6.2		6.8	1.07
18	GJ0601	1908	9.63	274		9.09	105.0	121.00	18.5	3.8	1.57	2.41	26.6			17.4	0.65

Ref.#	Sample	Ba	Be	Ce	Cl	Co	Cr	Cs	Cu	Dy	Er	Eu	Ga	Gd	Ge	Hf	Ho
18	GJ0602	1892	8.96	263		7.56	89.9	35.60	21.0	3.9	1.69	2.43	25.5			16.6	0.66
18	GJ0605	1904	9.44	273		9.73	88.6	52.50	11.6	4.1	1.80	2.54	26.5			17.7	0.68
18	GJ0606	1984	8.9	257		8.43	94.7	54.90	14.8	3.9	1.72	2.58	27.0			17.1	0.63
18	08YR04	1094	10.7	160		7.69	60.7	34.40	20.0	2.6	1.10	1.68	25.6			10.3	0.43
18	GJ0614	654	3.66	161		2.69	41.0	20.70	6.2	3.4	1.52	1.33	27.4			7.8	0.62
18	GJ0617	694	5.62	157		4.86	39.1	20.80	8.4	3.7	1.85	1.29	27.4			7.8	0.69
18	GJ0619	725	5.61	160		4.81	38.2	20.60	5.9	4.0	1.81	1.30	27.1			7.7	0.69
18	GJ0620	787	4.5	155		4.48	40.5	18.50	8.6	4.2	2.02	1.36	27.0			8.1	0.75
18	GJ0624	874	9.56	170		7.11	36.8	35.80	7.6	2.6	1.14	1.40	26.2			8.3	0.44
18	GJ0627	873	9.15	172		6.34	37.5	30.70	10.4	2.7	1.18	1.39	26.7			7.9	0.43
18	GJ0628	1333	13.1	273		9.32	53.0	50.90	14.7	3.9	1.78	2.11	39.9			12.0	0.69
18	GJ0629	875	7.62	159		6.21	36.0	21.20	8.9	2.5	1.13	1.41	26.6			7.1	0.42
18	10XB03	638	7.32	161		5.33	33.2	19.00	9.8	3.9	1.81	1.24	29.2			7.4	0.64
18	10XB04	650	7.06	170		4.66	35.6	19.10	12.7	3.5	1.53	1.28	30.8			7.4	0.55
18	10XB07	566	7.38	166		6.62	41.3	19.60	12.2	3.3	1.47	1.16	29.5			7.6	0.52
18	08YR05	1982	7.21	141		26.8	318.0	29.90	44.8	4.6	2.05	3.28	20.5			10.9	0.82
18	10XB10	2080	9.89	176		24.6	475.0	28.00	52.3	5.6	2.31	3.60	21.8			14.6	0.84
18	10XB12	2208	10.1	182		25.7	517.0	32.70	37.3	6.2	2.48	3.89	22.0			15.2	0.91
18	10XB13	2175	10	178		27.3	510.0	30.10	23.3	5.9	2.39	3.76	21.3			15.3	0.91
18	10YR01	2001	7.16	153		14.6	375.0	33.80	38.1	5.0	2.36	3.28	21.6			11.9	0.81
18	10YR02	1786	6.52	142		20.9	334.0	16.90	45.9	4.6	2.20	3.02	20.0			10.8	0.75
18	10YR04	1827	7.05	144		28.2	329.0	32.00	47.7	4.5	2.11	3.12	20.1			11.1	0.71
18	10YR04a	1760	6.76	141		27.1	296.0	31.00	45.9	4.4	2.04	3.10	19.6			10.8	0.70
18	10YR07	1824	7.45	143		25.4	325.0	31.80	43.6	4.5	1.99	3.11	20.2			11.0	0.69
19	MV1B	185		48				113.00				0.31				2.6	0.30
19	MV2	205		49				110.00				0.29				2.7	0.32
19	UM1B	172		55				113.00				0.26				2.7	0.33
19	UM3V	169		52				79.00				0.29				2.8	0.30
19	UMQP	210		50				78.00				0.30				2.7	0.37
19	UMVU	460		48				351.00				0.25				2.6	0.37

Ref.#	Sample	Ba	Be	Ce	Cl	Co	Cr	Cs	Cu	Dy	Er	Eu	Ga	Gd	Ge	Hf	Ho
20	TE008/93	2351	20	275	262	20	314.0		38.0	6.7	2.20	4.50	17.0	15.0		12.2	0.99
20	TE011/93	2715	21	251	212	20	332.0		31.0	6.6	2.30	2.80	22.0	16.0		13.0	0.91
20	TE125/93	1863	12	185	480	21	295.0		33.0	6.5	2.50	4.00	22.0	14.0		15.6	1.06
20	TE126/93	2718	14	284	246	25	496.0		55.0	6.2	2.20	4.40	21.0	16.0		17.7	0.81
20	TE127/93	2715	13	290	323	26	494.0		53.0	6.6	2.20	4.60	22.0	17.0		18.2	0.90
20	TE131/93	2397	14	269	230	30	384.0		73.0	5.6	2.00	4.30	20.0	15.0		19.1	0.79
20	TE137/93	3488	9	207	930	28	528.0		63.0	7.8	2.50	5.30	16.0	16.0		11.2	1.14
20	TE138/93	3416	9	206	1100	24	368.0		58.0	6.9	2.50	4.70	19.0	16.0		10.0	1.01
20	TE117/93	2160	11	197	330	21	377.0		53.0	6.6	2.30	4.80	20.0	15.0		12.5	0.91
20	TE118/93	2292	14	203	430	25	419.0		39.0	5.8	2.30	4.90	23.0	14.0		13.0	0.91
20	TE007/93	1562	14	178		13	129.0		28.0				17.0				
20	TE025/93	1165	12	173		17	82.0		14.0	2.9	1.10	1.80	25.0	6.0			0.45
20	TE136/93	1988	5	191		8	130.0		39.0	4.3	1.60	2.40	22.0	8.0		8.8	0.64
20	TE148/93	989	7	176		4	65.0		15.0	3.1	1.40	1.70	29.0	6.0		10.3	0.50
20	TE150/93	941	9	162		3	63.0		21.0	3.3	1.40	1.80	28.0	8.0		10.3	0.54
20	TE153/93	964	9	176		13	63.0		16.0	2.8	1.10	1.80	28.0	6.0		10.3	0.40
20	TE154/93	810	9	160		5	67.0		15.0	3.4	1.50	1.80	27.0	7.0		9.7	0.55
20	TE047/93	778	2	59		4	25.0		12.0	1.7	0.80	0.90	15.0	2.0		3.3	0.29
20	TE189/93	998	2	79		7	50.0		9.0	2.6	1.10	1.70	17.0	4.0		4.5	0.43
20	TE192/93	781	2	60		7	33.0		14.0	2.1	0.90	1.30	17.0	3.0			0.36
20	TE194/94	813	3	69		13	25.0		10.0	2.4	1.00	1.30	23.0	4.0			0.46
21	Y-2	2599	196.4				53.0			5.3	2.00	3.40	21.0	12.1		12.0	
21	Y-4	2258	114.6				28.0			3.2	1.20	2.10	18.0	6.9		7.0	
21	ZB1	2507	121.8				126.0			5.3	2.00	3.30	17.0	10.9		8.0	
21	ZB4	2823	138.9				138.0			5.9	2.30	3.70	21.0	12.4		10.0	
21	ZB10	2775	136.1				145.0			5.8	2.20	3.60	20.0	11.9		9.0	
21	ZB12	2919	138.1				116.0			6.1	2.30	3.50	21.0	12.0		12.0	
22	K732	1387		255								2.91					
22	K738	1635		233								2.92					
22	K89G185	1626		224								2.82					

Ref.#	Sample	Ba	Be	Ce	Cl	Co	Cr	Cs	Cu	Dy	Er	Eu	Ga	Gd	Ge	Hf	Ho
22	K89G200	1315		163								2.56					
22	K9007	1466		255								2.90					
22	K9008	1389		258								2.86					
22	K9021	2563		333								4.30					
22	K9024	2076		287								3.60					
22	K9031	2206		260								2.60					
22	K9038	1985		326								3.20					
23	Bb-105	2563		333								4.30				8.0	
23	Bb-107	2564		358						6.3	2.70	4.70		12.0		9.0	
23	Bb-109	2080		263						4.5	2.10	3.00		8.3		4.0	
23	Bb-114	2091		290						4.9	2.40	3.20		9.2		10.0	
23	Bb-88	1760		274								3.00				8.0	
23	Bb-89	86		103						1.0	1.00	0.20		1.0		8.0	
23	Bb94-2	2076		287								3.60				10.0	
23	Bb-95			388						5.7		4.10		15.1			
23	Bg121			260						3.1	1.40	2.80		58.0			
23	Bg124			234						3.6	1.50	2.70		6.6			
23	COUL311			230						4.6	1.80	3.40		8.0			
23	COUL326			260						3.7	1.60	3.20		7.4			
23	COUL328			300						4.2	1.80	3.00		7.8			
23	COUL338			280						4.2	1.90	2.90		7.2			
23	COUL339			300						4.1	1.90	3.00		7.3			
23	k705	1985		326						4.4	2.00	7.30		8.3			
23	k708	2206		260						3.8	1.70	2.60		6.4			
23	K713			320						4.1	1.70	2.90		8.3			
23	K716			319								3.40					
23	K718			276								2.80					
23	K720			260						6.2		3.30		10.9			
23	K723			229								4.10					
23	K732			288								3.70				9.0	

Ref.#	Sample	Ba	Be	Ce	Cl	Co	Cr	Cs	Cu	Dy	Er	Eu	Ga	Gd	Ge	Hf	Ho
23	K738			304								4.40				9.0	
23	K89G159	105		352						5.9	2.40	4.20		13.9			
23	K89G162			706								10.20				9.0	
23	K89G163			724								9.10				13.0	
23	K89G185			572								6.60				13.0	
23	K89G186											3.90				27.0	
23	K89G191											8.40				9.0	
23	K89G192											4.30				31.0	
23	K89G193											5.60				8.0	
23	K89G197											4.50				23.0	
23	K89G200	1454														11.0	
23	K9002	1387										2.90					
23	K9006	1466										2.90				11.0	
23	K9007	1267															
23	K9008	1398															
23	K9016	1389										2.90				11.0	
23	K9017	1611															
23	K9018	1527										2.70				9.0	
23	K9019	1626										2.80				9.0	
23	K9021	1814															
23	K9024	1315										2.60				7.0	
23	K9026	1479															
23	K9027	1635		233								2.90				9.0	
23	K9028	1631		232								2.90				10.0	
23	K9029	1596															
23	K9031	407															
23	K9032	1413															
23	K9038	1462															
23	K9039			72						4.3	2.80	0.70		4.4			
23	Kp35-10			56						1.3	0.60	0.90		2.3			

Ref.#	Sample	Ba	Be	Ce	Cl	Co	Cr	Cs	Cu	Dy	Er	Eu	Ga	Gd	Ge	Hf	Ho
23	Kp12-58			68						2.0	1.00	1.20		3.3			
23	Kp23-2			38						3.5	1.80	1.30		4.2			
23	Kp24-1			33						3.6	2.00	1.30		4.0			
23	Kp39-3	2131		177								2.30				12.0	
23	Kp47-2	2211		204								2.90				13.0	
23	Kp47-5	1860		181								2.40				12.0	
25	04wq-1	2999		519		38.2	461.0		31.5	6.3	2.62	4.92	17.7	11.2	1.78	7.4	1.00
25	04wq-2	2861		473		35.4	420.0		24.7	6.0	2.49	4.60	17.0	10.6	1.74	7.0	0.97
25	04wq-3	3153		609		40.7	433.0		45.5	7.0	2.81	5.44	17.8	12.7	1.82	7.5	1.08
25	04wq-4	3773		441		38.5	404.0		44.6	6.3	2.62	4.63	17.8	11.9	1.80	7.7	1.01
25	04wq-5	3092		609		40.7	427.0		45.6	7.0	2.83	5.70	18.3	13.2	1.88	7.5	1.10
25	04wq-6	2084		212		30.3	293.0		36.6	4.4	1.98	2.46	18.7	6.9	1.42	6.8	0.77
25	04wq-7	2056		211		31.1	288.0		22.2	4.4	2.00	2.54	18.8	6.6	1.52	6.9	0.76
25	4086-1	1998		209		30.8	307.0		37.4	4.3	1.97	2.51	19.5	6.4	1.42	6.8	0.75
25	8528	1533		118		33.6	445.0		22.5	4.2	2.09	2.24	17.2	6.3	1.30	7.0	0.79
25	8518-1	1255		108		16.9	127.0		25.7	3.3	1.54	1.68	20.9	4.7	1.39	6.3	0.59
25	8518-2	1239		107		16.2	125.0		24.3	3.3	1.53	1.62	21.0	5.0	1.32	6.1	0.58
25	9063-GS2	1473		93		22.7	217.0		30.8	2.9	1.38	1.78	18.4	3.9	1.34	4.7	0.55
25	9063-GS3	1537		73		20.8	267.0		24.5	2.5	1.21	1.75	19.9	3.5	1.24	4.6	0.47
25	D3145	1986		439		8.55	20.0		15.0	6.2	2.67	4.24	24.4	8.2	1.34	11.3	1.01
26	05S2-7	2939		123		21.5	278.0			4.7	1.79	3.83		11.9		19.1	0.72
26	05S2-8-1	3007		162		20.8	304.0			5.0	1.94	4.35		13.2		18.5	0.75
26	05SLP5-3	3028		175		17.8	271.0			5.6	2.26	5.40		14.6		17.2	0.89
26	05SLP5-05	2402		145		25.4	312.0			4.5	1.95	4.24		10.1		14.4	0.77
26	05SLP5-06	2458		175		22.3	344.0			4.0	1.65	3.76		9.4		14.2	0.66
26	05SLP5-7	2507		174		24.2	415.0			4.4	1.74	4.69		10.7		15.5	0.67
26	05SLP5-8	1979		163		20.3	244.0			3.7	1.66	3.67		9.1		13.8	0.62
26	05SLP5-09	2541		279		22.7	353.0			5.4	2.10	4.83		15.6		18.0	0.83
26	S05SLP5-10	3220		153		20.9	283.0			4.3	1.73	4.57		10.5		11.3	0.69
26	05SLP5-11	2691		114		21.8	271.0			3.3	1.34	4.14		8.1		13.7	0.52

Ref.#	Sample	Ba	Be	Ce	Cl	Co	Cr	Cs	Cu	Dy	Er	Eu	Ga	Gd	Ge	Hf	Ho
26	05SLP5-16	2567		132		31.5	460.0			5.1	2.07	4.30		11.3		15.7	0.83
26	05SLP4-01	12549		555		41.7	452.0			12.8	3.74	12.50		38.4		10.3	1.68
26	05SLP4-02	5569		303		30.9	290.0			7.4	2.34	6.81		20.3		17.1	1.07
26	05SLP4-03	6642		396		38.3	329.0			9.4	2.86	9.17		25.6		13.7	1.29
26	05SLP4-04	5794		294		31.7	321.0			7.0	2.28	6.58		18.9		17.4	0.99
27	WR-12-48	558		127		9.3	7.4			5.4	3.28	1.51		6.3		10.3	1.10
27	WR-12-47	65		50						6.9	4.31	0.09		7.1		2.6	1.43
27	WR-12-44	234		24		9.7				1.1	0.71	0.91		1.3		5.5	0.22
27	WR-12-45	118		35		35.7	67.8			4.0	2.31	1.38		4.4		2.3	0.78
27	WR-12-40	740		50		10.1				2.2	1.48	1.04		2.5		6.1	0.47
27	WR-12-42	274		39		27.4				3.5	2.05	1.17		4.1		2.4	0.70
27	WR-12-33	620		60		13.2	6.1			2.7	1.59	0.98		3.3		3.2	0.55
27	WR-12-35	294		72		32.5	22.1			5.4	3.10	1.33		6.7		3.8	1.06
28	T2A/98	4221		315						8.2	2.70	5.33		19.9		8.4	1.17
28	T3b/98	2696		199						7.1	2.96	3.49		12.7		9.6	1.19
28	T4A/98	2737		284						5.9	2.06	4.58		15.5		12.6	0.87
28	T5A/98	1593		124						4.2	1.84	2.17		7.9		6.9	0.72
28	T11B/98	740		56						1.7	0.73	1.11		3.1		3.6	0.29
28	JPT14.2	734		53						1.7	0.76	1.08		3.1		3.5	0.30
29	JPT24A	1003		147		16				4.2	1.80	1.90	23.8	8.1		7.5	0.70
29	JPT24B	1726		147		30.4				5.6	2.20	3.20	18.8	12.2		10.7	0.90
29	JPT24C	1640		139		27.6				5.2	2.10	3.10	18.1	11.7		10.2	0.80
29	JPT22	711		152		9				3.7	1.70	1.30	26.8	6.4		6.1	0.70
29	K89G162	1322		233		9.7				4.1	1.40	3.00	20.4	10.4		6.0	0.60
29	20E39A	948		98		32.4				4.8	2.30	2.20	16.3	6.7		4.7	0.90
29	JPT7	1878		116		19.5				4.1	1.80	2.00	12.7	7.4		6.4	0.70
29	T5B/98	1535		127		15				4.3	2.00	2.20	14.4	8.0		7.2	0.80
29	JPT14.1	847		65		14.4				2.1	1.00	1.20	21.4	3.6		3.1	0.40
29	JPT3	914		64		11.3				2.1	0.90	1.20	17.7	3.7		3.5	0.40
29	JPT4	761		42		3.7				0.9	0.40	0.60	16.3	1.8		1.2	0.20

Ref.#	Sample	Ba	Be	Ce	Cl	Co	Cr	Cs	Cu	Dy	Er	Eu	Ga	Gd	Ge	Hf	Ho
29	JPT5.2	1060		66		8.6				1.5	0.60	1.00	19.0	3.1		2.5	0.20
29	JPT8	963		89		3.7				0.7	0.40	0.40	18.9	1.1		2.1	0.10
29	95RAS11.3	877		51		3.1				1.2	0.60	0.50	11.2	2.0		1.9	0.20
29	T2A	4221		315		36				8.2	2.70	5.30	16.0	19.9		8.4	1.10
29	T3B	2696		199		25				7.1	3.00	3.50	18.0	12.7		9.6	1.20
29	T4A	2735		180		26				5.9	2.10	4.50	20.0	15.8		12.5	0.90
29	T5A	1594		124		19				4.2	1.80	2.20	13.0	7.9		6.9	0.70
29	912	2429		286		15.5				5.6	2.20	3.90	22.4	12.1		14.2	0.90
29	1105	599		69		15.1				4.2	2.30	1.10	16.6	5.0		2.4	0.80
29	K702	2133		275		19.5				6.0	2.30	3.90	19.5	13.3		9.6	1.00
29	K703	2131		318		19.4				6.9	2.60	4.50	22.2	15.1		11.5	1.10
29	K89G185	2854		373		31				6.9	2.50	5.10	21.7	15.6		9.6	1.10
29	K89G186	2697		349		31.9				6.2	2.20	4.70	20.5	14.2		9.4	0.90
29	K89G200	2287		310		20.7				5.2	1.90	3.90	21.4	11.8		8.1	0.80
29	KP12.6	1649		337		13.4				6.4	2.30	3.60	24.6	13.8		12.3	1.00
29	KP47-2			288								3.70				8.6	
29	KP47-5			304								4.40				9.4	
29	Bb124	1844		303		14.3				4.7	1.80	3.10	22.4	10.3		11.1	0.80
29	Bb121	1788		287		12.8				4.4	1.70	3.10	22.0	9.8		10.6	0.70
29	Bq137	1923		348		8.8				4.4	1.60	3.10	22.5	10.2		10.9	0.70
29	Bb119	2002		377		8.4				4.8	1.70	3.10	22.9	11.3		12.3	0.80
29	Bb122	1968		342		9.4				4.3	1.60	3.00	22.0	10.0		12.5	0.70
29	Bb135	1970		353		7.2				4.4	1.60	3.00	22.7	10.4		11.8	0.70
29	Bg142	1789		239		3.2				1.8	0.50	2.00	23.1	6.1		6.1	0.20
29	Bq140	1768		243		3				1.9	0.50	1.80	22.3	6.2		6.7	0.30
29	Bq141	1763		263		2.1				2.4	0.70	2.10	23.6	6.9		11.8	0.30
29	K9024	1606		214		17.7				4.7	2.10	2.60	18.9	8.7		8.6	0.80
29	K9026	1673		231		15				4.9	2.00	2.80	20.3	9.2		9.3	0.80
29	K9027	1610		225		14.5				4.8	2.00	2.70	19.4	8.7		9.0	0.80
29	K9028	1610		205		14.4				4.5	1.90	2.50	18.9	8.3		8.4	0.80

Ref.#	Sample	Ba	Be	Ce	Cl	Co	Cr	Cs	Cu	Dy	Er	Eu	Ga	Gd	Ge	Hf	Ho
29	K9029	1701		225		15.8				4.8	2.10	2.80	21.0	9.1		9.5	0.80
29	K9031	1732		229		17.7				4.9	2.10	2.80	20.1	9.1		9.4	0.80
29	K9032	1816		235		16.9				5.0	2.10	2.80	20.8	8.7		9.3	0.80
29	K9038	1427		164		19.3				4.6	2.00	2.40	19.2	7.7		7.1	0.80
29	K9039	1577		178		19.5				5.0	2.20	2.70	20.5	8.7		7.5	0.90
29	K9041	595		80		6.6				6.6	3.70	2.00	21.0	7.3		6.8	1.30
29	K9001	357		57		9.6				3.7	2.10	1.00	13.4	4.2		3.2	0.70
29	K9002	376		59		11				3.9	2.20	1.10	15.1	4.4		3.8	0.80
29	K9006	1640		281		11.2				5.6	2.20	3.00	24.7	10.8		11.0	0.90
29	K9007	1458		263		11.4				5.4	2.20	2.80	23.3	10.2		10.4	0.90
29	K9008	1507		254		10.3				5.3	2.10	2.90	23.2	10.5		10.2	0.80
29	K9016	1345		251		9.6				4.9	1.90	2.60	23.3	9.6		9.1	0.80
29	K9017	1461		264		9.5				5.3	2.20	2.80	23.2	10.1		10.1	0.90
29	K9018	1521		262		10.8				5.5	2.20	2.90	23.1	10.8		10.4	0.90
29	K9019	1542		266		11.9				5.3	2.10	2.90	22.9	10.5		10.1	0.90
29	K9021	1416		258		10.4				5.1	2.10	2.80	22.1	9.8		10.4	0.80
30	2007k251	4160		543	37.4	37.39	156.1	3.18	31.6	7.5	2.55	7.18	20.2	18.7		9.6	1.15
30	2007k252	5108		559	35.6	35.61	155.1	4.79	37.8	7.7	2.74	7.15	18.4	19.0		10.7	1.16
30	2007k253	4817		517	34.2	34.21	149.0	4.53	32.6	7.1	2.52	6.68	17.8	17.9		10.1	1.07
30	2007k254	4572		560	35.5	35.49	150.0	6.35	31.5	7.7	2.71	7.40	17.2	19.6		10.3	1.15
31	DHLT-10	2084		294						4.5	1.76	3.55		8.9		9.1	0.67
31	DHLT-2	2065		283						2.6	0.86	2.74		6.3		11.0	0.30
31	DHLT-4	3113		343						6.4	2.23	5.10		12.5		15.0	0.84
31	DHLT-5	2104		292						4.3	1.66	3.52		8.8		10.0	0.60
31	DHLT-7	2098		300						3.5	1.23	3.39		8.1		10.0	0.46
31	DHLT-9	2096		292						4.5	1.59	3.53		8.9		12.0	0.67
31	PL-12	1946		265						6.7	3.20	3.55		16.4		9.1	1.12
31	PL-2	2106		337						7.0	3.20	4.10		19.2		10.0	1.13
31	PL-3	2353		337						6.6	2.80	4.24		19.4		11.0	1.03
31	PL-5	2462		346						5.6	2.93	4.15		16.5		9.7	1.09

Ref.#	Sample	Ba	Be	Ce	Cl	Co	Cr	Cs	Cu	Dy	Er	Eu	Ga	Gd	Ge	Hf	Ho
31	PL-7	1900		249						5.9	2.60	3.36		15.4		9.4	1.04
31	PL-9	1815		282						6.9	3.20	3.73		17.7		9.1	1.18
31	YCN-1	1909		254						4.8	1.81	3.49		8.9		11.0	0.65
31	YCN-2	1973		249						4.1	1.43	3.34		8.1		11.0	0.61
31	YCN-3	1898		252						4.9	1.88	3.55		8.9		10.0	0.70
31	YCN-4	1879		265						5.3	2.04	3.76		9.4		10.0	0.76
31	YCN-6	1838		253						5.8	2.40	3.75		9.8		11.0	0.95
31	YCN-7	1789		262						5.9	2.44	3.81		9.9		8.1	0.93
31	YCN-8	2155		243						5.6	2.47	3.64		10.1		9.9	0.88
31	KP24-1			388						5.7	2.50	4.10		15.1			1.10
31	KP25-3			408						5.6	2.50	4.40		15.2			1.00
31	KP28-1			214						4.7	2.80	2.90		9.8			1.10
32	11UMT14	82		69				5.29		5.4	2.94	1.88		5.9		4.0	1.11
32	11UMT15	211		33				1.95		5.2	2.90	1.59		4.9		3.1	1.08
32	11UMT17-a	3033		244				4.21		5.9	2.37	3.86		9.8		5.3	1.02
32	12HG04	59		33			4.6	99.25	3.1	1.7	0.69	0.08	31.7	2.0		2.1	0.28
32	12HG06	195		56			3.9	55.40	5.1	1.8	0.47	0.30	26.8	3.3		3.2	0.23
32	12HXV01	3192		325			304.7	4.29	36.3	5.9	2.08	4.51	17.2	11.4		5.9	0.94
32	12HXV08	489		99			9.0	46.17	2.3	2.4	0.88	0.96	25.3	3.9		4.2	0.37
32	12HXV09	1944		321			17.1	1.18	12.2	6.2	2.40	3.48	20.6	9.8		12.0	1.02
32	12HXV12	1977		286			23.3	3.13	11.3	5.2	1.93	3.26	21.4	8.8		10.6	0.85
32	12HXV15	1728		301			22.3	3.61	14.8	5.4	2.03	2.95	23.1	9.0		10.3	0.89
32	12HXV19	1326		296			23.4	50.25	28.0	5.0	1.83	3.10	22.1	8.5		10.7	0.80
32	12HXV21A	1755		288			18.6	21.65	14.0	5.1	1.94	3.06	22.6	8.6		10.4	0.86
32	12HXV23	1653		311			25.7	8.20	17.5	4.9	1.91	2.86	22.6	8.2		10.0	0.82
32	12HXV24	446		113			8.2	44.39	0.9	2.6	1.04	0.88	24.7	4.0		4.2	0.43
32	12HXV32	501		104			9.3	37.16	4.0	2.5	0.91	0.95	25.7	4.0		4.2	0.38
32	12HXV33	3079		311			806.0	8.00		7.2	2.51	5.24		13.9		6.2	1.13
32	13DV05	1640		284		12	50.0	4.78	23.0	6.0	2.21	3.26	23.7	9.4		12.3	0.99
32	13DV04	1765		290		11	50.0	3.69	24.0	6.0	2.35	3.30	24.0	10.0		12.4	0.95

Ref.#	Sample	Ba	Be	Ce	Cl	Co	Cr	Cs	Cu	Dy	Er	Eu	Ga	Gd	Ge	Hf	Ho
32	13DV11	1645		295		14	50.0	5.75	21.0	6.2	2.48	3.33	23.7	10.1		12.5	1.02
32	13DV13	1565		281		15	60.0	4.80	50.0	5.5	2.23	3.24	23.9	9.1		11.6	1.00
32	13DV14	1430		252		14	50.0	3.85	17.0	5.2	2.27	2.71	22.3	8.3		10.6	0.89
32	13DV15	1555		282		13	50.0	4.88	45.0	5.8	2.53	3.03	23.9	9.4		11.4	1.00
32	13DV23	1480		186		19	80.0	5.48	27.0	5.1	2.31	2.71	22.8	7.7		9.4	0.88
32	13DV29	1220		179		19	90.0	4.22	27.0	5.1	2.31	2.58	21.6	7.3		8.6	0.89
32	13LG07	1805		282		4	30.0	4.73	15.0	3.9	1.67	2.45	22.8	7.2		12.8	0.66
32	13XV01	1405		269		11	50.0	4.52	8.0	5.1	2.08	2.74	25.2	8.7		11.0	0.83
32	13XV02	1625		291		13	30.0	4.12	12.0	5.6	2.38	3.19	24.9	9.3		12.4	0.98

Table B.4 – Trace element compositions of compiled lavas in the Tibetan Plateau, part 2. Data typically obtained via ICPMS.

Ref.#	Sample	La	Li	Lu	Nb	Nd	Ni	Os	P	Pb	Pr	Re	Rb	Sc	Sm	Sn	Sr
1	K89G185	176.7		0.20	31.2	142.0	72			28.9			122	10	20.2		2011
1	K89G186	183.0		0.19		141.0	64			30.4	37.4		177.8	13	20	0	1756
1	K89G189													10			1740
1	K89G190													10			1356
1	KB9G191	137.0		0.20		96.3	70			26.9	27.3		119.5	13	13	0	1410
1	K89G192	156.0		0.25		105.0	59			34.7	29.12		187.6	12	15	0	1397
1	K189G193	150.9		0.20	35.7	106.0	58			27.0			193	8.3	13.6		1368
1	K89G197	78.9		0.20		15.3	0			19.2	6.83		1139	3	1.69	8.7	64
1	K89G200	160.9		0.20	26	119.0	61			35.2			198	9.1	16.1		1567
2	05S2-4	73.6		0.24	34.3	148.0			2574.8	68.4	32.3		517	15	31.5		689
2	05S2-6	49.6		0.23	35.2	127.0			3273	61.3	26.2		662	15.4	28		704
2	05S2-9	31.2		0.21	30.6	59.2			480.04	85.1	12.4		488	17	15		851
2	05SLP5-1	75.8		0.24	28.7	128.0			2487.5	50.0	29		515	15.4	24.7		1031
2	05SLP5-2	69.9		0.20	30.5	118.0			1876.5	53.8	27.1		698	12.4	23.2		942
2	05SLP5-4	63.7		0.18	32.9	87.8			1571	50.2	21.2		498	15.6	16.5		969
2	CM10-04-04	114.0		0.20	53.2	138.0			1309.2	67.8	34.8		754	17.3	20.1		839
2	CM10-04-09	139.0		0.25	57.2	139.0			1178.3	123.0	38.6		855	20.7	20.5		1182
2	CM10-04-12	49.7		0.20	52.7	82.1			349.12	77.9	19.6		504	22.2	14.6		1000
2	04DYH-01	60.5		0.21	14.4	46.8			1221.9	15.5	12.9		88.26	16	7.13		1616
2	D3141	286.0		0.42	34.9	225.0			5018.6	94.1	64.5		141	28.3	34.2		2443
3	04LQS-2	56.1		0.14	7.56	36.6			261.84	36.6	10.27		84.24	10.93	5.39		2276
3	04LQS-3	47.7		0.14	8.31	26.4			261.84	40.4	7.59		95.07	10.28	3.93		2113
3	04LQS-6	73.1		0.24	11.87	51.2			2051.1	28.0	14.46		55.96	12.9	7.34		2118
3	04LQS-14	52.2		0.13	4.9	34.7			654.6	30.0	10.12		98.82	5.51	5.07		816
3	04LQS-16	18.2		0.17	5.53	13.0			130.92	25.5	3.43		72.56	10.53	2.45		1248
3	04YJL-05	45.0		0.19	9.61	28.7			174.56	62.6	7.98		84.64	16.65	4.66		1876
3	04YJL-07	69.8		0.15	14.52	43.6			349.12	40.2	12.89		157	8.51	6.13		1552
3	04YJL-06	60.2		0.13	13.62	38.4			392.76	37.8	11.18		158	6.92	5.22		1747

Ref.#	Sample	La	Li	Lu	Nb	Nd	Ni	Os	P	Pb	Pr	Re	Rb	Sc	Sm	Sn	Sr
3	04YJL-09	61.9		0.19	12.73	41.4			392.76	38.3	12.25		181	8.34	5.93		1095
3	04DN30-2	61.8		0.20	14.76	47.3			1091	17.5	13		86.55	17.77	7.11		1669
3	04DN30-3	52.4		0.15	9.81	31.1			349.12	32.5	9.37		118	10.59	4.4		1135
3	04DN31-1	43.9		0.12	10.6	24.3			218.2	26.0	7.25		100	9.4	3.46		1073
3	04DN32-1	25.1		0.13	7.78	17.2			174.56	7.0	4.75		98.51	10.17	3.01		959
3	04DN32-2	27.3		0.13	7.47	19.2			174.56	5.2	5.16		103	10.07	3.15		1030
3	04DN35-2	26.7		0.10	9.33	17.8			610.96	23.4	5.02		107	10.57	2.78		892
3	04DN36-3	43.2		0.16	9.17	30.2			916.44	31.5	8.38		113	11.26	4.82		917
3	04DN37-2	18.1		0.13	9.11	15.1			261.84	33.1	3.83		86.32	16.81	2.8		1281
3	04DN39	33.7		0.14	7.07	20.8			610.96	19.5	6.1		127	9.13	3.18		851
3	04DN40	50.1		0.14	8.48	35.1			218.2	35.4	10.37		117	7.02	5.13		1220
3	04DY44-2	41.6		0.17	9.53	31.8			829.16	40.8	8.94		109	13.82	4.84		1152
3	04DY44-4	50.6		0.14	7.57	33.2			567.32	30.3	9.7		127	8.54	4.77		1519
3	04DY44-7	49.2		0.13	8.9	28.3			87.28	13.7	8.3		105	10.84	4.18		1907
3	04D6441	49.4		0.18	14	27.7			130.92	24.0	8.34		154	13.62	4.12		1770
3	04D6437	66.5		0.17	16.29	39.3			349.12	40.5	11.24		108	14.67	5.82		2827
4	2T394	65.0		0.30	66	46.0			1789.2	6.9	12.4		8.8		7.9		1138
4	2T395	64.0		0.40	61	46.0			2269.3	7.2	12.2		8.6		8.1		1122
4	2T396	33.0		0.40	15	31.0			3491.2	8.6	8.2		10	29.9	6.3		741
4	98T03	37.0		0.50	18	34.0			2836.6	8.4	9		11	33	7.1		950
4	98T04	66.0		0.40	65	48.0			3709.4	7.5	12.9		9		8.1		1162
4	98T07	536.0		0.90	154	270.0			741.88	207.0	90		138	9.4	36.5		8102
4	98T15	359.0		0.60	59	211.0			1789.2	134.0	66.7		97	8	30.1		8843
4	98T16	683.0		0.90	101	303.0			130.92	316.0	112.6		137	5.4	39.5		12239
4	98T33	491.0		0.70	89	253.0			392.76	144.0	79.3		146	3.7	35.2		8614
4	98T38	755.0		1.10	116	341.0			218.2	339.0	126.8		137	5.7	44.1		6849
4	98T43	649.0		0.90	104	310.0			567.32	282.0	115.8		114	6.8	40.9		7309
4	98T44	760.0		1.00	92	310.0			1003.7	201.0	99.8		181	7.6	53.2		15881
4	98T46	639.0		0.90	97	268.0			43.64	276.0	107.2		122	3.3	33.7		11258
4	98T49	403.0		0.50	73	189.0			87.28	117.0	63.3		236	5.3	24		7998

Ref.#	Sample	La	Li	Lu	Nb	Nd	Ni	Os	P	Pb	Pr	Re	Rb	Sc	Sm	Sn	Sr
4	98T51	553.0		0.80	81	247.0			1265.6	249.0	89.7		161	4.7	30.8		5409
4	98T52	387.0		0.50	42	229.0			4451.3	81.0	70.1		317	9.1	31.4		11985
4	98T53	322.0		0.50	63	169.0			741.88	95.0	54.6		132	4.4	22.7		5150
4	98T54	237.0		0.20	18	158.0			4058.5	12.0	48		401	4	21		5619
4	98T57	538.0		0.70	69	257.0			480.04	167.0	75		101	4.5	34		15352
4	98T69	400.0		0.50	53	209.0			523.68	113.0	68		146	6	28		8933
4	98T70	356.0		0.50	62	184.0			523.68	95.0	59		605	5.8	25		9166
4	98T71	574.0		0.80	97	253.0			1571	173.0	96		133	5.4	34		5889
4	98T73	590.0		0.80	85	259.0			87.28	235.0	100		230	7.3	33		7592
4	99T132	232.0		0.20	73	203.0			5847.8	167.0	56		372		29		1377
4	99T134	288.0		0.20	50	253.0			1614.7	116.0	69		455		31		1077
4	99T145	292.0		0.30	106	246.0			1876.5	201.0	68		353		38		1760
4	99T152	254.0		0.20	43	207.0			2574.8	87.0	57		432		26		1028
4	99T154	247.0		0.20	53	213.0			3360.3	92.0	58		416		29		1907
4	99T53	142.0		0.30	25	156.0			2487.5	93.0	39		676		31		1490
4	99T56	97.0		0.10	23	77.0			2051.1	62.0	20		479		11		552
4	99T57	111.0		0.20	28	95.0			2443.8	54.0	25		506		17		745
4	99T60	110.0		0.20	29	118.0			2007.4	55.0	30		586		22		843
4	99T62	116.0		0.20	24	131.0			2923.9	113.0	32		619		25		1556
5	2002T1021	54.6		0.23	32.81	47.4			2574.8	11.3	12.59		14.92	18.6	9.06		1038
5	2002T1022	50.1		0.23	36.05	41.3			2662	9.7	11.47		25.49	18.46	7.54		1012
5	2002T1023	75.7		0.18	27.11	65.2			2312.9	23.9	17.4		53.13	13.95	9.86		1640
5	2002T1024	62.1		0.19	26.54	44.4			2574.8	24.9	12.68		85.68	11.98	7.05		834
5	2002T1025	67.4		0.14	25.54	46.6			2400.2	27.1	13.46		110.1	8.36	7.33		758
5	2002T1026	62.6		0.15	22.44	39.2			2531.1	30.8	11.8		134.8	7.57	6.51		555
5	2003T373	59.6		0.13	21.37	39.2			3491.2	30.0	11.3		141.8	7.8	6.1		564
5	2003T374	66.8		0.15	22.85	43.3			3316.6	27.3	12.86		108.1	9.02	7.13		594
5	2003T375	59.1		0.09	20.35	38.5			3796.7	32.8	11.32		174.9	5.78	6.49		435
5	2003T380	55.9		0.16	25.02	40.4			2574.8	26.0	11.46		120.1	12.69	6.71		640
5	2003T483	82.6		0.25	28.97	54.0			2269.3	28.3	16.38		123.1	12.2	8.52		838

Ref.#	Sample	La	Li	Lu	Nb	Nd	Ni	Os	P	Pb	Pr	Re	Rb	Sc	Sm	Sn	Sr
5	2003T485	86.5		0.23	29.42	63.6			1614.7	24.8	18.05		124.9	11.65	10.2		901
5	2003T486	86.8		0.23	29.47	63.4			1614.7	25.3	18.01		120.2	11.84	10.3		888
5	2003T487	86.6		0.25	29.34	63.3			1832.9	25.3	17.91		121.7	11.88	10.3		889
5	2003T488	86.4		0.24	29.65	63.0			1396.5	25.6	17.93		125.6	12.09	10.1		906
5	2003T492	87.2		0.26	29.88	64.0			1745.6	25.4	18.01		112.6	11.51	10.4		894
6	Tl/10	200.0		0.23	47.3	218.7	237			127.5	57.2		790	17.3	31.2		1421
6	Tl/11	200.0		0.23	48.8	217.1	227			128.5	57		550	16.9	31		1564
6	Tl/18	138.0		0.24	34	196.1	132			85.2	46.8		576	15	32		1196
6	Tl/13	165.0		0.27	34.9	168.6	175			107.7	44.8		391	17.6	24.6		1633
6	Tl/03	154.0		0.24	46.4	182.8	188			101.5	46.6		611	20.3	28.2		1260
6	Tl/08	133.0		0.24	34.5	189.6	125			89.4	45.8		598	14.8	30.8		1207
6	Tl/17	156.0		0.26	54.2	241.3	339			101.2	56.5		939	19.5	42.7		1004
6	Tl/06	241.0		0.19	63	185.6	56			132.8	54.5		441	8.7	22.9		1371
6	Tl/59	204.0		0.15	56.5	165.4	51			109.5	47.2		442	7.7	21.8		930
6	CHZ-1	139.0		0.33	73.2	244.0	186			166.0	54.7		880	18.8	46.4		810
6	CHZ-2	138.0		0.32	68.5	247.0	176			116.0	54.8		702	18.3	45.7		798
6	CHZ-3	139.0		0.31	66.3	231.0	158			81.2	52		784	18.5	42.9		704
6	CHZ-4	123.0		0.30	54.9	199.0	172			82.4	45.1		712	18.6	36.8		660
6	CHZ-5	133.0		0.34	57.9	215.0	202			105.0	48.2		781	20.1	40.6		739
6	CHZ-6	143.0		0.33	70.7	221.0	151			158.0	50.3		785	17.4	40.4		688
6	CHZ-7	140.0		0.33	65.8	236.0	179			150.0	53.5		871	19.3	45		844
6	CHZ-8	141.0		0.32	73.8	234.0	174			166.0	52.1		564	18.2	43.7		1072
6	CHZ-9	135.0		0.32	70.9	247.0	188			110.0	56.3		538	19.5	47.5		911
6	CHZ-10	139.0		0.32	75	243.0	188			144.0	54.2		529	19.1	45.7		861
6	CHZ-11	138.0		0.30	50.4	237.0	194			125.0	53.1		811	19.5	45.1		855
6	CHZ-12	140.0		0.35	80.6	254.0	193			147.0	56.3		795	20.1	48		790
7	AH-7	187.0		0.40	45.8	118.0			15187	36.2	38.9		149	10.4	20.4		994
7	G26	376.0		0.56	72.1	194.0			15492	116.5	71.5		213	9.42	28.7		8561
7	G68	348.0		0.64	75.9	166.0			13136	188.9	57.2		357	6.49	27.3		6369
7	G98-0	197.0		0.39	56.6	117.0			9339	38.9	38.6		166	15.3	22.9		3988

Ref.#	Sample	La	Li	Lu	Nb	Nd	Ni	Os	P	Pb	Pr	Re	Rb	Sc	Sm	Sn	Sr
7	G98-1	405.0		0.57	68.2	208.0			12612	68.6	65.3		119	23.3	34.7		2433
7	G98-14	366.0		0.56	78.6	172.0			16234	67.1	60.7		213	20.6	28.1		2047
7	G98-3	423.0		0.52	51.7	201.0			12874	76.3	72.5		138	25.6	38.1		2326
7	G98-6	401.0		0.67	70.9	215.0			10168	72.6	67.2		209	23.5	36.1		2664
7	G98-9	236.0		0.61	80.5	162.0			9906.3	68.2	51.7		246	21.6	28.1		2611
7	HH72	125.0		0.31	34.5	92.8			15798	36.9	26.5		121	27.8	14.7		1394
7	HS07	134.0		0.27	40.9	74.7			16452	37.2	23.5		111	14.2	13.6		866
7	HS-69	48.3		0.26	18.7	28.9			13921	35.5	8.11		79.4	24.7	5.16		684
7	JC9719	229.0		0.47	47.9	109.0			10517	64.9	33.8		304	22.6	18.7		1668
7	JC973	219.0		0.59	46.5	119.0			8946.2	58.5	37.2		279	18.2	21.4		1706
7	JC975	129.0		0.44	24.3	75.3			9469.9	53.6	22.9		359	22.1	15.1		1289
7	JC978	38.9		0.38	16.54	36.7			8946.2	50.7	9.61		388	20.5	8.51		946
7	JH6	154.0		0.30	43.8	73.4			16540	28.3	22.9		138	22.9	16.4		1698
7	KX84	136.0		0.27	41.7	104.0			14663	20.5	28.1		131	25.1	20.2		1681
7	PL-58	203.0		0.47	38.8	125.0			11346	35.3	37.5		102	11.3	22.7		1012
7	PL-7	124.0		0.51	37.4	92.5			15972	28.6	25.7		101	22.9	14.6		1068
7	QQ08	151.0		0.28	45.6	111.0			15405	31.1	33.4		158	7.64	13.8		1176
7	QS22	162.0		0.33	92.1	82.5			9382.6	51.6	25.2		126	24.4	19.6		1788
7	XT16	128.0		0.44	29.4	70.9			13790	39.3	21.7		138	18.3	13.5		1106
7	XT8	193.0		0.23	25.7	113.0			13747	26.9	36.4		96.8	22.1	22.3		1239
7	XY03	156.0		0.32	36.8	95.0			14358	74.6	27.2		174	22.8	15.3		1709
7	XY05	145.0		0.26	36.5	81.7			13136	23.5	27.3		238	7.14	15.1		887
7	YS02	216.0		0.21	44.6	100.0			16409	32.2	34.8		86.5	21.9	19		1138
7	YS72	166.0		0.18	28.9	103.0			15536	36.5	32.2		136	11.5	16.9		1507
7	ZF91	60.8		0.24	34.2	41.7			14838	35.7	12.6		100	11.1	7.94		694
7	ZF96	161.0		0.31	21.9	102.0			14488	42.0	35.3		119	15.5	17.7		2789
8	ZF09	32.6		0.13	7.76	26.9	19			35.2	6.84		135	5.95	5.47		819
8	GUO62	22.8		0.12	6.67	17.2	31			33.4	6.04		167	5.1	4.09		490
8	GUO51	27.1		0.11	7.83	18.4	17			29.1	5.83		188	4.88	3.55		689
8	GUO48	23.9		0.10	6.51	25.4	32			27.7	6.67		88.3	5.27	5.02		1024

Ref.#	Sample	La	Li	Lu	Nb	Nd	Ni	Os	P	Pb	Pr	Re	Rb	Sc	Sm	Sn	Sr
8	GUO37	18.1		0.09	4.85	19.2	39			19.2	5.01		92.8	6.75	3.77		1133
8	G09	18.3		0.09	15.2	20.7	33			28.9	5.82		252	5.05	3.21		785
8	ZFG17	18.2		0.11	5.34	19.3	20			40.9	4.71		188	4.82	3.64		889
8	G006	8.6		0.05	5.33	6.2	30			29.2	1.68		158	8.44	1.24		317
8	G019	28.1		0.06	8.05	20.8	24			68.6	5.74		369	3.95	3		448
8	G016	30.9		0.06	7.34	23.4	20			103.0	6.7		401	3.04	3.15		422
8	G025	36.0		0.08	4.98	26.5	28			31.5	7.62		84.2	6.46	4.14		1003
9	DY-7	312.6		0.26	89.6	341.2	182			176.8	72.9		471.3	18.57	40.8		1626
9	DC2	348.1		0.23	61.4	298.2	165			192.4	78.6		502.3	17.21	39.7		985
9	D509	253.4		0.17	75.3	222.5	247			259.3	59.6		326.4	21.6	28.1		821
9	DG43	429.7		0.21	132.6	397.1	225			108.5	108.2		478.7	17.39	56.8		2243
9	YE51	251.8		0.23	84.7	211.5	239			128.7	58.9		347.5	14.28	28.7		1039
9	YC08	191.4		0.20	50.1	175.3	163			179.2	52.8		462.8	13.21	26.7		1694
9	YG13	332.8		0.25	76.3	213.0	197			218.6	65.6		523.7	15.85	27.5		1825
9	YF12	312.7		0.27	64.1	203.1	175			236.5	57.8		387.2	14.27	26.4		886
9	YA32	180.3		0.19	41.3	152.1	181			78.3	43.6		326.1	12.46	23.8		1168
9	MH78	183.5		0.25	51.9	177.9	341			87.1	50.4		419.5	18.43	25.7		1327
9	MH69	235.7		0.20	65.2	191.2	373			124.4	57.6		883.1	22.59	31.9		986
9	MG-3	158.3		0.26	51.3	172.8	190			66.1	45.7		610.8	16.9	26.3		863
9	MY1	212.5		0.28	41.3	224.1	232			90.2	55.2		734	17.62	33.4		1082
9	MK09	141.7		0.24	30.9	147.2	315			156.1	39.8		522.3	17.11	26.9		1328
9	MR21	101.6		0.16	34.2	104.2	226			71.8	27.4		381.4	15.2	16.1		1037
9	MA75	224.9		0.26	57.8	192.4	386			104.3	51.1		1033	20.14	24.7		997
9	MX5	122.7		0.31	68.2	125.2	278			113.1	34.9		702.2	18.43	20.6		914
9	2003T534	125.0		0.23	33	181.0	263			87.0	43		588	19	31		932
9	2003T536	120.0		0.24	35	190.0	277			89.0	44		1511	19	31		927
9	2003T539	121.0		0.21	33	187.0	288			88.0	44		1924	19	30		923
9	G8	142.4		0.35	33.8	206.5	169			146.4	50.7		725.4	18.47	47.2		637
9	C10	131.6		0.37	27.7	182.5	185			98.6	46.3		938.3	16.39	42.4		879
9	CV5	118.2		0.34	46.5	201.9	144			157.6	45.7		826.9	17.11	38.3		758

Ref.#	Sample	La	Li	Lu	Nb	Nd	Ni	Os	P	Pb	Pr	Re	Rb	Sc	Sm	Sn	Sr
9	C76	140.7		0.39	55.4	184.5	176			125.1	45.9		1046	18.52	44.3		613
9	CH4	151.5		0.26	52.5	268.9	199			182.1	57.4		1359	19.37	51.2		1038
9	CH7	148.5		0.32	36.8	275.0	418			82.3	61.2		894.2	17.92	59.3		847
9	C03	150.3		0.31	61.6	236.9	386			157.6	54.7		1205	18.94	48.7		799
9	CX38	114.6		0.25	21.7	186.5	302			87.8	42.1		536.5	17.09	36.3		846
9	C25	102.7		0.27	26.5	139.3	187			71.7	34.1		498.4	18.63	29.5		676
10	CT09	130.1		0.24	37.3	108.5	104			39.2	31.2			15.2	14.9		1720
10	CT12	141.7		0.25	41.2	82.8	168			26.3	30.1			22.4	15.2		1817
10	CT17	68.8		0.26	25.8	60.5	173			31.7	18.4			24.7	11.3		1125
10	CT05	105.5		0.26	33.6	71.9	137			28.4	22.3			18.4	12.8		1328
10	CT23	128.6		0.23	30.9	90.1	159			37.6	26.8			21.9	13.7		1543
10	QS12	132.1		0.27	41	116.9	102			18.6	33.4			13.4	18.3		1428
10	QS27	113.7		0.25	35.7	101.7	143			24.0	29.8			25.6	19.5		1731
10	QS19	104.3		0.31	33.9	78.3	162			23.8	23.7			23.8	18.6		1647
10	QS23	101.4		0.28	30.8	77.2	136			31.2	26.9			22.1	14.3		1718
10	QS18	92.5		0.28	29.4	79.4	153			27.3	23.8			18.9	15.6		1752
10	QS24	71.8		0.26	37.4	69.3	148			25.4	20.6			22.7	10.9		1678
10	KY03	103.8		0.26	54.7	90.1	133			23.8	28.7			16.2	18.3		1820
10	KY02	92.9		0.28	45.1	79.3	146			26.5	23.4			18.9	18.7		2167
10	KY06	61.5		0.24	48.7	57.1	219			31.8	15.6			27.5	10.9		2280
10	KY01	115.2		0.23	46.9	101.4	172			18.9	31.9			17.8	21.7		1483
10	HS041	102.3		0.27	46.9	51.6	87			21.0	18.4			31	10.3		1247
10	HS046	96.7		0.23	34.1	58.2	122			38.6	19.3			16.6	11.8		849
10	HS047	118.4		0.22	42.9	69.3	184			30.9	25.8			19.5	13.2		752
10	HS028	76.5		0.23	20.3	46.7	341			27.5	13.5			26.7	9.63		760
10	AH607	137.7		0.33	55.9	126.1	115			37.4	37.2			24.2	18.9		1376
10	AH605	97.3		0.38	48.3	60.8	110			41.9	19.5			23.7	13.6		1528
10	AH609	95.8		0.31	52.4	86.9	94			26.8	24.1			17.9	14.6		1406
10	AH602	116.2		0.26	46.1	86.5	98			34.1	22.4			27.6	14.9		1390
10	AH618	105.9		0.24	49.6	73.8	105			31.7	21.3			24.4	12.3		1471

Ref.#	Sample	La	Li	Lu	Nb	Nd	Ni	Os	P	Pb	Pr	Re	Rb	Sc	Sm	Sn	Sr
10	AH615	103.6		0.35	53.2	92.3	114			41.0	23.7			28.3	15.1		1428
10	YS74	211.4		0.24	31.8	162.7	102			44.9	45.6			21.3	27.8		1381
10	YS78	198.5		0.25	29.4	131.3	95			43.6	40.1			23.7	24.7		1565
10	YS05	172.7		0.27	37.9	120.3	132			51.8	32.8			25.8	23.5		1872
10	YS79	232.9		0.23	30.6	171.3	89			36.3	50.2			15.2	31.4		1329
10	YS07	135.8		0.21	28.5	86.3	92			37.5	28.2			14.9	15.1		1417
10	KX44	117.8		0.33	37.2	122.5	184			27.7	30.7			23.5	28.1		1921
10	KX51	132.3		0.28	27.9	95.4	148			23.4	29			30.7	19.6		1729
10	KX80	131.8		0.31	28.4	114.7	153			27.9	31.5			28.1	21.8		1803
10	KX49	115.3		0.24	40.6	125.3	174			30.6	31.4			23.6	29.3		1846
10	KX62	136.2		0.30	33.9	121.6	168			35.1	34.9			29.3	23.8		1783
10	PL53	158.3		0.24	38.4	116.8	313			42.6	34.6			24.3	19.2		1028
10	PL61	172.8		0.21	36.3	109.5	295			47.4	35.7			25.7	20.2		1134
10	PL3	124.7		0.27	41	81.4	98			54.8	24.1			17.8	14.6		964
10	PL18	160.7		0.25	54.9	112.3	219			49.5	31.8			18.2	18.2		1273
10	PL92	176.2		0.23	51.5	116.9	183			50.3	36.8			20.5	21.8		1120
10	PL43	113.4		0.26	39.5	78.7	136			51.2	22.9			21.3	13.2		982
12	07-SA-21	40.4		0.15	4.979	39.3	127			36.0	9.98		49		6.62		968
12	07-SA-26A	27.4		0.04	6.356	26.8	24			18.0	6.863		3		4.32		453
12	07-SA-26B	26.4		0.06	5.866	26.3	14			9.0	6.56		0		4.28		1048
12	07-SG-03	60.0		0.11	12.59	45.7	12			6.0	12.56		151		6.86		1498
12	07-SG-04A	63.2		0.13	13.83	49.0	9			52.0	13.33		138		7.44		295
12	07-SG-05	69.2		0.16	12.51	53.1	17			26.0	14.46		132		8.24		1061
12	07-SG-06	63.1		0.12	13.06	48.8	9			38.0	13.2		159		7.59		467
12	07-SG-29	59.8		0.14	9.854	48.9	14			40.0	13.14		176		7.65		1177
12	07-SG-30	62.8		0.11	9.57	51.3	18			24.0	13.89		181		8		935
12	07-SG-31A	56.2		0.16	9.91	46.6	12			39.0	12.43		201		7.72		690
12	07-SG-31B	59.8		0.18	10.07	49.8	11			36.0	13.22		186		8.05		627
12	07-SG-48A	52.4		0.08	10.27	44.1	36			28.0	11.86		135		6.5		1034
12	07-SG-48B	53.4		0.09	4.952	45.7	13			42.0	12.08		138		6.97		954

Ref.#	Sample	La	Li	Lu	Nb	Nd	Ni	Os	P	Pb	Pr	Re	Rb	Sc	Sm	Sn	Sr
12	07-SG-52A	58.8		0.20	10.43	52.9	103			49.0	13.92		135		8.86		838
12	07-SG-66	25.7		0.06	5.122	23.2	10			75.0	5.966		159		4.08		884
12	06-SA-28C	23.7		0.13	8.27	26.0	97			46.0	6.27		48		4.63		262
12	06-SA-48A	21.7		0.06	7.52	22.3	68			14.0	5.46		0		3.77		941
12	06-SG-200	72.5		0.14	15.7	53.1	54			27.0	15.01		183		8.66		969
12	06-SG-201	69.8		0.16	13.22	52.4	29			16.0	14.39		136		8.41		973
13	NQ2-1*	188.0		0.31	30	171.0			4582.2		46		120		27		4357
13	NQ21-4*	139.0		0.28	25	93.0			1614.7		28		184		13		2513
13	NQ7-1*	52.0		0.20	9.7	46.0			785.52		12		165		7.2		1205
13	Y1-11	78.0		0.16	8.5	49.0			916.44	23.0	14		173		7.4		1024
13	Y1-12	74.0		0.17	9.6	53.0			960.08	20.0	15		183		8.1		956
13	Y1-13	66.0		0.16	9.2	47.0			872.8	26.0	13		185		7.2		937
13	Y1-14	57.0		0.17	9.6	44.0			872.8	26.0	12		183		7.3		1006
13	Y1-15	65.0		0.17	10	49.0			872.8	33.0	14		188		8		988
13	Y115-90								130.92								
13	Y1-16	31.0		0.09	9.7	24.0			523.68	19.0	6.8		190		3.2		924
13	Y1-18	48.0		0.12	9.1	36.0			1091	24.0	10		245		5.6		612
13	Y1-8	70.0		0.19	10	54.0			1003.7	25.0	15		170		8.7		993
13	Y1-9	75.0		0.19	9.4	50.0			916.44	27.0	15		181		7.7		999
13	Y2-1	53.0		0.16	9	39.0			829.16	30.0	10		190		6.2		742
13	Y2-2	49.0		0.16	9.8	40.0			960.08	30.0	11		239		6.6		737
13	Y2-3	43.0		0.16	8.2	32.0			698.24	28.0	8.6		187		5.4		852
13	Y2-4	44.0		0.15	8.6	34.0			741.88	29.0	9.1		197		5.5		763
13	Y2-5	45.0		0.16	7.9	37.0			741.88	24.0	10		212		5.7		772
13	Y2-6	54.0		0.15	8.9	41.0			872.8	62.0	11		196		6.1		799
13	Y2-7	43.0		0.15	8.5	35.0			741.88	24.0	9.4		198		5.5		868
13	Y2-8	50.0		0.14	8.1	36.0			698.24	45.0	10		229		5.9		648
13	Y2-9	42.0		0.15	8.2	33.0			741.88	30.0	8.7		208		4.7		840
13	Z96-2*	93.0		0.26	16	85.0			1745.6		24		168		13		1332
14	KK06003	147.0		0.24	37.6	101.0			3622.1	33.3	31.4		137	9.94	14.3		1118

Ref.#	Sample	La	Li	Lu	Nb	Nd	Ni	Os	P	Pb	Pr	Re	Rb	Sc	Sm	Sn	Sr
14	KK06004	138.0		0.21	36.4	94.3			3709.4	37.8	28.7		144	10.1	13.7		1126
14	KK06005	139.0		0.21	35.6	93.4			3753	24.9	29		133	9.89	14		1076
14	KK06006	137.0		0.23	37.4	97.0			3665.8	30.4	29.4		129	9.36	14.6		1072
14	KK06007	138.0		0.24	36.7	96.8			3360.3	26.7	29.8		155	9.32	13.9		1052
14	KK06008	153.0		0.24	38.2	105.0			3709.4	36.6	31.7		139	9.28	15.5		1165
14	KK06009	151.0		0.24	38.6	108.0			3753	34.7	32.2		143	10.4	15.9		1212
14	KK06010	138.0		0.25	39.4	103.0			3753	33.5	30.7		144	10.2	15.5		1180
14	KK06011	147.0		0.25	39.4	108.0			3796.7	33.4	32.4		148	10.3	15.9		1152
14	KK06012	145.0		0.23	38.7	98.2			3753	27.9	29.8		147	10.9	15.2		1206
14	KK06013	133.0		0.20	29.5	80.8			2225.6	28.4	25		180	9.34	11.3		1000
14	KK06014	138.0		0.20	29.8	84.6			2225.6	23.7	26.6		176	9.76	11.7		972
14	KK06016	131.0		0.18	29	72.4			2182	29.8	23.8		171	9.5	10.5		915
14	KK06018	133.0		0.18	29.8	80.5			2269.3	34.5	25.9		166	9.23	11.1		939
14	KK06019	138.0		0.21	28.6	77.1			2182	43.8	25.7		176	10.6	10.7		964
14	KK06022	134.0		0.21	28.5	79.4			2225.6	45.6	25.3		157	10	10.7		902
14	KK06024	138.0		0.21	29.6	82.9			2312.9	35.1	26.4		177	9.82	11.1		965
14	KK06025	164.0		0.27	44.2	120.0			4800.4	33.8	35		121	11.9	17.3		1334
14	KK06026	155.0		0.26	44.6	117.0			4800.4	28.9	34.4		124	9.9	16.9		1298
14	KK06027	154.0		0.25	43.6	103.0			4102.2	25.5	31.2		123	11.2	14.6		1092
14	KK06028	164.0		0.26	44.1	111.0			4145.8	41.7	33.3		135	10.8	15.5		1100
14	KK06029	147.0		0.26	44	102.0			4145.8	38.1	31.3		107	9.67	15.4		962
14	KK06030	138.0		0.26	44.1	97.3			4233.1	23.7	29		91	9.18	15.1		927
14	KK06031	154.0		0.25	42.9	107.0			4145.8	22.8	32.3		109	10.4	15.8		983
14	KK06032	48.6		0.11	13.1	43.4			1352.8	35.1	11.9		372	3.72	7.14		109
14	KK06033	50.2		0.10	12.9	44.3			1352.8	35.5	12.1		382	2.7	7.1		120
14	KK06034	49.2		0.11	13.2	44.2			1396.5	36.1	11.9		389	2.55	7.37		112
14	KK06038	144.0		0.25	37.2	98.4			3185.7	40.1	30.5		174	9.74	13.8		995
14	KK06039	153.0		0.25	41.9	104.0			3578.5	38.3	31.9		137	5.41	15.1		1145
14	KK06040	188.0		0.27	47.4	129.0			4102.2	46.2	39.6		146	6.17	18.3		1260
14	KK06041	172.0		0.26	49.4	121.0			4844	35.4	36.1		110	9.59	16.7		1227

Ref.#	Sample	La	Li	Lu	Nb	Nd	Ni	Os	P	Pb	Pr	Re	Rb	Sc	Sm	Sn	Sr
14	KK06042	164.0		0.24	43	114.0			3753	57.6	33.5		167	6.71	15.8		1126
14	KK06043	191.0		0.26	53.1	131.0			5062.2	44.6	39.6		131	8.05	19.6		1408
14	KK06046	161.0		0.23	43.7	111.0			3491.2	26.6	33.5		185	6.41	15.9		1135
14	KK06047	152.0		0.22	41.5	105.0			3534.8	27.9	31.7		174	7.83	14.9		1037
15	Z02H1	75.1		0.18	10.6	52.9			1658.3	28.4	14.3		100	11.8	7.57		1397
15	Z07H	24.7		0.23	6.13	18.6			610.96	36.2	5.05		147	8.15	3.36		632
15	Z07H1	68.8		0.21	9.23	51.6			1527.4	39.4	13.6		126	12.7	7.94		1238
15	Z07H2	68.7		0.20	9.21	51.6			1571	39.1	13.6		125	12.7	7.83		1230
15	Z07H3	50.4		0.21	7.01	35.1			916.44	44.7	9.55		108	13.3	5.51		1068
15	Z07H4	69.4		0.21	9.29	51.4			1571	39.1	13.6		122	13	7.9		1257
15	Z07H5	59.2		0.20	8.35	41.3			1134.6	38.4	11.1		140	12.4	6.27		998
15	Z07H6	58.0		0.19	8.07	40.8			1091	32.2	11		116	13.1	6.29		978
15	Z08H1	68.2		0.21	8.79	48.9			1352.8	37.6	13		115	11.3	7.36		1151
15	Z08H2	58.4		0.15	8.27	39.3			1134.6	34.3	10.7		122	12.7	5.93		1010
15	Z08H3	71.1		0.19	8.93	49.9			1352.8	37.9	13.4		117	11.4	7.54		1192
15	Z08H4	73.7		0.18	9.15	51.6			1396.5	38.7	13.8		121	11.7	7.74		1218
15	Z08H6	70.3		0.19	8.83	49.0			1352.8	37.8	13.1		113	12	7.35		1173
15	Z12H3	45.3		0.20	8.33	34.5			1178.3	30.3	9.03		110	15.9	5.71		914
15	Z15H1	56.9		0.23	7.43	44.8			916.44	39.0	11.5		121	12	7		1317
15	Z15H2	55.6		0.21	7.35	42.4			916.44	36.2	11.1		117	11.7	6.56		1269
15	Z15H3	56.1		0.22	7.5	43.6			872.8	39.4	11.3		118	12.1	6.69		1308
15	Z15H5	34.6		0.14	6.35	23.2			654.6	32.0	6.46		149	7.75	3.76		717
15	Z15H6	33.3		0.15	6.25	22.8			654.6	38.6	6.25		152	8.21	3.9		650
15	Z19H1	41.4		0.17	6.87	30.9			829.16	37.6	8.26		141	9.21	4.94		891
15	Z19H4	30.4		0.14	6.04	21.5			654.6	38.8	5.85		150	7.82	3.61		724
15	Z19H5	30.7		0.14	6.12	21.4			741.88	39.0	5.9		153	7.72	3.57		728
15	Z19H6	30.6		0.14	6.19	21.7			785.52	38.8	5.9		153	7.96	3.68		716
15	Z06H	63.8		0.21	9.52	45.1			1309.2	40.0	12.1		91.7	11.3	6.92		1081
15	Z08H5	76.5		0.18	9.25	54.0			1440.1	39.8	14.3		118	9.38	8.09		1228
15	Z10H	49.3		0.15	9.2	36.2			1265.6	34.2	9.62		126	9.11	5.8		985

Ref.#	Sample	La	Li	Lu	Nb	Nd	Ni	Os	P	Pb	Pr	Re	Rb	Sc	Sm	Sn	Sr
15	Z11H1	49.0		0.16	9.09	35.4			1309.2	31.9	9.47		124	10.5	5.63		963
15	Z11H2	49.2		0.18	8.9	37.1			1309.2	33.4	9.74		116	14.2	6.13		971
15	Z12H1	46.2		0.22	8.31	35.4			1178.3	28.4	9.26		110	16	5.84		927
15	Z12H2	48.5		0.16	8.81	36.1			1265.6	29.8	9.51		117	11	5.76		972
15	Z15H7	24.3		0.13	5.91	17.1			567.32	34.2	4.68		149	5.64	3.1		602
15	Z15H11	146.0		0.20	41.7	103.0			2967.5	36.3	28.2		175	7.35	14.3		681
16	ET021B	7.2		0.22	2.4	9.4			480.04	2.6	2.09		10.3	35.6	2.4		341
16	ET021C	16.8		0.30	5.3	17.0			610.96	11.5	4.19		65.7	16.6	3.78		333
16	ET022A	19.8		0.24	5.8	12.0			261.84	13.6	3.44		75.9	4.6	2.16		195
16	ET024	22.8		0.23	6.9	13.1			218.2	11.7	3.85		92.2	5.6	2.25		225
16	ST052B	73.0		0.43	19.9	49.9			392.76	33.2	14.2		334	7.2	8.57		433
16	ST053	76.1		0.41	18.6	52.8			567.32	35.5	14.9		321	7.9	9.1		641
16	ST054	79.3		0.40	19.3	54.3			480.04	36.2	15.4		335	9.6	9.37		534
16	ST055A	86.1		0.49	23.7	57.9			218.2	39.7	16.7		416	8.9	9.77		160
16	ST055B	78.5		0.45	21.1	53.7			349.12	38.2	15.3		374	9.4	9.27		367
16	ST055C	46.8		0.36	7.8	41.3			1658.3	32.6	10.3		160	20.7	8.22		1066
16	ST057A	58.6		0.36	13.7	46.6			1265.6	32.9	12.4		252	15.3	8.6		805
16	ST058	73.1		0.38	18.8	49.8			698.24	33.7	14.1		325	7.4	8.56		578
16	ST059A	58.0		0.44	16.1	43.7			523.68	4.3	11.9		220	15.5	7.98		130
16	ST060A	85.4		0.46	21.5	56.8			305.48	34.7	16.4		352	8.1	9.71		349
16	ST060C	89.2		0.54	24.6	62.1			305.48	23.6	17.8		426	11.6	10.7		378
16	ST061A	42.8		0.52	15.6	46.7			1178.3	10.7	11.5		392	19.7	10.3		393
16	ST062	106.0		0.52	28.3	68.3			654.6	45.5	20.2		454	9.5	11.4		350
16	ST101B	22.9		0.22	3.9	21.7			1178.3	5.3	5.39		24.9	10.3	4.04		607
16	ST102B	14.1		0.28	3	14.3			654.6	9.7	3.38		50.3	17	3.12		367
16	ST109	31.1		0.17	6.6	21.4			698.24	10.7	5.93		61	4.4	3.51		376
16	ST119A	14.8		0.39	5.2	20.7			1571	21.1	4.68		2.2	26	4.74		520
16	ST119B	37.6		0.66	10.5	46.8			3753	7.5	10.9		18.1	16.3	9.65		326
16	ST121	35.9		0.57	9.4	41.9			3491.2	6.2	9.88		23.6	14.6	8.68		534
16	ST122	24.1		0.38	6.9	25.6			2138.4	4.2	6.24		1.1	19.1	5.24		482

Ref.#	Sample	La	Li	Lu	Nb	Nd	Ni	Os	P	Pb	Pr	Re	Rb	Sc	Sm	Sn	Sr
16	T006B1	20.3		0.26	8.2	19.9			960.08	8.9	4.93		36.1	17.9	4.07		409
16	T006B2	20.8		0.35	12.1	20.9			1134.6	5.9	5.04		41	35.7	4.58		473
16	T034A	7.1		0.25	0.94	11.7			4800.4	4.3	2.52		10.1	24.9	2.93		280
16	T034B	6.9		0.23	1	11.5			436.4	4.7	2.45		4.6	27.4	2.89		254
16	T036D	8.0		0.20	2.2	12.6			1003.7	3.9	2.66		19.7	21.8	3.05		746
16	T038F	38.6		0.41	15.6	31.0			436.4	12.9	8.37		248	11.8	6		65
16	T038G	32.8		0.45	13.3	29.4			960.08	31.1	7.5		137	14.4	6.07		214
16	T038M	19.4		0.38	16.2	15.2			130.92	22.3	4.36		240	9.3	2.89		71
16	T039	25.2		0.37	12.7	20.6			261.84	56.8	5.52		183	10.5	4.18		283
16	T040A	30.3		0.32	10	27.5			960.08	19.8	7.09		110	14.7	5.37		453
16	T040B	34.8		0.35	11.8	31.5			698.24	123.0	8.18		131	14.41	6.05		427
16	T041J	8.4		0.21	2.1	12.0			960.08	4.1	2.58		16.4	17.4	2.89		691
16	T041F	8.5		0.21	1.9	12.1			1003.7	7.5	2.62		21.3	19.4	2.86		703
16	T041H	8.5		0.20	2.1	13.0			1003.7	3.6	2.77		10.8	16.6	3.15		926
16	T042C	27.0		0.56	12.3	32.3			1440.1	7.2	7.56		73	33.8	7.35		327
16	T042D	17.1		0.22	12	18.9			1440.1	3.8	4.37		15.7	46	4.21		445
16	T046A	17.8		0.31	6.3	20.9			1352.8	12.6	4.87		29.6	23.2	4.56		487
16	T047	26.3		0.31	10.1	27.6			1527.4	17.9	6.64		120	23.3	5.79		445
16	T048B	31.8		0.31	8.4	24.6			785.52	17.5	6.59		85.8	16.7	4.61		463
16	T049A	32.2		0.34	11.6	25.4			305.48	8.4	7.04		124	8.6	4.58		73
16	T049B	29.9		0.23	6.7	25.5			1178.3	18.6	6.62		70.3	9.8	4.73		643
16	T049C	32.3		0.25	7	27.5			1221.9	15.1	7.14		85.1	12.3	5.07		780
16	T051B	30.2		0.24	17	27.8			261.84	2.3	7.1		46.9	4.5	5.47		479
16	T051C	32.0		0.35	11.2	19.2			87.28	14.4	5.77		170	4.6	3.31		178
16	T052	39.0		0.34	10.7	28.4			480.04	16.0	7.95		145	7.9	5.13		342
16	T054A	18.1		0.39	5.2	23.8			1571	8.2	5.35		33.6	16.8	5.49		557
16	T055A	19.8		0.33	6.8	21.0			480.04	8.9	5.07		17.5	19.6	4.54		417
16	T055B	17.0		0.44	5.7	22.0			1003.7	13.4	4.99		68.6	23.9	5.08		432
16	T056A	9.9		0.28	3.6	13.6			741.88	9.3	3.03		22.5	25.5	3.16		663
16	T056B	12.2		0.38	4.8	15.7			872.8	7.4	3.58		12	18.4	3.62		266

Ref.#	Sample	La	Li	Lu	Nb	Nd	Ni	Os	P	Pb	Pr	Re	Rb	Sc	Sm	Sn	Sr
16	T062B	30.2		0.44	10.8	32.1			1309.2	34.4	7.78		83.8	16.1	6.57		404
16	T062C	17.7		0.26	5.2	19.7			1003.7	8.8	4.62		20.7	20.4	4.27		661
16	T063	25.6		0.26	8.3	22.8			916.44	10.0	5.79		83.1	19.1	4.66		667
16	T064A	22.2		0.24	6.6	19.6			829.16	15.1	5.05		63.7	16	3.85		502
16	T065A	35.3		0.33	12.9	29.1			436.4	39.3	7.85		131	11.7	5.46		108
16	T065B	36.0		0.45	13.6	30.7			305.48	37.9	8.39		183	6.3	5.55		131
16	T066	31.6		0.42	9.1	31.7			1221.9	20.4	7.86		55.2	26.6	6.4		353
16	T068	31.9		0.42	11.8	24.7			261.84	16.2	6.81		177	8.3	4.68		123
16	T070A	35.4		0.38	9.7	30.4			829.16	15.7	7.99		89.3	6.3	5.51		548
16	T072A	51.6		0.42	14.7	38.8			960.08	18.5	10.7		120	23.8	7		330
16	T072D	36.6		0.35	11.2	29.4			698.24	24.5	7.89		53.1	21	5.66		299
16	T072E	35.7		0.35	11	28.5			698.24	21.7	7.67		50.7	16.8	5.47		371
16	T073	35.2		0.34	11.5	28.1			741.88	26.5	7.59		149	16.2	5.41		233
16	T078B	30.6		0.12	9.9	24.6			741.88	19.0	6.87		25.3	3	3.43		763
16	T079A	11.5		0.25	5.2	17.6			829.16	6.2	3.77		22.1	64.2	4.58		482
16	T079B	19.6		0.34	4.7	22.2			1221.9	7.2	5.09		139	29.1	5.21		620
16	T079C	17.1		0.38	4.7	19.9			1178.3	9.7	4.52		9.7	25.1	4.83		874
16	T080	17.5		0.28	4	19.8			1658.3	6.1	4.52		42.5	28.5	4.54		245
16	T082A	36.4		0.23	7	20.4			218.2	11.4	6.29		106	3.1	3.09		176
16	T082B	35.8		0.24	8.2	20.4			218.2	20.1	6.25		115	5.4	3.17		153
16	T083B	36.8		0.39	9.3	29.7			130.92	32.3	8.19		242	6.3	5.39		112
16	T083C	21.5		0.39	4.9	24.7			1134.6	18.1	5.76		85.9	32.3	5.69		294
16	T084C	27.9		0.47	14	27.5			261.84	4.3	6.83		205	9	6.14		327
16	T102A	42.9		0.44	10	34.1			1178.3	11.3	8.95		361	10.2	6.48		299
16	T103	86.9		0.48	9	55.6			130.92	3.3	15.3		307	4.6	10.1		62
16	T104	42.8		0.45	11.1	31.0			130.92	5.5	8.5		306	8.6	5.98		41
16	T105A	39.5		0.58	10.6	43.0			1440.1	11.9	10.4		150	21.4	8.76		199
16	T110A	55.0		0.40	15	43.1			610.96	35.2	11.7		236	18.2	8.01		107
16	T110B	44.0		0.38	12.2	34.9			523.68	23.1	9.32		169	13	6.6		140
16	T111	28.5		0.21	7.9	19.5			349.12	24.2	5.51		170	6.2	3.49		318

Ref.#	Sample	La	Li	Lu	Nb	Nd	Ni	Os	P	Pb	Pr	Re	Rb	Sc	Sm	Sn	Sr
16	T112	62.9		0.51	15.5	48.9			741.88	28.4	13.1		161	19.6	9.31		251
16	T113	63.5		0.53	14	49.5			610.96	29.4	13.3		191	14.8	9.25		212
16	T116A	15.8		0.41	8.8	22.1			1789.2	5.6	4.86		20.2	33.1	5.36		591
16	T117	29.2		0.29	7.5	24.4			305.48	16.4	6.56		86	7.7	4.69		64
16	T127B	28.6		0.21	6.2	20.3			654.6	11.5	5.54		64.8	10.8	3.75		288
16	T129A	20.0		0.40	5.3	17.5			567.32	6.9	4.35		107	25.7	4.02		276
16	T130	24.2		0.65	18.2	22.1			43.64	13.0	5.79		296	7.2	4.67		49
16	T131A	55.6		0.45	8.5	34.0			305.48	14.8	9.35		15	12.5	6.37		143
16	T134	93.1		0.78	18.7	64.5			261.84	36.7	17.8		206	10.7	11.7		443
16	T136A	175.0		0.83	23	101.0			43.64	40.0	27.1		275	8.8	17.1		47
16	T136B	155.0		1.57	18	142.0			3098.4	78.7	33.1		242	18.1	58.8		53
16	T138D	7.4		0.04	4.5	5.9			305.48	11.4	1.55		140	2.9	1.15		582
16	T139	27.8		0.33	12.3	24.3			43.64	31.4	6.42		251	7.1	5.46		51
16	T140A	37.2		0.47	8.5	25.6			305.48	16.6	7.03		96.4	12.3	4.97		173
16	T140B	42.4		0.36	8.8	34.0			872.8	16.7	8.82		23.2	19.5	6.49		384
16	T140D	34.9		0.43	8.2	24.1			480.04	18.2	6.56		131	15.8	4.67		198
16	T140E	20.9		0.64	12	23.5			43.64	26.5	5.72		232	4.4	6.5		76
16	T142	34.7		0.47	8.7	26.9			436.4	6.8	7.18		104	7.2	5.3		262
16	T143	42.2		0.51	9	30.2			392.76	28.8	8.27		135	13.2	5.89		206
16	T144A	36.8		0.80	10.5	36.3			174.56	1.4	9.02		75.7	13.1	9.03		74
16	T144B	24.6		0.49	7.2	25.3			610.96	6.5	6.26		87.1	31.5	5.8		108
16	T144C	31.9		0.53	10.8	21.5			130.92	123.0	6.24		285	9.6	4.17		65
16	T144D	58.3		0.37	7	30.7			261.84	6.2	9.35		110	10.1	4.9		159
16	T146	24.8		0.54	9.7	23.2			436.4	15.2	5.97		106	11.4	5.05		146
16	T147	40.9		0.66	10.7	32.7			130.92	20.2	8.65		160	14	6.94		109
16	T151	40.5		0.39	12.6	40.4			1963.8	15.2	10		47.3	33.1	7.73		861
16	T152A	51.3		0.45	12.5	45.0			1352.8	15.7	11.5		142	18.1	8.45		571
16	T152B	18.3		0.28	5.4	20.8			1003.7	7.2	4.89		64	31.8	4.49		743
16	T155	61.3		0.40	14.5	43.3			567.32	19.3	12.1		203	9.5	7.86		393
16	T160A	34.6		0.45	11.4	31.6			872.8	21.9	8.06		148	18.8	6.68		363

Ref.#	Sample	La	Li	Lu	Nb	Nd	Ni	Os	P	Pb	Pr	Re	Rb	Sc	Sm	Sn	Sr
16	T160B	45.3		0.77	14.5	51.2			87.28	25.1	12.8		237	5.5	11.7		59
16	T169A	62.8		0.67	15.2	43.7			87.28	34.6	12.1		431	3.5	8.38		34
16	T169B	335.0		0.68	14.6	173.0			87.28	38.6	46.3		407	4.6	28.8		29
16	T169C	35.3		0.30	10.5	30.6			130.92	53.8	8.13		125	9.6	5.7		28
16	T233A	22.2		0.20	4.5	18.0			392.76	9.5	4.75		13.3	11.7	3.21		72
16	T233B	23.3		0.36	6.7	21.9			741.88	14.6	5.46		47.7	13.4	4.53		588
16	T233C	51.9		0.35	11	44.1			1483.8	12.5	11.3		19.1	21.4	9.13		962
16	T234A	50.6		0.30	10.1	41.1			1527.4	12.1	11		64.9	9.6	7.64		442
16	T234B	51.1		0.30	9.8	44.2			1832.9	9.2	11.6		53.4	12.1	8.3		1268
16	T234C	52.2		0.23	9.8	35.2			1134.6	14.9	9.77		46.5	10.9	6.23		120
16	T235A	47.7		0.44	9.9	42.1			43.64	12.1	11		131	5.4	7.9		94
16	T235B	47.4		0.41	9.1	37.8			43.64	10.5	9.92		130	5.6	6.95		103
16	T238B	20.8		0.36	5	21.2			916.44	14.6	5.16		5.2	19.4	4.65		638
16	T239	22.0		0.33	6.6	20.2			829.16	9.9	5.16		31.1	23	4.25		527
16	T240B	23.4		0.37	7	21.7			829.16	12.3	5.51		142	16	4.61		436
17	GGL01	46.2		0.35	16.51	38.4			1134.6	18.8	10.73		94.96	12.48	6.83		370
17	GGL02	54.2		0.48	20.42	46.6			1658.3	19.5	12.63		99.62	14.58	8.28		391
17	GGL03	48.3		0.38	19.65	44.0			1658.3	18.0	12.22		108.2	17.99	7.85		393
17	GGL04	53.1		0.55	19.67	47.8			1702	18.9	12.81		94.16	15.55	8.66		426
17	GGL05	43.1		0.46	16.8	39.5			1702	15.6	10.41		71.7	17.94	7.38		437
17	GGL06	42.0		0.44	16.96	37.8			1702	14.5	10.04		70.88	18	7		421
17	GGL07	43.2		0.43	17.12	38.8			1702	14.9	10.4		74.15	16.95	7.14		416
17	GGL08	39.6		0.42	16.28	36.0			1658.3	14.4	9.624		70.09	18.62	6.74		422
17	GGL09	45.5		0.45	18.26	40.5			1745.6	15.8	10.76		79.12	17.54	7.34		429
17	GGL10	45.9		0.46	17.47	41.8			1702	16.8	11.22		77.31	16.45	7.83		425
17	GGL11	44.6		0.43	17.97	40.4			1745.6	16.4	10.71		76.88	16.71	7.49		414
17	GGL12	43.9		0.45	17.52	39.7			1702	15.8	10.54		76.2	16.94	7.4		412
17	GGL13	45.1		0.47	17.64	42.3			1702	16.5	11.18		75.13	15.99	7.72		424
17	GGL14	46.4		0.47	17.88	42.1			1702	17.0	11.13		77.96	17.07	7.75		436
17	GGL15	44.8		0.40	18.31	40.2			1789.2	15.9	10.68		79.95	17.51	7.37		430

Ref.#	Sample	La	Li	Lu	Nb	Nd	Ni	Os	P	Pb	Pr	Re	Rb	Sc	Sm	Sn	Sr
18	GJ0601	135.0		0.17	31.9	108.0	18			85.9	30.4		457	12.2	15.1		491
18	GJ0602	137.0		0.20	31.2	106.0	17			88.1	30.5		442	10.8	15.2		487
18	GJ0605	147.0		0.20	32.6	110.0	12			90.7	32.1		419	11	15.5		508
18	GJ0606	138.0		0.21	33	106.0	19			90.4	30.9		465	11.2	15.1		505
18	08YR04	81.7		0.12	20.3	65.8	15			106.0	19.3		399	9.41	9.47		479
18	GJ0614	78.3		0.15	13.2	63.6	7			39.0	18.3		319	8.43	10.3		211
18	GJ0617	74.8		0.25	12.6	63.4	5			37.1	18		314	8.59	10.6		190
18	GJ0619	77.6		0.25	12.9	64.4	4			39.1	18		310	8.59	10.5		193
18	GJ0620	76.5		0.25	12.4	64.0	7			34.9	17.9		301	8.76	10.9		183
18	GJ0624	82.9		0.17	21.1	62.5	11			82.9	18.4		395	7.27	9.22		318
18	GJ0627	85.4		0.16	20.4	64.1	10			79.8	19		414	7.21	9.62		301
18	GJ0628	137.0		0.24	30.2	99.8	15			122.0	29.5		585	10.5	14.7		498
18	GJ0629	80.1		0.15	19.9	60.1	10			75.6	17.7		397	6.85	9.07		334
18	10XB03	76.4		0.21	11.5	69.3	14			38.3	20.5		337	7.27	11.9		167
18	10XB04	87.1		0.16	10.2	78.6	10			39.1	23.3		354	7.37	13.1		205
18	10XB07	77.9		0.17	9.85	71.9	10			38.5	20.9		341	7.56	12		192
18	08YR05	57.9		0.25	24.4	96.3	179			46.8	21.4		527	16.6	20		659
18	10XB10	64.4		0.24	34.1	128.0	240			86.6	27.9		453	15.6	23.8		755
18	10XB12	67.2		0.24	36.3	135.0	234			87.2	29.5		477	16.3	25.8		741
18	10XB13	65.6		0.24	37.4	132.0	256			83.0	29		456	16.3	24.6		734
18	10YR01	61.2		0.25	26.9	113.0	81			57.4	24.4		540	16.8	21.3		682
18	10YR02	55.8		0.26	23.8	97.9	147			41.5	22		450	16	18.6		637
18	10YR04	57.4		0.24	25.7	98.0	233			46.2	22.5		518	15.7	19.9		640
18	10YR04a	55.7		0.23	24.6	93.8	230			46.0	22.6		511	15.4	19.5		624
18	10YR07	57.3		0.23	25	105.0	192			46.5	22.4		523	15.5	19.8		636
19	MV1B	22.1		0.11		19.0			1221.9	39.0			458	2.19	4.5		54
19	MV2	21.9		0.11		19.0			1265.6	39.0			448	2.21	4.1		55
19	UM1B	22.5				22.0			0	36.0			479	2.3	4.4		51
19	UM3V	24.0		0.10		24.0			1221.9	37.0			468	2.3	4.1		57
19	UMQP	22.8		0.10		20.0			1309.2	39.0			510	2.32	4.03		54

Ref.#	Sample	La	Li	Lu	Nb	Nd	Ni	Os	P	Pb	Pr	Re	Rb	Sc	Sm	Sn	Sr
19	UMVU	19.6				20.0			1265.6				838	1.73	4.2		57
20	TE008/93	112.0		0.23	28	157.0	144			118.0	34		528	16	28		849
20	TE011/93	115.0		0.22	38	158.0	145			128.0	34		574	15	28		772
20	TE125/93	72.0		0.31	38	109.0	87			47.0	24		632	18	25		621
20	TE126/93	119.0		0.24	37	200.0	203			93.0	39		465	17	31		792
20	TE127/93	118.0		0.22	38	171.0	212			88.0	39		437	18	32		787
20	TE131/93	112.0		0.22	40	155.0	202			88.0	36		466	18	29		802
20	TE137/93	84.0		0.30	23	144.0	358			79.0	30		702	13	30		990
20	TE138/93	89.0		0.27	24	145.0	230			87.0	29		523	12	29		1042
20	TE117/93	81.0		0.25	29	145.0	193			52.0	29		753	12	31		842
20	TE118/93	85.0		0.24	26	135.0	169			53.0	30		712	14	30		802
20	TE007/93	95.0			21		54			125.0			386	10			684
20	TE025/93	87.0		0.15	22	68.0	17			109.0	19		438	10	11		500
20	TE136/93	93.0		0.21	17	83.0	74			67.0	22		340	9	15		772
20	TE148/93	87.0		0.19	14	73.0	22			83.0	19		381	9	11		415
20	TE150/93	92.0		0.19	14	78.0	19			85.0	20		411	7	12		425
20	TE153/93	84.0		0.14	14	68.0	21			80.0	19		396	8	11		418
20	TE154/93	89.0		0.22	18	75.0	21			85.0	20		413	7	12		420
20	TE047/93	29.0		0.13	8	22.0	8			31.0	6		155	5	4		452
20	TE189/93	40.0		0.14	8	35.0	17			28.0	9		156	6	6		969
20	TE192/93	30.0		0.12	6	28.0	14			45.0	7		118	6	5		756
20	TE194/94	34.0		0.16	8	30.0	16			53.0	8		145	7	5		675
21	Y-2	96.7		0.20	21	107.0	24			45.0	28		254		16.3		1007
21	Y-4	65.7		0.10	14	60.4	9			55.0	16.3		274		9.1		583
21	ZB1	62.2		0.20	34	86.6	83			77.0	19.8		350		16.8		1441
21	ZB4	72.0		0.30	38	97.9	92			79.0	22.8		379		19.1		1638
21	ZB10	67.6		0.30	36	93.2	96			78.0	21.7		357		18		1626
21	ZB12	69.4		0.30	50	91.2	72			119.0	21.7		425		17.9		1495
22	K732	136.0			39	97.9			0				198	8			686
22	K738	122.0			39	90.3			0				118	15			1025

Ref.#	Sample	La	Li	Lu	Nb	Nd	Ni	Os	P	Pb	Pr	Re	Rb	Sc	Sm	Sn	Sr
22	K89G185	116.0			39	86.5			4887.7				119	14			983
22	K89G200	82.4			36	67.7			5367.7				98	15			1075
22	K9007	133.0			39	97.5			3403.9				214	7			713
22	K9008	137.0			39	95.6			3665.8				211	10			686
22	K9021	177.0			31	142.0			3665.8				122	10			2011
22	K9024	161.0			26	119.0			3971.2				198	9			1567
22	K9031	148.0			44	129.2			3578.5				108.7	14			914
22	K9038	170.0			38	154.2			3622.1				137.4	12			1101
23	Bb-105	177.0		0.20	31	142.0			261.84	29.0				10	20.2		2011
23	Bb-107	183.0		0.20		141.0			6676.9	30.0	37			13	20		1756
23	Bb-109	137.0		0.20		96.0			261.84	27.0	27			13	13		1410
23	Bb-114	156.0		0.30		105.0			6546	35.0	29			12	15		1397
23	Bb-88	151.0		0.20	36	106.0			785.52	27.0				8	13.6		1368
23	Bb-89	79.0		0.20		15.0			6546	19.0	7			3	1.7		64
23	Bb94-2	161.0		0.20	26	119.0			480.04	35.0				9	16.1		1567
23	Bb-95	202.0		0.90		146.0			3622.1		40				21.2		1158
23	Bg121	154.0				120.0			2880.2						11.6		1250
23	Bg124	140.0				104.0			2836.6						12.3		
23	COUL311	146.0				100.0			87.28						14.7		
23	COUL326	154.0				116.0			698.24						14		
23	COUL328	162.0				126.0			1265.6						14.2		944
23	COUL338	154.0				120.0			1134.6						13		
23	COUL339	170.0				132.0			1178.3						13.3		
23	k705	170.0			38	164.0			4538.6					12	21.6		1101
23	k708	148.0			44	129.0			4014.9					14	19.2		914
23	K713	180.0		0.20		112.0			4844		34				16		
23	K716	162.0		0.20		117.0			4669.5						13.8		
23	K718	138.0		0.10		101.0			4931.3						12.3		
23	K720	134.0		0.60		98.0			4975		26				14.6		
23	K723	111.0		0.30		101.0			5062.2						17.1		

Ref.#	Sample	La	Li	Lu	Nb	Nd	Ni	Os	P	Pb	Pr	Re	Rb	Sc	Sm	Sn	Sr
23	K732	154.0		3.00		108.0			5367.7					19	17.3		1621
23	K738	165.0		0.30		114.0			4887.7					16	19.4		1562
23	K89G159	184.0		0.80		130.0					36				19.6		1379
23	K89G162	471.0		0.40		341.0								23	44.1		4810
23	K89G163	382.0		0.50		262.0								18	36.4		4735
23	K89G185	328.0		0.30		204.0								8	26		4040
23	K89G186	390.0		0.50		137.0								1	17.3		2306
23	K89G191	326.0		0.30		250.0								23	33.4		2941
23	K89G192	542.0		0.70		198.0								1	16.7		1700
23	K89G193	217.0		0.30		166.0								20	21.6		3214
23	K89G197	334.0		0.60		146.0								2	18.9		2295
23	K89G200				40					39.0				8			700
23	K9002	136.0		0.30	39	98.0			610.96	67.0				8	13.6		685
23	K9006	133.0		0.30	39	98.0			3753	29.0				7	13.4		713
23	K9007				37				3403.9	27.0				8			635
23	K9008				39				3665.8	36.0				12			713
23	K9016	137.0		0.30	39	96.0			3447.6	39.0				10	13.1		686
23	K9017				40				3709.4	27.0				11			1019
23	K9018	112.0		0.30	37	81.0			3709.4	25.0				13	11.4		987
23	K9019	116.0		0.30	39	87.0			3840.3	30.0				14	11.8		983
23	K9021				39				3665.8	30.0				11			1040
23	K9024	82.0		0.30	36	68.0			7375.2	21.0				15	9.8		1075
23	K9026				39				3665.8	22.0				14			1092
23	K9027	122.0		0.30	39	90.0			3753	32.0				15	12.3		1025
23	K9028	123.0		0.30	40	90.0			3316.6	35.0				12	12.2		1029
23	K9029				41				3316.6	29.0				13			1014
23	K9031				11				3578.5	12.0				9			196
23	K9032				40				3665.8	46.0				10			712
23	K9038				39				3622.1	38.0				9			747
23	K9039	36.0		0.50	14	26.0			3796.7		7				5.3		119

Ref.#	Sample	La	Li	Lu	Nb	Nd	Ni	Os	P	Pb	Pr	Re	Rb	Sc	Sm	Sn	Sr
23	Kp35-10	28.0		0.10	6	22.0			3753		6				3.7		762
23	Kp12-58	33.0		0.10	6	28.0			4364		7				5.1		893
23	Kp23-2	18.0		0.10	6	18.0			5236.8		4				43		772
23	Kp24-1	16.0		0.20	5	16.0			4669.5		3				3.8		770
23	Kp39-3	83.0		0.10	21	87.0			5629.6	114.0					4	12.7		984
23	Kp47-2	85.0		0.20	22	101.0			4451.3	102.0					7	16.6		976
23	Kp47-5	86.0			23	87.0			3971.2	107.0					6	12.7		816
24	2303								1091								
24	2509								1396.5								
24	1P2JD7-1								1702								
24	1P2JD7-1a								1527.4								
24	2011a								698.24								
24	2059a								1221.9								
24	2303a								1134.6								
24	2511-1								1396.5								
25	04wq-1	303.0		0.30	15.2	157.0	283			35.6	46.5		40.1	23	21.5	3910	
25	04wq-2	268.0		0.31	14.2	151.0	255			36.7	44.2		40.4	21	20.7	3546	
25	04wq-3	367.0		0.32	15.5	178.0	315			37.7	50.8		45.5	21.9	24.1	4366	
25	04wq-4	216.0		0.32	14.5	155.0	276			36.2	43.7		37.8	24.4	21.2	4424	
25	04wq-5	371.0		0.32	15.1	185.0	308			37.3	51.7		38.7	22.7	24.8	3979	
25	04wq-6	103.0		0.26	17.3	77.7	170			38.8	22		79.5	17.7	11.1	2085	
25	04wq-7	105.0		0.27	17.4	80.8	164			38.8	22.5		77.9	17.5	11.2	2094	
25	4086-1	101.0		0.26	16.9	75.3	170			47.6	22.1		78	17.9	11.2	1996	
25	8528	55.0		0.30	12.7	50.5	193			20.7	13.8		145	21.5	8.2	1263	
25	8518-1	58.1		0.22	10.7	46.0	83			27.6	12.8		82.6	11.1	7.2	1350	
25	8518-2	58.1		0.22	10.2	44.8	81			30.7	12.5		82	10.7	7.05	1354	
25	9063-GS2	50.9		0.24	7.29	38.3	126			29.2	10.6		70.3	16.9	6.19	1120	
25	9063-GS3	39.9		0.19	7.91	30.5	118			24.0	8.37		83.2	16.6	5.04	1223	
25	D3145	263.0		0.37	47	131.0	15			176.0	41		251	5.06	17.9	2012	
26	05S2-7	40.8		0.21	35.3	111.0	217			60.2	22.1		602	15.4	25.4		634

Ref.#	Sample	La	Li	Lu	Nb	Nd	Ni	Os	P	Pb	Pr	Re	Rb	Sc	Sm	Sn	Sr
26	05S2-8-1	56.7		0.23	34.9	132.0	219			65.4	27.8		6142	14.8	28.7		701
26	05SLP5-3	76.3		0.27	32.9	145.0	202			58.7	31.6		693	13.6	29.8		989
26	05SLP5-05	55.4		0.24	28.1	109.0	209	0.1067		44.4	23.8	0.294	580	14.9	21.9		920
26	05SLP5-06	73.8		0.22	31	111.0	192			51.0	26.4		459	14.2	20.8		956
26	05SLP5-7	67.8		0.21	30.9	121.0	112	0.0278		42.9	27.6	0.234	604	15.7	23.7		987
26	05SLP5-8	70.3		0.22	26.7	105.0	123			44.1	24.7		581	13.8	19.8		782
26	05SLP5-09	118.0		0.25	32.6	189.0	185			48.3	45		725	12.8	34.1		826
26	S05SLP5-10	63.9		0.21	28.6	102.0	88			74.5	23.4		389	13.2	19.9		1145
26	05SLP5-11	50.1		0.17	27.7	75.0	147			54.0	17.5		475	12.4	15.5		1005
26	05SLP5-16	46.3		0.24	35.3	109.0	142			60.7	22.7		476	20.5	23.6		854
26	05SLP4-01	268.0		0.34	17.8	319.0	254	0.0447		158.0	82	0.642	675	25.7	59		5274
26	05SLP4-02	150.0		0.26	31.9	191.0	216	0.0204		103.0	46.8	0.696	523	17.7	35		1728
26	05SLP4-03	188.0		0.29	26.4	238.0	257	0.0217		122.0	60.4	0.256	520	2.97	44.6		1519
26	05SLP4-04	142.0		0.26	32	185.0	231	0.0211		96.4	45.7	0.285	892	17.9	34.5		1626
26	05S2-7					111.0		0.1717		60.2		0.387	602		25.4		634
26	05S2-8-1					132.0		0.174		65.4		0.307	614		28.7		701
27	WR-12-48	65.2		0.54	28.7	44.2	5			15.0	12.1		220.2	9.15	7.98		446
27	WR-12-47	25.7		0.72	15	25.2	1			19.0	6.12		185.4	5.59	6.39		16
27	WR-12-44	13.7		0.15	2.8	8.2	4				2.27		40	7.59	1.39		374
27	WR-12-45	17.1		0.34	3.9	18.6	22				4.1		18.5	34.6	4.23		364
27	WR-12-40	28.7		0.32	9.7	16.7	7			10.0	4.83		97.5	9.32	2.93		447
27	WR-12-42	19.0		0.30	3.8	19.0	9				4.23		34.8	24.2	4.11		467
27	WR-12-33	30.9		0.25	6.9	23.2	6			12.0	5.98		95.5	10.6	4.22		542
27	WR-12-35	34.5		0.49	11.2	33.3	14			11.0	7.92		88	23.8	7.08		649
28	T2A/98	145.9		0.31	18.56	167.1				10.3	40.72		642.6		30.13		921
28	T3b/98	96.0		0.38	20.36	101.6				52.7	25.13		325.6		18.19		1115
28	T4A/98	133.7		0.24	23.78	165.0				59.8	40.47		401		27.24		699
28	T5A/98	56.4		0.24	14.40	67.0				47.0	16.12		283.9		11.90		767
28	T11B/98	28.5		0.09	6.22	26.3				25.8	6.78		99.76		4.28		996
28	JPT14.2	26.8		0.10	5.93	25.0				24.9	6.49		67.34		4.18		856

Ref.#	Sample	La	Li	Lu	Nb	Nd	Ni	Os	P	Pb	Pr	Re	Rb	Sc	Sm	Sn	Sr
29	JPT24A	68.3		0.20	18.5	73.4			1745.6	43.7	18.7		359.9	9.5	13.2		372
29	JPT24B	62.5		0.30	28.8	94.8			3054.8	47.3	21.2		462.2	14.4	20.3		733
29	JPT24C	58.6		0.30	27.2	90.2			3054.8	44.5	20.1		438.2	14	19.2		724
29	JPT22	73.5		0.20	14.4	65.6			872.8	43.6	18.1		326.5	7.7	10.3		222
29	K89G162	110.2		0.10	33.5	117.5				113.8	29.7		540.7	6	18.5		575
29	20E39A	49.3		0.30	11.8	48.5			1309.2	21.0	12.1		66.7	24.8	8.6		660
29	JPT7	54.3		0.20	13.6	64.1			3054.8	50.6	15.4		257.8	9.7	11.3		716
29	T5B/98	56.8		0.30	15.4	67.7			3491.2	49.0	16.5		276	10.6	12.1		470
29	JPT14.1	34.1		0.10	8.1	30.1			872.8	28.4	7.9		91	7.6	4.9		949
29	JPT3	30.9		0.10	4.7	31.1			1309.2	33.0	7.8		116.2	6.4	5.3		803
29	JPT4	22.8		0.10	6.3	17.0			436.4	36.5	4.8		146.8	2.3	2.6		651
29	JPT5.2	33.3		0.10	14.2	30.0			872.8	44.2	8		206.2	4.8	4.7		472
29	JPT8	22.3		0.10	5.8	11.4			872.8	60.5	3.5		314.6	2.6	1.6		158
29	95RAS11.3	26.8		0.10	18.6	19.4			436.4	41.2	5.6		70.6	1.6	2.9		3353
29	T2A	145.8		0.30	20.3	167.1			5673.2	10.3	40.7		642.6	14	30.1		921
29	T3B	95.9		0.40	23.7	101.6			3491.2	52.7	25.1		325.6	16	18.1		1115
29	T4A	134.3		0.20	14.4	164.9			4364	59.6	40.5		398	15	27.2		694
29	T5A	56.4		0.20		67.0			3054.8	47.0	47		283.9	10	11.9		768
29	912	141.2		0.30	45.1	123.3			4800.4	30.0	33.3		236	10.7	18.1		1387
29	1105	36.1		0.40	14.2	29.3			3054.8	22.8	7.8		123.7	14	5.5		296
29	K702	153.0		0.30	43.6	129.9			7418.8	34.4	35.4		113.9	10.3	18.8		1217
29	K703	177.6		0.30	49.5	148.5			5236.8	40.4	40.9		126.3	11.1	21.3		1177
29	K89G185	190.2		0.20	42.3	163.8				34.0	43.6		132.4	9.9	23.3		2120
29	K89G186	178.6		0.20	39.3	150.2				31.5	40.4		121.9	9.7	21.4		1968
29	K89G200	162.9		0.20	36	126.7				38.4	34.8		207.9	9.1	18		1682
29	KP12.6	173.0		0.30	63.5	139.7			3927.6	34.4	38.7		182.3	7	19.9		813
29	KP47-2	154.0		0.30		108.0			4800.4				103	19	17.3		1621
29	KP47-5	165.0		0.30		113.5			3927.6				144	16	19.4		1562
29	Bb124	160.0		0.20	38.1	112.7			3054.8	35.0	32.7		144.5	8.1	14.9		1135
29	Bb121	152.4		0.20	36.8	109.3			3054.8	31.6	31.4		122.5	8.1	14.7		1065

Ref.#	Sample	La	Li	Lu	Nb	Nd	Ni	Os	P	Pb	Pr	Re	Rb	Sc	Sm	Sn	Sr
29	Bq137	186.1		0.20	37.3	123.7			3054.8	40.5	36.8		173.4	5.9	15.8		906
29	Bb119	204.8		0.20	37.6	134.8			5673.2	36.0	39.3		175.7	6.6	16.9		921
29	Bb122	184.2		0.20	35.8	121.3			436.4	42.2	36.1		162	7.1	15.5		934
29	Bb135	191.2		0.20	37.6	123.3			5236.8	42.4	37		182.6	6.1	15.7		861
29	Bg142	138.1		0.00	11.3	79.1			872.8	71.1	24.4		236.7	0.7	10.1		652
29	Bq140	137.9		0.00	10.7	79.6			1309.2	76.0	24.3		235	0.9	10.1		634
29	Bq141	151.4		0.10	13.7	85.5			1745.6	97.8	26.5		239.4	1.3	11		720
29	K9024	113.6		0.20	40.9	84.4			3927.6	31.1	23.5		109.8	9.6	11.8		982
29	K9026	122.7		0.30	44.9	90.4			3491.2	25.9	25.9		116.4	8.9	12.8		899
29	K9027	118.4		0.20	42.6	87.6			3927.6	32.2	24.6		111.3	8.2	12.2		969
29	K9028	108.7		0.20	40.6	81.0			3491.2	25.0	22.8		106.7	8.2	11.3		968
29	K9029	119.7		0.30	46.6	88.3			3491.2	28.6	24.9		126.2	8.7	12.4		1078
29	K9031	120.7		0.30	43.7	90.7			3491.2	31.9	25.3		118.4	11.7	12.8		1001
29	K9032	123.4		0.30	43.9	89.9			3491.2	25.9	26.1		118.6	11.2	13.2		1057
29	K9038	81.9		0.30	39.2	70.5			3927.6	21.3	19		93.6	11.4	10.4		1074
29	K9039	89.1		0.30	43	76.3			3927.6	22.4	20.9		92.6	12.2	11.4		1003
29	K9041	37.8		0.50	17	38.9			1309.2	20.9	9.7		185.8	13.9	7.8		234
29	K9001	29.1		0.30	10.3	26.1			436.4	8.9	6.9		69.6	6.9	4.8		223
29	K9002	29.6		0.30	11.6	27.4			436.4	12.7	7.1		99.6	8.3	5.2		198
29	K9006	148.9		0.30	48.6	108.5			3927.6	41.7	30.6		226.6	7.3	15.3		755
29	K9007	138.6		0.30	44.5	101.9			3491.2	69.9	28.9		199.2	7.2	14.7		699
29	K9008	138.7		0.20	45.1	102.8			3927.6	29.4	29.8		207.7	7	14.7		650
29	K9016	131.4		0.20	42.7	97.4			3491.2	28.9	27.6		237.8	6.1	13.8		624
29	K9017	139.6		0.20	45	100.9			3927.6	44.9	28.9		213.5	6.6	14.5		718
29	K9018	145.0		0.30	45.8	105.6			3927.6	37.1	30.6		209.2	7.2	15.1		666
29	K9019	140.1		0.20	45.7	102.1			3927.6	38.2	28.9		192.8	6.9	14.8		774
29	K9021	136.8		0.20	43	99.5			3491.2	39.5	28.1		204	6.4	14		669
30	2007k251	269.2		0.25	65.86	221.7	151			34.7	59.61		100.7	15.68	30.9	4682	
30	2007k252	266.5		0.27	73.5	251.2	141			44.8	65.92		132.5	15.51	29.7	4777	
30	2007k253	243.6		0.24	67.94	226.4	138			38.5	58.14		119.5	15.1	27.9	4370	

216

Ref.#	Sample	La	Li	Lu	Nb	Nd	Ni	Os	P	Pb	Pr	Re	Rb	Sc	Sm	Sn	Sr
30	2007k254	265.1		0.26	63.43	253.2	143			36.0	65.92		124.4	15.73	30.7	4668	
31	DHLT-10	152.0		0.18	28	105.0			0.89	38.0	28		204	7.5	14.6		1438
31	DHLT-2	149.0		0.08	30	93.2			0.81	27.0	26.6		213	6.7	12		1426
31	DHLT-4	163.0		0.22	32	137.0			1.49	54.0	34.1		255	9.5	20.4		2021
31	DHLT-5	151.0		0.16	28	105.0			0.9	31.0	27.8		199	7.3	14.3		1420
31	DHLT-7	156.0		0.11	30	105.0			0.96	62.0	29.2		189	7.7	14.2		1444
31	DHLT-9	150.0		0.18	30	104.0			0.86	45.0	27.7		190	7.3	14.9		1414
31	PL-12	136.5		0.31	42	92.3			0.96	31.0	24.64		123	18	13.8		1163
31	PL-2	172.3		0.27	46	112.6			1.15	31.0	30.8		113	15	16.6		1286
31	PL-3	174.5		0.24	50	113.1			1.17	39.0	30.69		119	16	16.1		1414
31	PL-5	176.9		0.30	44	114.8			1.18	31.0	31.41		125	18	17.5		1476
31	PL-7	126.2		0.24	38	86.5			1.03	28.0	23.32		115	16	13.2		1171
31	PL-9	144.0		0.31	41	96.3			0.94	26.0	25.74		119	16	14.6		1060
31	YCN-1	125.0		0.18	43	95.9			1	31.0	25.5		99	11	14.3		1239
31	YCN-2	125.0		0.14	48	93.4			1	25.0	25		103	11	13.8		1281
31	YCN-3	125.0		0.19	44	96.0			1	30.0	25.5		107	11	14.6		1266
31	YCN-4	131.0		0.21	42	101.0			1	29.0	26.7		101	10	15.3		1235
31	YCN-6	126.0		0.26	45	98.6			0.99	22.0	25		98	11	15.2		1203
31	YCN-7	131.0		0.26	31	101.0			1.02	24.0	26.4		102	10	15.3		1155
31	YCN-8	122.0		0.24	41	96.0			0.99	27.0	23.7		132	14	14.6		1370
31	KP24-1	202.0		0.86		146.0					40.2				21.2		
31	KP25-3	219.0		0.81		148.0					41.1				21.7		
31	KP28-1	115.0		0.25		84.4					22.2				12.8		
32	11UMT14	32.5		0.43	13.89	32.5			2400.2	27.6	8.34		2.67	21.3	6.55		672
32	11UMT15	14.6		0.41	7.18	18.8			1309.2	25.7	4.39		19.27	28.94	4.6		706
32	11UMT17-a	110.2		0.28	30.75	103.7			5455	149.2	28.16		112.1	33.79	15.4		2685
32	12HG04	15.4		0.08	30.68	12.4	3		1316.6	21.6	3.64		851.4	1.8	2.78		36
32	12HG06	25.0		0.04	16.35	22.7	4		1304.3	35.4	6.5		567.7	1.6	4.87		24
32	12HXV01	176.2		0.23	16.31	123.7	103		4061	51.6	34.42		105.7	15	19.4		2942
32	12HXV08	51.8		0.11	20.87	35.6	6		1311.1	39.9	10.6		341.3	3.2	6.13		284

Ref.#	Sample	La	Li	Lu	Nb	Nd	Ni	Os	P	Pb	Pr	Re	Rb	Sc	Sm	Sn	Sr
32	12HXV09	179.9		0.26	46.27	108.5	8		3594.8	33.7	32.5		139.1	7.9	16		1011
32	12HXV12	145.7		0.21	39.11	101.5	16		3726.6	26.2	29.76		154.8	8.8	14.9		1210
32	12HXV15	150.0		0.22	38.38	105.6	15		3183.8	30.1	31.42		174.1	7.8	15.3		1057
32	12HXV19	168.1		0.20	42.15	104.3	23		3271.8	38.2	31.15		106.2	7.6	14.9		1153
32	12HXV21A	147.7		0.22	38.65	99.8	14		3458.9	35.0	29.49		178.1	7.7	14.7		1078
32	12HXV23	178.7		0.21	36.91	100.7	16		3104	26.2	30.42		178.3	7.8	14.4		962
32	12HXV24	58.5		0.13	24.72	39.0	2		1165.6	52.6	11.77		404	3.1	6.42		248
32	12HXV32	53.9		0.10	21.2	37.5	2		1311.4	41.6	11.28		356.9	2.7	6.35		283
32	12HXV33	159.6		0.25	15.79	128.1	186		4888.1	43.7	33.98		164.2	19.8	22.2		2485
32	13DV05	145.5	30	0.24	45.6	105.5	19		3927.6	36.0	30.2		140	9	15.1	4	798
32	13DV04	149.5	30	0.26	46.2	108.0	17		3971.2	32.0	30.7		136.5	9	15.8	4	831
32	13DV11	150.5	40	0.25	45.8	108.5	17		4014.9	33.0	30.8		143.5	9	16	4	864
32	13DV13	147.0	40	0.25	45.8	100.5	28		3971.2	36.0	29.5		133	9	14.8	4	821
32	13DV14	133.5	40	0.26	42.6	90.3	22		3578.5	39.0	26.3		148.5	9	13.2	4	730
32	13DV15	148.0	30	0.28	45.8	101.5	23		3753	32.0	29.3		154.5	9	14.9	4	790
32	13DV23	100.0	30	0.22	43.8	74.7	44		3578.5	22.0	20.9		109.5	13	11.6	3	816
32	13DV29	93.2	40	0.24	45.9	69.9	53		3360.3	23.0	19.65		98.7	12	10.9	4	763
32	13LG07	154.0	30	0.18	32.9	93.0	9		2618.4	30.0	28.2		182	7	12.5	4	759
32	13XV01	141.5	40	0.22	41.3	95.1	20		3229.4	30.0	28.2		197	8	14	4	754
32	13XV02	152.0	30	0.27	46.9	104.0	19		3796.7	39.0	30.1		163.5	9	14.8	5	856

Table B.5 – Trace element compositions of compiled lavas in the Tibetan Plateau, part 3. Data typically obtained via ICPMS

Ref.#	Sample	Ta	Tb	Th	Ti	Tm	U	V	W	Y	Yb	Zn	Zr
1	K89G185	1.6	1.3	26.5	11090		2.8		4.3	31.6	1.5	111.9	411.8
1	K89G186			23.6	10611		0.0	127		17	1.51	97.7	358
1	K89G189				10731								
1	K89G190				7973								
1	KB9G191			48.2	8153		0.0	95		2t.00	1.59	84.6	230
1	K89G192			49	7913		0.0	97		24	1.83	101.8	318
1	K189G193	2.3	0.9	49.5	7853		0.0		6.6	23	1.6	79.2	368.1
1	K89G197			66.1	599		97.8	3		9	1.25	29.4	27
1	K89G200	1.5	1.0	44.4	8573		6.8		7.9	23.4	1.4	96.5	407.2
2	05S2-4	1.9	1.5	225	8992	0.26	36.8			26.4	1.71		694
2	05S2-6	2.0	1.3	241	8812	0.24	38.0			23.2	1.58		706
2	05S2-9	1.7	0.9	180	7973	0.21	26.2			18.5	1.39		563
2	05SLP5-1	1.6	1.2	165	8872	0.25	21.8			24.7	1.65		571
2	05SLP5-2	1.7	1.0	186	8213	0.21	26.6			19.9	1.39		709
2	05SLP5-4	1.9	0.8	152	8693	0.19	21.7			17.5	1.26		579
2	CM10-04-04	3.5	1.0	118	9951	0.22	4.1			15	1.3		953
2	CM10-04-09	3.0	1.1	135	10671	0.26	15.5			18.6	1.56		988
2	CM10-04-12	3.0	0.8	166	9352	0.21	16.3			12.8	1.36		741
2	04DYH-01	0.8	0.6	21.2	6055	0.2	4.8			14.9	1.25		314
2	D3141	1.4	2.3	83.5	7314	0.45	13.4			35.9	2.7		475
3	04LQS-2	0.5	0.4	16.95	2997	0.13	3.2			8.99	0.89		183
3	04LQS-3	0.5	0.3	15.79	3297	0.12	2.6			7.85	0.83		199
3	04LQS-6	0.7	0.7	14.88	4616	0.21	3.5			16.6	1.45		217
3	04LQS-14	0.3	0.4	19.65	2638	0.12	4.1			8.49	0.79		239
3	04LQS-16	0.4	0.3	8.73	3297	0.14	2.7			7.77	0.98		157
3	04YJL-05	0.7	0.5	13.44	4736	0.19	3.8			11.96	1.21		211
3	04YJL-07	1.1	0.5	29.08	4976	0.15	8.7			11.74	0.96		299
3	04YJL-06	1.0	0.4	23.61	4976	0.12	7.4			9.58	0.79		306

Ref.#	Sample	Ta	Tb	Th	Ti	Tm	U	V	W	Y	Yb	Zn	Zr
3	04YJL-09	1.0	0.5	22.74	4196	0.19	6.3			13.23	1.17		282
3	04DN30-2	0.9	0.6	22.38	6115	0.21	4.9			15.4	1.33		305
3	04DN30-3	0.6	0.4	22.99	4436	0.14	5.0			9.89	0.91		263
3	04DN31-1	0.7	0.3	19.08	4976	0.12	4.4			8.07	0.73		273
3	04DN32-1	0.5	0.3	13.06	4136	0.13	3.1			8.47	0.81		206
3	04DN32-2	0.5	0.3	13.31	4136	0.13	2.8			8.36	0.81		198
3	04DN35-2	0.6	0.3	16.11	4736	0.1	4.1			6.63	0.63		221
3	04DN36-3	0.7	0.5	15.79	5515	0.16	4.3			11.75	1.01		228
3	04DN37-2	0.7	0.3	11.16	5395	0.12	3.9			7.98	0.76		231
3	04DN39	0.5	0.3	17.71	5036	0.14	5.0			8.82	0.87		180
3	04DN40	0.6	0.4	17.5	3297	0.15	4.6			10.33	0.91		217
3	04DY44-2	0.7	0.5	16.08	5275	0.17	4.5			12.03	1.05		217
3	04DY44-4	0.5	0.4	19.19	3597	0.14	5.1			10.14	0.9		212
3	04DY44-7	0.5	0.4	13.44	4916	0.12	3.8			8.33	0.77		207
3	04D6441	0.9	0.4	20.45	4616	0.15	4.6			10.26	1.08		185
3	04D6437	0.9	0.5	23.02	5755	0.14	5.6			10.97	1.02		302
4	2T394	4.2	1.0	8.3	7014	0.4	2.0			25	2.1		253
4	2T395	3.9	1.1	8.3	10671	0.4	2.1			25	2.4		250
4	2T396	0.8	1.0	4.7	12889	0.4	1.2			31	2.9		170
4	98T03	1.3	1.0	5.5	12889	0.5	1.5			35	3.2		204
4	98T04	4.5	1.1	8.9	13788	0.4	2.2			26	2.3		259
4	98T07	6.2	3.4	191	6594	1	19.0			82	6		1178
4	98T15	3.5	2.7	69	7014	0.7	6.7			60	4.4		785
4	98T16	2.8	3.5	195	4736	1	18.0			86	6.3		1103
4	98T33	4.0	2.7	134	6894	0.7	7.1			57	4.5		726
4	98T38	3.4	4.0	219	4916	1.2	21.0			95	7.1		1205
4	98T43	3.3	3.6	194	5216	1	23.0			82	6.3		1052
4	98T44	6.3	4.1	62	6235	1.1	11.0			89	6.8		1064
4	98T46	3.2	3.0	178	4796	1	12.0			76	6.1		1098
4	98T49	3.3	2.0	59	5815	0.6	5.8			45	3.6		653

Ref.#	Sample	Ta	Tb	Th	Ti	Tm	U	V	W	Y	Yb	Zn	Zr
4	98T51	2.6	2.7	148	4256	0.8	10.0			62	5		853
4	98T52	3.2	2.5	52	6774	0.6	5.8			50	3.5		555
4	98T53	2.7	1.9	48	5395	0.5	7.8			42	3.1		542
4	98T54	0.5	1.4	34	1978	0.3	1.7			25	1.5		113
4	98T57	4.0	2.9	96	5515	0.8	15.0			66	5		882
4	98T69	3.6	2.4	57	6055	0.6	9.3			50	3.7		624
4	98T70	3.0	2.0	50	6355	0.5	11.0			42	3.2		552
4	98T71	3.5	2.8	160	4916	0.8	11.0			62	5.2		1011
4	98T73	2.8	2.8	157	4316	0.8	19.0			67	5.3		926
4	99T132	4.3	1.7	214	6474	0.2	23.0			20	1.7		1154
4	99T134	5.2	2.0	223	3957	0.3	12.0			23	1.8		929
4	99T145	5.2	2.2	283	3957	0.4	43.0			30	2.1		1534
4	99T152	3.7	1.8	160	5875	0.2	5.2			18	1.2		786
4	99T154	3.3	1.8	176	5815	0.3	4.8			22	1.7		679
4	99T53	1.6	2.5	129	7434	0.4	18.0			40	2.3		511
4	99T56	1.6	0.9	108	7314	0.2	17.0			14	1		197
4	99T57	2.4	1.4	145	8573	0.2	21.0			22	1.4		271
4	99T60	2.1	1.5	117	7554	0.3	25.0			23	1.6		352
4	99T62	1.9	1.9	116	7554	0.3	8.4			27	1.7		428
5	2002T1021	2.5	0.9	5.2	8033	0.28	1.2			21.07	1.7		277.6
5	2002T1022	5.9	0.8	4.44	7973	0.27	1.5			20.57	1.59		280.84
5	2002T1023	1.5	0.8	7.3	7793	0.21	1.3			18.09	1.28		291.47
5	2002T1024	1.9	0.7	7.54	7913	0.23	2.2			17.71	1.39		271.13
5	2002T1025	1.5	0.6	11.92	7913	0.16	3.1			14.07	1.01		302.7
5	2002T1026	1.8	0.5	16.27	7973	0.16	4.8			11.88	1.02		280.18
5	2003T373	1.4	0.5	14.28	12469	0.14	4.1			12.02	0.9		266.74
5	2003T374	1.4	0.6	13.68	11750	0.16	3.1			12.64	1.02		305.49
5	2003T375	1.4	0.5	18.26	9472	0.12	1.9			9.97	0.69		183.12
5	2003T380	1.6	0.6	17.33	7014	0.19	3.3			14.55	1.12		238.25
5	2003T483	1.6	0.9	13.15	7014	0.27	2.1			20.36	1.58		378.94

Ref.#	Sample	Ta	Tb	Th	Ti	Tm	U	V	W	Y	Yb	Zn	Zr
5	2003T485	2.0	0.9	15.63	5156	0.26	2.7			19.36	1.64		366.33
5	2003T486	1.8	0.9	15.65	5096	0.27	2.7			19.56	1.62		369.88
5	2003T487	1.8	0.9	15.41	5695	0.28	2.7			20.69	1.77		369.5
5	2003T488	1.8	0.9	15.31	4316	0.27	2.7			19.27	1.7		380.25
5	2003T492	1.8	0.9	15.66	7134	0.29	2.8			23.6	1.81		370.53
6	Tl/10	2.5	1.6	130.7	10071	0.285	14.0	131.3	4.67	25	1.65		974
6	Tl/11	2.5	1.6	131.9	9712	0.282	9.6	128	0.74	25.2	1.65		994
6	Tl/18	1.9	1.5	150.8	9472	0.298	13.7	124.3	2.71	25.4	1.74		784
6	Tl/13	1.8	1.4	112	8693	0.313	10.9	119.7	2.34	25.8	1.87		862
6	Tl/03	2.5	1.4	183.1	8573	0.279	17.0	140	3.57	23.9	1.69		783
6	Tl/08	1.9	1.4	152	9652	0.283	13.6	114.3	2.53	24.1	1.7		787
6	Tl/17	2.9	1.9	224.3	6355	0.317	22.0	122.3	2.47	28.6	1.88		966
6	Tl/06	3.2	1.2	145.1	7314	0.229	16.0	70.6	2.63	19.9	1.37		990
6	Tl/59	2.9	1.1	153	5515	0.183	14.5	65	5.59	16.9	1.07		340
6	CHZ-1	4.1	2.4	204.4	9592	0.406	22.4	136	4.07	36.1	2.43		1101
6	CHZ-2	3.9	2.4	187.6	9712	0.389	28.2	137	4.13	34.9	2.36		893
6	CHZ-3	3.8	2.2	154	9951	0.373	23.7	141	3.98	32.2	2.27		806
6	CHZ-4	3.2	2.0	166.6	9172	0.345	20.2	147	6.17	29.6	2.13		834
6	CHZ-5	3.4	2.2	202.3	9052	0.403	23.3	164	5.85	32.9	2.4		884
6	CHZ-6	3.6	2.2	184.1	9112	0.397	27.7	134	5.58	32.7	2.33		917
6	CHZ-7	3.6	2.4	219.1	9532	0.393	23.9	151	3.3	35.5	2.34		983
6	CHZ-8	3.7	2.3	202.3	9592	0.391	29.4	137	4.05	35.4	2.3		1000
6	CHZ-9	3.9	2.5	213.5	9712	0.4	21.9	135	5.29	35.6	2.36		935
6	CHZ-10	4.2	2.5	139.3	9772	0.404	24.5	145	4.59	35.5	2.31		965
6	CHZ-11	2.7	2.4	231.7	9592	0.377	18.2	142	2.71	34.5	2.15		749
6	CHZ-12	4.5	2.5	198.6	9652	0.422	24.0	152	1.86	37.4	2.5		853
7	AH-7	2.2	1.7	34.2	6295	0.41	4.5			28.4	2.65		521
7	G26	3.7	2.4	75.3	7853	0.66	7.5			74.2	4.18		697
7	G68	3.4	2.0	56.9	6954	0.61	12.8			56.8	4.12		787
7	G98-0	2.4	1.4	59.6	8273	0.43	8.9			33.8	2.68		241

Ref.#	Sample	Ta	Tb	Th	Ti	Tm	U	V	W	Y	Yb	Zn	Zr
7	G98-1	1.0	2.3	134.1	7194	0.58	10.6			38.2	3.84		428
7	G98-14	2.4	1.8	158.5	8153	0.59	6.9			33.5	3.95		442
7	G98-3	1.1	2.4	139.2	6414	0.61	8.4			32.4	3.63		401
7	G98-6	1.7	2.1	116.7	4496	0.64	8.3			37.5	4.31		549
7	G98-9	3.0	1.4	146.2	8693	0.61	7.7			35.9	3.89		475
7	HH72	2.1	1.1	32.6	9292	0.34	3.0			27.8	1.98		339
7	HS07	1.7	0.9	28.2	9592	0.28	6.6			17.6	1.84		315
7	HS-69	1.9	0.6	13.6	8573	0.27	7.6			27.2	1.76		415
7	JC9719	2.3	1.1	108.9	8752	0.52	6.3			34.7	3.11		317
7	JC973	2.7	1.6	126.9	8333	0.63	5.7			31.7	4.07		338
7	JC975	2.3	1.0	25.9	9112	0.46	5.9			30.1	2.96		494
7	JC978	2.3	0.7	21.6	9592	0.38	6.0			30.9	2.54		389
7	JH6	3.2	1.0	24.5	8872	0.29	4.7			23.6	1.96		346
7	KX84	2.8	0.8	14.4	8333	0.28	3.4			23.5	1.78		415
7	PL-58	2.3	1.9	37.9	10071	0.43	7.4			28.6	2.86		394
7	PL-7	1.9	1.6	26.3	10071	0.46	5.1			28.3	2.97		401
7	QQ08	2.2	1.2	30.1	7074	0.29	5.8			28.2	1.94		438
7	QS22	2.7	1.0	59.24	9412	0.3	7.3			25.7	2.14		369
7	XT16	2.5	1.2	28.5	6774	0.4	5.0			18.6	2.87		254
7	XT8	0.7	1.2	19.6	6474	0.22	2.4			22.8	1.47		239
7	XY03	2.5	1.2	42.9	9652	0.33	5.3			29.8	2.17		404
7	XY05	3.1	1.1	34.7	8633	0.28	5.5			22.7	1.66		352
7	YS02	1.3	1.0	28.5	6295	0.26	5.5			21.5	1.54		217
7	YS72	1.3	1.3	40	7074	0.24	6.3			20.4	1.27		472
7	ZF91	0.8	0.6	42.9	4376	0.25	3.5			13.6	1.61		261
7	ZF96	1.3	1.1	46.8	7314	0.38	5.3			34.2	2.13		202
8	ZF09	0.8	0.4	16.5	5455		13.3	41.9		11	0.88	26.4	130
8	GUO62	0.9	0.4	16.7	3837		20.3	58.5		11.2	0.76	22.3	135
8	GUO51	0.9	0.3	21.4	2878		15.3	45.1		8.9	0.73	25.2	122
8	GUO48	0.4	0.4	10.1	5096		2.1	70.6		8.53	0.67	23.8	126

Ref.#	Sample	Ta	Tb	Th	Ti	Tm	U	V	W	Y	Yb	Zn	Zr
8	GUO37	0.4	0.4	3.14	4436		0.9	72.1		10.1	0.71	23.8	114
8	G09	0.8	0.4	42.3	3777		3.7	38.6		12.9	0.65	33.4	173
8	ZFG17	0.4	0.4	21.6	3897		4.1	57.5		10.1	0.68	24.4	167
8	G006	0.5	0.1	12.6	2758		1.8	55.5		4.17	0.33	21.5	92.6
8	G019	0.7	0.2	16.4	2878		5.4	42.2		5.51	0.44	47.5	109
8	G016	0.8	0.2	29.8	1379		8.5	34.8		6.23	0.48	53.6	124
8	G025	0.5	0.3	10.4	2638		2.1	48		6.18	0.56	63.2	185
9	DY-7	4.8	2.3	268.5	8752	0.32	36.7	132.53		19.4	1.92	61.96	1318.5
9	DC2	3.9	2.2	187.3	9412	0.24	10.5	141.06		16.2	1.57	75.35	827.9
9	D509	5.3	1.3	171.5	10671	0.18	27.2	156.47		13.8	1.11	72.12	1037.2
9	DG43	6.0	2.0	327.4	9292	0.22	14.1	138.68		24.1	1.37	78.42	1728.4
9	YE51	4.1	1.7	236.3	7733	0.23	17.2	131.63		17.4	1.54	83.1	1102.1
9	YC08	3.4	1.7	161.4	8633	0.22	12.6	116.84		22.9	1.44	59.52	817.4
9	YG13	5.2	1.5	195.8	9172	0.31	21.0	125.61		25.6	1.82	72.01	1482.9
9	YF12	3.1	1.4	131.2	9712	0.28	16.3	120.42		18.4	1.79	74.29	782.3
9	YA32	2.4	1.3	144.6	10191	0.21	15.4	108.79		28.7	1.28	65.25	653.1
9	MH78	2.8	1.5	113.7	9772	0.31	20.6	161.07		24.3	1.82	84.52	891.5
9	MH69	3.4	1.0	148.9	9652	0.21	26.1	157.91		27.9	1.35	89.37	1005.3
9	MG-3	2.6	1.4	138.6	9891	0.29	8.8	124.08		19.2	1.72	71.58	523.7
9	MY1	2.0	1.5	135.7	10131	0.31	14.1	131.45		21.2	1.84	77.36	718.6
9	MK09	1.7	1.3	113.2	9652	0.26	17.9	133.73		18.6	1.65	80.02	415.7
9	MR21	1.8	0.7	95.4	9832	0.17	11.5	117.1		11.6	1.04	76.34	472.3
9	MA75	2.2	1.2	167.2	8393	0.25	21.7	142.85		30.1	1.73	86.41	969
9	MX5	3.3	1.2	81.3	8213	0.34	17.9	147.68		33.8	2.19	95.3	621.7
9	2003T534	1.9	1.4	163	8812	0.28	15.0	148			1.74		722
9	2003T536	2.6	1.4	160	8992	0.27	17.0	132			1.75		722
9	2003T539	1.9	1.3	158	8872	0.25	15.0	119			1.5		747
9	G8	2.2	2.4	138.7	6714	0.38	21.9	136.23		34.2	2.31	58.32	838.1
9	C10	1.8	2.7	123.3	8573	0.46	21.8	151.79		46.8	2.68	21.97	481.2
9	CV5	2.7	2.6	162.9	7853	0.44	17.1	146.68		39.7	2.57	13.8	645.3

Ref.#	Sample	Ta	Tb	Th	Ti	Tm	U	V	W	Y	Yb	Zn	Zr
9	C76	3.2	1.9	247.9	9112	0.39	26.7	137.09		31.6	2.38	52.14	979.5
9	CH4	3.0	2.5	252.9	9292	0.32	33.2	148.86		35.4	1.88	67.83	1082.9
9	CH7	2.8	3.1	211.9	8693	0.37	24.8	131.9		29.6	2.19	88.23	809.5
9	C03	3.5	2.4	231.7	9772	0.35	27.8	128.77		37.9	2.12	74.5	621.3
9	CX38	1.6	1.7	138.3	8932	0.31	23.1	140.58		21.3	1.79	17.52	502.1
9	C25	1.7	1.4	149.3	9712	0.28	16.5	131.47		24.6	1.77	14.31	412.7
10	CT09	1.7	1.4	26.4	9112	0.3	5.8	124.1		25.7	1.71	124.7	392.5
10	CT12	1.9	1.3	61.6	9472	0.31	4.9	143.5		28.3	1.76	168.5	517.4
10	CT17	1.8	1.1	21.1	9891	0.29	3.7	162.3		31.7	1.72	152.1	429.7
10	CT05	1.4	1.2	25.3	8633	0.32	5.5	132.8		23.9	1.81	115.2	416.2
10	CT23	1.7	1.2	41.7	10551	0.28	8.4	157.2		33.6	1.64	162.3	468.3
10	QS12	1.4	1.4	28.3	8093	0.36	2.8	157.9		18.3	1.98	182.3	319
10	QS27	2.1	1.7	37.5	8992	0.33	4.2	172.4		31	1.87	127.5	362
10	QS19	1.3	1.5	85.2	8393	0.39	4.3	169.5		28.6	2.12	132.3	417
10	QS23	1.3	1.7	81.8	9472	0.37	6.3	201.7		23.5	2.11	159.3	393
10	QS18	2.8	1.4	42.5	10011	0.35	3.1	179.1		28.7	1.96	141.8	368
10	QS24	1.8	1.3	53.9	10311	0.31	2.4	182.6		31.6	1.76	146.2	401
10	KY03	2.1	1.4	43.7	9832	0.34	3.4	151.8		21.8	2.19	125.8	525
10	KY02	1.3	1.4	51.9	10971	0.37	6.1	122.5		36.2	2.21	167	476
10	KY06	2.0	1.4	65.9	6894	0.34	4.4	180.2		33.4	1.98	219.2	551
10	KY01	2.6	1.6	48.7	8153	0.31	5.5	156.4		26.9	1.77	156.5	382
10	HS041	2.4	1.1	18.6	10071	0.31	5.3	153.1		25.6	1.82	129.6	543.1
10	HS046	1.9	0.9	25	10551	0.28	6.5	117.4		31.9	1.71	96.4	618.5
10	HS047	2.6	1.0	26.2	12649	0.29	3.8	124.3		27.4	1.68	103.8	508.2
10	HS028	1.5	0.9	48.3	9832	0.28	4.2	201.9		24.6	1.67	90.7	317.1
10	AH607	3.2	1.4	15.1	11390	0.32	3.8	162.3		19.4	1.86	117.4	317
10	AH605	2.6	0.8	16.6	14328	0.41	3.7	234.9		23.6	2.63	125	289
10	AH609	3.3	1.6	15.3	11570	0.34	3.9	136.2		21.7	1.78	109.2	351
10	AH602	3.6	1.4	14.8	15047	0.29	3.9	157.8		20.8	1.69	114.3	324
10	AH618	2.7	1.1	15.7	14268	0.33	4.1	215.3		22.4	1.72	105.5	305

Ref.#	Sample	Ta	Tb	Th	Ti	Tm	U	V	W	Y	Yb	Zn	Zr
10	AH615	3.9	1.6	13.9	13009	0.37	3.5	190.6		21.3	1.91	132.6	326
10	YS74	1.4	1.9	31.7	8633	0.35	7.3	168.5		30.5	1.81	138.3	393
10	YS78	1.3	1.7	35.8	8093	0.3	8.8	177.1		35.8	1.69	90.2	416
10	YS05	1.7	1.7	21.4	9472	0.31	11.3	236.2		27.9	1.79	207.9	448
10	YS79	1.6	1.8	23	8153	0.28	6.4	139.5		17.3	1.65	126.6	329
10	YS07	1.0	1.2	36.1	8513	0.23	8.3	128.7		18.4	1.52	119.7	410
10	KX44	2.4	2.1	13.2	11390	0.36	3.3	231.7		28.4	2.19	156.2	536
10	KX51	1.1	0.9	8.2	9232	0.29	4.7	262.3		32.5	1.98	201.3	520
10	KX80	1.3	1.8	10.6	8872	0.31	3.4	251.4		33.6	1.89	208.5	516
10	KX49	2.2	2.0	14.2	11150	0.38	4.6	250.7		31.7	1.92	141.4	472
10	KX62	1.3	1.5	12.9	11450	0.35	5.2	254.5		28.3	1.79	219.8	418
10	PL53	1.0	1.7	17.2	10731	0.32	4.3	158.6		25.6	1.89	126.8	415
10	PL61	1.2	1.7	15.1	10971	0.28	5.4	162.3		27.1	1.66	131.4	482
10	PL3	1.3	1.2	12.8	12889	0.29	3.0	114.3		23.3	1.79	101.2	349
10	PL18	2.1	1.8	21.6	12289	0.32	3.2	116.6		24.8	1.83	105.3	510
10	PL92	2.4	1.5	24.5	11630	0.29	3.2	131.4		27.6	1.78	98.6	534
10	PL43	1.4	1.2	13.9	13069	0.27	3.0	103.7		22.9	1.68	120.5	378
12	07-SA-21	0.3	0.5	9.311	5515	0.15		102		11.365	0.989	84	182.41
12	07-SA-26A	0.3	0.3	4.101	5455	0.048		94		6.989	0.281	77	176.93
12	07-SA-26B	0.3	0.4	4.009	5335	0.075		86		6.772	0.396	81	174.21
12	07-SG-03	0.8	0.5	28.669	4556	0.105		93		10.38	0.724	49	202.76
12	07-SG-04A	0.9	0.6	31.518	4616	0.164		82		10.813	0.822	53	214.92
12	07-SG-05	0.8	0.6	29.059	4736	0.153		98		11.936	0.974	73	183
12	07-SG-06	0.8	0.6	30.025	4796	0.139		86		10.786	0.844	72	198
12	07-SG-29	0.6	0.6	31.928	3537	0.156		71		12.529	0.948	56	210
12	07-SG-30	0.5	0.6	32.577	3477	0.14		59		11.993	0.9	50	220
12	07-SG-31A	0.6	0.6	32.801	3357	0.169		59		11.961	1.05	41	204
12	07-SG-31B	0.6	0.6	33.561	3477	0.19		50		12.873	1.11	43	214
12	07-SG-48A	0.6	0.4	22.096	4376	0.088		64		8.554	0.567	61	186.32
12	07-SG-48B	0.3	0.4	21.817	4496	0.104		70		8.678	0.682	71	178.2

Ref.#	Sample	Ta	Tb	Th	Ti	Tm	U	V	W	Y	Yb	Zn	Zr
12	07-SG-52A	0.6	0.7	32.91	5695	0.225		131		14.143	1.385	78	230
12	07-SG-66	0.3	0.3	9.942	3177	0.077		70		6.368	0.419	75	148
12	06-SA-28C	0.4	0.4	4.86	5515	0.132		125		10.5	0.924	86	151
12	06-SA-48A	0.4	0.3	3.51	5275	0.069		82		6.3	0.423	80	153
12	06-SG-200	1.0	0.6	35.142	5156	0.149		93		12.472	0.9	64	223
12	06-SG-201	0.8	0.6	31.021	4676	0.174		95		13.458	1.061	61	207.24
13	NQ2-1*	1.2	1.9	19	4496	0.35	5.0			34	2.1		340
13	NQ21-4*	1.4	1.0	34	3177	0.31	5.1			26	1.9		449
13	NQ7-1*	0.7	0.6	15	2458	0.2	5.1			16	1.3		175
13	Y1-11	0.8	0.6	21	2338	0.19	6.2			13	1.1		242
13	Y1-12	0.8	0.7	23	2398	0.2	3.9			13	1.1		254
13	Y1-13	0.8	0.6	22	2218	0.18	5.1			12	1		238
13	Y1-14	0.9	0.6	24	2218	0.2	5.8			13	1.1		297
13	Y1-15	0.9	0.6	22	2338	0.2	5.4			13	1.1		248
13	Y115-90				3117								
13	Y1-16	0.8	0.2	15	2218	0.1	3.6			5.1	0.53		270
13	Y1-18	0.8	0.4	22	2218	0.14	6.7			8.9	0.8		249
13	Y1-8	0.9	0.7	24	2398	0.24	4.6			16	1.4		297
13	Y1-9	0.8	0.6	25	2338	0.2	5.5			14	1.2		371
13	Y2-1	0.8	0.5	22	2218	0.18	5.8			12	1.1		254
13	Y2-2	0.9	0.6	22	2458	0.19	7.1			12	1.1		297
13	Y2-3	0.8	0.5	20	2038	0.17	7.0			11	1		347
13	Y2-4	0.9	0.5	20	2098	0.17	7.4			11	0.97		313
13	Y2-5	0.8	0.5	22	2038	0.17	7.1			11	1		322
13	Y2-6	0.9	0.5	21	2338	0.1	7.1			12	1		343
13	Y2-7	0.8	0.5	20	2038	0.16	6.3			11	0.93		289
13	Y2-8	0.8	0.5	21	1978	0.17	5.6			11	0.94		244
13	Y2-9	1.0	0.5	21	2038	0.17	6.9			11	0.95		264
13	Z96-2*	1.1	1.0	23	2997	0.26	7.6			22	1.8		209
14	KK06003	2.2	1.2	33.1	9532	0.28	5.3			21.7	1.65		482

Ref.#	Sample	Ta	Tb	Th	Ti	Tm	U	V	W	Y	Yb	Zn	Zr
14	KK06004	2.1	1.1	30.4	9472	0.25	4.9			20.1	1.48		473
14	KK06005	2.0	1.1	30.2	9472	0.25	4.8			20.3	1.48		455
14	KK06006	2.2	1.1	31.8	9472	0.26	5.2			20.9	1.57		479
14	KK06007	2.2	1.1	36.4	8812	0.27	6.1			20.3	1.57		471
14	KK06008	2.1	1.2	33.4	9652	0.27	5.3			21.5	1.66		489
14	KK06009	2.1	1.2	33.7	9772	0.28	5.4			21.7	1.71		497
14	KK06010	2.2	1.2	33.8	9652	0.28	5.7			20.9	1.65		508
14	KK06011	2.2	1.2	34.6	9772	0.28	5.6			21.6	1.7		514
14	KK06012	2.2	1.2	33.2	9652	0.27	5.3			21.3	1.62		496
14	KK06013	1.6	0.8	51.5	6534	0.22	6.0			16.6	1.4		393
14	KK06014	1.6	0.9	50.8	6474	0.23	5.9			17	1.4		403
14	KK06016	1.6	0.8	50.5	6534	0.22	6.7			16.3	1.39		400
14	KK06018	1.6	0.8	49.9	6714	0.21	5.7			15.9	1.3		387
14	KK06019	1.5	0.9	49.6	6474	0.24	6.0			17.5	1.54		390
14	KK06022	1.6	0.9	49.3	6654	0.24	5.9			17.5	1.49		392
14	KK06024	1.6	0.9	51.1	6894	0.23	7.2			17.2	1.43		401
14	KK06025	2.6	1.4	20.8	11090	0.32	3.9			26	1.88		472
14	KK06026	2.6	1.4	20.8	11150	0.32	4.1			25.3	1.94		469
14	KK06027	2.4	1.2	29.2	10491	0.29	4.4			23.1	1.72		517
14	KK06028	2.4	1.3	28.9	10431	0.31	4.5			25	1.96		522
14	KK06029	2.3	1.3	29.9	10611	0.3	4.5			24	1.82		527
14	KK06030	2.4	1.2	27.4	10491	0.3	4.4			23.8	1.88		529
14	KK06031	2.3	1.3	28.1	10611	0.29	4.3			24	1.81		508
14	KK06032	1.5	0.5	48.2	2338	0.12	16.0			9.06	0.77		197
14	KK06033	1.5	0.5	49.9	2278	0.11	8.4			8.25	0.7		183
14	KK06034	1.4	0.6	48.5	2278	0.12	16.2			9.15	0.8		185
14	KK06038	2.1	1.2	36.9	7613	0.28	6.1			22.3	1.72		425
14	KK06039	2.5	1.3	37.3	8333	0.31	5.4			25.3	1.82		495
14	KK06040	2.6	1.4	38.3	8812	0.32	7.0			25.4	1.88		532
14	KK06041	3.0	1.4	30.5	10191	0.33	5.1			25.6	1.85		517

Ref.#	Sample	Ta	Tb	Th	Ti	Tm	U	V	W	Y	Yb	Zn	Zr
14	KK06042	2.4	1.2	38.7	8633	0.29	6.2			22.7	1.7		499
14	KK06043	2.9	1.5	31.9	10611	0.32	5.3			25.9	1.9		553
14	KK06046	2.5	1.2	36.6	8513	0.27	6.8			21.4	1.59		483
14	KK06047	2.4	1.2	40.8	8033	0.25	6.2			20.9	1.49		456
15	Z02H1	0.7	0.6	22.6	4196	0.2	4.7			15.2	1.22		233
15	Z07H	0.6	0.4	11.4	2578	0.24	4.5			14.9	1.48		134
15	Z07H1	0.6	0.7	22.7	4316	0.23	4.4			17.4	1.37		204
15	Z07H2	0.6	0.7	22.7	4256	0.23	4.4			17.1	1.35		205
15	Z07H3	0.5	0.6	21.4	3537	0.23	4.4			16.1	1.43		189
15	Z07H4	0.6	0.7	22.5	4256	0.23	4.4			17.7	1.39		206
15	Z07H5	0.6	0.6	22.9	3897	0.22	4.6			16.5	1.38		200
15	Z07H6	0.6	0.6	22.3	3897	0.21	4.3			15.9	1.29		196
15	Z08H1	0.6	0.7	24	4136	0.24	4.6			17.7	1.43		204
15	Z08H2	0.6	0.6	23	4017	0.18	3.8			13.3	1.08		200
15	Z08H3	0.6	0.7	24.7	4196	0.22	4.7			16.7	1.34		211
15	Z08H4	0.6	0.7	25.5	4316	0.21	4.4			16.4	1.25		216
15	Z08H6	0.6	0.7	24.5	4076	0.22	4.6			19.1	1.32		207
15	Z12H3	0.6	0.6	16.8	4316	0.22	4.4			16	1.34		177
15	Z15H1	0.6	0.6	19.2	3177	0.25	5.0			17.7	1.51		153
15	Z15H2	0.6	0.6	18.7	3177	0.23	5.0			16.4	1.41		154
15	Z15H3	0.6	0.6	19.1	3297	0.24	5.1			17.3	1.47		160
15	Z15H5	0.6	0.4	15.2	2698	0.15	3.0			10.6	0.92		146
15	Z15H6	0.6	0.4	15.2	2638	0.17	5.1			12	1.03		152
15	Z19H1	0.6	0.5	15.9	2878	0.19	5.3			13.6	1.14		160
15	Z19H4	0.6	0.4	15	2398	0.15	5.4			11	0.93		137
15	Z19H5	0.5	0.4	14.9	2398	0.15	5.4			11	0.93		138
15	Z19H6	0.6	0.4	14.9	2338	0.15	5.4			11.1	0.94		144
15	Z06H	0.6	0.7	27.3	4556	0.24	3.7			17.2	1.41		213
15	Z08H5	0.6	0.7	25.9	4316	0.22	4.4			16.8	1.28		217
15	Z10H	0.7	0.6	19.1	4796	0.18	4.5			13.9	1.05		190

Ref.#	Sample	Ta	Tb	Th	Ti	Tm	U	V	W	Y	Yb	Zn	Zr
15	Z11H1	0.6	0.6	18.9	4856	0.19	4.2			14.4	1.13		191
15	Z11H2	0.6	0.6	18	4676	0.21	3.8			16	1.23		189
15	Z12H1	0.6	0.6	17	4376	0.24	3.8			17.1	1.5		179
15	Z12H2	0.6	0.6	17.7	4676	0.2	3.1			14.6	1.1		184
15	Z15H7	0.6	0.4	11	2458	0.15	4.7			10.1	0.92		129
15	Z15H11	2.3	1.2	33.9	10311	0.27	4.1			24.1	1.47		629
16	ET021B	0.2	0.5	1.1	4556	0.23	0.37			15	1.47		41.9
16	ET021C	0.5	0.6	0.43	4676	0.3	1.5			20.6	1.97		20.9
16	ET022A	0.5	0.3	7.8	1858	0.21	2.0			12.7	1.45		59
16	ET024	0.6	0.3	8.9	1379	0.2	2.0			13.2	1.42		50.4
16	ST052B	1.6	1.0	44.1	3177	0.43	6.9			31.3	2.8		288
16	ST053	1.5	1.1	38.8	3777	0.42	7.4			31.1	2.7		246
16	ST054	1.5	1.1	41.2	3657	0.42	5.7			32	2.68		127
16	ST055A	1.9	1.2	54.6	2698	0.5	9.7			36.4	3.26		301
16	ST055B	1.7	1.1	45.5	3177	0.46	8.2			32.9	2.97		274
16	ST055C	0.6	1.0	10.1	5515	0.38	2.1			29	2.37		139
16	ST057A	1.0	1.0	27.3	4796	0.38	4.8			28.5	2.43		250
16	ST058	1.5	1.0	37.6	4256	0.39	5.2			29.5	2.54		167
16	ST059A	1.4	1.1	21	3777	0.46	2.3			31.9	2.89		160
16	ST060A	1.7	1.1	48.1	2878	0.47	7.4			34.4	3.04		208
16	ST060C	1.9	1.3	54.5	2818	0.54	8.2			39.7	3.56		254
16	ST061A	1.3	1.4	32.7	6175	0.59	3.7			40.6	3.7		183
16	ST062	2.6	1.3	92	3597	0.55	8.9			40.5	3.52		42.6
16	ST101B	0.3	0.5	4.2	4976	0.22	0.92			14.7	1.39		105
16	ST102B	0.2	0.5	3.5	4556	0.28	0.92			18.3	1.79		87.7
16	ST109	0.5	0.4	8.3	2758	0.17	1.5			11.3	1.11		67.5
16	ST119A	0.4	0.8	1.1	9712	0.4	0.41			26.9	2.53		152
16	ST119B	0.7	1.4	3	10791	0.67	0.96			45.8	4.23		312
16	ST121	0.6	1.3	2.5	10071	0.59	0.76			40.7	3.76		263
16	ST122	0.4	0.8	1.7	8333	0.37	0.51			24.6	2.41		184

Ref.#	Sample	Ta	Tb	Th	Ti	Tm	U	V	W	Y	Yb	Zn	Zr
16	T006B1	0.5	0.6	0.79	5575	0.26	1.1			19.1	1.7		140
16	T006B2	0.7	0.8	1.2	7613	0.36	0.4			25.2	2.33		33.3
16	T034A	0.1	0.5	1.4	3117	0.24	0.4			15.5	1.63		75.4
16	T034B	0.1	0.5	1.2	2997	0.24	0.4			16	1.54		57.1
16	T036D	0.1	0.5	1.5	5635	0.21	0.2			14.7	1.37		12.1
16	T038F	1.1	0.9	0.66	4376	0.41	2.5			28.9	2.71		148
16	T038G	1.0	0.9	0.48	6295	0.44	3.7			33.8	2.93		170
16	T038M	1.8	0.5	1.9	1439	0.34	5.7			17.1	2.43		20.8
16	T039	1.1	0.7	17.3	1739	0.37	2.8			26.1	2.46		73
16	T040A	0.7	0.7	0.88	4556	0.33	2.5			24.8	2.15		127
16	T040B	0.7	0.8	0.54	3957	0.36	2.1			28.7	2.36		63
16	T041J	0.1	0.5	13	5695	0.22	0.1			15.6	1.45		28.5
16	T041F	0.1	0.5	8.3	5216	0.21	0.1			15.4	1.38		31.9
16	T041H	0.1	0.5	1.5	5515	0.22	0.2			16.3	1.36		14.6
16	T042C	0.9	1.2	4.1	7494	0.6	0.8			40.1	3.76		222
16	T042D	0.6	0.6	1.1	5395	0.24	0.6			18.2	1.53		53.7
16	T046A	0.4	0.7	3.4	5635	0.32	1.0			23.9	2.04		113
16	T047	0.6	0.9	0.57	7434	0.35	1.0			26.1	2.24		89.5
16	T048B	0.6	0.7	0.61	4856	0.31	2.2			22.2	2.03		186
16	T049A	0.9	0.7	0.52	2338	0.33	2.3			22.2	2.21		99.1
16	T049B	0.5	0.6	0.65	5275	0.23	2.1			16.5	1.52		151
16	T049C	0.5	0.6	0.51	5635	0.26	2.2			18.3	1.67		160
16	T051B	1.0	0.6	0.62	2278	0.25	1.2			17.8	1.62		45.9
16	T051C	1.1	0.5	0.53	959	0.3	5.2			17.3	2.18		112
16	T052	1.0	0.7	0.22	2578	0.34	3.2			23.5	2.28		52.1
16	T054A	0.3	0.9	1.2	7254	0.4	0.7			27.7	2.61		108
16	T055A	0.5	0.7	0.53	5575	0.33	0.6			24.1	2.16		135
16	T055B	0.3	0.9	0.67	7554	0.44	0.8			30.4	2.84		118
16	T056A	0.3	0.5	2	6414	0.27	0.5			18.8	1.82		106
16	T056B	0.3	0.6	0.79	5216	0.35	0.5			22.5	2.36		120

Ref.#	Sample	Ta	Tb	Th	Ti	Tm	U	V	W	Y	Yb	Zn	Zr
16	T062B	0.7	0.9	10.8	5455	0.44	2.5			31.2	2.86		195
16	T062C	0.3	0.6	4.1	6235	0.28	1.1			20.7	1.78		111
16	T063	0.5	0.7	7.4	4076	0.27	1.7			21.1	1.75		105
16	T064A	0.5	0.5	8.1	3957	0.24	2.2			17.3	1.57		85.4
16	T065A	1.0	0.8	15.4	3057	0.36	2.0			26.2	2.26		72.8
16	T065B	1.1	0.8	21.1	1739	0.43	2.2			29.6	2.89		78.6
16	T066	0.6	0.9	11.4	7673	0.43	2.8			31.6	2.73		170
16	T068	0.9	0.7	20.7	1559	0.41	2.7			26.7	2.77		67.2
16	T070A	0.6	0.7	10.7	2638	0.37	2.2			25.8	2.45		158
16	T072A	1.1	0.9	26.8	4916	0.43	3.9			29.3	2.77		226
16	T072D	0.9	0.8	20.6	4496	0.37	3.6			26	2.35		162
16	T072E	0.9	0.8	21	4496	0.36	3.6			24.5	2.3		165
16	T073	0.9	0.8	22.4	4556	0.35	3.3			24.8	2.28		163
16	T078B	0.5	0.3	6.6	2098	0.11	2.4			8.2	0.77		131
16	T079A	0.3	0.7	2.8	8812	0.28	0.61			20.3	1.73		45.4
16	T079B	0.3	0.8	6.6	6774	0.35	1.4			24.2	2.24		96.5
16	T079C	0.3	0.8	6.1	6175	0.38	0.9			26.9	2.49		97.9
16	T080	0.2	0.7	2.5	6594	0.31	0.75			21.7	1.88		60.8
16	T082A	0.6	0.4	14	1079	0.21	2.4			14	1.45		44.3
16	T082B	0.6	0.4	13.4	1379	0.22	3.6			14.6	1.54		46.7
16	T083B	0.8	0.7	20.4	779	0.38	2.5			25.5	2.53		70.4
16	T083C	0.3	0.9	5.9	7673	0.42	2.5			30.3	2.64		35.8
16	T084C	1.0	0.9	25	2578	0.46	5.2			32.4	3		148
16	T102A	0.7	0.9	12.7	3897	0.45	1.8			33.4	2.94		26.3
16	T103	0.7	1.4	16.3	1319	0.53	1.7			42	3.26		94.9
16	T104	1.0	0.9	19.8	1739	0.46	2.9			32.3	2.96		105
16	T105A	0.7	1.3	12.9	7134	0.61	3.4			43.9	3.86		315
16	T110A	1.2	1.0	22.7	4136	0.43	2.2			31.1	2.65		121
16	T110B	1.1	0.9	17	3597	0.41	2.0			29.1	2.61		125
16	T111	0.8	0.5	13.3	1559	0.22	1.3			15.2	1.41		46.6

Ref.#	Sample	Ta	Tb	Th	Ti	Tm	U	V	W	Y	Yb	Zn	Zr
16	T112	1.2	1.3	20.8	4496	0.56	2.7			37.7	3.43		143
16	T113	1.1	1.3	22.6	3897	0.57	3.0			39.1	3.65		141
16	T116A	0.5	0.9	0.93	11570	0.44	0.8			32.2	2.82		60.1
16	T117	0.6	0.6	9.9	2038	0.29	1.5			20.1	1.92		140
16	T127B	0.6	0.5	9.8	2997	0.21	2.0			15.4	1.35		127
16	T129A	0.5	0.7	7.6	5995	0.39	1.5			26.7	2.59		101
16	T130	1.4	0.8	18.3	599	0.63	2.4			36.2	4.22		120
16	T131A	0.8	1.0	17.8	1978	0.47	1.8			38.6	2.98		100
16	T134	1.3	1.7	26	1679	0.83	3.1			56.7	5.23		164
16	T136A	1.6	2.1	28.1	779	0.84	3.5			53.9	5.58		155
16	T136B	1.6	17.6	25	4196	2.42	5.8			415	12.3		199
16	T138D	0.3	0.2	2.7	1079	0.05	1.0			4.4	0.27		25
16	T139	1.0	0.7	26.2	480	0.31	3.3			16.4	2.07		84.2
16	T140A	0.8	0.8	13.8	2278	0.45	2.5			29.7	2.94		194
16	T140B	0.6	0.9	9	6295	0.38	0.9			27.1	2.4		211
16	T140D	0.7	0.8	12.9	3057	0.41	2.3			27.3	2.73		151
16	T140E	1.1	1.2	25.7	420	0.66	3.6			48.5	4.3		74.2
16	T142	0.7	0.9	15.1	2638	0.47	2.5			31.6	3.12		85.4
16	T143	0.9	0.9	16.4	2458	0.51	2.7			33	3.34		91.9
16	T144A	0.8	1.8	14.7	1559	0.89	2.6			54.4	5.5		170
16	T144B	0.5	1.0	7.7	4256	0.49	1.3			34.9	3.19		160
16	T144C	1.5	0.6	27.5	719	0.45	5.0			24.3	3.25		83.7
16	T144D	0.6	0.7	16.8	1918	0.36	2.2			23.1	2.39		82.9
16	T146	0.9	0.9	9.8	3117	0.54	2.7			28.8	3.53		237
16	T147	1.1	1.2	20.6	1019	0.66	2.9			43.7	4.4		122
16	T151	0.7	1.0	4.6	7733	0.42	0.8			31.1	2.64		219
16	T152A	1.0	1.1	11.8	5875	0.47	2.1			32.7	2.97		349
16	T152B	0.4	0.7	2.6	5875	0.3	0.5			20.7	1.89		99.1
16	T155	1.2	1.0	24.1	2638	0.41	2.9			28.6	2.71		87.7
16	T160A	1.0	1.0	9.8	4976	0.47	3.1			29.8	2.99		195

Ref.#	Sample	Ta	Tb	Th	Ti	Tm	U	V	W	Y	Yb	Zn	Zr
16	T160B	1.4	1.5	21.8	480	0.81	3.1			49	5.28		85.7
16	T169A	1.8	1.2	36.1	959	0.66	7.7			43.1	4.37		164
16	T169B	1.8	3.5	34	959	0.82	4.5			78.6	4.84		166
16	T169C	0.8	0.7	9.3	2997	0.32	2.0			25.9	2.05		119
16	T233A	0.3	0.4	4.7	2818	0.19	1.4			13	1.31		84.5
16	T233B	0.5	0.7	7.7	4436	0.35	2.2			23.6	2.3		126
16	T233C	0.5	1.2	10.3	6175	0.39	2.0			32.4	2.37		119
16	T234A	0.5	0.9	13.3	4076	0.31	2.8			24.3	1.99		168
16	T234B	0.5	1.0	11.3	4976	0.31	2.4			25.6	2.01		158
16	T234C	0.6	0.7	16	3297	0.25	3.4			19.7	1.52		174
16	T235A	0.8	1.1	15.4	719	0.44	3.7			35.2	2.94		141
16	T235B	0.7	0.9	14.3	719	0.41	3.3			31.4	2.77		106
16	T238B	0.3	0.7	4.8	5455	0.37	1.2			25.7	2.34		161
16	T239	0.5	0.6	7.3	5395	0.34	1.7			23.2	2.09		188
16	T240B	0.6	0.7	7.9	5036	0.38	1.8			26.6	2.4		199
17	GGL01	1.2	0.9	14.23	4856	0.36	11.0			22	2.18		216.7
17	GGL02	1.4	1.1	14.05	7134	0.49	2.2			32.7	3.06		279.7
17	GGL03	1.4	1.1	13.76	7254	0.415	2.2			26.8	2.653		275.1
17	GGL04	1.4	1.2	14.54	7494	0.549	2.0			35.07	3.453		278.9
17	GGL05	1.3	1.1	11.46	8273	0.447	2.0			27.84	2.936		240.7
17	GGL06	1.2	1.0	10.49	8333	0.433	1.7			30.66	2.803		236.9
17	GGL07	1.2	1.0	11.09	8213	0.453	1.9			30.92	2.784		239.5
17	GGL08	1.1	1.0	10.2	8033	0.426	1.6			27.31	2.623		226.3
17	GGL09	1.3	1.0	11.67	7913	0.45	2.0			30.09	2.869		258.1
17	GGL10	1.3	1.1	12.49	8033	0.475	2.1			29.45	2.954		245.8
17	GGL11	1.2	1.0	11.65	8213	0.441	1.8			28.73	2.777		250
17	GGL12	1.2	1.1	11.31	7973	0.447	1.9			29.9	2.818		249.5
17	GGL13	1.3	1.1	12.53	7913	0.479	2.0			28.29	2.991		250
17	GGL14	1.3	1.1	12.66	8033	0.474	2.2			30.11	3.03		254.5
17	GGL15	1.3	1.0	11.8	8513	0.389	1.6			26.48	2.535		258.4

Ref.#	Sample	Ta	Tb	Th	Ti	Tm	U	V	W	Y	Yb	Zn	Zr
18	GJ0601	3.6	0.9	58.9		0.19	12.0	83.6		16.7	1.23	83.8	563
18	GJ0602	3.4	0.9	57.2		0.22	12.4	76.2		17.8	1.39	68.9	562
18	GJ0605	3.5	0.9	58.9		0.23	13.3	76.8		18.5	1.43	77.4	603
18	GJ0606	3.5	0.9	59.5		0.22	13.6	69.4		17.8	1.4	67.1	570
18	08YR04	2.1	0.6	44.5		0.15	10.8	59.4		11.7	0.84	68.5	377
18	GJ0614	1.1	0.7	39.9		0.18	5.1	51.5		16.5	1.21	44.9	267
18	GJ0617	1.1	0.8	39.8		0.26	8.3	62.6		18.8	1.68	68.8	268
18	GJ0619	1.1	0.8	40		0.26	8.2	60.1		18.9	1.65	69.5	268
18	GJ0620	1.0	0.8	38.5		0.27	7.5	58		20.3	1.69	52	286
18	GJ0624	2.0	0.6	55.2		0.17	14.1	50.4		12	1.06	63.5	271
18	GJ0627	2.0	0.6	57.8		0.17	13.3	53.1		12.5	1.12	61.1	256
18	GJ0628	3.0	0.9	85.9		0.25	22.3	75.5		18.7	1.63	93.4	398
18	GJ0629	1.9	0.6	51.9		0.15	12.4	51.2		12	0.98	60.5	228
18	10XB03	0.9	0.9	40.4		0.24	8.8	51.5		18.5	1.4	84.8	266
18	10XB04	0.8	0.9	42.9		0.19	7.4	54.1		16.4	1.19	80.5	269
18	10XB07	0.7	0.8	41.9		0.19	8.6	60.2		15	1.14	84	266
18	08YR05	1.3	1.1	135		0.29	17.9	131		22.7	1.76	75.9	390
18	10XB10	2.0	1.4	116		0.27	17.8	112		24.9	1.59	66.9	496
18	10XB12	2.2	1.6	127		0.29	16.0	109		27.3	1.7	75.1	508
18	10XB13	2.2	1.5	123		0.28	16.8	110		26.6	1.69	74.3	513
18	10YR01	1.4	1.2	140		0.29	21.1	139		24.3	1.7	84.3	433
18	10YR02	1.3	1.1	122		0.28	16.8	131		22.6	1.6	81	392
18	10YR04	1.3	1.1	131		0.26	17.5	130		21.7	1.53	77.9	405
18	10YR04a	1.3	1.1	131		0.24	17.4	126		21.3	1.5	75.4	395
18	10YR07	1.3	1.1	131		0.26	17.4	127		21.4	1.56	78.9	407
19	MV1B	7.8	0.3	22.7	1499		26.0			25	0.49		78
19	MV2	8.1	0.3	22.9	1319		26.0			25	0.5		87
19	UM1B	8.2	0.3	23.5	1259		18.0			26	0.48		81
19	UM3V	7.6	0.3	23.9	1439		17.0			27	0.53		83
19	UMQP	7.9	0.4	23.4	1379		16.0			27	0.5		86

Ref.#	Sample	Ta	Tb	Th	Ti	Tm	U	V	W	Y	Yb	Zn	Zr
19	UMVU	11.2	0.4	23.2	1439		12.0			44	0.35		77
20	TE008/93	1.8	1.7	114	5156	0.23	23.0	107		25	1.6	68	446
20	TE011/93	1.8	1.7	136	6055	0.26	27.0	111		25	1.4	76	418
20	TE125/93	2.8	1.5	114	7913	0.33	25.0	133		27	2	87	511
20	TE126/93	2.5	1.5	192	8033	0.23	20.0	128		24	1.3	74	635
20	TE127/93	2.7	1.7	188	8213	0.26	21.0	130		24	1.4	77	609
20	TE131/93	2.8	1.5	160	7733	0.23	22.0	109		26	1.3	56	589
20	TE137/93	1.3	1.8	169	5455	0.31	22.0	115		30	2.1	72	392
20	TE138/93	1.3	1.7	157	5216	0.29	20.0	109		28	1.9	75	387
20	TE117/93	1.6	1.6	165	6055	0.26	23.0	120		27	1.7	62	461
20	TE118/93	1.6	1.5	186	6175	0.28	26.0	128		28	1.6	80	454
20	TE007/93			106	4316			83		18		59	285
20	TE025/93		0.7	47	3537	0.13		76		14	1	67	412
20	TE136/93	1.4	0.9	104	3777	0.19	17.0	67		17	1.4	65	316
20	TE148/93	1.4	0.7	35	3717	0.15	9.0	52		14	1	78	358
20	TE150/93	1.4	0.8	39	3537	0.18	11.0	49		17	1.2	78	364
20	TE153/93	1.4	0.7	34	3657	0.14	10.0	63		11	0.8	76	370
20	TE154/93	1.3	0.7	45	3537	0.19	7.0	74		13	1.3	72	373
20	TE047/93	0.8	0.3	18	1858	0.11	21.0	36		8	0.8	28	117
20	TE189/93	0.8	0.5	10	4136	0.15	3.0	94		12	0.9	39	175
20	TE192/93		0.4	9	3537	0.13	10.0	57		12	0.8	48	123
20	TE194/94		0.5	12	3537	0.15	10.0	68		14	1.1	67	128
21	Y-2	1.1	1.2	63	4796		11.0	88		24	1.6		419
21	Y-4	0.8	0.7	49	2698		7.0	48		15	1		255
21	ZB1	1.8	1.2	56	7434		15.0	113		26	1.7		298
21	ZB4	2.0	1.3	64	7494		15.0	124		28	1.9		335
21	ZB10	1.9	1.3	59	7374		16.0	125		28	1.9		334
21	ZB12	2.8	1.3	94	7494		21.0	112		29	1.9		424
22	K732		1.1	31	13668		5.0			28	2.13		504
22	K738		1.0	23	13908		3.0			26	1.9		433

Ref.#	Sample	Ta	Tb	Th	Ti	Tm	U	V	W	Y	Yb	Zn	Zr
22	K89G185		1.0	22	11090		3.0			25	1.75		433
22	K89G200		0.9	9	8573		0.0			25	1.88		328
22	K9007		1.1	33	9232		5.0			26	1.95		507
22	K9008		10.5	32	9712		6.0			27	2.11		514
22	K9021		1.3	27	9412		2.8			32	1.5		411
22	K9024		1.0	44	9472		6.8			23	1.4		407
22	K9031		0.8	33	9292		3.0			32	1.2		55
22	K9038		1.2	27	9532		2.0			28	1.3		461
23	Bb-105	1.6	1.3	27	2458		3.0			32	1.5		412
23	Bb-107			24	7434					17	1.5		358
23	Bb-109			48	2098					21	1.6		230
23	Bb-114			49	10311					24	1.8		318
23	Bb-88	2.3	0.9	50	7793					23	1.6		368
23	Bb-89			66	11690		98.0			9	1.3		27
23	Bb94-2	1.5	1.0	44	3357		7.0			23	1.4		407
23	Bb-95		2.1		5575						2.4		488
23	Bg121				8992					13	0.8		
23	Bg124				7554					16	1.1		
23	COUL311				1619					18	1.3		
23	COUL326				2758					17	1.1		
23	COUL328				3537					18	1.1		
23	COUL338				6115					18	1.3		
23	COUL339				6295					18	1.3		
23	k705			27	11210					28	1.3		461
23	k708			33	11090					32	1.2		550
23	K713		1.0		13608						1.3		
23	K716				13369						1.4		
23	K718				12709						1.4		
23	K720		1.5		13369						3.2		
23	K723		1.4		13369						1.8		

Ref.#	Sample	Ta	Tb	Th	Ti	Tm	U	V	W	Y	Yb	Zn	Zr
23	K732	2.3	1.4	9	13668						1		348
23	K738	1.5	1.5	18	13908						1.9		399
23	K89G159		2.0		4436						2.7		
23	K89G162	4.9	2.6	67	4856						2.5		985
23	K89G163	2.5		80	4616						3		695
23	K89G185	1.8	1.9	114	11090						2.5		587
23	K89G186	1.9		216	10611						5.1		1828
23	K89G191	1.3	2.5	89	8153						2.3		443
23	K89G192	5.1	1.7	267	7913						5.3		
23	K89G193	1.9		76	7853						2.1		509
23	K89G197	2.6	1.7	145	599						3.6		1360
23	K89G200			32	8573		5.0			26			509
23	K9002	2.5	1.1	31	3777		6.0			28	2.1		604
23	K9006	2.6	1.1	33	9592		5.0			26	2		507
23	K9007			34	9232		8.0			26			469
23	K9008			31	9712		6.0			27			501
23	K9016	2.5	1.1	32	8812		6.0			27	2.1		514
23	K9017			23	9352		2.0			26			460
23	K9018	2.2	1.0	21	9532		1.0			26	1.8		411
23	K9019	2.2	1.0	22	9772		3.0			25	1.8		433
23	K9021			23	9412					28			445
23	K9024	2.2	0.9	9	10071					25	1.9		328
23	K9026			13	10131					27			338
23	K9027	2.4	1.0	23	10071		3.0			26	1.9		433
23	K9028	2.3	1.0	23	9172		1.0			27	2		452
23	K9029			21	9772		3.0			24			436
23	K9031			9	9292		1.0			24			215
23	K9032			32	9772		6.0			26			499
23	K9038			30	9532		4.0			26			495
23	K9039				10251						3		187

Ref.#	Sample	Ta	Tb	Th	Ti	Tm	U	V	W	Y	Yb	Zn	Zr
23	Kp35-10				11270						0.6		149
23	Kp12-58				10491						0.9		141
23	Kp23-2				14028						1		122
23	Kp24-1				11390						1.6		116
23	Kp39-3	1.4	0.7	107	11330		8.0			16	1.2		422
23	Kp47-2	1.6	0.7	116	9292		8.0			16	1		426
23	Kp47-5	1.4	0.6	106	9412		11.0			14	1.1		400
24	2303				2338								
24	2509				1379								
24	1P2JD7-1				719								
24	1P2JD7-1a				659								
24	2011a				659								
24	2059a				1319								
24	2303a				2218								
24	2511-1				2578								
25	04wq-1	0.7	1.4	23.9		0.343	4.8	162		29.8	2		315
25	04wq-2	0.7	1.3	22.9		0.334	4.5	148		28.4	1.93		293
25	04wq-3	0.7	1.6	23.9		0.35	4.7	160		31.6	2.03		308
25	04wq-4	0.7	1.4	24.1		0.339	4.7	158		29.2	2.03		304
25	04wq-5	0.7	1.6	25		0.336	5.0	165		31.2	2.13		309
25	04wq-6	1.0	0.9	23.8		0.276	5.3	144		22.1	1.69		289
25	04wq-7	0.9	0.9	23.9		0.275	5.5	143		22.6	1.67		296
25	4086-1	0.9	0.9	23.6		0.278	5.2	145.8		22.3	1.67		287
25	8528	0.7	0.8	14.1		0.31	3.4	154.6		20.7	1.91		295
25	8518-1	0.6	0.6	16.1		0.229	3.7	95.72		17.8	1.38		247
25	8518-2	0.6	0.6	15.8		0.217	3.7	96.77		17.1	1.33		243
25	9063-GS2	0.5	0.6	14.2		0.213	3.5	125		15.1	1.43		208
25	9063-GS3	0.5	0.5	14.2		0.183	3.5	122		12.2	1.18		196
25	D3145	2.5	1.3	109		0.36	14.6	70.6		29.1	2.41		565
26	05S2-7	2.1	1.2	232		0.23	34.4	111		21.7	1.53		722

Ref.#	Sample	Ta	Tb	Th	Ti	Tm	U	V	W	Y	Yb	Zn	Zr
26	05S2-8-1	2.0	1.3	240		0.25	37.4	104		24.3	1.6		717
26	05SLP5-3	1.8	1.5	188		0.29	28.6	90.2		29.9	1.89		717
26	05SLP5-05	1.6	1.2	160		0.26	22.0	121		22.6	1.67		603
26	05SLP5-06	1.8	1.0	153		0.24	20.6	109		20.7	1.5		603
26	05SLP5-7	1.7	1.1	178		0.23	23.5	132		21.7	1.52		651
26	05SLP5-8	1.5	0.9	150		0.23	21.7	113		19.6	1.48		589
26	05SLP5-09	1.8	1.5	184		0.27	24.6	100		27.8	1.77		746
26	S05SLP5-10	1.6	1.1	138		0.23	16.7	116		21.6	1.49		509
26	05SLP5-11	1.6	0.8	126		0.18	19.2	111		16.3	1.18		593
26	05SLP5-16	2.2	1.2	169		0.28	20.2	159		24.8	1.71		633
26	05SLP4-01	1.1	3.8	136		0.41	12.4	188		55.1	2.6		501
26	05SLP4-02	1.8	2.0	151		0.29	12.8	164		32.8	1.88		734
26	05SLP4-03	1.5	2.7	55.9		0.33	11.3	158		34.1	2.13		657
26	05SLP4-04	1.8	2.0	143		0.28	12.6	159		33.1	1.88		745
26	05S2-7			232			34.4						
26	05S2-8-1			240			37.4						
27	WR-12-48	1.6	1.0	44.1		0.512	6.9	72		33	3.45		554
27	WR-12-47	1.8	1.2	27.9		0.703	4.0			48	4.64		66
27	WR-12-44	0.3	0.2	3.68		0.116	1.2	63		7	0.85		257
27	WR-12-45	0.3	0.7	1.82		0.339	0.7	293		21	2.17		103
27	WR-12-40	0.5	0.4	8.67		0.242	2.5	84		14	1.72		251
27	WR-12-42	0.2	0.6	1.9		0.299	0.5	269		20	1.87		101
27	WR-12-33	0.7	0.5	20.1		0.237	3.9	113		16	1.57		135
27	WR-12-35	0.9	1.0	8.68		0.481	3.2	186		32	3.14		158
28	T2A/98	1.0	2.1	117.98	5755	0.35	13.6			36.34	2.15		323.33
28	T3b/98	1.3	1.5	68.32	6295	0.42	10.4			35.82	2.55		367.91
28	T4A/98	1.3	1.5	146.91	5995	0.27	21.3			26.98	1.64		484.50
28	T5A/98	0.8	0.9	79.29	4094	0.27	13.9			22.31	1.62		253.46
28	T11B/98	0.4	0.4	9.37	4376	0.10	2.0			8.82	0.61		139.34
28	JPT14.2	0.4	0.4	9.20	4616	0.11	2.0			9.17	0.65		130.45

Ref.#	Sample	Ta	Tb	Th	Ti	Tm	U	V	W	Y	Yb	Zn	Zr
29	JPT24A	1.4	0.9	54	4796	0.3	11.3			21.6	1.7		263.3
29	JPT24B	1.9	1.3	86.2	6594	0.3	18.2			26.8	2		400.8
29	JPT24C	1.8	1.2	81.6	6594	0.3	17.2			25.5	1.9		377.2
29	JPT22	1.2	0.8	40.4	3597	0.3	8.3			19.9	1.6		206.7
29	K89G162	2.0	1.0	135.9	4796	0.2	11.0			18.1	1.1		154.4
29	20E39A	0.8	0.9	19.1	5395	0.3	1.6			26.1	2.1		182.5
29	JPT7	0.7	0.9	75	4796	0.2	13.2			21.3	1.6		238.8
29	T5B/98	0.8	0.9	84.1	4796	0.3	14.1			23.1	1.7		269.1
29	JPT14.1	0.6	0.4	16	4196	0.1	2.7			11.2	0.8		109.1
29	JPT3	0.7	0.4	19.3	4196	0.1	3.7			11	0.8		122.3
29	JPT4	0.4	0.2	16.4	2398	0.1	3.7			4.8	0.4		27.4
29	JPT5.2	0.5	0.3	23.9	3597	0.1	2.2			7.4	0.5		78.8
29	JPT8	1.2	0.1	56.2	2398	0.1	8.1			4.5	0.6		47.4
29	95RAS11.3	0.5	0.2	17.8	1798	0.1	4.7			7.1	0.6		50.7
29	T2A	1.0	2.0	118	5995	0.4	13.6			36.3	2.1		323
29	T3B	1.3	1.5	68.3	6594	0.4	10.4			35.8	2.6		367.9
29	T4A	1.3	1.5	146.7	6594	0.3	21.2			26.7	1.6		482.4
29	T5A	0.8	0.9	78.3	4196	0.3	13.9			22.3	1.6		253.4
29	912	2.5	1.3	30.5	10791	0.3	5.6			27.4	1.8		600.1
29	1105	1.3	0.7	18	4196	0.4	4.4			24.9	2.4		72
29	K702	2.1	1.4	27	11390	0.3	4.3			28.1	1.8		432.5
29	K703	2.4	1.6	31.9	11990	0.4	4.8			31.7	2		532
29	K89G185	2.0	1.6	29.4	10791	0.3	4.2			32	1.8		451.9
29	K89G186	1.9	1.5	27.5	11390	0.3	4.4			27.6	1.6		451.7
29	K89G200	1.8	1.2	46.3	8393	0.2	9.7			24.4	1.4		327.6
29	KP12.6	3.2	1.5	37.7	11990	0.3	7.5			30.1	1.9		572.9
29	KP47-2	2.3	1.4	9	9592						2		348
29	KP47-5	1.5	1.5	18	9592						1.9		399
29	Bb124	1.8	1.1	38.5	7793	0.2	6.3			23	1.5		524.8
29	Bb121	1.8	1.1	37.3	8992	0.2	5.1			20.9	1.4		500.2

Ref.#	Sample	Ta	Tb	Th	Ti	Tm	U	V	W	Y	Yb	Zn	Zr
29	Bq137	1.7	1.1	48.7	8992	0.2	6.1			20.5	1.3		484.7
29	Bb119	1.8	1.2	49	9592	0.2	6.3			22.3	1.2		565.9
29	Bb122	1.7	1.0	49.2	8992	0.2	7.5			20.1	1.3		596.9
29	Bb135	1.8	1.1	52.6	8992	0.2	7.8			20.4	1.3		535.9
29	Bg142	0.5	0.6	61.6	4796	0.1	5.9			7.4	0.3		239.8
29	Bq140	0.5	0.6	60.7	4796	0.1	9.3			7.9	0.4		268.9
29	Bq141	0.6	0.7	68.2	4796	0.1	11.1			10.2	0.5		639
29	K9024	2.0	1.0	19.6	9592	0.3	3.5			24.1	1.7		412.2
29	K9026	2.3	1.0	21.3	10191	0.3	3.4			24	1.7		432.4
29	K9027	2.1	1.0	20.5	10191	0.3	3.3			23.4	1.7		426.1
29	K9028	2.1	1.0	19.4	9592	0.3	3.4			23	1.6		400.7
29	K9029	2.3	1.0	21.7	10191	0.3	3.6			24.6	1.7		461.6
29	K9031	2.2	1.0	21.1	9592	0.3	3.4			24.8	1.8		440.5
29	K9032	2.2	1.0	20.9	9592	0.3	3.5			25.6	1.8		443.8
29	K9038	2.1	0.9	11.6	9592	0.3	2.3			23.4	1.7		323.7
29	K9039	2.3	1.0	12.7	10791	0.3	2.3			25.7	1.9		341.1
29	K9041	1.8	1.1	13.2	4796	0.6	5.8			40.2	3.5		282
29	K9001	0.8	0.6	9.6	3597	0.3	2.1			21.9	2.2		109.2
29	K9002	0.8	0.7	9.8	3597	0.3	2.2			23.8	2.2		137.7
29	K9006	2.7	1.2	32.1	9592	0.3	8.2			27.8	1.8		523.1
29	K9007	2.4	1.2	30.5	9592	0.3	6.6			26.7	1.8		491.8
29	K9008	2.6	1.2	30.1	9592	0.3	7.4			24.6	1.6		480.6
29	K9016	2.6	1.1	29.3	8992	0.3	8.4			23.5	1.5		407
29	K9017	2.6	1.2	30.4	9592	0.3	7.7			26.2	1.7		486
29	K9018	2.6	1.2	30.9	9592	0.3	7.5			26.6	1.8		492.4
29	K9019	2.4	1.2	28.6	10191	0.3	6.9			26.3	1.7		484.6
29	K9021	2.4	1.1	30.1	9592	0.3	7.5			24.8	1.6		486.1
30	2007k251	2.9	1.8	20.06	8633	0.309	4.7	148.1			1.845	103.8	437.2
30	2007k252	3.7	1.7	20.82	8633	0.323	5.0	149			1.993	100.8	440.4
30	2007k253	3.3	1.6	18.82	8693	0.294	4.6	137.3			1.792	92.92	419.2

Ref.#	Sample	Ta	Tb	Th	Ti	Tm	U	V	W	Y	Yb	Zn	Zr
30	2007k254	3.5	1.8	20.81	8693	0.316	5.1	141.3			1.932	95.53	419.6
31	DHLT-10	1.0	1.2	34	8273	0.18	8.6			18.7	1.31		307
31	DHLT-2	1.0	0.6	34	7853	0.07	9.0			9.06	0.59		368
31	DHLT-4	1.2	1.7	26	10191	0.26	6.1			25.7	1.66		486
31	DHLT-5	0.8	1.3	33	8333	0.14	8.1			17.1	1.17		335
31	DHLT-7	0.7	0.8	27	8812	0.08	4.8			12.7	0.82		352
31	DHLT-9	0.7	1.1	32	8213	0.17	8.2			18.7	1.3		425
31	PL-12	1.9	1.6	29	11810	0.39	4.4			23.79	2.01		381
31	PL-2	1.4	1.7	30	13009	0.42	4.3			23.58	1.86		411
31	PL-3	1.1	1.7	31	13488	0.39	4.6			22.21	1.67		448
31	PL-5	1.6	1.6	31	13488	0.33	4.5			23.55	1.84		403
31	PL-7	2.1	1.7	27	12289	0.33	3.7			21.73	1.78		370
31	PL-9	3.2	1.7	25	11630	0.42	3.7			24.59	2.05		369
31	YCN-1	1.7	1.1	12	11690	0.15	2.6			18.2	1.32		379
31	YCN-2	1.7	1.1	12	11750	0.15	2.8			15	1.08		408
31	YCN-3	1.4	1.0	13	11990	0.21	2.7			18.9	1.4		365
31	YCN-4	1.6	1.3	12	12050	0.2	2.7			20.5	1.53		362
31	YCN-6	1.5	1.2	12	11870	0.29	2.6			24.5	1.91		395
31	YCN-7	1.4	1.2	12	12349	0.29	2.6			24.6	1.89		285
31	YCN-8	1.5	1.3	14	11990	0.11	2.7			23.4	1.83		362
31	KP24-1		2.1			0.4					2.4		
31	KP25-3		2.2			0.42					2.7		
31	KP28-1		1.3			0.5					2.6		
32	11UMT14	0.8	0.9	3.35	6235	0.43	0.3			27.65	2.66		173.85
32	11UMT15	0.4	0.8	0.98	7434	0.42	0.2			26.5	2.58		124.69
32	11UMT17-a	1.5	1.2	13.06	6714	0.32	2.6			24.85	1.9		206.19
32	12HG04	6.7	0.3	17.81	713	0.1	9.7	3		8.51	0.64	66	55
32	12HG06	2.6	0.4	31.38	1181	0.06	11.5	6		6.69	0.35	35	97
32	12HXV01	0.7	1.3	29.41	4376	0.27	5.4	118		24.86	1.58	69	245
32	12HXV08	2.6	0.5	26.95	2668	0.12	13.5	22		10.78	0.79	68	156

Ref.#	Sample	Ta	Tb	Th	Ti	Tm	U	V	W	Y	Yb	Zn	Zr
32	12HXV09	2.3	1.2	32.82	9526	0.31	4.9	97		26.75	1.83	88	563
32	12HXV12	2.1	1.1	33.68	9238	0.25	5.4	99		22.2	1.51	102	482
32	12HXV15	2.2	1.1	37.22	8411	0.27	6.5	95		23.22	1.57	95	462
32	12HXV19	2.3	1.0	34.19	10941	0.24	5.1	85		20.69	1.41	144	491
32	12HXV21A	2.2	1.1	38.52	8782	0.25	7.0	80		22.32	1.51	115	470
32	12HXV23	2.2	1.0	42.94	8099	0.24	9.0	89		21.18	1.48	102	447
32	12HXV24	3.4	0.5	32.83	2452	0.15	8.8	18		11.99	0.91	60	155
32	12HXV32	2.8	0.5	28.68	2632	0.12	9.0	17		10.61	0.77	46	157
32	12HXV33	0.7	1.6	27.13	4994	0.31	4.4			29.64	1.76		255
32	13DV05	2.2	1.2	25.1	11270	0.29	4.6	110	2	25.9	1.75	126	591
32	13DV04	2.3	1.3	25.1	11510	0.32	4.3	114	8	26	1.83	132	590
32	13DV11	2.2	1.3	25.5	11510	0.34	4.4	110	2	26.6	1.68	128	585
32	13DV13	2.3	1.2	28	10491	0.32	5.9	104	10	25.1	1.61	141	553
32	13DV14	2.2	1.1	27.7	9772	0.3	6.3	95	2	23.8	1.64	124	492
32	13DV15	2.3	1.2	29	10131	0.3	6.2	105	7	25.7	1.81	115	546
32	13DV23	2.4	1.0	17.15	11270	0.31	3.4	134	2	23.8	1.73	102	407
32	13DV29	2.3	1.0	16.6	10971	0.28	3.3	130	6	23.5	1.7	115	383
32	13LG07	1.4	0.9	51.8	7254	0.21	6.6	72	2	18	1.34	89	617
32	13XV01	2.0	1.0	36.2	8872	0.24	6.9	93	6	23.1	1.73	109	526
32	13XV02	2.2	1.2	32.8	10491	0.32	5.9	108	2	26.1	1.76	143	591

Table B.6 – Isotopic compositions of lavas in the Tibetan Plateau, part 1. See references for methods.

Ref. #	Sample	87Rb/86Sr	87Sr/86Sr	147Sm/144Nd	143Nd/144Nd	206Pb/204Pb	207Pb/204Pb	208Pb/204Pb
1	K89G185	0.060700	0.708080		0.512330	18.7140	15.6910	39.1200
1	K89G186		0.708070		0.512370	18.6800	15.6560	39.0150
1	K89G189		0.708020		0.512390	18.7500	15.7120	39.2080
1	K89G190		0.708190		0.512350	18.7130	15.6650	39.0330
1	KB9G191		0.708170		0.512339	18.7190	15.6770	39.0280
1	K89G192		0.708120		0.512358	18.7390	15.7050	39.1150
1	K189G193	0.141100	0.708150		0.512330	18.7560	15.7080	39.1160
1	K89G197		0.713720		0.512353	18.8870	15.6740	39.0130
1	K89G200	0.126400	0.708190		0.512310	18.7470	15.7180	39.3040
2	CM10-04-04		0.719695		0.511965			
2	CM10-04-09		0.719266		0.511933			
2	CM10-04-12		0.719869		0.511935			
2	D3141		0.709443		0.512262			
3	04LQS-6		0.706538		0.512461			
3	04LQS-14		0.706662		0.512454			
3	04LQS-16		0.706750		0.512440			
3	04YJL-05		0.707200		0.512445			
3	04YJL-07		0.706421		0.512459			
3	04YJL-06		0.706269		0.512370			
3	04YJL-09		0.707048		0.512382			
3	04DN30-2		0.707061		0.512360			
3	04DN30-3		0.707746		0.512287			
3	04DN31-1		0.706884		0.512436			
3	04DN32-2		0.707270		0.512386			
3	04DN37-2		0.707023		0.512434			
3	04DN39		0.707697		0.512369			
3	04DN40		0.705651		0.512461			
3	04D6437		0.706525		0.512417			

Ref. #	Sample	87Rb/86Sr	87Sr/86Sr	147Sm/144Nd	143Nd/144Nd	206Pb/204Pb	207Pb/204Pb	208Pb/204Pb
4	2T396		0.705930		0.512438	18.8880	15.6050	38.8910
4	98T03		0.706060		0.512461	18.8130	15.5560	38.9620
4	98T04		0.704640		0.512657	18.2140	15.5010	38.4200
4	98T07		0.704710		0.512711	18.4140	15.5130	38.6200
4	98T15		0.704600		0.512658	18.3870	15.4900	38.5630
4	98T16		0.709030		0.512213	18.9640	15.7020	39.3150
4	98T33		0.709030		0.512228	19.1050	15.8280	39.6870
4	98T38		0.709160		0.512195	19.0120	15.7310	39.4110
4	98T43		0.709060		0.512218	18.8830	15.6420	39.1390
4	98T44		0.709210		0.512166	19.0520	15.7660	39.5570
4	98T46		0.709100		0.512192	18.9840	15.6960	39.3250
4	98T49		0.709060		0.512187	18.9360	15.6750	39.2390
4	98T51		0.709060		0.512206	19.0580	15.7610	39.5100
4	98T52		0.708830		0.512197	18.9460	15.6760	39.2740
4	98T53		0.708960		0.512205	18.9670	15.7040	39.3430
4	98T54		0.708980		0.512233	18.9660	15.6990	39.3460
4	98T57		0.709010		0.512232	18.9440	15.6670	39.2110
4	98T69		0.709050		0.512215	18.9870	15.7300	39.4270
4	98T70		0.709110		0.512172	19.0260	15.7440	39.4370
4	98T71		0.709150		0.512208	19.0220	15.7320	39.4060
4	98T73		0.709110		0.512207	18.9090	15.6550	39.2250
4	99T132		0.708940		0.512219	18.9480	15.6760	39.2490
4	99T134		0.709010		0.512205	19.0900	15.8000	39.6050
4	99T145		0.722160		0.511883	18.4800	15.7720	39.5200
4	99T152		0.722180		0.511888	18.8810	15.7450	39.2880
4	99T154		0.724380		0.511875	18.4210	15.6900	39.3000
4	99T53		0.718450		0.511893	18.4200	15.6980	39.2710
4	99T56		0.720520		0.511893	18.4530	15.7250	39.4380
4	99T57		0.720360		0.511985	18.8080	15.7160	39.4310

Ref. #	Sample	87Rb/86Sr	87Sr/86Sr	147Sm/144Nd	143Nd/144Nd	206Pb/204Pb	207Pb/204Pb	208Pb/204Pb
4	99T60		0.718430		0.512021	18.8200	15.7330	39.5030
4	99T62		0.718200		0.511996	18.9480	15.7420	39.6330
5	2002T1021	0.389055	0.706721	0.096493	0.512544	18.8680	15.7500	39.4910
5	2002T1022	0.389752	0.706432	0.096532	0.512601	18.8760	15.7650	39.5950
5	2002T1023	0.386279	0.706543	0.096719	0.512538			
5	2002T1024	0.392318	0.706631	0.103465	0.512491			
5	2002T1025	0.410781	0.706578	0.091478	0.512576			
5	2002T1026	0.367869	0.706496	0.090153	0.512503			
5	2003T373	0.033303	0.704798	0.106282	0.512609			
5	2003T374	0.069461	0.704682	0.107895	0.512696			
5	2003T375	0.092903	0.705472	0.091530	0.512565			
5	2003T380	0.299610	0.705278	0.093622	0.512670			
5	2003T483	0.384922	0.705468	0.092453	0.512526			
5	2003T485	0.608987	0.705653	0.096935	0.512552			
5	2003T486	0.666921	0.705667	0.093533	0.512511			
5	2003T487	0.486867	0.705577	0.092556	0.512563			
5	2003T488	1.057487	0.705991	0.094233	0.512482			
5	2003T492	0.486430	0.705368	0.098162	0.512525			
6	TI/10		0.719154		0.511956	18.5500	15.8400	40.0600
6	TI/11		0.718477		0.511946	18.5200	15.8100	39.7000
6	TI/18		0.719612		0.511817	18.5200	15.7700	39.7500
6	TI/13		0.716764		0.511979	18.4600	15.7900	39.5600
6	TI/03		0.719945		0.511959	18.5600	15.8100	39.7200
6	TI/08		0.719518		0.511880	18.4800	15.7700	39.7200
6	TI/17		0.726580		0.511832	18.5800	15.8000	39.8600
6	TI/06		0.719806		0.511943	18.5700	15.8200	39.7900
6	TI/59		0.718240		0.511963	18.5300	15.8000	39.6500
6	CHZ-1		0.736476		0.511876	18.7700	15.6800	39.4800
6	CHZ-2					18.8200	15.7300	39.6700

Ref. #	Sample	87Rb/86Sr	87Sr/86Sr	147Sm/144Nd	143Nd/144Nd	206Pb/204Pb	207Pb/204Pb	208Pb/204Pb
6	CHZ-3					18.8900	15.7100	39.7300
6	CHZ-4					18.9100	15.7300	39.8000
6	CHZ-5		0.730948		0.511866	18.8500	15.6800	39.5900
6	CHZ-6					18.9300	15.7800	39.9100
6	CHZ-7					18.7800	15.7200	39.6000
6	CHZ-8		0.731065		0.511867	18.7600	15.7000	39.5600
6	CHZ-9					18.7800	15.7100	39.5800
6	CHZ-10		0.736455		0.511865	18.7700	15.7100	39.5600
6	CHZ-11					18.7600	15.7200	39.5800
6	CHZ-12		0.736385		0.511856	18.8200	15.7100	39.6500
7	AH-7		0.706578		0.512576			
7	G26		0.706496		0.512503			
7	G68	0.422700	0.709103	0.108500	0.512226			
7	G98-0	0.070000	0.709021	0.092800	0.512324			
7	G98-1	0.158000	0.708684	0.103200	0.512146			
7	G98-14	0.117400	0.708324	0.122800	0.512385			
7	G98-3	0.138400	0.707982	0.104700	0.512307			
7	G98-6	0.294000	0.708862	0.102400	0.512106			
7	G98-9	0.167300	0.708243	0.118900	0.512318			
7	HH72	0.221200	0.708249	0.105400	0.512213			
7	HS07	0.265700	0.708019	0.108500	0.512039			
7	HS-69	0.244700	0.707076	0.099600	0.512361			
7	JC9719	0.359900	0.708201	0.114300	0.512438			
7	JC973	0.327200	0.706538	0.112200	0.512529			
7	JC975	0.514100	0.707819	0.107800	0.512407			
7	JC978	0.461600	0.708746	0.112900	0.512229			
7	JH6	0.786300	0.707638	0.125900	0.512488			
7	KX84	1.156700	0.708418	0.145400	0.512162			
7	PL-58	0.229200	0.707016	0.140000	0.512441			

Ref. #	Sample	87Rb/86Sr	87Sr/86Sr	147Sm/144Nd	143Nd/144Nd	206Pb/204Pb	207Pb/204Pb	208Pb/204Pb
7	PL-7	0.219800	0.706689	0.121900	0.512442			
7	QQ08	0.284200	0.709029	0.114000	0.512113			
7	QS22	0.266600	0.708819	0.099100	0.512326			
7	XT16	0.378700	0.709713	0.078100	0.512206			
7	XT8	0.198800	0.707210	0.149100	0.512429			
7	XY03	0.351900	0.708095	0.119500	0.512393			
7	XY05	0.220400	0.707618	0.123900	0.512381			
7	YS02	0.287100	0.707307	0.101100	0.512506			
7	YS72	0.756500	0.710573	0.116200	0.511945			
7	ZF91	0.214100	0.707512	0.119200	0.512246			
7	ZF96	0.254500	0.708394	0.103000	0.512266			
8	ZF09		0.708124		0.512237	18.4030	15.6090	38.3140
8	GUO62		0.707423		0.512354	18.2560	15.5800	38.2670
8	GUO51		0.709188		0.512249	18.3110	15.6120	38.3080
8	GUO48		0.706812		0.512147	18.5130	15.6400	39.0840
8	GUO37		0.706639		0.512506	18.5100	15.6090	38.4230
8	G09		0.706004		0.512588	18.3140	15.5780	38.1560
8	ZFG17		0.704807		0.512798	18.3040	15.5040	38.2510
8	G006		0.704911		0.512604	18.2130	15.5040	38.1250
8	G019		0.708114		0.512544	18.6680	15.7260	38.8330
8	G016		0.707937		0.512511	18.7300	15.7080	38.7210
8	G025		0.705516		0.512508	18.4120	15.5880	38.5010
9	DY-7		0.712847		0.512056	18.3200	15.7100	39.3500
9	DC2		0.718046		0.511965	18.3600	15.6600	39.2200
9	D509		0.716054		0.512026	18.4000	15.6900	39.1300
9	DG43		0.714758		0.511941	18.3700	15.6800	39.4200
9	YE51		0.718364		0.511913	18.4000	15.7200	39.2300
9	YC08		0.718469		0.511917	18.4000	15.7500	39.3600
9	YG13		0.717351		0.511936	18.3800	15.7400	39.3700

Ref. #	Sample	87Rb/86Sr	87Sr/86Sr	147Sm/144Nd	143Nd/144Nd	206Pb/204Pb	207Pb/204Pb	208Pb/204Pb
9	YF12		0.719673		0.511983	18.4200	15.7500	39.4400
9	YA32		0.719041		0.511964	18.4400	15.7000	39.4100
9	MH78		0.719877		0.511926	18.4900	15.7500	39.5800
9	MH69		0.721486		0.511992	18.6100	15.7600	39.4800
9	MG-3		0.719649		0.511961	18.5800	15.7500	39.6100
9	MY1		0.722672		0.511934	18.5400	15.7800	39.6200
9	MK09		0.720948		0.511926	18.6000	15.7700	39.7200
9	MR21		0.725133		0.511854	18.6300	15.8000	39.5800
9	MA75		0.720861		0.511847	18.5700	15.7300	39.8500
9	MX5		0.718768		0.511928	18.5300	15.7300	39.5100
9	2003T534		0.719910		0.511844			
9	2003T536		0.720660		0.511822			
9	2003T539		0.720930		0.511815			
9	G8		0.729418		0.511856	18.8000	15.7000	40.0600
9	C10		0.735896		0.511874	18.9400	15.8200	39.9900
9	CV5		0.733316		0.511852	18.8600	15.8300	39.6300
9	C76		0.730484		0.511793	18.9600	15.8400	39.1900
9	CH4		0.733043		0.511924	18.9000	15.8200	39.6300
9	CH7		0.726819		0.511828	18.8800	15.7500	39.6100
9	C03		0.723169		0.511894	18.7600	15.7800	39.4800
9	CX38		0.721648		0.511887	18.8200	15.7200	39.9500
9	C25		0.736552		0.511826	18.9900	15.8500	39.4000
10	CT09	0.191400	0.708172	0.083000	0.512335	18.7420	15.7270	39.1840
10	CT12	0.171900	0.711863	0.111000	0.512241	18.7360	15.6840	39.1320
10	CT17	0.224500	0.708194	0.112900	0.512305	18.7040	15.7130	39.1450
10	CT05	0.227500	0.707962	0.107600	0.512218	18.7270	15.6730	39.2270
10	CT23	0.246000	0.707685	0.091900	0.512441	18.8860	15.6910	39.2160
10	QS12	0.189800	0.707816	0.094700	0.512156	19.0690	15.7460	39.3140
10	QS27	0.190900	0.708529	0.115900	0.512341	18.7140	15.6960	39.1150

Ref. #	Sample	87Rb/86Sr	87Sr/86Sr	147Sm/144Nd	143Nd/144Nd	206Pb/204Pb	207Pb/204Pb	208Pb/204Pb
10	QS19	0.224100	0.712843	0.143600	0.512167	18.9420	15.6740	38.9860
10	QS23	0.201000	0.713148	0.112000	0.512328	18.8810	15.6580	39.0370
10	QS18	0.179400	0.709648	0.118800	0.512236	18.8120	15.7150	39.2760
10	QS24	0.217700	0.710213	0.095100	0.512148	18.8940	15.6430	39.0280
10	KY03	0.186600	0.708454	0.122800	0.512207	18.7260	15.6300	38.8250
10	KY02	0.165500	0.709312	0.142600	0.512316	18.7510	15.6410	39.0570
10	KY06	0.131000	0.709471	0.115400	0.512127	18.9050	15.5930	39.0160
10	KY01	0.159000	0.708103	0.129400	0.512249	18.8770	15.6340	38.9450
10	HS041	0.302900	0.707849	0.120700	0.512258	18.9420	15.8670	39.4610
10	HS046	0.335000	0.710381	0.122600	0.512105	18.9750	15.9480	39.5830
10	HS047	0.279500	0.709417	0.115200	0.512263	19.0120	15.8270	39.1260
10	HS028	0.341600	0.710824	0.124700	0.512237	19.0140	15.7460	38.8300
10	AH607	0.207100	0.709036	0.090600	0.512387	18.7830	15.6850	38.9510
10	AH605	0.214400	0.709531	0.135300	0.512129	18.8180	15.6640	38.9750
10	AH609	0.205000	0.707619	0.101600	0.512483	18.7050	15.6730	38.9040
10	AH602	0.227300	0.707319	0.104200	0.512474	18.7660	15.6490	38.9830
10	AH618	0.205600	0.709224	0.100800	0.512116	18.8370	15.6820	39.0640
10	AH615	0.224100	0.710308	0.098900	0.512402	18.7140	15.6270	38.8100
10	YS74	0.518200	0.710016	0.103300	0.512287	18.7130	15.6570	38.7020
10	YS78	0.427800	0.707924	0.113800	0.512395	18.7520	15.6830	38.9470
10	YS05	0.404800	0.707637	0.118100	0.512412	18.7810	15.6720	38.8230
10	YS79	0.295900	0.708453	0.110800	0.512462	18.7640	15.7050	38.9470
10	YS07	0.261000	0.708134	0.105800	0.512395	18.7760	15.7310	39.2150
10	KX44	0.396600	0.708143	0.138700	0.512179	18.8190	15.6540	38.9950
10	KX51	0.404500	0.708247	0.124200	0.512062	18.7760	15.6310	38.8630
10	KX80	0.383200	0.707967	0.114900	0.512148	18.8040	15.5850	38.6720
10	KX49	0.421800	0.708645	0.141400	0.512097	18.8070	15.6790	38.8460
10	KX62	0.270000	0.708317	0.118300	0.512124	18.8120	15.6470	38.8090
10	PL53	0.243200	0.708761	0.099400	0.512179	18.7760	15.6530	38.7210

Ref. #	Sample	87Rb/86Sr	87Sr/86Sr	147Sm/144Nd	143Nd/144Nd	206Pb/204Pb	207Pb/204Pb	208Pb/204Pb
10	PL61	0.223300	0.708827	0.111500	0.512053	18.7520	15.6910	38.6570
10	PL3	0.338000	0.708562	0.108500	0.512427	18.7870	15.5720	39.1350
10	PL18	0.213000	0.708004	0.098000	0.512013	18.7510	15.6750	38.9780
10	PL92	0.235900	0.708951	0.112800	0.512338	18.7850	15.6280	38.8240
10	PL43	0.335300	0.708845	0.101400	0.512309	18.8150	15.6370	38.9460
11	G10	1.640000	0.705360	0.073000	0.512790			
11	G15A	0.350000	0.704640	0.124000	0.512780			
11	S70C	7.730000	0.715810	0.127000	0.512260			
11	S70D	3.240000	0.709150	0.103000	0.512290			
12	07-SA-21	0.146500	0.707283	0.101000	0.512439			
12	07-SA-26A	0.019200	0.708139	0.102900	0.512419			
12	07-SG-31B	0.858700	0.712301	0.097900	0.512298			
12	07-SG-48B	0.418600	0.709154	0.092900	0.512339			
12	07-SG-52A	0.466300	0.711372	0.102000	0.512305			
12	07-SG-66			0.106300	0.512358			
12	06-SG-200	0.546600	0.711453	0.095000	0.512167			
12	07-SA-25			0.211300	0.513083			
13	NQ2-1*	0.404900	0.710108	0.119500	0.512012			
13	NQ21-4*	0.120500	0.709506	0.108900	0.512342			
13	NQ7-1*		0.705616		0.512603	18.6450	15.5540	38.5390
13	Y1-11		0.705227		0.512578	18.7610	15.5750	38.6560
13	Y1-12		0.705190		0.512473	18.8590	15.5780	38.7470
13	Y1-13	0.520800	0.706862		0.512487	18.7509	15.6728	38.9631
13	Y1-15	0.612200	0.707306		0.512486	18.7358	15.6609	38.9371
13	Y1-8	0.739800	0.706958		0.512478	18.7125	15.6456	38.8668
13	Y1-9	1.359000	0.707075		0.512486	18.8240	15.6650	38.9990
13	Y2-2	0.445100	0.706771		0.512482	18.7136	15.6578	38.8947
13	Y2-3	1.054000	0.707462		0.512478	18.7307	15.6610	38.9235
13	Y2-4	0.971300	0.707260		0.512513	18.7180	15.6522	38.8951

Ref. #	Sample	87Rb/86Sr	87Sr/86Sr	147Sm/144Nd	143Nd/144Nd	206Pb/204Pb	207Pb/204Pb	208Pb/204Pb
13	Y2-6	0.841900	0.707197		0.512465	18.7195	15.6544	38.8943
13	Y2-9	0.738200	0.706880		0.512482	18.7177	15.6456	38.8744
14	KK06003		0.707909		0.512386	18.6740	15.6500	38.9760
14	KK06004		0.707866		0.512362	18.7250	15.7160	39.2030
14	KK06006		0.707882		0.512403	18.7390	15.7330	39.2490
14	KK06010		0.707893		0.512371	18.7660	15.7600	39.3510
14	KK06011		0.707947		0.512399	18.7340	15.7220	39.2200
14	KK06018		0.707346		0.512411	18.7110	15.7240	39.2390
14	KK06022		0.707371		0.512448	18.6940	15.7090	39.1640
14	KK06024		0.707358		0.512416	18.7090	15.7130	39.2040
14	KK06027		0.708529		0.512368	18.7760	15.7490	39.3490
14	KK06028		0.708469		0.512349	18.7460	15.7200	39.2390
14	KK06029		0.708440		0.512350	18.7340	15.7060	39.2100
14	KK06030		0.708471		0.512374	18.7350	15.6980	39.1860
14	KK06032		0.714915		0.512281	18.7040	15.6910	39.1090
14	KK06038		0.708041		0.512404	18.7540	15.7550	39.3180
14	KK06041		0.707834		0.512392	18.7340	15.6890	39.0990
14	KK06042		0.707906		0.512432	18.6800	16.6650	39.0140
15	Z02H1	0.720000	0.709057	0.090000	0.512282			
15	Z07H3	0.292570	0.707509	0.094900	0.512375	18.7802	15.7191	39.2050
15	Z07H4	0.294020	0.707500	0.091730	0.512347	18.7499	15.7197	39.1660
15	Z07H6	0.343160	0.707258	0.093200	0.512337	18.7777	15.7097	39.1810
15	Z08H1	0.289070	0.707259	0.090990	0.512369	18.7620	15.7109	39.1700
15	Z08H6	0.278710	0.707279	0.090680	0.512321	18.7606	15.7107	39.1690
15	Z08H5	0.278010	0.707502	0.090570	0.512350	18.7569	15.7189	39.1780
15	Z12H2	0.348250	0.707412	0.096460	0.512433	18.8417	15.7290	39.2620
15	Z15H7	0.716140	0.708284	0.109590	0.512393	18.8189	15.7314	39.1830
16	ET021B	0.685100	0.709412	0.086790	0.512591	18.7995	15.6884	39.2146
16	ET021C	0.874400	0.709566	0.088140	0.512334	18.7635	15.6675	39.1356

Ref. #	Sample	87Rb/86Sr	87Sr/86Sr	147Sm/144Nd	143Nd/144Nd	206Pb/204Pb	207Pb/204Pb	208Pb/204Pb
16	ET022A	0.087000	0.704563	0.155000	0.512672			
16	ET024	0.572000	0.704639	0.135000	0.512737			
16	ST052B	1.125000	0.707115	0.109000	0.512630			
16	ST053	1.188000	0.707376	0.104000	0.512495			
16	ST055A	1.448000	0.708107	0.104000	0.512317			
16	ST055C	7.523000	0.717727	0.102000	0.512324			
16	ST058	0.434000	0.706480	0.120000	0.512472			
16	ST059A	0.905000	0.708656	0.112000	0.512361			
16	ST060A	1.628000	0.754776	0.104000	0.511676			
16	ST060C	4.907000	0.708236	0.110000	0.512647			
16	ST062	3.259000	0.708870	0.104000	0.512373			
16	ST101B	2.886000	0.708851	0.133000	0.512339			
16	ST102B	3.758000	0.709576	0.101000	0.512294			
16	ST109	0.119000	0.704472	0.113000	0.512725			
16	ST119A	0.396000	0.704574	0.133000	0.512796			
16	ST121	0.012000	0.703481	0.138000	0.512961			
16	T006B2	0.007000	0.703776	0.124000	0.512889			
16	T034A	0.256000	0.705951	0.124000	0.512558			
16	T034B	0.251000	0.707243	0.133000	0.512399			
16	T036D	0.104000	0.703814	0.151000	0.512925			
16	T038G	0.076000	0.704302	0.147000	0.512799			
16	T038M	10.990000	0.715798	0.117000	0.512362			
16	T041 J	0.704000	0.705970	0.118000	0.512560			
16	T042C	0.088000	0.704031	0.142000	0.512800			
16	T042D	0.034000	0.704054	0.146000	0.512829			
16	T046A	0.647000	0.708556	0.138000	0.512522			
16	T047	0.176000	0.703779	0.132000	0.512814			
16	T051C	0.131000	0.706038	0.139000	0.512662			
16	T054A	2.754000	0.707360	0.105000	0.512529			

Ref. #	Sample	87Rb/86Sr	87Sr/86Sr	147Sm/144Nd	143Nd/144Nd	206Pb/204Pb	207Pb/204Pb	208Pb/204Pb
16	T055B	0.174000	0.705779	0.139000	0.512556			
16	T056A	0.121000	0.705156	0.131000	0.512651			
16	T062C	0.317000	0.706418	0.112000	0.512530			
16	T063	0.600000	0.705532	0.124000	0.512587			
16	T065A	0.361000	0.705562	0.124000	0.512582			
16	T066	3.500000	0.760054	0.113000	0.511908			
16	T068	4.046000	0.707747	0.109000	0.512638			
16	T072E	1.052000	0.713173	0.109000	0.512082			
16	T078B	0.396000	0.712857	0.116000	0.511985			
16	T080	0.649000	0.705626	0.142000	0.512616			
16	T083C	2.181000	0.707916	0.094000	0.512454			
16	T102A	0.783000	0.705841	0.127000	0.512635			
16	T105A			0.109000				
16	T127B	0.846000	0.705341	0.139000	0.512626			
16	T131A	1.124000	0.727732	0.139000	0.512269			
16	T136B	1.348000	0.713115	0.109000	0.512030			
16	T138D	17.110000	0.737603	0.103000	0.512009			
16	T139	13.170000	0.739981	0.251000	0.511994			
16	T144C			0.116000				
16	T152A	0.303000	0.713131	0.113000	0.512193			
16	T160B	1.499000	0.706855	0.110000	0.512475			
16	T234B	0.057000	0.704850	0.125000	0.512778			
16	T235B	0.120000	0.705179	0.107000	0.512667			
16	T239	3.088000	0.708966	0.112000	0.512563			
16	T240B	0.023000	0.705082	0.132000	0.512636			
17	GGL01	0.171000	0.706282	0.127000	0.512489			
17	GGL03					18.6770	15.6670	39.0780
17	GGL05	0.796600	0.707520	0.107968	0.512437	18.6730	15.6660	39.0710
17	GGL06					18.6730	15.6670	39.0680

Ref. #	Sample	87Rb/86Sr	87Sr/86Sr	147Sm/144Nd	143Nd/144Nd	206Pb/204Pb	207Pb/204Pb	208Pb/204Pb
17	GGL07	0.475000	0.706690	0.112824	0.512461	18.6830	15.6760	39.1010
17	GGL08	0.487400	0.706750	0.112020	0.512464	18.6660	15.6650	39.0600
17	GGL09	0.516300	0.706720	0.111252	0.512469	18.6820	15.6730	39.0960
17	GGL10	0.480700	0.707380	0.113300	0.512473	18.6800	15.6670	39.0800
17	GGL11	0.534700	0.707810	0.109441	0.512470			
17	GGL12	0.527200	0.707950	0.113191	0.512462	18.6770	15.6710	39.0830
17	GGL13					18.6790	15.6680	39.0850
17	GGL14	0.535500	0.706800	0.112530	0.512445	18.6810	15.6670	39.0800
17	GGL15	0.513600	0.707070	0.110243	0.512467			
18	GJ0601		0.740593		0.511957	18.8250	15.7880	39.6090
18	GJ0602		0.739577		0.511958	18.8240	15.7870	39.6040
18	GJ0605				0.511965	18.8280	15.7880	39.6110
18	GJ0606		0.739035		0.511985	18.8310	15.7890	39.6080
18	08YR04		0.735859		0.511952	18.8260	15.7820	39.5860
18	GJ0614		0.734442		0.511911	18.8590	15.7950	39.7250
18	GJ0617		0.736300		0.511903	18.8760	15.7970	39.7370
18	GJ0619		0.735886		0.511898	18.8740	15.7960	39.7330
18	GJ0620		0.732696		0.511898	18.8750	15.7960	39.7360
18	GJ0624		0.733256		0.511950	18.8130	15.7860	39.6210
18	GJ0627		0.732916		0.511954	18.8130	15.7850	39.6300
18	GJ0628		0.732819		0.511962	18.8110	15.7840	39.6230
18	GJ0629		0.732739		0.511955	18.8080	15.7850	39.6270
18	10XB03		0.740400		0.511879	18.9090	15.7540	39.6590
18	10XB04		0.730801		0.511903	18.8660	15.7420	39.6100
18	10XB07		0.731030		0.511913	18.8430	15.7170	39.5150
18	08YR05		0.718822		0.511924	18.6710	15.7510	39.7450
18	10XB10		0.717902		0.512008	18.6950	15.6840	39.3060
18	10XB12		0.720027		0.511977			
18	10XB13		0.720312		0.511978	18.6910	15.6960	39.3580

Ref. #	Sample	87Rb/86Sr	87Sr/86Sr	147Sm/144Nd	143Nd/144Nd	206Pb/204Pb	207Pb/204Pb	208Pb/204Pb
18	10YR01		0.719501		0.511921	18.6300	15.6800	39.4830
18	10YR02		0.718966		0.511933	18.6460	15.6980	39.5760
18	10YR04		0.719616		0.511923	18.6410	15.7000	39.5800
18	10YR07		0.719596		0.511923	18.6330	15.6900	39.5470
19	MV1B	0.517600	0.706840	0.111193	0.512451			
20	TE011/93	2.092000	0.722540	0.095400				
20	TE125/93	2.893000	0.720260	0.124900				
20	TE126/93	1.701000	0.720570	0.091100		18.5630	15.6986	39.4228
20	TE137/93	1.957000	0.722340	0.130100		18.5211	15.7332	39.7556
20	TE138/93	1.408000	0.717650	0.119600		18.4571	15.6795	39.5534
20	TE117/93	2.591000	0.719910					
20	TE118/93	2.603000	0.720090	0.126300		18.6034	15.7231	39.5820
20	TE025/93	2.528000	0.738410	0.092900		18.7968	15.7579	39.4821
20	TE136/93	1.303000	0.717950					
20	TE150/93	2.854000	0.733440	0.087500		18.5892	15.6761	39.1361
20	TE153/93	2.908000	0.733760	0.082700				
20	TE154/93	2.852000	0.733550					
20	TE047/93	0.996000	0.709560	0.096900				
20	TE189/93	0.449000	0.709140	0.105400				
20	TE192/93	0.470000	0.709780	0.107400				
20	TE194/94	0.656000	0.709670	0.099300				
22	K89G185		0.709180		0.512290			
22	K89G200		0.708370		0.512320			
22	K9007		0.709160		0.512330			
22	K9008		0.708030		0.512290			
22	K9021		0.709100		0.512270			
22	K9024		0.709160		0.512310			
22	K9031		0.708080		0.512330			
22	K9038		0.708190		0.512310			

Ref. #	Sample	87Rb/86Sr	87Sr/86Sr	147Sm/144Nd	143Nd/144Nd	206Pb/204Pb	207Pb/204Pb	208Pb/204Pb
23	Bb-105		0.710050		0.512370			
23	Bb-107		0.710540		0.512220			
23	Bb-109		0.708070		0.512330	18.7140	15.6910	39.1200
23	Bb-114		0.708050		0.512370	18.6800	15.6560	39.0150
23	Bb-88		0.708150		0.512340	18.7190	15.6770	39.0280
23	Bb-89		0.708120		0.512360	18.7390	15.7050	39.1150
23	Bb94-2		0.708120		0.512330	18.7560	15.7080	39.1160
23	Bb-95		0.713700		0.512350	18.8870	15.6740	39.0130
23	Bg 121		0.708170		0.512310	18.7470	15.7180	39.3040
23	Bg 124		0.710340		0.512263	18.8340	15.6890	39.1900
23	COUL311		0.710373		0.512265			
23	COUL326		0.710230		0.512277			
23	COUL328		0.710360		0.512259			
23	COUL338		0.709911		0.512282			
23	COUL339		0.709875		0.512264			
23	k705		0.709832		0.512272			
23	k708		0.709960		0.512291			
23	K713		0.710540		0.512221			
23	K716		0.710051		0.512365			
23	K720		0.708670		0.512326	18.7180	15.6910	39.0860
23	K723		0.708770		0.512293	18.7040	15.6690	39.0300
23	K732		0.708490		0.512371	18.7180	15.6870	39.1310
23	K9002		0.708230		0.512318	18.7280	15.7250	39.2960
23	K9006		0.708248		0.512251			
23	K9007		0.709175		0.512292	18.7420	15.6870	39.1680
23	K9008		0.709103		0.512265	18.7700	15.7130	39.2600
23	K9016		0.709229		0.512243	18.7760	15.7090	39.2170
23	K9017		0.709068		0.512292			
23	K9018		0.709155		0.512308	18.7690	15.7060	39.3240

Ref. #	Sample	87Rb/86Sr	87Sr/86Sr	147Sm/144Nd	143Nd/144Nd	206Pb/204Pb	207Pb/204Pb	208Pb/204Pb
23	K9019				0.512334			
23	K9021		0.708198		0.512337			
23	K9024		0.709158		0.512333	18.7420	15.6940	39.1780
23	K9026				0.512338	18.7120	15.8920	39.1350
23	K9027		0.708026		0.512294	18.6750	15.6790	39.0010
23	K9029		0.708374		0.512333	18.7140	15.6890	39.1400
23	K9031		0.708189		0.512333			
23	Kp12-58		0.707970		0.512650	18.6720	15.6070	38.9120
23	Kp23-2		0.705900		0.512480	18.4880	15.6550	38.8570
23	Kp24-1		0.706410		0.512470	18.5260	15.6760	38.9790
23	Kp39-3		0.704930		0.512700	18.6100	15.6080	38.7610
23	Kp47-2		0.704800		0.512710	18.5910	15.5920	38.7300
23	Kp47-5		0.704810		0.512070	18.6930	15.7810	39.6090
24	2303		0.715520		0.512030	18.7210	15.7690	39.6990
24	2509				0.512040			
25	04wq-1	0.029600	0.706886	0.083400	0.512419			
25	04wq-3	0.030100	0.707008	0.082600	0.512415			
25	04wq-4	0.024700	0.707395	0.083200	0.512422			
25	04wq-6	0.110300	0.707035	0.087100	0.512414			
25	4086-1	0.113100	0.706982	0.090600	0.512423			
25	8528	0.331400	0.707212	0.098800	0.512406			
25	8518-1	0.176900	0.706975	0.095300	0.512471			
25	8518-2	0.175300	0.707211	0.095700	0.512462			
25	9063-GS2	0.181500	0.707247	0.098300	0.512442			
25	9063-GS3	0.196800	0.707322	0.100600	0.512434			
25	D3145	0.360800	0.708426	0.083340	0.512278			
26	05SLP5-05	1.823600	0.719589	0.122700	0.511877	18.4220	15.6870	39.4680
26	05SLP5-7	1.769000	0.719274	0.119000	0.511880	18.7870	15.7490	39.6890
26	05SLP4-01	0.370100	0.718783	0.112600	0.511969	18.4890	15.7230	39.4410

Ref. #	Sample	87Rb/86Sr	87Sr/86Sr	147Sm/144Nd	143Nd/144Nd	206Pb/204Pb	207Pb/204Pb	208Pb/204Pb
26	05SLP4-02	0.874800	0.714699	0.111200	0.512040	18.4310	15.6930	39.4390
26	05SLP4-03	0.988600	0.716930	0.114000	0.511996	18.4140	15.6930	39.7650
26	05SLP4-04	1.585200	0.715106	0.113700	0.512037			
26	05S2-7	2.745600	0.728008	0.139600	0.511852	18.7120	15.7030	39.7070
26	05S2-8-1	2.532100	0.727871	0.132100	0.511850	18.7030	15.6970	39.6660
27	WR-12-48	1.427000	0.705490	0.109100	0.512601			
27	WR-12-47	34.628000	0.735180	0.153000	0.512591			
27	WR-12-45	0.147000	0.704590	0.137400	0.512604			
27	WR-12-40	0.631000	0.705000	0.105900	0.512600			
27	WR-12-42	0.216000	0.704620	0.130600	0.512643			
27	WR-12-33	0.510000	0.706640	0.109800	0.512404			
28	T2A/98		0.739716		0.511737			
28	T3b/98		0.712352		0.511878			
28	T4A/98		0.712004		0.511980			
28	T5A/98		0.716194		0.511914			
28	T11B/98		0.706927		0.512085			
28	JPT 14.2		0.706957		0.512320			
29	JPT24C	2.800000	0.715271	0.110000	0.511955			
29	JPT22	1.820000	0.715276	0.130000	0.511914			
29	K89G162	1.750000	0.715049	0.130000	0.511767			
29	20E39A	4.260000	0.735148	0.090000	0.512121			
29	T5B/98	0.290000		0.110000	0.512419			
29	JPT4	0.280000	0.707216	0.100000	0.512021			
29	JPT5.2	0.420000	0.706694	0.100000	0.512357			
29	JPT8	0.650000	0.706764	0.090000	0.512431			
29	95RAS11.3	1.260000	0.706945	0.090000	0.512307			
29	T2A	5.750000	0.711373	0.080000	0.512028			
29	K702	0.490000	0.708373	0.090000	0.512152			
29	K703	1.210000	0.710180	0.110000	0.512013			

Ref. #	Sample	87Rb/86Sr	87Sr/86Sr	147Sm/144Nd	143Nd/144Nd	206Pb/204Pb	207Pb/204Pb	208Pb/204Pb
29	K89G185	0.270000	0.710180	0.090000	0.511985			
29	K89G186	0.310000		0.090000	0.512110			
29	Bq141	1.050000	0.709992	0.080000	0.512110			
29	K9026	0.960000	0.709821	0.080000	0.512126			
29	K9028	0.370000	0.708164	0.090000	0.512334			
29	K9032	0.340000	0.708242	0.080000	0.512362			
29	K9039	0.320000	0.708233	0.090000	0.512338			
29	K9001	0.270000	0.707939	0.090000	0.512371			
29	K9007	1.450000	0.714156	0.110000	0.511949			
29	K9019	0.860000	0.708976	0.090000	0.512296			
30	2007k251	0.058250	0.708582	0.083200	0.512354			
31	DHLT-10		0.708148		0.512370	18.8069	15.7424	38.7910
31	DHLT-2		0.708218		0.512550	18.7854	15.7090	38.7284
31	DHLT-4		0.708138		0.512440	18.7886	15.7437	39.2886
31	DHLT-7		0.708077		0.512465	18.7650	15.7018	39.1210
31	PL-12		0.708759		0.512403	18.6027	15.6026	38.6998
31	PL-2		0.708653		0.512391	18.7140	15.5774	38.6607
31	PL-3		0.708846		0.512362	18.2615	15.4798	38.3023
31	PL-5		0.708974		0.512289	18.7511	15.6083	38.7351
31	PL-7		0.708733		0.512283	18.7670	15.5860	38.7042
31	PL-9		0.708628		0.512192	18.8260	15.6225	38.8080
31	YCN-1		0.708634		0.512213	18.7026	15.6800	38.8855
31	YCN-3		0.709631		0.512419	18.7627	15.6746	38.8988
31	YCN-6		0.708643		0.512356	18.7287	15.6662	38.8511
31	YCN-7		0.708703		0.512443	18.7409	15.6491	38.8183
32	11UMT17-a		0.706296		0.512524	18.7285	15.6621	38.9532
32	12HG04		0.726296		0.512236	18.7117	15.6785	39.0090
32	12HG06		0.720432		0.512292	18.7067	15.6557	38.8898
32	12HXV01		0.706971		0.512471	18.6120	15.6614	38.9244

Ref. #	Sample	87Rb/86Sr	87Sr/86Sr	147Sm/144Nd	143Nd/144Nd	206Pb/204Pb	207Pb/204Pb	208Pb/204Pb
32	12HXV08		0.709936		0.512305	18.6754	15.6654	38.9561
32	12HXV09		0.708426		0.512385	18.7658	15.7003	39.2226
32	12HXV12		0.707812		0.512413	18.7069	15.6771	39.0788
32	12HXV15		0.707843		0.512398	18.7048	15.6754	39.0702
32	12HXV19		0.707858		0.512400	18.6986	15.6770	39.0650
32	12HXV21A		0.707845		0.512403	18.6921	15.6735	39.0505
32	12HXV23		0.707870		0.512412	18.7047	15.6724	39.0531
32	12HXV24		0.710250		0.512320	18.6552	15.6637	38.9511
32	12HXV32		0.710129		0.512316	18.6553	15.6626	38.9437
32	12HXV33		0.707065		0.512485	18.6103	15.6568	38.9296

Table B.7 – Isotopic compositions of lavas in the Tibetan Plateau, part 2. See references for methods.

Ref. #	Sample	175Hf/177Hf	238U/204Pb	235U/204Pb	232Th/204Pb	187Os/188Os	187Re/188Os	187Os/188Os(i)
7	AH-7		4.07	0.03	42.17			
7	G26		4.26	0.03	19.50			
7	G68		6.876	0.051	118.069			
7	G98-0		9.62	0.07	126.21			
7	G98-1		7.16	0.05	104.40			
7	G98-14		6.31	0.05	149.54			
7	G98-3		6.91	0.05	136.47			
7	G98-6		14.33	0.11	98.68			
7	G98-9		6.03	0.04	139.37			
7	HH72		6.05	0.04	107.32			
7	HS07		6.84	0.05	31.27			
7	HS-69		7.398	0.054	27.667			
7	JC9719		6.033	0.044	77.456			
7	JC973		7.882	0.058	72.321			
7	JC975		4.433	0.033	36.802			
7	JC978		14.424	0.106	94.443			
7	JH6		5.012	0.037	55.858			
7	KX84		10.554	0.078	56.911			
7	PL-58		11.745	0.086	62.704			
7	PL-7		13.178	0.097	24.224			
7	QQ08		11.011	0.081	48.716			
7	QS22		10.233	0.075	55.664			
7	XT16		5.466	0.04	46.473			
7	XT8		7.991	0.059	46.893			
7	XY03		7.728	0.057	60.78			
7	XY05		8.792	0.065	74.141			
7	YS02		10.759	0.079	70.93			
7	YS72		10.279	0.076	45.328			

Ref. #	Sample	175Hf/177Hf	238U/204Pb	235U/204Pb	232Th/204Pb	187Os/188Os	187Re/188Os	187Os/188Os(i)
7	ZF91		11.201	0.082	59.549			
7	ZF96		13.135	0.096	69.708			
10	CT09		9.182	0.067	42.97			
10	CT12		11.527	0.085	149.442			
10	CT17		7.167	0.053	42.469			
10	CT05		12	0.088	56.839			
10	CT23		13.81	0.101	70.761			
10	QS12		9.228	0.068	97.078			
10	QS27		10.779	0.079	99.694			
10	QS19		11.025	0.081	228.407			
10	QS23		12.546	0.092	167.281			
10	QS18		7.101	0.052	99.328			
10	QS24		5.737	0.042	135.395			
10	KY03		8.716	0.064	117.153			
10	KY02		14.259	0.105	124.959			
10	KY06		8.446	0.062	132.223			
10	KY01		18.032	0.132	164.405			
10	HS041		15.494	0.114	56.512			
10	HS046		10.381	0.076	41.324			
10	HS047		7.633	0.056	54.099			
10	HS028		9.34	0.069	112.063			
10	AH607		6.257	0.046	25.76			
10	AH605		5.467	0.04	25.278			
10	AH609		8.962	0.066	36.425			
10	AH602		6.989	0.051	27.692			
10	AH618		8.005	0.059	31.6			
10	AH615		5.21	0.038	21.631			
10	YS74		10.066	0.074	45.046			
10	YS78		12.391	0.091	52.389			
10	YS05		13.457	0.099	26.359			

Ref. #	Sample	175Hf/177Hf	238U/204Pb	235U/204Pb	232Th/204Pb	187Os/188Os	187Re/188Os	187Os/188Os(i)
10	YS79		10.852	0.08	40.427			
10	YS07		13.731	0.101	61.422			
10	KX44		7.266	0.053	30.405			
10	KX51		12.454	0.091	22.359			
10	KX80		7.413	0.054	24.241			
10	KX49		9.302	0.068	29.608			
10	KX62		9.112	0.067	23.449			
10	PL53		6.203	0.046	25.761			
10	PL61		6.982	0.051	20.326			
10	PL3		3.346	0.025	14.903			
10	PL18		4.041	0.03	27.842			
10	PL92		3.879	0.028	31.077			
10	PL43		3.63	0.027	17.322			
17	GGL06	0.282674						
20	TE126/93		15.78					
20	TE137/93		23.51					
20	TE138/93		17.12					
20	TE118/93		36.65					
20	TE025/93		13.73					
20	TE150/93		9.6					
26	05SLP5-05					0.16812	13.35385	0.16421
26	05SLP5-7					0.38678	41.81012	0.37454
26	05SLP4-01					0.16205	69.44532	0.14067
26	05SLP4-02					0.16036	165.16091	0.1095
26	05SLP4-03					0.16652	57.08475	0.14895
26	05SLP4-04					0.17031	65.24389	0.15022
26	05S2-7					0.14869	10.89194	0.1455
26	05S2-8-1					0.14775	8.51367	0.14526
32	11UMT17-a	0.282862						
32	12HG04	0.282595						

Ref. #	Sample	175Hf/177Hf	238U/204Pb	235U/204Pb	232Th/204Pb	187Os/188Os	187Re/188Os	187Os/188Os(i)
32	12HG06	0.282656						
32	12HXV01	0.2828						
32	12HXV08	0.282639						
32	12HXV09	0.282697						
32	12HXV12	0.282702						
32	12HXV15	0.282707						
32	12HXV19	0.282705						
32	12HXV21A	0.282711						
32	12HXV23	0.282711						
32	12HXV24	0.282657						
32	12HXV32	0.282642						
32	12HXV33	0.28279						

Table B.8 – Calculated values for lavas in the Tibetan Plateau

Ref. #	Sample	Mg# (85% FeO)	Dy/Dy*	K	FeO(t)	d7/4	d8/4
1	K89G185	70.4		39599	6.0	17.14	86.78
1	K89G186	77.2	0.694346	39018	5.9	14.01	80.39
1	K89G189	71.7		38935	5.9	18.85	91.22
1	K89G190	75.5		36112	5.1	14.55	78.20
1	KB9G191	72.5	0.522637	39433	5.1	15.69	76.97
1	K89G192	70.2	0.49499	42753	5.1	18.27	83.25
1	K189G193	72.1		41425	5.1	18.38	81.30
1	K89G197	4.7	0.155729	40678	2.9	13.56	55.16
1	K89G200	74.7		44829	5.3	19.48	101.19
2	05S2-4	74.4	0.704385	68737	5.1		
2	05S2-6	75.3	0.787574	70979	5.3		
2	05S2-9	71.4	0.780018	60768	6.1		
2	05SLP5-1	70.2	0.643684	52383	6.2		
2	05SLP5-2	74.6	0.627347	67741	5.0		
2	05SLP5-4	70.6	0.594452	54126	5.9		
2	CM10-04-04	73.4	0.631546	57198	5.5		
2	CM10-04-09	72.9	0.590344	21418	5.0		
2	CM10-04-12	68.3	0.647389	50723	6.8		
2	04DYH-01	67.2	0.559768	27727	6.5		
2	D3141	73.2	0.634014	30965	8.5		
3	04LQS-2	72.5	0.414763	27478	4.3		
3	04LQS-3	65.9	0.414794	29222	4.3		
3	04LQS-6	63.8	0.48999	20671	5.5		
3	04LQS-14	53.7	0.455444	26814	3.0		
3	04LQS-16	53.6	0.488157	22829	4.1		
3	04YJL-05	65.0	0.48331	24324	6.5		
3	04YJL-07	65.9	0.489389	35531	4.7		
3	04YJL-06	63.8	0.484341	34618	4.2		
3	04YJL-09	66.0	0.490418	36942	4.0		
3	04DN30-2	66.4	0.529495	27976	6.4		
3	04DN30-3	65.3	0.45613	29139	5.0		
3	04DN31-1	60.1	0.468181	27312	4.7		
3	04DN32-1	49.5	0.541979	25901	4.3		
3	04DN32-2	46.3	0.522151	26316	4.5		
3	04DN35-2	53.3	0.534704	27395	4.7		
3	04DN36-3	62.6	0.552097	28059	5.1		
3	04DN37-2	63.3	0.627026	28142	5.1		
3	04DN39	53.3	0.460411	27312	5.1		
3	04DN40	63.2	0.483271	29471	3.5		
3	04DY44-2	60.4	0.539227	27312	5.3		
3	04DY44-4	63.8	0.464575	29554	4.0		
3	04DY44-7	60.9	0.453811	33871	4.9		
3	04D6441	63.8	0.412494	40263	5.2		
3	04D6437	60.7	0.462541	39101	5.5		
4	2T394	58.1	0.601147	4151	10.6		
4	2T395	59.2	0.594741	5562	10.5		
4	2T396	58.0	0.66334	7804	10.7	6.65	42.84
4	98T03	69.9	0.630252	4151	8.6	2.57	59.01
4	98T04	67.4	0.629226	5562	8.9	3.56	77.23
4	98T07	27.5	0.470732	63756	5.6	2.59	73.05

Ref. #	Sample	Mg# (85% FeO)	Dy/Dy*	K	FeO(t)	d7/4	d8/4
4	98T15	43.1	0.515276	40595	6.9	0.58	70.61
4	98T16	18.1	0.436019	49062	8.4	15.53	76.05
4	98T33	17.8	0.46834	55289	7.1	26.60	96.21
4	98T38	11.0	0.43055	48398	8.1	17.91	79.85
4	98T43	11.1	0.445692	48398	8.0	10.41	68.25
4	98T44	25.4	0.472727	70647	6.5	20.98	89.61
4	98T46	16.7	0.395366	52798	7.2	14.71	74.63
4	98T49	21.8	0.420272	56700	5.4	13.13	71.84
4	98T51	18.2	0.406101	54542	6.8	20.41	84.19
4	98T52	56.1	0.507057	26648	6.0	13.13	74.13
4	98T53	24.0	0.465759	66994	6.5	15.70	78.49
4	98T54	34.4	0.591196	77869	2.4	15.21	78.91
4	98T57	16.7	0.44741	54625	6.8	12.25	68.07
4	98T69	23.9	0.464409	66081	6.3	18.08	84.47
4	98T70	27.9	0.457744	61100	6.2	19.06	80.76
4	98T71	19.1	0.393999	49976	6.8	17.90	78.14
4	98T73	4.9	0.417693	57945	6.5	11.43	73.70
4	99T132	69.1	0.517468	51221	6.7	13.10	71.39
4	99T134	45.1	0.448454	54292	2.8	23.96	89.82
4	99T145	50.8	0.522516	61266	3.1	27.78	155.07
4	99T152	64.9	0.570603	62511	4.3	20.73	83.39
4	99T154	65.7	0.479902	67990	5.0	20.22	140.20
4	99T53	56.1	0.869884	87582	3.4	21.03	137.42
4	99T56	63.1	0.621811	93310	3.8	23.37	150.13
4	99T57	59.8	0.675117	71560	4.6	18.62	106.51
4	99T60	65.3	0.72832	96797	3.7	20.19	112.26
4	99T62	66.3	0.74529	83763	3.7	19.70	109.79
5	2002T1021	43.3	0.638643	31048	5.9	21.37	105.26
5	2002T1022	44.8	0.664862	30799	6.1	22.78	114.69
5	2002T1023	47.7	0.602946	31048	6.6		
5	2002T1024	41.1	0.546823	30550	6.8		
5	2002T1025	39.9	0.572304	31131	6.2		
5	2002T1026	38.6	0.517267	30301	6.5		
5	2003T373	59.9	0.541597	16105	8.9		
5	2003T374	63.5	0.538582	20256	8.8		
5	2003T375	46.9	0.596522	27229	7.2		
5	2003T380	50.8	0.587885	27146	5.7		
5	2003T483	43.2	0.544013	27976	4.8		
5	2003T485	51.2	0.514787	31795	3.8		
5	2003T486	51.1	0.527933	32127	4.0		
5	2003T487	52.6	0.505441	29222	4.4		
5	2003T488	40.6	0.51248	35365	2.0		
5	2003T492	25.6	0.518663	29305	5.1		
6	Tl/10	81.8	0.636405	37108	5.6	33.82	200.61
6	Tl/11	86.1	0.636405	60851	5.5	31.14	168.23
6	Tl/18	79.1	0.664811	66579	5.4	27.14	173.23
6	Tl/13	87.1	0.588845	58028	5.8	29.79	161.49
6	Tl/03	88.2	0.619415	52632	6.1	30.71	165.40
6	Tl/08	85.5	0.655403	66828	5.5	27.58	175.07
6	Tl/17	75.8	0.721817	68156	4.1	29.49	176.98
6	Tl/06	82.3	0.504244	76126	3.8	31.60	171.19

Ref. #	Sample	Mg# (85% FeO)	Dy/Dy*	K	FeO(t)	d7/4	d8/4
6	Tl/59	76.3	0.578581	72556	3.4	30.03	162.02
6	CHZ-1	77.4	0.822272	67243	6.0	15.43	116.01
6	CHZ-2	78.6	0.835669	65749	5.8	19.89	128.96
6	CHZ-3	74.5	0.779924	68820	5.9	17.13	126.50
6	CHZ-4	73.2	0.764132	62262	6.3	18.92	131.08
6	CHZ-5	73.6	0.758927	63258	6.3	14.57	117.34
6	CHZ-6	74.5	0.761063	68073	5.8	23.70	139.66
6	CHZ-7	78.6	0.83337	66745	5.9	19.32	126.80
6	CHZ-8	78.7	0.812177	68654	5.7	17.54	125.22
6	CHZ-9	79.7	0.858166	69401	5.8	18.32	124.80
6	CHZ-10	80.0	0.856067	71477	5.8	18.43	124.01
6	CHZ-11	79.4	0.857585	63922	5.9	19.54	127.22
6	CHZ-12	78.0	0.828049	69069	5.9	17.89	126.96
7	AH-7	47.8	0.587797	38602	8.3		
7	G26	55.4	0.501996	55455	6.1		
7	G68	21.1	0.43107	40263	7.1		
7	G98-0	57.4	0.518369	35199	8.9		
7	G98-1	70.8	0.435112	52466	7.3		
7	G98-14	63.3	0.405522	39931	8.7		
7	G98-3	60.4	0.476442	27478	11.1		
7	G98-6	63.3	0.387047	32210	11.0		
7	G98-9	63.2	0.373581	36693	9.8		
7	HH72	68.9	0.536599	37440	8.0		
7	HS07	56.5	0.45452	29720	8.4		
7	HS-69	66.5	0.492748	46406	9.2		
7	JC9719	70.1	0.381171	39018	8.2		
7	JC973	58.9	0.433806	40512	9.3		
7	JC975	67.0	0.442218	39433	9.5		
7	JC978	60.7	0.525811	40595	10.4		
7	JH6	65.2	0.46036	39516	9.3		
7	KX84	67.3	0.452216	40678	8.9		
7	PL-58	51.7	0.604523	32044	8.1		
7	PL-7	66.1	0.609403	32210	9.9		
7	QQ08	53.0	0.555631	33206	5.8		
7	QS22	65.1	0.377214	36693	8.3		
7	XT16	58.7	0.459145	35614	8.6		
7	XT8	58.3	0.579172	30467	9.6		
7	XY03	66.6	0.518012	35116	6.7		
7	XY05	38.2	0.621187	35365	6.2		
7	YS02	64.4	0.519063	38685	8.1		
7	YS72	60.2	0.829553	61017	5.9		
7	ZF91	47.9	0.511863	31961	4.9		
7	ZF96	54.5	0.548478	32957	6.0		
8	ZF09	68.6	0.629829	28890	2.1	12.31	43.78
8	GUO62	61.9	0.667491	18596	2.6	11.00	56.85
8	GUO51	63.9	0.503657	23494	2.7	13.61	54.30
8	GUO48	62.3	0.681795	23161	3.5	14.22	107.48
8	GUO37	53.7	0.671927	13947	5.3	11.15	41.74
8	G09	58.5	0.655879	30716	2.2	10.18	38.74
8	ZFG17	71.9	0.667843	17848	2.1	2.88	49.45
8	G006	61.9	0.467709	27478	1.8	3.87	47.85

Ref. #	Sample	Mg# (85% FeO)	Dy/Dy*	K	FeO(t)	d7/4	d8/4
8	G019	70.6	0.523473	44580	1.5	21.14	63.64
8	G016	68.1	0.474475	56202	1.3	18.67	44.94
8	G025	59.0	0.468077	19758	2.5	10.11	61.39
9	DY-7	73.6	0.531795	76707	5.1	23.31	157.41
9	DC2	69.9	0.51155	88661	5.5	17.88	139.58
9	D509	73.8	0.569476	78450	5.3	20.44	125.74
9	DG43	73.1	0.51604	74382	5.6	19.77	158.37
9	YE51	74.8	0.602223	66994	5.1	23.44	135.74
9	YC08	71.9	0.670749	77703	5.4	26.44	148.74
9	YG13	77.2	0.495546	82103	4.8	25.66	152.16
9	YF12	74.8	0.497732	71560	5.2	26.23	154.32
9	YA32	67.8	0.596454	64586	6.2	21.01	148.90
9	MH78	75.9	0.591306	49228	5.9	25.47	159.86
9	MH69	79.6	0.45579	53711	5.0	25.17	135.35
9	MG-3	72.7	0.625647	66994	5.2	24.49	151.98
9	MY1	71.5	0.56735	67658	6.2	27.93	157.81
9	MK09	73.7	0.561155	62179	6.1	26.28	160.56
9	MR21	74.5	0.598293	57032	5.5	28.95	142.93
9	MA75	74.5	0.48706	59605	6.6	22.60	177.19
9	MX5	75.9	0.514821	56949	5.4	23.03	148.02
9	2003T534	74.1	0.627127	53877	6.1		
9	2003T536	75.1	0.609949	53794	6.4		
9	2003T539	75.9	0.664377	53047	6.2		
9	G8	68.8	0.783409	43915	5.6	17.11	170.38
9	C10	69.0	0.827191	59439	5.8	27.59	146.45
9	CV5	67.8	0.824489	52881	5.9	29.46	120.13
9	C76	68.7	0.662429	50059	6.1	29.37	64.04
9	CH4	68.2	0.977466	44414	6.6	28.02	115.29
9	CH7	76.7	0.869482	48398	6.7	21.24	115.71
9	C03	78.9	0.88689	42670	6.0	25.54	117.22
9	CX38	68.6	0.743264	39931	6.8	18.89	156.96
9	C25	73.6	0.739498	53877	5.0	30.05	81.41
10	CT09	63.1	0.652712	43998	6.7	20.44	89.79
10	CT12	63.2	0.544117	34701	7.8	16.20	85.32
10	CT17	63.0	0.710831	40180	7.9	19.45	90.49
10	CT05	65.2	0.647518	46655	6.6	15.20	95.91
10	CT23	64.8	0.574812	48315	7.3	15.28	75.58
10	QS12	58.1	0.613131	29886	8.7	18.79	63.26
10	QS27	58.2	0.634006	32044	9.8	17.64	86.28
10	QS19	57.4	0.630973	35697	9.7	12.97	45.81
10	QS23	61.5	0.848624	38519	9.3	12.03	58.29
10	QS18	62.0	0.804409	30882	9.4	18.48	90.53
10	QS24	62.3	0.814344	31546	9.1	10.39	55.82
10	KY03	64.0	0.861557	35282	6.8	10.91	55.83
10	KY02	58.2	0.755911	36278	7.4	11.74	76.00
10	KY06	62.3	0.838155	40180	7.8	5.27	53.29
10	KY01	63.3	0.830709	37440	6.9	9.67	49.57
10	HS041	57.2	0.5519	30550	8.4	32.27	93.31
10	HS046	54.6	0.572818	27063	8.3	40.01	101.52
10	HS047	55.2	0.567027	30965	8.5	27.51	51.35
10	HS028	59.4	0.623134	28890	8.5	19.39	21.51

Ref. #	Sample	Mg# (85% FeO)	Dy/Dy*	K	FeO(t)	d7/4	d8/4
10	AH607	61.2	0.606175	36112	9.7	15.79	61.54
10	AH605	63.5	0.435286	39350	10.3	13.31	59.70
10	AH609	62.4	0.756142	36942	8.6	15.44	66.27
10	AH602	66.4	0.657957	36610	9.0	12.38	66.79
10	AH618	66.6	0.573785	39350	9.2	14.91	66.31
10	AH615	67.0	0.710777	37523	9.3	10.74	55.78
10	YS74	61.8	0.762948	52051	7.6	13.75	45.10
10	YS78	64.7	0.727495	43002	6.5	15.93	64.88
10	YS05	61.6	0.778425	60021	8.0	14.51	48.98
10	YS79	60.4	0.772281	44497	5.9	18.00	63.43
10	YS07	60.8	0.626957	48647	5.4	20.47	88.78
10	KX44	69.3	0.799483	47402	8.2	12.30	61.58
10	KX51	67.4	0.482025	38851	8.4	10.47	53.58
10	KX80	68.2	0.761619	40346	8.1	5.56	31.10
10	KX49	69.1	0.938366	47900	8.2	14.93	48.13
10	KX62	69.0	0.709082	44081	8.3	11.68	43.83
10	PL53	67.1	0.730691	36444	8.4	12.67	39.38
10	PL61	66.5	0.747731	40595	8.5	16.73	35.88
10	PL3	54.8	0.603314	35448	7.6	4.45	79.45
10	PL18	57.7	0.635635	33871	7.8	15.14	68.10
10	PL92	58.0	0.544541	35614	7.9	10.07	48.59
10	PL43	58.0	0.593522	39682	7.1	10.65	57.17
11	G10						
11	G15A						
11	S70C						
11	S70D						
12	07-SA-21	65.4	0.606082	20422	5.0		
12	07-SA-26A	55.4	1.022128	830	4.1		
12	07-SA-26B	52.5	0.855083	581	4.0		
12	07-SG-03	51.7	0.670272	27146	3.9		
12	07-SG-04A	57.2	0.662705	35033	3.9		
12	07-SG-05	55.5	0.605974	28641	4.3		
12	07-SG-06	56.7	0.628877	39599	4.1		
12	07-SG-29	51.2	0.604909	40180	3.1		
12	07-SG-30	51.2	0.597593	39267	3.1		
12	07-SG-31A	52.0	0.584023	37523	2.8		
12	07-SG-31B	52.3	0.560744	37938	2.9		
12	07-SG-48A	48.2	0.639002	32044	3.1		
12	07-SG-48B	48.0	0.566548	32957	3.2		
12	07-SG-52A	63.3	0.570053	27146	5.5		
12	07-SG-66	53.3	0.712865	30384	2.9		
12	06-SA-28C	67.3	0.697912	25154	5.2		
12	06-SA-48A	52.1	0.766526	830	4.0		
12	06-SG-200	60.3	0.606891	33704	4.3		
12	06-SG-201	53.4	0.581428	28142	4.3		
12	07-SA-25						
13	NQ2-1*	80.9	0.659026	37274	6.1		
13	NQ21-4*	82.4	0.489524	48564	4.0		
13	NQ7-1*	70.4	0.556393	37025	2.8	4.19	37.02
13	Y1-11	70.0	0.497993	39433	1.5	5.03	34.70
13	Y1-12	63.7	0.506126	37357	2.7	4.27	31.95

Ref. #	Sample	Mg# (85% FeO)	Dy/Dy*	K	FeO(t)	d7/4	d8/4
13	Y1-13	65.3	0.520018	40844	2.2	14.92	66.63
13	Y1-14	67.6	0.528863	37357	2.4		
13	Y1-15	64.1	0.54554	38685	2.5	13.89	65.85
13	Y115-90	71.4		35448	2.9		
13	Y1-16	76.6	0.430827	40595	1.4		
13	Y1-18	76.1	0.514898	57198	1.4		
13	Y1-8	69.0	0.529049	36610	2.4	12.62	61.64
13	Y1-9	66.1	0.491522	39350	2.5	13.35	61.38
13	Y2-1	75.4	0.480743	34618	2.1		
13	Y2-2	73.1	0.533533	41010	2.2	13.82	64.30
13	Y2-3	65.1	0.502021	39682	2.1	13.96	65.11
13	Y2-4	66.8	0.509106	36942	2.4	13.22	63.80
13	Y2-5	67.5	0.51755	36195	2.3		
13	Y2-6	70.6	0.531864	36693	2.2	13.42	63.54
13	Y2-7	63.0	0.527888	39267	2.1		
13	Y2-8	70.1	0.52297	40346	2.2		
13	Y2-9	65.6	0.500132	38519	2.2	12.56	61.77
13	Z96-2*	72.8	0.527161	45493	4.0		
14	KK06003	49.2	0.549324	35780	5.7	13.47	77.21
14	KK06004	46.3	0.573521	36776	5.7	19.52	93.75
14	KK06005	44.9		36610	5.7		
14	KK06006	49.7	0.575168	36195	5.3	21.07	96.65
14	KK06007	45.0	0.562218	37938	5.4		
14	KK06008	48.1		36527	5.8		
14	KK06009	48.1		35531	5.9		
14	KK06010	45.5		37025	5.8	23.48	103.59
14	KK06011	48.3	0.565154	36776	5.7	20.02	94.36
14	KK06012	46.6	0.559821	36942	5.7		
14	KK06013	46.7		36527	4.3		
14	KK06014	47.9		35863	4.4		
14	KK06016	48.6	0.460357	36444	4.4		
14	KK06018	52.9		36361	4.0	20.47	99.04
14	KK06019	50.4		35780	4.4		
14	KK06022	49.1	0.475968	35780	4.6	19.16	93.60
14	KK06024	54.5		35033	4.3	19.39	95.78
14	KK06025	39.2	0.594607	33372	7.2		
14	KK06026	28.1	0.58423	34203	7.2		
14	KK06027	40.4	0.572744	34037	6.3	22.27	102.18
14	KK06028	42.0		34701	6.3	19.69	94.81
14	KK06029	41.7	0.575233	33871	6.4	18.42	93.36
14	KK06030	40.8	0.568353	34286	6.3	17.61	90.84
14	KK06031	40.4	0.553896	34120	6.4		
14	KK06032	40.4		42670	1.8	17.25	86.89
14	KK06033	40.4		43417	1.3		
14	KK06034	40.5		42421	1.7		
14	KK06038	47.7	0.545791	36195	4.4	23.11	101.74
14	KK06039	35.7	0.571256	37938	3.1		
14	KK06040	43.5		37772	2.7		
14	KK06041	36.1	0.576952	36361	6.5	16.72	82.26
14	KK06042	43.6	0.544348	36195	4.8	114.91	80.29
14	KK06043	30.6		37689	5.6		

Ref. #	Sample	Mg# (85% FeO)	Dy/Dy*	K	FeO(t)	d7/4	d8/4
14	KK06046	28.4	0.556858	37938	5.2		
14	KK06047	29.5	0.570567	38353	4.5		
15	Z02H1	65.5	0.50918	27146	4.1		
15	Z07H	50.1	0.464186	26399	3.0		
15	Z07H1	70.5	0.543083	28890	4.8		
15	Z07H2	72.0	0.537652	29056	4.8		
15	Z07H3	65.7	0.480094	27312	4.6	19.23	87.27
15	Z07H4	71.3	0.529955	28225	4.6	19.62	87.04
15	Z07H5	71.1	0.498084	27644	3.6		
15	Z07H6	63.4	0.526934	26482	4.4	18.32	85.18
15	Z08H1	67.9	0.520899	27395	3.8	18.61	85.97
15	Z08H2	58.3	0.523764	27644	4.1		
15	Z08H3	60.3	0.534747	28225	4.0		
15	Z08H4	52.3	0.554949	28641	3.6		
15	Z08H6	60.1	0.526042	27893	4.3	18.61	86.04
15	Z12H3	57.1	0.561128	25154	4.7		
15	Z15H1	59.1	0.502058	26067	4.1		
15	Z15H2	56.7	0.495301	26316	4.1		
15	Z15H3	58.4	0.505658	26233	4.3		
15	Z15H5	55.9	0.46008	28558	3.1		
15	Z15H6	62.3	0.503079	29222	3.1		
15	Z19H1	68.6	0.520796	29471	3.4		
15	Z19H4	65.2	0.501896	30633	2.8		
15	Z19H5	65.5	0.489735	31131	2.8		
15	Z19H6	65.6	0.507768	31214	2.8		
15	Z06H	24.7	0.514603	22995	5.4		
15	Z08H5	43.3	0.563849	29471	2.9	19.47	87.39
15	Z10H	13.2	0.581691	28308	4.7		
15	Z11H1	16.7	0.565984	28142	5.0		
15	Z11H2	26.7	0.59944	26067	5.7		
15	Z12H1	43.7	0.547875	24739	5.4		
15	Z12H2	44.6	0.580507	26897	2.8	19.56	85.54
15	Z15H7	22.7	0.507163	27395	1.9	20.04	80.39
15	Z15H11	32.9	0.641902	37191	5.1		
16	ET021B	67.5	0.809044	2324	9.0	15.95	85.90
16	ET021C	60.6	0.668856	18596	6.4	14.25	82.35
16	ET022A	37.2	0.427807	20920	1.7		
16	ET024	44.3	0.422134	24656	1.0		
16	ST052B	33.9	0.499072	52300	2.0		
16	ST053	37.2	0.513952	48813	2.5		
16	ST054	36.3	0.523471	51138	2.2		
16	ST055A	26.9	0.492819	55787	1.6		
16	ST055B	31.5	0.503332	54874	2.0		
16	ST055C	54.6	0.654479	36610	7.2		
16	ST057A	45.8	0.566591	44248	5.2		
16	ST058	57.5	0.512334	31463	5.3		
16	ST059A	35.8	0.559006	49810	2.5		
16	ST060A	42.0	0.495441	55621	2.1		
16	ST060C	42.9	0.488936	53130	2.3		
16	ST061A	41.3	0.718673	37938	8.0		
16	ST062	42.0	0.493336	47402	3.4		

Ref. #	Sample	Mg# (85% FeO)	Dy/Dy*	K	FeO(t)	d7/4	d8/4
16	ST101B	51.0	0.580015	10377	6.3		
16	ST102B	50.8	0.68125	15524	7.2		
16	ST109	45.6	0.476116	24905	2.8		
16	ST119A	61.6	0.789804	1992	7.6		
16	ST119B	54.4	0.708859	10958	6.6		
16	ST121	47.7	0.689467	18679	6.3		
16	ST122	61.5	0.658535	1162	7.1		
16	T006B1	66.3	0.649045	12867	6.6		
16	T006B2	57.7	0.679935	7554	10.6		
16	T034A	57.9	0.750132	9049	6.3		
16	T034B	59.6	0.771559	4317	5.8		
16	T036D	57.8	0.823303	5977	9.5		
16	T038F	50.1	0.563097	36693	4.3		
16	T038G	42.0	0.603304	22165	5.4		
16	T038M	27.8	0.43512	43085	0.9		
16	T039	35.1	0.568269	42255	1.5		
16	T040A	44.1	0.598393	26399	4.1		
16	T040B	39.2	0.608837	30135	3.5		
16	T041 J	46.2	0.770119	6392	9.9		
16	T041F	45.8	0.776856	8302	9.5		
16	T041H	44.8	0.842846	6060	8.8		
16	T042C	49.3	0.751582	6807	9.5		
16	T042D	77.1	0.733739	4815	8.9		
16	T046A	45.0	0.698014	8717	7.0		
16	T047	46.0	0.712343	21169	6.8		
16	T048B	50.8	0.561331	18264	5.5		
16	T049A	56.3	0.517152	24407	2.5		
16	T049B	39.1	0.557626	13864	6.6		
16	T049C	39.9	0.566098	17599	8.0		
16	T051B	0.0	0.579291	17848	1.7		
16	T051C	28.6	0.387568	45742	0.8		
16	T052	39.0	0.515676	34535	2.8		
16	T054A	41.7	0.758732	8800	8.0		
16	T055A	42.2	0.6918	5147	6.7		
16	T055B	21.8	0.751692	17931	9.5		
16	T056A	31.5	0.728318	6226	8.3		
16	T056B	34.0	0.682839	2740	9.3		
16	T062B	39.2	0.62682	31463	6.0		
16	T062C	50.4	0.712113	7887	8.3		
16	T063	47.2	0.630482	22829	4.7		
16	T064A	47.5	0.587356	17267	5.5		
16	T065A	57.1	0.581871	25652	3.6		
16	T065B	19.2	0.508642	37523	1.9		
16	T066	47.4	0.630862	10958	9.1		
16	T068	6.9	0.510291	35697	1.7		
16	T070A	47.3	0.523711	22746	3.0		
16	T072A	60.8	0.525352	21667	4.9		
16	T072D	58.2	0.574683	16520	5.5		
16	T072E	59.9	0.567427	13781	5.8		
16	T073	54.1	0.567865	26399	4.8		
16	T078B	43.9	0.412935	6641	2.5		

Ref. #	Sample	Mg# (85% FeO)	Dy/Dy*	K	FeO(t)	d7/4	d8/4
16	T079A	60.3	0.918378	5064	10.9		
16	T079B	49.8	0.713289	18596	10.0		
16	T079C	47.9	0.712282	5811	10.5		
16	T080	55.6	0.75027	18097	9.5		
16	T082A	28.7	0.397433	30467	1.2		
16	T082B	25.7	0.399273	34618	1.5		
16	T083B	19.1	0.496042	50308	1.2		
16	T083C	41.4	0.742765	13532	10.7		
16	T084C	31.0	0.621383	45576	2.0		
16	T102A	34.1	0.570401	23826	5.6		
16	T103	60.8	0.579809	47485	0.4		
16	T104	38.0	0.544421	35863	2.6		
16	T105A	38.5	0.656513	19260	8.3		
16	T110A	48.5	0.578584	37025	6.4		
16	T110B	51.2	0.597109	27229	4.5		
16	T111	46.1	0.504257	30301	1.8		
16	T112	37.9	0.594077	29720	4.9		
16	T113	36.5	0.592168	29969	3.9		
16	T116A	57.5	0.805913	10128	10.1		
16	T117	48.9	0.585827	17516	2.2		
16	T127B	54.3	0.554837	16852	3.7		
16	T129A	39.4	0.636601	22746	7.8		
16	T130	7.8	0.529685	56119	0.5		
16	T131A	23.4	0.561356	2241	2.5		
16	T134	67.2	0.547724	44331	0.6		
16	T136A	2.3	0.473182	42836	1.8		
16	T136B	22.2	2.086707	31463	4.0		
16	T138D	59.8	0.727782	26316	1.2		
16	T139	5.4	0.51726	42172	0.7		
16	T140A	25.2	0.525864	17184	2.7		
16	T140B	45.0	0.59131	3072	6.6		
16	T140D	33.4	0.531747	21999	4.0		
16	T140E	5.3	0.731712	30965	0.8		
16	T142	32.2	0.557723	22082	3.2		
16	T143	34.6	0.540773	29471	2.9		
16	T144A	44.0	0.85311	22663	2.0		
16	T144B	55.8	0.673658	24241	6.8		
16	T144C	34.1	0.401537	52798	1.0		
16	T144D	47.0	0.429681	27063	2.3		
16	T146	35.5	0.615192	32957	3.2		
16	T147	15.2	0.589073	29056	1.8		
16	T151	62.8	0.639753	14196	8.1		
16	T152A	40.2	0.593049	29305	5.7		
16	T152B	64.6	0.710567	13698	8.0		
16	T155	39.7	0.519182	42421	2.6		
16	T160A	38.5	0.626344	33538	5.1		
16	T160B	16.5	0.599664	43832	1.0		
16	T169A	1.3	0.515781	52217	1.6		
16	T169B	5.8	0.651575	49312	1.0		
16	T169C	32.0	0.58416	24075	0.9		
16	T233A	54.1	0.528919	3570	5.5		

Ref. #	Sample	Mg# (85% FeO)	Dy/Dy*	K	FeO(t)	d7/4	d8/4
16	T233B	48.1	0.609887	19592	5.5		
16	T233C	40.8	0.708633	9298	9.3		
16	T234A	47.9	0.597113	26067	6.5		
16	T234B	44.3	0.628569	19675	8.0		
16	T234C	33.7	0.564685	16022	4.5		
16	T235A	40.7	0.60342	25818	1.2		
16	T235B	41.3	0.541444	23327	1.0		
16	T238B	47.8	0.671586	2075	7.4		
16	T239	50.4	0.638045	12369	5.9		
16	T240B	47.9	0.640933	27810	5.6		
17	GGL01	36.1	0.616918	26399	4.7		
17	GGL02	12.9	0.601508	27561	4.5		
17	GGL03	30.1	0.612532	26233	7.3	15.14	87.05
17	GGL04	25.4	0.603925	25901	2.7		
17	GGL05	49.4	0.638619	20339	6.0	15.08	86.83
17	GGL06	48.8	0.632015	20007	6.4	15.18	86.53
17	GGL07	48.0	0.651771	21086	5.8	15.98	88.63
17	GGL08	52.6	0.64758	19675	6.6	15.06	86.58
17	GGL09	47.0	0.634183	21833	6.3	15.69	88.25
17	GGL10	47.0	0.648054	21667	6.3	15.11	86.89
17	GGL11	43.3	0.629181	22248	6.0		
17	GGL12	46.7	0.651168	21584	6.3	15.54	87.55
17	GGL13	50.2	0.629611	21335	6.0	15.22	87.51
17	GGL14	45.1	0.632856	21833	5.8	15.10	86.77
17	GGL15	38.6	0.637899	23078	4.4		
18	GJ0601	55.4	0.525615	72058	3.5	25.64	122.26
18	GJ0602	53.2	0.497301	70979	3.6	25.55	121.88
18	GJ0605	59.5	0.500359	70481	3.5	25.60	122.09
18	GJ0606	44.0	0.49247	74714	3.7	25.67	121.43
18	08YR04	54.1	0.543105	57779	2.6	25.03	119.84
18	GJ0614	32.4	0.568751	38104	2.8	25.97	129.75
18	GJ0617	53.6	0.497208	36195	2.7	25.98	128.89
18	GJ0619	54.1	0.534114	37689	2.7	25.91	128.73
18	GJ0620	36.9	0.551566	36776	2.4	25.89	128.91
18	GJ0624	57.8	0.456669	51719	2.3	25.57	124.91
18	GJ0627	56.9	0.456087	49478	2.5	25.47	125.81
18	GJ0628	56.2	0.445379	47734	2.4	25.39	125.35
18	GJ0629	54.5	0.477734	48979	2.7	25.52	126.11
18	10XB03	49.0	0.586188	42006	2.8	21.33	117.10
18	10XB04	42.2	0.574711	40263	2.6	20.59	117.40
18	10XB07	54.2	0.567604	42421	2.9	18.34	110.68
18	08YR05	72.1	0.644818	47236	5.5	23.61	154.48
18	10XB10	69.6	0.815699	54542	4.8	16.65	107.67
18	10XB12	71.7	0.852681	56617	5.2		
18	10XB13	71.5	0.827706	55040	5.3	17.89	113.36
18	10YR01	72.8	0.711701	54126	3.6	16.95	133.23
18	10YR02	71.1	0.693633	47817	4.8	18.58	140.60
18	10YR04	72.4	0.698368	50889	5.3	18.83	141.60
18	10YR04a	71.8	0.697081	52881	5.1		
18	10YR07	72.4	0.686341	52300	5.3	17.92	139.27
19	MV1B	24.5		40678	1.2		

Ref. #	Sample	Mg# (85% FeO)	Dy/Dy*	K	FeO(t)	d7/4	d8/4
19	MV2	15.0		40844	1.2		
19	UM1B	21.2		40678	1.2		
19	UM3V	18.2		40346	1.1		
19	UMQP	14.0		74382	1.0		
19	UMVU	22.3		41093	1.0		
20	TE008/93	68.2	0.822503	51719	5.0		
20	TE011/93	67.3	0.8815	56949	5.2		
20	TE125/93	62.8	0.783296	62594	5.9		
20	TE126/93	68.2	0.862547	52632	6.7	19.54	135.31
20	TE127/93	68.2	0.874543	54791	6.5		
20	TE131/93	70.3	0.793744	49644	6.0		
20	TE137/93	78.1	0.86664	55704	6.0	23.45	173.66
20	TE138/93	72.5	0.807158	51387	5.7	18.78	161.18
20	TE117/93	73.1	0.858383	53794	5.3		
20	TE118/93	71.6	0.775089	52217	5.6	21.55	146.35
20	TE007/93	59.6		36527	4.2		
20	TE025/93	54.9	0.532755	56617	3.4	22.93	112.98
20	TE136/93	48.1	0.613085	42338	3.2		
20	TE148/93	37.4	0.569497	52300	3.2		
20	TE150/93	34.5	0.525241	51968	3.1	17.00	103.48
20	TE153/93	35.7	0.606832	50308	3.1		
20	TE154/93	49.0	0.517235	49893	3.2		
20	TE047/93	30.5	0.511066	24075	2.0		
20	TE189/93	43.4	0.652552	31131	2.3		
20	TE192/93	40.1	0.624765	23411	1.5		
20	TE194/94	45.7	0.551106	29388	3.2		
21	Y-2	29.1	0.680717	50308	4.8		
21	Y-4	41.8	0.64092	50806	1.4		
21	ZB1	60.0	0.747659	54209	5.9		
21	ZB4	60.9	0.736693	53213	5.8		
21	ZB10	61.2	0.738396	52466	5.9		
21	ZB12	60.6	0.770335	54292	5.6		
22	K732	43.5		33538	7.9		
22	K738	43.7		28142	9.9		
22	K89G185	49.4		39599	8.6		
22	K89G200	58.2		44829	6.6		
22	K9007	41.6		32625	5.5		
22	K9008	31.5		34950	5.6		
22	K9021	41.1		34203	5.3		
22	K9024	51.5		31629	6.3		
22	K9031	53.2		31795	6.2		
22	K9038	50.1		30799	5.3		
23	Bb-105	14.8		58775	4.5		
23	Bb-107	67.3	0.69534	32293	8.9		
23	Bb-109	15.9	0.51922	58194	4.1	17.14	86.78
23	Bb-114	55.7	0.500687	11207	8.9	14.01	80.39
23	Bb-88	51.9		35282	13.3	15.69	76.97
23	Bb-89	59.5	0.15781	31712	8.6	18.27	83.25
23	Bb94-2	26.9		63756	3.9	18.38	81.30
23	Bb-95	30.4	0.440776	64005	6.7	13.56	55.16
23	Bg 121	40.6	0.557539	31961	7.2	19.48	101.19

Ref. #	Sample	Mg# (85% FeO)	Dy/Dy*	K	FeO(t)	d7/4	d8/4
23	Bg 124	47.7	0.534815	30550	5.5	15.64	79.27
23	COUL311	21.3	0.60093	37855	2.4		
23	COUL326	40.6	0.533786	37108	2.5		
23	COUL328	47.5	0.59655	28807	3.7		
23	COUL338	47.5	0.539743	16437	7.3		
23	COUL339	47.4	0.511108	10045	7.6		
23	k705	47.1	0.548506	31795	7.5		
23	k708	41.5	0.522514	36278	7.4		
23	K713	42.7	0.502198	30633	7.2		
23	K716	48.4		35780	7.3		
23	K718	36.0		34203	8.4		
23	K720	46.5	0.445742	30052	7.9	17.10	82.89
23	K723	45.4		29637	8.0	15.05	78.99
23	K732	39.6		33538	7.9	16.70	87.39
23	K738	39.7		28142	9.9		
23	K89G159	41.0	0.432766	60270	2.6		
23	K89G162	56.9		59938	3.1		
23	K89G163	52.1		53379	3.1		
23	K89G185	45.4		39599	8.7		
23	K89G186	54.9		39018	8.2		
23	K89G191	50.6		39433	6.6		
23	K89G192	49.1		42753	6.2		
23	K89G193	50.7		41425	6.4		
23	K89G197	45.6		40678	0.9		
23	K89G200	54.2		44829	6.6		
23	K9002	41.0		19094	3.9	20.39	102.68
23	K9006	36.5		34369	5.4		
23	K9007	37.6		32625	5.5	16.44	88.19
23	K9008	28.1		34950	5.6	18.73	94.01
23	K9016	35.6		34950	5.1	18.27	88.98
23	K9017	35.5		34452	5.4		
23	K9018	36.2		34535	5.5	18.04	100.53
23	K9019	36.8		33289	5.6		
23	K9021	33.6		34203	6.2		
23	K9024	47.4		46821	6.3	17.14	89.19
23	K9026	44.6		34618	6.1	37.26	88.52
23	K9027	45.5		34120	6.1	16.36	79.59
23	K9028	46.2		30052	5.7		
23	K9029	45.2		33704	6.0	16.94	88.78
23	K9031	49.2		31795	6.2		
23	K9032	44.2		33289	6.5		
23	K9038	46.0		30799	5.3		
23	K9039	24.4	0.484391	30799	6.7		
23	Kp 35-10	43.7	0.482121	32210	5.8		
23	Kp12-58	35.2	0.532572	35946	7.3	9.20	71.06
23	Kp23-2	46.9	1.044084	33704	8.5	15.99	87.80
23	Kp24-1	48.8	0.804258	35780	7.2	17.68	95.41
23	Kp39-3	63.0		43334	8.2	9.97	63.45
23	Kp47-2	51.7		33704	6.6	8.57	62.65
23	Kp47-5	49.2		34701	7.8	26.37	138.22
24	2303	44.9		43417	1.2	24.86	143.83

Ref. #	Sample	Mg# (85% FeO)	Dy/Dy*	K	FeO(t)	d7/4	d8/4
24	2509	28.9		42172	1.3		
24	1P2JD7-1	34.8		32791	1.0		
24	1P2JD7-1a	3.4		34369	1.2		
24	2011a	65.1		34286	0.3		
24	2059a	16.6		41757	2.5		
24	2303a	38.5		44995	1.7		
24	2511-1	42.2		45410	1.6		
25	04wq-1	76.0	0.487887	13117	7.1		
25	04wq-2	75.7	0.49294	23494	6.9		
25	04wq-3	76.7	0.502926	25818	7.3		
25	04wq-4	76.1	0.534182	26067	6.9		
25	04wq-5	76.7	0.484143	24158	7.3		
25	04wq-6	69.6	0.536074	27893	6.6		
25	04wq-7	68.6	0.531244	27893	6.5		
25	4086-1	68.1	0.526558	27395	6.5		
25	8528	73.2	0.570374	31048	6.9		
25	8518-1	63.6	0.550897	25237	4.6		
25	8518-2	63.3	0.558323	25403	4.7		
25	9063-GS2	66.7	0.497242	21501	5.4		
25	9063-GS3	66.8	0.52681	22580	5.1		
25	D3145	21.0	0.438647	62096	4.3		
26	05S2-7	75.4	0.818903	70813	5.2		
26	05S2-8-1	75.6	0.758341	66745	5.1		
26	05SLP5-3	68.0	0.691841	62843	5.1		
26	05SLP5-05	73.6	0.671905	54542	6.0	19.91	156.88
26	05SLP5-06	73.9	0.583807	54375	5.5		
26	05SLP5-7	74.8	0.656115	58526	5.9	22.15	134.85
26	05SLP5-8	71.0	0.551777	52881	5.1		
26	05SLP5-09	75.5	0.61056	62760	5.4		
26	S05SLP5-10	69.6	0.657545	52881	6.2		
26	05SLP5-11	70.2	0.642601	53213	6.1		
26	05SLP5-16	73.1	0.787741	55953	6.9		
26	05SLP4-01	77.8	0.858435	53296	8.2	22.78	146.08
26	05SLP4-02	75.5	0.739613	60851	6.9	20.41	152.89
26	05SLP4-03	75.0	0.805429	73884	8.0	20.59	187.55
26	05SLP4-04	74.2	0.714429	69069	7.2		
26	05S2-7					18.36	145.72
26	05S2-8-1					17.86	142.71
27	WR-12-48	40.2	0.455714	50640	4.5		
27	WR-12-47	9.8	0.633823	37523	0.8		
27	WR-12-44	39.7	0.392132	10543	5.1		
27	WR-12-45	52.2	0.703685	6641	10.4		
27	WR-12-40	42.5	0.397664	26399	4.3		
27	WR-12-42	46.5	0.67336	9630	8.3		
27	WR-12-33	47.5	0.499111	27146	4.8		
27	WR-12-35	50.9	0.599378	14362	8.0		
28	T2A/98	80.5	0.7564	63839	5.8		
28	T3b/98	64.4	0.659194	49478	6.1		
28	T4A/98	72.6	0.677684	54126	5.4		
28	T5A/98	70.7	0.637229	41757	3.8		
28	T11B/98	56.8	0.619707	23411	3.6		

Ref. #	Sample	Mg# (85% FeO)	Dy/Dy*	K	FeO(t)	d7/4	d8/4
28	JPT 14.2	55.4	0.615101	22414	3.6		
29	JPT24A	62.6	0.575673	39848	3.5		
29	JPT24B	69.2	0.70487	48979	5.0		
29	JPT24C	70.7	0.691762	48979	5.2		
29	JPT22	54.7	0.517071	35697	2.6		
29	K89G162	60.5	0.655645	61432	3.1		
29	20E39A	37.1	0.628341	29056	6.7		
29	JPT7	69.1	0.628913	44829	4.3		
29	T5B/98	67.4	0.623781	43168	4.0		
29	JPT14.1	61.9	0.600619	24075	3.9		
29	JPT3	38.2	0.619109	38187	4.4		
29	JPT4	48.2	0.47078	34037	1.8		
29	JPT5.2	52.2	0.598353	39018	2.9		
29	JPT8	40.0	0.278437	43168	1.9		
29	95RAS11.3	53.8	0.451074	20754	1.4		
29	T2A	80.4	0.768904	66413	6.0		
29	T3B	64.3	0.653256	51470	6.3		
29	T4A	72.4	0.684937	57281	5.8		
29	T5A	70.9	0.636774	45659	4.0		
29	912	58.2	0.590036	41508	6.5		
29	1105	42.5	0.551694	35697	5.4		
29	K702	58.2	0.61676	31546	6.5		
29	K703	54.1	0.629814	34037	7.1		
29	K89G185	58.7	0.663333	40678	8.5		
29	K89G186	49.6	0.65932	39848	8.7		
29	K89G200	58.1	0.623953	44829	6.7		
29	KP 12.6	39.3	0.6102	33206	6.5		
29	KP47-2	55.7		34867	6.8		
29	KP47-5	53.5		35697	8.0		
29	Bb 124	53.4	0.540633	31546	5.3		
29	Bb121	46.6	0.538895	31546	6.5		
29	Bq137	61.3	0.533446	35697	5.0		
29	Bb119	30.9	0.597241	30716	6.6		
29	Bb122	42.0	0.522971	34037	5.2		
29	Bb135	42.3	0.529027	35697	4.9		
29	Bg142	42.6	0.66016	44829	2.0		
29	Bq140	46.6	0.571252	42338	2.9		
29	Bq141	30.6	0.600777	36527	3.3		
29	K9024	51.6	0.550855	32376	6.5		
29	K9026	49.0	0.560839	34867	6.1		
29	K9027	49.5	0.555457	34037	6.2		
29	K9028	50.6	0.557534	31546	5.9		
29	K9029	49.0	0.553594	34037	6.1		
29	K9031	53.1	0.541812	32376	6.3		
29	K9032	48.1	0.549119	34037	6.6		
29	K9038	49.8	0.596236	31546	5.5		
29	K9039	28.2	0.584695	31546	6.9		
29	K9041	25.3	0.65827	24905	5.6		
29	K9001	47.5	0.55159	15773	3.2		
29	K9002	44.8	0.578366	19094	3.9		
29	K9006	41.1	0.580474	34037	5.4		

Ref. #	Sample	Mg# (85% FeO)	Dy/Dy*	K	FeO(t)	d7/4	d8/4
29	K9007	41.3	0.572226	33206	5.7		
29	K9008	32.5	0.609209	35697	5.7		
29	K9016	39.5	0.598847	34867	5.1		
29	K9017	39.8	0.583008	34867	5.4		
29	K9018	40.4	0.574783	34867	5.6		
29	K9019	41.3	0.582367	34037	5.7		
29	K9021	41.1	0.588714	34867	5.4		
30	2007k251	84.5	0.639574	41259	8.4		
30	2007k252	80.5	0.620786	42255	7.4		
30	2007k253	82.1	0.635635	40429	7.6		
30	2007k254	80.5	0.636477	46074	7.4		
31	DHLT-10	84.6	0.580122	43251	5.7	21.27	42.65
31	DHLT-2	72.5	0.576509	44248	5.5	18.17	38.99
31	DHLT-4	77.8	0.68665	55372	7.1	21.60	94.62
31	DHLT-5	69.9	0.599407	43500	5.7		
31	DHLT-7	72.4	0.61988	41259	6.2	17.67	80.71
31	DHLT-9	83.8	0.584294	42919	5.7		
31	PL-12	61.0	0.661849	33704	8.0	9.51	58.21
31	PL-2	75.2	0.681062	34286	8.0	5.78	40.85
31	PL-3	72.6	0.689361	34286	8.2	0.93	59.71
31	PL-5	62.6	0.537346	34369	8.3	8.47	43.80
31	PL-7	70.1	0.650698	33040	7.8	6.07	38.79
31	PL-9	56.8	0.657538	34369	7.8	9.08	42.04
31	YCN-1	68.6	0.645408	30965	7.4	16.16	64.71
31	YCN-2	67.1	0.645004	31048	7.5		
31	YCN-3	64.1	0.636569	32708	7.6	14.97	58.77
31	YCN-4	62.8	0.634687	32708	7.6		
31	YCN-6	59.5	0.611629	33040	7.7	14.50	58.11
31	YCN-7	73.3	0.610855	32874	7.6	12.66	53.36
31	YCN-8	92.7	0.612333	32708	7.7		
31	KP24-1	53.4	0.440776	35780	7.1		
31	KP25-3	47.3	0.389332	34784	6.7		
31	KP28-1	50.7	0.408933	35199	6.3		
31	KP33-3	59.2		34452	8.9		
31	KP39-1	78.5		19094	8.3		
31	KP39-4	57.7		26897	4.1		
31	KP47-1	51.3		37108	1.9		
31	KP47-4	54.5		36278	5.9		
31	KP47-7	64.2		36278	7.7		
32	11UMT14	41.0	0.682074	1411	8.2		
32	11UMT15	56.9	0.862966	6060	8.8		
32	11UMT17-a	72.7	0.64305	26399	8.1	14.09	68.35
32	12HG04	39.8	0.742325	47900	1.1	15.92	75.96
32	12HG06	31.9	0.982068	60187	1.1	13.69	64.64
32	12HXV01	70.8	0.635534	41010	5.3	15.28	79.55
32	12HXV08	44.9	0.608985	41923	1.8	14.99	75.06
32	12HXV09	34.5	0.594573	36278	5.8	17.51	90.77
32	12HXV12	44.1	0.615212	38187	5.9	15.83	83.52
32	12HXV15	43.9	0.611668	39682	5.4	15.68	82.91
32	12HXV19	42.2	0.591294	26814	5.9	15.91	83.14
32	12HXV21A	51.5	0.603172	39267	4.4	15.63	82.48

Ref. #	Sample	Mg# (85% FeO)	Dy/Dy*	K	FeO(t)	d7/4	d8/4
32	12HXV23	44.2	0.554376	39433	5.3	15.38	81.21
32	12HXV24	52.6	0.580435	42836	1.1	15.05	76.99
32	12HXV32	52.0	0.624861	42089	1.1	14.94	76.24
32	12HXV33	77.3	0.746105	33704	6.4	14.84	80.28
32	13DV05	42.4	0.639773	32625	6.3		
32	13DV04	40.3	0.61717	32708	6.5		
32	13DV11	44.8	0.674063	34867	6.5		
32	13DV13	47.5	0.614948	31878	6.2		
32	13DV14	43.6	0.597963	33871	5.9		
32	13DV15	43.9	0.595884	33704	6.1		
32	13DV23	37.6	0.609354	29554	7.1		
32	13DV29	51.0	0.635272	28890	7.1		
32	13LG07	35.6	0.49456	37274	4.7		
32	13XV01	47.6	0.553036	35199	5.4		
32	13XV02	47.9	0.581665	33455	5.9		

B.2 References

Arnaud, N.O., Vidal, P., Tapponnier, P., Matte, P., and Deng, W.M., 1992, The high K2O volcanism of northwestern Tibet: Geochemistry and tectonic implications: Earth and Planetary Science Letters, v. 111, p. 351–367, doi: 10.1016/0012-821X(92)90189-3.

Chen, J., Wu, J., Xu, J., Dong, Y., Wang, B., and Kang, Z., 2013, Geochemistry of Eocene high-Mg# adakitic rocks in the northern Qiangtang terrane, central Tibet: Implications for early uplift of the plateau: Geological Society of America Bulletin, v. 125, p. 1800–1819, doi: 10.1130/B30755.1.

Chen, J.-L., Xu, J.-F., Wang, B.-D., and Kang, Z.-Q., 2012, Cenozoic Mg-rich potassic rocks in the Tibetan Plateau: Geochemical variations, heterogeneity of subcontinental lithospheric mantle and tectonic implications: Journal of Asian Earth Sciences, v. 53, p. 115–130, doi: 10.1016/j.jseaes.2012.03.003.

Ding, L., Kapp, P.A., Yue, Y., and Lai, Q., 2007, Postcollisional calc-alkaline lavas and xenoliths from the southern Qiangtang terrane, central Tibet: Earth and Planetary Science Letters, v. 254, p. 28–38, doi: 10.1016/j.epsl.2006.11.019.

Ding, L., Kapp, P.A., Zhong, D., and Deng, W., 2003, Cenozoic Volcanism in Tibet: Evidence for a Transition from Oceanic to Continental Subduction: Journal of Petrology, v. 44, p. 1833–1865, doi: 10.1093/petrology/egg061.

Gao, Y., Hou, Z., Kamber, B.S., Wei, R., Meng, X., and Zhao, R., 2007, Lamproitic Rocks from a Continental Collision Zone: Evidence for Recycling of Subducted Tethyan Oceanic Sediments in the Mantle Beneath Southern Tibet: Journal of Petrology, v. 48, p. 729–752, doi: 10.1093/petrology/egl080.

Guo, Z., Wilson, M., and Liu, J., 2007, Post-collisional adakites in south Tibet: Products of partial melting of subduction-modified lower crust: Lithos, v. 96, p. 205–224, doi: 10.1016/j.lithos.2006.09.011.

Guo, Z., Wilson, M., Liu, J., and Mao, Q., 2006, Post-collisional, Potassic and Ultrapotassic Magmatism of the Northern Tibetan Plateau: Constraints on Characteristics of the Mantle Source, Geodynamic Setting and Uplift Mechanisms: Journal of Petrology, v. 47, p. 1177–1220, doi: 10.1093/petrology/egl007.

Guo, Z., Wilson, M., Zhang, M., Cheng, Z., and Zhang, L., 2013, Post-collisional, K-rich mafic magmatism in south Tibet: constraints on Indian slab-to-wedge transport processes and plateau uplift: Contributions to Mineralogy and Petrology, v. 165, p. 1311–1340, doi: 10.1007/s00410-013-0860-y.

Guo, Z., Wilson, M., Zhang, L., Zhang, M., Cheng, Z., and Liu, J., 2014, The role of subduction channel mélanges and convergent subduction systems in the petrogenesis of post-collisional K-rich mafic magmatism in NW Tibet: Lithos, v. 198-199, p. 184–201, doi: 10.1016/j.lithos.2014.03.020.

Harris, N.B.W., Ronghua, X., Lewis, C.L., Hawkesworth, C.J., and Yuquan, Z., 1988, Isotope Geochemistry of the 1985 Tibet Geotraverse, Lhasa to Golmud: Philosophical Transactions of the Royal Society A: Mathematical, Physical and Engineering Sciences, v. 327, p. 263–285, doi: 10.1098/rsta.1988.0129.

Hébert, R., Guilmette, C., Dostal, J., Bezard, R., Lesage, G., Bédard, É., and Wang, C., 2014, Miocene post-collisional shoshonites and their crustal xenoliths, Yarlung Zangbo Suture Zone southern Tibet: Geodynamic implications: Gondwana Research, v. 25, p. 1263–1271, doi: 10.1016/j.gr.2013.05.013.

Jiang, Y.-H., Jiang, S.-Y., Ling, H.-F., and Dai, B.-Z., 2006, Low-degree melting of a metasomatized lithospheric mantle for the origin of Cenozoic Yulong monzogranite-porphyry, east Tibet:

Geochemical and Sr–Nd–Pb–Hf isotopic constraints: Earth and Planetary Science Letters, v. 241, p. 617–633, doi: 10.1016/j.epsl.2005.11.023.

Jiang, D., Liu, J., and Ding, L., 2008, Geochemistry and petrogenesis of Cenozoic potassic volcanic rocks in the Hoh Xil area, northern Tibet plateau: Acta Petrologica Sinica, v. 24, p. 279–290, doi: CNKI:SUN:YSXB.0.2008-02-010.

Lai, S., and Qin, J., 2013, Adakitic rocks derived from the partial melting of subducted continental crust: Evidence from the Eocene volcanic rocks in the northern Qiangtang block: Gondwana Research, v. 23, p. 812–824, doi: 10.1016/j.gr.2012.06.003.

Lee, H.-Y., Chung, S.-L., Ji, J., Qian, Q., Gallet, S., Lo, C.-H., Lee, T.-Y., and Zhang, Q., 2012, Geochemical and Sr–Nd isotopic constraints on the genesis of the Cenozoic Linzizong volcanic successions, southern Tibet: Journal of Asian Earth Sciences, v. 53, p. 96–114, doi: 10.1016/j.jseaes.2011.08.019.

Li, Y., He, J., Wang, C., Santosh, M., Dai, J., Zhang, Y., Wei, Y., and Wang, J., 2013, Late Cretaceous K-rich magmatism in central Tibet: Evidence for early elevation of the Tibetan plateau? Lithos, v. 160-161, p. 1–13, doi: 10.1016/j.lithos.2012.11.019.

Liu, F., Yang, J.S., Dilek, Y., Xu, Z.Q., Xu, X.Z., Liang, F.H., Chen, S.Y., and Lian, D.Y., 2014, Geochronology and geochemistry of basaltic lavas in the Dongbo and Purang ophiolites of the Yarlung-Zangbo Suture zone: Plume-influenced continental margin-type oceanic lithosphere in southern Tibet: Gondwana Research, v. 27, p. 701–718, doi: 10.1016/j.gr.2014.08.002.

McKenna, L.W., and Walker, J.D., 1990, Geochemistry of crustally derived leucocratic igneous rocks from the Ulugh Muztagh Area, Northern Tibet and their implications for the formation of the Tibetan Plateau: Journal of Geophysical Research, v. 95, p. 21483, doi: 10.1029/JB095iB13p21483.

Miller, C., Schuster, R., Klotzli, U., Frank, W., and Purtscheller, F., 1999, Post-Collisional Potassic and Ultrapotassic Magmatism in SW Tibet: Geochemical and Sr-Nd-Pb-O Isotopic Constraints for Mantle Source Characteristics and Petrogenesis: Journal of Petrology, v. 40, p. 1399–1424, doi: 10.1093/petroj/40.9.1399.

Nomade, S., Renne, P.R., Mo, X., Zhao, Z., and Zhou, S., 2004, Miocene volcanism in the Lhasa block, Tibet: spatial trends and geodynamic implications: Earth and Planetary Science Letters, v. 221, p. 227–243, doi: 10.1016/S0012-821X(04)00072-X.

Turner, S., Arnaud, N., Liu, J., Rogers, N., Hawkesworth, C., Harris, N., Kelley, S.P., van Calsteren, P., and Deng, W., 1996, Post-collision, Shoshonitic Volcanism on the Tibetan Plateau: Implications for Convective Thinning of the Lithosphere and the Source of Ocean Island Basalts: Journal of Petrology, v. 37, p. 45–71, doi: 10.1093/petrology/37.1.45.

Turner, S., Hawkesworth, C., Liu, J., Rogers, N., Kelley, S.P., and van Calsteren, P., 1993, Timing of Tibetan uplift constrained by analysis of volcanic rocks: Nature, v. 364, p. 50–54, doi: 10.1038/364050a0.

Wang, B., Chen, J., Xu, J., and Wang, L., 2014, Geochemical and Sr–Nd–Pb–Os isotopic compositions of Miocene ultrapotassic rocks in southern Tibet: Petrogenesis and implications for the regional tectonic history: Lithos, v. 208-209, p. 237–250, doi: 10.1016/j.lithos.2014.09.008.

Wang, Q., Chung, S.-L., Li, X., Wyman, D.A., Li, Z.-X., Sun, W., Qiu, H.-N., Liu, Y.-S., and Zhu, Y., 2012, Crustal Melting and Flow beneath Northern Tibet: Evidence from Mid-Miocene to Quaternary Strongly Peraluminous Rhyolites in the Southern Kunlun Range: Journal of Petrology, v. 53, p. 2523–2566, doi: 10.1093/petrology/egs058.

Wang, Q., Wyman, D. a., Li, Z.-X., Sun, W., Chung, S.-L., Vasconcelos, P.M., Zhang, Q., Dong, H., Yu, Y., and Pearson, N., 2010, Eocene north–south trending dikes in central Tibet: New

constraints on the timing of east–west extension with implications for early plateau uplift? Earth and Planetary Science Letters, v. 298, p. 205–216, doi: 10.1016/j.epsl.2010.07.046.

Wang, R., Richards, J.P., Hou, Z., An, F., and Creaser, R. a., 2015, Zircon U–Pb age and Sr–Nd–Hf–O isotope geochemistry of the Paleocene–Eocene igneous rocks in western Gangdese: Evidence for the timing of Neo-Tethyan slab breakoff: Lithos, v. 224-225, p. 179–194, doi: 10.1016/j.lithos.2015.03.003.

Williams, H.M., Turner, S.P., Pearce, J.A., Kelley, S.P., and Harris, N.B.W., 2004, Nature of the Source Regions for Post-collisional, Potassic Magmatism in Southern and Northern Tibet from Geochemical Variations and Inverse Trace Element Modelling: Journal of Petrology, v. 45, p. 555–607, doi: 10.1093/petrology/egg094.

Yang, D., and Ding, L., 2013, Geochronology and geochemistry of the high magnesium and high potassium ultrabasic leucite basanite in northern Tibetan Plateau: Chinese Journal of Geology, v. 48, p. 449–467.

Zhang, Z., Xiao, X., Wang, J., Wang, Y., and Kusky, T.M., 2008, Post-collisional Plio-Pleistocene shoshonitic volcanism in the western Kunlun Mountains, NW China: Geochemical constraints on mantle source characteristics and petrogenesis: Journal of Asian Earth Sciences, v. 31, p. 379–403, doi: 10.1016/j.jseaes.2007.06.003.